IMPROVED SCALING LAWS FOR STAGE INERT MASS OF SPACE PROPULSION SYSTEMS

Volume II - System Modeling & Weight Data

June 1971

PREPARED
FOR

NATIONAL AERONAUTICS AND SPACE ADMINISTRATION
AMES RESEARCH CENTER
MOFFETT FIELD, CALIFORNIA 94035

CONTRACT NAS2-6045

APPROVED BY

J. A. BODDY
STUDY MANAGER

Space Division
North American Rockwell

SD71-534-2

FOREWORD

The Improved Scaling Laws for Stage Inert Mass of Space Propulsion Systems Study was conducted by the Space Division of the North American Rockwell under Contract NAS2-6045 for the Advanced Concepts and Missile Division of the National Aeronautics and Space Administration. The contract involved a study for the development of improved scaling laws for stage inert mass of future planetary vehicle systems. The laws were to consider the effects of mission profiles, propulsion/propellant combinations and advanced structural concepts.

This report is submitted in three volumes -

I. (SD71-534-1) Summary Report

II. (SD71-534-2) System Modeling and Weight Data

III. (SD71-534-3) Propulsion Synthesis Program - Programmers and Users Manual

This volume details the technical models and analytical approaches used to develop the weight data for vehicle system concepts using advanced technology. Weight data are supplied for the following major system elements: engine, pressurization, propellant containers, structural shells and secondary structure, and environmental protection shields for the meteoroid and thermal design requirements. Scaling laws, improved and a simplified set, were developed from the system weight data. The laws consider the implications of the major design parameters and mission requirements on the stage inert mass.

ACKNOWLEDGEMENTS

The following North American Rockwell, Space Division, personnel were the major contributors to the technical contents of this volume:

C. M. McCrary	Propulsion and Fluid Systems
C. K. McBaine	Weight Prediction
B. J. Hamry	Structural Synthesis
A. J. Richardson	Penetration Mechanics
J. P. Sanders	Meteoroid Structures
J. A. Boddy	Thermal Insulation
C. W. Martindale	Synthesis Program Development
J. A. Boddy	System Modeling

The Contracting Officer Representative for the National Aeronautics and Space Administration, Duane W. Dugan of the Advanced Concepts and Mission Division, provided valuable guidance and direction throughout the study.

CONTENTS

Preceding page blank

CONTENTS (CONT'D)

ILLUSTRATIONS

ILLUSTRATIONS (CONT.)

ILLUSTRATIONS (CONT.)

ILLUSTRATIONS (CONT.)

APPENDIX A. STRUCTURAL SHELL ANALYSIS

APPENDIX A. STRUCTURAL SHELL ANALYSIS (CONT'D)

APPENDIX B. METEOROID SHIELDING

APPENDIX B. METEOROID SHIELDING

APPENDIX C. THERMAL INSULATION OPTIMIZATION FOR PROPELLANT TANK

APPENDIX D. OPTIMUM THERMAL SHIELDING FOR TANK SUPPORTS

TABLES

TABLES (CONT'D)

1.0 INTRODUCTION

Scaling laws currently used in weight prediction are based upon specific basepoint designs developed to reflect existing technology. The application of these laws to advanced systems is not always meaningful. Future propulsion systems will utilize advanced design concepts and technology improvements. Some of these advanced designs are currently under development but no historical hardware data exists to permit statistical analysis for weight-scaling relationships. Experience relating to advanced space system designs has been accumulated during many studies in the past few years that will assist in fulfilling the requirements of this study. Both manned and unmanned space vehicles have been studied utilizing many different engine systems and design concepts for the propulsion stages.

Comparative vehicle performance can be based on the relative weight of various concepts, but absolute weight in a usable form is required to identify overall system performance. Reasonably accurate laws are necessary to generate confidence in the performance evaluation of advanced space systems. These scaling laws must be more sophisticated than simple gross laws and must reflect the effects of several design parameters. An error of a few percent in the element weights of the stage mass fraction can make the difference between a merely feasible concept and a more efficient concept. Any attempt at weight estimation in the early design phases should provide accuracy, flexibility, and technical depth in sufficient detail to measure the sensitivity of the individual design parameter to the subsystem and to the overall system.

Weight-scaling laws for the major subsystems and structural elements must be sufficiently comprehensive to differentiate between types of engines and propellants, types of subsystems and their usage, stage geometric characteristics, special design constraints, and overall mission performance requirements. Scaling laws for structural components must reflect the time period in which the components are to be designed, developed, and utilized.

The conventional methods of using historical data for existing launch vehicle components, such as the present Saturn-class vehicles, are of limited value in deriving scaling laws for components consisting of advanced materials and/or construction concept. Many weight prediction tools are used to extrapolate beyond the allowable region of the basepoint design. Items such as minimum feasible weight due to design constraints, manufacturing constraints, etc., are ignored by the prediction laws and models. It was the intent of this study to overcome some of these problems by providing weight modeling of the various systems and subsystem elements of space propulsion

modules and to identify the major design parameters that influence the scaling laws. Scaling relationships developed were correlated with actual design systems and compared with design studies for future vehicle systems.

Design information relating to future systems, where no historical data are available, were mathematically modeled and data synthesized by the NR Space Division's Computer Aided Design programs. Detailed parametric weights data were generated to encompass system concepts considering various insulation concepts, meteoroid protection designs, and engine systems. Tankage and structural arrangements were evaluated for storable and cryogenic systems using both clustered and tandem vehicle staging. Realistic design data developed, provided a foundation for the derivation of structural-scaling laws for components consisting of advanced materials and/or constructions. The generated data for the future theoretical subsystem were screened and adjusted with their appropriate non-optimum weight factors in order to reflect actual fabricated subsystem weights.

This volume details the analytical models employed for the data generation and data reduction, parametric weight data for the different systems and the resulting improved scaling laws for stage inert mass. These laws apply to vehicle systems employing pressure- or pump-fed engines using cryogenic or storable propellant combinations with the stages constructed from current or future types of material or construction, and capable of fulfilling a vast spectrum of mission objectives. The improved scaling laws are incorporated into a computer program devised to size space propulsion systems for a wide variety of applications.

For those who, from necessity or preference, would use a manual method rather than the computer code, the improved scaling laws are presented in a simplified version by means of graphs, nomograms, step-by-step procedures, equations and other devices designed to make the task of assessing the performance of a space propulsion system for a given application as convenient as is possible without sacrificing the degree of accuracy attained with the more detailed treatment offered by the computer program.

2.0 STUDY APPROACH

Weight estimating is essentially limited to prediction procedures that cannot be directly substantiated by test. A large portion of this effort is directed toward the development and refinement of rather sophisticated analytical tools, which, in order to be accurate, accountable, and sensitive to the parameters that affect weight, must be expressed in terms of the very load-geometry-configuration-environment parameters that are so difficult to quantify in the early conceptual stages of a design. It cannot be used without a degree of good engineering judgement; and insofar as is possible, should be closely coordinated with the other disciplines contributing to a particular design analysis.

Weight prediction methods to support this effort were derived from:

1. Actual weights (known weights of off-the-shelf components)
2. Empirical analysis (weights based upon experience and past designs with statistical correlations)
3. Prediction models (development of analytical models to represent the system in terms of system weight and major design parameters)

None of these approaches can completely satisfy requirements for improved scaling laws, because actual weights of future space vehicle elements are not available. Detailed analysis requires design-strength and performance analysis, and definition of a detailed design environment; an in-depth analysis is usually not warranted. Historically based empirical scaling laws are useful when components used are similar to those from which the empirical relationships were derived, however, extrapolation beyond appropriate ranges is always hazardous. Weight contingencies and weight growth must be included in some fashion in the prediction technique and must be apportioned to the subsystem if accurate system performance estimates are to be obtained.

A weight prediction system that is statistical-analytical, as opposed to purely empirical, is based on the correlation of actual in-service hardware by function and structural penalty with logical combinations of identifiable design parameters of the following four types:

1. Load (gross weight, major externally applied acceleration loads, fuel pressures)

2. Geometry (external exposed area, structural members, tankage arrangement, thickness)

3. Configuration (type of construction, material, structural arrangement, cut-out size)

4. Environment (temperature, internal pressure, meteoroid flux)

Any of the prediction models for the subsystems must include configuration penalties and special penalties for non-optimum weight factors. Configuration penalties include materials required to accommodate the portions of component weight set by specific requirements and/or classes of vehicles; (e.g., docking, tankage arrangement, payload attachment, etc.) Special penalties are represented by the portions component weight required to accommodate special and unique environmental-usage requirements and criteria; (e.g., manned or unmanned, meteoroid and thermal protection, fatigue, and reliability requirements). This category of weight cannot normally be predicted by statistical-analytical means; usually, an allowance or estimate is made in the early stages.

The various weight prediction models used in this study include the following:

1. Element analytical modeling for subsystems amenable to this technique.

2. Statistical and historical scaling for elements not amenable to modeling.

3. Correlation of Items 1 and 2 with detailed design data.

4. Recognition of mission-dependent and design-dependent parameters.

5. Inclusion of weight contingency and growth patterns.

Major load-carrying structures, thermal and meteoroid protection, and propulsion systems can be included in the analytical models. Secondary structure (i.e., supports, cut-outs for doors, electronic equipment, electrical system, and power supplies are more adaptable to the statistical approach than to detailed analysis.

The study approach, Figure 1, was to collect and generate parametric weight data for the various vehicle systems, reduce the data to a series of improved scaling laws for stage inert mass and define the procedures used

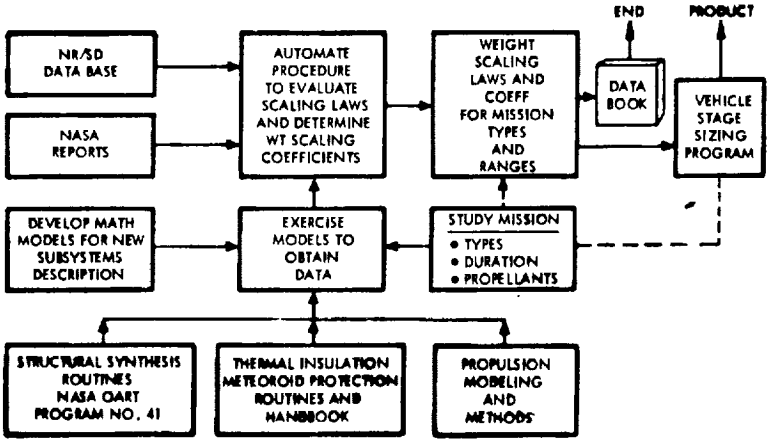

Figure 1. Study Approach Logic

to synthesize the vehicle systems both manually and with a computer program. Data were collected and reviewed, the sources included the NR/SD data bank, on-going NASA studies, and in-house studies relating to advanced propulsion systems. Appropriate rocket-engine manufacturers were surveyed to obtain the most current engine data and weight/performance predictions for future systems. The major weight elements and design parameters were identified for the various types of propulsion subsystems. These elements include, where applicable, engine, propellant feed, pressurization, plumbing, and controls. Scaling models were devised for these elements which incorporate the pacing design parameters. Models were provided for the various tankage arrangements, common/separate bulkheads, clustered/tandem staging, and geometric models describing volumes, surface areas, etc., Structural synthesis programs were exercised to determine typical weights for bulkheads, pressurized and unpressurized shells, and thrust structures fabricated from conventional and advanced composite materials/construction. Thermal insulation models were developed to determine system requirements and weight budgets for the spectrum of anticipated missions, environments, and stage sizes. Meteoroid protection concepts were described and analyzed with acceptable penetration mechanics theories and for a series of meteorcid flux models.

The theoretical weight data obtained were reviewed and edited, and non-optimum weight factors, secondary structure, and weight budgets were included based on experience and existing historical data. Data were

conditioned and reduced statistically to weight-scaling laws for the various subsystem elements for a spectrum of propulsion/propellant modules and a family of missions. The range of application for each series of scaling coefficients was identified together with the concept type and technology advancement.

An NR/SD parametric stage synthesis program was developed which included routines capable of accepting the improved subsystem-scaling laws and an executive main program supplied to control concept selection.

The study requirements were to investigate the effects of mission and design selection on various stage modules and develop a series of improved scaling laws which describe the stage inert mass. Mission and design selection were meant to include

1) Mission Objectives
   a) Trajectory profile, duration and velocity requirements
   b) Performance and payload requirements
2) Design Concepts
   a) Engine type
   b) Propellant combination
   c) Stage configuration and arrangement
3) System Elements
   a) Construction method
   b) Material selection
   c) Protection concept
4) Design Environment
   a) External loading
   b) Internal pressure
   c) Meteoroid flux
   d) Thermal flux

5) Design Criteria

   a) Structural integrity

   b) Margins-of-safety

   c) Penetration probability

   d) Design constraints

6) Technology Base

   a) Current and existing

   b) Advanced

The stage propulsion modules are best analyzed by subdividing them into independent but interrelated subsystems. In order to completely describe the propulsion module, four major subsystems will be used and weight scaling developed for the subsystem and/or its primary elements, Table 1.

Table 1. Major Subsystem and Primary Weight Elements

Engine Module	Propellant Module	Environmental Protection	Other Subsystems
Thrust Chamber Assembly Turbo Pump Thrust Vector Controls Plumbing Propellant-Feed Aft Skirt Enclosing Engines Thrust-Structure	Tank Wall Bulkheads Slosh/Vortex Baffles Secondary Structure Tank Supports Forward Skirt Intertank Aft Skirt Pressurization System Payload Adaptor	Cryogen Insulation Insulation Attachment Meteoroid Bumpers Secondary Structure	Guidance and Navigation Attitude Control Docking Electrical & Power Instrumentation Interstage Structure for Tandem or Parallel

The engine module weight is affected by the type of engine system used, its thrust level and overall length. An outer support structure encloses the engine and is a function of the engine length. A second module consists of the structure required to contain the propellants and its associated structure. Weights for the environmental protection are based upon the exposed surface areas of both the engine and propellant modules, the propellant characteristics and the mission profile. The remainder of the stage inert mass has been assigned to the fourth weight module. The scaling laws used in the stage mass prediction are based upon design data from specific base-point designs reflecting existing hardware, and advanced design concepts.

This stage synthesis approach, Figure 2, was able to consider different vehicle models and subsystems subjected to a series of design load environments. The synthesis procedure is an iterative approach which cycles through several analytical steps to define a vehicle which is derived from the scaling laws, consistent with the design environment, and capable of fulfilling the mission objectives. The analytical steps include determining the vehicle's lump-mass propellant requirements, the stage shape and dimensions, the design environment experienced throughout the mission, and weight estimates for the various subsystems of the vehicle.

Vehicle synthesis approaches were provided to minimize the vehicle's gross lift-off weight for a fixed payload, or maximize the payload capability for a fixed gross lift-off weight. Elements of the synthesis program were used during the study to provide parametric data of the integrated meteoroid flux for the simplified scaling laws. The interaction between the synthesis program and other detailed design programs is shown in Figure 3, and shows how the parametric data are prepared for the different structural elements and design concepts.

Design synthesis routines of the NR Computer Aided Design library were modified and used to provide design data for the major structural elements subjected to boost acceleration and pressure-induced loads. Figure 4 is an example of the procedure used for structural optimization. Design weight requirements for various meteoroid shielding concepts were obtained from existing programs which optimize the design arrangement by considering the penetration mechanics involved with successfully stopping the impacting meteoroid particles.

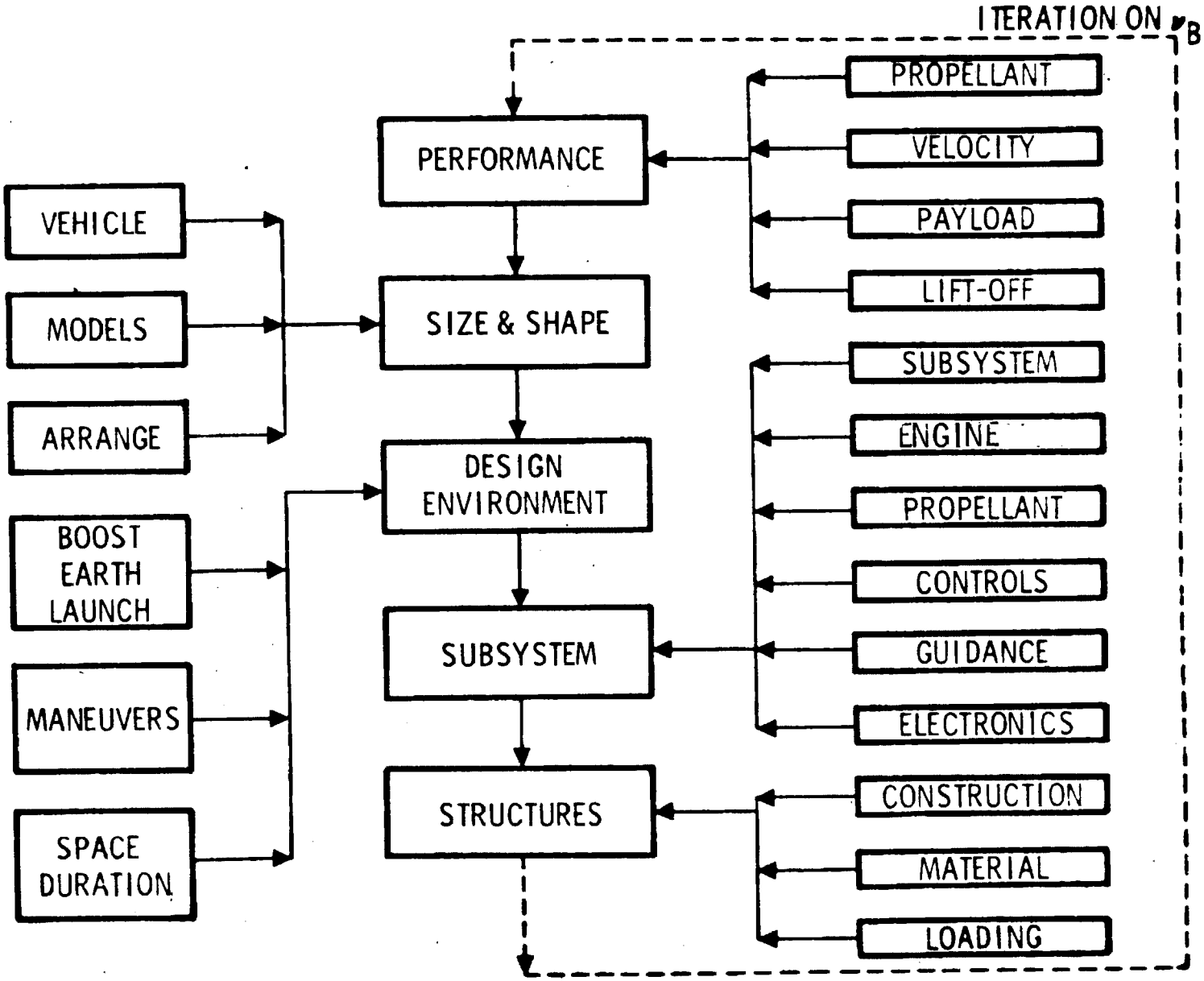

Figure 2. Iterative Procedure for Stage Synthesis

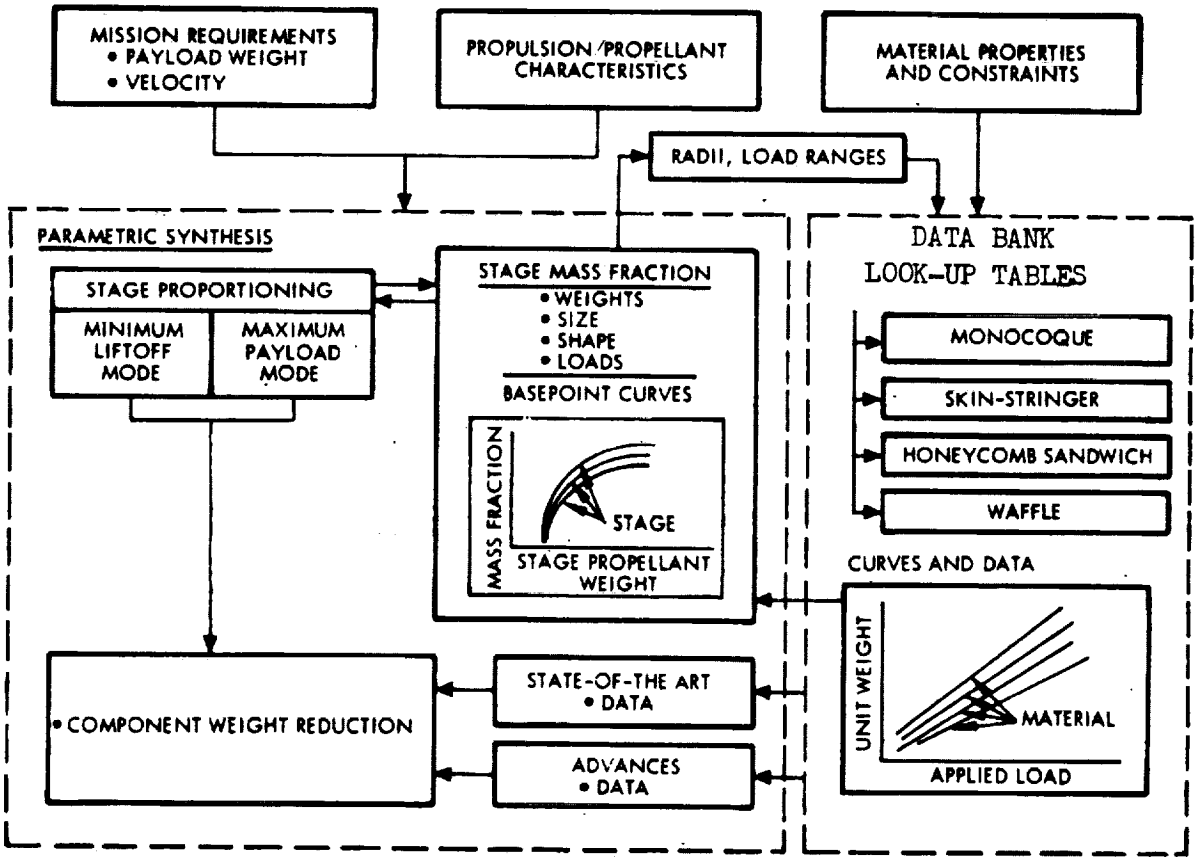

Figure 3. Parametric Synthesis and Data Bank Coupling

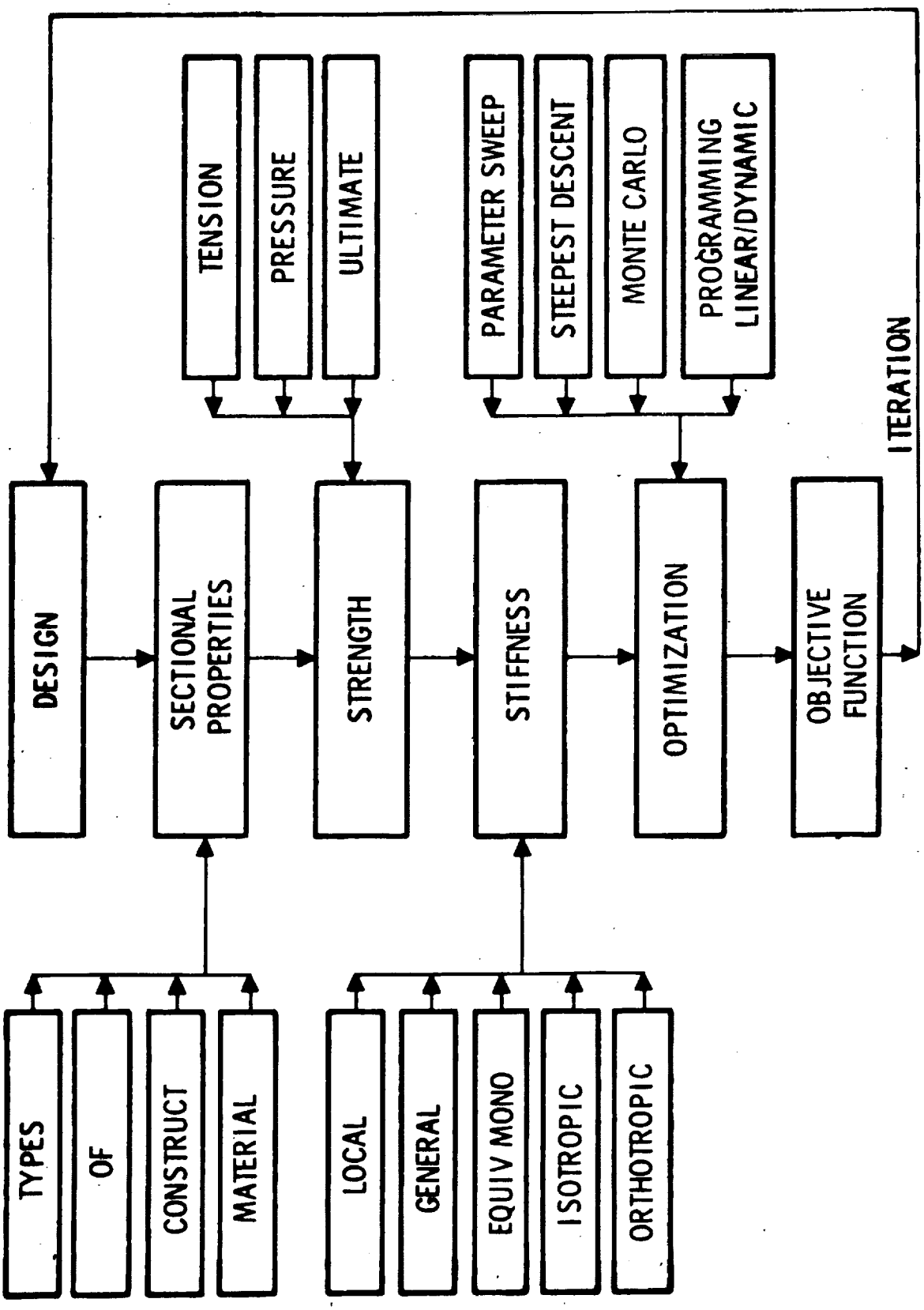

Figure 4. Structural Synthesis Procedure

THIS PAGE LEFT

INTENTIONALLY BLANK.

3.0 DATA REDUCTION

The improved scaling laws were developed both from historical data and information derived from mathematical models which were exercised by various synthesis computer programs. Most of the raw parametric data obtained represented design weights for specific design basepoints or limited ranges of individual parameters. The study required developing scaling laws embracing completely the specified design spectrum reflecting the variations due to the major parameters. Data that were obtained from numerous sources have been screened and statistically reduced to derive the appropriate scaling relationships. The method of data reduction employed was a constrained multi-linear regression analysis together with various equational forms which were felt to provide a "good fit" to the available data. An example of fitting engine weight data is shown to indicate the procedure, method of "tailoring" data and back substitution to indicate the goodness of fit. This procedure with slight variations has been applied to the structural elements and other subsystems which comprise the propulsion module.

The scaling equations for the engine systems were derived from parametric data supplied by the engine manufacturers and from existing engine systems. Parameters having the greatest influence on engine weight are thrust (F), engine chamber pressure (P_c), and nozzle area ratio (ε). For ablatively-cooled engines, engine life is a significant auxiliary term for the burn-time requirements. Most of the parametric data are based on the use of pressure-fed engines for the low-thrust range, and pump-fed systems for the larger engines. The foremost design parameter affecting the weight data was the engine thrust level, whereas the pressure and expansion ratio parameters had secondary effects. It was the prime intent of the scaling equations to match the data as closely as possible to the prime parameter, thrust level, with slight perturbations to account for variations due to changes in chamber pressure, expansion ratio, and burn-time.

There are many forms for the scaling equations; each type of equation has its relative merits in terms of goodness of fit to the weight data. Scaling law relationships fitted with polynomial expressions, second- or higher-order, have a serious deficiency in that inflection points can occur within their range of application resulting in two different engine systems having the same weight. This effect can be corrected by using a linear expression, which however, seriously limits the shape of the curve. Another approach would be to represent the engine weight by the design parameters raised to some exponential power. This form of the equation has several advantages:

1. It is assured of being monotonic throughout a single-parameter range.

2. The engine has a finite weight throughout the specified thrust range for the scaling law.

3. Depending on the sign and the magnitude of the exponents, this curve can assume many varied shapes.

Fitting a curve to an exponential expression with a weighted least squares approach will allow for wide ranges of design parameters and will produce only small magnitude errors in the resulting system weight. If a simple polynomial expression is used and an unweighted least squares is adopted, the results will produce large magnitude differences for the low-weight engine systems. This approach produces extremely large percentage errors for small engines and insignificant percentage errors for the larger engines. It is better from the weight scaling approach to minimize the deviation of percentage changes of engine weight. Transforming the data to the logarithmic domain and applying a multi-linear regression analysis minimize the percentage differences throughout the range of engine weight. The resulting scaling law can then be measured as a percentage difference based on the actual engine weight rather than on an explicit magnitude difference. The general form of the weight-scaling equation used to define the engine system is shown in Equation 1.

$$W_{ENG} = K\,(F)^{a}\,(P_c)^{b}\,(\varepsilon)^{c}\,(t_b)^{d}$$

K = equation coefficient

F = thrust

P_c = chamber pressure

ε = expansion ratio

t_b = burn time

a,b,c,d = exponents

A typical procedure for fitting these data is outlined to demonstrate the systematic approach to defining the scaling equation that best represents the particular engine data. Data for a FLOX/methane propellant combination from References 1 and 2 have been used to indicate the systematic data reduction. Visual inspection of the data (Figure 5) clearly indicated that, for the large-thrust levels, the weight was nearly linearly dependent upon thrust level. A multiple regression analysis was performed to derive the required coefficients for Equation 1, which would result in a good representation of these data. The resulting equation and its coefficients are given by Equation 2.

$$W_{ENG} = 0.4105\,(F)^{0.9269}\,(P_c)^{-0.467}\,(\varepsilon)^{0.094} \qquad (2)$$

$$40{,}000 \leq F \leq 250{,}000 \text{ lbf}$$

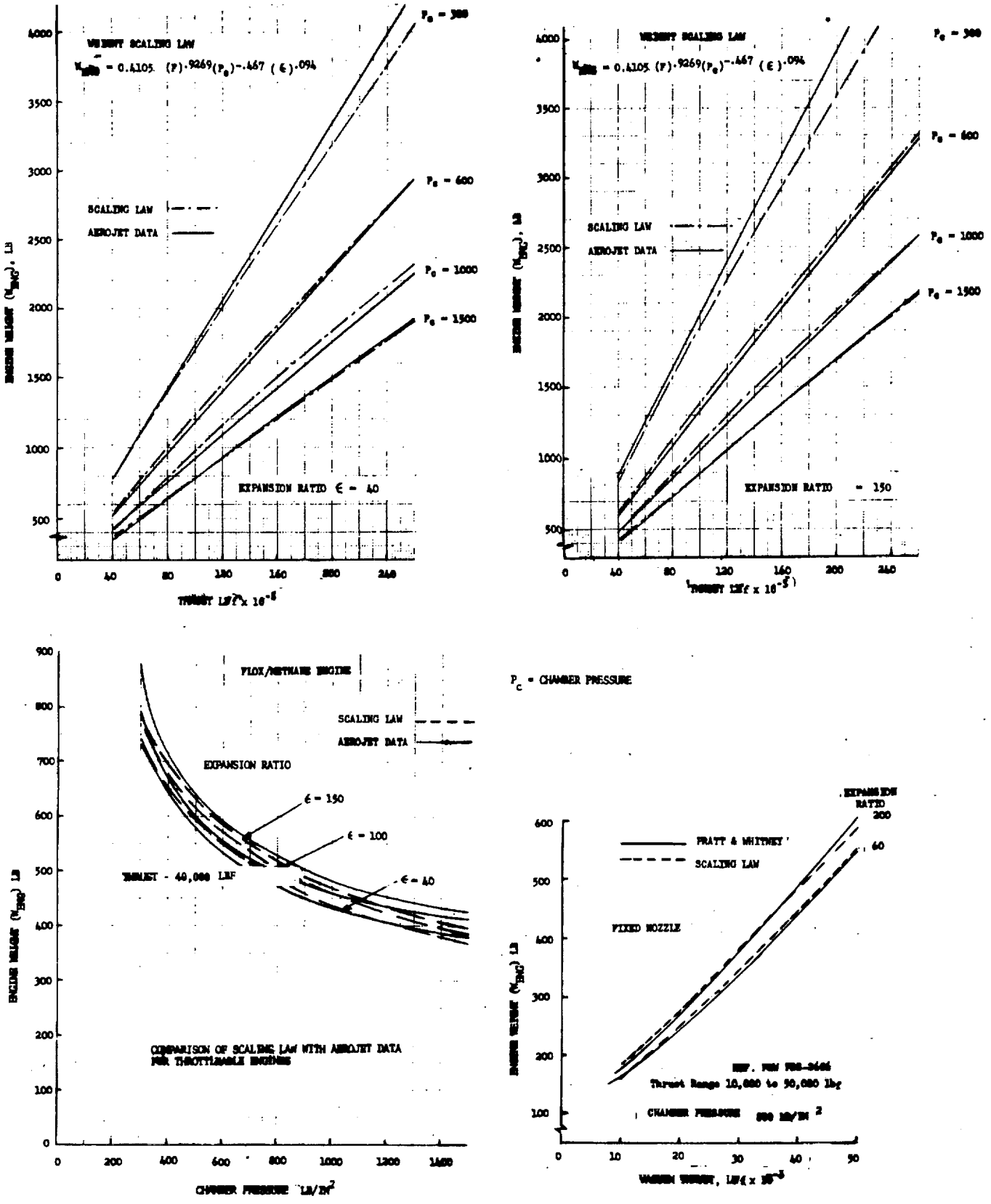

Figure 5. Parametric Weight Data for FLOX/Methane Engines

This scaling law equation has been transposed onto the original data (Figure 5) to indicate the goodness-of-fit. It is to be recognized that other FLOX/Methane engine systems with different chamber pressures and different expansion ratios are completely described from the standpoint of weight by this equation.

For the lower-thrust engines there were insufficient data points to produce a multi-parameter scaling law using statistical analysis and have the law provide a good fit to the original data. The existing data points are used with a constrined regression analysis and *a posteriori* information from other similar systems. The Aerojet General data, at a constant thrust level of 40,000 lbf (Figure 5) were used to obtain correlation between the remaining parameters.

$$W_{ENG}\Big|_{F=40,000} = K^{*} \quad (P_c)^{-0.43} \quad (\varepsilon)^{0.05} \tag{3}$$

The two exponents of Equation 3 were systematically applied to the remaining weight data for the low-thrust engines. Initially all the data were modified to a nominal expansion ratio of 160

$$W_{ENG}\Big|_{\varepsilon = 160} = W_{ENG}\Big|_{\varepsilon} \quad \left(\frac{160}{\varepsilon}\right)^{0.05} \tag{4}$$

A further reduction of this modified data were conducted to a nominal chamber pressure of 800 lb/in^2.

$$W_{ENG}\Big|_{\substack{\varepsilon=160 \\ P_c=800}} = W_{ENG}\Big|_{\substack{\varepsilon=160 \\ P_c}} \quad \left(\frac{800}{P_c}\right)^{-0.43} \tag{5}$$

The data modification process provides sufficient information to determine the remaining exponent and coefficient for the engine weight-scaling.

$$W_{ENG} = 1.1819 \ (F)^{0.814} \ (\varepsilon)^{0.05} \qquad F < 40,000 \text{ lbf} \tag{6}$$

The engine weights from this scaling equation, Figure 5, indicate the comprehensive representation with the original data and that the errors are within acceptable limits.

4.0 STRUCTURAL SYNTHESIS

The major structural elements of any propulsion stage are the propellant containers, the unpressurized components (skirts, interstage) and the thrust structure. Weight allowances must be assigned to each of these major elements to account statistically for the secondary structure and ancillary equipment. Each of the structural components is divided into its element models, each element is defined analytically, and a preliminary design synthesis is conducted on the individual elements to identify minimum weights for feasible designs. Different types of construction and materials are considered for the range of mission parameters, environments and design criteria. Design data thus derived are subjected to a multi-linear regression analysis to define an appropriate scaling law for each element. Combination of these element laws will provide a relationship for the major components. A correlation factor (non-optimum weight, etc.) is applied to these laws based on historical data pertinent to the type of material, construction, and complexity of the structural component.

The structural modeling consists of the derivation of the parametric equations that describe the structural weight of the stage in terms of its various components for a range of propellant combinations and loadings and for specific geometries.

The components investigated included:

1. Tankage (Bulkheads, tank wall)
2. Intertank Structure
3. Forward Skirt
4. Interstage Structure
5. Thrust and Engine Mounting Structures

The structural requirements for the payload were not analyzed because of lack of definition of the payload. Weight allowances for the payload adaptor were included in the forward skirt of the upper stage to account for bolting rings and variations between the stage and payload diameters.

The structural shells of the propulsion stage are a major contributor to the stage's inert weight. Improved weight-scaling laws defining the structural contribution must differentiate between the effects of stage diameter, loading environment, types of construction and materials, and weight reduction predictions for future technology. Weight data for the structural shells were generated using existing detail design synthesis programs, Reference 3. These data are used to derive the structural scaling laws.

Design loading for the structural elements are considered for earth launch or space launch conditions. Compressive load intensities are due to:

1. Axial loads caused by maximum longitudinal acceleration during earth launch when the stage is boosted into orbit. Propellant tanks could be full or empty.

2. Body bending if the stage is subjected to lateral accelerations during ascent. The mode of transportation to orbit will influence the lateral forces; wind and drag loads if the stage is the payload (upper stage) of the launch vehicle, or reaction loads from support cradles if carried in the cargo bay of the reusable space shuttle vehicle.

3. Engine thrust loads during space operation of the stage or parent vehicle system.

Engine net-positive-suction-head requirements will determine the tank pressure schedule and impose design conditions on the tank wall and bulkhead thicknesses.

The design synthesis programs considered the structural strength and stiffness requirements resulting from compressive and pressure design criteria. Details of the strength and stability analysis for skin stringer and waffle design concepts are given in Appendix A of this report. Instability failure modes considered are:

1. Panel buckling of the skin

2. Panel buckling of stiffener elements

3. Crippling load of combined stiffener elements

4. Column buckling of combined stiffener and attached skin

5. General shell instability

Various combinations of structural concepts, material properties and design parameters have been investigated to determine their effects, if any, on the weight data. The range of parameters considered were:

1. Construction

   Skin-stringer, top-hat and integral stiffeners

   Waffle grid pattern

2. Material

   Aluminum alloy 2014-T6

   Titanium alloy 6AL-4V

   Projected improved alloys

3. Geometry

   50 to 300 inch radius

4. Loading environment

   Ultimate compressive loading intensity

   500 to 10,000 lb/in

   Internal burst pressure

   15 to 300 lb/in^2

   Temperatures range from cryogenic to room temperature

4.1 STRUCTURAL SHELLS

The structural synthesis programs using the shell analysis discussed in the Appendix A were used to define the unit shell weight for unpressurized and pressurized shells fabricated from aluminum, titanium, and beryllium. The unit weights were obtained for a series of shell radii, pressure levels, material property changes with temperature, and compressive load intensities. Typical unit shell weight data are shown in Figures 6 through 10 as a function of the compressive load intensity and other design parameters. A comprehensive list of structural-weight data is provided in Appendix A. The weight data obtained were statistically reduced to provide the appropriate scaling relationships.

Unit weight for unpressurized shell is

$$W_{shell} = K_1 N_x^{K_2} \sigma^{K_3} (R+K_4)^{K_5} E^{K_6}$$

N_x = compressive load intensity

σ = material working stress

E = Young's Modulus of the material

R = shell radius

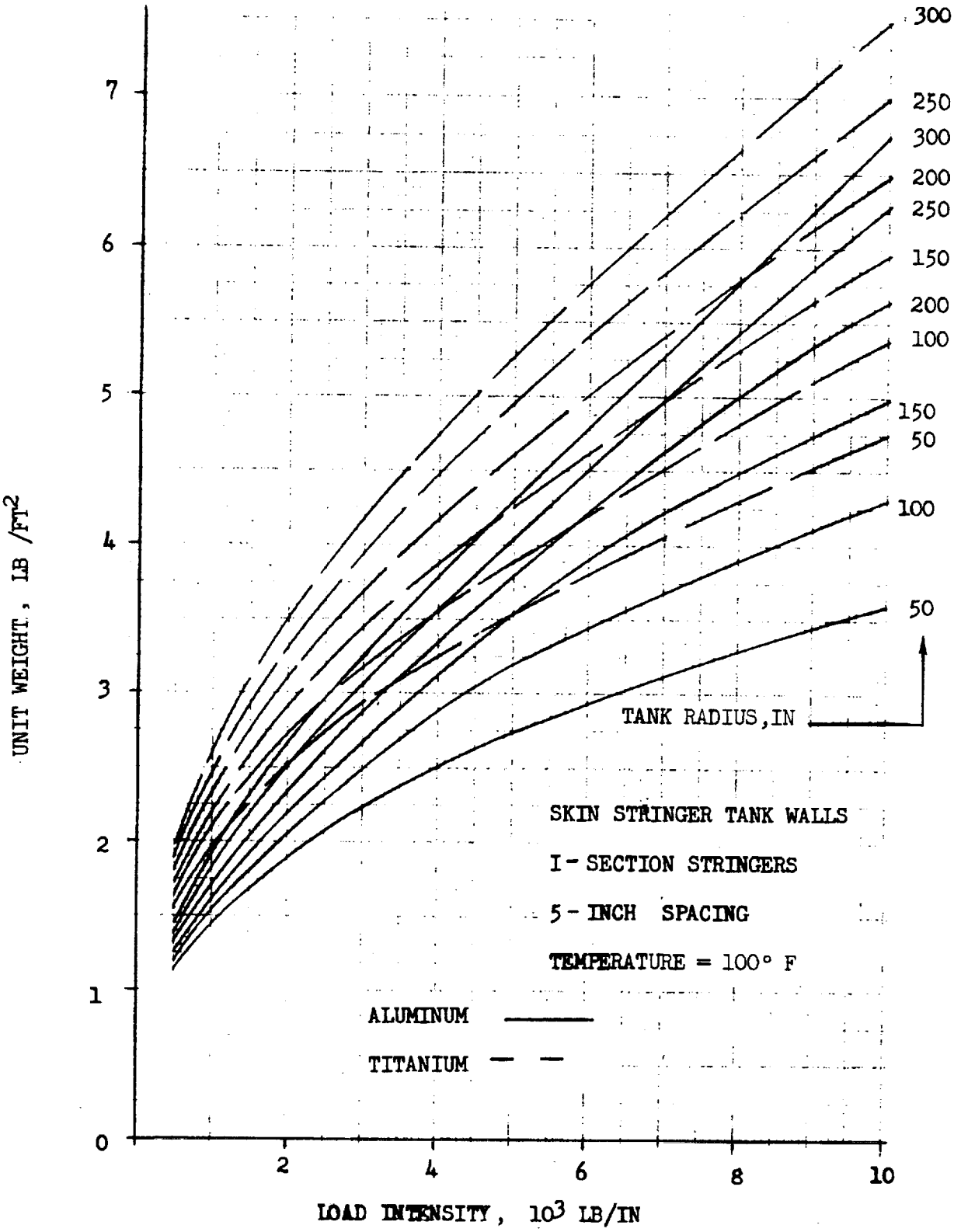

Figure 6. Skin-Stringer Tank Wall Unit Weight for Unpressurized Tanks — Aluminum and Titanium

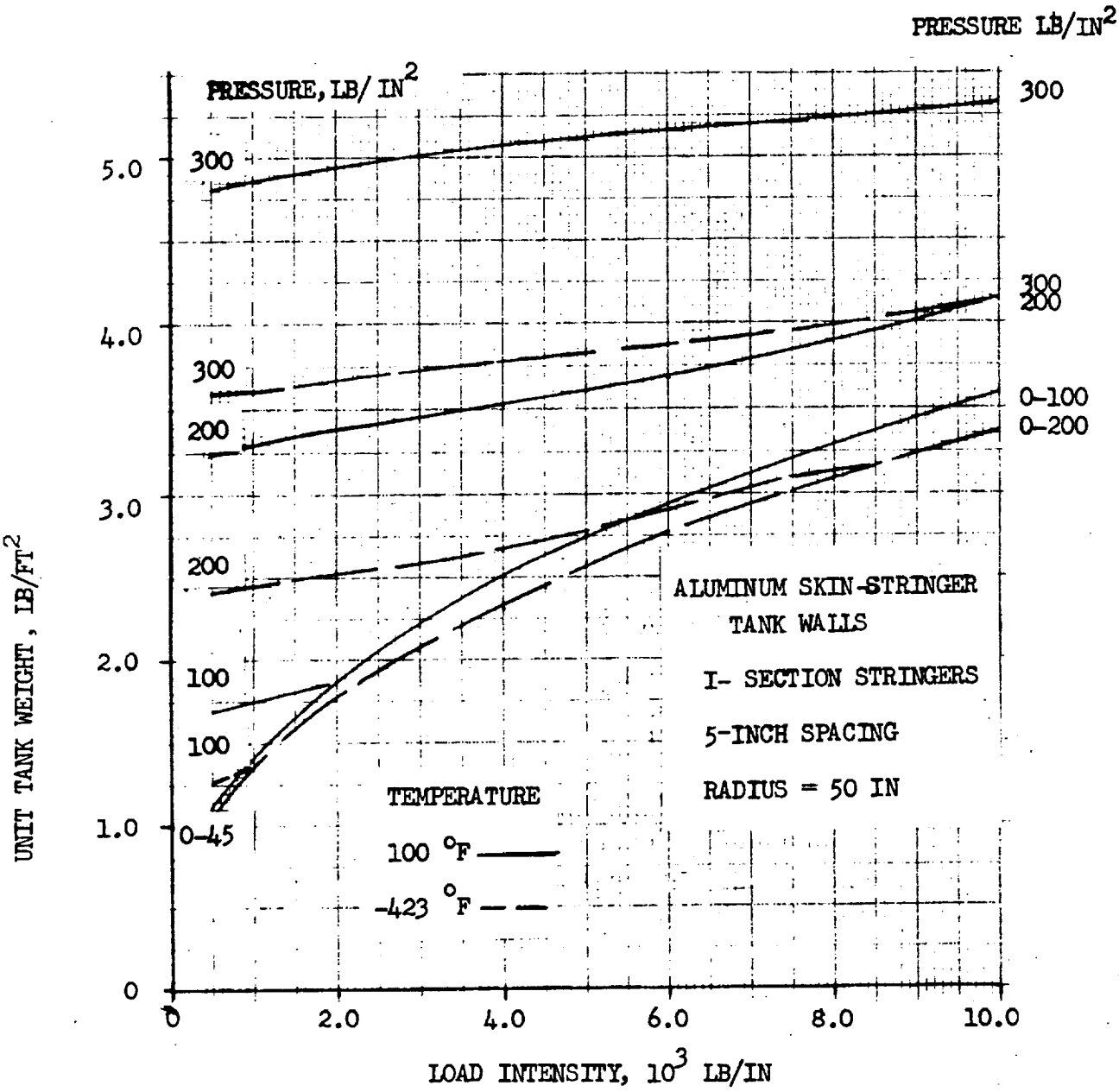

Figure 7. Skin-Stringer Tank Wall Unit Weight for Pressurized Aluminum Tanks of 50-Inch Radius

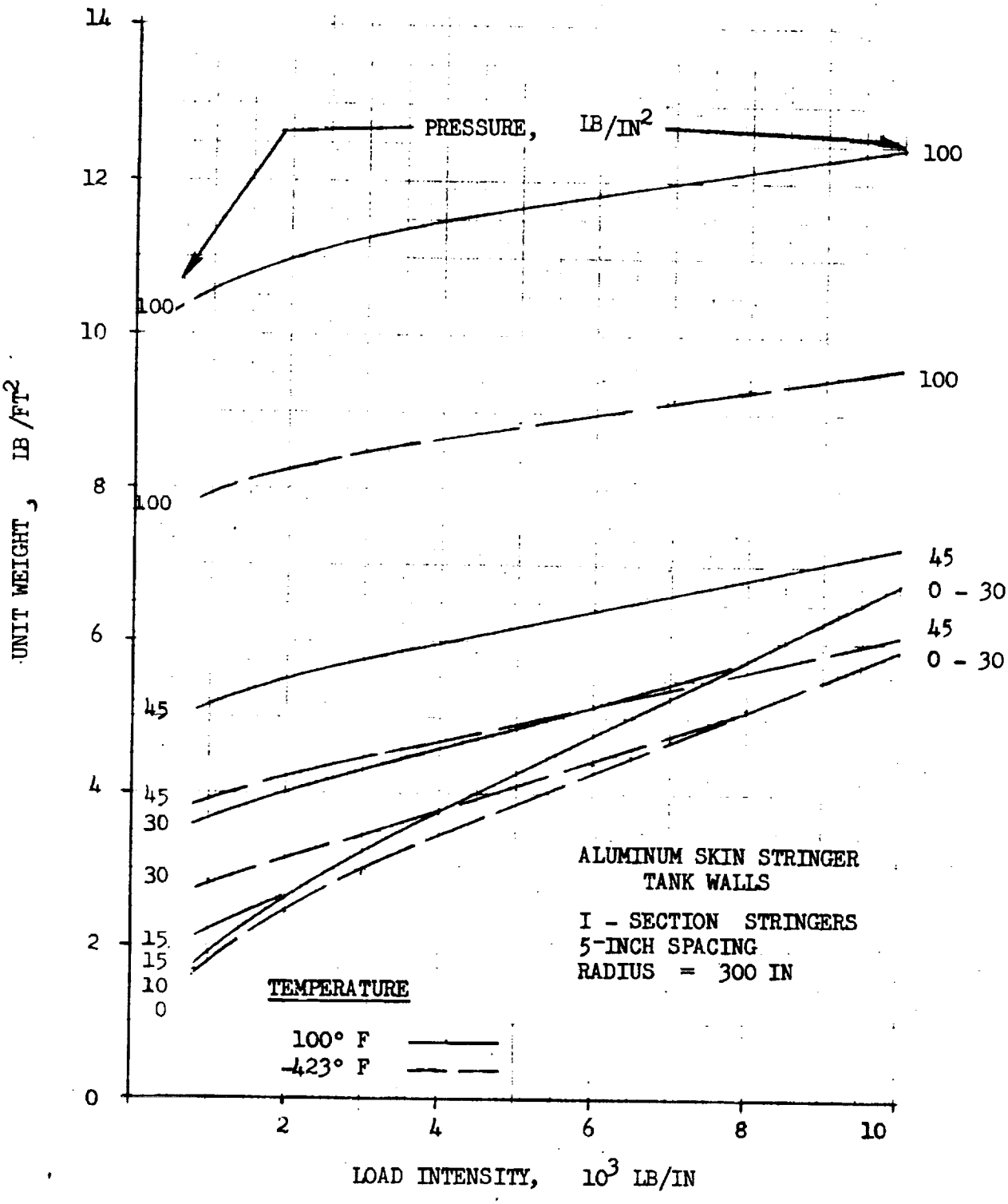

Figure 8. Skin-Stringer Tank Wall Unit Weight for Pressurized Aluminum Tanks of 300-Inch Radius

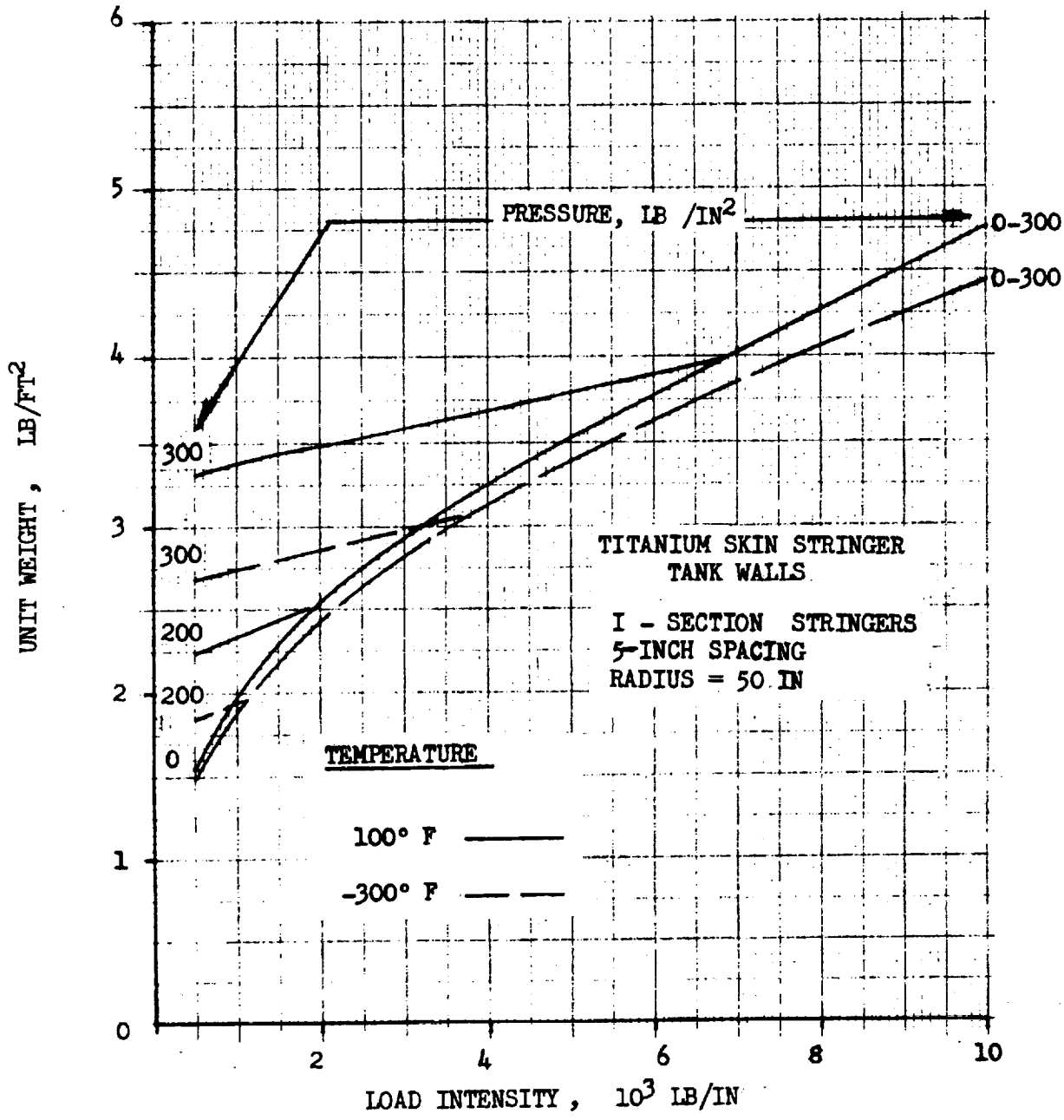

Figure 9. Skin-Stringer Tank Wall Unit Weight for Pressurized Titanium Tanks of 50-Inch Radius

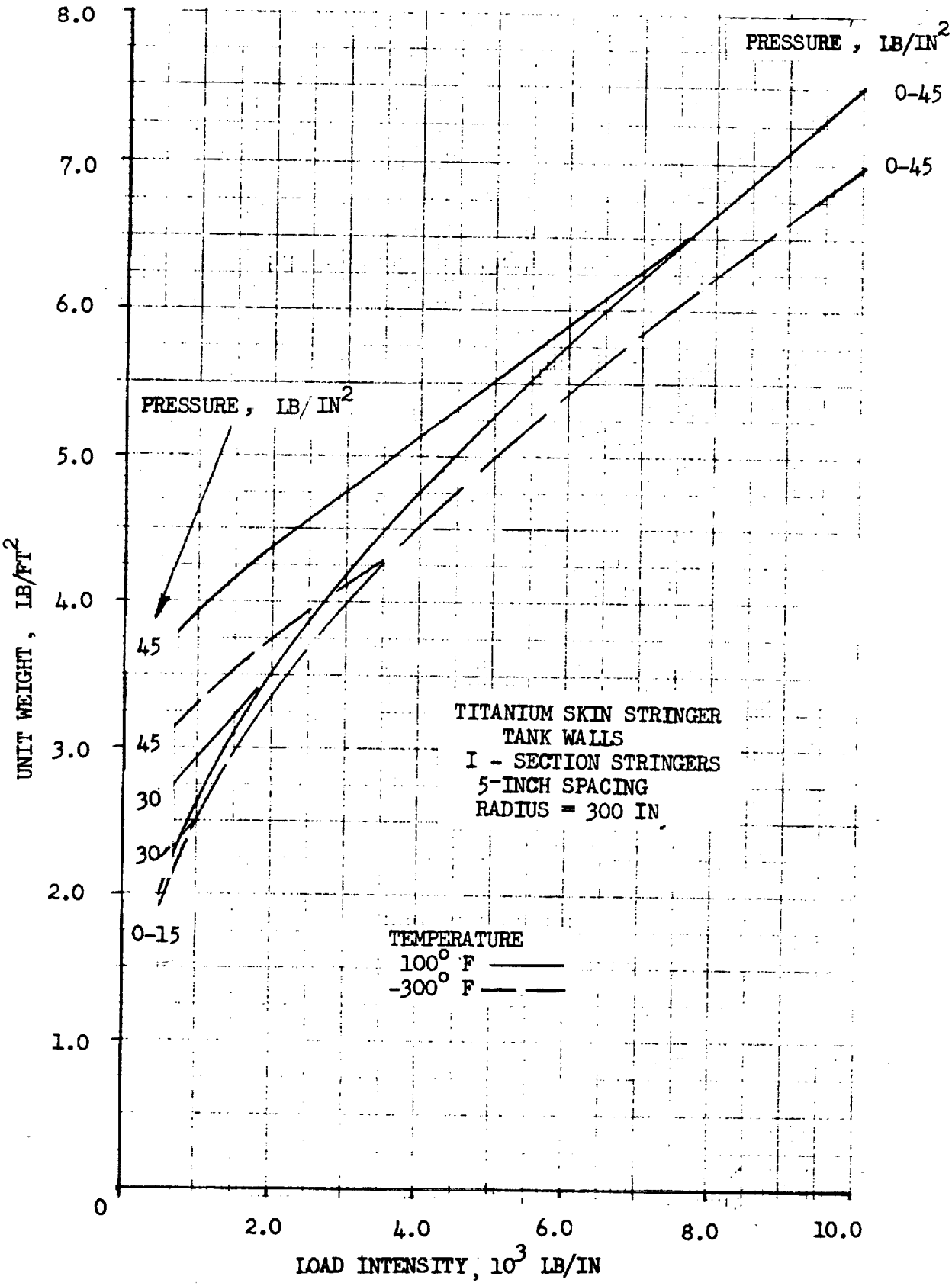

Figure 10. Skin-Stringer Tank Wall Unit Weight for Pressurized Titanium Tanks of 300-Inch Radius

and the unit weight for pressurized tank walls is

$$W_{tank} = \frac{K_1 P R}{\sigma} + K_2 N_x^{K_3} R^{K_4} P^{K_5} \left(\frac{E}{10^6}\right)^{K_6} \qquad (7)$$

Values of the coefficients for different materials and types of construction are given in Tables 2 through 5. The unit weight for the tank wall when it is subjected to a compressure load intensity, N_x, and an internal pressure is the maximum unit weight from either W_{tank} or W_{shell}.

In the following example, unit weights for structural shells of waffle construction are computed in English units from the proper weight-scaling laws. For comparison purposes, three materials were used in the example - aluminum, titanium, and beryllium. In each case the unpressurized, pressurized, and minimum gage weights must be computed from the scaling laws to determine the design weight.

$$\text{Shell Weight} = \text{Maximum} \left\{ \begin{array}{c} \text{Unpressurized} \\ \text{Weight} \end{array} , \begin{array}{c} \text{Pressurized} \\ \text{Weight} \end{array} , \begin{array}{c} \text{Minimum Gage} \\ \text{Weight} \end{array} \right\}$$

Structural Shell Design Parameters

Radius ; R = 200 in

Pressure ; P = 100 lb/in^2

Load Intensity (Ultimate) ; N_x = 6000 lb/in

Temperature ; T = 70°F

		Aluminum	Titanium	Beryllium
Working Stress (psi)	; σ =	47,100	111,000	50,000
Modulus of Elasticity (psi)	; E =	10.65×10^6	16.2×10^6	40.0×10^6
Material Density (lb/in^3)	; ρ =	0.101	0.160	0.066

Factor of Safety FS_u = 1.40 ultimate ; FS_y = 1.1 yield

Table 2. Scaling Laws for Unpressurized Shell Weights
(Metric Units)

$$W_{shell} = K_1 \, N_x^{K_2} \, \sigma^{K_3} \, (R+K_4)^{K_5} \, E^{K_6}$$

Material	Construction	K_1	K_2	K_3	K_4	K_5	K_6
Aluminum	Skin I Stringers	42.42	0.44	0	127.0	0.335	-0.519
	Skin Hat Stringers	9.338	0.540	0	127.0	0.430	-0.519
	Waffle	3.704	0.530	0	127.0	0.591	-0.519
Titanium	Skin I Stringers	54.756	0.4031	0	127.0	0.3026	-0.465
	Skin Hat Stringers	47.466	0.410	0	127.0	0.295	-0.465
	Waffle	1.314	0.535	0	127.0	0.712	-0.465
Beryllium	Skin I Stringers	0.3748	1.00	0	127.0	0.189	-0.500
	Skin Hat Stringers	0.3326	1.00	0	127.0	0.189	-0.500
	Waffle	0.3424	1.00	0	127.0	0.189	-0.500

Note: Weights are subject to minimum gage weight constraints.

Table 3. Scaling Laws for Unpressurized Shell Weights
(English Units)

$$W_{shell} = K_1 \, N_x^{K_2} \, \sigma^{K_3} \, (R + K_4)^{K_5} \, E^{K_6}$$

Material	Construction	K_1	K_2	K_3	K_4	K_5	K_6
Aluminum	Skin I Stringers	60.8	0.44	0	50.0	0.335	-0.519
	Skin Hat Stringers	15.5	0.540	0	50.0	0.430	-0.519
	Waffle	7.1	0.530	0	50.0	0.591	-0.519
Titanium	Skin I Stringers	64.46	0.4031	0	50.0	0.3026	-0.465
	Skin Hat Stringers	55.80	0.410	0	50.0	0.295	-0.465
	Waffle	2.45	0.535	0	50.0	0.712	-0.465
Beryllium	Skin I Stringers	0.617	1.00	0	50.0	0.189	-0.500
	Skin Hat Stringers	0.549	1.00	0	50.0	0.189	-0.500
	Waffle	0.563	1.00	0	50.0	0.189	-0.500

Note: Weights are subject to minimum gage weight constraints.

Table 4. Scaling Laws for Pressurized Shell Weight
(Metric Units)

$$W = K_1 PR\ \sigma^{-1} + K_2 N_x^{K_3} R^{K_4} P^{K_5} \left(\frac{E}{10^6}\right)^{K_6}$$

Material	Construction	K_1	K_2	K_3	K_4	K_5	K_6
Aluminum	Skin I Stringer	20.0	0.000202	0.533	0.778	0	-3.00
	Skin Hat Stringer	20.0	0.000212	0.533	0.778	0	-3.00
	Waffle	20.0	0.0000123	0.650	0.778	0	-3.00
Titanium	Skin I Stringer	31.6	0.00271	0.325	0.915	0	-3.00
	Skin Hat Stringer	31.6	0.00114	0.660	0.600	0	-3.00
	Waffle	31.6	0.0000856	1.37	-.30	0	-3.00
Beryllium	Skin I Stringer	13.05	0.01888	0	1.0	1.0	-3.00
	Skin Hat Stringer	13.05	0.0200	0	1.0	1.0	-3.00
	Waffle	13.05	0.0174	0	1.0	1.0	-3.00

Note: Weights are subject to minimum gage weight constraints.

Table 5. Scaling Laws for Pressurized Shell Weights
(English Units)

$$W_{tank} = K_1 PR\sigma^{-1} + K_2 N_x^{K_3} R^{K_4} P^{K_5} \left(\frac{E}{10^6}\right)^{K_6}$$

Material	Construction	K_1	K_2	K_3	K_4	K_5	K_6
Aluminum	Skin I Stringer	10.40	0.332	0.533	0.778	0	-3.00
	Skin Hat Stringer	10.40	0.350	0.533	0.778	0	-3.00
	Waffle	10.40	0.0216	0.650	0.778	0	-3.00
Titanium	Skin I Stringer	16.44	4.50	0.325	0.915	0	-3.00
	Skin Hat Stringer	16.44	1.72	0.660	0.600	0	-3.00
	Waffle	16.44	.084	1.37	-0.30	0	-3.00
Beryllium	Skin I Stringer	6.78	1.98	0	1.0	1.0	-3.00
	Skin Hat Stringer	6.78	2.10	0	1.0	1.0	-3.00
	Waffle	6.78	1.82	0	1.0	1.0	-3.00

Note: Weights are subject to minimum gage weight constraints

The working stress is obtained from the material's ultimate stress Ft_u and yield stress Ft_y.

$$\sigma = \text{Min} \left\{ \frac{Ft_u}{FS_u} \quad , \quad \frac{Ft_y}{FS_y} \right\}$$

Unpressurized Shell Weights (Table 3)

$W_{SHELL} = (7.1)\ (6000)^{.53}\ (250)^{.591}\ (10.65 \times 10^6)^{-.519}$

$W_{SHELL} = 4.21\ lb/ft^2$ Aluminum

$W_{SHELL} = (2.45)\ (6000)^{.535}\ (250)^{.712}\ (16.2 \times 10^6)^{-.465}$

$W_{SHELL} = 5.83\ lb/ft^2$ Titanium

$W_{SHELL} = (.563)\ (6000)\ (250)^{.189}\ (40 \times 10^6)^{-.500}$

$W_{SHELL} = 1.51\ lb/ft^2$ Beryllium

Pressurized Weights (Table 5)

$W_{TANK} = (10.40)\ (100)\ (200)\ (47{,}100)^{-1}$
$+ (.0216)\ (6000)^{.650}\ (200)^{.778}\ (10.65)^{-3}$ Aluminum

$W_{TANK} = 4.75\ lb/ft^2$

$W_{TANK} = (16.4)\ (100)\ (200)\ (111{,}000)^{-1}$
$+ (.084)\ (6000)^{1.37}\ (200)^{-.3}\ (16.2)^{-3}$ Titanium

$W_{TANK} = 3.56\ lb/ft^2$

$W_{TANK} = (6.78)\ (100)\ (200)\ (50000)^{-1}$
$+ (1.82)\ (200)\ (100)\ (40)^{-3}$ Beryllium

$W_{TANK} = 3.28\ lb/ft^2$

A summary of the computed theoretical unit shell weights is shown in the table below.

Table 6. Design Unit Weight for Test Example

	UNIT WEIGHT , lb/ft^2		
Construction	Unpressurized	Pressurized	Design
Aluminum Waffle	4.21	4.75	4.75
Titanium Waffle	5.83	3.56	5.83
Beryllium Waffle	1.51	3.28	3.28

The summary table shows that the aluminum and beryllium unit weights were dictated by the pressurized-scaling laws and the titanium unit weight by the unpressurized scaling law. The titanium shell weight is dictated by the design requirement of satisfying shell instabilities imposed by the compressive load intensity. This design requirement more than satifies the pressure design requirements.

The methods presented in Appendix A can be used to synthesize the nonpressurized composite shell structures (interstages, skirts, etc.). The principal modification required to use these methods is the replacement of the modulus of elasticity of the metallic shell with an effective modulus of elasticity for the composite shell. For instance the general instability equation for the metallic shell can be written as:

$$\sigma_{CR} = kE\frac{t}{R}$$

Where k is an experimental buckling coefficient, t is the material gage, R is the radius of the cylinder and E is the modulus of elasticity of the material. The corresponding equation for the composite shell is (Reference 4).

$$\sigma_{CR} = k\left(\frac{t}{R}\right)\left[\frac{E_L E_T}{3}\left(1 - V_{LT}\,V_{TL}\right)\right]^{1/2}\Phi$$

where Φ is the smaller of

$$\Phi = \left[2\, G_{LT} \frac{\left\{ 2 + (V_{LT}\, V_{TL})^{1/2} \right\}}{(E_L\, E_T)^{1/2}} \right]^{1/2}$$

or

$$\Phi = 1$$

where

E_L E_T = longitudinal (transverse) modulus of elasticity of the composite material

V_{LT} = composite's Poisson ratio

G_{LT} = shear modulus of the composite material

The influence of changes in material on the weight of flat panels are presented in Figures 11 and 12. The weight curves for the composite materials with honeycomb sandwich have discontinuities due to discrete number of lay up tapes in the surface panels. Unit weight curves for the cylindrical shells for glass epoxy and boron epoxy are given in Figures 13 and 14.

4.2 STRUCTURAL BULKHEAD

The ellipsoidal bulkheads for the propellant tanks have been designed as minimum weight membranes subjected to internal pressures (ullage for the forward bulkhead and ullage plus hydrostatic head for the aft bulkhead). Appendix A contains the bulkhead analysis used to compute the required thicknesses at several points around the ellipsoidal dome. Aspect ratios less than 0.707 produce compressive stresses in the bulkhead and have been considered for shell stability. Table 7 is a typical computer print-out from the bulkhead synthesis program.

Since the theoretical methods of computing ellipsoidal dome bulkhead weights require lengthy calculations, an empirical approximation more suitable for weight scaling has been provided. Theoretical membrane weight data were computed according to the analytical methods presented in Appendix A. The theoretical weight of ellipsoidal dome bulkheads is dependent upon five parameters: tank material, design temperature, bulkhead aspect ratio (b/a), tank radius (R), and tank pressure (P).

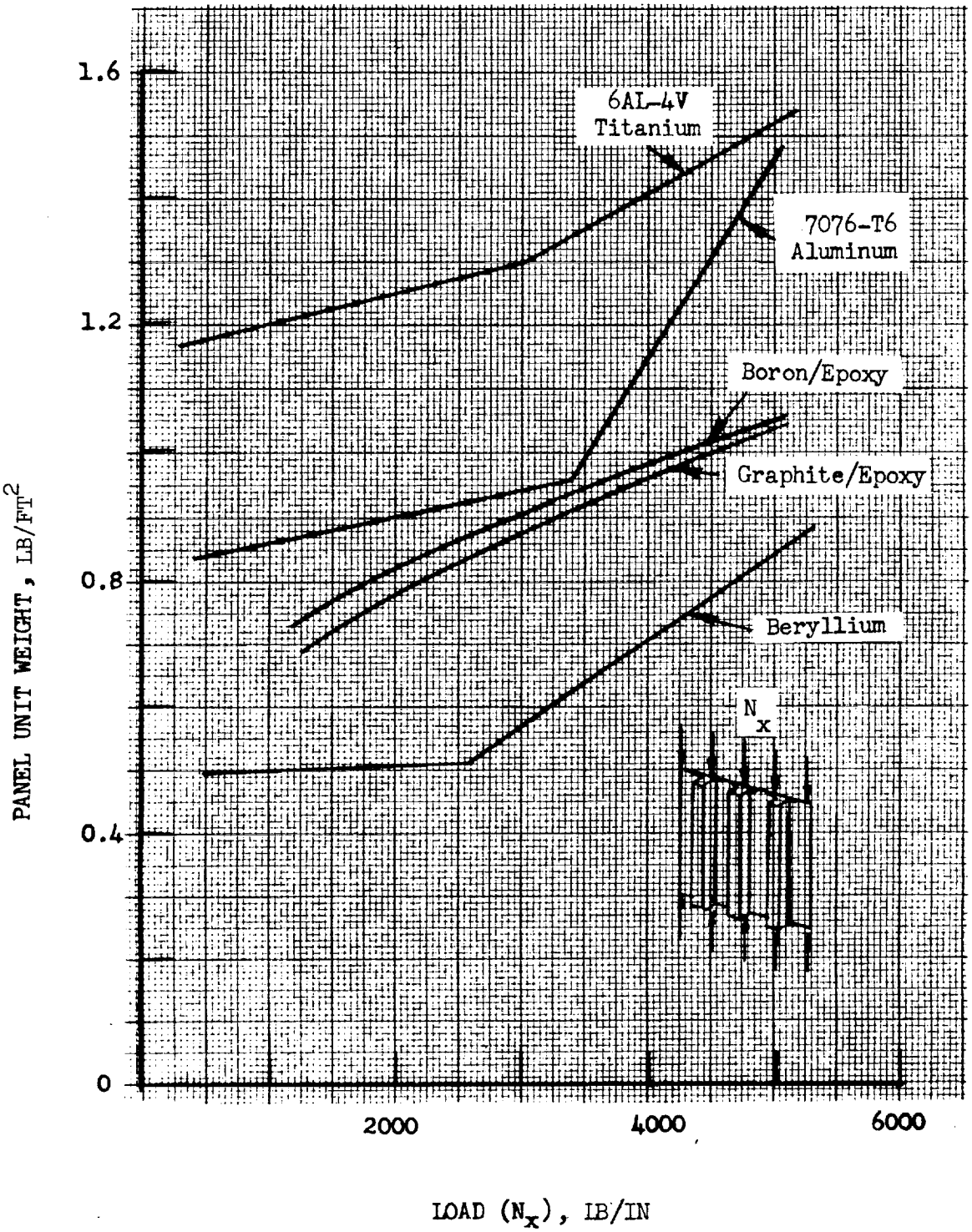

Figure 11. Comparison of Materials, Skin-Stringer Panels

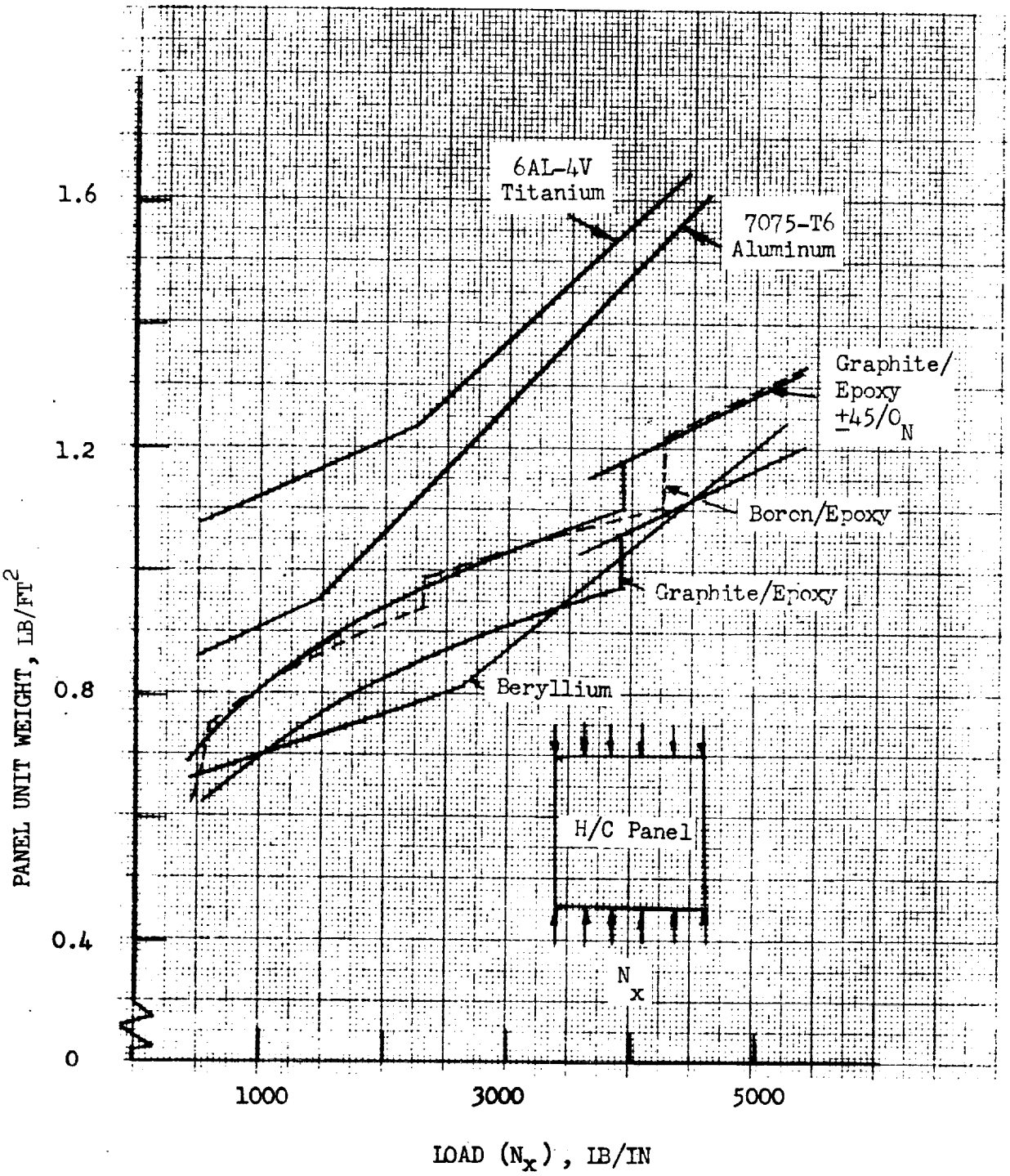

Figure 12. Comparison of Skin Materials, Honeycomb Sandwich Panels

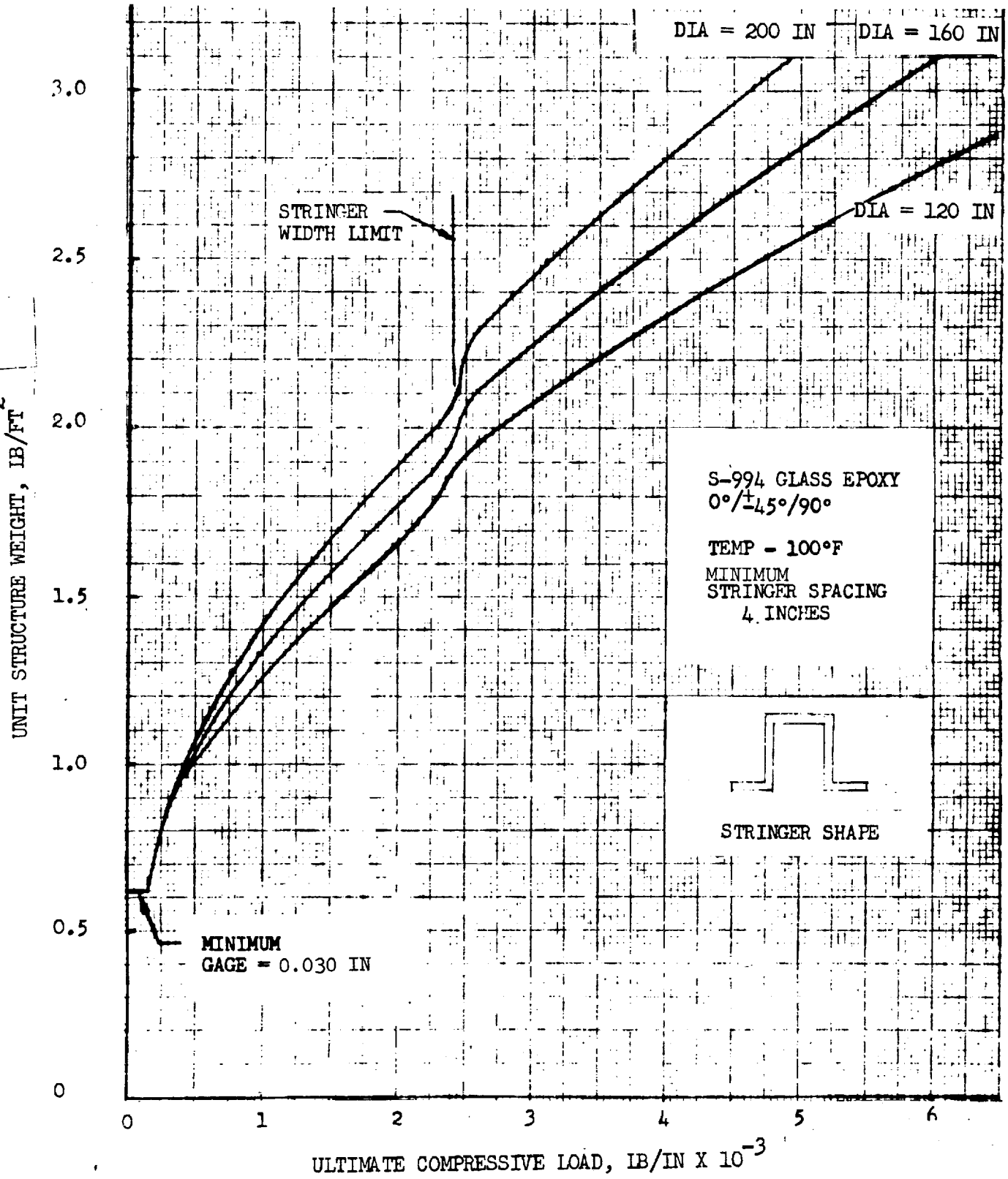

Figure 13. Weight of Unpressurized Cylindrical Shells Subjected to Axial Compression Load — Skin Stringer Construction (S-994 Glass Epoxy)

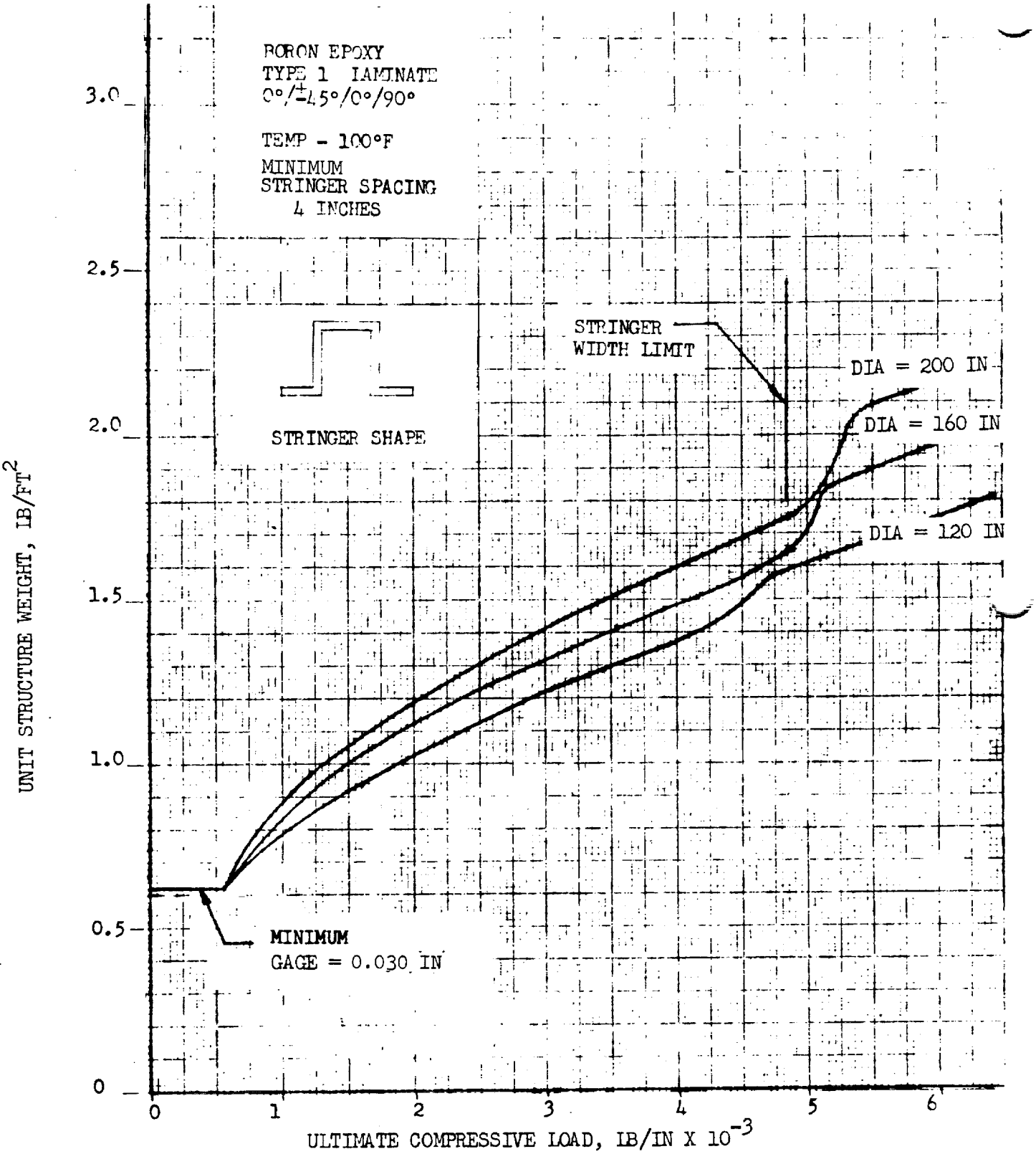

Figure 14. Weight of Unpressurized Cylindrical Shells Subjected to Axial Compression Load – Skin Stringer Construction (Boron Epoxy)

Table 7. CONSTRUCTION - ELLIPTICAL DOME BULKHEAD

MATERIAL - AL 2219 (72 DEG)

YIELD STRESS	49800.0	MATERIAL DENSITY	0.1020	LIMIT LOAD FACTOR	1.1
ULTIMATE STRESS	62000.0	TEMPERATURE	72.0000	ULT LOAD FACTOR	1.4
YOUNGS MODULUS	10500000.0	MIN SKIN THICKNESS	0.0100		

MAJOR RADIUS	MINOR RADIUS	NET PRESSURE	BULKHEAD SKIN THICKNESS EQUATOR	MID-POINT	APEX	WEIGHT	AREA
75.0	60.0	50.0	0.0529	0.0438	0.0368	139.5	30736.9
75.0	60.0	150.0	0.1588	0.1315	0.1103	418.6	30736.9
75.0	60.0	200.0	0.2117	0.1754	0.1470	558.2	30736.9
75.0	60.0	300.0	0.3175	0.2630	0.2206	837.2	30736.9
75.0	60.0	400.0	0.4234	0.3507	0.2941	1116.3	30736.9
75.0	53.0	20.0	0.0240	0.0176	0.0169	57.1	28682.4
75.0	53.0	30.0	0.0359	0.0264	0.0254	85.6	28682.4
75.0	53.0	40.0	0.0479	0.0353	0.0339	114.1	28682.4
75.0	53.0	50.0	0.0599	0.0441	0.0424	142.7	28682.4
75.0	53.0	150.0	0.1797	0.1322	0.1271	428.0	28682.4
100.0	90.0	30.0	0.0376	0.0346	0.0307	205.4	58687.4
100.0	90.0	40.0	0.0502	0.0461	0.0409	273.8	58687.4
100.0	90.0	50.0	0.0627	0.0577	0.0511	342.3	58687.4
100.0	90.0	150.0	0.1882	0.1730	0.1534	1026.8	58687.4
100.0	90.0	200.0	0.2509	0.2307	0.2045	1369.1	58687.4
150.0	150.0	20.0	0.0339	0.0339	0.0339	488.4	141371.5
150.0	150.0	30.0	0.0508	0.0508	0.0508	732.6	141371.5
150.0	150.0	40.0	0.0677	0.0677	0.0677	976.8	141371.5
150.0	150.0	50.0	0.0847	0.0847	0.0847	1221.0	141371.5

Theoretical weights were computed for 2219 Aluminum and 6Al-4V Titanium for the following parameter ranges:

Temperature	72 to 400 F
Pressure	20 to 400 lb/in^2
Major Radius	25 to 200 in
Bulkhead Aspect Ratio	0.5 to 1.0

The theoretical data were plotted to estimate the type of curve fit required for the weight-scaling relationships. Bulkhead weights for titanium and aluminum are presented in Figures 15 through 18 and 19 through 22, respectively. The figures show that a slope discontinuity occurs in the weight plotted as a function of bulkhead aspect ratio. This discontinuity is at a bulkhead aspect ratio of 0.707 and is the result of the internal pressure causing a compressive stress in the bulkhead and the skin thickness is based on a stability criteria. Another slope discontinuity occurs for bulkheads with minimum gages. A plot of the minimum gage weight for aluminum and titanium is presented in Figure 23. The weight-scaling law is

$$W = A_c \rho t R^2 \tag{8}$$

where A_c is a bulkhead shape factor (Figure 24).

Temperature was related to material properties for the purpose of correlating the theoretical data. The yield stress, ultimate stress, actual working stress, and modulus of elasticity are presented in Table 8.

A multi-regression analysis was performed on the theoretical weight data to determine if curve fitting of the following form were feasible:

$$W = K_1 \rho \left(\frac{b}{a}\right)^{K_2} \sigma^{K_3} R^{K_4} P^{K_5}$$

where

K_i = weight scaling coefficient or exponents

Separate scaling relationships were determined for bulkhead aspect ratios on either side of the discontinuity value of b/a = 0.707. For bulkhead aspect ratios $b/a \geq 0.707$, the following relationship was used.

$$W = 3.12 \rho \left(\frac{b}{a}\right)^{0.2} R^3 P \sigma^{-1} \text{ (lb)} \tag{10}$$

for the following aspect ratio range

$$0.707 \leq \left(\frac{b}{a}\right) \leq 1.0$$

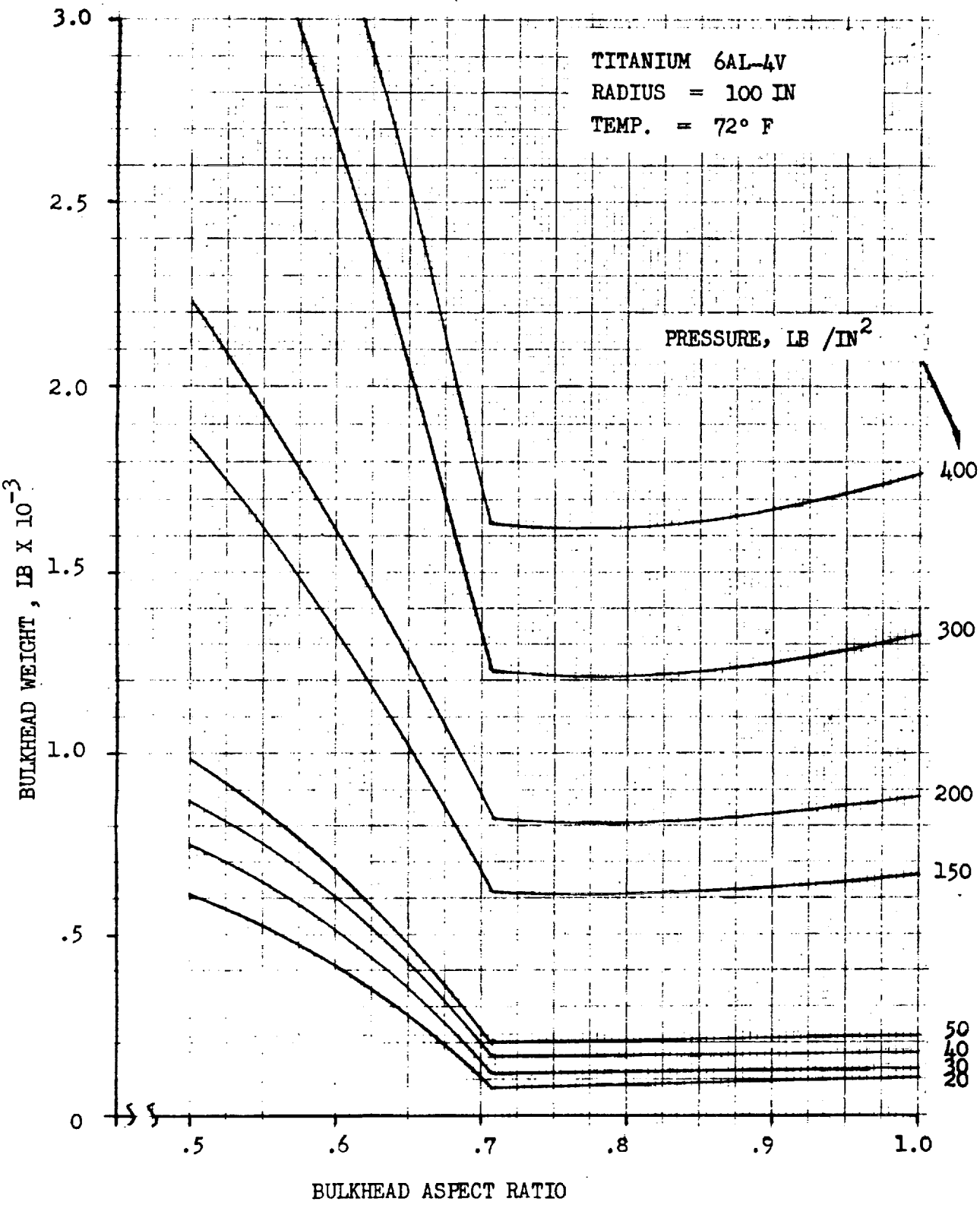

Figure 15. Effects of Pressure and Aspect Ratio on the Weight of Ellipsoidal Dome Bulkheads with Fixed Radii - Titanium 6AL-4V

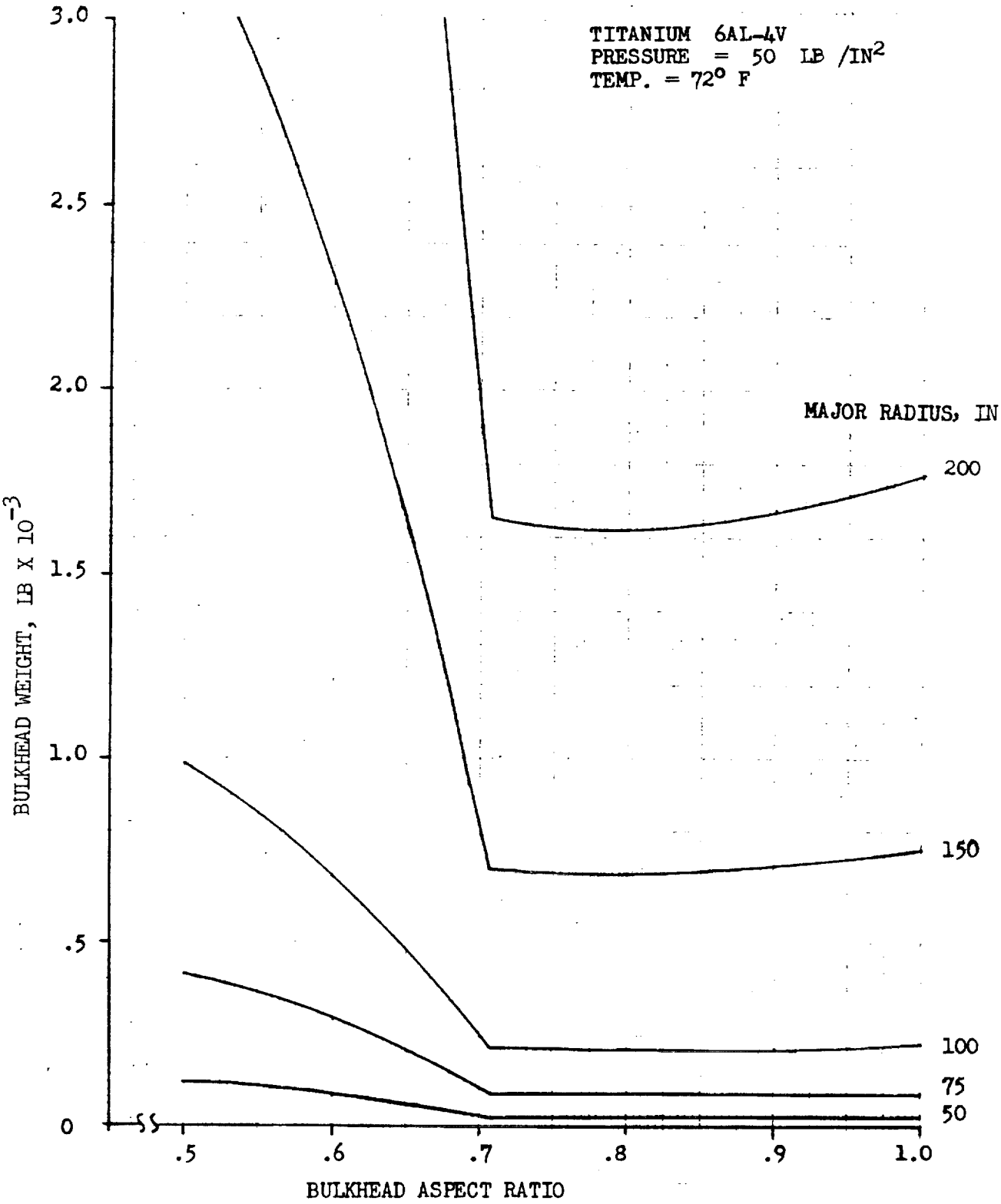

Figure 16. Effects of Radius and Aspect Ratio on the Weight of Ellipsoidal Dome Bulkheads for Fixed Pressure - Titanium 6AL-4V

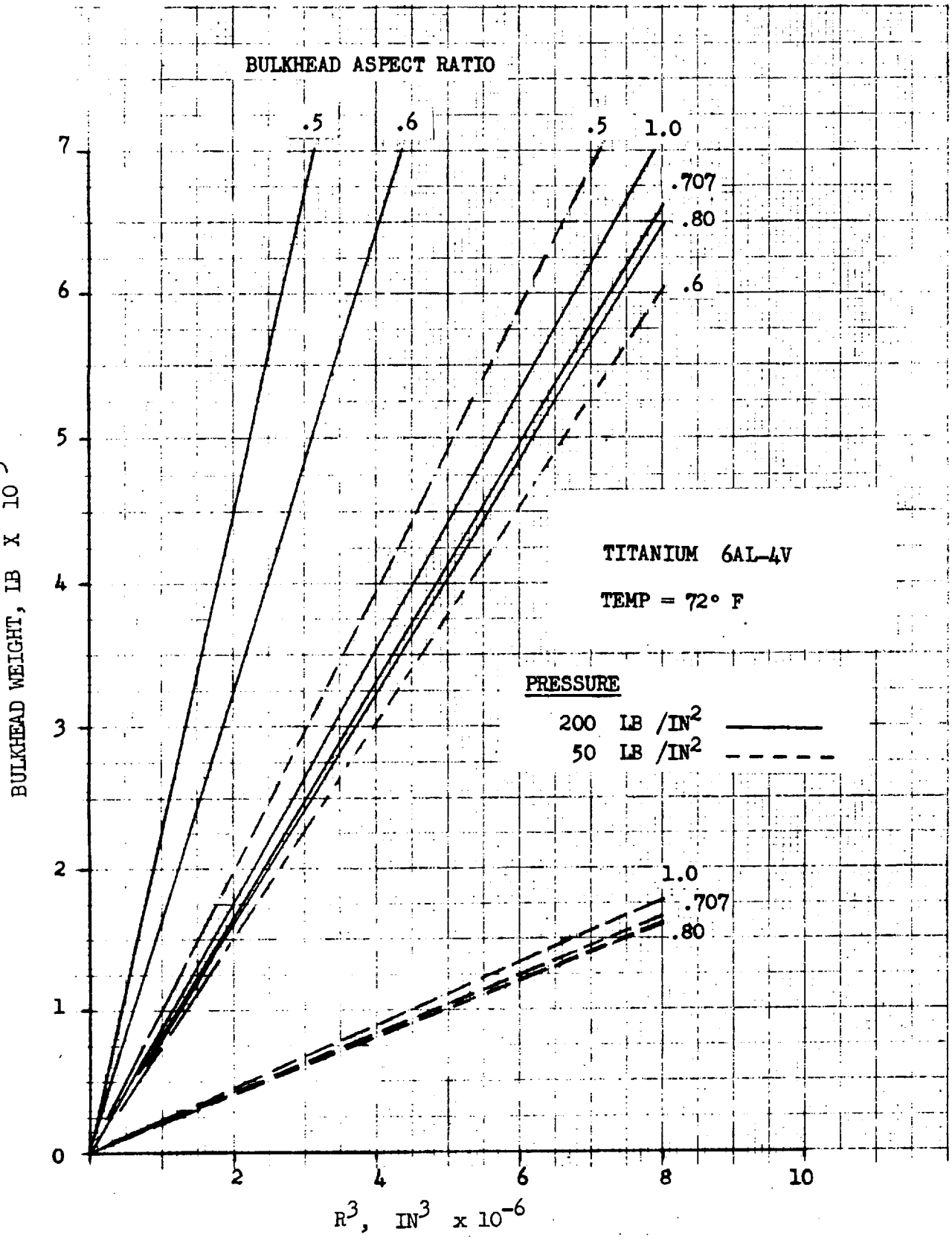

Figure 17. Effects of Major Radius and Aspect Ratio on Weight of Ellipsoidal Dome Bulkheads - Titanium 6AL-4V

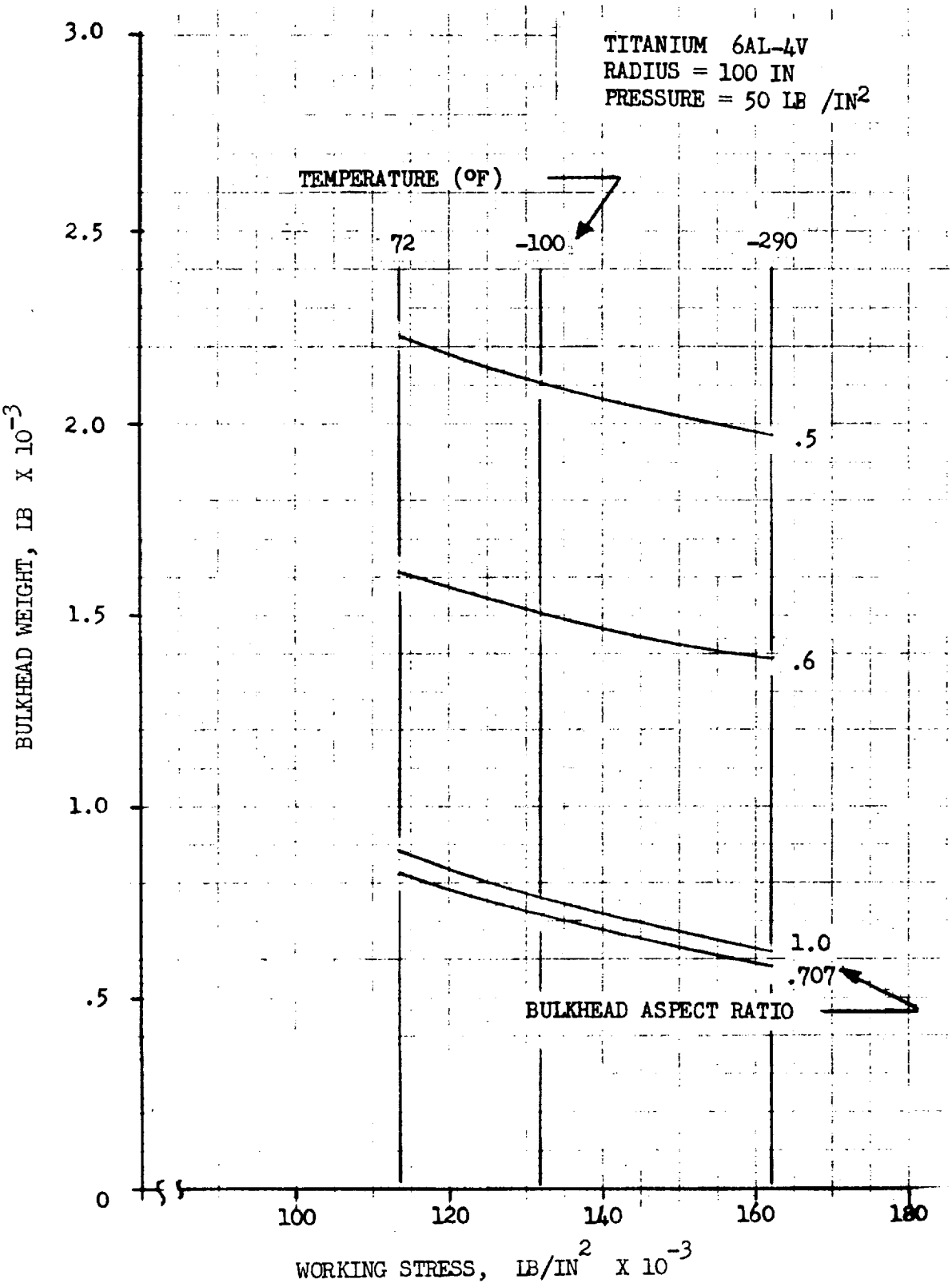

Figure 18. Effects of Working Stress and Temperature on the Weight of Ellipsoidal Dome Bulkheads - Titanium 6AL-4V

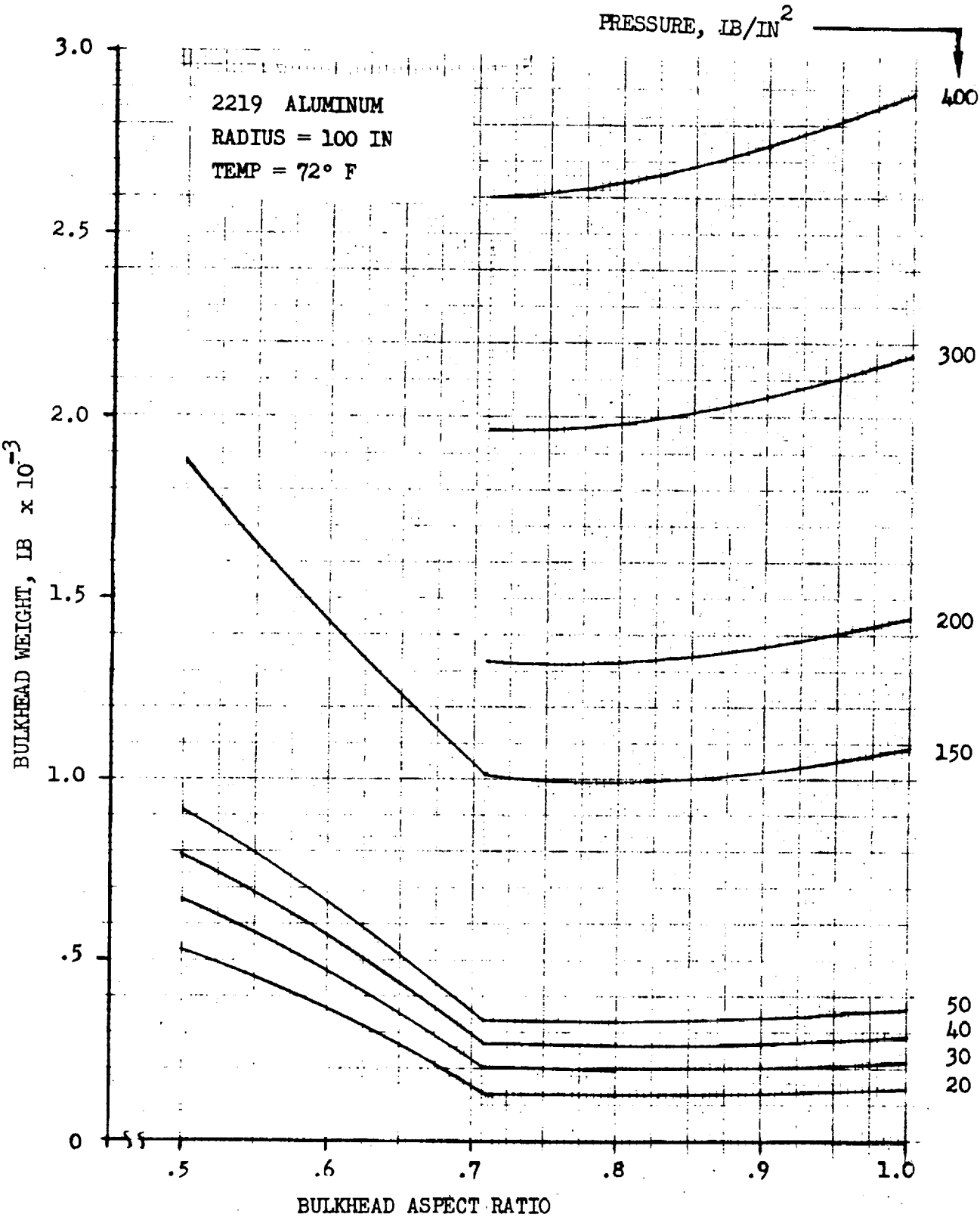

Figure 19. Effect of Pressure and Aspect Ratio on the Weight of Ellipsoidal Dome Bulkheads with Fixed Radii - Aluminum AL 2219

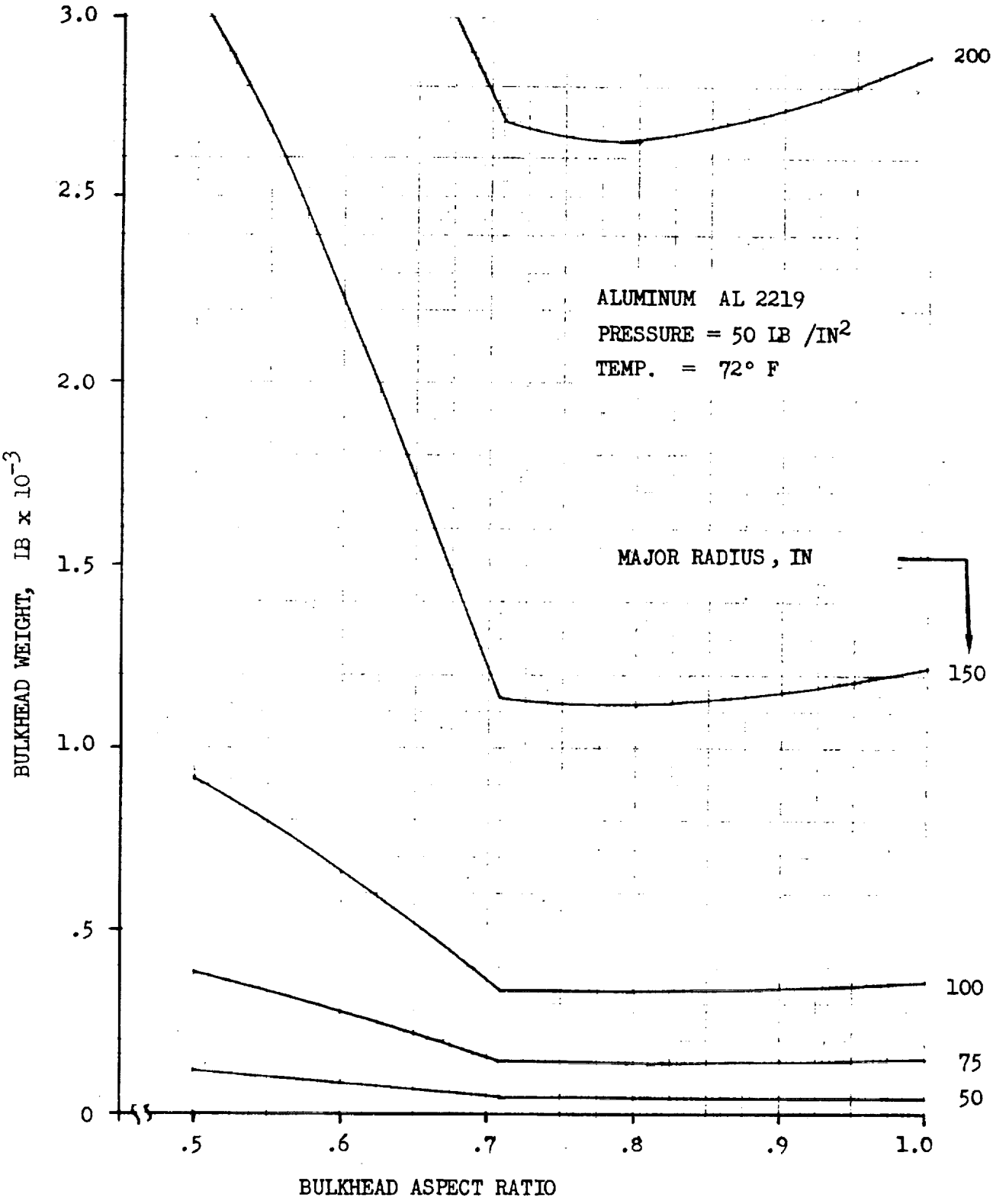

Figure 20. Effects of Radius and Aspect Ratio on Weight of Ellipsoidal Dome Bulkheads Fixed Pressure - Aluminum AL 2219

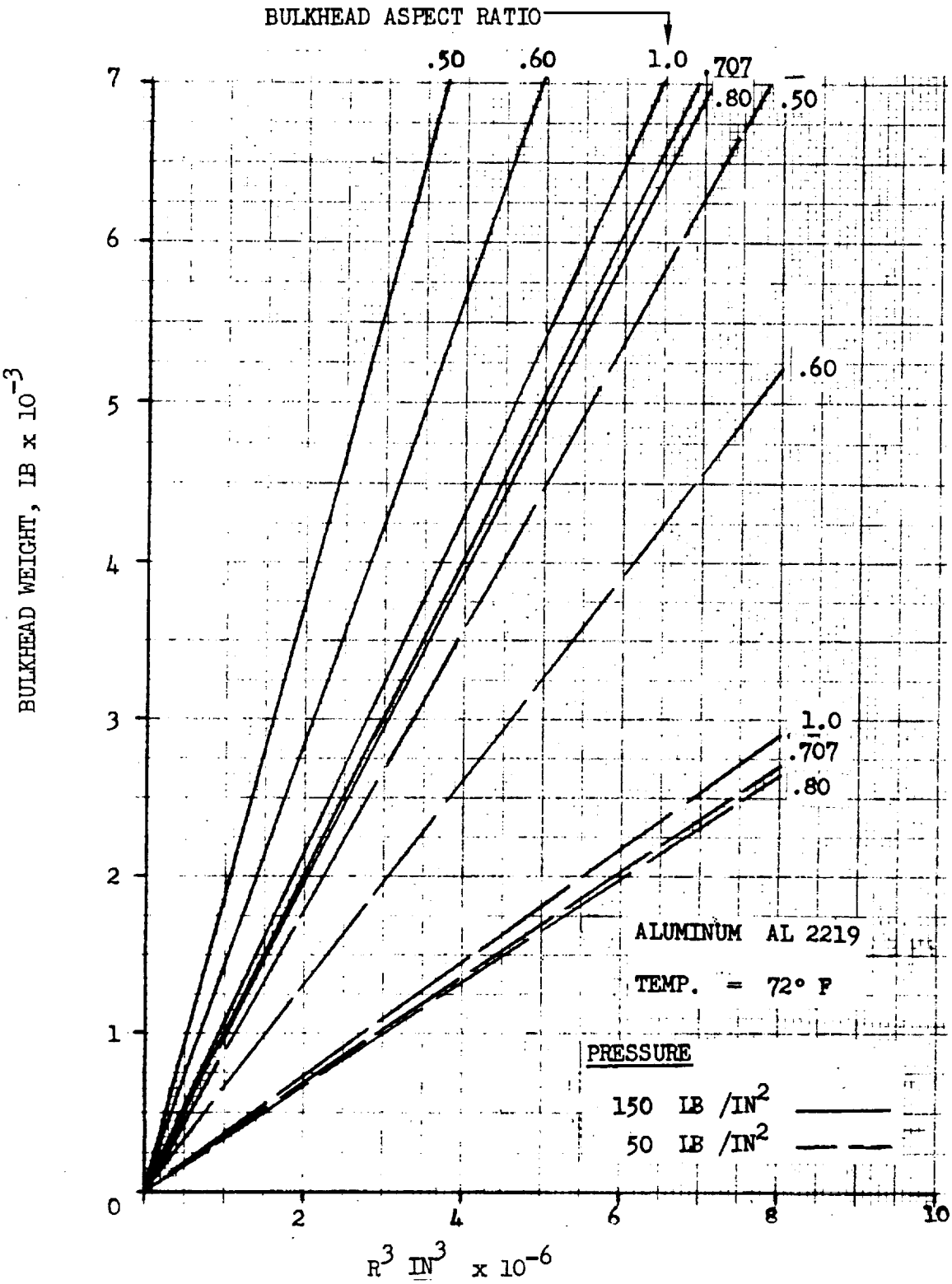

Figure 21. Effect of Radius and Aspect Ratio on the Weight of Ellipsoidal Dome Bulkheads - Aluminum AL 2219

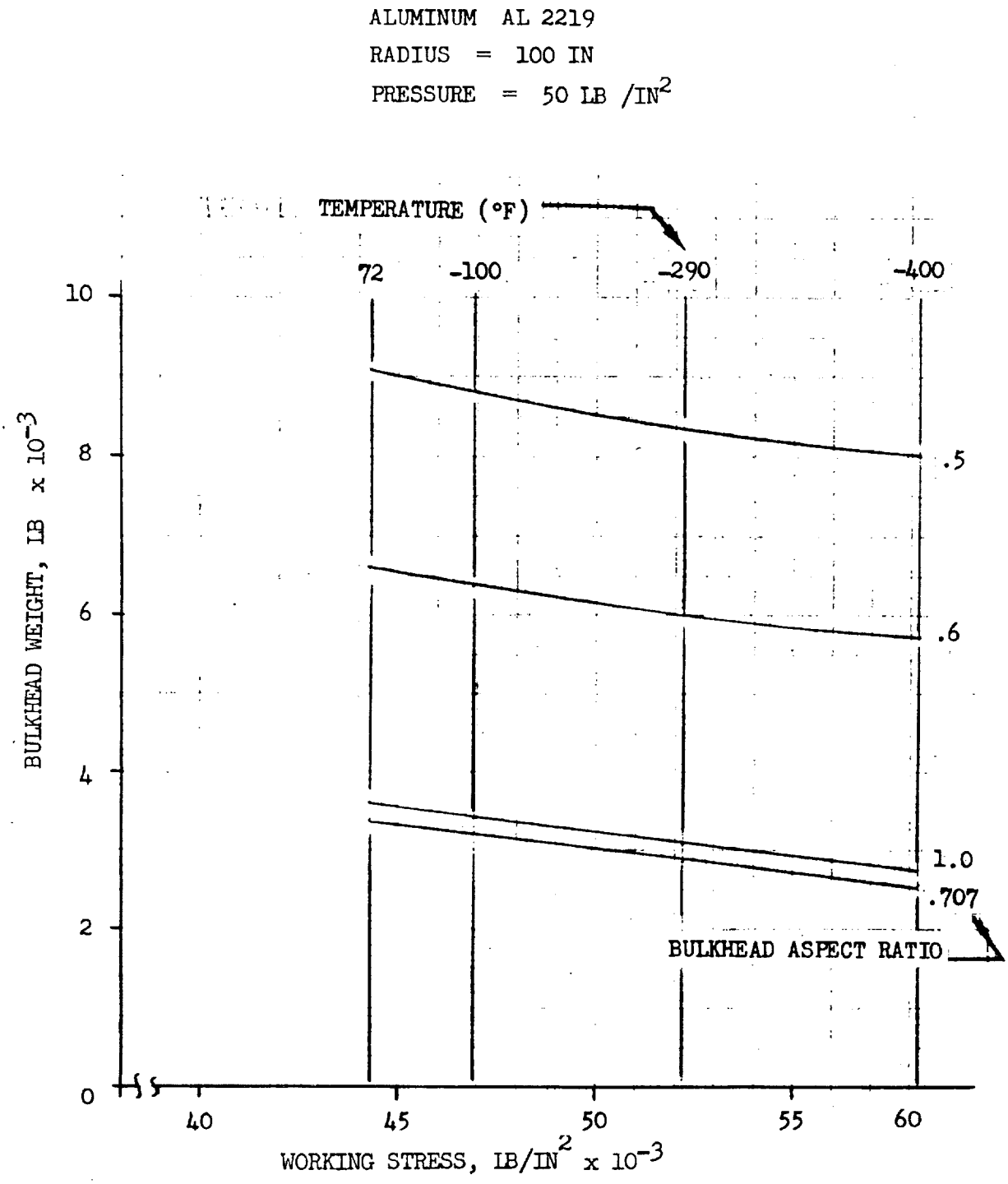

Figure 22. Effect of Working Stress and Temperature on the Weight of Ellipsoidal Dome Bulkheads - Aluminum AL 2219

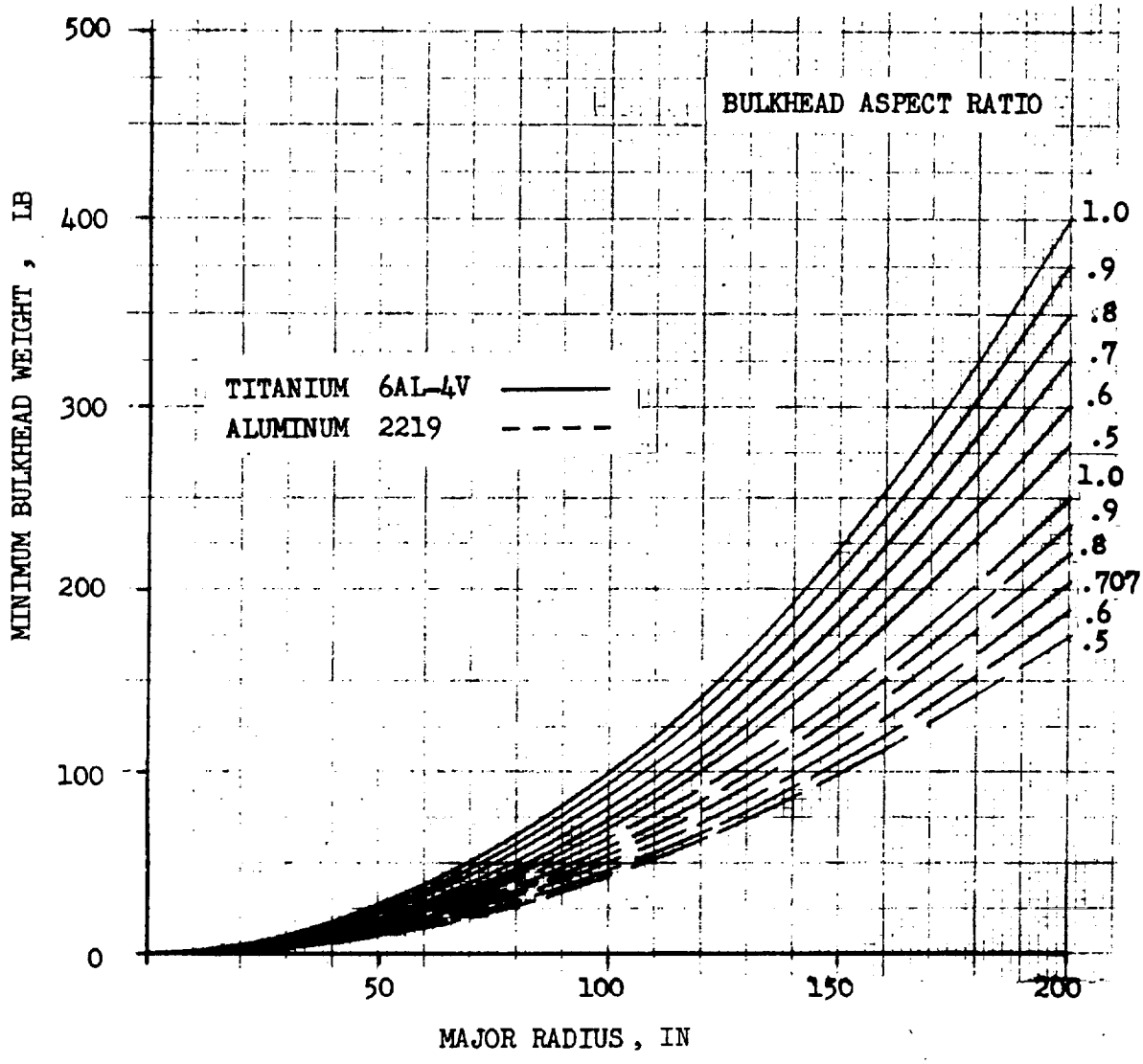

Figure 23. Minimum Weight of Ellipsoidal Dome Bulkheads Titanium 6AL-4V and Aluminum AL 2219

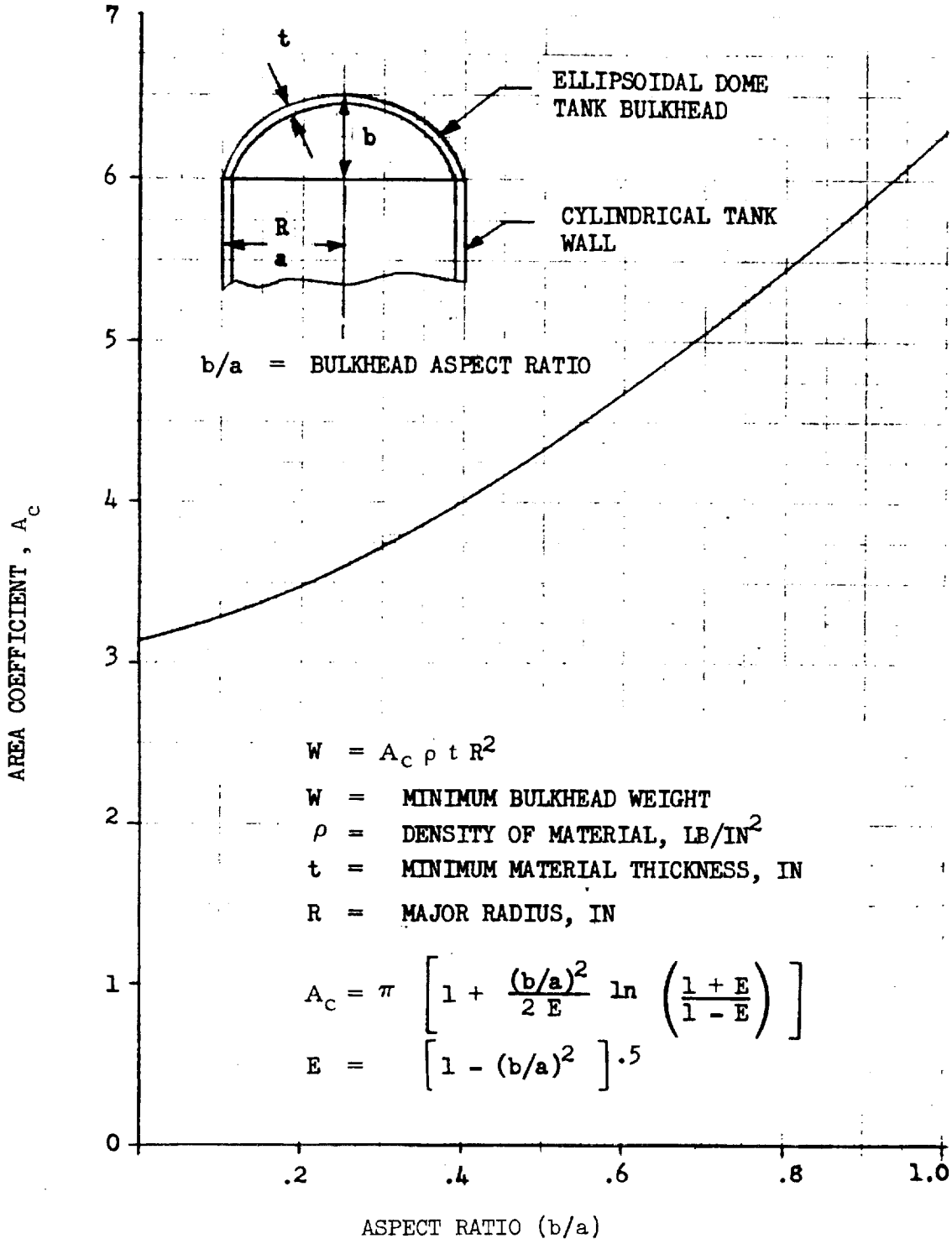

Figure 24. Minimum Weight Coefficient Versus Bulkhead Aspect Ratio

Table 8. Working Stress Versus Temperature for Aluminum and Titanium Ellipsoidal Dome Bulkheads

Temperature °C (°F)	$Ft_y \times 10^{-3}$ kg/cm^2 (lb/in^2)	$Ft_u \times 10^{-3}$ kg/cm^2 (lb/in^2)	$\sigma \times 10^{-3}$ kg/cm^2 (lb/in^2)	$E \times 10^{-6}$ kg/cm^2 (lb/in^2)	$Ft_y \times 10^{-3}$ kg/cm^2 (lb/in^2)	$Ft_u \times 10^{-3}$ kg/cm^2 (lb/in^2)	$\sigma \times 10^{-3}$ kg/cm^2 (lb/in^2)	$E \times 10^{-6}$ kg/cm^2 (lb/in^2)
22.2 (72)	3.5 (49.8)	4.36 (62.0)	3.11 (44.3)	0.74 (10.50)	10.09 (143.5)	11.18 (159.0)	7.99 (113.6)	1.15 (16.35)
-73.3 (-100)	3.73 (53.0)	4.61 (65.6)	3.30 (46.9)	0.77 (10.95)	11.84 (168.5)	12.97 (184.5)	9.27 (131.8)	1.20 (17.15)
-178.9 (-290)	4.08 (58.0)	5.14 (73.1)	3.62 (52.2)	0.82 (11.70)	14.48 (206.0)	15.96 (227.0)	11.39 (162.0)	1.26 (17.95)
-240 (-400)	4.50 (64.0)	6.21 (88.3)	4.09 (58.2)	0.86 (12.20)	-	-	-	-
	ALUMINUM				TITANIUM			

This scaling law produced extremely good fit to the design data. Weight variation between scaled and design data did not exceed three percent

For the aspect ratio b/a < 0.707, the bulkhead weights were not amenable to a scaling law of the above general form. The data in Figures 15 through 22 indicated that the scaling law should have the pressure parameter modified by a function of the aspect ratio and there is also a weight cut-off where the curves tend to zero at b/a = 0.75. The resulting scaling law is

$$W = K_1 \rho \left(\frac{b}{a}\right)^{K_2} R^3 \left(K_3 - b/a\right)^{K_4} P^{\left(K_5 + b/a\right)^{K_6}} E^{K_7} \qquad (11)$$

for the following parameter limits:

$$0.500 \leq (b/a) \leq 0.707$$

$$0 \leq P \leq 7.03 \text{ kg/cm}^2 \ (100 \text{ lb/in}^2)$$

Values for K_1 through K_7 are given in Tables 9 and 10.

The pressure should be limited to less than 7.03 kg/cm^2 (100 lb/in^2) for the low-aspect ratio bulkheads, since the weight increases significantly at higher pressures, more than offsetting the benefits derived from the reduced height and shortened unpressurized outer shell.

For the bulkhead design, the weight to be used is the maximum of that obtained from minimum thickness (Equation 8) or weight from Equation 10 or 11. These three scaling equations reflect the weight of only the bulkhead. Non-optimum weight allowances will be included to account for manifolds and attachment of the bulkhead membrane to the main tank wall.

4.3 PROPELLANT TANKAGE

The propellant containers to be considered are cylindrical tanks with spherical or ellipsoidal bulkheads, spherical and toroidal tanks. Tankage geometry will follow the present-day design philosophy in constraining the propulsive stage to a L/D ratio of the overall length to diameter which minimizes the effects of bending and dynamic loads during boost ascent from the Earth's surface.

Loading conditions considered for the sizing of the tanks are based on the following:

Table 9. Scaling Laws for Tank Bulkhead Weights (Metric Units)

$$W = K_1 \rho (b/a)^{K_2} R^3 P \sigma^{-1} \qquad .707 \leq (b/a) \leq 1.0$$

$$W = K_1 \rho (b/a)^{K_2} R^3 (K_3 - b/a)^{K_4} P^{(K_5 + b/a)^{K_6}} E^{K_7} \qquad 0.5 \leq (b/a) \leq .707$$

	K_1	K_2	K_3	K_4	K_5	K_6	K_7
$\frac{b}{a} > 0.707$	3.14	0.20	-	-	-	-	-
$\frac{b}{a} < 0.707$	307,000	-2.634	0.75	1.049	0.293	0.888	-1.056

Table 10. SCALING LAWS FOR TANK BULKHEAD WEIGHTS (English Units)

$$W = K_1 \rho (b/a)^{K_2} R^3 P \sigma^{-1} \qquad .707 \leq (b/a) \leq 1.0$$

$$W = K_1 \rho (b/a)^{K_2} R^3 (K_3 - b/a)^{K_4} P^{(K_5 + b/a)^{K_6}} E^{K_7} \qquad 0.5 \leq (b/a) \leq .707$$

	K_1	K_2	K_3	K_4	K_5	K_6	K_7
b/a > .707	3.14	0.20	-	-	-	-	-
b/a < .707	19780	-2.634	0.75	1.049	0.293	0.888	-1.056

NOTE: Weights are subject to minimum gage weight constraints.

1. Maximum differential pressure for engine requirements (net-positive-suction head)

2. Maximum axial acceleration during launch if the stage is launched into orbit with full tanks. General equations are derived for the cylindrical tanks which are applicable to the chemical stages.

These equations are dependent upon the following parameters:

W_P = Propellant weight, kg (lb)

W_O = Gross weight of stage, kg (lb)

P_L = Propellant loading factor, (W_P/W_O)

MR = Mixture ratio by weight, oxidizer/fuel

ρ_{ox}, ρ_f = Density of oxidizer or fuel, kg/m^3 (lb/ft^3)

b/a = Ratio of minor to major axis of an ellipse

ρ_m = Material density, kg/m^3 (lb/ft^3)

σ = Stress level allowable, kg/m^2 (lb/ft^2)

P = Tank pressure, kg/m^2 (lb/ft^2)

η_x = Axial acceleration factor

General equation for the Volume V, of a bi-propellant systems is

$$V_{ox} = \frac{W_O P_L}{\rho_{ox}} \left(\frac{MR}{MR+1}\right)(1 + UF_{ox}) \quad \text{for the oxidizer}$$

and

$$V_f = \frac{W_O P_L}{\rho_f} \left(\frac{1}{MR+1}\right)(1 + UF_f) \quad \text{for the fuel}$$

where UF is the ullage volumetric factor

If $K_v = \frac{V_{ox}}{V_f}$ is the ratio of the volumes,

then if $K_v < 1.0$, V_{ox} is the smaller of the two volumes

and if $K_v > 1.0$, V_f is the smaller volume

Without imposing any restrictions on the diameter, D, or the cylindrical length of the tank, L, the volume equation of either tank with ellipsoidal bulkheads is given by:

$$V = \frac{\pi D^3}{6} \left[\frac{3}{2} \left(\frac{L}{D}\right) + \left(\frac{b}{a}\right) \right]$$

For an ellipsoidal tank with no tank wall, the volume is:

$$V = \frac{\pi D^3}{6} \left(\frac{b}{a}\right)$$

The maximum diameter for the oxidizer tank when $K_v < 1.0$ is

$$D_{Max} = \left[\frac{6 W_o P_L}{\pi \rho_{ox}} \left(\frac{a}{b}\right) \left(\frac{MR}{MR + 1}\right) (1 + UF_{ox}) \right]^{1/3}$$

If the maximum diameter is constrained to D_c, $< D_{MAX}$, then the corresponding slenderness ratio (L/D) can be expressed as:

$$\left(\frac{L}{D}\right)_{ox} = \frac{2}{3} \left[\left(\frac{D_{MAX}}{D_c}\right)^3 - 1 \right] \left(\frac{b}{a}\right)$$

The corresponding $(L/D)_f$ of the fuel tank for the constrained diameter is given by:

$$\left(\frac{L}{D}\right)_f = \frac{1}{K_v} \left(\frac{L}{D}\right)_{ox} + \frac{2}{3} \left(\frac{b}{a}\right) \left(\frac{1}{K_v} - 1\right)$$

A necessary step in the derivation of weight equations is the determination of design pressure and loads, surface areas, material and wall thickness distribution. The thickness of the lower bulkhead is a function of the bulkhead pressure, P_{LB}, which includes the inertia effects of the head of propellant

$$P_{LB} = P_u + D\left[\left(\frac{L}{D}\right)_{ox,f} + \frac{b}{a}\right] \rho_{ox,f}\ \eta_x$$

where $D = D_{Max}$ or D_C

The thickness of the cylindrical segment is determined from the tank design pressure P_A, which is the average pressure between the top and bottom of the cylindrical portion of the tank

$$P_A = P_u + \left\{\frac{D}{2}\left[\left(\frac{L}{D}\right)_{ox,f} + \left(\frac{b}{a}\right)\right]\right\} \rho_{ox,f}\ \eta_x$$

The design pressure for the upper bulkhead considers the tank ullage pressure P_u.

The surface area for each ellipsoidal dome is:

$$S_D = \frac{D^2}{4} Ac$$

where A_C is a surface coefficient for ellipsoidal bulkheads and is shown in Figure 24

The cylindrical surface area is:

$$S_c = \pi D^2 \left(\frac{L}{D}\right)_{ox,f}$$

The tank weight is the sum of products of the surfaces areas, thickness and material density of the bulkheads and cylindrical wall.

$$\text{Tank Weight}\quad W_{T_{ox,f}} = \left(S_c W_{SHELL} + W_{BULK_1} + W_{BULK_2}\right)\ OF$$

where OF = Non-optimum weight factor which in this analysis accounts for joints, material tolerance, etc.

W_{BULK} = Bulkhead weights obtained from Tables 9 or 10 using the appropriate design pressures.

W_{SHELL} = Tank wall unit weight obtained from Tables 4 or 5 and using design loads and pressures.

Bulkhead - Tank Wall Intersection

Another significant weight item is the joining segment at the intersection of the propellant tank bulkhead, tank wall and unpressurized shell. There is a load-discontinuity effect at this junction which requires additional structural material. The intersection weight is dependent on the internal pressure of the tank and the compressive-load intensity in the shell. The weight for the intersection of the aft bulkhead and the tank will be greater than the weight for the forward bulkhead and skirt intersection. Weights for the two combined intersection joints has been derived from historical data, Figure 25, and can be represented by

$$W_{Intersection} = 3.07 \times 10^{-4} F^{1.083} \left(\frac{P_u}{39}\right)^{0.5}, \text{ lb} \qquad (12)$$

where F = total stage thrust

4.4 MATERIAL IMPROVEMENTS

The effect of future material technology can be assessed by considering weight reductions arising from improved material properties. For the design synthesis, only improvements in the physical strength and stiffness properties of the material are considered. The effect of the manufacturing difficulties, fabrication limitations, and cost considerations are not considered. Based on current concepts and research trends, and on the rate of improvement in the past decade, predictions of future strength property changes for aluminum and titanium alloys are presented in Figures 26 and 27 respectively. The use of aluminum alloys has proven acceptable for tankage containing LH_2, LOX, LF_2 and MMH. Current titanium alloys do not possess sufficient toughness below -320F. The impact sensitivity of titanium alloys in contact with oxidizers (LOX) limits their use to specific propellant tanks.

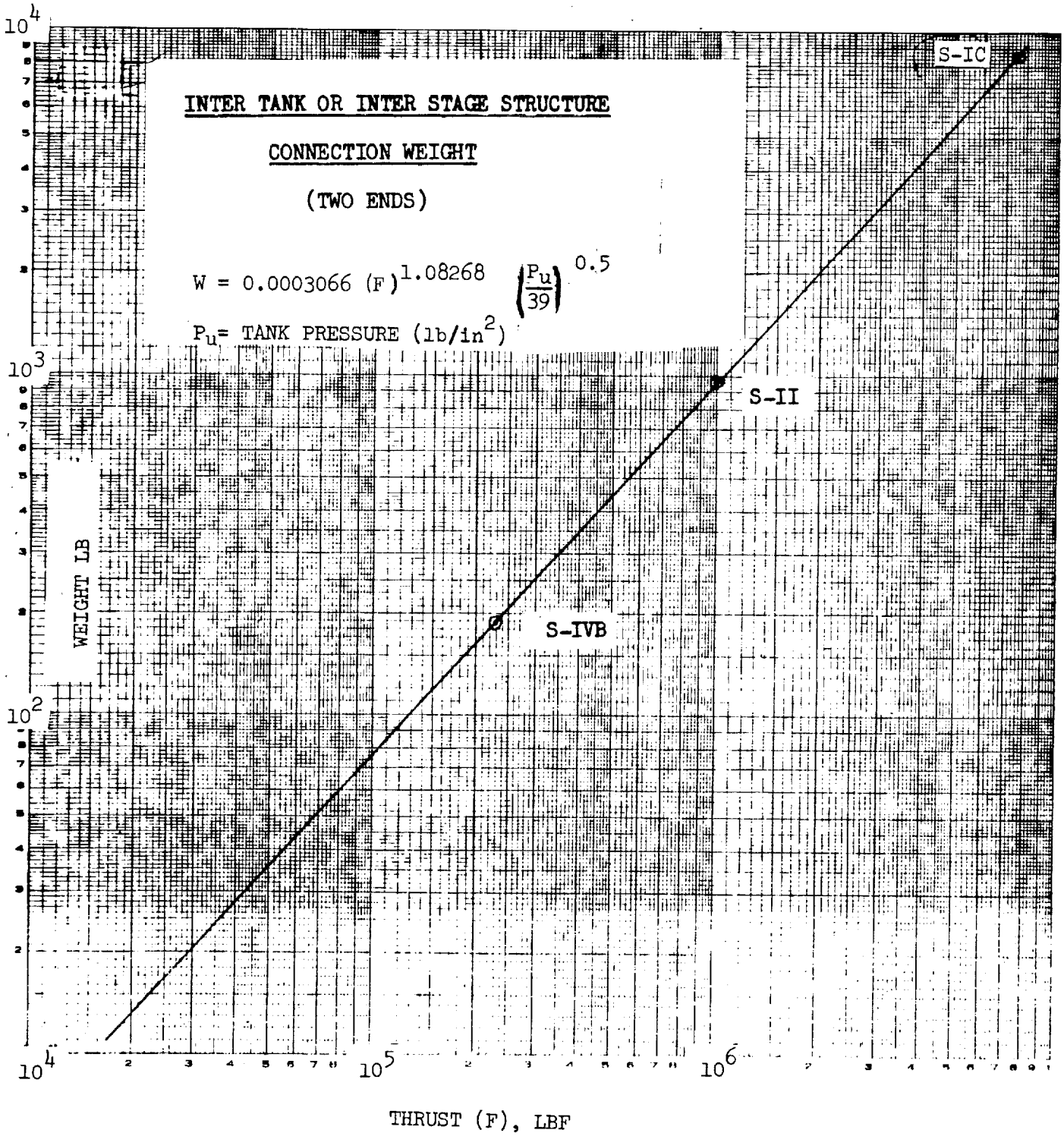

Figure 25. Scaling Law for Additional Structural Weights Required at Intersection of Tank Walls and Bulkheads

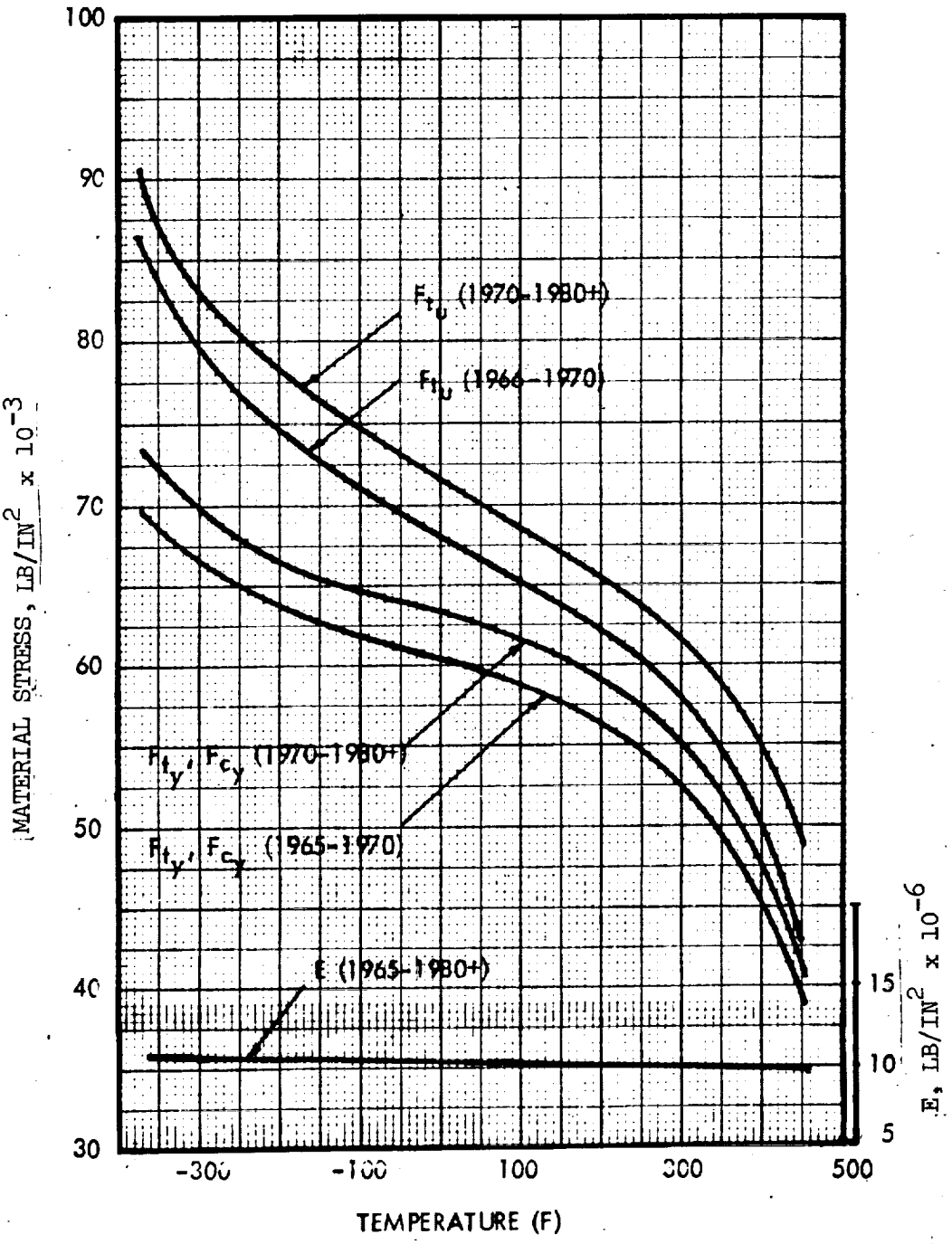

Figure 26. Future Strength Properties of a High-Strength Aluminum Alloy

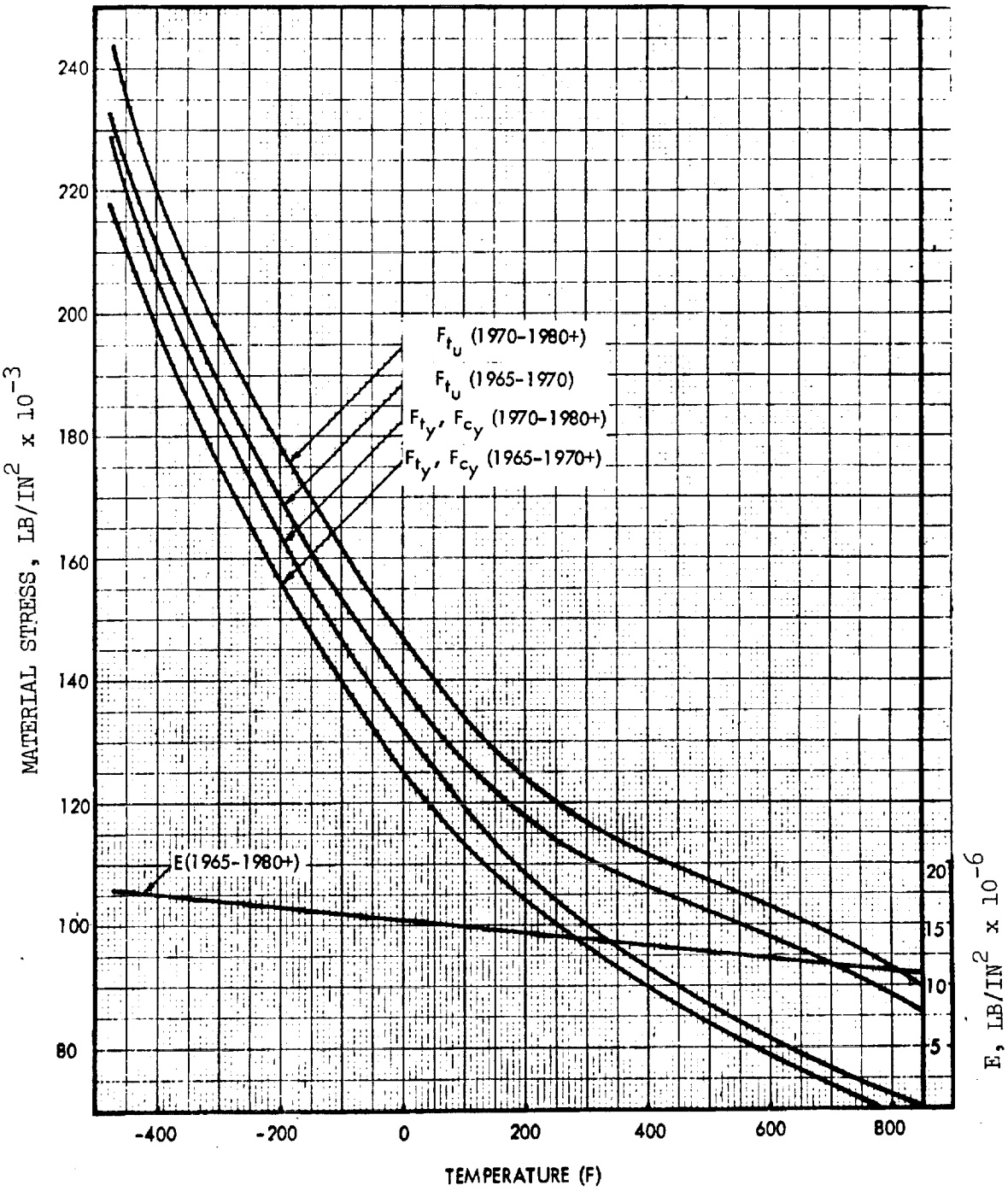

Figure 27. Future Strength Properties of a Titanium Alloy

The property improvements of projected materials are expressed as a percentage increase of a nominal compression yield and tensile ultimate strength of current materials. The shape of the stress-strain diagram for the plasticity considerations for advanced alloy materials is assumed to be identical to that of the current material. The plasticity curve of the material is expressed mathematically for inclusion in the computer subroutines to provide access to the plasticity correction factors for the various materials. Design synthesis analyses to evaluate minimum weight for the structural components must consider materials in the elastic range and plastic range. To benefit from the improved material yield and ultimate properties, the design has to have the capability of working at a stress level above the elastic range. Figure 28 indicates the relative small weight reductions to be anticipated for improvements in both titanium and aluminum alloys for unpressurized components. These weight reductions are the best obtainable for an efficient honeycomb sandwich design where the skins can reach a high stress level. For both skin stringer and waffle construction which are heavier than the sandwich concept, the working stress level will be lower and the weight reductions due to material improvements noticeably lower. Figure 29 shows the similar effects for pressurized shells (50 lb/in^2). These reductions are applicable for a limited range of load intensities. Aluminum achieves weight improvements for all radii but the magnitude of improvement is a function of the radii. The benefits obtained from the 270-inch radius design with aluminum are appreciable since the shell skins are completely determined by the large hoop stress design criteria. The values quoted in Figure 29 are the maximum compressive loading intensities where any material improvement will produce a weight reduction. For load intensities above these values, improvements results in a smaller weight reduction due to the design being primarily dictated by the compression criteria. In heavily loaded components, the skin thickness associated with minimum weight for both the pressurized and unpressurized design is similar. No reduction in design weight can be obtained with the smaller radii for material improvement using titanium. For a 270-inch diameter vehicle, there is a slight improvement for components where the loading intensity is N_x of 8,000 lb/in.

The form of the weight-scaling law will allow for weight variation due to material property increases if the design condition is principally pressure-dependent (high pressure and large diameter). For most space propulsion stages, the anticipated compressive load ranges should be less than 5,000 lb/in.

It can be seen from the previous data that there are only small weight reductions to be expected by improving the strength properties of aluminum or titanium. Anticipated strength improvements during the next decade are less than ten percent and will involve considerable material research. Increases in strength properties often have the adverse side effect of making the material more difficult to use during fabrication. The utility of advanced materials and their small weight reductions have to be evaluated against the extra costs involved with fabrication, design changes, and learning processes. Cost of research and development of new materials should not be amortized over a particular design when considering the material's cost effectiveness. Usually the material is available and the choice is where to apply the material in the most cost-effective manner.

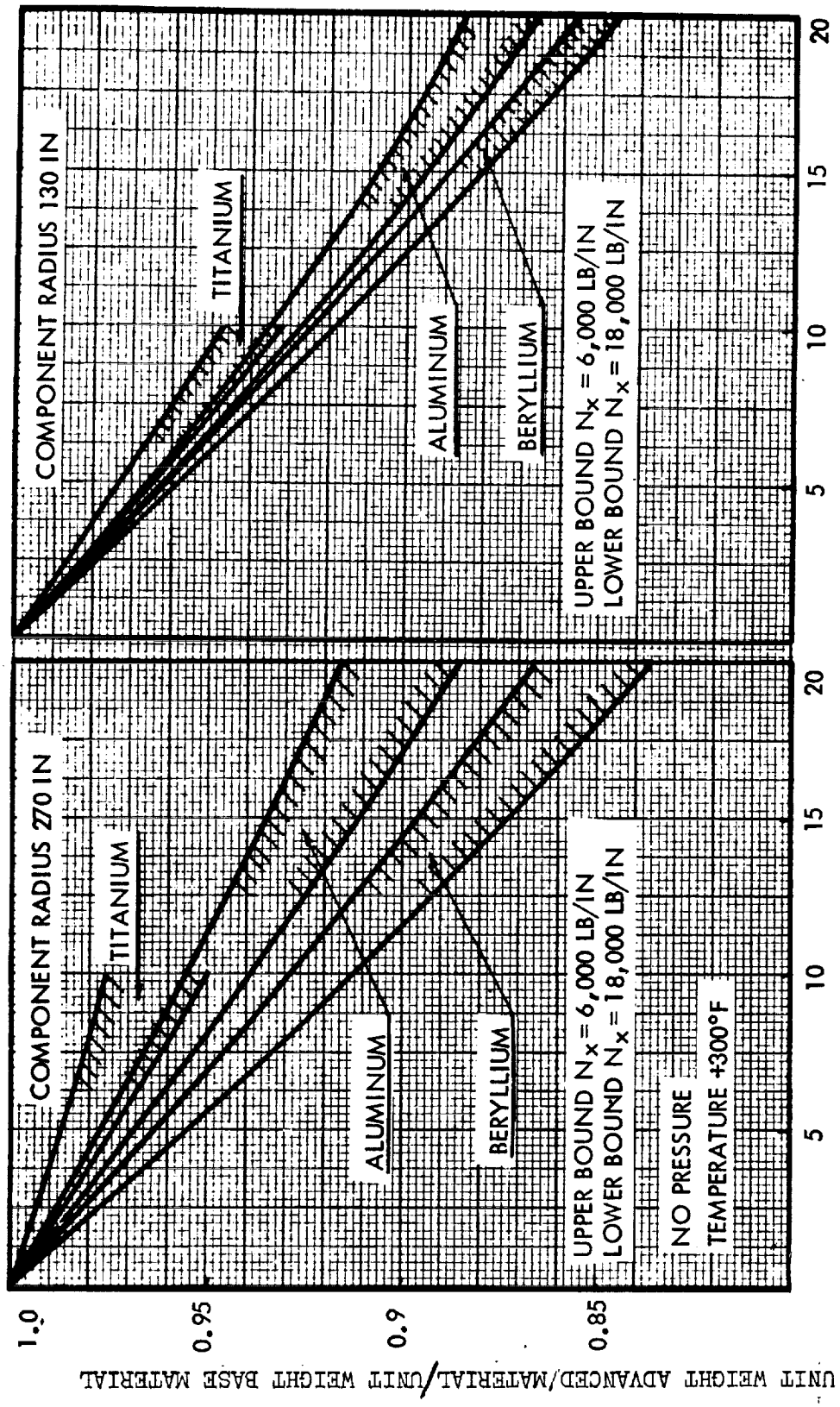

Figure 28. Unit Weight Reductions Resulting from Material Improvements

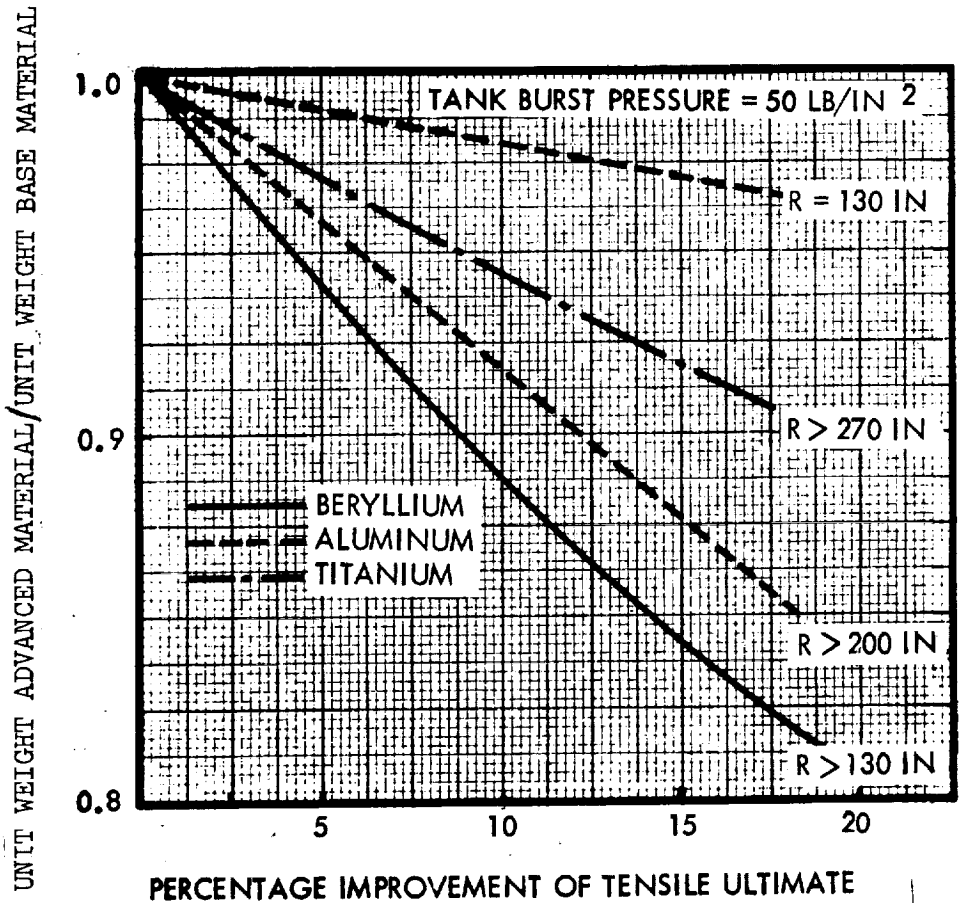

MATERIAL	STRINGER SECTION	RADIUS IN	LOAD INTENSITY N_x^* (LB/IN)
ALUMINUM	'Z'	130 200 270	5,000 12,000 20,000
TITANIUM	'Z'	130 200 270	0 0 8,000
BERYLLIUM	⊓	130 200 270	20,000 20,000 20,000

N_x^* MAXIMUM LOAD INTENSITY WHERE MATERIAL IMPROVEMENT REDUCES UNIT WEIGHT

Figure 29. Effect of Material Improvements in Pressure Tanks

THIS PAGE LEFT

INTENTIONALLY BLANK

5.0 ENVIRONMENTAL SHIELDS

5.1 METEOROID SHIELDING

In the weight estimation and sizing of the propulsion modules, it is necessary to consider the meteoroid environment to which the stage will be exposed during its mission. Additional shielding may be required to ensure adequate protection of the various subsystem components and preclude any catastrophic meteoroid penetration of the structure. Shielding requirements will be based on the vehicle's mission, the various types of meteoroid environments, and the penetration probability criteria.

The meteoroid shielding requirement evaluation is divided into three separate steps, as shown in Figure 30. This stepwise procedure is efficient as it separates the mission integration of the flux densities from the iteration step of the propulsion stage sizing and weight optimization to meet specified mission requirements.

The initial step is that portion of the analysis that is dependent only on the mission profile and flux models. The mission is subdivided into a series of elliptic heliocentric arcs for the transplanetary portion of the mission and additional arcs for the planetary stay times. A time/position/velocity history for the mission is developed and the flux intensity at the various positions along the trajectory identified. Three different flux models are used to represent the sporadic asteroidal, sporadic cometary, and stream cometary meteoroidal environments. The flux densities and relative velocities are integrated for each leg of the mission.

Step two considers the effects that the design criteria (probability of no penetration) and the propulsion stage size have on the design requirements for the shielding. The duration that any particular stage is subjected to the space environment must be considered to ensure there is adequate protection from the meteoroid flux until its useful life is complete and the stage is jettisoned. A weighted average throughout the mission is obtained for the flux density and its relative velocity.

Probabilities are assigned to the different types of meteoroids in an optimum fashion to ensure a minimum weight shielding design. The maximum meteoroid particle that will be encountered is identified by its diameter, velocity and density, the shielding must resist this particle without penetration.

Step three uses the penetration mechanics for the various shielding concepts to determine the required material thicknesses for the bumper and back-up sheets. Shielding thickness allowances are made for existing insulation and or structure which will contribute towards the meteoroid shield. The additional structural weights to meet the meteoroid shielding requirements are considered for the three design concepts (single sheet, single bumper, multi-bumper) and the lightest weight design can be selected.

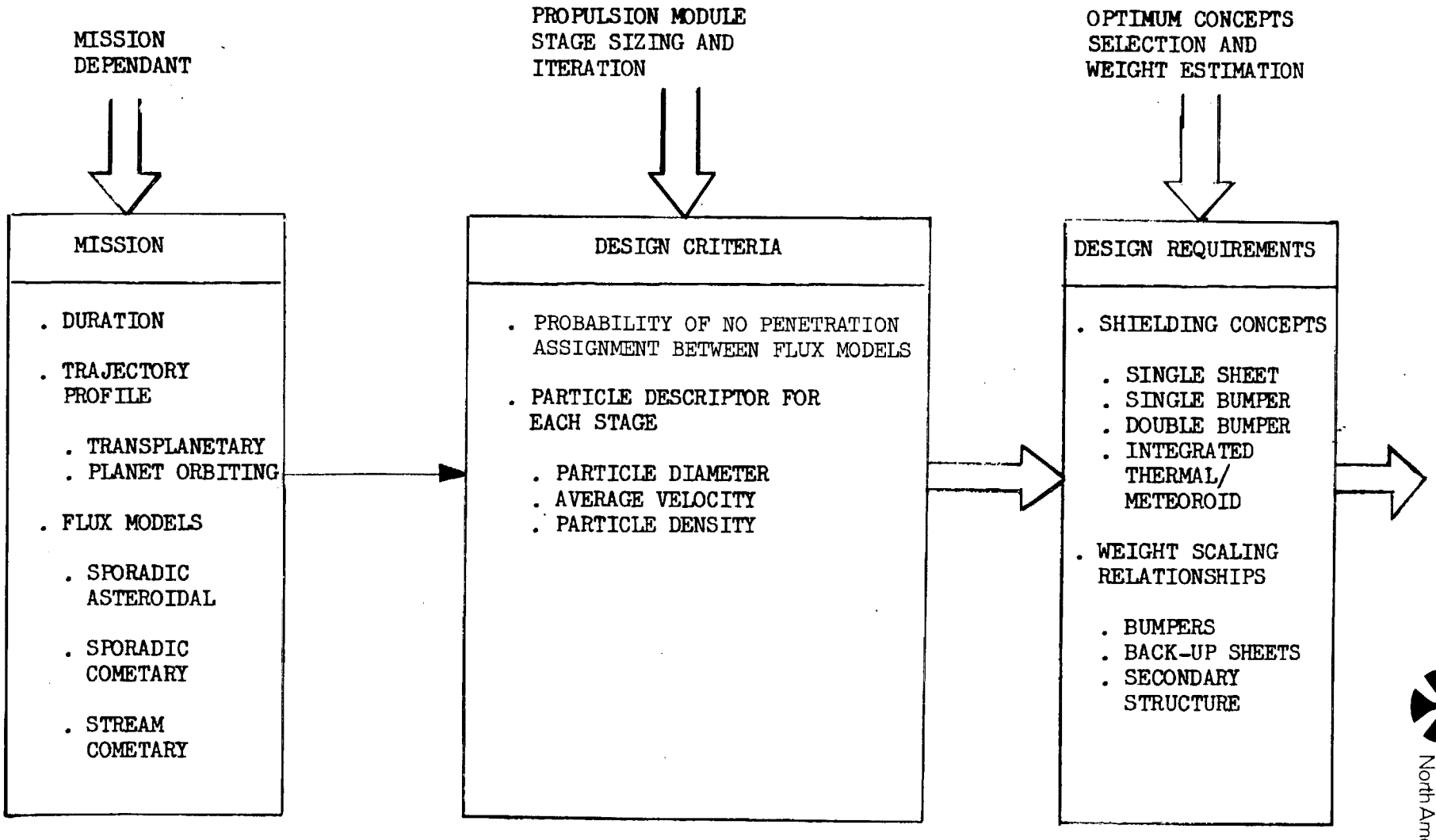

Figure 30. Stepwise Procedure for Meteoroid Protection Evaluation

The vehicle synthesis computer program will perform these three steps in its evaluation and sizing of a propulsion module. Elements of this program have been used to provide data for ranges of missions; these data are used as look-up curves for the simplified scaling laws.

5.1.1 Meteoroid Flux Models

The meteoroid population within the solar system is presently divided into three separate environments: the sporadic cometary environment, the sporadic asteroidal environment, and the cometary stream environment. Current models of the sporadic cometary environment define the population as highest near the sun and falling off slowly with distance from the sun. Asteroid particle models show virtually all particles to be concentrated in the asteroid belt between Mars and Jupiter. The current model of the stream particles has them grouped in clusters which orbit the sun; therefore, a spacecraft may or may not encounter a major stream depending on its mission trajectory.

Three models are used to represent the flux density distribution for the three types of meteoroids, with each model varying the flux with solar distance and velocity of encounter.

The general equation for the particle flux distribution is given by

$$\mathrm{Log}_{10} F = K_1 + K_2 \, \mathrm{Log}_{10} \, m + f(R) + \mathrm{Log}_{10} \, \overline{V} \qquad (13)$$

where

$\overline{V}$ = relative velocity between particle and spacecraft, m/sec

F = flux of particles of mass $\geq m$, m^{-2} -sec^{-1}

m = meteoroid mass, grams

K_1, K_2 = empirical constants

$f(R)$ = solar system location function

R = distance from the sun, AU

5.1.1.1 Sporadic Asteroidal Meteoroids

These particles are concentrated in a belt located between 1.5 and 3.5 AU. They travel in circular orbits at low angles of inclination to the ecliptic plane. Information on these particles is obtained almost solely by telescope examinations of the visible asteroids. Due to the minimal data

available, definition of the model for this environment is uncertain, particularly in regard to the particle flux. The fluxes defined by several candidate models are compared in Figure 31 . Two of these models, NASA/MSC 1964 (Reference 5) and NASA/MSFC 1969 (Reference 6) greatly limit the range of AU in which they are applicable. The other three models show general agreement. The NR model (Reference 7) was the first of this type to be developed. The NASA 1970 model (Reference 8) has received considerable development effort and is used for the weight scaling study.

For the asteroidal flux the constants are defined in Table 11, and the function f(R) is illustrated in Figure 32. The asteroidal flux is applied to the total spacecraft surface. Reference 8 approximates the relative velocity ($\bar{V}$) between the meteoroid and the spacecraft by

$$\bar{V} = R^{-\frac{1}{2}} u_1 (u_2 - u_3 \sigma \cos \gamma + \sigma^2)^{\frac{1}{2}} \qquad (14)$$

where

σ = ratio of vehicle speed to circular speed

γ = angle between vehicle velocity vector and circular velocity vector

Empirical values for u_1, u_2, and u_3 for the asteroidal model are quoted in Table 12 .

5.1.1.2 Sporadic Cometary Meteoroids

These particles result from disintegration of comets, and like comets are distributed throughout the solar system. They travel in a full spectrum of orbit shapes and at all inclinations to the ecliptic plane. The environment model selected for this type particle is that of Reference 8. The particle flux is given by Equation 13 with constants as given in Table 11. Radial distribution of the sporadic cometary meteoroids can be represented by

$$f(R) = -1.5 \, \mathrm{Log}_{10} R \qquad (15)$$

The sporadic cometary particle impact velocity is given by Equation 14 and the coefficients are given in Table 12. The sporadic cometary flux is applied to the total spacecraft surface.

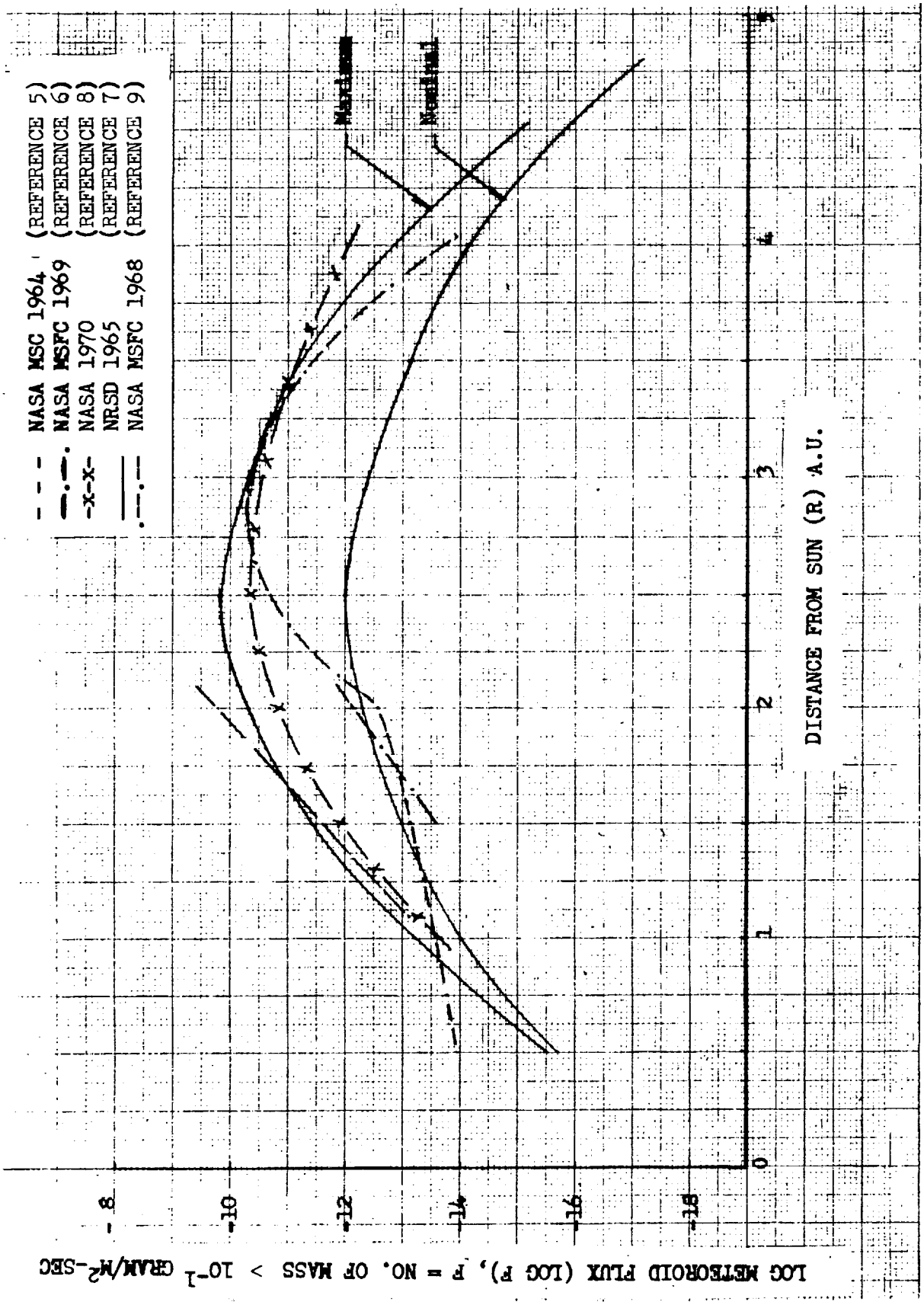

Figure 31. Comparison of Asteroidal Flux Models

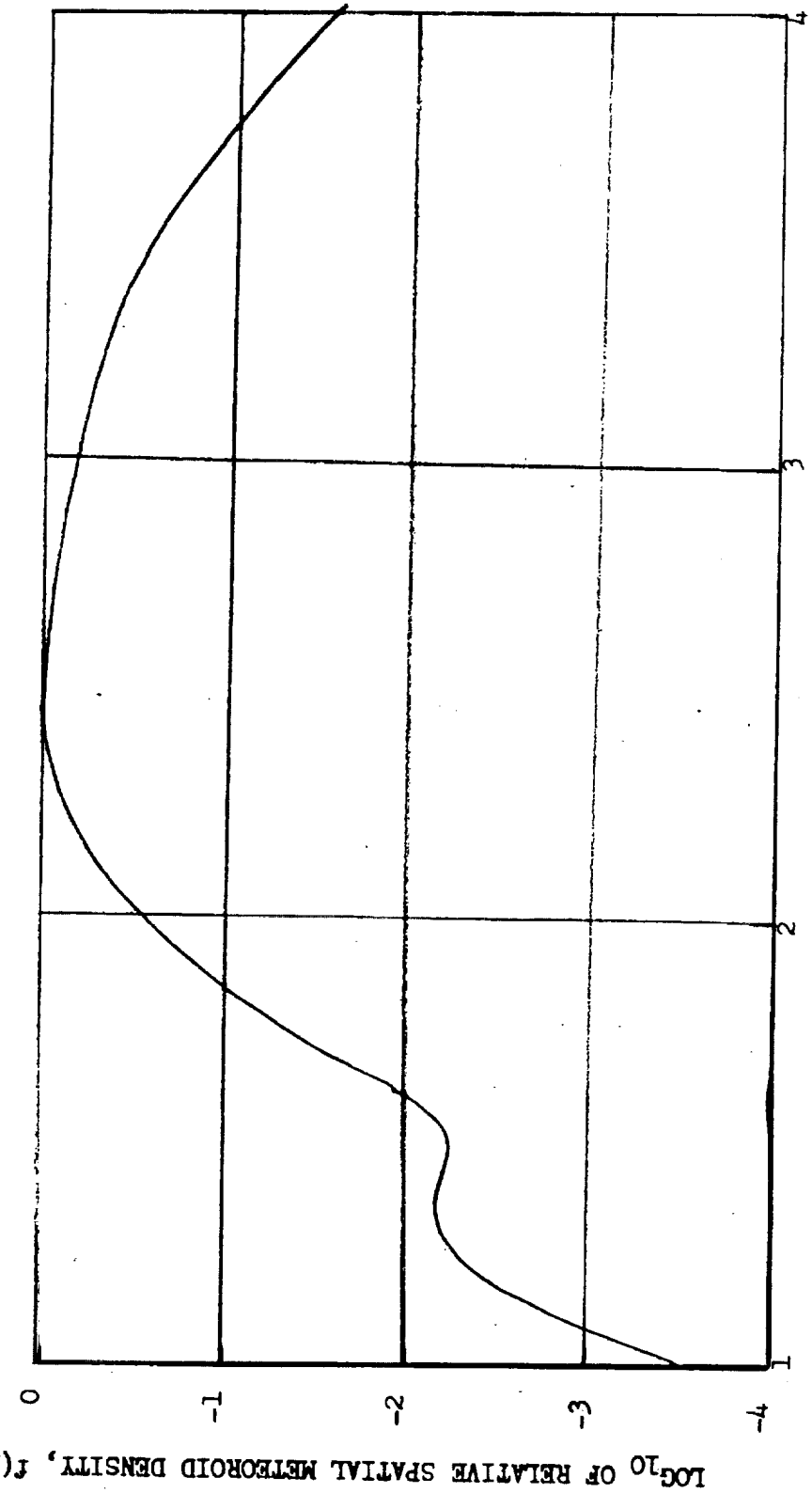

Figure 32. Asteroidal Meteoroid Radial Distribution

Table 11. Meteoroid Environment Constants

Flux density coefficients

Environment (1)	Mass Range Grams	K_1	K_2	Density Gram/cm^3
Cometary	$10^{-6} \leq m \leq 10^{2}$	-18.776	-1.213	0.5
Asteroidal	$10^{-9} \leq m \leq 10^{2}$	-16.392	-0.84	3.5
Stream	$10^{-6} \leq m \leq 10^{2}$	-11.475	-1.213	0.5

Table 12. Empirical Velocity Coefficients

R	u_1	u_2	u_3	Meteoroids
1.7 AU	30.05×10^{3}	1.2292	2.1334	Asteroidal
2.5 AU	29.84×10^{3}	1.0391	1.9887	Asteroidal
4.0 AU	29.93×10^{3}	0.9593	1.9230	Asteroidal
-	31.29×10^{3}	1.30	1.9235	Cometary

5.1.1.3 Cometary Stream Meteoroids

These particles, like the sporadic cometary particles, also result from comet disintegration, but they remain closely grouped in stream formations following the parent comet orbit. Streams are divided into major and minor streams, the first having an existing parent comet and the second being without a parent comet. Certain major streams have been located by telescope observation of the comet. The environment model selected to define the major stream meteoroid environment is that of Reference 10. This model predicts the location of the known major meteoroid streams and their intersection with the ecliptic plane.

Figure 33 is a map of these known streams. The solid dots indicate streams into the plane, the open circles signify the streams out of the plane towards the reader. Although this figure shows many streams, their presence will not be coincidental. The periodicities of the streams range up to 100 years, a fact that will greatly reduce the probability of encountering a stream for a well planned mission. A typical Grand Tour trajectory has been super-imposed upon Figure 33, and while it appears that the trajectory crosses the orbit path of two streams, their appearance does not remotely coincide with the mission launch date. They appear years away from this particular trajectory. The flux density due to the stream cometary model is given by

$$\text{Log}_{10}F = K_1 + K_2 \text{ Log}_{10}m \tag{16}$$

The stream cometary model is simplified by considering the velocity $\overline{V}$ for a near Earth environment; therefore

$$K_1 = K_1^* + \log_{10} \overline{V}$$

where K_1, K_2 are given in Table 11,

and

$$V = \text{particle impact velocity} = 20{,}000/\sqrt{R}, \text{m/sec}$$

There exists a remote possibility of a chance encounter with an unknown stream. There is no method of explicitly determining the probability of encounter. Each mission could consider the unknown stream encounter to determine its effect on the meteoroid shielding requirements.

5.1.1.4 Meteoroid Environment Near Planets

The meteoroid environment modeling of Reference 8 is applied to define the sporadic asteroidal and cometary particle environment. Modification to the predictions of these models must be made in the vicinity of the planets to take into account the planetary shielding and gravitational effects. To take into account the increase in flux due to gravitational attraction, the general flux equation is multiplied by

$$G = 1 + 0.76 \frac{RV_p^2 r_p}{V_e^2 r} \tag{17}$$

and to take into account the decrease due to shielding the flux is multiplied by the factor

$$\eta = \frac{1}{2} + \frac{1}{2}\left(1 - \frac{r_p^2}{r^2}\right)^{\frac{1}{2}} \tag{18}$$

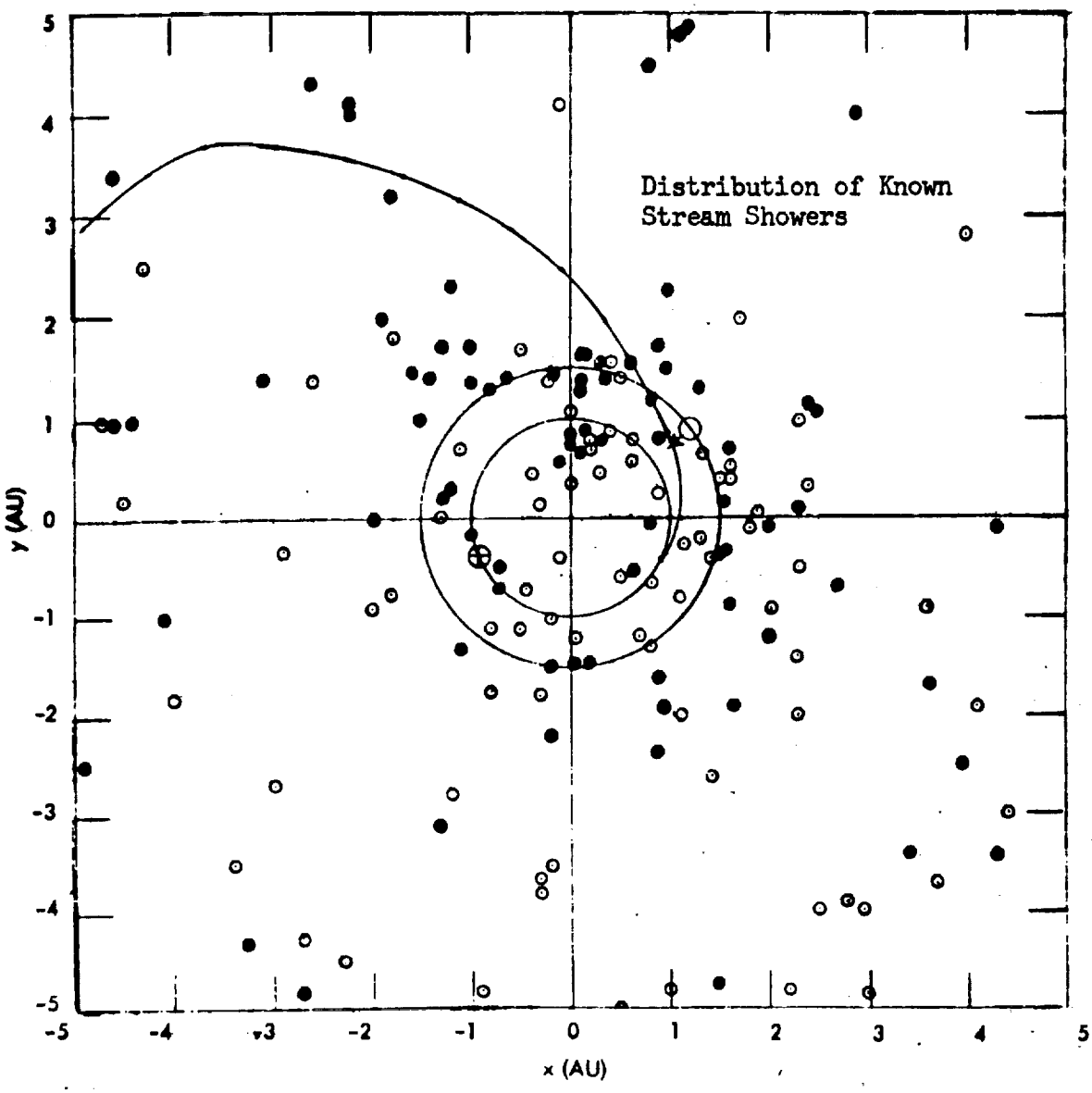

Figure 33. Grand Tour Trajectory Relative to Meteoroid Shower Zones

where

η = shielding factor due to presence of planet

G = flux increase factor due to planet gravity

r_p = radius of the planet

r = spacecraft's distance from the planet's center

R = distance of the planet from the sun in astronomical units (AU)

V_e = escape velocity from the earth's surface

V_p = escape velocity from the planet's surface

The average velocity relative to the spacecraft is

$$\overline{V} = \sqrt{\frac{r_p}{r} V_p^2 + V_s^2}$$

where

$\overline{V}$ = average relative velocity to a spacecraft near a large planet (m/sec)

V_s = velocity of spacecraft relative to the planet (m/sec)

The presence of the planet increases the average velocity $\overline{V}$ by about 3 percent for the small planets (Mercury, Venus, Earth and Mars), while for the larger planets $\overline{V}$ approaches the escape velocity of the planet. The escape velocities for the planets are given in Table 13.

5.1.2 Particle Penetration Mechanics

5.1.2.1 Meteoroid Particle Encounter

The main meteoroid hazard to spacecraft is the chance encounter with a single large particle. The approach taken is to provide information such that the probability of failure due to this source is equal to, or lower than, some prescribed value. To obtain gross sizing of the structure, it is

Table 13. Escape Velocities from the Surface of the Planets

Planet	Average Distance from Sun (AU)	V_p (m/sec)
Mercury	0.39	4.3×10^3
Venus	0.72	10.4×10^3
Earth	1.00	11.2×10^3
Mars	1.52	5.1×10^3
Jupiter	5.20	61.0×10^3
Saturn	9.54	36.7×10^3
Uranus	19.19	22.4×10^3
Neptune	30.07	25.6×10^3

convenient to work in terms of a design meteoroid particle. This particle will impact the structure without puncturing the inner wall. The maximum particle's size is related to the probability of encounter by the Poisson probability law.

A spacecraft is normally composed of several modules, the number of which may increase or decrease during a given mission with resulting variation in total surface area. The mission also may require travel in both orbit and deep space, which would vary the amount of planetary shielding. To account for variations, the mission is divided into n phases, and the probability of no failure of the spacecraft during phase i is given by

$$P_{o_i} = \exp\left(-F_i A_i T_i\right)$$

or

$$P_{o_i} = 1 - F_i A_i T_i$$

where A_i = the exposed surface area of the spacecraft during the i^{th} mission phase

T_i = the duration of the i^{th} mission phase

The probability of no failure of the spacecraft for the total mission duration is

$$P_o = 1 - \sum_{i=1}^{n} F_i A_i T_i \qquad (19)$$

Using equation 19 and the general flux equation 13

$$P_o = 1 - \sum_{i=1}^{n} 10^{K_1} \bar{V} 10^{f(R)} A_i T_i m^{K_2}$$

and, on rearranging, the design meteoroid mass (m_p) is given by

$$m_p = \left[\sum_{i=1}^{n} \frac{10^{K_1} \bar{V} 10^{f(R)} A_i T_i}{(1 - P_o)} \right]^{-1/K_2} \quad ; P_o > 0.9 \qquad (20)$$

The variation of the particle mass with the exposure factor is shown in Figure 34. The meteoroid shape is assumed to be spherical and its diameter (d_p) is given by

$$d_p = \left(\frac{6m_p}{\pi \rho_p} \right)^{1/3} \qquad (21)$$

and is shown in Figure 35 as a function of m_p for the particle densities ρ_p of the various flux models shown in Table 11. Figures 36 and 37 are used to determine the particle diameter as a function of the parameter $\sum$FAT for a range of probabilities of no penetration and for both the asteroidal and cometary meteoroid flux.

5.1.2.2 Single Sheet Penetration Mechanics

Numerous methods have been used to describe the penetration mechanics of the meteoroid particles impacting upon quasi-infinite and finite metal targets. In the past, most investigators have chosen to relate penetration depth to the various projectile and target parameters by power expressions (References 11 and 12). Others (References 13 and 14) have chosen to use a combination of power and logarithmic expressions.

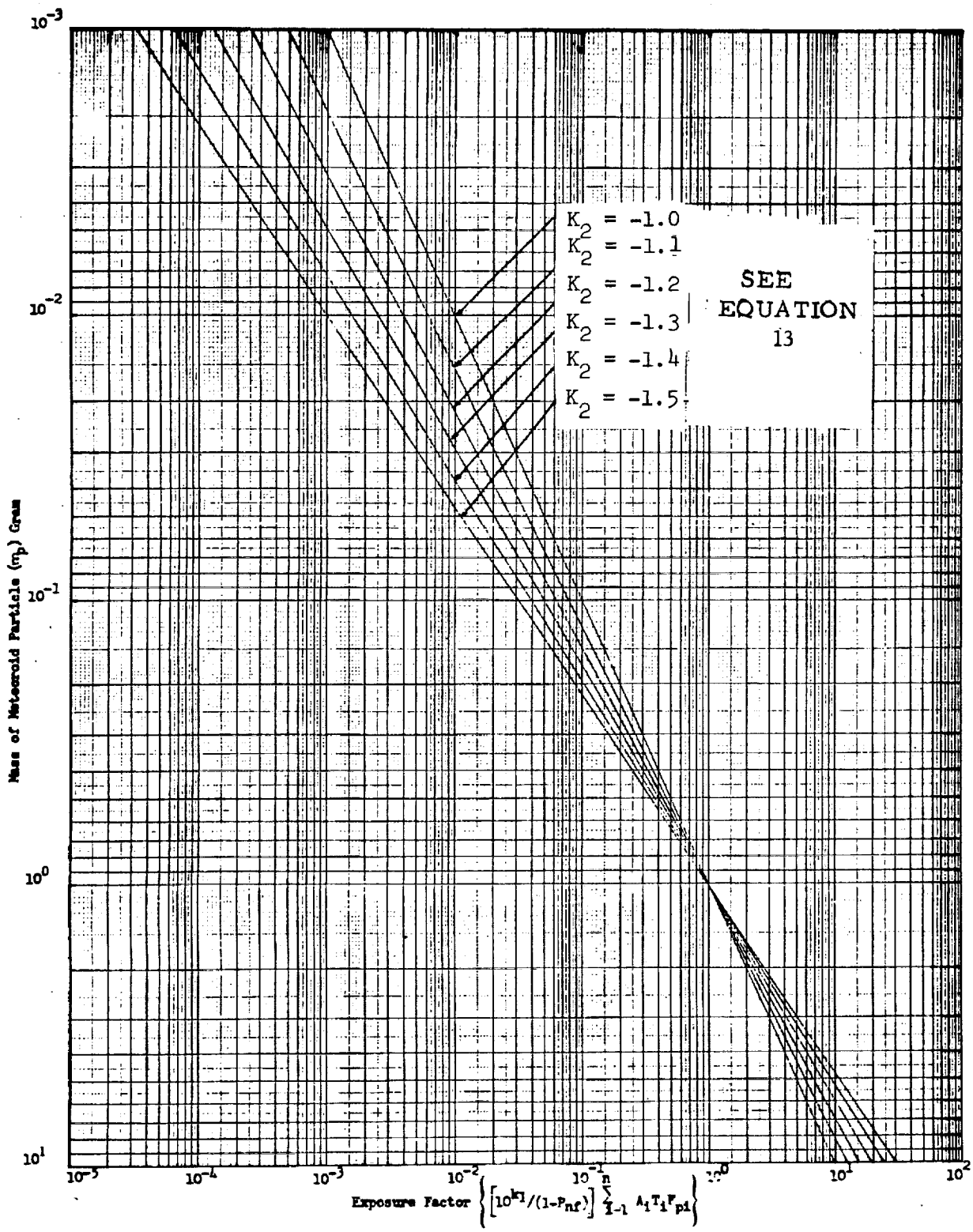

Figure 34. Exposure Factor for Meteoroid Penetration Shielding

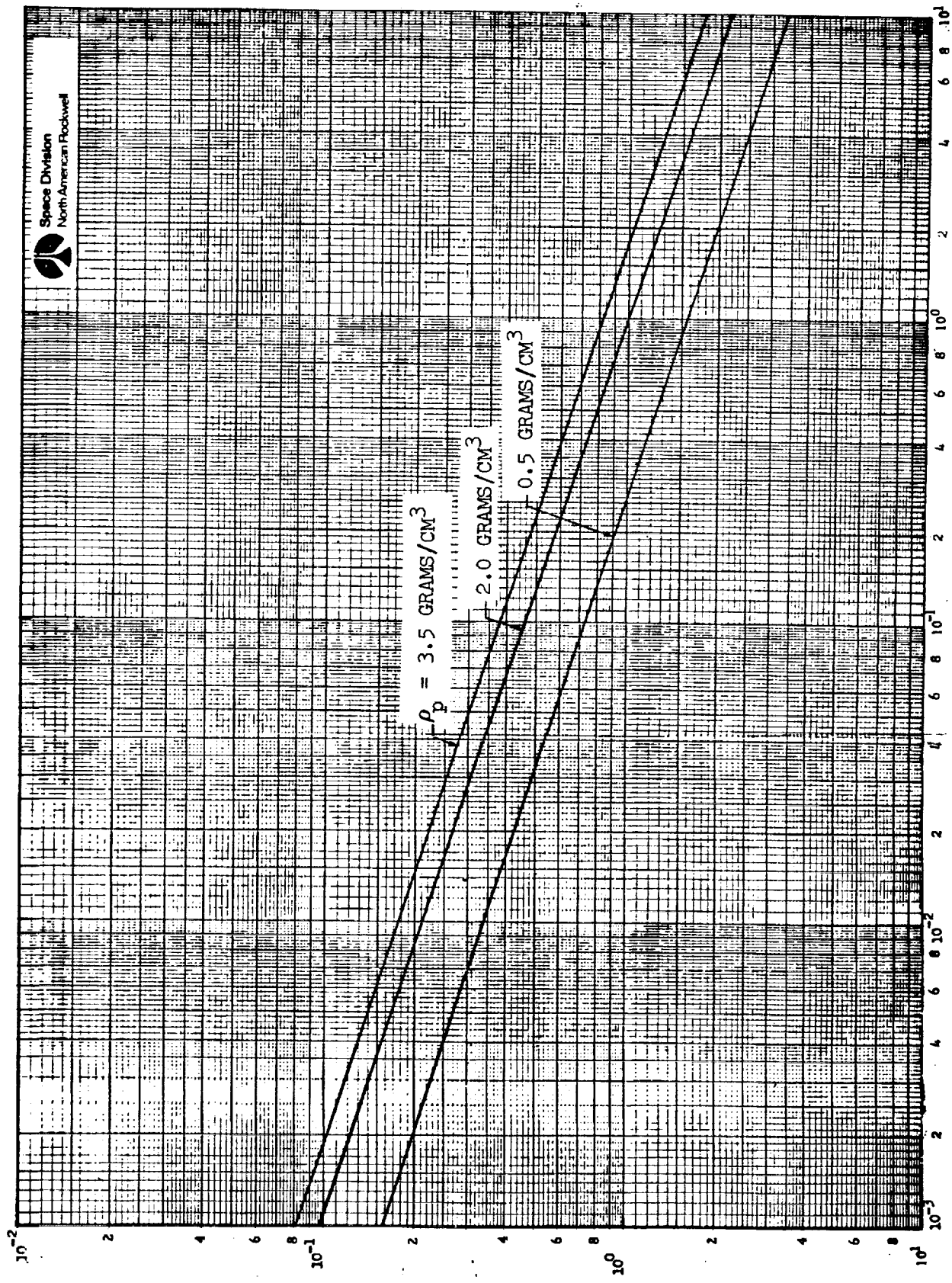

Figure 35. Meteoroid Mass and Diameter

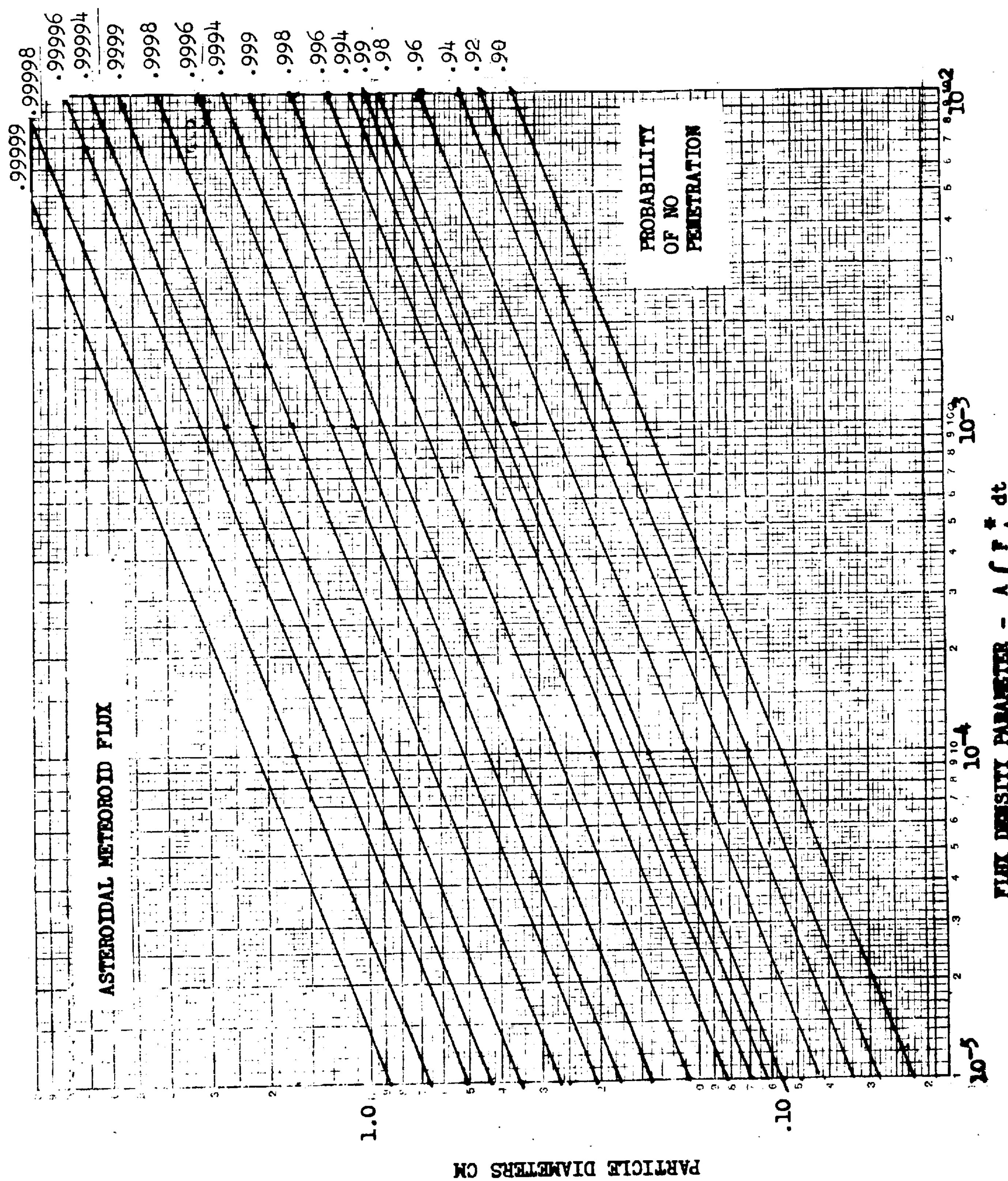

Diameter Determination for Asteroidal Flux

Figure 37. Particle Diameter Determination for Cometary Flux

Hypervelocity impact tests were initiated by NASA and Space Division Apollo Engineering for the shielding analysis of the Apollo command module. Numerous types of materials and structures were tested; among them were included quasi-infinite and finite metal targets. These tests were made to establish the basic equations describing penetration and rear spall resulting from a single hypervelocity particle impact. Early in the testing it became apparent that none of the numerous penetration equations available described the results being obtained on these targets.

Extensive hypervelocity particle impact tests have been conducted at several facilities: the North American Rockwell Space Division Space Sciences Laboratory (SSL), General Motors Defense Research Laboratory (DRL), and the Naval Research Laboratory (NRL). Projectiles were launched by gas gun, shaped charge and electrothermal gun. The power relationship was used to reduce the data chiefly because they were conservative. The general form of the equation selected is

$$P_\infty = \frac{K\, d_p^{\,a}\, \rho_p^{\,b}\, V_p^{\,c}}{\rho_t^{\,d}\, H_t^{\,e}}$$

The penetration equation considered the properties of the meteoroid particle and the target material. A multiple regression analysis was performed on the available data. The results (Reference 15) were

$$P_\infty = \frac{1.33\, d_p^{\,1.12}\, \rho_p^{\,0.588}\, V_p^{\,0.674}}{\rho_t^{\,0.1625}\, H_t^{\,0.261}} \quad ; \text{ (cm)} \qquad (22)$$

Multiple correlation coefficient = 0.99983

Residual variance = 0.000406

The exponents of Equation 22 imply greater accuracy than is justified. A more appropriate form has been adopted for use in shielding design.

$$P_\infty = \frac{1.38\, d_p^{\,1.1}\, \rho_p^{\,1/2}\, V_p^{\,2/3}}{\rho_t^{\,1/6}\, H_t^{\,1/4}} \qquad (23)$$

At this point, it is appropriate to compare Equation 23 with the work of other investigators to establish differences and their effects. Perhaps the most meaningful comparison is the predicted penetration of a cometary meteoroid (0.5 gram/cm^3) impacting on an aluminum surface. The depths of penetration predicted by several well known equations are compared in Figure 38. Figure 38 shows that penetration laws developed by Hermann and Jones are relatively nonconservative for the higher particle velocities and that the penetration of Summers is ultraconservative compared with the NR exponential data. As indicated, differences in these penetration equations result in substantially different predictions.

The differences in the numerous power type penetration equations available can be readily determined by use of the matrix in Table 14. The equations presented include most of the better known power equations. Each is distinguished as being of empirical or theoretical origin. It should be noted that the parameter, target speed of sound (C_t), has been eliminated by substitution of the equivalent E_t and ρ_t relationship. Examination of the matrix indicates general agreement between all equations. Closer examination reveals

1. There are significant differences regarding the choice of a target strength term.

2. There are significant differences in the choice of exponents.

3. The more recent equations appear to be in close agreement.

The penetration mechanics used for this study were from Reference 16 which has a simplified expression for the penetration with an empirical coefficient K. K is determined experimentally for the particular target material.

The penetration depth for a quasi-infinite sheet is

$$P_\infty = K\, m_p^{0.352}\, \rho_p^{1/6}\, \bar{V}_p^{2/3} \qquad (24)$$

Typical values for K are 0.42 for several different aluminum alloys (Reference 16).

In meteoroid protection analysis of the spacecraft, it is necessary to be able to compute the minimum thickness of the material able to resist perforation by a given hypervelocity particle. Sufficient test data are available for this target to provide a gross understanding of the perforation process. As target thickness is reduced toward the minimum thickness that

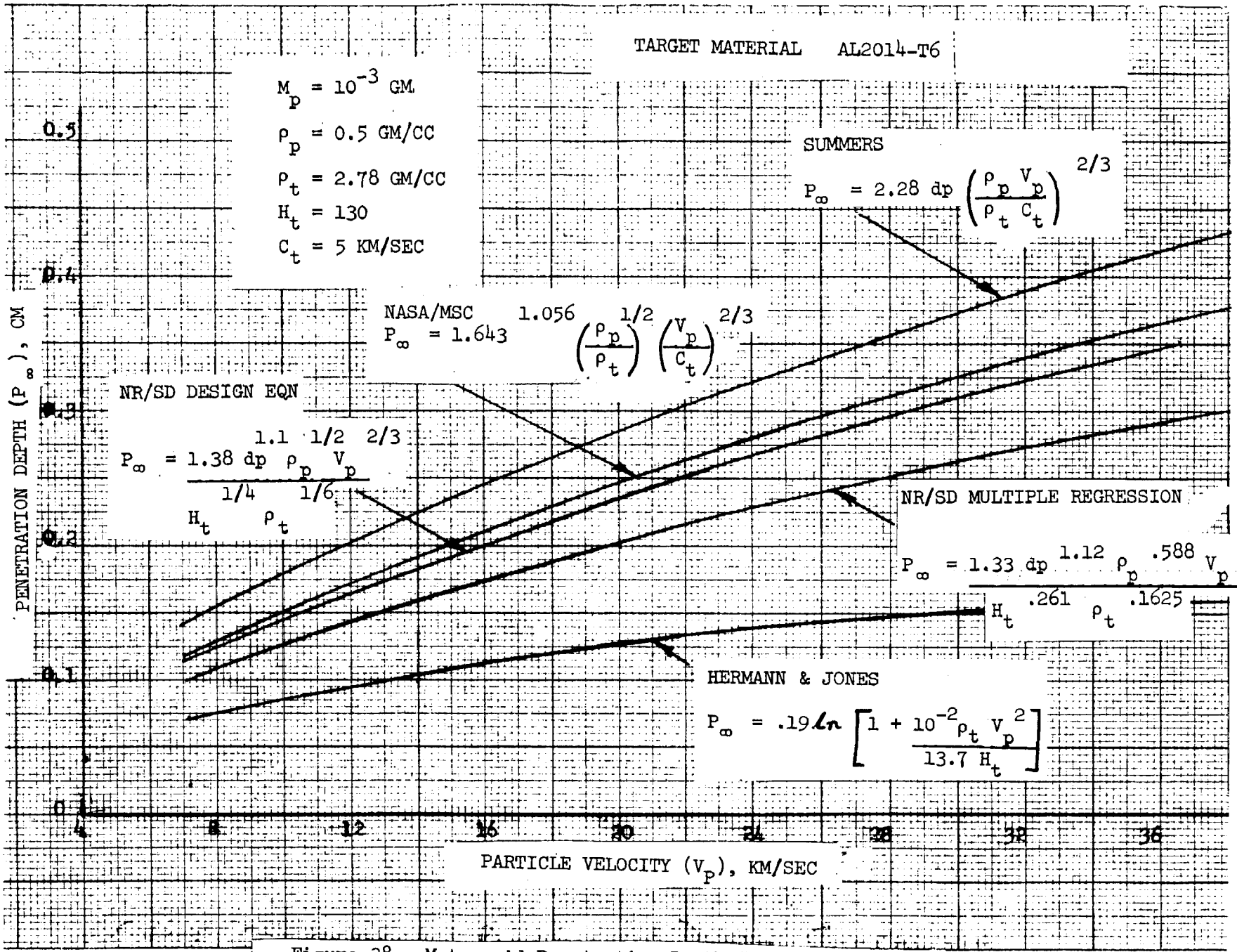

Figure 38. Meteoroid Penetration Depth Comparison

Table 14 . Comparison of Penetration Equation Parameters

PARAMETER	EXPONENT	VALUE OF EXPONENT										
		BJORK (9) Theo.	WALSH & JOHNSON (11) Theo.	RINEY & HEYDA (12) Theo.	HERRMANN & JONES (5) Emp.	GMC-DRL (1) Emp.	(1958) CHARTERS & SUMMERS (3) Emp.	(1959) CHARTERS & SUMMERS (4) Emp.	BRUCE (10) Emp.	SORENSON (13) Emp.	NASA-MSC (14) Emp.	EQUATION No. 3 Emp.
PROJECTILE DIAMETER	a	1.0	1.0	1.0	1.0	1.0	1.0	1.0	1.0	1.0	1.056	1.1
PROJECTILE DENSITY	b	-	1/3	1/3	2/3	1/2	2/3	2/3	1/2	.449	1/2	1/2
PROJECTILE VELOCITY	c	1/3	.58	2/3	2/3	2/3	2/3	2/3	2/3	.564	2/3	2/3
TARGET DENSITY	d	-	.04	-	1/3	1/3	1/3	1/3	1/2	1/6	1/6	1/6
TARGET BRINELL HARDNESS	e	-	-	-	1/3	1/4(a)	-	1/3(b)	-	-	-	1/4
TARGET MODULUS	f	-	.29	-	-	-	1/3	-	-	-	1/3	0(e)
PROJECTILE MODULUS	g	-	-	-	-	-	-	-	-	-	-	0(d)
TARGET SHEAR STRENGTH	h	-	-	-	-	-	-	-	-	.282	-	(c)

(a) Converted from H_{tmax}
(b) Deformation strength term
(c) This parameter was not included in this analysis.
(d) Penetration was found to be virtually unrelated to this parameter.
(e) Penetration was found to be effectively not a function of this parameter when preceding parameters are all included.

will just resist perforation (limit thickness), the projectile impact causes penetration and removal of material from the target rear surface. The amount of material removed can be substantial, the thickness in some cases being as much as 80 percent of the depth of penetration.

Early tests by Kinard (Reference 17) on aluminum targets indicated single finite sheet requirements to resist penetration were 1.5 times that of a quasi-infinite target. The NASA monograph, Reference 16, has been used for this study to determine the single sheet requirements, and the empirical equation is

$$t_{ss} = K_1 \, m_p^{0.352} \, \rho_p^{1/6} \, \bar{V}_p^{0.875} \qquad (25)$$

where the coefficient K_1 is based on test results for various materials as shown in Table 15.

5.1.2.3 Multi-Sheet Penetration Mechanics

The penetration mechanics for the multi-sheet concept are based upon the NR developed approach of penetration damage of multi-sheet structures from discrete particles, Reference 18. An expanding cloud of discrete fragments is used to model the fragmentation and scattering of the particle and first-sheet material following initial impact. The damage to the structure is expressed in terms of the bumper hole size and depth of penetration into the rear sheet(s). The empirical constants identified in the method have been correlated with numerous available test data on a variety of structure/projectile combinations.

The NR penetration mechanics and shielding protection weight data are detailed in Appendix B. These data were obtained from an existing NR/SD penetration mechanics program which is used to select the most efficient spacing and thicknesses of the various sheets to attain overall minimum weight concept. The weight for the total shielding (W_{mp}) can be expressed as:

$$W_{mp} = W_B + W_m + W_s \qquad (26)$$

where

W_B = Unit weight of outer bumper

W_m = Unit weight of rear sheets

W_s = Weight of support structure required to ensure bumper spacing.

Table 15. Single Sheet Penetration Coefficient K_1

Material	K_1	
	Visual	Pressure
2024 T3, T4 7075 T6 6061 T6	0.54	0.57
304 316	----	0.32
17-4 PH (annealed)	----	0.38
Magnesium Lithium 141-A	----	0.80
Columbium alloy CB-IZR	----	0.34

The treatment for the multi-sheet shielding considers the case where the projectile and the mass of shield material it removes are fragmented into smaller projectiles which constitute the debris cloud impacting the subsequent sheets. For low velocity projectiles and/or thin outer-bumper sheets, this fragmentation does not occur. Figures 39 and 40 clearly demonstrate this effect with resulting increase in penetration depth for the lower impact velocity particles. These data were obtained from actual test shots and tend to confirm that there is a no fragmentation/fragmentation cross-over to consider in the analysis. The cross-over that occurs at the velocity of 6 k m/sec (Figure 39) was for a test specimen with an extremely thin outer sheet. A more practical and minimum weight design would have a thicker outer bumper such as the test specimens used for the data in Figure 40.

Most of the available test data used impacting velocities less than 10 km/sec. The theoretical penetration equation indicates decreasing penetration depth with increasing impacting velocity. It is felt at NR/SD that extrapolation of theoretical results beyond the 8 km/sec test range is premature and has not been substantiated adequately with experimental test data. Therefore, the penetration theory for allowable hole size of the outer bumper is modified for impacting velocities in excess of 8 km/sec and the resulting penetration depth correlation shown in Figure 40 is conservative and should be used for design and weight estimating purposes.

The performance of the multi-sheet concepts can be improved by utilizing the effective stopping power of the thermal insulation around the cryogenic tanks. The insulation will significantly reduce the impacting velocity of the smaller particle debris cloud after the original projectile has been fragmented by the outer bumper. Tests at NR/SD have verified the effectiveness of the insulation and corroborated the method of analysis for the multi-sheet penetration mechanics. Appendix B indicates how the reduction of the particle velocity impacting the rear sheets can be used to define the unit weights required for the shielding concepts which include insulation.

The meteoroids can damage the thermal insulation and provide additional heat leaks into the propellant tanks. Preliminary analysis conducted at NR/SD for a Space Station complex in Earth orbit, showed that the insulation surface area damaged by meteoroids during a ten-year exposure amounted to approximately 0.2%. This damage to the multi-layer high performance insulation results in exposure of the tank wall. Test results from meteoroid shielding concepts penetrated by meteoroids have shown that the damaged area of the insulation has clean edges and there were no direct contacts between individual metallic layers.

It is felt from previous investigation that the heat leak through the damaged area would not approach the total heat leak through the undamaged insulation. Additional detailed study beyond the scope of this contract is required to determine whether these heat leaks can be neglected.

5.1.2.4 Probability Assignment

The improved scaling laws for the structural shielding requirements for meteoroid protection consider the effect of the vehicle exposure to the time varying flux environment. The penetration equation requires a knowledge of the anticipated particle size which has to be resisted without penetration, the particle density, and its relative velocity. There are three different meteoroid models which must be considered (sporadic asteroidal, sporadic cometary and stream cometary). Each model imposes individual design criteria on the shielding requirements depending upon the mission profile. The effects of all models must be assessed and the most effective shielding requirements defined to provide an overall probability of no penetration for the total stage.

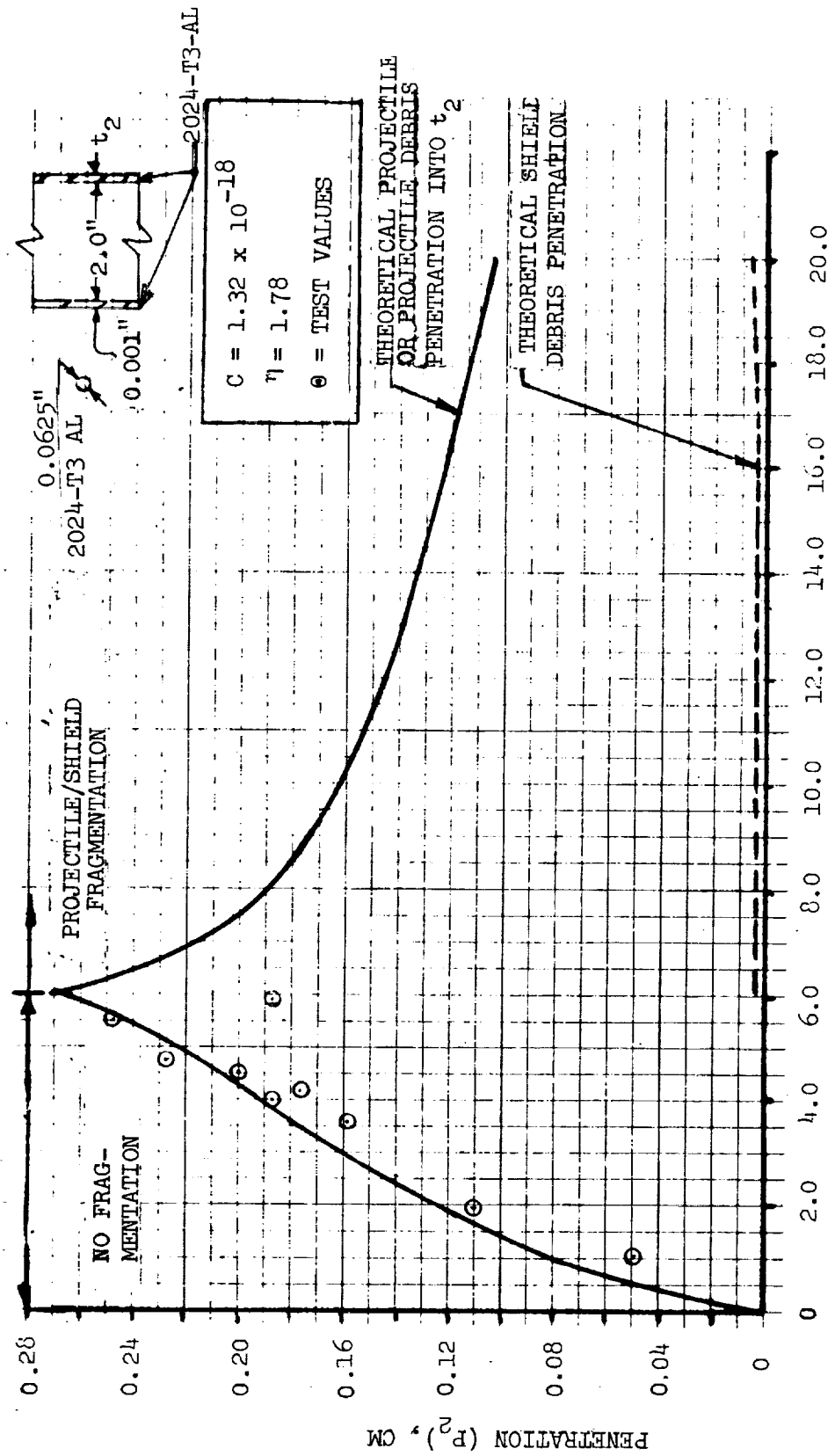

Figure 39. Effect of Impact Velocity on Damage - $t_1/d = 0.016$

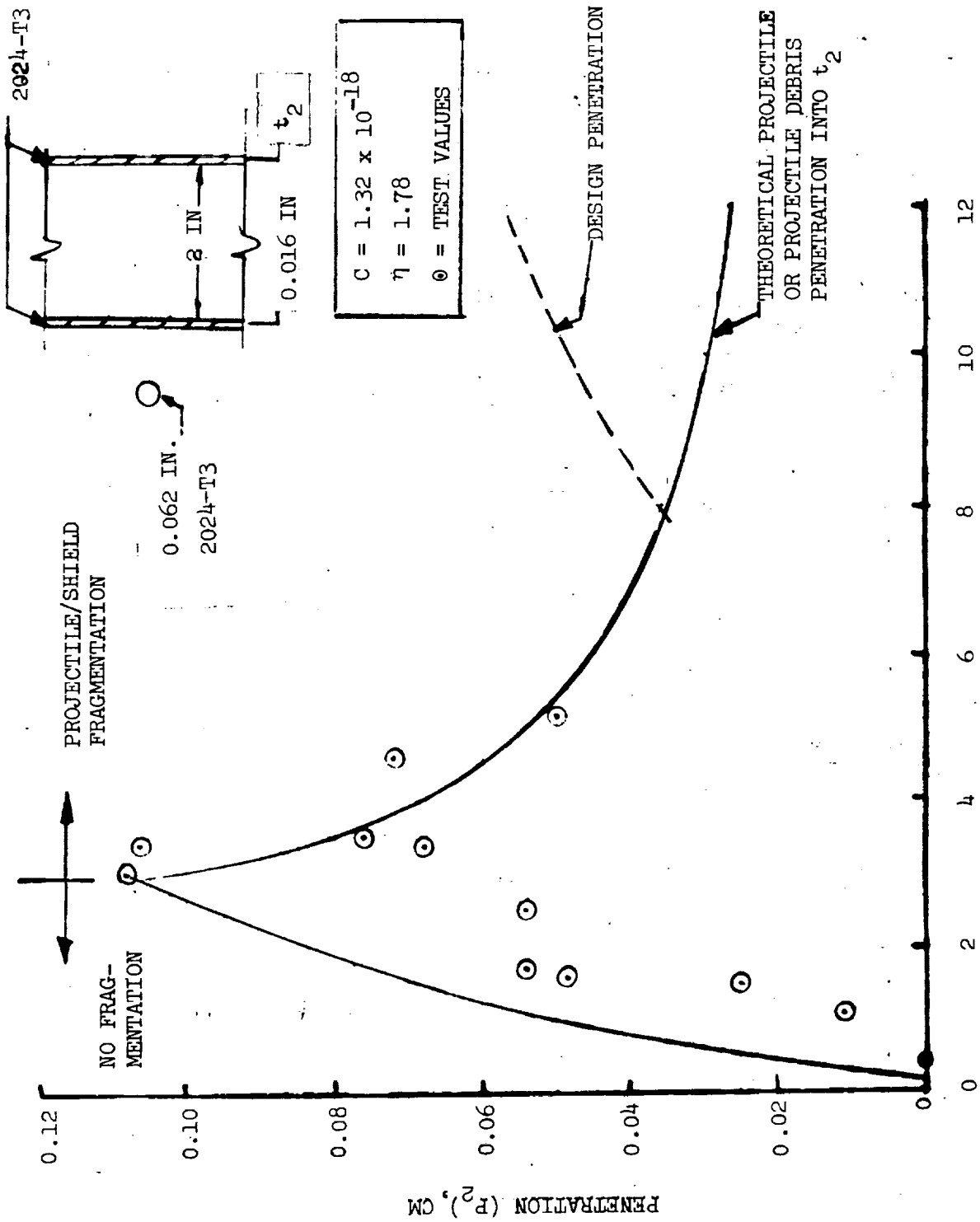

Figure 40. Effect of Impact Velocity on Damage - $t_1/d = 0.256$

depending upon the mission profile. The effects of all models must be assessed and the most effective shielding requirements defined to provide an overall probability of no penetration for the total stage.

The flux density (F) is obtained from Equation 13.

$$F_{a,c} = 10^{K1_{a,c}} m_{a,c}^{K2_{a,c}} 10^{f(R)_{a,c}} V_{a,c} \qquad (27)$$

where the subscripts refer to sporadic asteroidal (a) and cometary (c) meteoroids.

For a required probability of no penetration (P_o) the design meteoroid mass and hence the shielding requirements can be determined. The probability criteria for each of the three flux models must be combined to provide the required overall probability (P_o).

$$P_o = P_{oa} \; P_{oc} \; P_{os} \qquad (28)$$

Probabilities must be assigned to each flux model, considering the varying flux densities and their effects, to achieve the lightest weight shielding design.

For the sporadic models of both the asteroidal and cometary meteoroids, the particle velocities are functions of solar position and spacecraft relative velocity. An averaging of the particle velocity throughout the mission is weighted by the particle flux density.

$$\overline{V}_{a,c} = \frac{\int_o^T V_{a,c} F_{a,c} \, dt}{\int_o^T F_{a,c} \, dt} \qquad (29)$$

where $\overline{V}$ is the weighted average velocity. Equation 29 cannot be directly evaluated because the flux density $F_{a,c}$ requires the design meteoroid mass. Equation 27 and Equation 29 can be combined to give

$$\overline{V}_{a,c} = \frac{\int_o^T V_{a,c} F^*_{a,c} \, dt}{\int_o^T F^*_{a,c} \, dt} \tag{30}$$

where

$$F^*_{a,c} = \frac{F}{m^{K2_{a,c}}}$$

$$= 10^{K1_{a,c}} \, 10^{f(R)_{a,c}} V_{a,c} \tag{31}$$

To obtain the most effective allocation of penetration criteria P_{oa} and P_{oc}, the resulting shielding thicknesses tss_a and tss_c must be equal. Using the assumption of equal shielding thickness required for both the asteroidal and cometary flux models, Equation 25 can be used to develop an auxilliary equation for the probability assignment.

$$d_{Pa}^3 \rho_{pa}^{1.4735} \overline{V}_a^{2.486} = d_{pc}^3 \rho_{pc}^{1.4735} \overline{V}_c^{2.486} \tag{32}$$

where the particle diameters assuming spherical meteoroids are

$$\left.\begin{aligned} d_{pa} &= \left(\frac{6m_a}{\pi\rho_a}\right)^{1/3} \\ d_{pc} &= \left(\frac{6m_c}{\pi\rho_c}\right)^{1/3} \end{aligned}\right\} \tag{33}$$

The probability of no penetration is approximated by

$$P_o = 1 - \int_0^T FA\, dt \tag{34}$$

where

A = spacecraft exposed surface area

T = Pertinent exposure time

Combining Equation 31 and Equation 34, the meteoroid mass is obtained as

$$\left.\begin{aligned} m_a &= \left(\frac{(1 - P_{oa})}{A \int_o^T F_a^* \, dt} \right)^{1/K_{2a}} \\ m_c &= \left(\frac{(1 - P_{oc})}{A \int_o^T F_c^* \, dt} \right)^{1/K_{2c}} \end{aligned}\right\} \tag{35}$$

Expressions for the mass Equation 35 can be substituted into Equations 32 and 33 as follows:

$$K_a^* (1 - P_{oa})^{1/K_{2a}} = K_c^* (1 - P_{oc})^{1/K_{2c}} \tag{36}$$

where

$$\left.\begin{aligned} K_a^* &= \frac{\rho_a^{.4735}\,\overline{V}_a^{\,2.486}}{\left(A\int_o^T F_a^* \, dt\right)^{1/K_{2_a}}} \\ K_c^* &= \frac{\rho_c^{.4735}\,\overline{V}_c^{\,2.486}}{\left(A\int_o^T F_c^* \, dt\right)^{1/K_{2_c}}} \end{aligned}\right\} \qquad (37)$$

Also, if the stream flux is neglected, Equation 28 can be rewritten as

$$P_o = P_{oa}\, P_{oc} \qquad (38)$$

Solution of Equations 37 and 38 will define the optimum penetration criteria for assignment to the two sporadic flux density models. The ranges of the two probabilities are bounded by

$$P_o \leq P_{oa},\ P_{oc} \leq 1.0$$

The optimums obtained, P_{oa} and P_{oc}, will allow the required shielding thicknesses to be subsequently evaluated.

The flux density estimated by the present stream cometary model is rather severe when compared with the other two models. The spatial occurrences of these meteoroid streams are shown in Figure 33. Their passage is periodic in nature. When a particular mission profile and departure time have been selected, the likelihood of encounter with any meteoroid stream must be determined. Meteoroid shielding requirements are defined with and without encountering cometary stream fluxes. Whether these streams are encountered will be specified by the user, both for the synthesis program and the selection of the appropriate scaling relationships. The sphere of influence for each of these streams is dependent upon the size of the cometary tail and the intersection of the vehicle flight path with a particular meteoroid stream. For the purposes of preliminary sizing, the vehicle is assumed to be in the cometary stream flux for an average distance of 0.1 AU.

Probability assignment when the stream flux is included can be considered in a similar fashion as described previously. Additional equations required are as follows:

$$K_s^* (1-P_{os})^{1/K_{2_s}} = K_c^* (1-P_{oc})^{1/K_{2_c}}$$

where

$$K_s^* = \frac{\rho_s^{.4735} \bar{V}_s^{2.486}}{\left[10^{K_{1_s}} A_s T_s\right]^{1/K_{2_s}}}$$

$$\bar{V}_s = 20000/R_s^{1/2} \text{ M/sec}$$

R_s = average AU distance of meteoroid stream at the point of encounter with the vehicle

T_s = time required for the vehicle to travel 0.1 AU distance

A_s = Projected lateral area of stage

Program subroutines have been developed that evaluate the mission position/velocity history and integrate the effects of the respective flux density models. This technique results in the identification of the assigned probabilities and the shielding requirements for the synthesis programs. Exercising of the subroutines provided a summary of the shielding requirements for a range of typical planetary missions and provided data for the simplified meteoroid shielding scaling laws. For the purposes of the improved scaling laws, these subroutines are included in the synthesis computer program.

5.1.2.5 Mission Environment Integration

During the planetary missions, the meteoroid and thermal environments will affect the inert weight requirements. Both the thermal and meteoroid fluxes vary with the mission trajectory profile and will require the synthesis program to integrate the effects during the mission duration. The mission trajectory is defined as arc segments of a sun-centered ellipse. A planetary mission with a stopover and return would be specified by the trip time and orbit parameters for each mission leg (outbound, planet capture phase, and return). If there is an auxiliary planet swingby, the mission

segment involving the swingby is divided into two arc segments. The orbit parameters required for the flux integration routine are the semi-major axis (a), eccentricity (e), departure planet and the trip time. The eccentric anomaly (E) at the start of the mission segment is obtained from

$$E = \cos^{-1}\left(\frac{1}{e} - \frac{R}{ea}\right) \tag{39}$$

where R is the departure planet distance from the sun, in AU. The time (T) since perihelion passage, years, for the planet departure is

$$T = \frac{a^{3/2}}{2\pi}(E - e \sin E) \tag{40}$$

The integration procedure takes time increments along the arc segment and evaluates vehicle position and velocity. The position is calculated as a function of time from Equation 40, which is a transcendental equation. With an initial estimate for the anomaly (E) from the previous time step, a recursive relationship is used.

$$E_{K+1} = \frac{e(\sin E_K - E_K \cos E_K) + \frac{2\pi(T + \Delta T)}{a^{3/2}}}{1 - e \cos E_K} \tag{41}$$

The vehicle position vector (R_t) and velocity (V) are obtained from Equations 39 and 41.

$$R_t = a(1 - e \cos E) \tag{42a}$$

$$V = \sqrt{\mu\left(\frac{2}{R_t} - \frac{1}{a}\right)} \tag{42b}$$

A ratio of vehicle speed to circular orbit speed is

$$\sigma = \sqrt{2 - \frac{R_t}{a}} \tag{43}$$

and the angle between the vehicle velocity vector and the circular velocity vector is given by

$$\gamma = \tan^{-1}\left[\frac{e}{\sqrt{1 - e^2}} \sin E\right] \tag{44}$$

This procedure from Equations 41 through 44 is repeated along the entire mission segment.

Thermal effects on the vehicle are evaluated by considering the vehicle's time-distance history (Equation 42a), and the solar heat flux variation with solar distance. A weighted average should be used to determine the tank wall equilibrium temperature. Heat flux into the propellant tanks is evaluated using a one-dimensional thermal analysis model for the tank wall, section 5.2.3.

The meteoroid model integration requires an evaluation of the total number of impacts (N) for the mission, and is obtained from

$$N = A \int F(R, V)\, dt \tag{45}$$

The meteoroid flux distribution is considered to vary with the radial distance from the sun and the effect has to be integrated throughout the mission profile during which the stage is exposed to the environment. A comprehensive approach has been formulated in this section and is used for the Propulsion Module Synthesis computer program. Elements of this program can provide an integrated data map for the mission fluxes for various types of missions. Such data is used to develop a simplified approach to estimation of meteoroid shielding requirements.

The total mission flux, Equation 45, is not a linear function with mission duration due to the radial distribution of the flux models. In fact the trajectory parameters influence the flux integral and velocity evaluation as seen in Figures 41 and 42. A simplified time flux product estimation of the flux integral is impractical. Figures 41 through 44 provide a quick graphical aid to a fairly accurate evaluation of the flux integration, for the simplified version of the scaling laws.

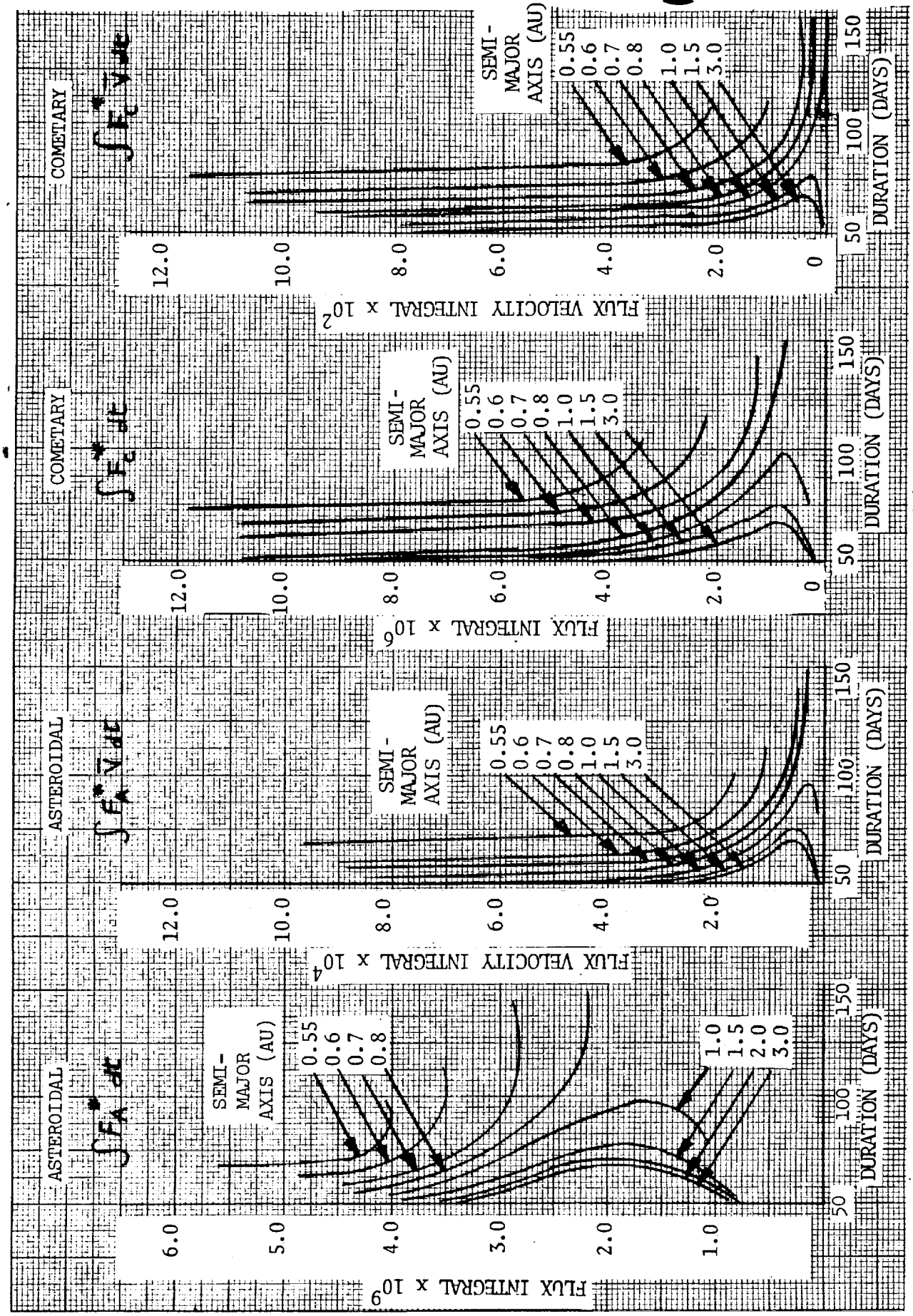

Figure 41. Flux and Flux Velocity Integral - Earth/Venus Mission

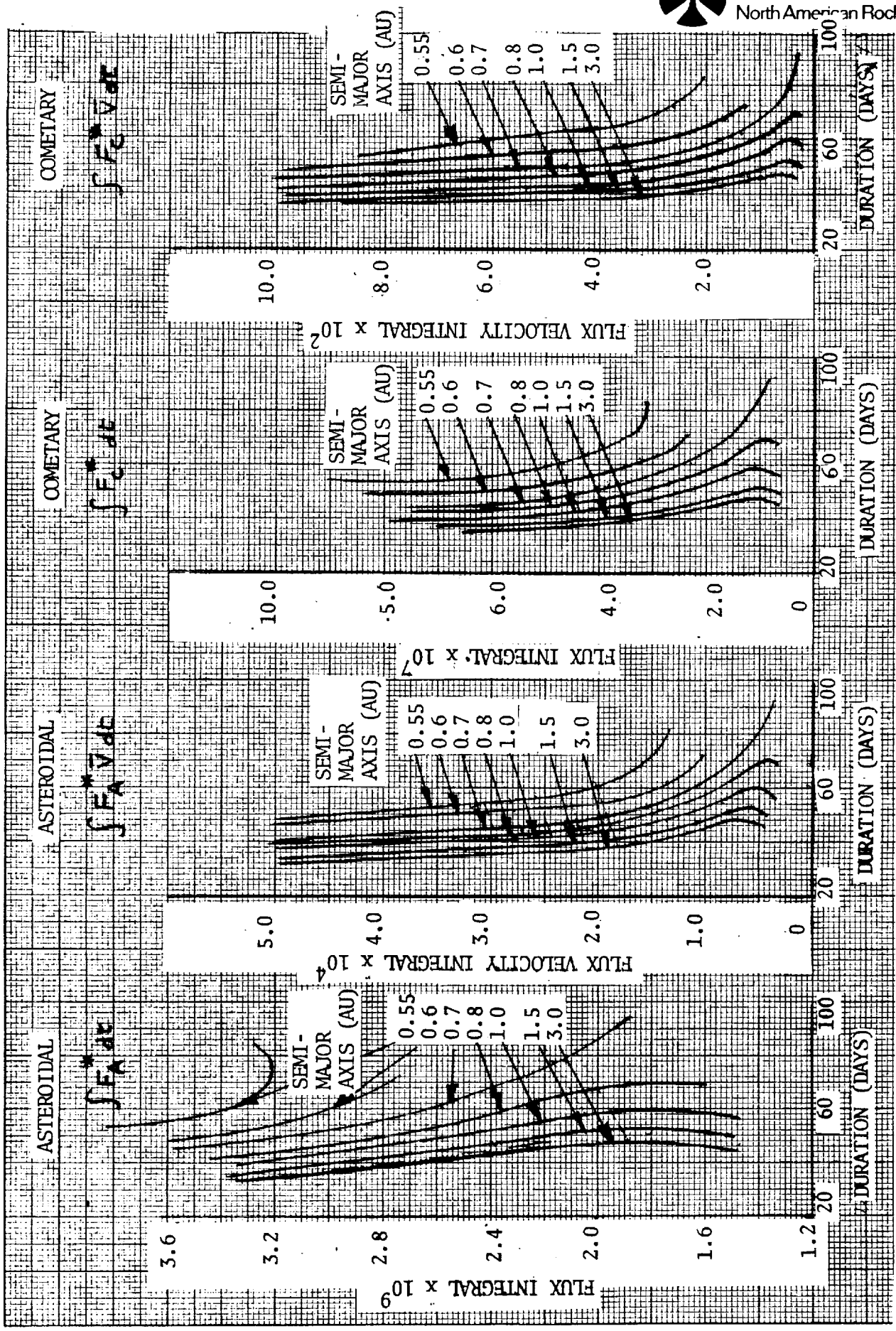

Figure 42. Flux and Flux Velocity Integral - Earth/Mercury Mission

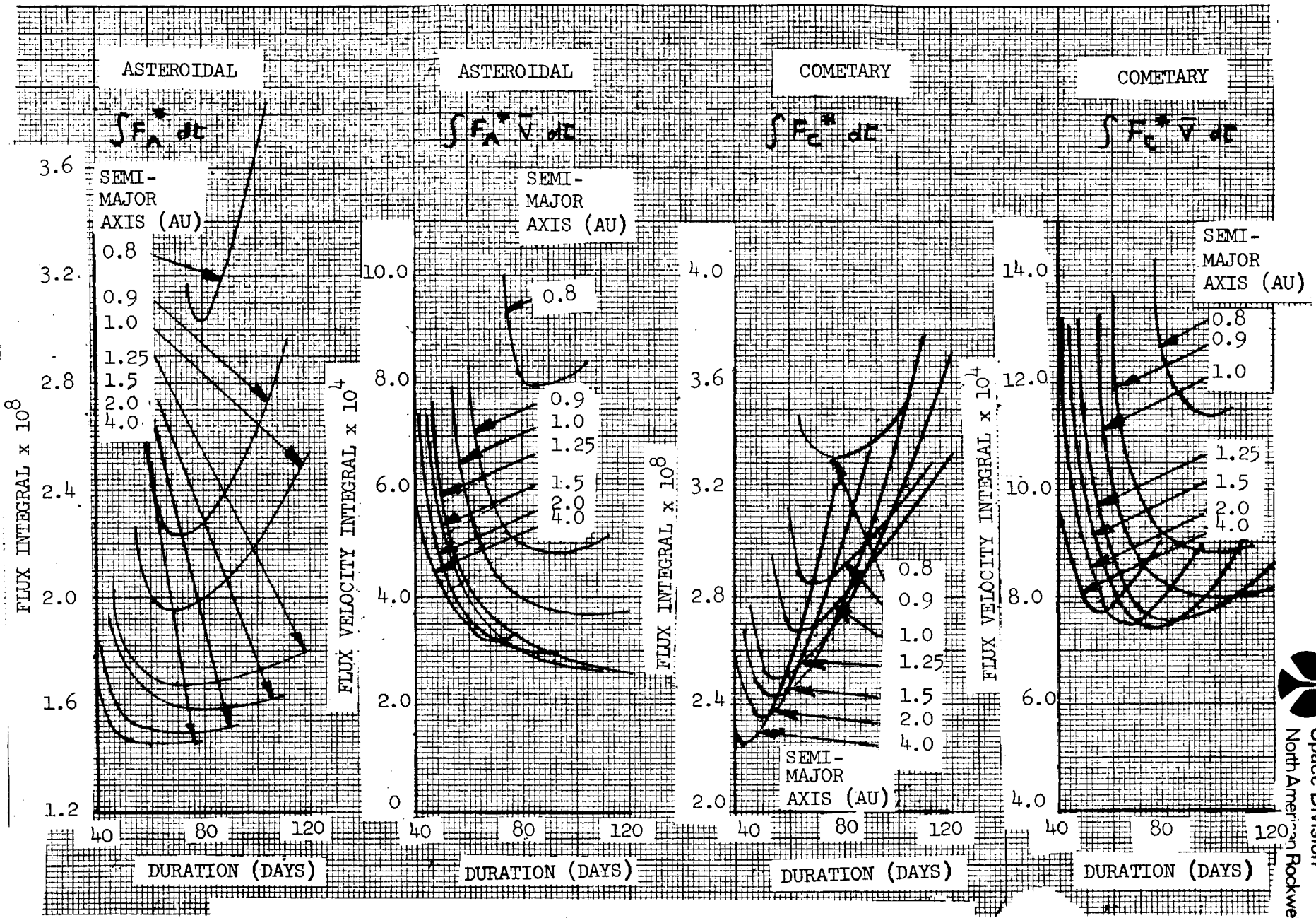

Figure 43. Flux and Flux Velocity Integral - Venus/Mars Mission

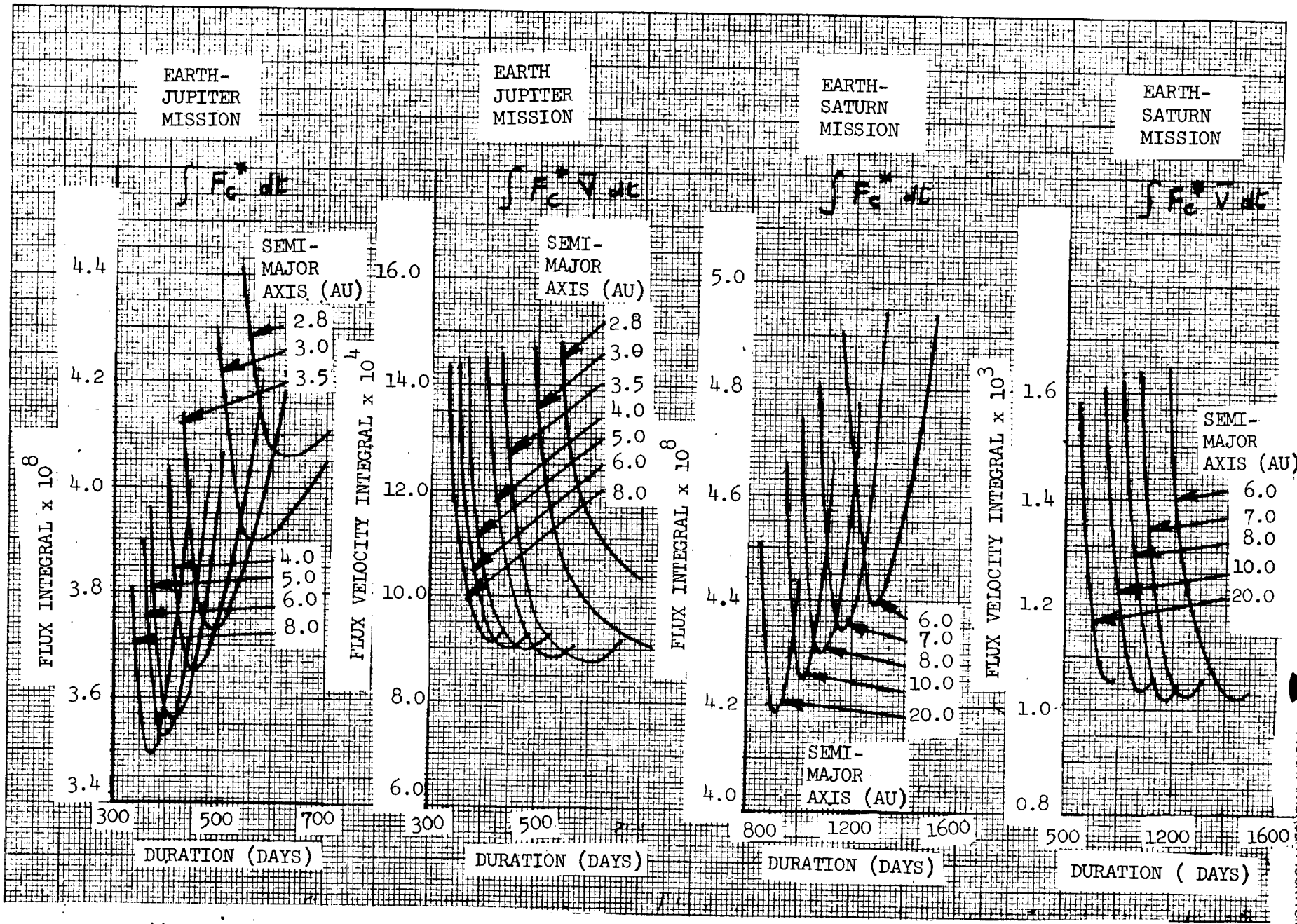

Figure 44. Cometary Flux and Flux Velocity Integral - Earth/Jupiter and Earth/Saturn Missions

The average particle velocity, V_p is obtained from

$$V_p = \frac{\int F^* \bar{V}\, dt}{\int F^*\, dt} \tag{46}$$

The flux integral in conjunction with either Figures 36 or 37 and a specified penetration probability criteria determine the largest diameter particle to be encountered by the propulsion stage through its mission. With a knowledge of the particle diameter, its average velocity and the shielding-weight-scaling law, a weight estimate can be obtained for the meteoroid shielding. The procedure is explained more fully in Section 9.4.1.

During the planet stop-over time, the spacecraft experiences a spatial flux distribution modified by the presence of a planet. The flux modification factor ($G\eta$), section 5.1.1.4, depends on the planet and the space altitude.

$$G\eta = \left\{1 + 0.76R\, \frac{V_p^2\, r_p}{V_e^2\, r}\right\}\left\{\frac{1}{2} + \frac{1}{2}\left(1 - \frac{r_p^2}{r^2}\right)^{1/2}\right\} \tag{47}$$

The modification factor variation with the radii ratio is presented for several planets in Figure 45. If the spacecraft is in an elliptic orbit around the planet, then $G\eta$ will vary during the planet stop-over mission. Since the expressions for G and η are approximations, an average attitude should suffice to estimate the appropriate modification factor. For the planets Neptune, Jupiter, Saturn and Uranus with $1.5 < r/r_p < 30$, the modification factor can be represented more simply as

$$G\eta = A\left(\frac{r}{r_p}\right)^{-0.88}$$

and the average modification factor between any two different altitude ratios will be

$$G\eta_{AV} = \frac{\int_{r_1/r_p}^{r_2/r_p} A\left(\frac{r}{r_p}\right)^{-0.88} d\left(\frac{r}{r_p}\right)}{\left(\frac{r_2}{r_p} - \frac{r_1}{r_p}\right)}$$

which upon integration will produce a weighted average factor suitable for the manual method of applying the simplified scaling laws.

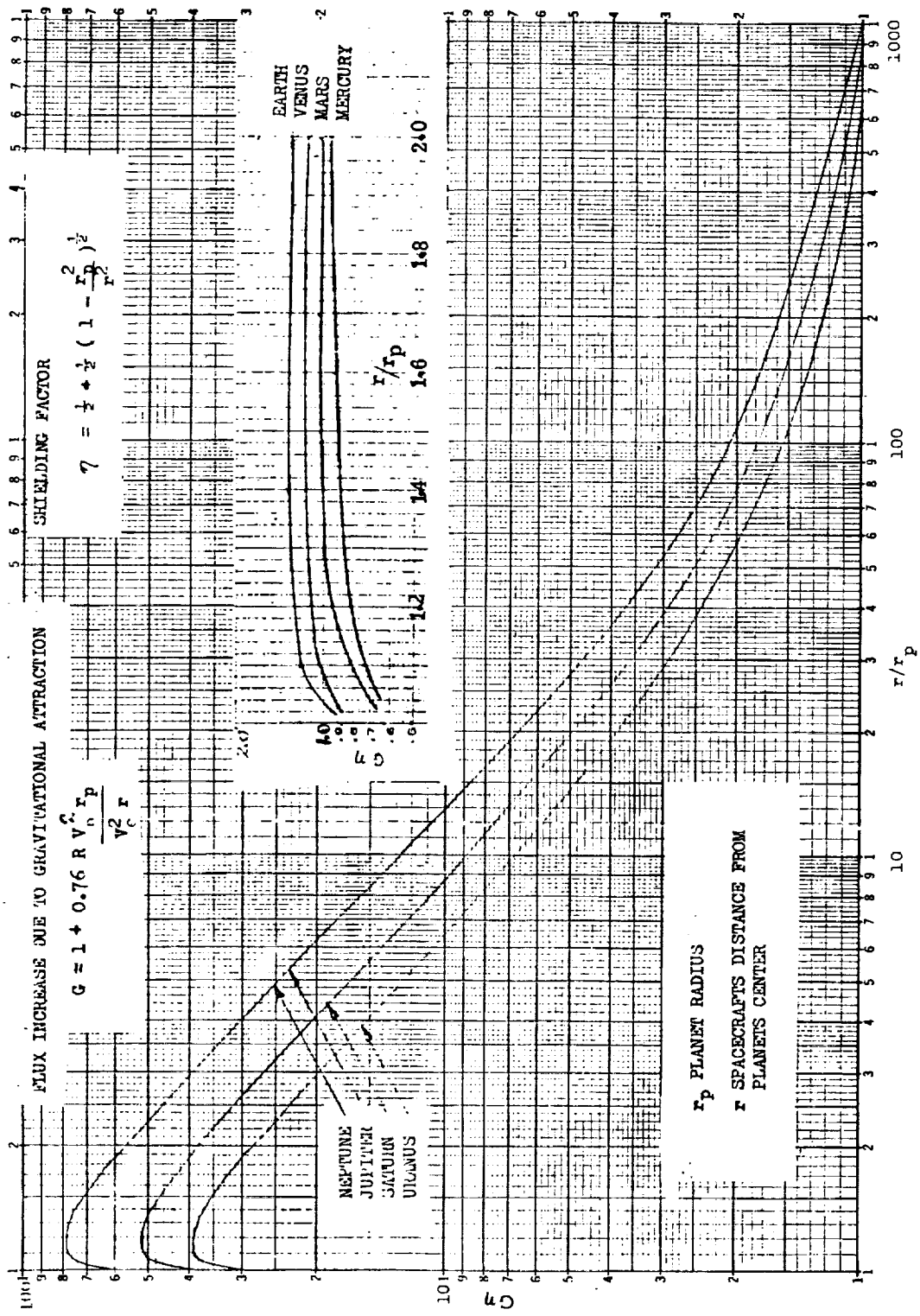

Figure 45. Meteoroid Flux Modification Factor in Vicinity of Planet

$$G\eta_{av} = 8.3 \frac{\left[G\eta_1 \left(\frac{r_2}{r_p}\right) - G\eta_2 \left(\frac{r_1}{r_p}\right) \right]}{\left(\frac{r_2}{r_p} - \frac{r_1}{r_p}\right)} \quad ; \text{ for manual method}$$

For the improved scaling laws included in the computer program, a mean value of Gη, applicable to elliptical orbits about any planet, is derived from integration of Equation 47 rather than the simplified equation. The expression obtained is

$$G\eta_{av} = \frac{1}{2} + \frac{1}{2(X_2 - X_1)} \left[\sqrt{X_2^2 - 1} \left(1 - \frac{C}{X_2}\right) - \sqrt{X_1^2 - 1} \left(1 - \frac{C}{X_1}\right) + \cos^{-1}\left(\frac{1}{X_1}\right) - \cos^{-1}\left(\frac{1}{X_2}\right) + C \ln\left(\frac{X_2\left(X_2 + \sqrt{X_2^2 - 1}\right)}{X_1\left(X_1 + \sqrt{X_1^2 - 1}\right)} \right) \right]$$

where

$$C = 0.76\ R \left(\frac{V_P}{V_e}\right)^2 \quad ; \quad X = \frac{r}{r_P}$$

The mission integrated flux about the planet during the spacecraft stopover time is in both methods

$$\int F_p^* \, dt = F^* \, T \, G \, \eta_{av}$$

where F* - the undisturbed flux at the planets solar distance; Table 16

T - Planet stay time (years)

Table 16. Undisturbed Flux at Planet Distances

PLANET	COMETARY FLUX		ASTEROIDAL FLUX	
	F_{pc} * Particles / m^2 Year	$\bar{V}$ m/sec	F_{pA} * Particles / m^2 Year	$\bar{V}$ m/sec
Mercury	6.822×10^{-7}	31000	-	14900
Venus	1.955×10^{-7}	22700	1.399×10^{-10}	10900
Earth	1.021×10^{-7}	19300	3.761×10^{-9}	9300
Mars	4.399×10^{-8}	15600	6.365×10^{-8}	7500
Jupiter	3.774×10^{-9}	8450	1.0105×10^{-10}	2580
Saturn	1.123×10^{-9}	6240	-	1850
Uranus	2.777×10^{-10}	4400	-	1300
Neptune	1.131×10^{-10}	3500	-	1040
Pluto	6.569×10^{-11}	3070	-	910

Meteoroid Flux During Approach to Planet

During approach and departure from a planet, a spacecraft is exposed to a meteoroid environment which is generally more severe than that in interplanetary space at the same heliocentric distance. The impact of such exposure on meteoroid shielding for capture missions is assessed in the following way.

The product of the flux and time of exposure to the flux during approach or departure will vary with the distance from the planet as shown in Figure 45. The value of the flux-time product during arrival from a distance of r_2 from a planet to capture in an orbit of periapsis r_1 on a hyperbolic trajectory is

$$G\eta F^* t = \int_o^t G\eta dt = \int_{x_1}^{x_2} G\eta dx$$

$$= 1/2 \frac{r_p}{V_\infty} \int_{x_1}^{x_2} \left[\frac{x}{\sqrt{X}} + \frac{\sqrt{x^2-1}}{\sqrt{X}} + C\left(\frac{1}{\sqrt{X}} + \frac{\sqrt{x^2-1}}{x\sqrt{X}} \right) \right] dx$$

F^* = meteoroid flux at solar distance of planet but unmodified by planet

where

$$x = r/r_p$$

$$dt = \frac{r_p}{V} \frac{x}{\sqrt{X}} dx$$

$$X = x^2 + 2ax - a^2 (e^2-1)$$

$$a = \frac{1}{2} \left(\frac{V_p}{V_\infty} \right)^2$$

$$e = 1 + \frac{x_1}{a}$$

$$C = 0.76 \left(\frac{V_p}{V_e} \right)^2 R$$

However, $G\eta F^* t$ does not represent a net increase in the meteoroid hazard, since as described earlier in Section 5.1.2.5, the integration of the interplanetary trajectory includes the distance from r_2 to the center of a massless target planet. If F^* is taken as a constant value for the flux in the neighborhood of the planet, then the net increase in the flux-time product is given by

$$\Delta(F^* t) = F^* \left(\int_o^t G\eta dt - \frac{r_2 - r_1}{V_\infty} \right)$$

This net increase may be expressed as an equivalent exposure in a circular parking orbit of radius r_1. Thus,

$$t_{eq}\, G\eta(r_1/r_p)\, F^* = \Delta(F^*t)$$

or

$$t_{eq} = \frac{\int_0^{t_1} G\eta dt - \frac{r_2 - r_1}{V_\infty}}{8.64 \times 10^4 \left(G\eta\,(r_1/r_p)\right)} \quad \text{days} \qquad (48)$$

The equivalent stay time (Equation 48) and the flux modification factor, $G\eta$, result in a flux addition during the approach and departure from the planets. This additional flux is equivalent to approximately 35 days (Jupiter), 20 days (Saturn and Neptune) and 15 days (Uranus) of transplanetary flight in the undisturbed flux environment. Considering the mission trip times to these four planets and the uncertainties in the flux models, it is possible to neglect the additional flux during approach and departure.

5.1.3 Shielding Weight Requirements

The shielding weight requirements are dependent on the type, diameter and impacting velocity of the meteoroid that must be resisted by the shielding concepts. Single sheet shielding could be adequate for small vehicle stages on certain missions, but would provide a prohibitive weight penalty for other long duration mission. To help reduce the shielding weight penalties, advanced shielding concepts have been proposed; these include designs with single and dual bumpers.

Weight data for the various designs are generated based on the penetration mechanics proposed for this study. The weight data presented in Appendix B are statistically reduced to provide the required scaling laws. Shielding weight is separated into two sections, outer bumper W_B and rear sheets(s) W_m. An additional weight allowance is provided for the secondary support structure

$$W_S = \text{MAX}\,(0.00085\, h^2,\ 0.05) \qquad kg/m^2$$

h = spacing between outer bumper and rear sheet, cm.

The support weight is based on use of the post type supports described in Section 5.2.1, Thermal Protection.

The single bumper concept used in Appendix B has an outer bumper thickness (t_1) and a rear sheet thickness (t_2). The rear sheet is located against the tank wall or could be introduced as a thickening of the tank wall. The bumper is spaced three inches (or a distance h, whichever is greater) from the tank wall. The three-inch space is for insulation and the h spacing maximizes the scattering effect of impact debris particles.

The bumper thickness is sized to provide a ratio of mass of the bumper material removed to the mass of the original particle of 0.8, which has been shown theoretically to be a good choice to minimize the total weight addition to the spacecraft. A minimum gage limit of 0.025-inch is established for the aluminum bumper and 0.016-inch for the titanium bumper. These thicknesses are established as being required to survive boost loads; and/or aerodynamic pressures.

The rear sheet thickness is designed to prevent maximum penetration of twenty-five percent of the tank wall thickness. Both bulge failure and penetration failure of the pressure wall are considered. The penetration failure is found to be the first mode. The shielding weight is computed for a case where two inches of insulation were present in the space between the tank and bumper.

For all cases treated, the shielding weight for the low impact velocity (4 Km/sec) is relatively high compared with that required for the higher impact velocities, due to the incomplete meteoroid fragmentation associated with the low impact velocity.

The following scaling laws apply to the different shielding concepts. The empirical coefficients and exponents are found in Tables 17 through 19.

Single Sheet

$$W_B = 0$$

$$W_m = K_1 d_p^{1.0535} V_p^{0.667}; \ kg/m^2$$

Coefficient K_1 is quoted in Table 17.

Single Bumper

$$W_B = \text{Maximum } (K_2 d, K_3); \ kg/m^2$$

$$W_m = K_1 d_p^{\alpha} V_p^{\beta}; \ kg/m^2$$

Coefficients K_1 through K_3 and exponents α and β are quoted in Table 18.

Dual Bumper

$$W_B = \text{Maximum } \left\{ K_2 d_p, K_3 + \left(\frac{K_4 - d_p}{K_5} \right) \left(\frac{V_p - K_6}{V_p} \right) \right\}; \ kg/m^2$$

$$W_m = K_1 d_p^{\alpha} V_p^{\beta}; kg/m^2$$

Coefficients K_1 through K_6 and exponents α and β are quoted in Table 19.

Table 17. Single Sheet Scaling Coefficient (K_1)

K_1	Material	Meteoroid
0.713	Aluminum	Asteroidal
0.825	Titanium	Asteroidal
0.600	Glass Epoxy	Asteroidal
0.259	Aluminum	Cometary
0.300	Titanium	Cometary
0.218	Glass Epoxy	Cometary

The rear sheet unit weights, W_m, are for a pressurized tank where a 25 percent penetration depth is allowed. For the unpressurized shell where full penetration is permissible, the rear sheet weights can be modified by

$$W_{m\ \text{unpressurized}} = 0.445\ W_{m\ \text{tank}}$$

Both the pressurized tank and the unpressurized shell have a minimum skin thickness for structural integrity based on design loads and internal pressures. Any additional material added to meet the meteoroid shielding unit weight requirements is considered as the weight penalty W_m^* due to meteoroid shielding.

Therefore

$$W_m^* = W_m - 10\rho_t\ T_t\ \text{kg/m}^2$$

where ρ_t = density of tank material (gm/cm^3)

T_t = skin thickness from structural considerations (cm)

Design weights of the rear sheet for the single and dual bumper have been based on the propellant tank always being fabricated from aluminum. If tank is made from other materials, its weight requirements will be

$$W_{m_{tank}} = K_1 W_m$$

K_1 = 1.0, Aluminum; 1.15, Titanium; 0.83, Glass Epoxy

Table 18. Scaling Coefficients for Single Bumper Concept

METEOROID	MATERIAL	VELOCITY m/sec	K_1	K_2	K_3	α	β
Cometary	Aluminum	$V > 8000$	0.0412	1.77	1.71	1.12	0.667
Cometary	Aluminum	$V \leq 8000$	2225	1.77	1.71	1.12	-0.546
Cometary	Titanium	$V > 8000$	0.0332	3.18	2.77	1.11	0.667
Cometary	Titanium	$V \leq 8000$	4360	3.18	2.77	1.11	-0.645
Cometary	Glass Epoxy	$V > 8000$	0.0467	2.28	1.27	1.09	0.667
Cometary	Glass Epoxy	$V \leq 8000$	1092	2.28	1.27	1.09	-0.453
Asteroidal	Aluminum	$V > 8000$	0.105	5.5	1.71	1.11	0.667
Asteroidal	Aluminum	$V \leq 8000$	8960	5.5	1.71	1.11	-0.6
Asteroidal	Titanium	$V > 8000$	0.0866	7.7	2.77	1.12	0.667
Asteroidal	Titanium	$V \leq 8000$	7270	7.7	2.77	1.12	-0.595
Asteroidal	Glass Epoxy	$V > 8000$	0.139	8.01	1.27	1.09	0.667
Asteroidal	Glass Epoxy	$V \leq 8000$	4205	8.01	1.27	1.09	-0.485

Table 19. Scaling Coefficients for Dual Bumper Concept

METEOROID	MATERIAL	VELOCITY m/sec	K_1	K_2	K_3	K_4	K_5	K_6	α	β
Cometary	Aluminum	$V > 8000$	0.0073	3.01	2.71	0.9	0.52	15000	1.15	0.667
Cometary	Aluminum	$V \leq 8000$	7.445×10^{9}	3.01	2.71	0.9	0.346	3550	1.15	-2.45
Cometary	Titanium	$V > 8000$	0.0062	2.32	2.32	1.0	0.286	7350	1.09	0.667
Cometary	Titanium	$V \leq 8000$	1.42×10^{10}	2.32	2.32	1.0	1.8	4000	1.09	-2.5
Asteroidal	Aluminum	$V > 8000$	0.0165	6.87	2.71	0.3	2.0	0	1.04	0.667
Asteroidal	Aluminum	$V \leq 8000$	3.77×10^{10}	6.87	2.71	9.3	2.01	16000	1.04	-2.5
Asteroidal	Titanium	$V > 8000$	0.0098	9.9	4.95	0.5	2.0	0	1.12	0.667
Asteroidal	Titanium	$V \leq 8000$	5.59×10^{10}	9.9	4.95	0.5	4.0	0	1.12	-2.6

When the meteoroid shielding properties of the tank insulation are taken into account, the rear sheet requirements, W_m, for the single bumper concepts can be significantly reduced and the weights can be obtained from

$$W_m = \frac{K_1 \, d_p^{\alpha} \, V_p^{\beta}}{EXP\left[14.9 \, (\rho_{ins} \, \tau_{ins}/d^*\right]}$$

where ρ_{ins} = insulation density (gm/cm^3)

τ_{ins} = insulation thickness (cm)

d^* = max (d_p,1.0) (cm)

and the coefficients (K_1, α and β) are defined in Table 18 for the single bumper concepts.

Consider the meteoroid shielding requirements for an unpressurized shell fabricated from 0.09 cm of titanium and covered by 5 cms of insulation with a density of 0.03 km/cm^3. The cometary meteoroid particle is 2.5 cm and has a velocity of 10 km/sec. A single bumper concept is used for the meteoroid protection. The weight of the titanium bumper, W_B, is found from Table 18 to be

$$W_B = \text{Maximum } (3.18 \, d_p, \, 2.77)$$

$$W_B = 3.18 \times 2.5 = 7.45 \text{ kg/m}^2$$

The rear sheet thickness using Table 18 is

$$W_m = 0.332 \, d_p^{1.11} \, V_p^{0.667}$$

$$W_m = 42.8 \text{ kg/m}^2$$

The insulation thickness will help reduce the rear sheet requirements

$$W_{m_{insulated}} = \frac{W_m}{EXP\left[14.9 \, (0.03 \times 5.0/2.5)\right]}$$

$$W_{m_{insulated}} = \frac{42.8}{EXP\,(0.893)} = 17.5 \text{ kg/m}^2$$

For the unpressurized shell

$$W_{m_{SHELL}} = 0.445 \times 17.5 = 7.8 \text{ kg/m}^2$$

Unit weight of existing shell is

$$W_{SHELL} = \rho\, t$$

ρ = density of titanium, 4610 kg/m^3

$$W_{SHELL} = 4610 \times \frac{0.09}{100} = 4.16 \text{ kg/m}^2$$

Therefore the unit weight penalty of the rear sheet for meteoroid protection is

$$W_m^* = 7.8 - 4.16 = 3.64 \text{ kg/m}^2$$

and the total unit weight penalty, W_{mp}, required for meteoroid protection is

$$W_{mp} = W_m^* + W_B$$

$$W_{mp} = 3.64 + 7.45 = 11.09 \text{ kg/m}^2$$

5.2 THERMAL ENVIRONMENT AND PROTECTION

The objective of the thermal analysis is to establish overall heat balances as well as heat-rejection and thermal-insulation requirements for the space propulsion modules. This problem is discussed in two parts, the first dealing with heat balances throughout the mission profile, and the second dealing with insulation requirements to optimize the stage's performance.

Weight-scaling laws for the propellant tankage insulation requirements are based on passive thermal-control techniques for the tank walls, bulkheads, intertank structure and tank supports. Typical insulation systems consist of an external thermal-control-surface finish and various types of insulation which are used to minimize heat transfer into the propellant, or used to maintain the propellants within their liquid range. The main source of heat transfer will be through the tank wall and bulkheads. Additional heat leak paths will arise from the support members of the tank, and from the load-carrying structure between tanks and the payload, engine or another tank.

5.2.1 Insulation Concepts

The basic thermal protection proposed for advanced mission usage is the passive system composed of high-performance insulation (HPI) coupled with heat blocks at all structural attachments to the propellant tanks. This system is under consideration for propellant temperature control for space storable propellants as well as cryogenic propellants. The components required for such a system are shown in Figure 46. As indicated, the barrier to radiation heat transfer is the multilayered HPI combined with a vent space and an atmosphere control barrier. The latter component is required to retain helium or similar atmosphere control gas in the insulation during periods when the tank contains cryogenic propellant and is in the earth's atmosphere. The vent space is required to permit thorough venting of the atmosphere control gas when in space so that maximum insulation performance is obtained. Heat blocks are formed in the support structure by use of low-conductivity structural material covered on either side by HPI.

Proposed HPI installations for advanced propulsion modules are based on use of preassembled panels of 1.25- to 2.5 cms thickness, which would be used to build up the desired overall insulation thickness. Panel construction falls into two categories - rigid and soft. There is one accepted candidate in the first category, the Goodyear GAC series, which is composed of alternating layers of foam spacers and aluminized mylar radiation shields. There are at this time several competing candidates of the soft type which use a variety of spacer and radiation shield combinations. In each case, additional components are required to form the radiation shields and spacers into a panel (Figure 47). These include straps to provide inplane tensile strength, pins to join the layers together (in the case of the soft types), reinforcement of hole openings for attachment posts, and Velcro fasteners at pin locations to join panels together or to join the inner panels to the structure.

Panels would be installed on the structure by Velcro pads, then panel connectors would be attached to join strap ends. The inherent shear and compressive strength of the rigid insulation plus the straps retain this type of insulation against boost loads. The soft insulation would be installed over tubular, insulation-filled posts which retain the insulation against shear loads.

The atmosphere control barrier can be supported either by spacers on the rigid insulation or by the posts of the soft insulation. The barrier construction employed for the exterior insulation is dependent on whether the propulsion module is shrouded or unshrouded during boost. A membrane is sufficient in the first case. For unshrouded boost, a concept for a lightweight honeycomb panel which is able to withstand the boost aerodynamic environment has been developed at NR SD. An alternate barrier for the external insulation is a self-supporting shell, attached to the primary structure at the ends of the tank supports.

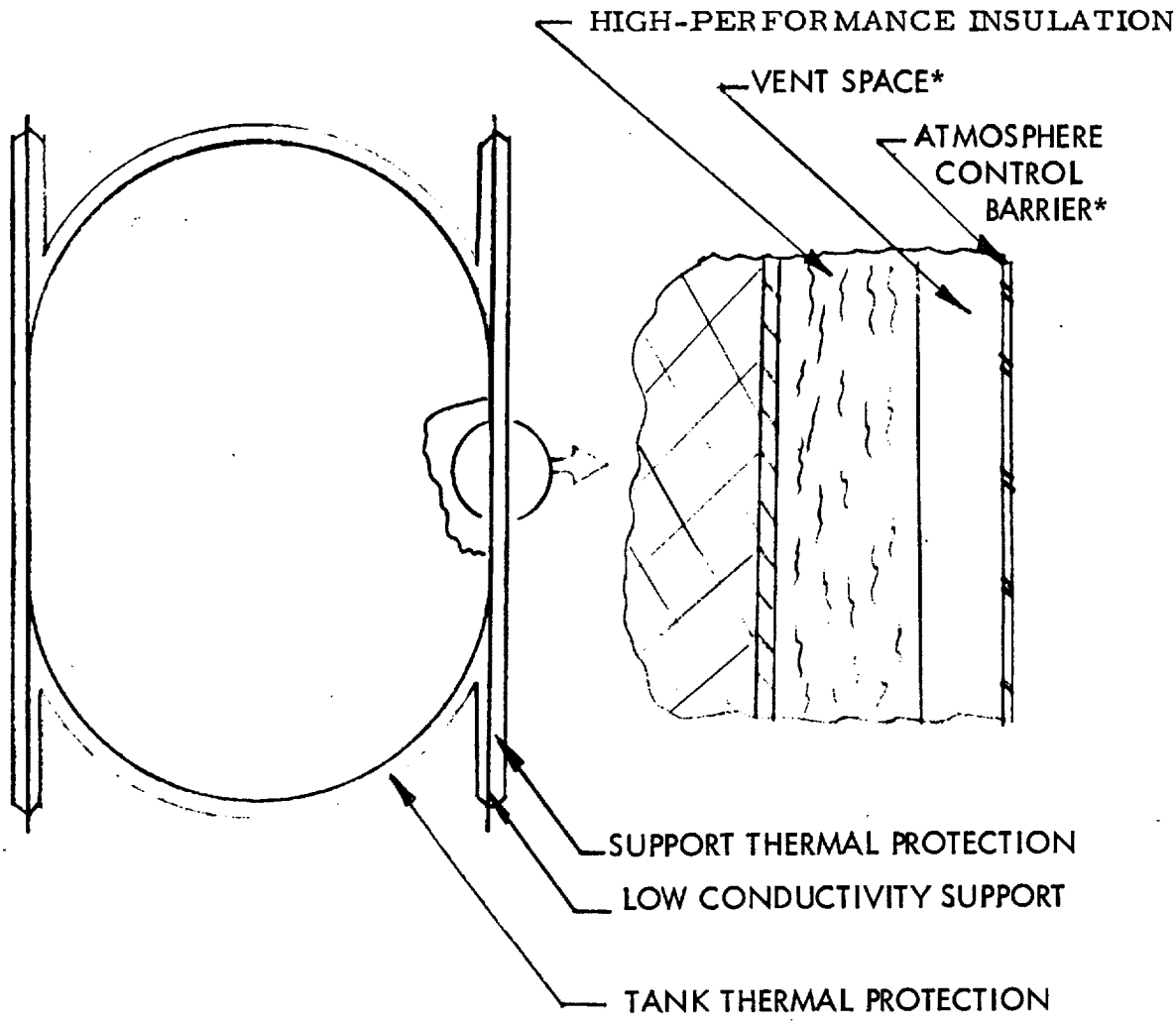

*NOT REQUIRED FOR NON-CRYOGENIC PROPELLANTS

Figure 46. Thermal Protection System Components

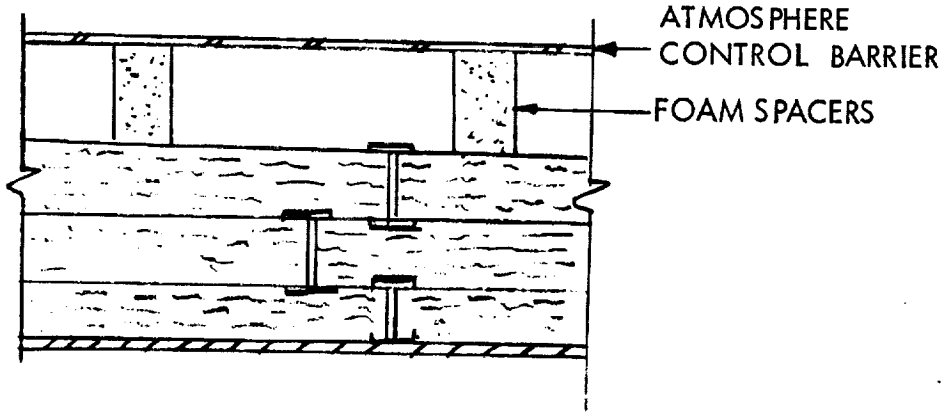

(c) RIGID INSULATION INSTALLATION

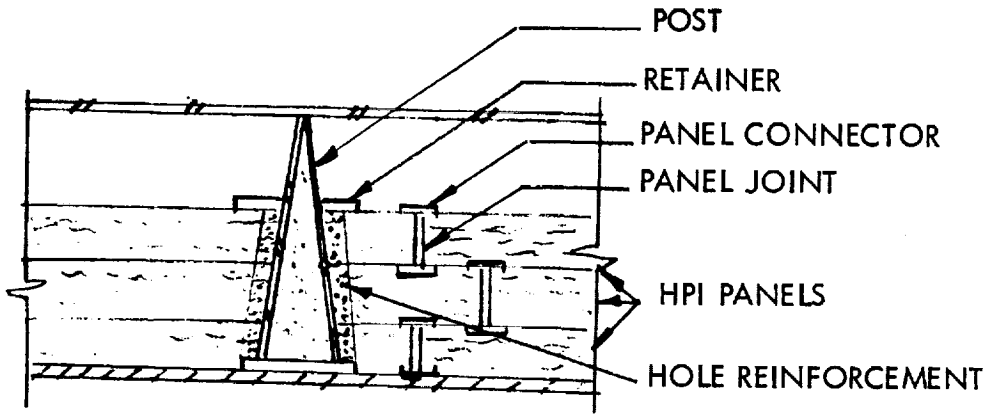

(b) SOFT INSULATION INSTALLATION

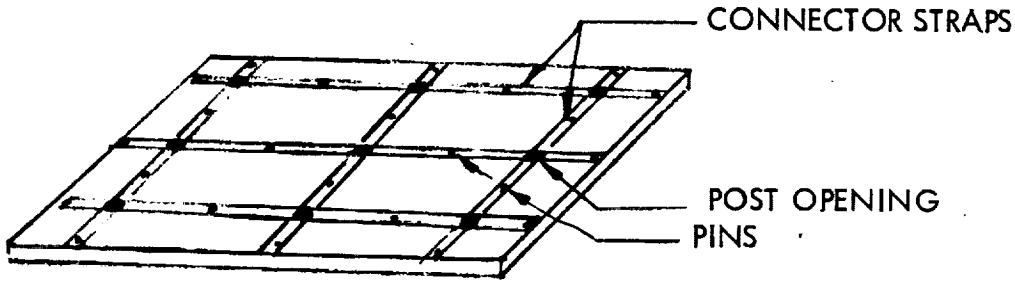

(a) TYPICAL HPI PANELS

Figure 47. High Performance Insulation Installation

5.2.2 Insulation Properties

Various types of superinsulation are available for application encompassing ranges of installed densities from 1.6 lb/ft^3 to 3.0 lb/ft^3. Most of the high performance insulations are a multi-layer type using insulated layers with reflective surfaces and some form of spacer between the layers. The thermal conductivity for these multi-layer insulations is strongly dependent on the surface temperature and the temperature drop across the insulation. Figure 48 shows the integrated heat flow for a type of NRC-2 superinsulation versus insulation temperature range. These data were obtained from tests performed at SD. Conductivity ranges for typical HPI are shown in Table 20, together with their material density and actual installed density based upon NR test data for subscale insulated tank models.

An analytical representation for the insulation's thermal conductivity is given by

$$K = A^*T + B\,T^3 \qquad (49)$$

where $A^* = K_c\,(1.168 \times 10^{-13})\,N^{2.725}$

$B = K_r\,(8.68 \times 10^{-12})\,N^{-1}$

T = the average temperature of any insulation layer, °K (°R)

N = the number of insulation layers per cm (in)

Table 21 gives the conductivity properties of the individual layers for the different insulations. For typical HPI with the layer density shown in Table 20, the resulting coefficients A* and B for the conductivity equation are quoted in Table 21. The total heat flow (H) into the propellant is given by

$$H = \frac{A}{d}\int_{T_C}^{T_H} K\,dT \quad ; \text{ watts (Btu/HR)} \qquad (50)$$

where A = the surface area requiring internal protection, cm^2 (ft^2)

d = the insulation thickness, cm (ft)

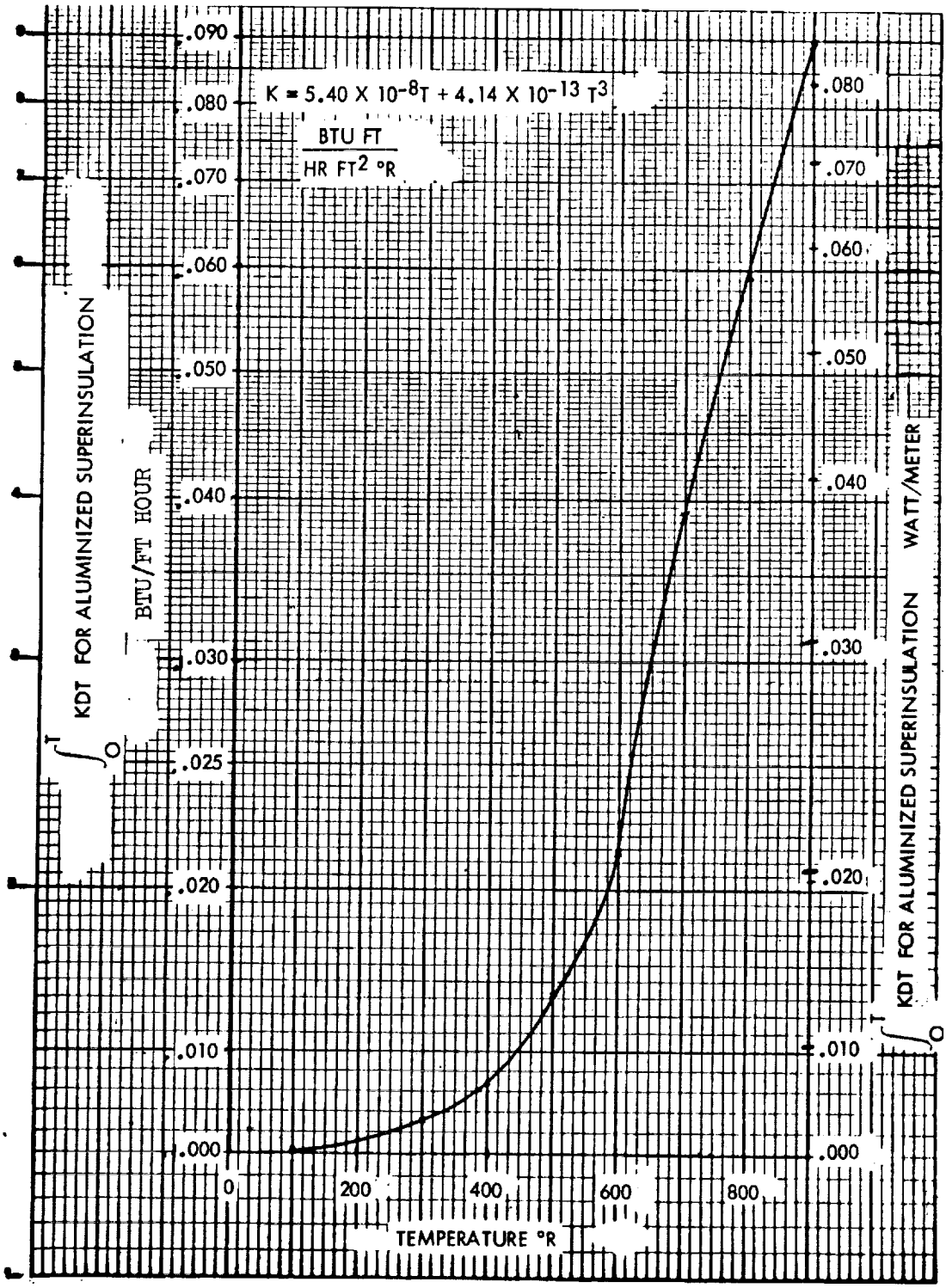

Figure 48. NRC-2 Superinsulation Integrated Heat Flow Versus Temperature

Table 20. High Performance Insulation Characteristics

Insulation	Radiation Shield	Spacer	Shield Spacing Layers Per Inch (CM)	Shield and Spacer Density LB/Ft^3 (Kg/M^3)	Installed Density LB/Ft^3 (Kg/M^3)	Conductivity $\frac{Btu}{Hr\text{-}Ft^2}$ or $\frac{WATT}{M^2\ ^oK} \times 10^5$	
						Shuttle Mission at $383^oR(213^oR)$	Mars Mission at $331^oR(184^oR)$
GAC-9	DAM	Foam Layer	38 (15)	2.18(34.92)	2.71 (43.4)	2.73 (4.78)	2.32(4.06)
Superflac	DAM	Dacron tufts	38 (15)	0.58(9.29)	1.64 (26.27)	2.48 (4.34)	2.21(3.87)
NAR SAM	Embossed SAM	None	93 (37)	1.28 (20.50)	2.22 (35.56	1.59 (2.78)	1.27 (2.22)
NRC 2	NRC 2	None	80 (31)	1.10 (17.62)	2.17 (34.76)	1.35 (2.36)	1.03 (1.80)
DAM/ NM	DAM	Nylon mesh	50 (20)	2.40 (38.44)	2.94 (47.09)	0.81 (1.42)	0.54 (0.95)

(1) Performance based on the outside surface temperature shown.

DAM = Doubly aluminized Mylar; NRC-2 = crinkled aluminized Mylar;
SAM = Singly aluminized Mylar
NM = Nylon Mesh

Table 21. High Performance Insulation Thermal Conductivity Factors

HPI	K_c	K_r	Number of Layers / Cm (Inch)	A * $\frac{\text{Watt-cm}}{\text{cm}^2\ {}^\circ\text{K}^2}\left(\frac{\text{Btu Ft}}{\text{HR FT}^2\ {}^\circ\text{R}^2}\right)$	B $\frac{\text{Watt-cm}}{\text{cm}^2\ {}^\circ\text{K}^4}\left(\frac{\text{Btu Ft}}{\text{HR FT}^2\ {}^\circ\text{R}^4}\right)$
DAM/NM	0.00722 (1.0)	0.00339 (4.7)	20 (50)	1.71×10^{-12} (5.49×10^{-9})	8.24×10^{-14} (8.16×10^{-13})
Superfloc	0.25559 (35.4)	0.00139 (1.922)	12 (30)	1.48×10^{-11} (4.77×10^{-8})	5.61×10^{-14} (5.56×10^{-13})
GAC-9	0.46930 (65.0)	0.0081 (1.118)	15 (38)	5.22×10^{-9} (1.6779×10^{-7})	2.58×10^{-14} (2.554×10^{-13})
NRC-2	0.02137 (2.96)	0.00390 (5.12)	31 (80)	1.835×10^{-11} (5.919×10^{-8})	5.61×10^{-14} (5.56×10^{-13})
NARSAM	0.01362 (1.885)	0.00166 (2.3)	39 (93)	1.785×10^{-11} (5.703×10^{-8})	2.17×10^{-14} (2.147×10^{-13})

Substituting Equation 49 into Equation 50 and integrating result in the heat flow (H) as follows:

$$H = \frac{A}{d}\left[T_H^2 - T_C^2\right]\left[\frac{A}{2} + \frac{B}{4}\left(T_H^2 + T_C^2\right)\right] \tag{51}$$

T_C will be essentially the cryogen temperature while T_H is the time varying temperature of outer surface of the propellant module. If the surface temperatures of the propellants are taken to be their boiling temperatures for nominal vapor pressures (not super-cooled propellants), the thermal conductivity integral can be evaluated for the various types of insulation. The normalized heat flux is given by

$$H_n = \frac{dH}{A} \tag{52}$$

These results are presented in Figures 49 and 50 for the different insulations and propellants. The normalized heat flow, H_n, multiplied by the mission duration (hours) and divided by the insulation thickness will provide an estimate of the amount of heat input per unit surface area through the insulation covering the propellant tanks.

5.2.3 Mission Profile Heat Balance

The modules will experience a varying heat flux depending upon the solar distance of the transplanetary flight profile and the planets albedo during the stop-over portions of the mission. Each leg of the mission will affect the propellant boil-off to a different degree and has to be considered systematically in order to identify the insulation-weight-scaling requirements and the overall stage performance.

The solar heat flux (S) is

$$S = \frac{S_\oplus}{R^2}\cos\phi \tag{53}$$

where R = the solar distance of the spacecraft in astronomical units (AU)

$S_\oplus$ = the solar heat flux at 1AU distance

ϕ = the angle between the local surface normal and the direction vector to the sun.

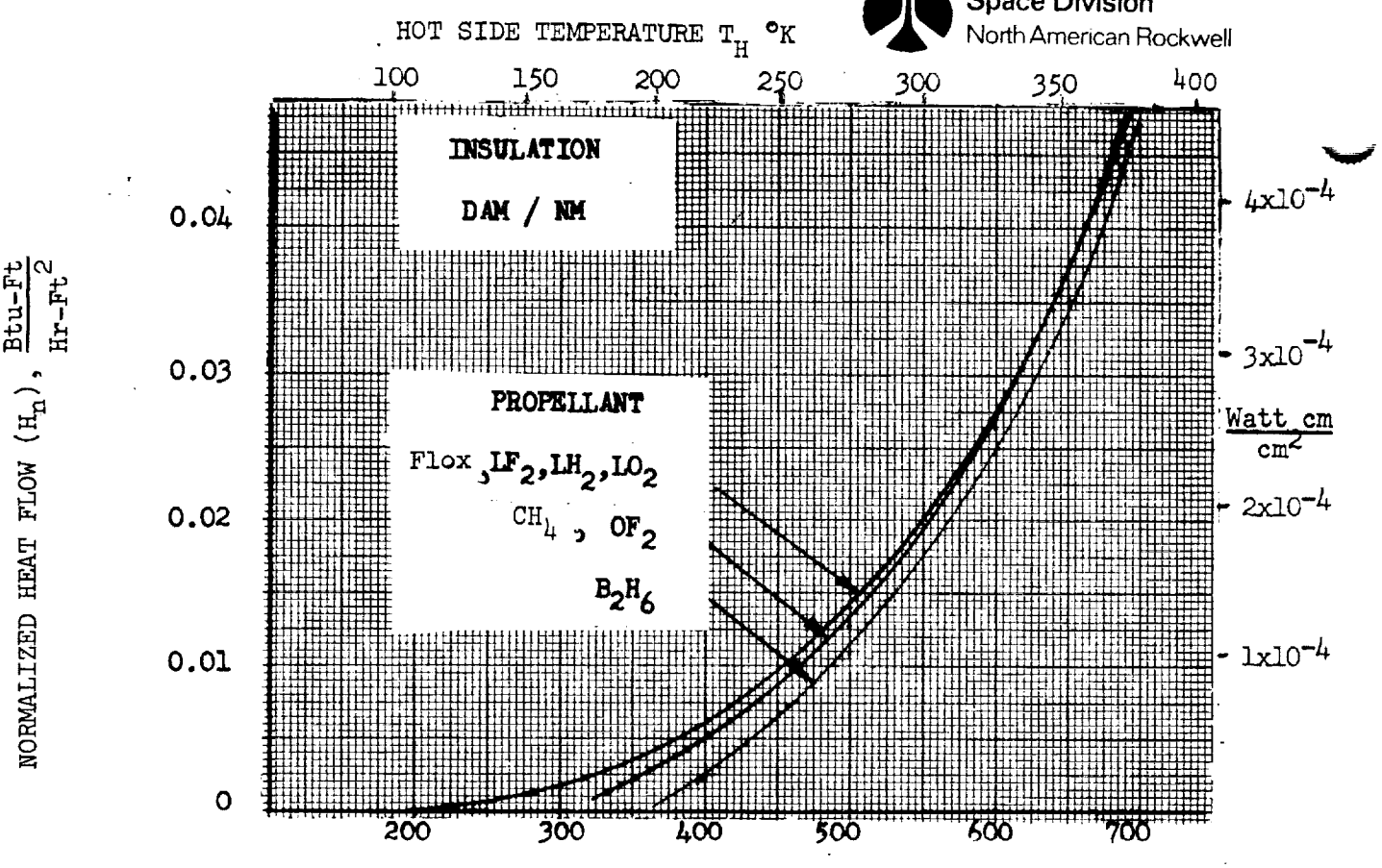

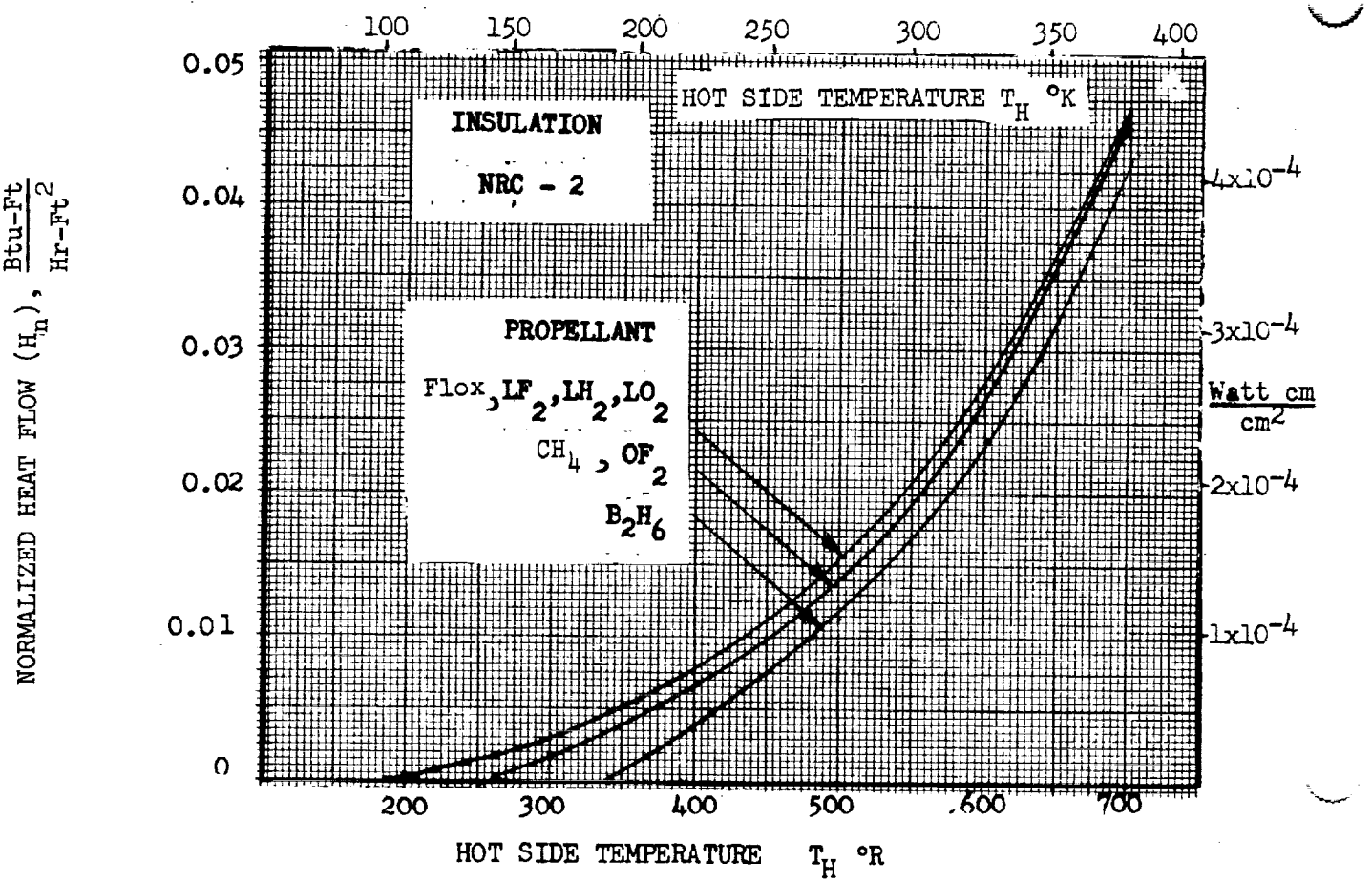

Figure 49. Heat Flux for DAM/NM & NRC-2 Insulation

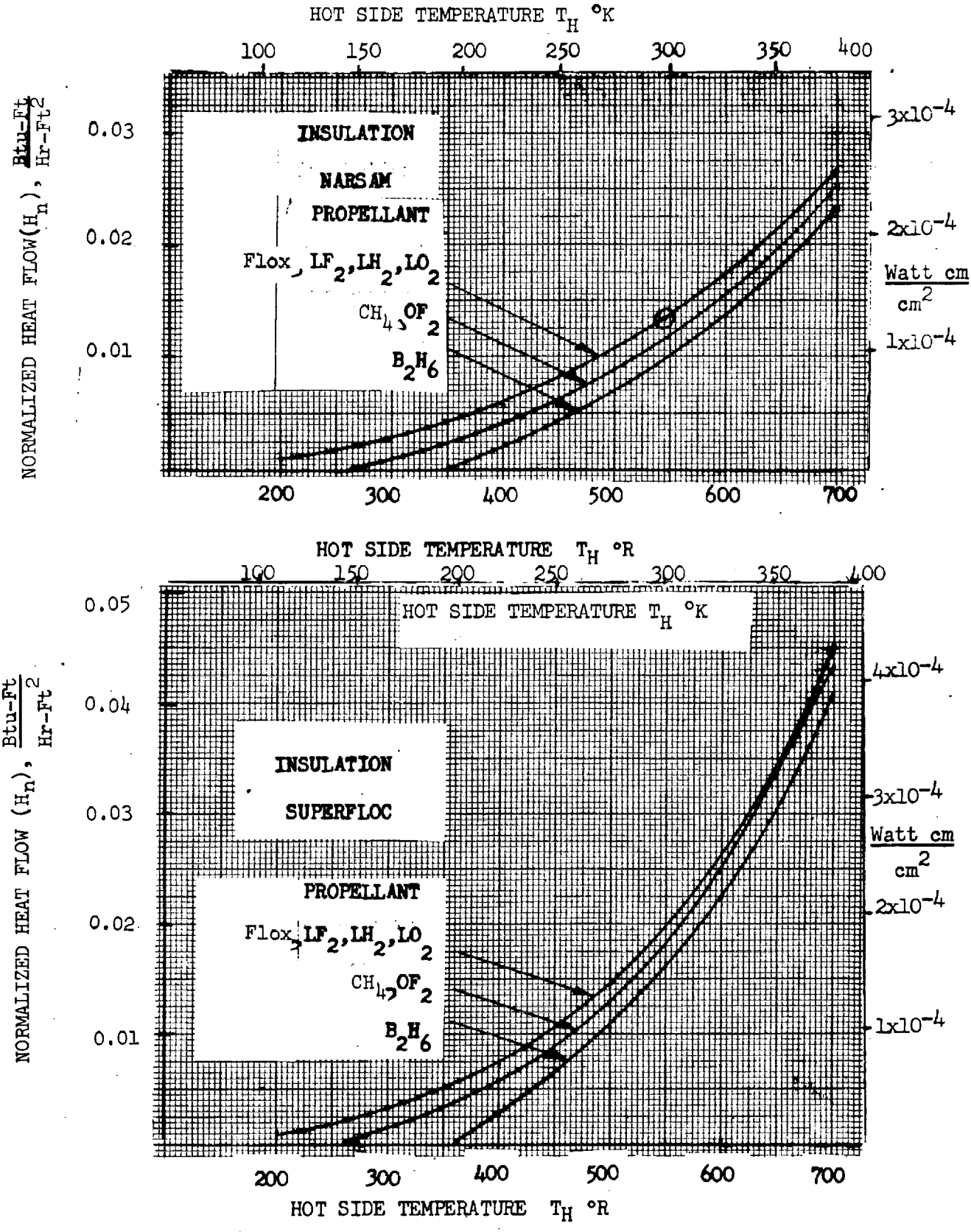

Figure 50. Unit Heat Flux for NARSAM & Superfloc Insulation

The total incident solar heat (Q) over the trajectory is

$$Q = \int_{t_1}^{t_2} S \, dt \tag{54}$$

The above integration is performed over the elapsed time in flight (for example the time from Earth departure t_1 to Mars arrival t_2). The actual propellant heating is a function of many other parameters, but the inverse square solar heating integral is a good indication of the relative severity of various portions of an interplanetary mission.

A simplified approach is used to determine the equilibrium wall temperature at the departure and arrival points for the mission. This approach considers an average surface temperature throughout the entire mission leg. The surface temperature (T_H) is assumed to be equal to the equilibrium wall temperature, which is given by

$$T_H = \left[\frac{\alpha_s}{\varepsilon} \frac{A_A}{A_E} \frac{S}{\sigma} \right]^{1/4} \tag{55}$$

where α_s = the surface coating absorptivity

ε = the surface coating emissivity

A_A = the effective absorbing area

A_E = the effective emitting area

S = the solar constant

σ = the Stefan-Boltzmann constant

Equilibrium temperature results for rotating spheres and surfaces normal to the sun's rays which radiate from the front only are shown in Figures 51 and 52, respectively. These plots bound the equilibrium temperatures that will be experienced by the modules during the mission profiles. Figures 51 and 52 show the equilibrium temperature as a function of heliocentric distance, and include effects of the ratio α_s/ε. It should be noted that to achieve a ratio of α_s/ε as small as 0.2, it is necessary to use a white surface coating such as zinc oxide which is highly reflective to incident solar radiation wave lengths and highly emissive for long wave length surface radiation. To approach a ratio of 5, a very specular surface is required: one which is capable of reflecting a great deal of the incident

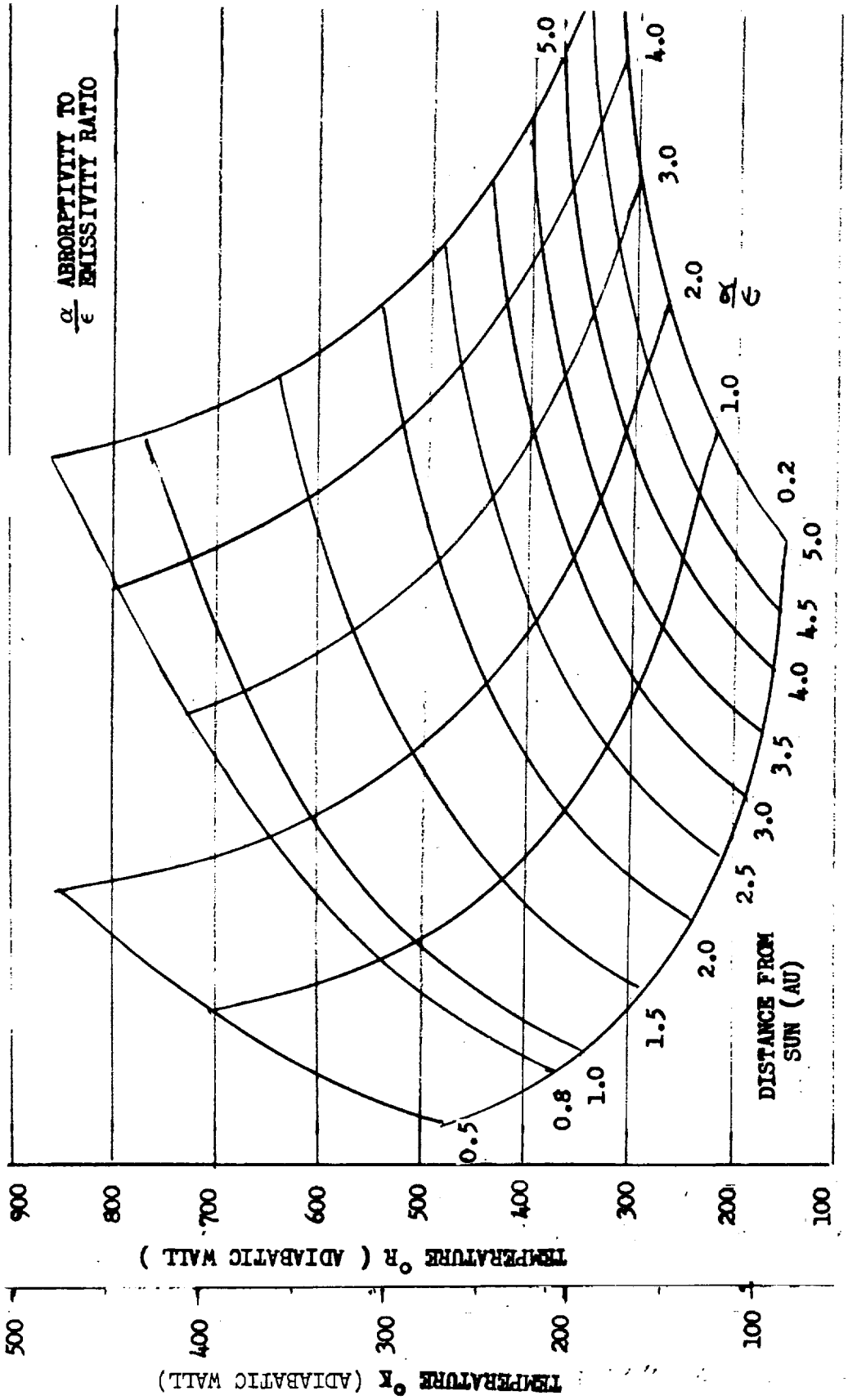

Figure 51. Equilibrium Wall Temperature~Rotating Sphere

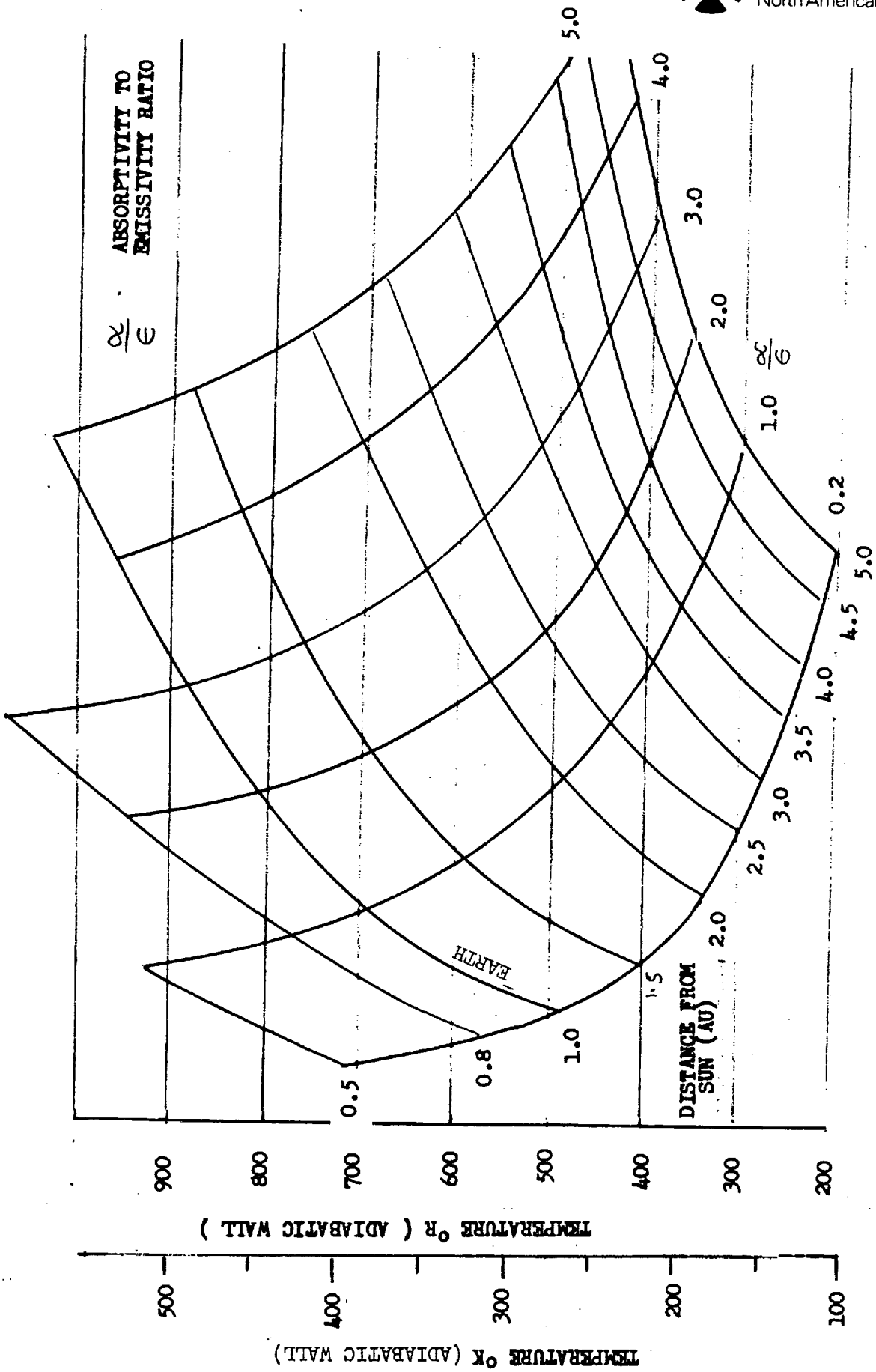

Figure 52. Equilibrium Wall Temperature - Spacecraft Surface Normal to Sun

solar radiation but is not capable of emitting at low temperatures even as much energy as it absorbs. Similarly, for a ratio of 1, it is necessary to have surfaces such as black lacquers, deposited carbon black, or other materials which emit and absorb all wave lengths equally.

An absorptivity/emissivity ratio of $\alpha_s/\varepsilon = 0.2$ is considered representative of the lowest practically obtainable ratios available in the current technology. This ratio is currently being approached on slab-sided spacecraft. With improvements in the state-of-the-art, it may be possible to reduce this ratio to a smaller value and work has been going on for many years in this direction. Concepts involving diffraction gratings and very selective materials have been the subject of much research in the aerospace industry, but to the present there has been no significant breakthrough in achieving a very low ratio. Figures 51 and 52 show that a ratio of 0.2 produces a much lower surface temperature than a ratio of 5, which is beneficial for cryogenic storage.

The presence of a planet will affect the heating flux experienced by the spacecraft. In addition to the solar flux, there are planet reflected and emitted heating fluxes. The total heat flux, S_{ABS}, is given by

$$S_{ABS} = \alpha_s S \left[1 + \left(\frac{S_R}{S}\right) + \left(\frac{\varepsilon_R}{\alpha_s}\right)\left(\frac{S_E}{S}\right)\right]$$

S_R = planet reflected heating rate

S_E = planet emitted heating rate

The value of S_{ABS} can be used to replace S in Equation 55 to account for the thermal contribution of the planet.

The albedo of a planet is the sum of the reflected and scattered solar radiation and a table of the albedo B for the various planets is given below.

Table 22. Near Planet Albedo and Surface Temperatures

Planet	Mercury	Venus	Earth	Mars	Jupiter	Saturn	Uranus	Neptune	Pluto
Albedo	0.058	0.76	0.39	0.15	0.51	0.50	0.66	0.62	0.16
Maximum Surface Temp °F	750	210	140	90	-200	-240	-270	-330	-370

The effective radiation received by the spacecraft due to the reflected radiation is

$$B_{eff} = B\, f(\theta) g \cos \delta$$

where $f(\theta)$ = geometry factor dependent on the angle between the spacecraft axis and radius vector to the planet

g = function of altitude (h)

δ = angle between radius vector and sun vector

The altitude function, g, for a simple sphere is

$$g = 1 - \frac{\sqrt{h(2r_p + h)}}{r_p + h}$$

where r_p is the planet radius.

The angle between the radius vector and the sun vector changes throughout the orbit period around the planet and with the orbital inclination with respect to the sun vector. If $f(\theta)$ and cos δ are taken as unity we have

$$B_{eff} = B\, g \tag{56}$$

The heat emitted from each planet is assumed to be constant over its surface, where the average surface temperature is defined as

$$T_p = \frac{394\ (1 - B)^{1/4}}{\sqrt{2R_p}}$$

and the planet emitted radiation E_{ff}, can be expressed as

$$E_{ff} = Z g T_p^{\ 4}$$

The view factor, Z, is 1.0 and 0.5 for single and clustered tanks, respectively. The solar flux heating will be increased during planet stop-over; the equilibrium wall temperature during planet stop-over is given by

$$T_H = \left[\left(\frac{\alpha_s}{\varepsilon}\right)\left(\frac{A_A}{A_E}\right)\left(\frac{S(1+B_{eff})}{\sigma} + E_{ff}\right)\right]^{1/4} {}^{\circ}K \tag{57}$$

For the spatially varying solar heat flux, Equations 49, 53, and 55 for normal incidence ($\phi = 0$) will produce the following:

$$\int_{T_C}^{T_H} KdT = \frac{C_1}{R} + \frac{C_2}{R^2} - C_3 \qquad (58)$$

where

$$C_1 = \frac{A^*}{2}\left[\left(\frac{\alpha_s}{\epsilon}\right)\left(\frac{A_A}{A_E}\right)\left(\frac{S_\oplus}{\sigma}\right)\right]^{1/2}$$

$$C_2 = \frac{B}{4}\left[\left(\frac{\alpha_s}{\epsilon}\right)\left(\frac{A_A}{A_E}\right)\left(\frac{S_\oplus}{\sigma}\right)\right]$$

and

$$C_3 = \frac{A^*}{2} T_c^2 + \frac{B}{4} T_c^4$$

The total heat input (Q_{IN}) is

$$Q_{IN} = \frac{A}{d} \int_{t_1}^{t_2} \int_{T_C}^{T_H} KdTdt;$$

or. from Equation 58

$$Q_{IN} = \frac{A}{d} \int_{t_1}^{t_2} \left(\frac{C_1}{R} + \frac{C_2}{R^2} - C_3\right) dt; \qquad (59)$$

where $t_2 - t_1$ is the exposure time of the propellant module under consideration. Integration of Equation 59 throughout the mission leg results in

$$Q_{IN} = \frac{8766\,A}{2\pi\,d}\left[\frac{C_1\ a\sqrt{1-e^2}\ (\Delta E) + C_2\ (\Delta \nu)}{\sqrt{a(1-e^2)}} - C_3\ (\Delta t)\right] \text{ BTU} \qquad (60)$$

where

a = semimajor axis of the heliocentric conic , AU

e = eccentricity

ΔE = change in eccentric anomaly

$\Delta \nu$ = change in true anomaly

Δt = exposure time (hours)

The changes in anomalies are evaluated from the departure (R_0) and arrival points (R_f) of the mission leg.

$$E = \cos^{-1} \quad (1/e - R/ea)$$

$$\nu = \cos^{-1} \left(\frac{\cos E - e}{1 - e \cos E} \right)$$

and

$$\Delta t = \frac{8766\ a^{3/2}}{2\pi} \left[E_f - E_0 - e \quad (\sin E_f - \sin E_0) \right] \text{ hours} \qquad (61)$$

5.2.4 Thermal Model Analysis

Weight scaling of the propellant modules requires an effective but simple method to estimate weight requirements for the tank insulation, the heat input into the propellant and the amount of ensuing propellant boil-off. Thermal models used for the family of vehicles, propellant combinations and mission profiles should represent the design concept as closely as possible and use thermal calculations simple enough to permit a rapid investigation over a wide range of design parameters, shapes and sizes.

Multi-layer vacuum insulations used are highly anisotropic with respect to their thermal conductivity. These high performance insulations have a thermal conductivity approaching 10^{-5} Btu/hr ft °R in the direction normal to the layers. This anisotropic effect would not be noticeable if the vehicle were subjected to a uniformly distributed heat flux. An interplanetary vehicle experiences a highly nonuniform thermal environment when exposed to solar radiation on one side and essentially absolute zero effective deep space temperature on the other side.

Multilayer insulation utilizing electrodeposited aluminum films on insulated materials such as Mylar have composite lateral conductivities 10^3 times larger than the normal thermal conductivity (Reference 19). This composite lateral conductivity does not include the "radiation tunneling" effect of heat transfer parallel to the layers by combined emission and reflection of radiation. These high values of the lateral conductivity are important to the anisotropic effect of the insulation.

Reference 20 considered several thermal models to determine the effect of the insulations lateral conductivity. The calculations were performed on a 32-foot diameter tank which was oriented broadside to the sun at 1.0 AU solar distance. Insulation depth was taken as 1.0 inch and the conductivities were 2.5×10^{-5} Btu/hr ft °R normal to the surface and 10^6 times this value parallel to the surface. Surface coating absorptivity was 0.25 and the emissivity was 0.9. Reference 20 used a two-dimensional multi-nodal model and found that the propellant heating per cylinder length yielded 7.52 Btu/hr.ft. A second method considered the lateral conductivity to be infinite which results in the outside insulation temperature being uniform. This can be achieved by rotating the space vehicle. This simplification allows a one dimensional model to be used and the resulting heat transfer into the propellant was 10.94 Btu/hr.ft, a value approximately 45 percent higher than the result obtained with the two-dimensional analysis.

A third model assumes the illuminated side to be isothermal and the non-illuminated side is ignored. This model produced heat transfer 15% lower than the two-dimensional model. Considering the uncertainties with respect to the installed performance of multi-layer insulation and the somewhat arbitrary method of accounting for thermal shorts, it is more desirable to use the conservative but much simpler model.

Actual normal thermal conductivity of the installed insulation is influenced by the method of insulation lay-up, panel sizes and heat shorts through the insulation due to stand-off supports and secondary structures. High performance insulation design and testing conducted at NR/SD have shown that the method of joining insulation panels produce noticeable heat

leak paths. Figure 53 shows four methods of joining panels which result in heat leak over the basic insulation ranging from 6 to 50 percent. Reference 21 considered the effect of insulation panel sizes on the overall thermal conductivity into the propellant containers. Figure 54 shows the increase in conductivity due to the panel area to joint length ratio.

Using a one dimensional thermal model will provide a representative assessment of the insulation requirements and the heat input into the propellant tanks. The optimum relationship between the boil-off propellant and the insulation thickness is obtained by minimizing the total vehicle mass.

The optimized propellant boil-off for a two-stage vehicle which has one or two cryogenic propellants can be evaluated by considering each propellant separately. The optimization model used in Appendix C, shows independency of the propellants for the optimization process. In principle the procedure given in Appendix C can be applied to multiple stage with multiple burns. The current version of the computer program however, considers a single stage with a single burn.

The optimum insulation thicknesses, d_{opt}, required for single burns in each stage are given below.

Stage One

$$d_{1_{opt}} = \frac{f_1 K_1}{L_1} + \frac{1}{L_1}\sqrt{\frac{L_1 K_1}{\rho_{ins}}\left(G_1 + \frac{1}{\mu_1}\right) + f_1^2 K_1^2} \qquad (62)$$

Stage Two

$$d_{2_{opt}} = \frac{f_2 K_2}{L_2} + \frac{1}{L_2}\sqrt{\frac{L_2 K_2}{\rho_{ins}}\left[G_2 + \frac{1}{\mu_1 \mu_2}\left\{1 + \frac{K_{21}}{K_2}\left(\mu_1 - 1\right)\right\}\right] + f_2^2 K_2^2}$$

THE FOLLOWING DATA ARE BASED ON EXPERIMENTS PERFORMED IN 1965 ON TWO SIDES OF A 4-FT BY 4-FT SPECIMEN - TWO JOINTS, EACH FOUR-FEET LONG.

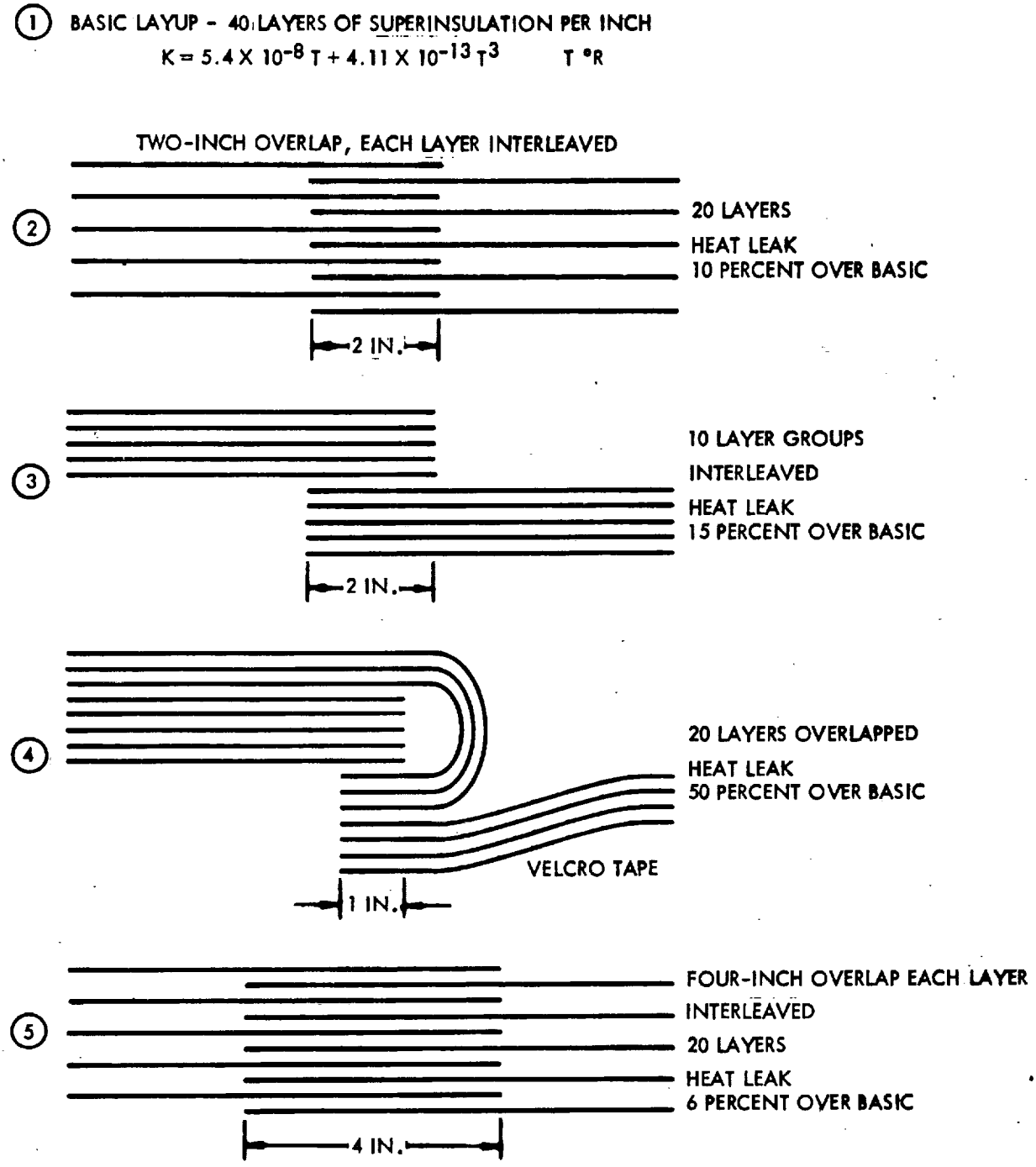

Figure 53 Interrelationships of Joints on Heat Leak

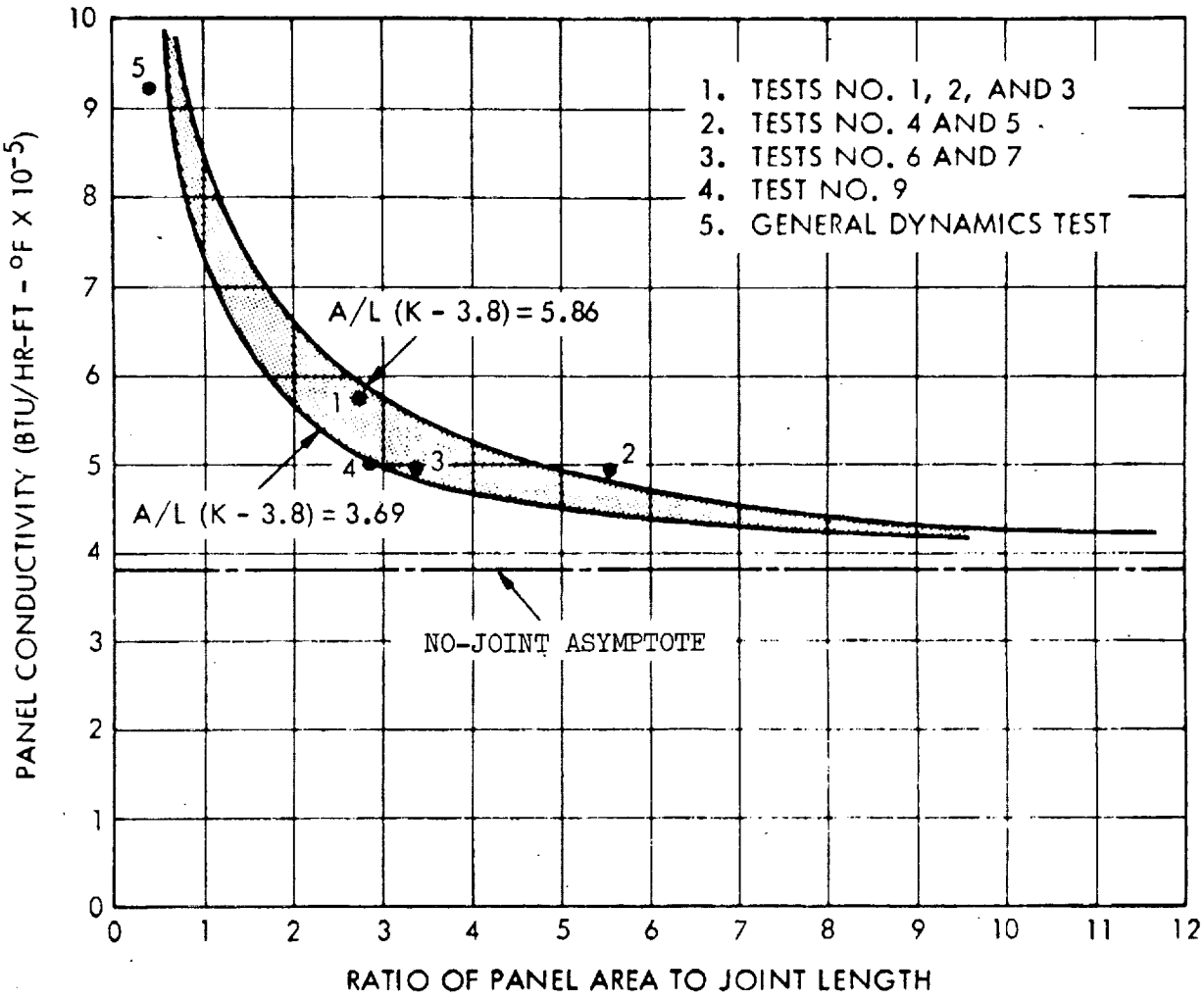

(Ref: Goodyear Aerospace
GER 11676 S/36)

Figure 54. Panel Conductivity Versus Ratio of Panel Area to Joint Length

and the propellant boil-offs resulting from these thicknesses of insulation are:

Stage One

$$W_{B_{1_{opt}}} = A_1 \sqrt{\frac{K_1 \rho_{ins} \mu_1}{L_1(G_1 \mu_1 + 1) + f_1^2 K_1 \mu_1 \rho_{ins}}} \qquad (63)$$

Stage Two

$$W_{B_{2_{opt}}} = A_2 \sqrt{\frac{K_2 \rho_{ins} \mu_1 \mu_2}{\left\{ L_2 \left[G_2 \mu_1 \mu_2 + 1 + \frac{K_{21}}{K_2}(\mu_1 - 1) \right] + f_2 \tilde{} K_2 \mu_1 \mu_2 \rho_{ins} \right\}}}$$

where $K = Q_{IN} \frac{d}{A}$

$$G = \frac{W_{ST}}{W_B}$$

$$f = \frac{A}{W_B}$$

L - heat of vaporization

K_i - total normalized heat absorbed by the i^{th} stage.

K_{ij} - normalized heat absorbed by the i^{th} stage between the j^{th} and $j + i^{th}$ burn of the entire vehicle

μ_i - the performance mass ratio for the i^{th} stage

ρ_{ins} - installed density of the insulation

The tank support structure, Figure 55, will also contribute to heat leaks into the propellant tanks and will require additional insulation. Heat input should be minimized by heat blocks.

Although an analysis lead to an optimum uniform thickness of insulation for propellant tanks and tank supports is given in Appendix D, from considerations of practicality, this analysis is modified for inclusion in computer code as follows.

First, the total heat input including heat leaks is assumed to be 1.5, 1.4, or 1.25 times the sum of all heat inputs Q_{IN} calculated earlier for stage propellant tanks, depending upon whether the material used for the tank supports (e.g. tank skirt) is aluminum, titanium, or whether heat blocks are used respectively. Hence the heat leak through the tank support is taken to be 0.5, 0.4, 0.25 of the heat absorbed through the insulated tank walls into the propellant. For a single tank support, such as the aft skirt, the heat leak Q_2 is calculated from

$$Q_2 = \frac{W_{BO}\ FACT}{2\ L}$$

where W_{BO} is the weight of propellant boil-off calculated previously for a given tank, L is the heat of vaporization of the propellant and FACT is the factor 0.5, 0.4, 0.25 given above.

The average rate of heat flow $\dot{Q}_2$ through the support into the tank is obtained by dividing Q_2 by the exposure time of a given stage. The optimum length L_2 of insulation to be used on each side of the support is then obtained as

$$L_2 = \frac{1.61\ K_2\ \bar{t}_2\ \omega_2\ \Delta T}{\dot{Q}_2}$$

where

K_2 = thermal conductivity of support structure

t_2 = thickness of support structure

ω_2 = perimeter of propellant tank πD

ΔT = temperature differences between hot and cold temperatures of support structure

The additional weight of insulation W_{ins_S} for each tank support is then

$$W_{ins_S} = 2\rho_{ins}\ d_{ins}\ \omega_2\ L_2$$

where ρ_{ins} is the density of the insulation used for both tank and supports, and d_{ins} is the thickness of insulation found necessary for the propellant.

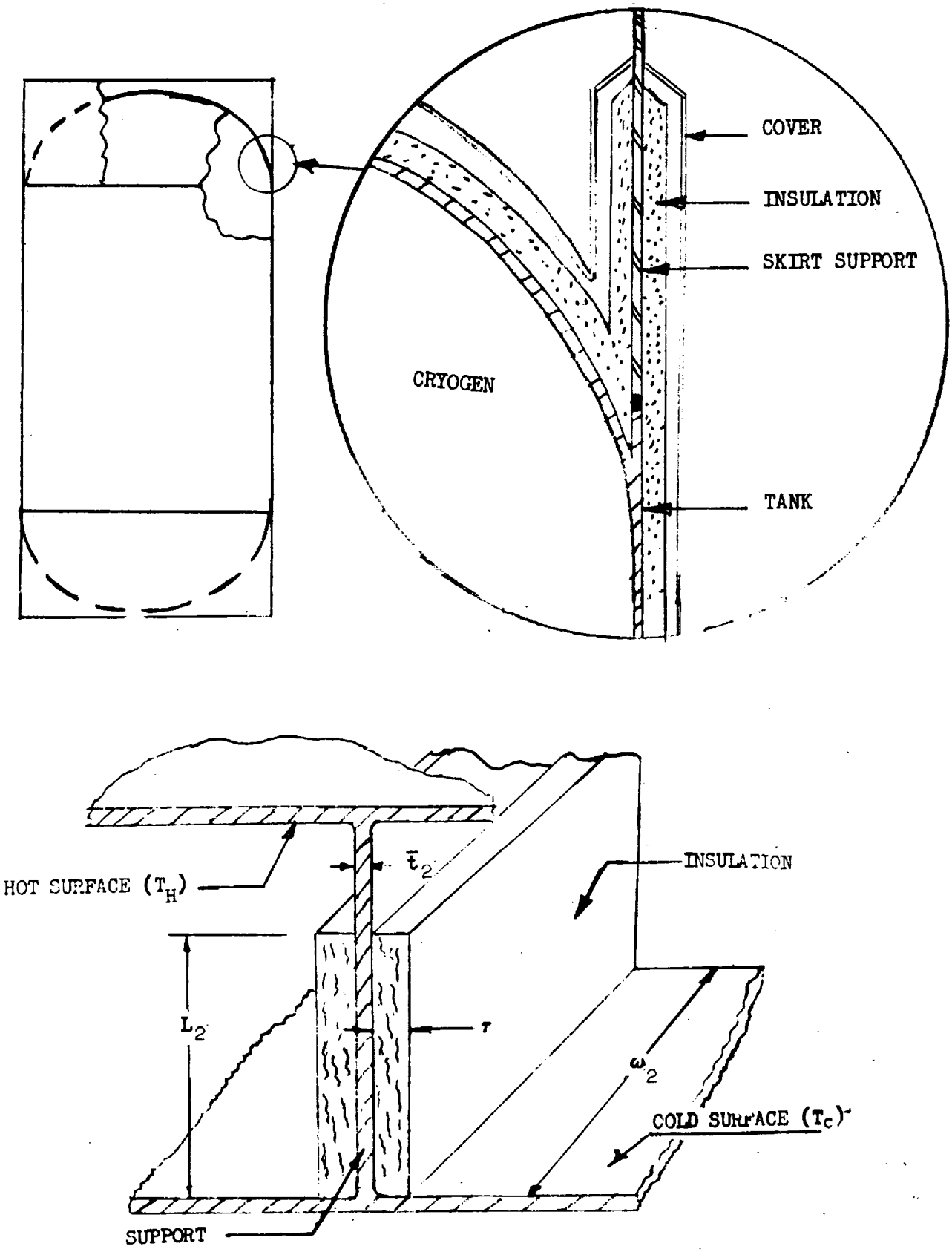

Figure 55. Heat Transfer Model for Tank Support Components

5.2.5 No Propellant Boil-off

An alternative approach to venting the propellant is to allow the tank pressure to increase, thereby supressing the fuel vaporization but requiring thicker tank shells. Restraining the boil-off will result in a smaller volume tank, thicker tank walls, but the overall effect could be an improvement in the vehicle's performance. For long duration missions, the tanks will be insulated with high performance insulation and the resulting heating rate into the tanks from the solar flux will be significantly smaller. Since the heat rate is small, it will be assumed that the liquid and ullage volume of the tanks will be in equilibrium. The heat input will raise the temperature of both the propellant and the pressurization gas, subsequently increasing the tank pressure and boiling point of the propellant. No propellant will be vaporized due to the raising of the boil ing point. The heat input, Q, into the propellant and ullage gas is given by

$$Q = W_P C_s (T_2 - T_1) + W_G C_v (T_2 - T_1) \quad (68)$$

where T_1 = the initial temperature of the tank contents; e.g., boiling point of propellant at one atmosphere.

T_2 = final temperature of contents when pressure has risen to required value.

C_s = specific heat of propellant.

C_v = specific heat of gas

W_P = weight of propellant

W_G = weight of ullage gas

The initial volume of the propellant and gas will be

$$Vol = \frac{W_P}{\rho_{L_1}} + \frac{W_G}{\rho_G}$$

where ρ_{L_1} = initial density of propellant at temperature T_1

ρ_G = initial density of gas at one atmosphere and T_1

Since the contents are contained in the propellant tanks, the tank volume is assumed not to change with the small increase in temperature or pressure. Therefore, the volume can be expressed in terms of the final parameters if the weights of propellant and gas remain constant.

$$\text{Vol} = \frac{W_P}{\rho_{L_2}} + \frac{W_G}{\rho_G}\left(\frac{P_1 T_2}{P_2 T_1}\right)$$

ρ_{L_2} = density of propellant at final temperature

P_1 = initial pressure of ullage gas

P_2 = final pressure of ullage gas

Combining the two volume equations produces

$$\frac{W_P}{\rho_{L_1}}\left(1 - \frac{\rho_{L_1}}{\rho_{L_2}}\right) = \frac{W_G}{\rho_G}\left(\frac{P_1 T_2}{P_2 T_1} - 1\right) \tag{69}$$

The initial volumes are given by

$V_L = \frac{W_P}{\rho_{L_1}}$ volume of propellant

$V_G = \frac{W_G}{\rho_G}$ volume of ullage gas

Substituting for the volumes, Equation 69 can be rearranged.

$$\left(\frac{V_L}{V_G} + 1\right)\rho_{L_2} - \rho_{L_2}\left(\frac{P_1 T_2}{P_2 T_1}\right) - \frac{V_L \rho_{L_1}}{V_G} = 0 \tag{70}$$

For the range of interest of temperature and pressure changes of the propellants, the propellant density can be expressed as a linear function of the absolute temperature,

$$\rho_L = K_1 - K_2 T \tag{71}$$

values for K_1 and K_2 for the various propellants are shown in Table 23.

Substituting Equation 71 into Equation 70 and solving for the final temperature yield

$$T_2 = \frac{1}{2}(B - \sqrt{B^2 + 4C})$$

where

$$B = \frac{P_2 T_1}{P_1}\left(\frac{V_L}{V_G} + 1\right) + \frac{K_1}{K_2}$$

$$C = \frac{P_2 T_1}{P_1}\left(\frac{V_L T_1}{V_G} + \frac{K_1}{K_2}\right) \tag{72}$$

The only unknown quantities present in Equation 72 are the final pressure and the ratio (V_L/V_G) which will be considered to be specified. On solving Equation 72, the allowable heat input per unit volume ratio is

$$\frac{Q}{V_L} = \rho_{L_1} C_s T_1 \left(\frac{T_2}{T_1} - 1\right) + \frac{V_G}{V_L} T_1 \rho_G C_v \left(\frac{T_2}{T_1} - 1\right) \tag{73}$$

Both the density and specific heat (C_s) in Equation 73 vary with the temperature as shown in Table 23.

The ratio V_G/V_L is the tankage ullage ratio and is usually about 5 percent for cryogenic tankage. Figures 56 and 57 provide estimates for the allowable heat input per unit volume for a series of ullage factors, propellants, and range of pressures up to 7.03×10^4 kg/m^2 (100 lb/in^2). The allowable total heat input per unit surface area H_{allow} is given by

$$H_{allow} = (Q/V_L)\frac{V_L}{A_s}$$

where A_s = total surface area of the stage absorbing solar heat flux.

From the data from Figures 56 and 57 we get the form of the empirical scaling law for the allowable heat input per unit volume.

$$Q/V_L = K_1 \text{ EXP } \left(\frac{K_2}{K_3 - P}\right) UF^{1.25}$$

Table 23. Propellant Property Variation With Temperature

PROPELLANT TYPE	PROPELLANT PROPERTY	K_1	K_2	K_3
LH_2	Density	6.328	0.052	-
LO_2	Density	99.91	0.180	-
LF_2	Density	134.2	0.2624	-
B_2H_6	Density	43.1	0.04608	-
LH_2	Specific Heat	7.0532	0.3004	0.00469
LO_2	Specific Heat	0.5572	0.00192	0.000006
LF_2	Specific Heat	0.38749	0.000684	0.000004
B_2H_6	Specific Heat	0.634	0.0	0.0
LH_2	Pressure	222.212	13.446	0.2127
LO_2	Pressure	731.736	9.5293	0.0315
LF_2	Pressure	697.35	9.778	0.03475

Density	$\rho = K_1 - K_2T$	lb/ft^3
Specific Heat	$C_s = K_1 - K_2T + K_3T^2$	$Btu/lb_m - °R$
Pressure	$P = K_1 - K_2T + K_3T^2$	lb/in^2
	T = Temperature °R	

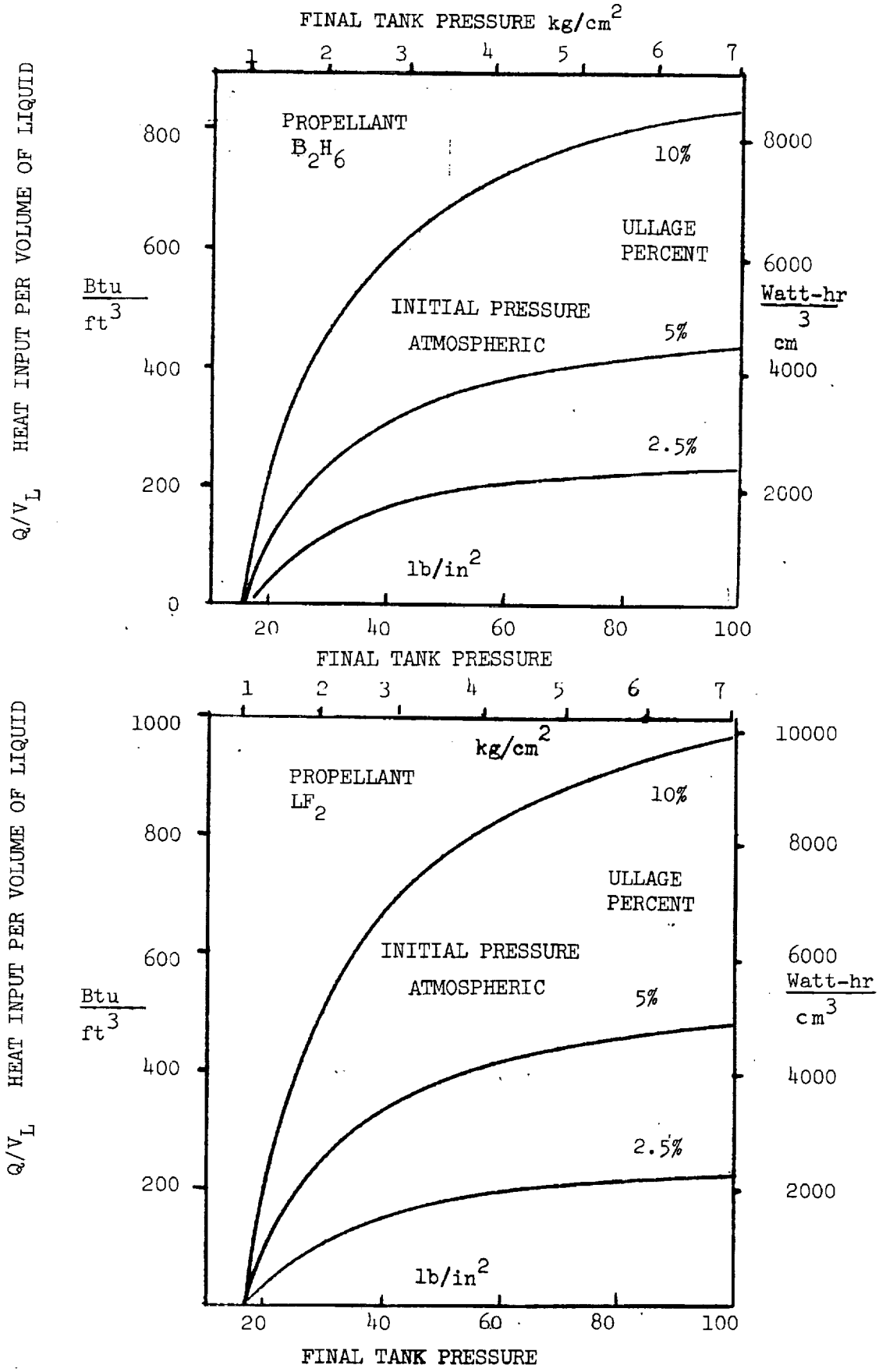

Figure 56. Allowable Heat Input - B_2H_6 and LF_2

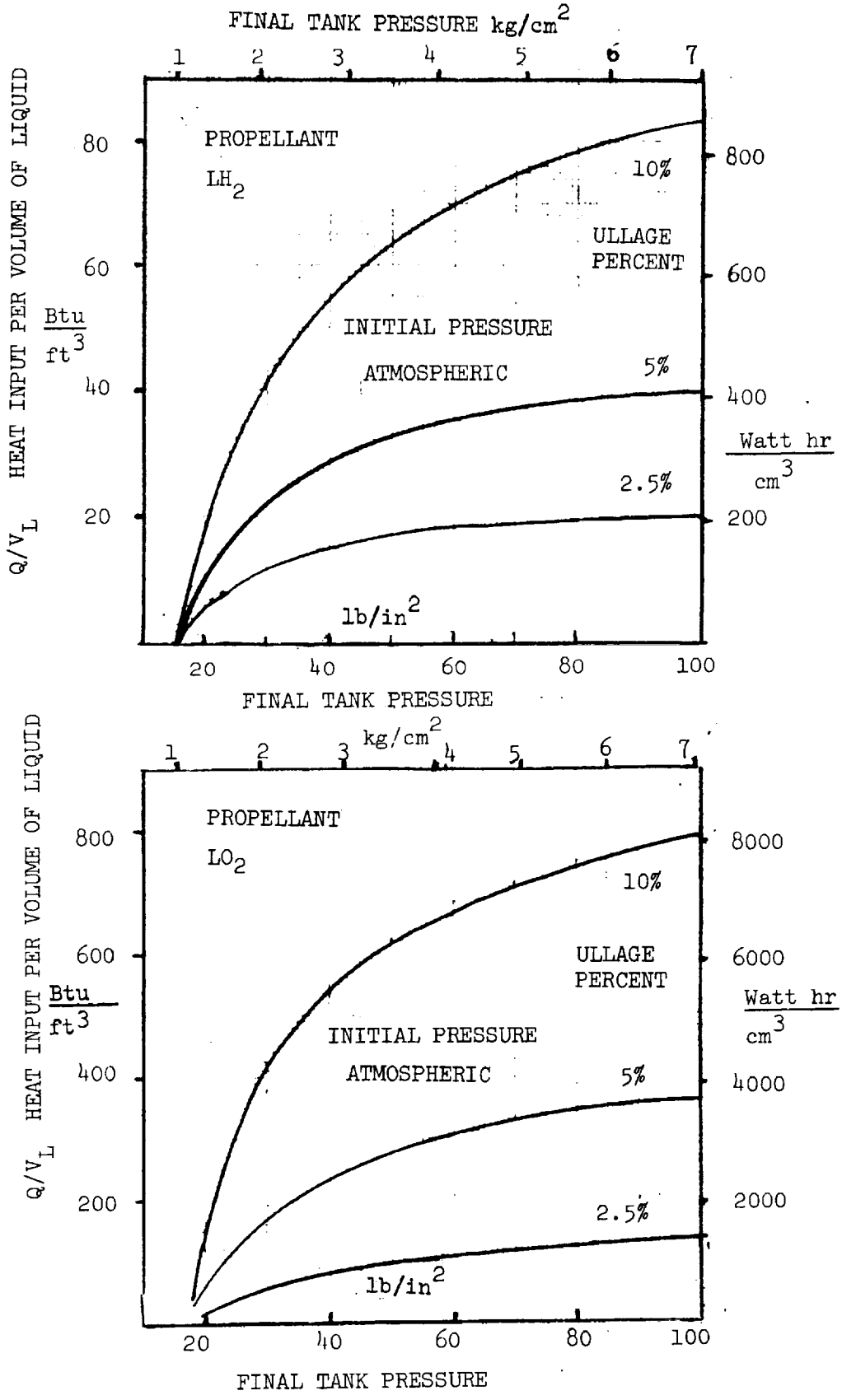

Figure 57. Allowable Heat Input - LH_2 and LO_2

THIS PAGE LEFT

INTENTIONALLY BLANK

6.0 SUBSYSTEM MODELING

The inert mass of the Space propulsion system consists of various functional subsystems, together with the major structural shell elements for the propellant containers. These additional subsystems provide a significant contribution to the stage's inert mass and have been considered in the following three categories.

1) Propulsion

   a) Main rocket engines
   b) Pressurization and feed system

2) Guidance and Control

   a) Intelligence module
   b) Attitude control and separation

3) Power and Communications

   a) Electrical power for stage systems
   b) Telemetry and wiring

Each of the individual systems has been considered and an appropriate scaling relationship developed to identify their respective weight requirements.

6.1 ENGINE MODULE

6.1.1 Main Rocket Engines

The major sources of engine system data were the major manufacturers of rocket engines (Pratt & Whitney, Aerojet, Rocketdyne, TRW, and Bell). Their contributions included design data for existing hardware and engines; projected weight, performance, and sizes of improved and updated versions of current hardware; and their best estimates of future engine systems. Some of the most useful information consisted of parametric weight data derived from consideration of paper engines (future design basepoints) and weight changes from small perturbations of the major design parameters for existing engines, References 22 through 37. The weight changes were reflected as a function of engine chamber pressures, expansion ratios, and thrust levels.

A summary of the data obtained from TRW, Aerojet General, Bell Aerospace, Pratt & Whitney, and Rocketdyne, and the range of engine parameters are identiified in Table 24.

A typical example of the parametric data received is illustrated in Figure 58 for a Pratt & Whitney pressure-fed, regeneratively-cooled rocket engine employing OF_2/CH_4 space-storable propellants. The parametric

Table 24. Engine Data Summary

Manufacturer	Propellant Combination	Thrust Range 1000 kg_f (lb_f)	Chamber Pressures kg/cm^2 (lb/in^2)	Propellant Feed	Expansion Ratio	Engine Cooling
Aerojet	OF_2/CH_4	0.45-3.6 (1-8)	3.52-105.5 (50-1500)	Press-Fed	20-150	Ablative-Rad
	Flox/CH_4	6.8-22.7 (15-50)		Pump-Fed (Stage Comb. Cycle)		Transpiration
	OF_2/B_2H_6	113.4 (250)				
	LO_2/LH_2	181.4 (400)	211 (3000)	Pump-Fed	50-200	Regen.
		453.6 (1000)	211 (3000)	Pump-Fed	50-200	Regen.
	N_2O_4/MMH	0.0451-2.175 (0.1-7)	7.03-35.2 (100-500)	Press-Fed	10-60	Regen. Adiabatic Wall Bimetallic
Bell	LF_2/LH_2	18.14 (40)	35.2-211 (500-3000)	Pump-Fed	50-300	Transpiration-radiation
	LF_2/LH_2	1.36-5.4 (3-12)	3.52-35.2 (500-1500)	Pump & Press-Fed	30-70	Regen-Radiation Ablative
Pratt & Whitney	OF_2/CH_4	0.45-22.7 (1-50)				Regenerative, Dump/Radiation Cooling
	Flox/CH_4	113.4 (250)	35.2-105.5 (500-1500)	Pump-Fed	60-400	
	LO_2/LH_2	0.45-22.7 (1-50)	35.2-105.5 (500-1500)	Pump-Fed	60-400	
	LF_2/LH_2	113.4 (250)	186.3 (2650)			
TRW	N_2O_2/MMH Descent Lemde	2.3-13.6 (5-30)	7.3 (104)	Press-Fed	47.5	Ablative
	O_2/H_2	0.23-1.4 (0.5-3)	2.03-35.2 (100-500)	Press-Fed	40	Ducted Cooled
	N_2O_4/UDMH	90.7-907 (200-2000)	17.6 (250)	Press-Fed	30-80	Ablative
Rocketdyne	$LF_2/LL_1/LH_2$	1.4-22.7 (3-50)	7.03-70.3 (100-1000)	Press-Fed Pump-Fed	40-150	Regen.
	N_2O_4/MMH, OF_2/B_2H_6, Flox/CH_4	.9-9.1 (2-20)	7.03-21.1 (100-300)	Press-Fed	40-100	Ablative-Radiation

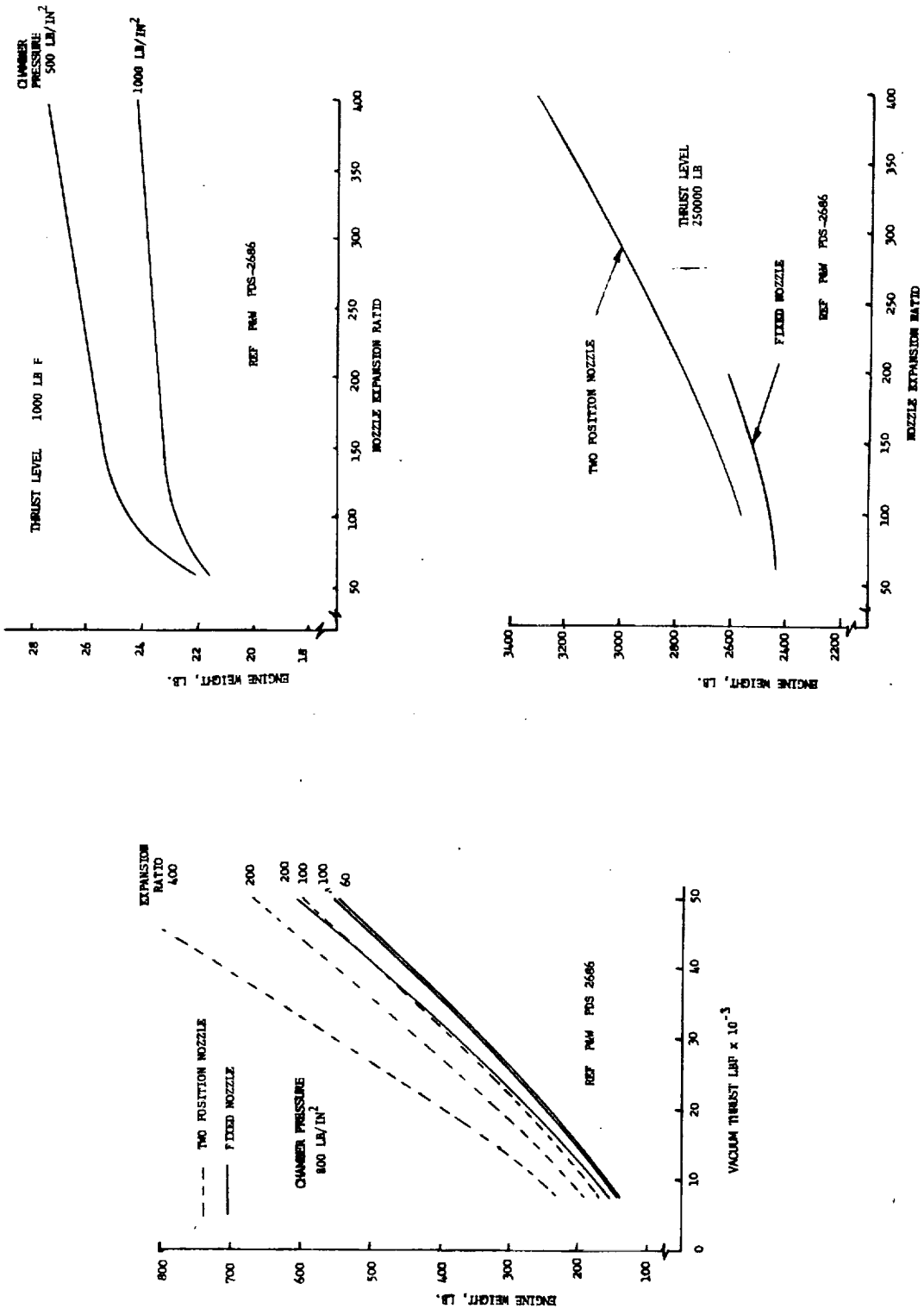

Figure 58 Parametric Engine Weight Data - Flox/Methane

data were for six specific thrust levels ranging from 4536 to 133,980 kgf (1000 to 250,000 lbf), engine expansion ratios from 50 to 400, and chamber pressures of 42.18 and 56.24 kg/cm^2 (600 and 800 lb/in^2).

Information obtained from engine manufacturers' design data handbooks, which are used for preliminary weight evaluation of engine systems, were used to assist in understanding the type of simple analytical modeling that is involved and the methods of estimating engine systems weight.

Some of the propellant combinations and engine sizes required for this study are proposed systems and have not been developed beyond the conceptual design phase. Any scaling laws derived from such information, therefore, would have a lower confidence level as there is no existing identifiable hardware design against which these individual laws can be checked. At best, these laws will provide estimates for trends of future systems and how the engine weights will vary with perturbations of the major design parameters of the engine. Actual engine weights can be adjusted easily as additional information becomes available or when these types of systems are developed.

The reports obtained were thoroughly reviewed, and the appropriate results were thoroughly interrogated to provide the basic design data from which the scaling laws are obtained. The engine system data have been segregated into the various types of engine systems ranging from pump-fed to pressure-fed systems and from regeneratively to transpirationally cooled systems.

Preliminary cataloging and statistical evaluation of these data were conducted to initially identify the subclass divisions and pertinent differences that can be anticipated between the various classes of engine systems. This approach permits identification of the types of engine systems that will be applicable to any specified scaling relationship and the range of application of each law.

The propulsion systems were divided into the four major subsystems: rocket engine assembly, propellant storage, propellant feed, and pressurization. Each of these subsystems was further divided into its component parts levels to identify the components and the subsystem parameters that significantly influence subsystem weight. These elements are illustrated in Figure 59. The propulsion system has been considered in terms of engine types, propellant combinations, and performance levels, including investigation of thrust ranges, mixture ratio ranges, pressure ranges, and changes in expansion ratio. These categories are used to organize data from the engine manufacturing sources, statistically reduce this data, and derive weight-scaling laws that include identification of the form of the equation, its coefficients, and its range of application. These laws are unique to the particular systems identified for each set of coefficients.

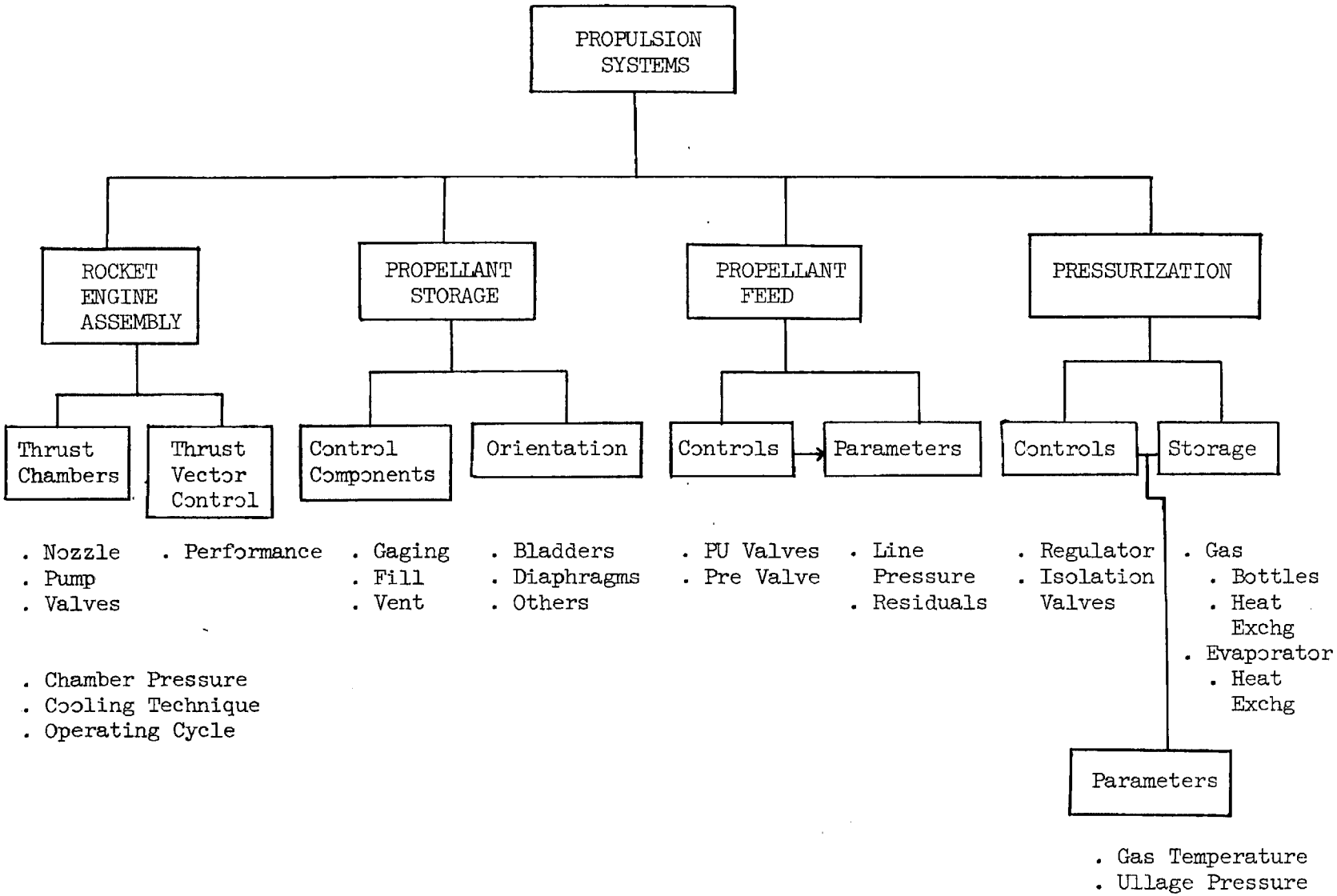

Figure 59. Propulsion System Elements

6.1.1.1 Engine Classes

Both pressure-and pump-fed rocket engine systems were considered during the study. Pressure-fed engines included ablation-cooled types with ablative or radiation-cooled nozzle extensions and a regeneratively cooled thrust chamber with a radiation-cooled nozzle extension. Pump-fed systems consisted of those with either regeneratively cooled thrust chambers and nozzles or radiation-cooled nozzle extensions, and those with transpiration-cooled thrust chambers and radiation-cooled nozzle extensions. In cases where extendible engine nozzles are employed, dump nozzle cooling is used. For pressure-fed engines, ablative cooling has inherent limits with regard to the combustion temperature, chamber pressure, duty cycle, and engine operating time and makes this concept unsatisfactory for high-energy propellants under most conditions. The temperature differentials between the flame temperature and the melting point of ablative materials is almost doubled by changing from earth-storable propellants to the more advanced space-storable propellant combination. Because of this increase in temperature difference, ablation rates are increased beyond tolerable limits causing additional ablation weight. Ablative-cooled rocket engines, therefore, are primarily limited to the lower temperature combustion processes associated with earth-storable combinations.

Regenerative cooling is an attractive method of engine cooling, because it provides a lightweight design, has unlimited burn-time capability, and has little performance loss. Unfortunately, there are inherent limitations to its use for some fuels, such as boron hydrides, which decompose so readily that tube fouling may occur. Other fuels, such as hydrazine-based fuels, decompose explosively in the vapor phase and require thrust-chamber pressures to prevent fuel vaporization. The transpiration-cooled thrust chambers used on pump-fed systems overcome some of the limitations associated with certain propellant combinations used in regeneratively cooled thrust chambers. Consideration was given to these different types of engines to account for noticeable weight variations.

Not all combinations of propellants and engine classes were considered in this study; certain feasible limitations were applied and the scaling laws developed for those engine concepts which have either been flight tested or were considered practicable. The pressure-fed engine laws were limited to working chamber pressures of 21 kg/cm^2 (300 lb/in^2) and a maximum thrust of 13,600 kg_f (30,000 lb_f). These limitations were considered due to the pressure effects on the structural/weight requirements for the propellant tankage. For propulsion modules having thrust levels exceeding 13,600 kg_f (30,000 lb) and a thrust-to-weight ratio of less than 0.5, the stage diameter is in excess of 5 m (15 ft) and would require skin gages greater than 2 cm (3/4 in) for the pressurized tanks.

The pump-fed engines, although heavier, are used with chamber-pressures of 21 kg/cm^2 to 211 kg/cm^2 (300 lb/in^2 to 3000 lb/in^2 to increase the deliverable specific impulse and improve the overall efficiency of the engine performance. The propellant combination of oxygen difluoride/diborane is not considered for the pump-fed engine concepts due to its possible clogging of the pump and feed systems. The high-pressure pump-fed engines are based on the engine designs for the Space Shuttle.

The range of engine operating pressures and thrust levels for pressure-fed and pump-fed engines have been categorized into the following ranges based on the data supplied by the engine manufacturers (Table 25). Thrust levels greater than 450,000 kgf will use a multiple engine installation.

Table 25 Engine Parameter Matrix

	Thrust kgf(lbf)x10^{-3}	Chamber Pressure kg/cm^2 (lb/in^2)	Expansion Ratio
Pressure-Fed	0.91-13.6(2-30)	7-21 (100-300)	100
Pump-Fed	1.4-22.6(3-50)	21-105(300-1500)	150
Pump-Fed	22.6-114(50-250)	105-211(1500-3000)	150
Pump-Fed	114-454(250-1000)	140-281(2000-4000)	150

Since the pressure-fed engines are limited to the lower chamber pressures, the average nozzle expansion ratio for the space engine performance should be about 100. High expansion ratio would make the overall thrust chamber assembly (TCA) excessively long and incur unwarranted weight penalties. The pump-fed engines can have expansion ratios from 150 to 400 depending on the engine size and performance improvement. A nominal value of $\varepsilon = 150$ will be used for the simplified scaling laws without compromising the weight laws significantly.

6.1.1.2 Propellant Combinations

Propellants used for this study range from earth- and space-storables to low-density cryogens. Basic characteristics for this range of propellants are given in Table 26. The effects of these propellant properties on the

TABLE 26 PROPELLANT CHARACTERISTICS

PROPELLANT POINT	FREEZING POINT °C (°F)	BOILING POINT °C (°F)	DENSITY kg/m^3 ($lb.ft^3$)	HEAT OF VAPORIZATION $\frac{Watt\text{-}Sec}{gm}$ (BTU/lb)	SPECIFIC HEAT $\frac{Watt\text{-}Sec}{gm\,^{\circ}C}$ (BTU/lb-°F)
Liquid Fluorine LF_2	-219 (-363.6)	-188 (-306.5)	1510 (94.3)	218.7 (94.1)	1.53 (0.365)
Liquid Hydrogen LH_2	-259 (-434.8)	-252.5 (-423.8)	70.4 (4.4)	454 (195)	0.98 (0.234)
Liquid Oxygen LO_2	-218 (-362)	-183 (-297.5)	1142 (71.3)	213 (91.6)	1.69 (0.405)
FLOX 85% O_2	-219 (-361.9)	-187.1 (-305.2)	1457 (91)	179 (77)	1.56 (0.373)
Nitrogen Tetroxide N_2O_4	-24.3 (-11.8)	21 (70)	1430 (89.3)	414 (178.1)	1.56 (0.373)
Monomethyl Hydrozine MMH	-52.4 (-62.5)	89.9 (192.5)	874 (54.6)	790 (340)	0.293 (0.070)
Diborane B_2H_6	-165 (-265.9)	-92.4 (-134.5)	450. 28.1)	521 (224.3)	2.6 (0.634)
Liquid Lithium LL_1	181.6 (359.2)	1332 (2430)	535 (33.4)	19376 (8338)	4.09 (0.979)
Oxygen Diflouride OF_2	-223 (-371)	-145 (-230)	1520 (94.9)	190 (81.9)	1.41 (0.338)
Methane CH_4	-182.5 (-296.5)	-161.1 (-258.9)	371 (23.2)	509 (219.2)	3.43 (0.82)

propulsion stage are given in Table 27. Combinations of propellants to be used for representative engine systems include LO_2/LH_2, LF_2/LH_2, $LF_2/Li - \% H_2$, OF_2/B_2H_6, OF_2/CH_4, FLOX/CH_4 and N_2O_4/MMH. Not all of these propellant combinations have resulted in current hardware engine systems.

Rocket engine technology for the propellant combinations identified in the study is in various stages of development. In the area of space storable propellants, sources of data for comparing actual hardware design and performance parameters with parametric data are few. Technology is being developed for pressure-fed ablatively cooled OF_2/B_2H_6 rocket engines at the 450 kg_f-thrust level and for a pump-fed regeneratively cooled FLOX/CH_4 engine at the 2270 kg_f-thrust level. Because no hardware data are available within the thrust ranges considered, the parametric data will have a low confidence level.

A major portion of the high (210 kg/cm^2) chamber pressure LO_2/LH_2 rocket engine hardware development program was conducted by Pratt & Whitney under Air Force sponsorship; but the data, although available, are not presented here because of the classified nature of the program. Studies being conducted by Aerojet, Pratt & Whitney, and Rocketdyne in support of the Space Shuttle program will reflect realistic hardware weights, thereby placing a higher confidence in the parametric data.

Technology development programs are being conducted for LF_2/LH_2 rocket engines under a classified Air Force contract. Data pertaining to the design and performance parameters are not included; however, the similarities of the LF_2/LH_2 engine design to LO_2/LH_2 engine design would place a relatively high degree of confidence in the parametric weight data.

The tripropellant rocket engine is in the early technology development stage, and changes in engine parameters are likely to occur as the technology progresses.

A high confidence level is placed in the parametric data for ablative-cooled pressure-fed engines employing N_2O_4/MMH propellants. Good correlation is shown between actual hardware weight and parametric data for thrust levels ranging 850 to 8500 kg_f, and it is believed that extrapolation of data up to 13,600 kg_f of thrust could be accomplished with a high degree of confidence.

To synthesize a propulsion module, weight relationships for the various subsystems and performance characteristics of the recommended engine system are required. Just as the engine weight is a function of the types of propellants and the major design parameters, the engine performance is influenced by these and a few additional parameters. Performance-data input to the parametric synthesis program will be made on an individual basis for each propellant combination and set of engine design parameters for which

TABLE 27. PROPELLANT PROPERTIES AND SYSTEM EFFECTS

PROPELLANT PROPERTIES	TANKAGE	PRESSURIZATION	FEED SYSTEM
Density	Tank volume Ullage volume	Pressurant Weight	Line Sizes & Pressure Drop
Vapor Pressure	Tank Pressure Level Tank Volume (pressurant volume)	Pressurant Weight Pressurant Volume - (stored gas)	
Heat of Vaporization	Tank Volume (boil off) Tank Weight (Insulation)	Vent vs. non-vent Pressure Concept (store gas vs. evaporative system)	Component cool-down
Specific Heat	Tank Volume (boil-off) Tank Weight (heat sink vs. insulation)	Vent reqmts Heat exchanger weights Pressurant Weight (ullage collapse factor)	Weight (Insulation)
Liquid Range	Weight (insulation) Design (supports & penetration)	Pressurant choice (He, N_2) Pressurant weight (ullage collapse factor)	Weight (Insulation)

the propulsion weight synthesis program is run. Theoretical vacuum specific impulses for FLOX/CH_4 and OF_2/B_2H_6 propellant combinations as functions of mixture ratio, expansion ratio, and chamber pressure are shown in Figure 60. The theoretical performance values are based on adiabatic combustion at constant pressure, isentropic expansion of perfect gases, no friction, homogeneous mixing and one dimensional flow. The data illustrates the performance regimes associated with the pressure-fed space-storable systems. Appropriate efficiency factors relating to the combustion and expansion processes must be applied to predict deliverable performance.

Estimated delivered vacuum specific impulse for LO_2/LH_2 and LF_2/LH_2 propellant combinations are shown in Figure 61 as a function of the mixture ratio and expansion ratios for thrust levels of 8000 and 50,000 lbf. The data generated by Pratt & Whitney are for pump-fed engines employing an expander propellant feed cycle. The performance is based on advanced but realistic combustion and nozzle efficiencies.

Rocketdyne tripropellent engine vacuum impulse is shown in Figure 62 for a pump-fed engine with a staged combusion cycle and for a pressure-fed engine. Specific impulse is presented as a function of nozzle expansion ratio and percent hydrogen for a fluorine/lithium mixture ratio of 2.74, chamber pressures of 100, 500, 750 and 1000 lb/in^2, and a thrust level of 10,000 lbf. The pressure-fed system is indicated for chamber pressures of 100, 300, and 500 lb/in^2 only. The higher chamber pressure performance data are applicable to a pressure-fed engine; however, the tank pressures would be prohibitively high. Summary performance data (deliverable specific impulses) are presented in Section 6.1.1.5.

6.1.1.3 Engine Weight Data

The engine weight data that were received indicated that for the purposes of weight estimation the engine propellant combinations could be represented by the following four types:

Earth Storable	-	N_2O_4/MMH; N_2O_4/UDMH
Space Storable	-	OF_2/CH_4; FLOX/CH_4; OF_2/B_2H_6
Cryogens	-	LO_2LH_2; LF_2/LH_2
Tripropellant	-	$LF_2/L_i/LH_2$

The engine weight data displayed in this section are as received from the engine manufacturers in English units; the final scaling laws developed from this data are quoted in both the English and metrie system of units.

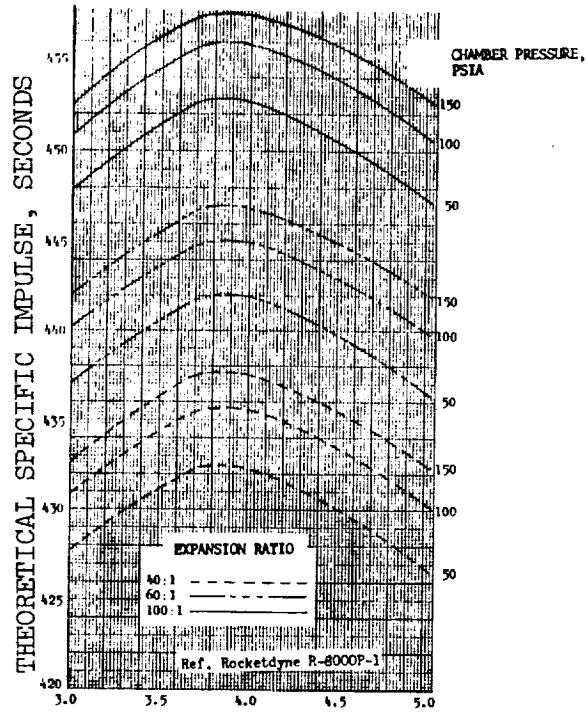

THEORETICAL VACUUM SPECIFIC IMPULSE VS
MIXTURE RATION FOR OF_2/H_2H_6

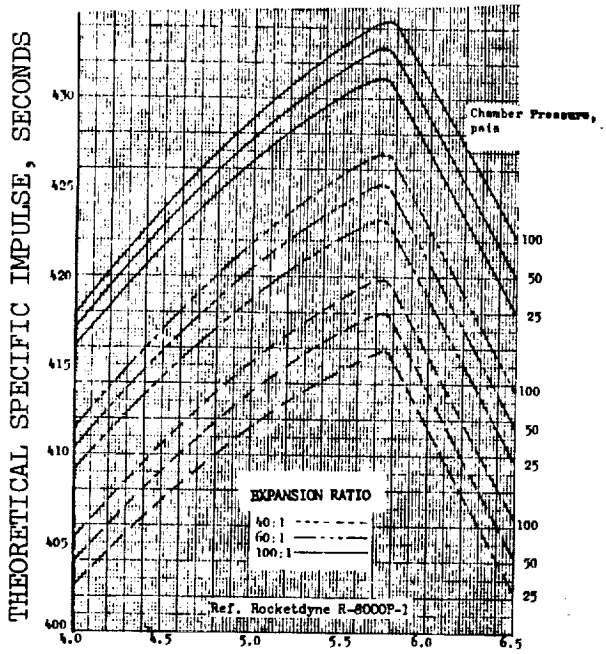

THEORETICAL VACUUM SPECIFIC IMPULSE VS
MIXTURE RATIO FOR FLOX $(0.826\text{-}0.174)/CH_4$

Figure 60 Theoretical Specific Impulse OF_2/B_2H_6 and Flox/CH_4

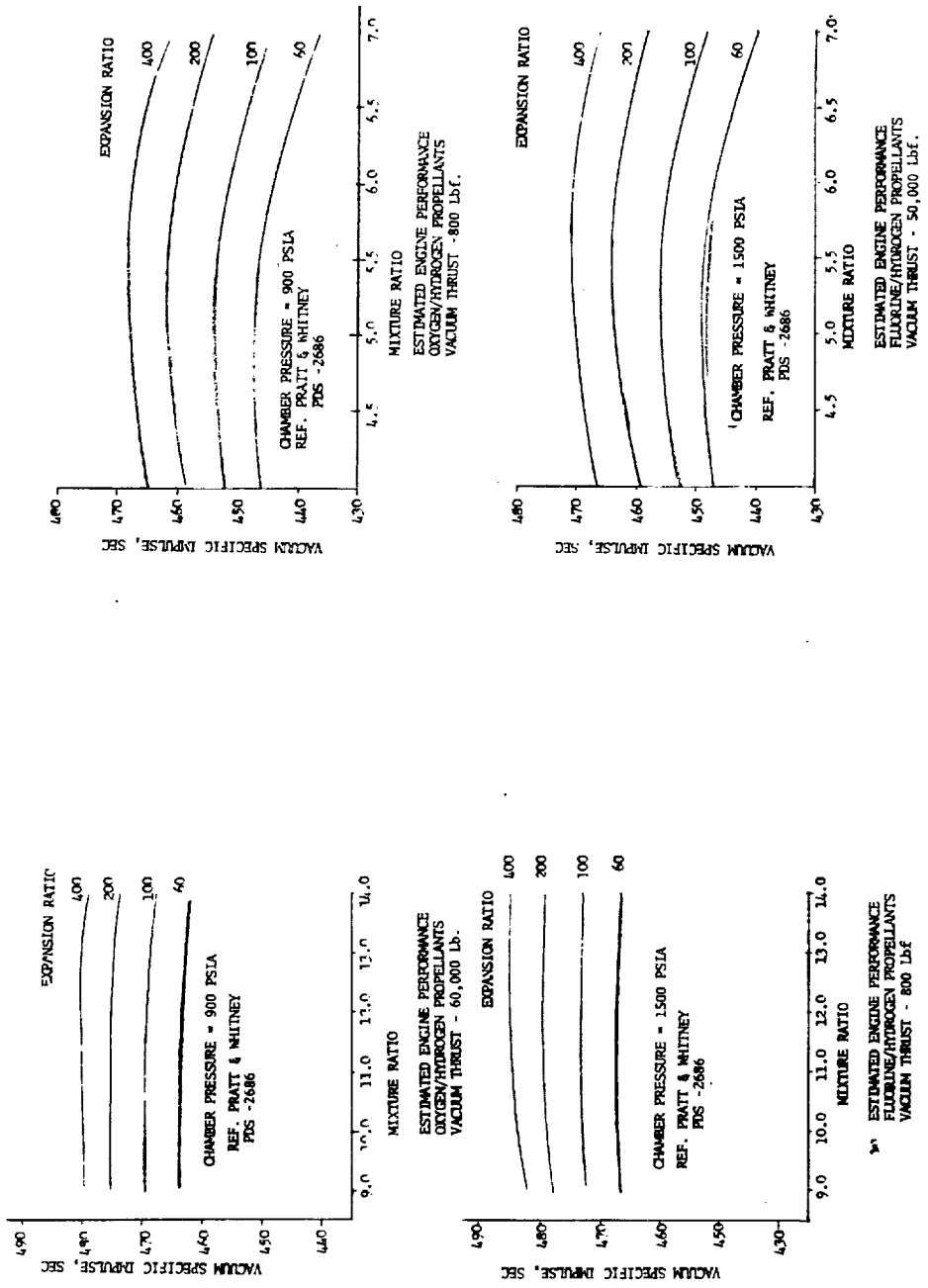

Figure 61. Vacuum Specific Impulse (LF_2/LH_2 and LO_2/LH_2)

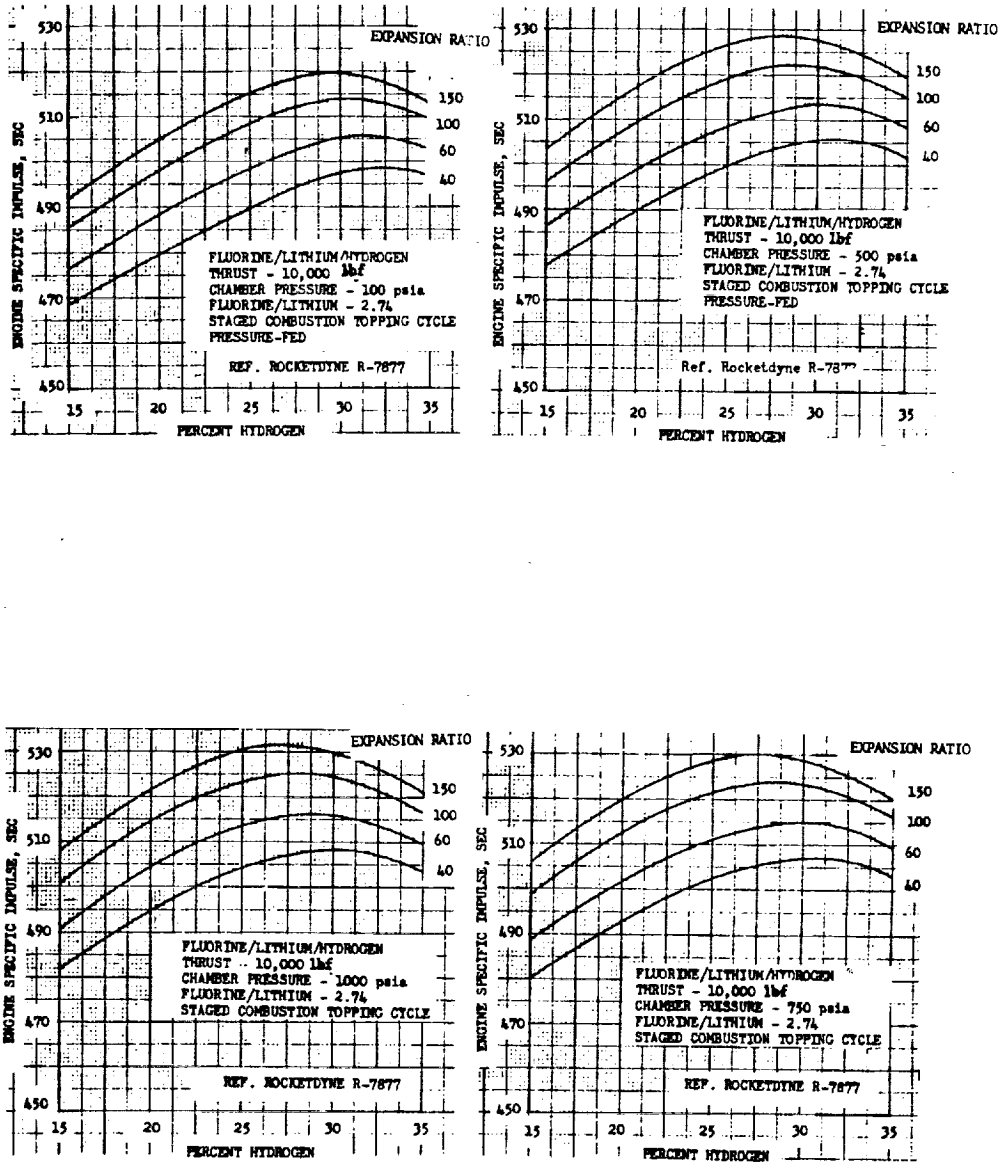

Figure 62. Delivered Specific Impulse (Tripropellant Engine)

Both the pump-fed and pressure-fed engine weights were estimated for fixed and two-position nozzles. The two-position nozzles are practical only for expansion ratio greater than 100 for which the reduced engine length will compensate for the additional engine system weight.

Pressure-fed engines with the lower thrust levels were considered to have ablative nozzles. Reference 31 indicates that the engine systems using halogen family oxidizers have been found to be more compatible with ablative nozzle construction of phenolic-impregnated carbon cloth or graphite fiber materials. Weight estimates for this chamber type may be computed by finding the appropriate thrust chamber assembly (TCA) weight for silica refrasil used for earth-and space-storable propellants and multiplying by a weight factor of 1.2 to compensate for density and char-rate differences.

The major design parameter reflected in the current weight-scaling laws for engine systems is limited to the thrust level. The thrust level and the engine-type are, in fact, but two of the important design parameters that influence the weight of an engine system. The screening and cataloging of the engine data have clearly indicated that other important parameters (chamber pressure and the expansion ratio) must be included. Both of these parameters have measurable effects on the parametric weight relationship of the engine systems. For engine systems of the ablative type, it is also recognized that the burning time plays an important part in weight scaling.

The major amount of unclassified information is pertinent to the smaller thrust levels for most of the engine systems. Information relating to engines that have thrusts in the range of 45360 kgf to 453600 kgf shows considerable variation in the weight data. This result is due primarily to major reliance on data for individual hardware designs and the lack of overall parametric scaling data. The engine systems were originally divided into several distinct components: engine nozzle, turbo machinery, combustion chamber, and thrust vector control. Unfortunately, detailed data relating to each of these identifiable systems are not available with any degree of consistency. It is further believed that, because of this lack of component information, the engine system should be described as a total subsystem. Any variation in the scaling laws due to combinations of component weight would be within acceptable noise levels anticipated for parametric scaling relationships.

The engine dry weight represented by the scaling laws is considered to include the following items.

Single-point thrust attachment

Turbo-pumps

Preburner assembly (where applicable)

Combustion chamber assembly

Expansion nozzle

Nozzle translating mechanisms (where applicable)

Controls, shut-off valves, and engine plumbing

The additional weight associated with the thrust vector control mechanism is quoted separately as a function of the engine thrust.

Weight data for the pressure-fed engines are based on the parametric data from Reference 31 for an ablative TCA and an ablative TCA with a radiation skirt. This latter concept is slightly lighter than the all-ablative nozzle. Figure 63 shows the weight variation with thrust level variation for the ablative nozzle with the radiation skirt and for an engine burn time of 100 seconds. A power series expression is used to represent the weight data and for the ablative engine the scaling law is

$$W_{ENG} = 0.1324 \; F^{0.853} \; P_c^{-0.757} \; \varepsilon^{0.24} \; ; \quad kg \qquad (74)$$

$$W_{ENG} = 1.11 \; F^{0.853} \; P_c^{-0.757} \; \varepsilon^{0.24} \; ; \quad lb$$

where

F = engine design thrust
P_c = engine design chamber pressure

For engine systems with longer than 100 seconds burn times, the engine weight will be modified by the longer burn time design requirements imposed on the ablative nozzle. The ablative thickness, which is a function of the char-rate and the burn time (t_b), is shown on Figure 64. A weight/burn-time modification factor is given by

$$(W)_{time} = \left(\frac{t_b}{100}\right)^{0.297} (W)_{100} \qquad (75)$$

and the weight-scaling relationship for the pressure-fed engines is

$$W_{ENG} = 0.0336 \; F^{0.853} \; P_c^{-0.757} \; \varepsilon^{0.24} \; t_b^{0.297} \; ; \quad kg \qquad (76)$$

$$W_{ENG} = 0.282 \; F^{0.853} \; P_c^{-0.757} \; \varepsilon^{0.24} \; t_b^{0.297} \; ; \quad lb$$

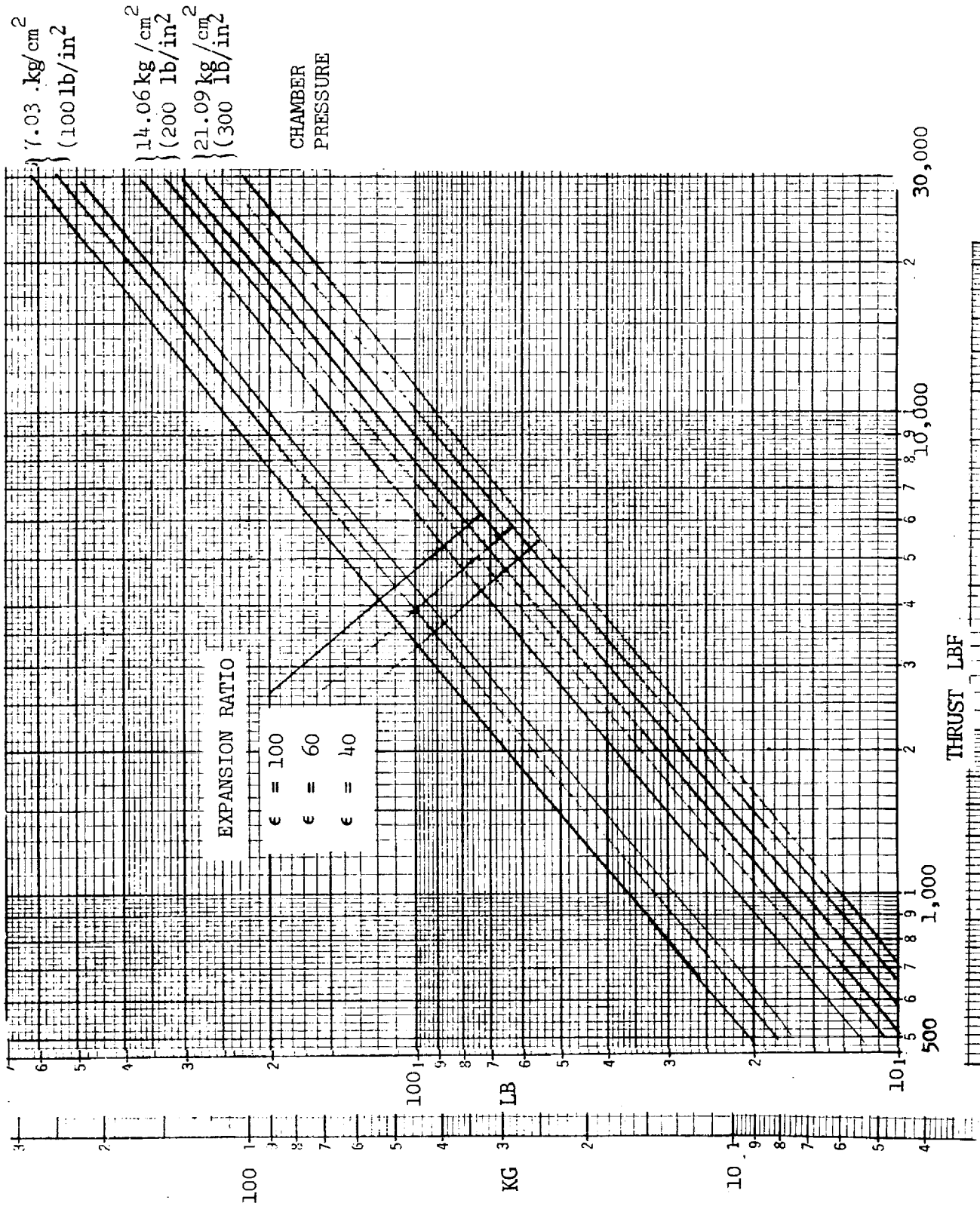

Figure 63 Parametric Weight for Ablative TCA With Radiative Skirt

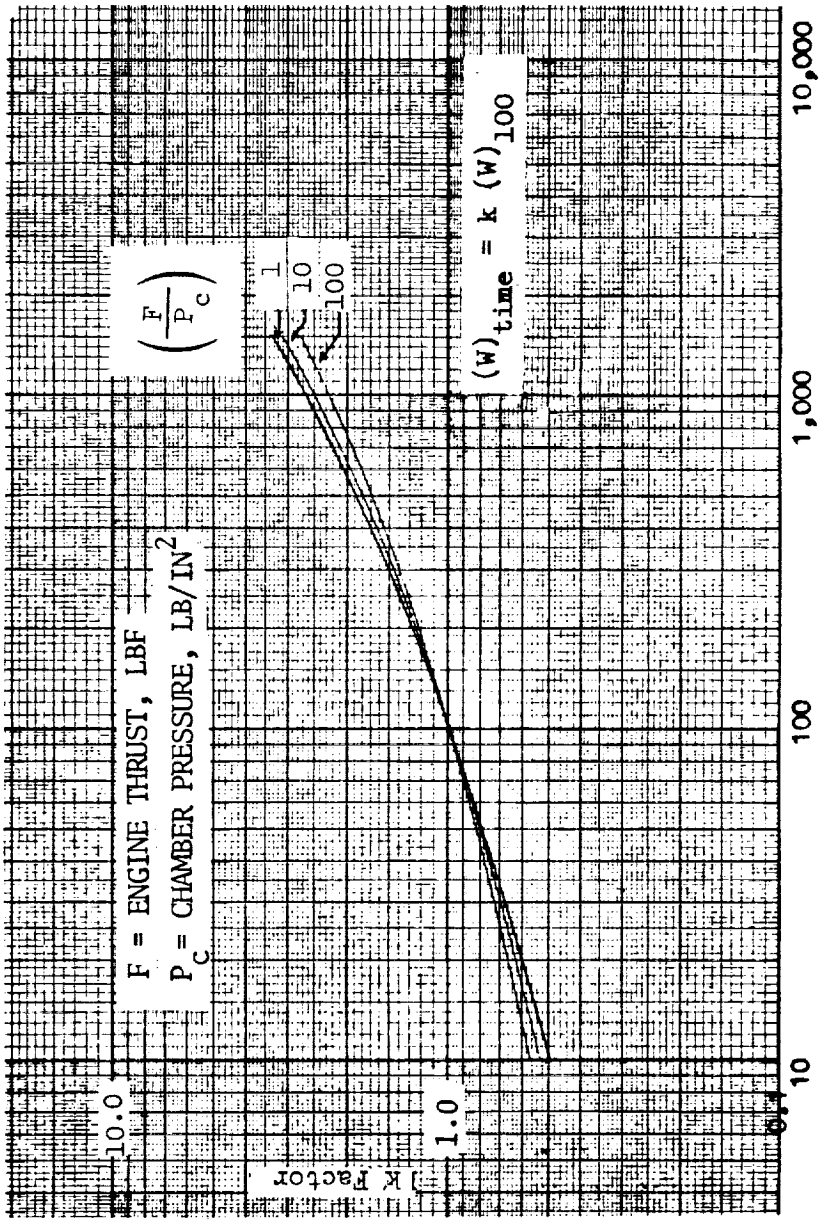

Figure 64. Effect of Burn Time on Weight of Thrust Chamber Assemblies With Ablative Nozzle.

The goodness of fit to the original weight data from Reference 31 is seen in Figure 65 which indicates maximum weight errors of 3 percent, well within acceptable limits for parametric weight estimation of engine systems. The ablative-nozzle-scaling law is compared in Figure 66 with several existing hardware engine systems listed in Table 28.

Table 28. Ablative Pressure-Fed Engines

Engine	F750L Apollo Subscale	Model 8258 Lunar Ascent	AJ10-138 Titon Transtage	SE10 Lunar Descent	AJ10-137 Apollo SPC
Thrust kgf (lbf)	1043 (2300)	1587 (3500)	3628 (8000)	4762 (10500)	9752 (21500)
Chamber Pressure kg/cm^2 (lb/in^2)	7.03 (100)	8.44 (120)	7.38 (105)	10.19 (145)	7.17 (102)
Expansion Ratio	40	40	40	53	62.5
Burn Time/ secs.	750	525	500	730	750
Weight kg (lb)	581 (128)	916 (202)	103 (227)	158 (350)	352 (777)

The most serious discrepancy appears to be the Lunar Ascent engine which is an early engine and was conservatively built to insure reliability.

The ablative pressure-fed engine weight can be reduced if the nozzle combines both ablation and radiation cooling. Radiation cooling is employed for the larger aft section of the nozzle to reduce the weight of the ablative material. Engine weight data for the ablative-radiation NTO/MMH pressure-fed system were obtained from Reference 31 and are presented in Figure 67. For the thrust levels above 4536 kgf (10000 lbf), the weight of engines with combined nozzle cooling is 50 percent or less than those with all-ablatively cooled nozzles.

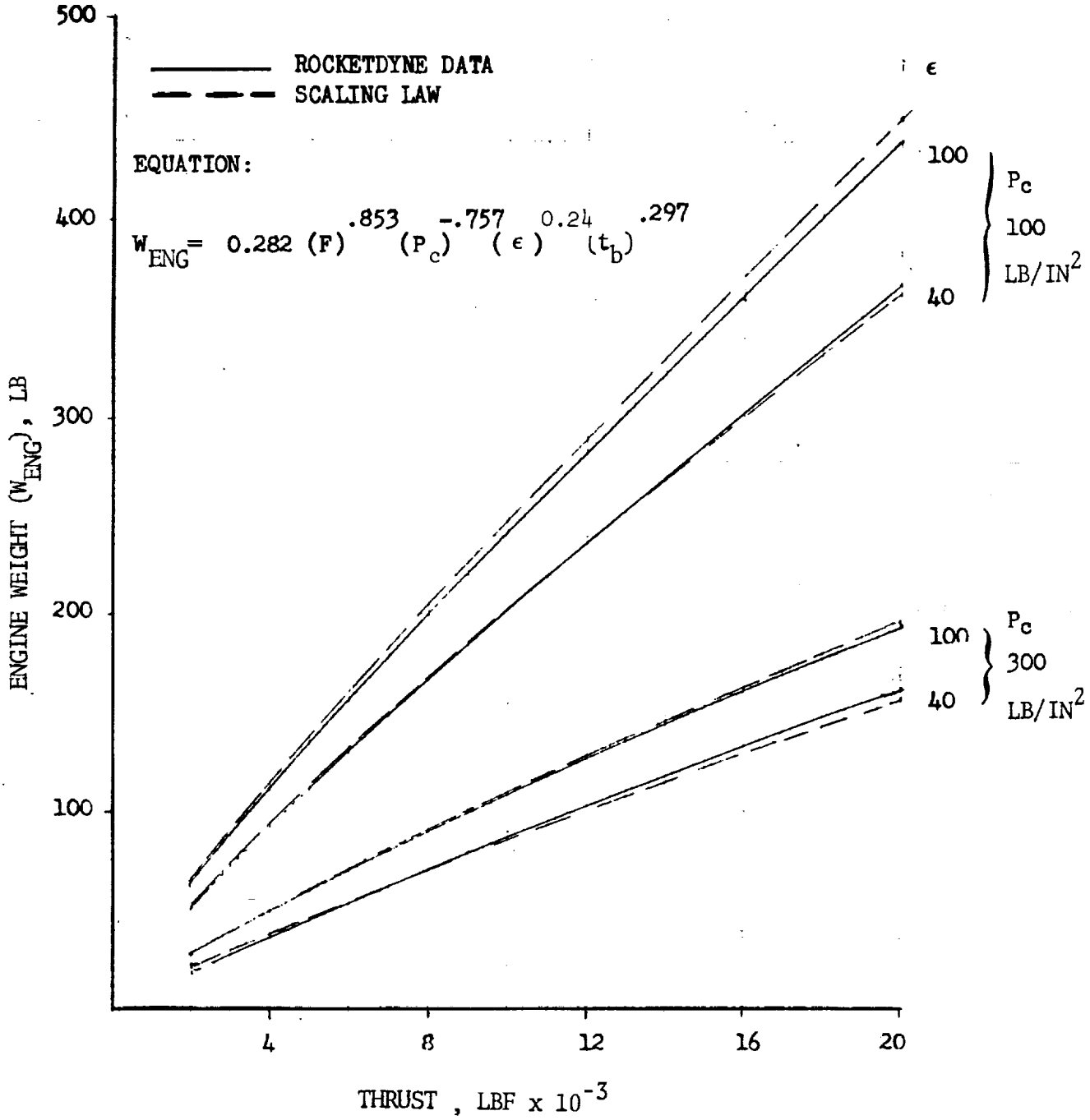

Figure 65. All-Ablative NTO/MMH Engine Weight Comparison (Pressure-Fed)

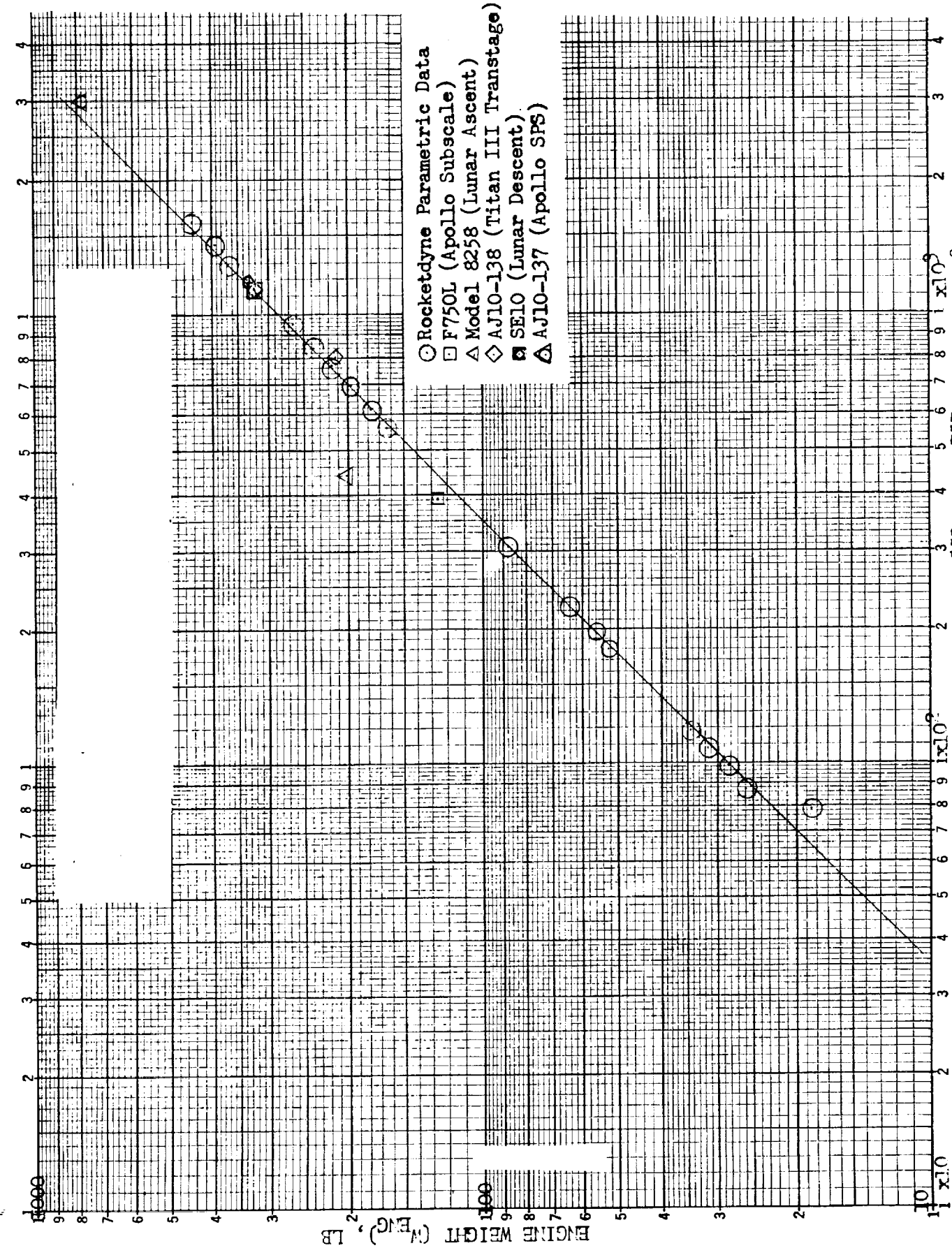

Figure 66. Ablative Pressure-Fed Engine Weight Parameter vs. Engine Weight

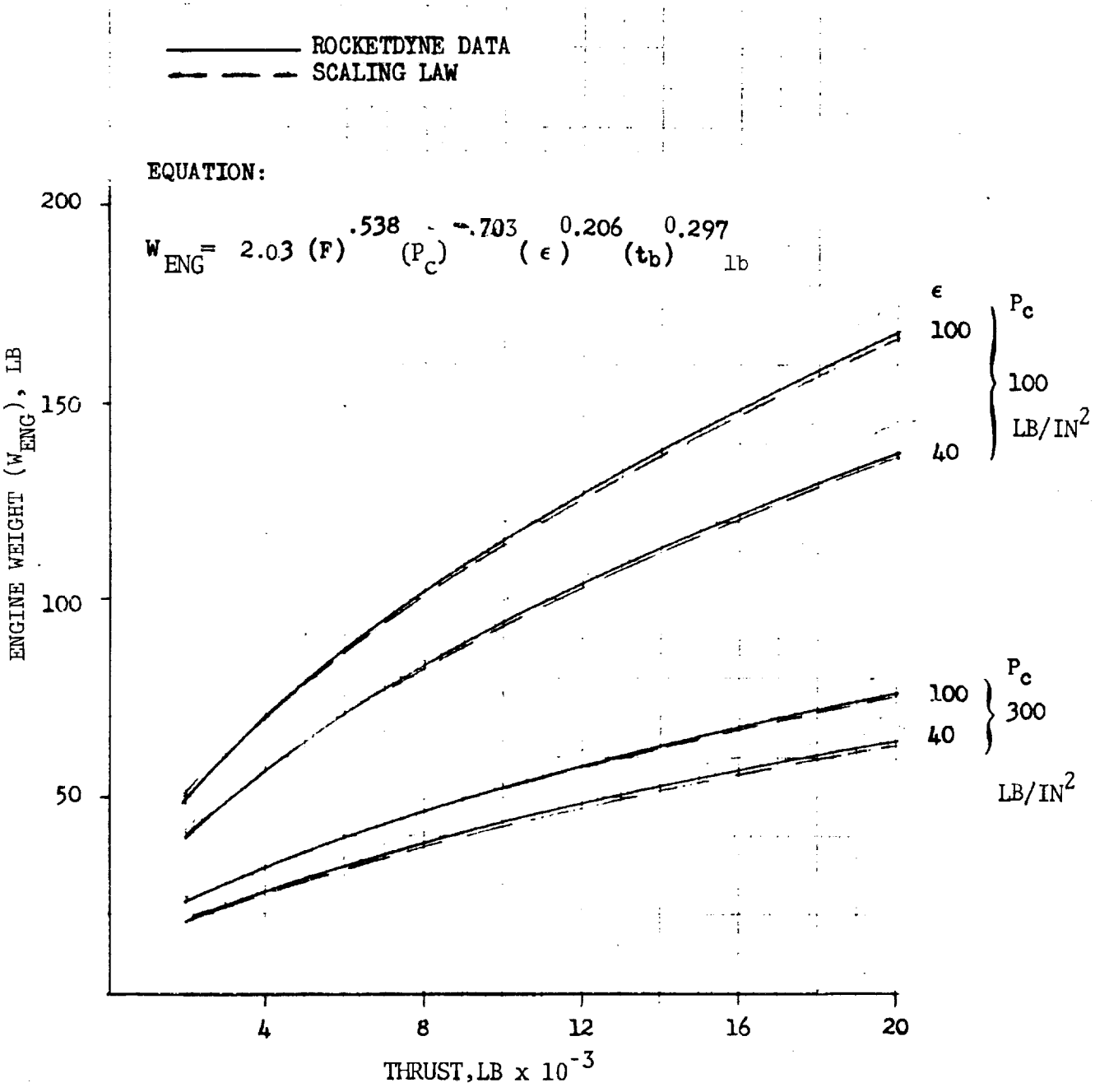

Figure 67. Ablative-Radiation NTO/MMH Engine Weight Comparison (Pressure-Fed)

A statistical reduction of this weight data provides a scaling law for the ablative/radiation pressure-fed engine.

$$W_{ENG} = 0.218 \; F^{0.538} \; P_c^{-.703} \; \varepsilon^{0.206} \; t_b^{0.297} \quad ; \; kg$$

$$W_{ENG} = 2.03 \; F^{0.538} \; P_c^{-.703} \; \varepsilon^{0.206} \; t_b^{0.297} \quad ; \; lb \qquad (71)$$

Pressure-fed TCA's could possibly have two-position nozzles for the higher thrust engines. Weight data for stowed nozzle pump-fed engines were obtained from References 1 and 2; the weight variation for the stowed-nozzle should be similar for the pressure-fed engines. The fixed nozzle weight equations were slightly modified for the two-position nozzle, and are:

All Ablative TCA (Pressure-Fed)

$$W_{ENG} = 0.037 \; F^{0.853} \; P_c^{-0.757} \; \varepsilon^{0.24} \; t_b^{0.297} \quad ; \; kg$$

$$W_{ENG} = 0.31 \; F^{0.853} \; P_c^{-0.757} \; \varepsilon^{0.24} \; t_b^{0.297} \quad ; \; lb \qquad (78)$$

Ablative TCA with Radiation Nozzle - (Pressure-Fed)

$$W_{ENG} = 0.24 \; F^{0.538} \; P_c^{-.703} \; \varepsilon^{0.206} \; t_b^{0.297} \quad ; \; kg$$

$$W_{ENG} = 2.23 \; F^{0.538} \; P_c^{-.703} \; \varepsilon^{0.206} \; t_b^{0.297} \quad ; \; lb \qquad (79)$$

Equations 78 and 79 will represent the weight-scaling relationships for the following propellant combinations:

Cryogens - LO_2/LH_2

Earth Storable - N_2O_4/MMH and N_2O_4/UDMH

The propellant combinations which have a halogen-family oxidizer have had their weights increased by 20 percent to account for the different ablative materials used, as suggested by Reference 31. This weight increase is considered to apply to

Cryogens - LF_2/LH_2

Space Storable - OF_2/CH_4; OF_2/B_2H_6; $FLOX/CH_4$

Engine design weights for the space storable pump-fed engines were obtained from References 1 and 2. The thrust/weight ratio as a function of the thrust level, Figure 68, shows that the T/W ratio is influenced by the chamber pressure, thrust level and expansion ratio. It was found that the thrust range of 453 to 22680 kgf (1000-50000 lbf) can be represented by

$$W_{ENG} = 0.3257 \; F^{.814} \; P_c^{-0.43} \; \varepsilon^{.05} \; ; \text{kg}$$

$$(453 \text{ kgf} < F < 22680 \text{ kgf}) \qquad (80)$$

$$W_{ENG} = 1.1819 \; F^{.814} \; P_c^{-0.43} \; \varepsilon^{.05} \; ; \text{lb}$$

$$(1000 \text{ lbf} < F < 5000 \text{ lbf})$$

and the higher-thrust engine weight is

$$W_{ENG} = 0.112 \; F^{.9269} \; P_c^{-.467} \; \epsilon^{.094} ; \text{ kg}$$

$$(22680 \text{ kgf} < F < 113400 \text{ kgf})$$

$$W_{ENG} = 0.41054 \; F^{.9269} \; P_c^{-.467} \; \epsilon^{.094} \; ; \text{lb}$$

$$(50000 \text{ lbf} < F < 250000 \text{ lbf})$$

The correlation between the scaling law and the original weight data from Aerojet-General produced an extremely good fit (maximum error less than 8 percent)as shown in Figure 68.

Weight data for the two-position nozzle engine were obtained from Reference 1 and the weight scaling laws were modified for the stowed nozzle engine as follows:

$$W_{ENG} = .3908 \; F^{0.814} \; P_c^{-0.43} \; \varepsilon^{0.05} ; \text{kg} \; (453 \text{ kgf} < F < 22680 \text{ kgf})$$

$$W_{ENG} = 1.30 \; F^{0.814} \; P_c^{-0.43} \; \varepsilon^{0.05} ; \text{lb} \; (1000 \text{ lbf} < F < 50000 \text{ lbf})$$

$$W_{ENG} = 0.117 \; F^{0.9269} \; P_c^{-0.407} \; \varepsilon^{0.094} ; \text{kg} \; (22680 \text{ kgf} < F < 113400 \text{ kgf}) \qquad (81)$$

$$W_{ENG} = 0.43 \; F^{0.9269} \; P_c^{-0.407} \; \varepsilon^{0.094} ; \text{lb} \; (50000 \text{ lbf} < F < 250000 \text{ lbf})$$

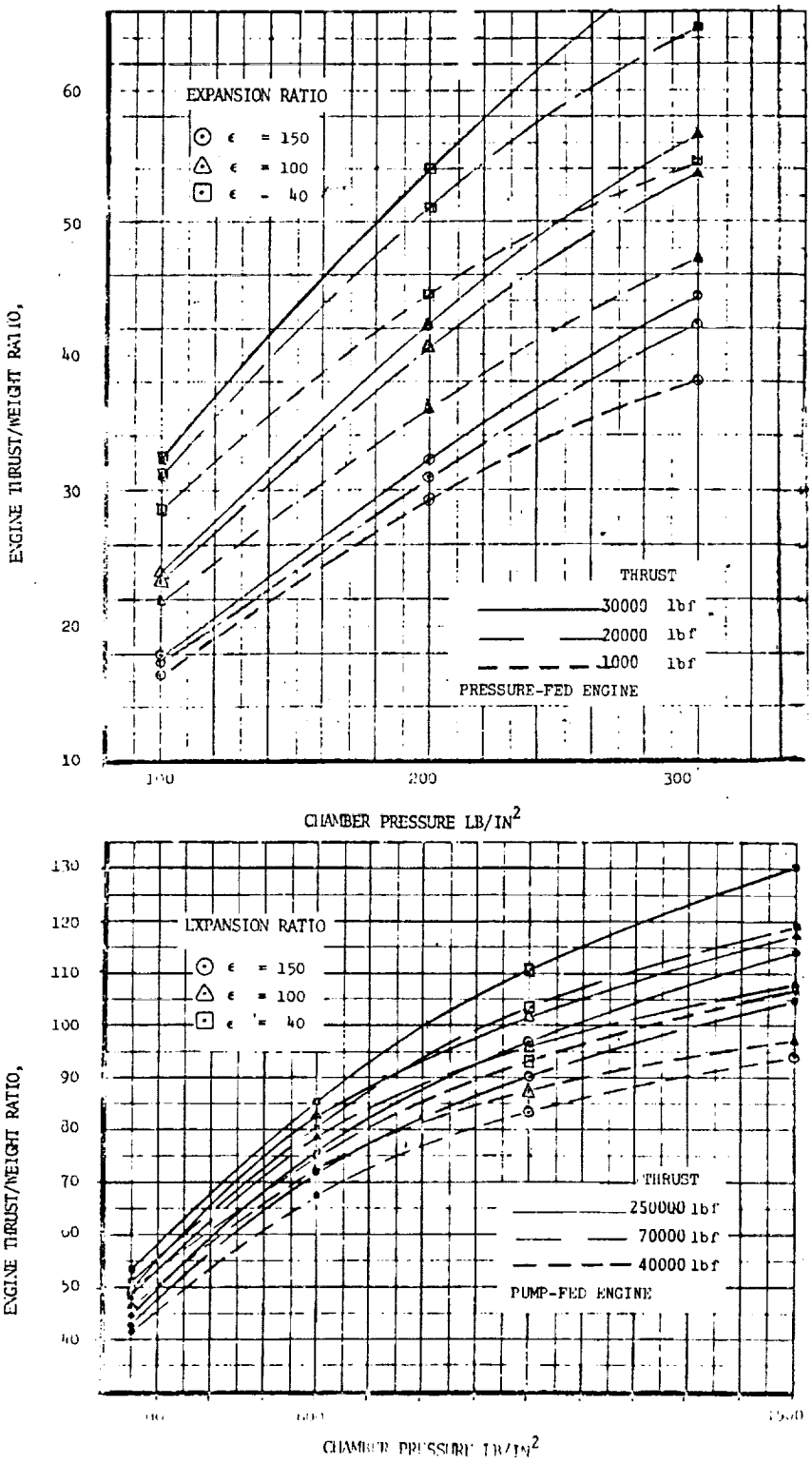

Figure 68. Engine Thrust/Weight Data - Flox/Methane

The oxygen-difluoride/diborane and earth-storable propellant combinations have not been considered for the pump-fed engine system and are reserved for the lower-thrust engines which are pressure fed.

The cryogen and tripropellant engine systems' weight data are reduced to a series of scaling laws that are not of the exponential form. The scaling laws are specially tailored to match the parametric data.

Reference 38 supplied the weight data for the LO_2/LH_2 and LF_2/LH_2 engine combinations and showed that there were no noticeable weight changes between the two different cryogenic propellant combinations. Figure 69 shows weight data for engines using cryogenic propellants.

Fixed Nozzle - Pump-Fed

$$W_{ENG} = 2.268 + 0.0183\,F + 1.7575 \times 10^{-6}\left(\frac{F\varepsilon^2}{P_c}\right);\ kg \quad (454\ kgf < F < 3629\ kgf)$$

$$W_{ENG} = 5.0 + 0.0183\,F + 2.5 \times 10^{-5}\left(\frac{F\varepsilon^2}{P_c}\right);\ lb \quad (1000\ lbf < F < 8000\ lbf)$$

$$W_{ENG} = 36.3 + 0.0105\,F + 1.7575 \times 10^{-6}\left(\frac{F\varepsilon^2}{P_c}\right);\ kg \quad (3629\ kg_f < F < 13608\ kgf) \qquad (82)$$

$$W_{ENG} = 80 + 0.0105\,F + 2.5 \times 10^{-5}\left(\frac{F\varepsilon^2}{P_c}\right);\ lb \quad (8000\ lbf < F < 30000\ lbf)$$

$$W_{ENG} = 49.9 + 0.00966F + 1.7575 \times 10^{-6}\left(\frac{F\varepsilon^2}{P_c}\right);kg \quad (13608\ kgf < F < 113398\ kgf)$$

$$W_{ENG} = 110 + 0.00966F + 2.5 \times 10^{-5}\left(\frac{F\varepsilon^2}{P_c}\right);lb \quad (30{,}000\ lbf < F < 250000\ lbf)$$

The high pressure 210 kg/cm^2 (3000 lb/in^2))pump-fed cryogen engine system is based upon Pratt & Whitney parametric performance data for the space shuttle engines, Figure 70. The scaling law derived is applicable to the thrust ranges shown below

$$W_{ENG} = 454 + 2.5\,\varepsilon + \frac{(1.065 + 0.002\varepsilon)}{P_c} 10^{-6} F^{1.5};kg \quad (90000\ kgf < F < 340000\ kg_f)$$

$$W_{ENG} = 1000 + 2.5\,\varepsilon + \frac{(1.02 + 0.002\varepsilon)10^{-5}}{P_c} F^{1.5};\ lb \quad (200000\ lb_f < F < 750000\ lb_f) \qquad (83)$$

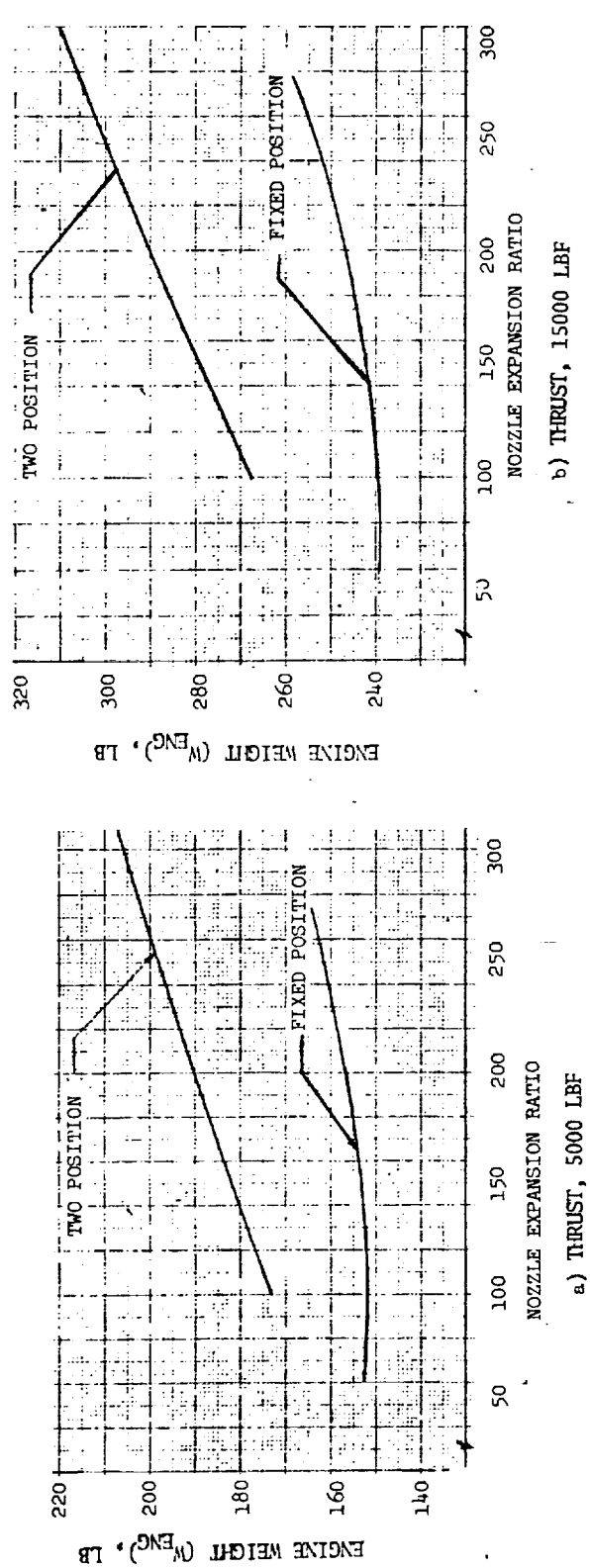

Figure 69. Cryogen Engine Weight (Fixed & Two-Position Nozzles)

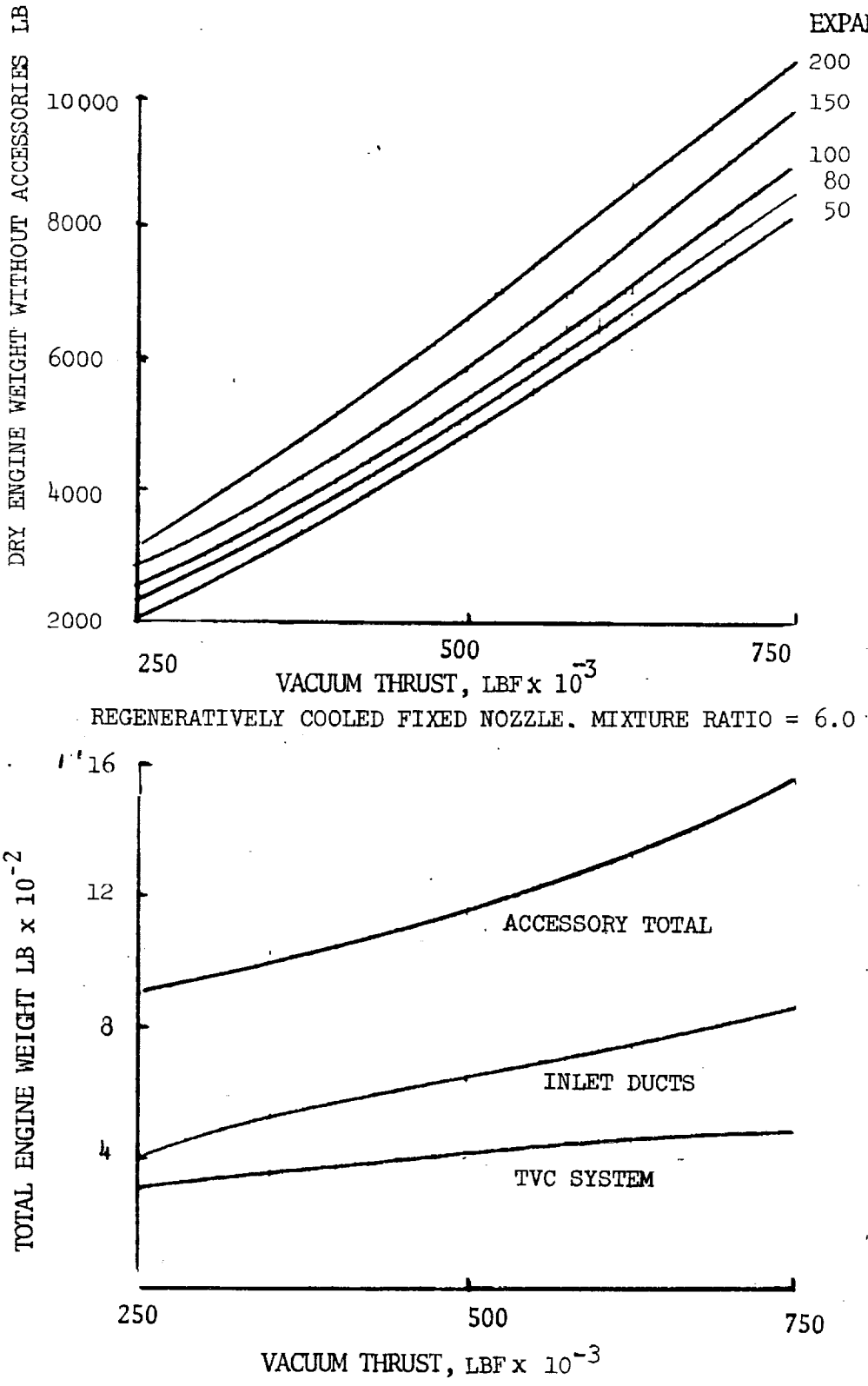

Figure 70. Space Shuttle Rocket Engine Parametric Weight Data

The data supplied with the high-pressure engine included additional weights to account for the thrust-vector control (TVC) system whose prime function is to gimbal the engine system and thus deflect the thrust vector. It appears logical that the TVC weight would be proportional to the reaction force (engine thrust). A TVC-weight-scaling law will be applicable to all types of engines

$$W_{TVC} = 0.002209\ F \quad ; kg \quad (F > 13600\ kgf)$$

$$W_{TVC} = 0.002209\ F \quad ; lb \quad (F > 30000\ lbf) \qquad (84)$$

$$W_{TVC} = 22.7 + 0.000542\ F \quad ; kg \quad (F \leq 13600\ kgf)$$

$$W_{TVC} = 50 + 0.000542\ F \quad ; lb \quad (F \leq 30000\ lbf)$$

The tripropellant engine was considered to be sufficiently different from a weight aspect that separate scaling relationships were developed for both the pressure-fed and pump-fed design. Figure 71 shows the weight data variation with pressure; these data were obtained from Reference 22. For the area of interest in the pressure range of 7 kg/cm^2 to 35 kg/cm^2 (100 lb/in^2 to 500 lb/in^2) an appropriate scaling law is

$$W_{ENG} = 9.07 + \frac{0.00161\ F^{1.22}\ \varepsilon^{0.5}}{P_c^{0.7}} \quad ; kg$$

$$W_{ENG} = 20 + \frac{0.008672\ F^{1.22}\ \varepsilon^{0.5}}{P_c^{0.7}} \quad ; lb \qquad (85)$$

For the pump-fed engine system, an increase in chamber pressure produces both a reduction in thrust chamber weight and an increase in the turbo machinery weight. At low chamber pressures, the thrust chamber is the dominant component, and an increase in chamber pressure results in a reduced system weight, Figure 72. As the chamber pressure is further increased, the turbo machinery becomes the dominant component and the system weight increases. The minimum weight chamber pressure is a function of the relative weights of the thrust chamber and turbo machinery. The optimum thrust/weight ratios for the staged combustion topping cycle system are shown in Figure 73. These ratios occur at chamber pressures ranging from 25 kg/cm^2 to 35 kg/cm^2 (350 lb/in^2 to 500 lb/in^2) and affect the delivered specific impulse by less than 4 seconds (0.8 percent).

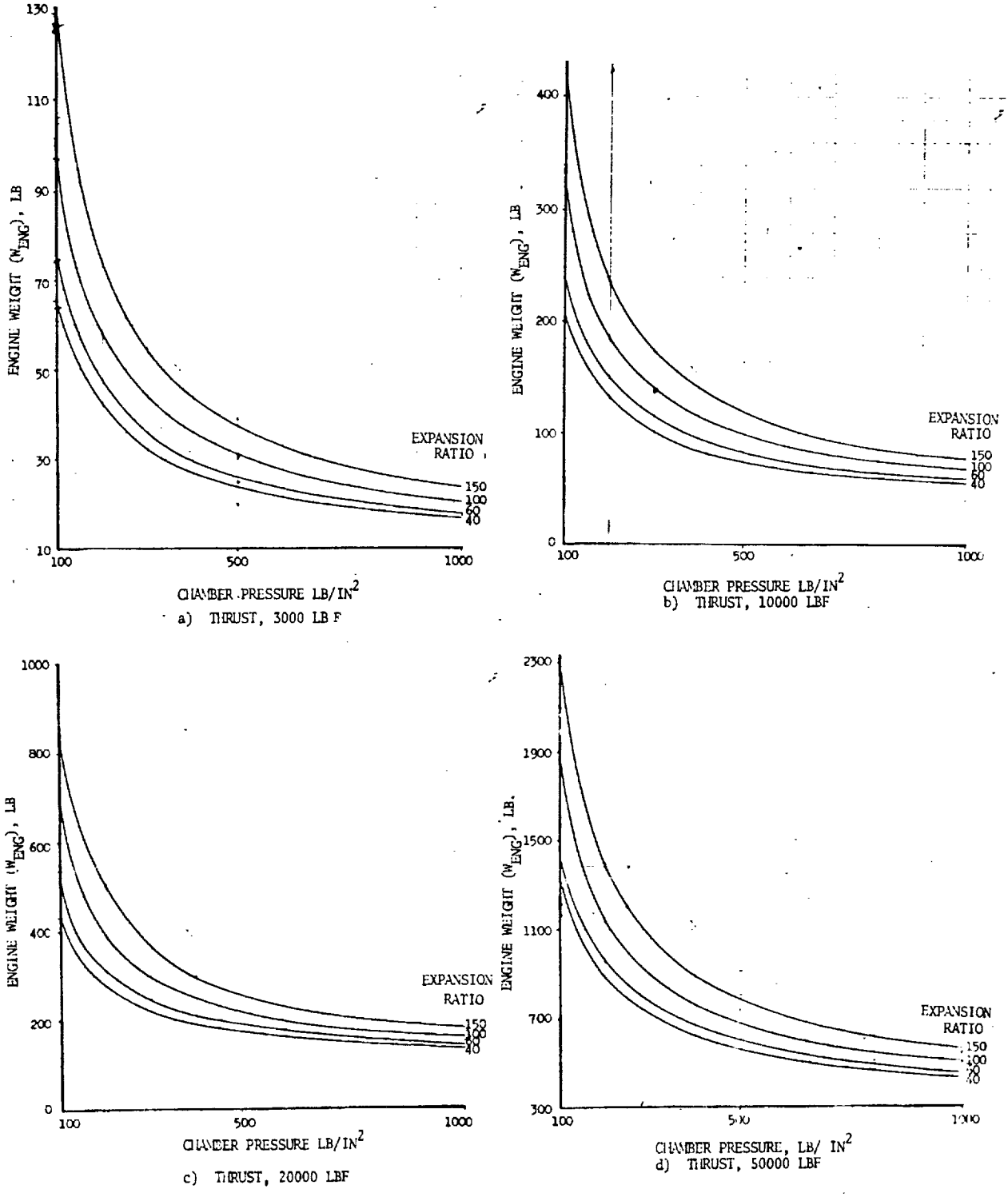

Figure 71. Tripropellant Engine Weight (Pressure-Fed)

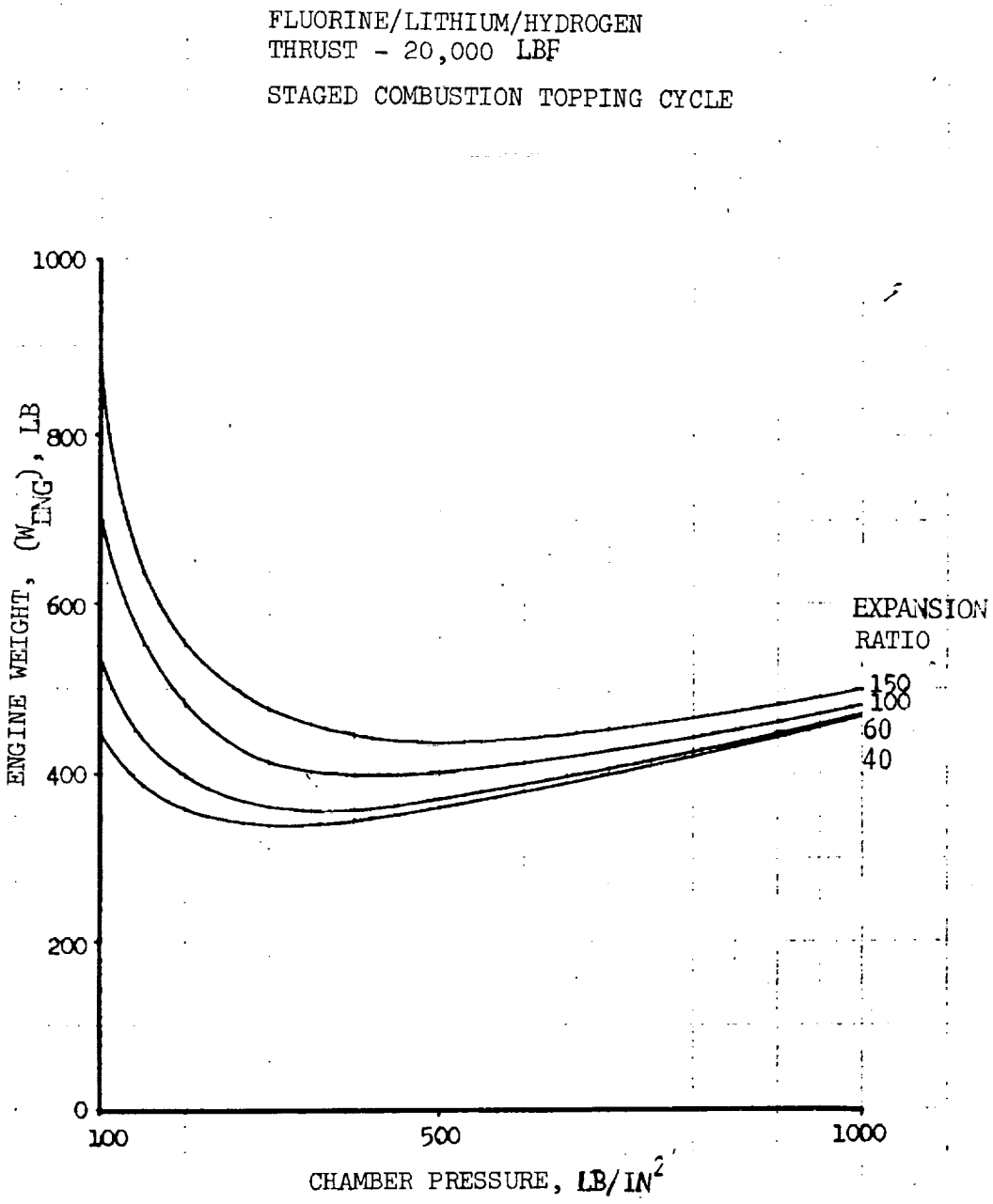

Figure 72. Chamber Pressure for Minimum Engine Weight (Tripropellants)

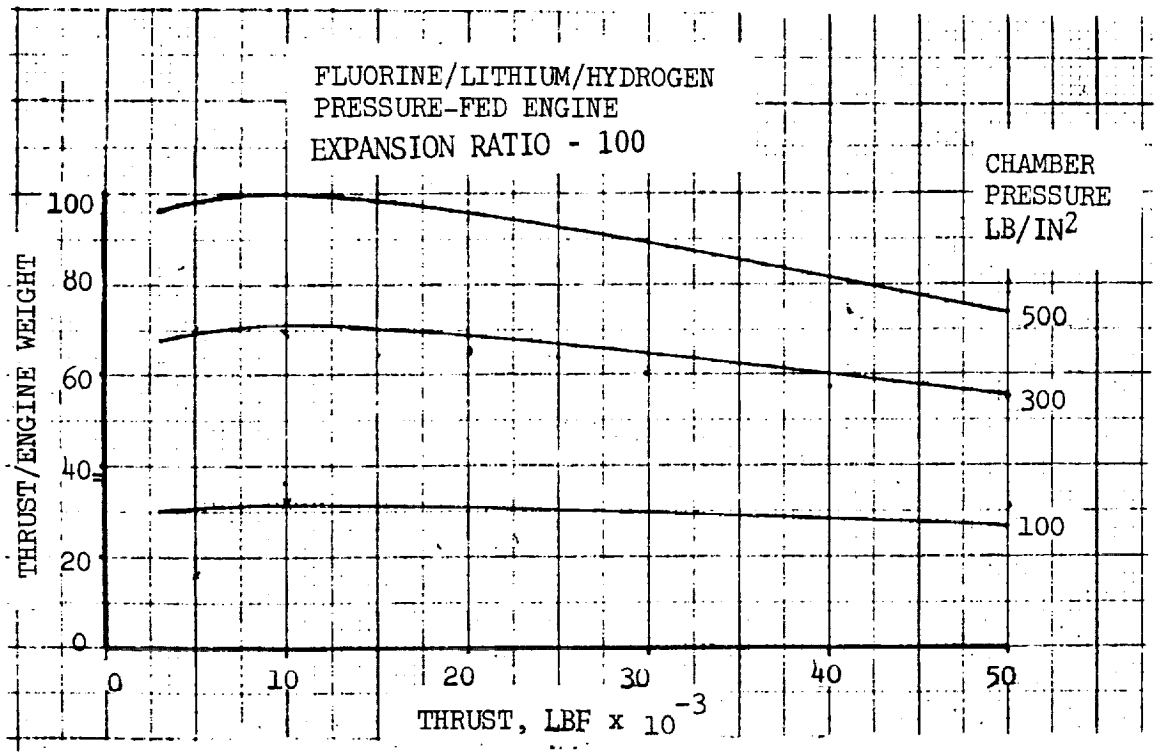

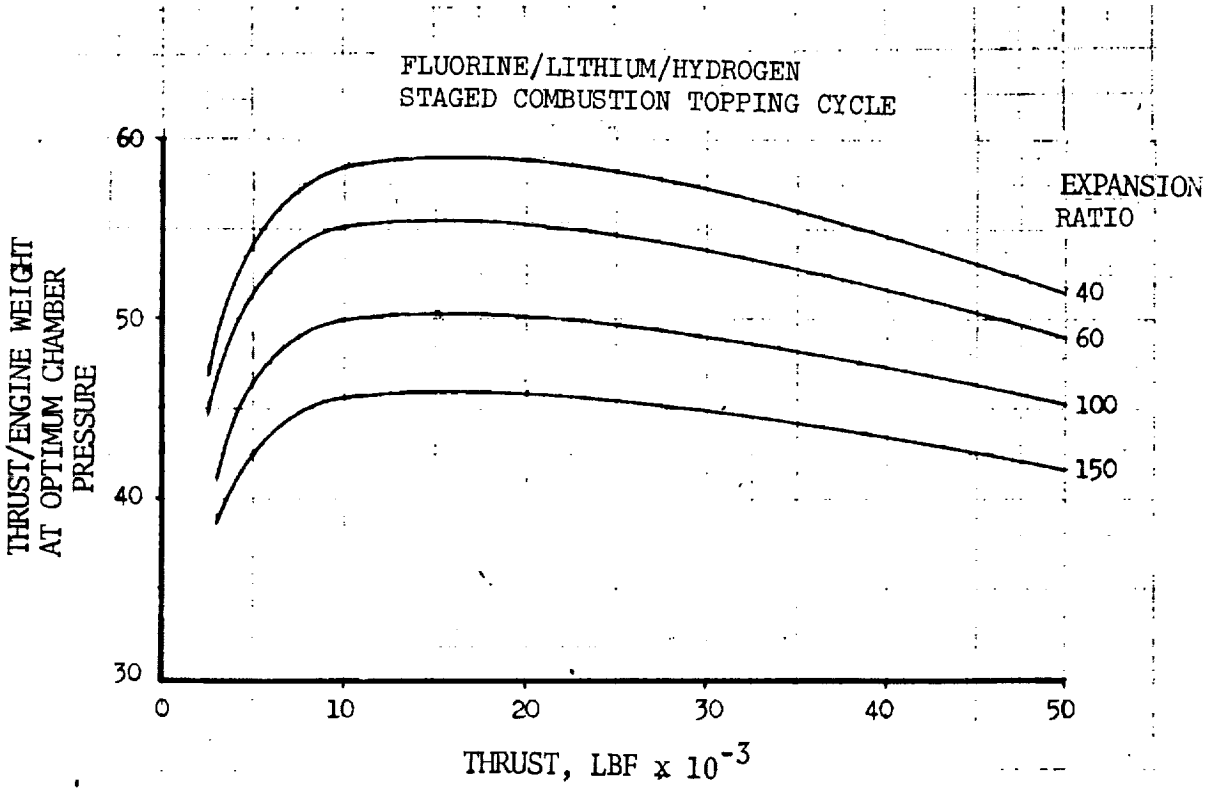

Figure 73. Thrust/Weight for Tripropellant Engines

6.1.1.4 Engine Dimensional Data

The stage inert mass is influenced by the engine overall length as well as the engine weight. Engines with larger expansion ratios have higher specific impulses and performance but their increased length results in a heavier interstage structure to enclose the engine system. The interstage length can be decreased by having a two-position nozzle with a heavier TCA. There is a trade-off between the weight reduction of the interstage and weight increase of the TCA. The optimum combination to maximize stage performance will depend on the stage size and characteristics, and the mission requirements.

Two approaches are considered for deriving the engine-sizing equations. One is similar to that followed in the derivation of engine weight scaling equations; namely, curve fitting of parametric and actual engine geometry data (Figure 74). The engine design parameters used in this approach are chamber pressure, nozzle expansion ratio, and engine thrust.

The second approach is based on the following engine combustion-chamber and nozzle design parameters for determining the engine geometry:

Internal Volume of Chamber (V_c)

Nozzle expansion ratio (ε)

Contraction ratio (C_R)

Characteristic chamber length (L^*)

Nozzle half angle (θ)

Percent equivalent to conical nozzle length (α)

The nozzle throat area (A_t) is determined from the thrust coefficient, chamber pressure, and engine thrust by:

$$A_t = \frac{F}{P_c C_F}$$

where

F = thrust

P_c = chamber pressure

C_F = thrust coefficient

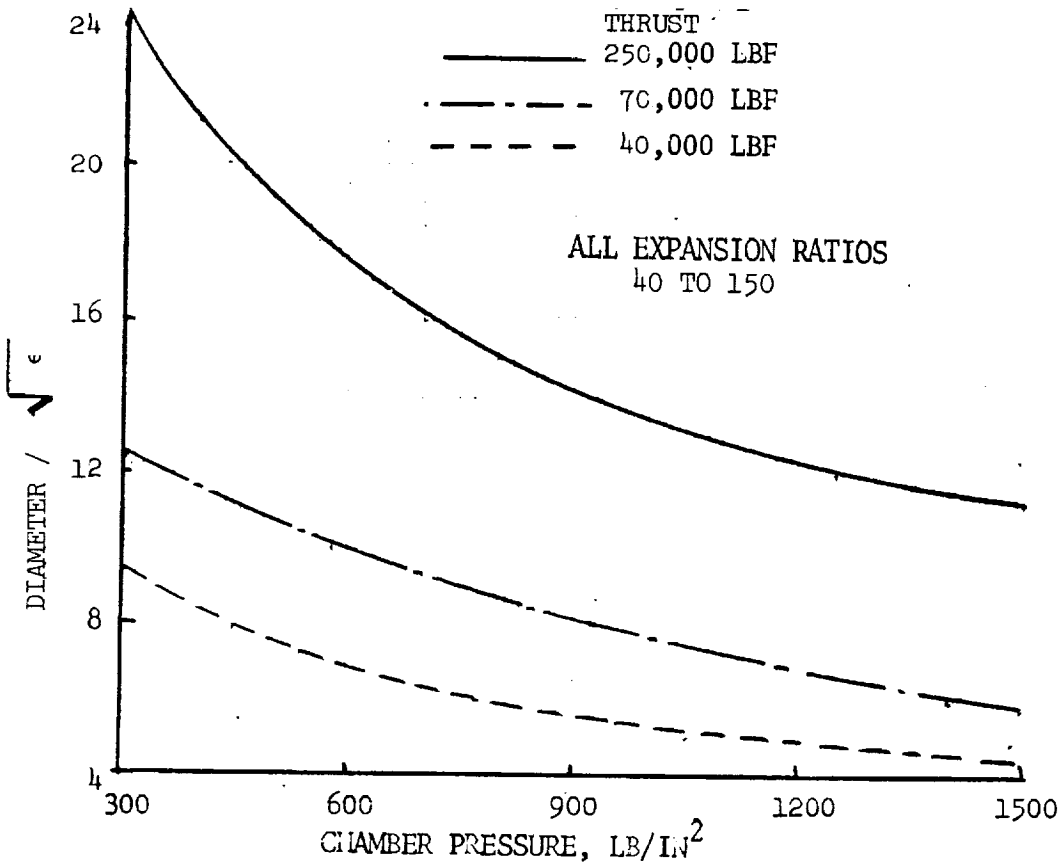

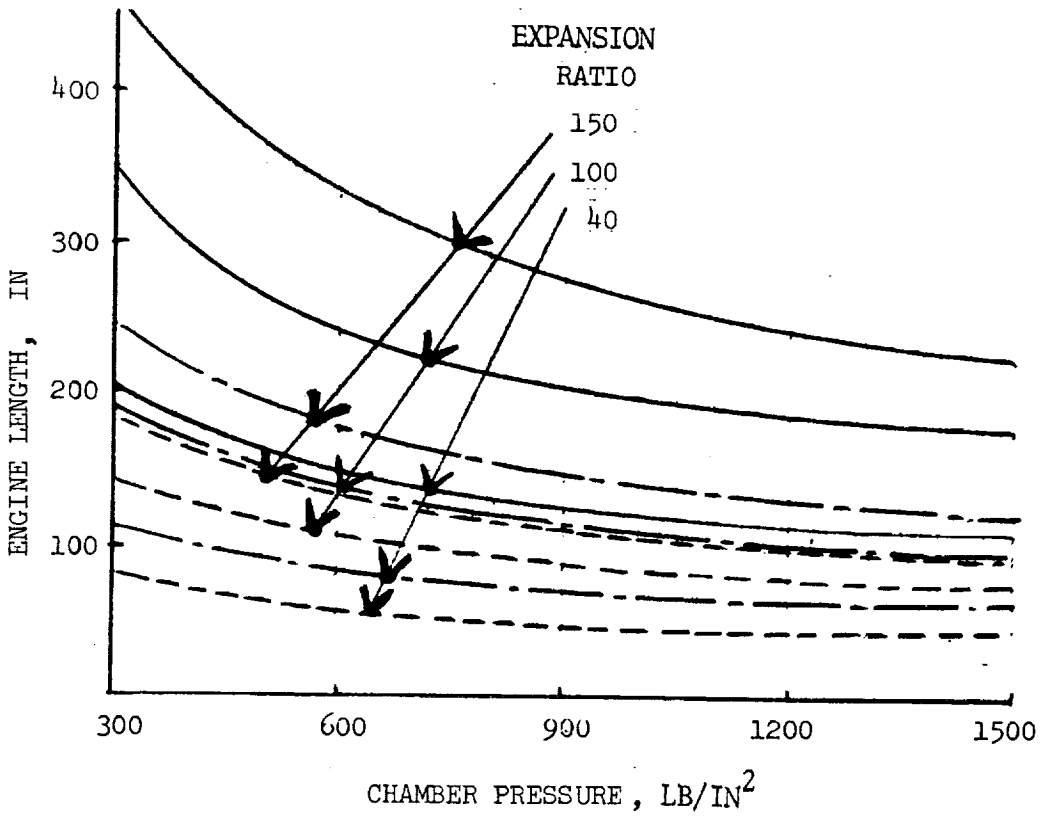

Figure 74. Engine Diameter & Length (Space Storable Propellants)

The thrust coefficient is based on the expansion ratio, specific heat, engine pressure ratio, and appropriate thrust-coefficient efficiency.

The characteristic chamber length and contraction ratio can be approximated for specific ranges of engine chamber pressures and propellant combinations based on past and current design practices, which are fairly consistent for specific classes of engines throughout the industry.

$$L^* = V_c/A_t$$

Typical values of L* range from 40 to 50 for a pump-fed earth storable engine operating at a chamber pressure of 800 lb/in^2 to a L* of 10 to 15 for a pump-fed space-storable engine for a chamber pressure of 1500 lb/in^2.

Nozzle half-angle is typically 15 degrees, the most commonly used percent equivalent conical nozzle length for 80-percent bell engines.

The application of the foregoing definitions to the nozzle and combustion chamber geometries are as follows:

Nozzle throat radius

$$R_c = \left(\frac{F}{C_F \pi P_c}\right)^{1/2}$$

Exit diameter

$$D_E = 2\varepsilon^{1/2} R_c$$

Nozzle length

$$L_n = \alpha R_c (\varepsilon^{1/2} - 1) / \tan \theta$$

Chamber length

$$L_c = K_1 L^*/C_R$$

K_1 = factor to account for chamber convergent section

The overall TCA length can be represented as

$$L_{Eng} = C_1 + C_2 \left(\frac{F}{P_c}\right)^{1/2} (\varepsilon^{1/2} - 1)$$

where C_1 and C_2 are determined in this study from the engine length data obtained from References 1, 2, 28, 29, 31 and 38.

Diameter data from Reference 2 and shown in Figure 74 indicates that for large engines with expansion ratios suitable for space propulsion ($\varepsilon > 50$), the engine diameter is determined by the exit diameter of the nozzle and can be represented by

$$D_{ENG} = 0.815\left(\frac{F\varepsilon}{P_c}\right)^{1/2} \quad \text{cm ; in} \tag{86}$$

and will apply to all pump-fed engine systems. The diameter should be increased slightly for the lower thrust pressure-fed systems to

$$D_{ENG} = 0.86\left(\frac{F\varepsilon}{P_c}\right)^{1/2} \quad \text{cm. ; in}$$

A design nomograph for engine length (Reference 31) is shown in Figure 75 and the appropriate derived relationship from this figure is used for the pressure-fed engines with a fixed nozzle

$$L_{ENG} = 102 + 1.05\left(\frac{F}{P_c}\right)^{1/2}(\varepsilon^{1/2} - 1) \quad ; \text{ cm} \quad (F \geq 4536 \text{ kgf})$$

$$L_{ENG} = 40 + 1.05\left(\frac{F}{P_c}\right)^{1/2}(\varepsilon^{1/2} - 1) \quad ; \text{ in} \quad (F \geq 100000 \text{ lbf})$$

$$L_{ENG} = 12.7 + 1.45\left(\frac{F}{P_c}\right)^{1/2}(\varepsilon^{1/2} - 1) \quad ; \text{ cm} \quad (F < 4536 \text{ kgf}) \tag{87}$$

$$L_{ENG} = 5 + 1.45\left(\frac{F}{P_c}\right)^{1/2}(\varepsilon^{1/2} - 1) \quad ; \text{ in} \quad (F < 10000 \text{ lbf})$$

The engine length can be reduced with the two-positioned nozzle; the lengths of the stowed nozzle-engine were obtained from References 1 and 38. Figure 76 shows the length of the LO_2/LH_2 engine with both fixed- and two-position nozzle. The latter is shown for both the stowed and extended positions. The stowed length remains constant at expansion ratios less than 150.

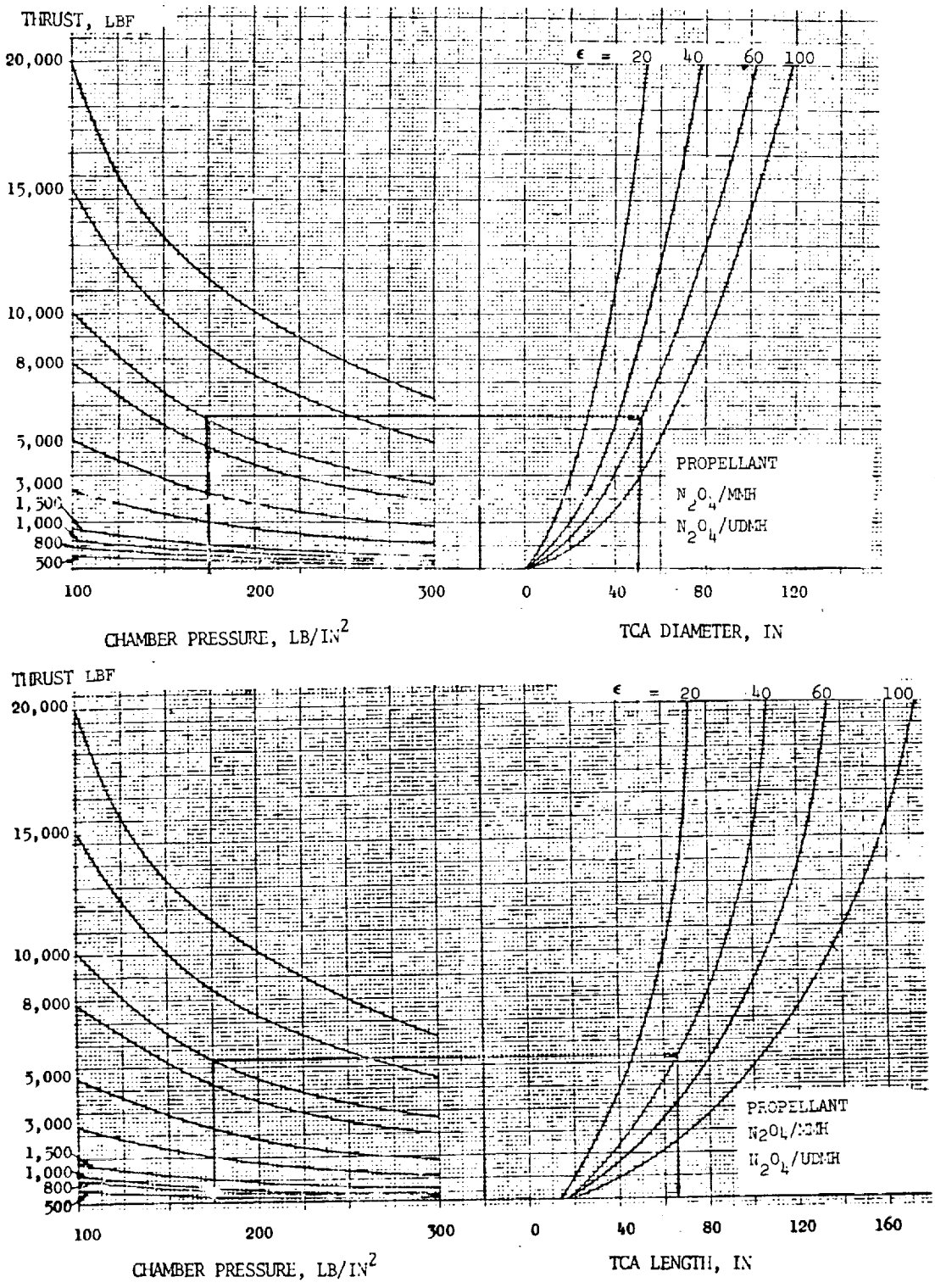

Figure 75. Thrust Chamber Assembly Diameter and Length for Pressure-Fed Earth Storable Engine Systems (Fixed Nozzle)

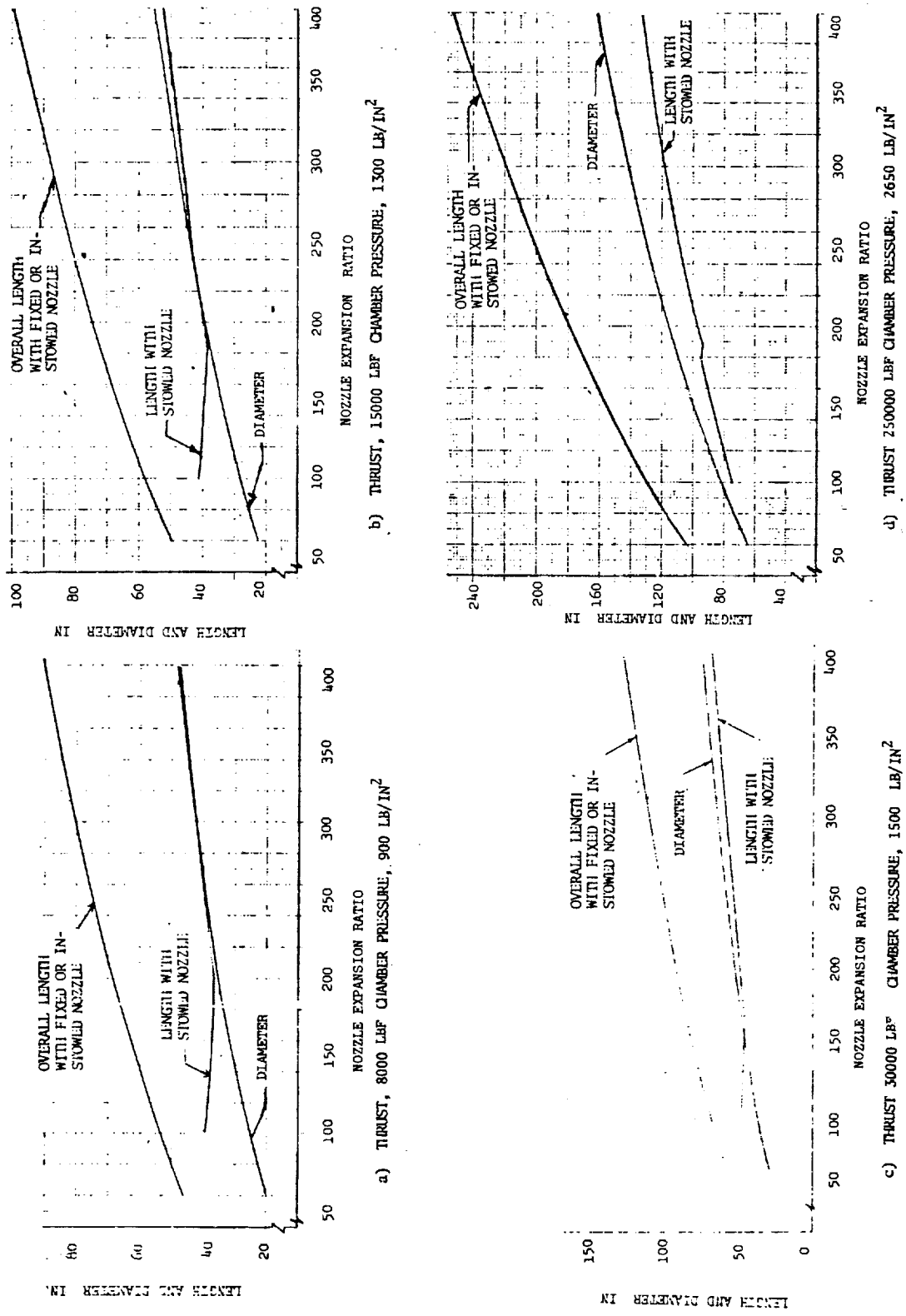

Figure 76. Cryogen Engine Length and Diameter for Fixed and Stowed Nozzles

Engine length with stowed nozzle ($\varepsilon \geq 150$)

$$L_{ENG} = 102 + 0.53\left(\frac{F}{P_c}\right)^{1/2} \left(\varepsilon^{1/2} - 1\right) \quad ; \text{ cm} \quad (F > 4536 \text{ kgf})$$

$$L_{ENG} = 40 + 0.53\left(\frac{F}{P_c}\right)^{1/2} \left(\varepsilon^{1/2} - 1\right) \quad ; \text{ in} \quad (F > 10000 \text{ lbf}) \qquad (88)$$

$$L_{ENG} = 12.7 + 0.73\left(\frac{F}{P_c}\right)^{1/2} \left(\varepsilon^{1/2} - 1\right) \quad ; \text{ cm} \quad (F < 4536 \text{ kgf})$$

$$L_{ENG} = 5 + 0.73\left(\frac{F}{P_c}\right)^{1/2} \left(\varepsilon^{1/2} - 1\right) \quad ; \text{ in} \quad (F < 10000 \text{ lbf})$$

Length data for the tripropellant engine, Reference 22, are shown in Figure 77. The form of scaling law is modified slightly to agree with the data as follows:

Tripropellant ($LF_2/LLi/LH_2$) Engine Length

$$L_{ENG} = 2.31\left(\frac{F}{P_c}\right)^{1/2} \varepsilon^{0.4} \quad \text{cm (in)} \qquad (89)$$

6.1.1.5 Engine Performance

The engine performance varies with the basic engine parameters (thrust, chamber pressure and expansion ratio), and with propellant mixture ratio. The optimum mixture ratio will provide the highest specific impulse for a specific combination of expansion ratio and chamber pressure. The data obtained clearly indicate that the specific impulse does not vary noticeably with thrust levels above 4536 kgf (10000 lbf) and would decrease by only about 10 secs. when the thrust level drops from 4536 kgf (10000 lbf) to 454 kfg (1000 lbf). Changes in chamber pressure modify the specific impulse Isp slightly; for pump-fed engines the Isp improves less than 5 sec when the pressure changes from 55 kg/cm^2 to 110 kg/cm^2.

Specific impulse for space-storable engines are shown in Figures 78 and 79. Values for the small-thrust pressure-fed engines are shown for expansion ratios from 20 to only 100. For the low chamber pressures, the expansion ratio should not exceed 100; otherwise the engine will be too big and heavy when compared with its available thrust. A maximum specific impulse is obtained for a mixture ratio of 5.8 for Flox/Methane, 5.5 Oxygen-Difluoride/Methane and 3.8 for Oxygen-Difluoride/Diborane.

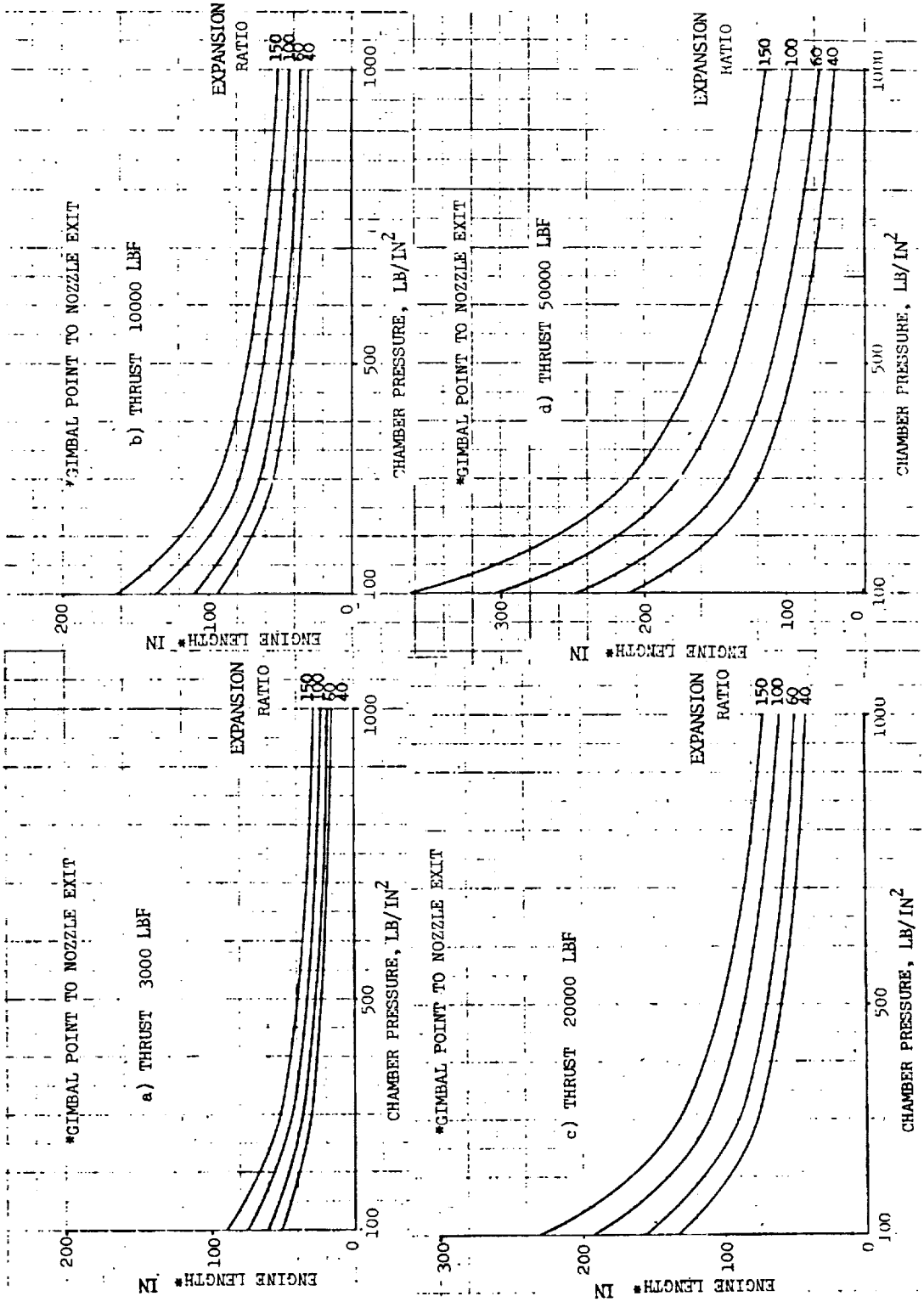

Figure 77. Tripropellant (Fluorine/Lithium/Hydrogen) Engine Length (Staged Combustion Topping Cycle)

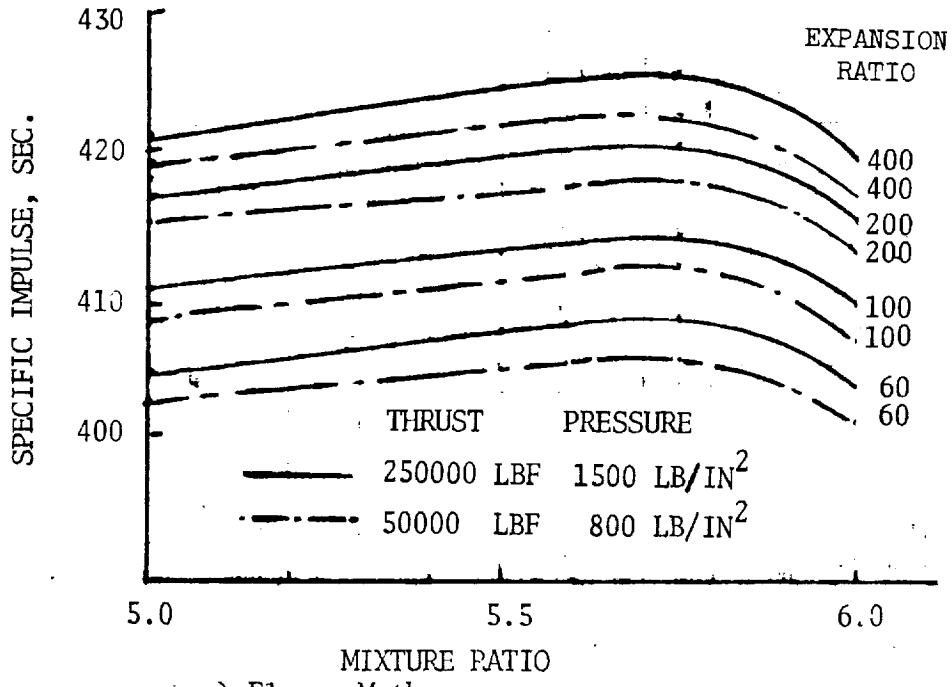

a) Flox Methane

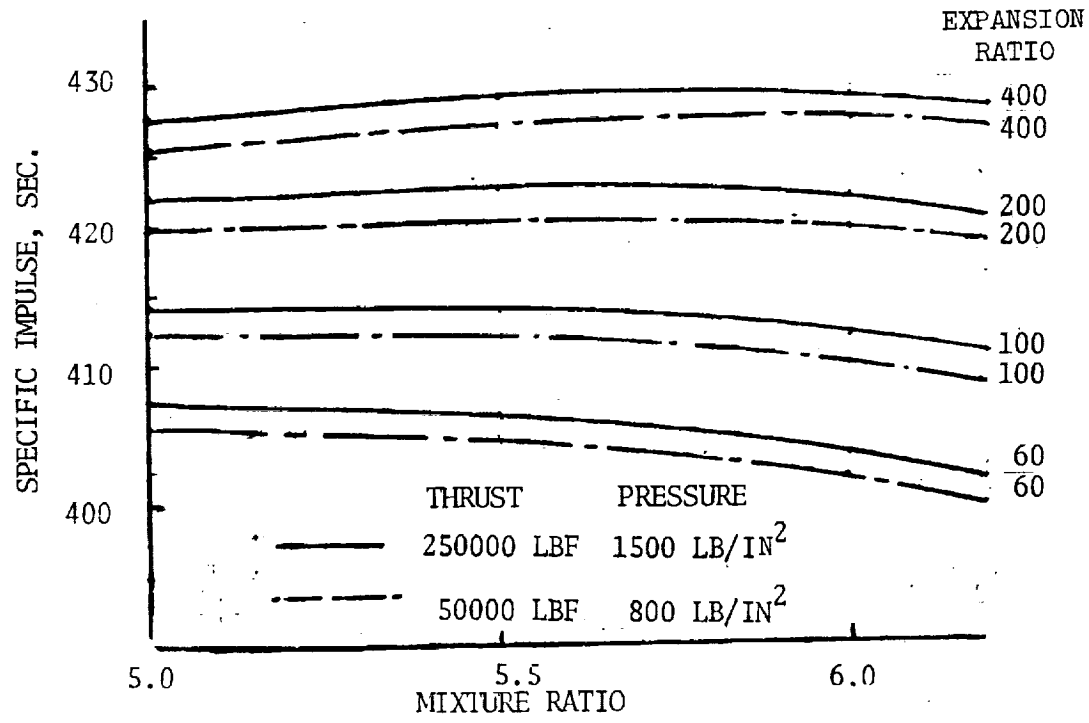

b) Oxygen-Difluoride/Methane

Figure 78. Specific Impulse (Flox/Methane and Oxygen-Difluoride/Methane)

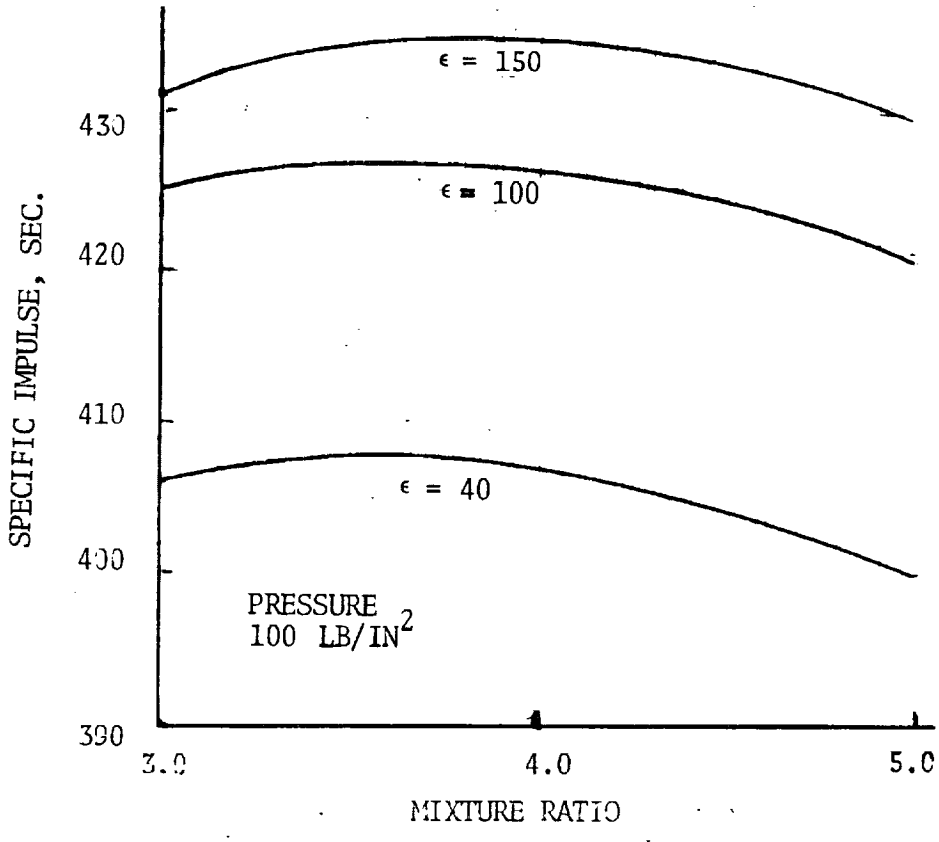

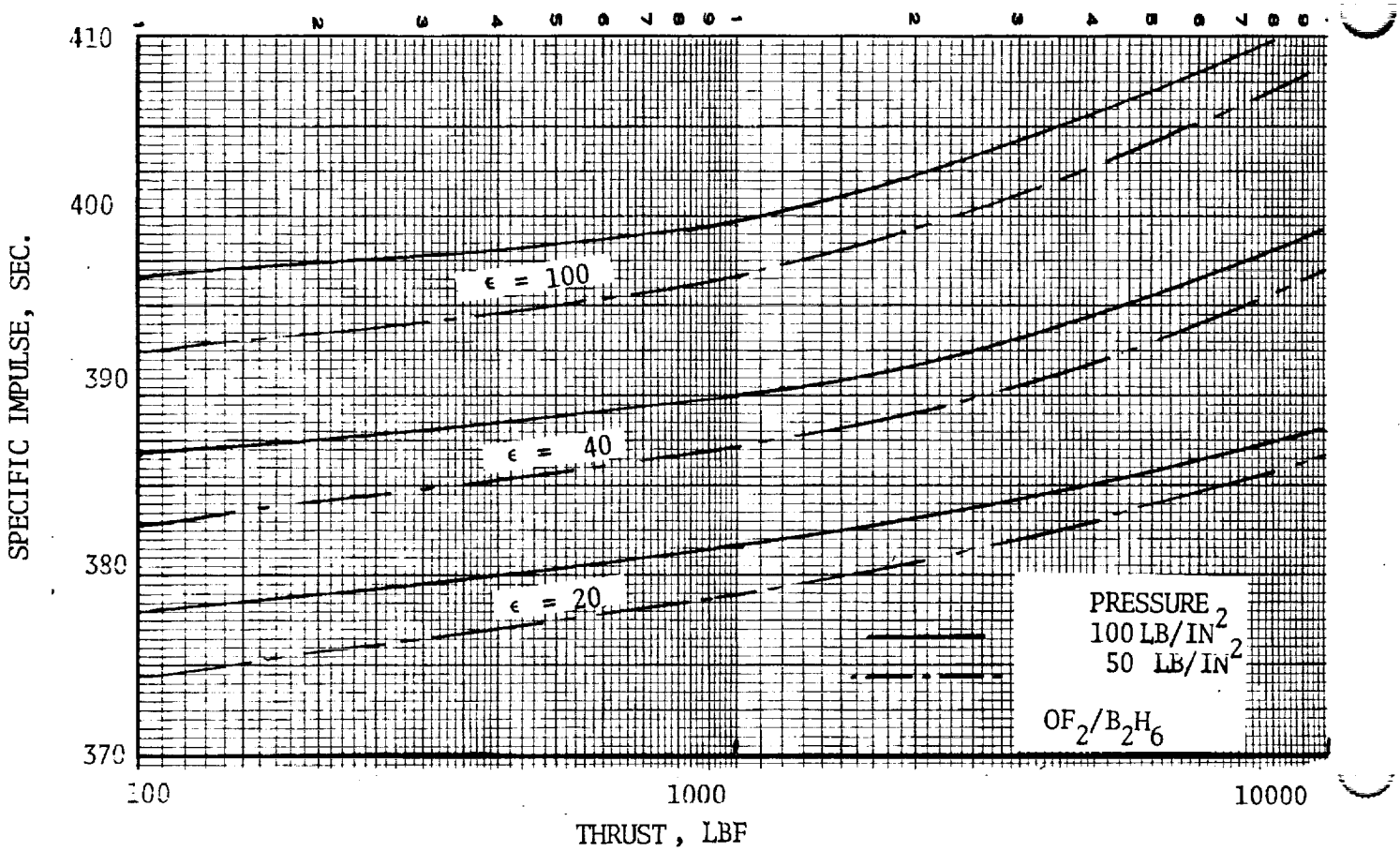

Figure 79. Specific Impulse (Oxygen-Difluoride/Diborane)

Variations of specific impulse with mixture ratio for Oxygen/Hydrogen and Fluorine/Hydrogen are given in Figure 80 with maximum values obtained at 5.6 and 11 respectively. Although the mixture ratio that yields the maximum specific impulse is recommended for earth- and space-storable engines, the mixture ratio for the maximum Isp with cryogens does not necessarily give the best overall performance of the stage. A somewhat larger value will often decrease the required volume of the low density LH_2 tank and thus, lower the associated structural, and thermal/meteoroid protection weights. The lower Isp combined with the lower inert weight could possibly result in an improvement of the vehicle's mission performance. The Isp variation with thrust, Figure 80 , shows nearly constant performance for thrust levels above 4540 kgf (10000 lbf).

Figure 81 shows the theoretical shifting-equilibrium performance for Oxygen/Hydrogen and Fluorine/Hydrogen. The latter combination can be significantly improved with the addition of lithium. The optimum combination is 2.74 Fluorine/Lithium with about 28 percent hydrogen, Figure 82. The maximum Isp does not vary between the pressure-fed system ($p = 14$ kg/cm^2, 200 lb/in^2) and the pump-fed ($p = 70.3$ kg/cm^2, 1000 lb/in^2), although there is a slight decrease of mixture ratio where the maximum occurs (31 percent hydrogen (pressure-fed), 27 percent hydrogen (pump-fed)).

6.1.2 Propellant and Engine Module Subelements

6.1.2.1 Propellant Baffles

Propellant slosh suppression devices are required in propellant tanks where it is necessary to prevent instability in the vehicle orientation, structure failure, premature engine shutdown, and other potential failures in the propulsion system as a result of propellant sloshing.

Even in low or near-zero gravity conditions where slosh frequencies are relatively low, some of the above mentioned failures could occur if amplitudes were to build up due to long term motion. In zero gravity there is also the requirement of producing a propellant head before engine operation. This problem might be integrated with the slosh problem in specific cases, but this particular analysis confines itself to slosh suppression under normal accelerations likely to be encountered in space, or earth boost systems.

Although there have been numerous design concepts on propellant slosh suppression, only the ring baffle concept appears to have had any extensive study or application. This analysis is for cylindrical tank slosh suppression device weight.

There are several design parameters affecting the sizing geometry, and thus weight, of the ring baffle, but the required ratio of damping to critical damping (ζ) is the prime parameter. This will be a required parameter for specific configurations and is thus assumed to be a known value in this analysis. An acceptable value would be $\zeta = 0.1$.

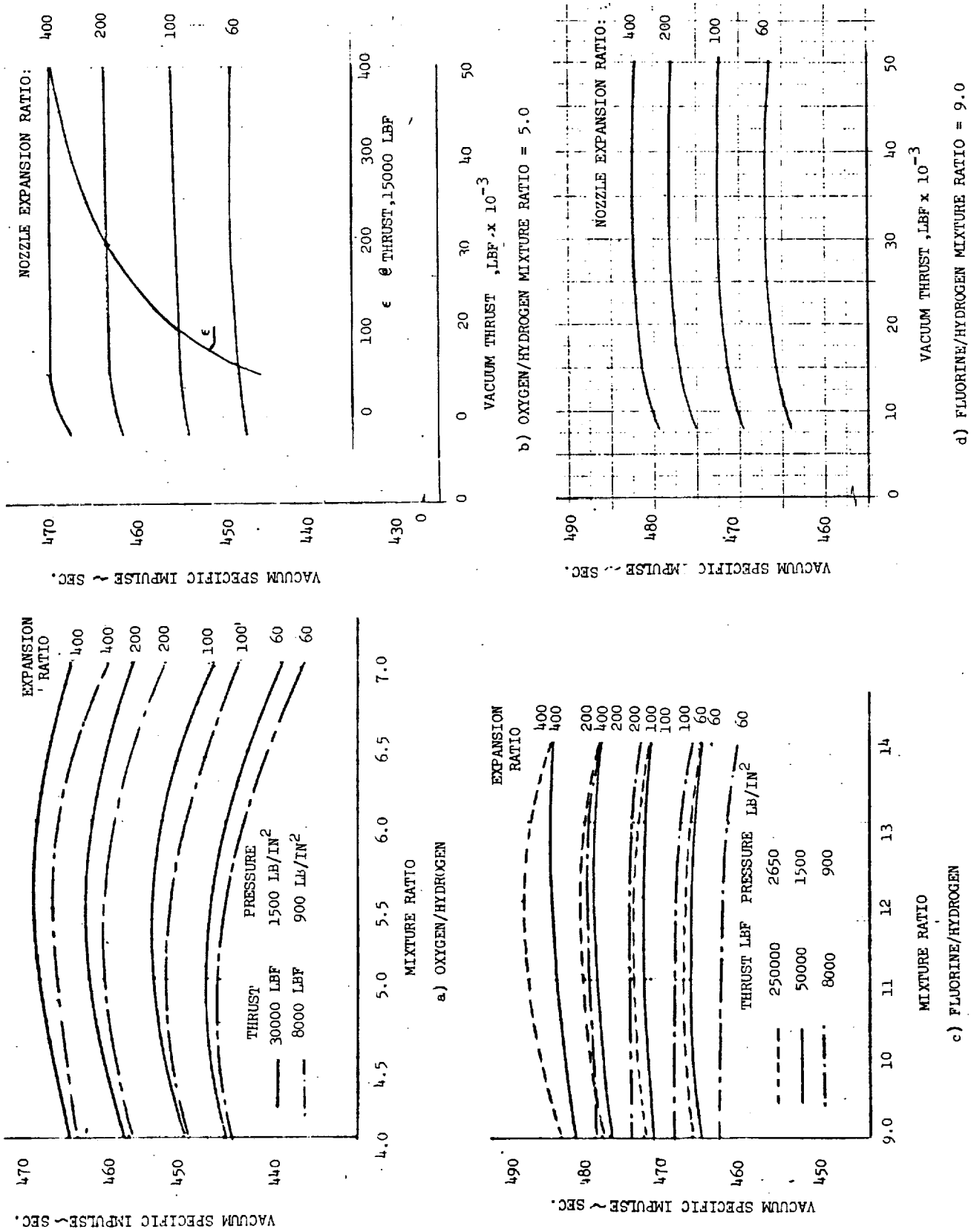

Figure 80. Specific Impulse (Oxygen/Hydrogen and Fluorine/Hydrogen)

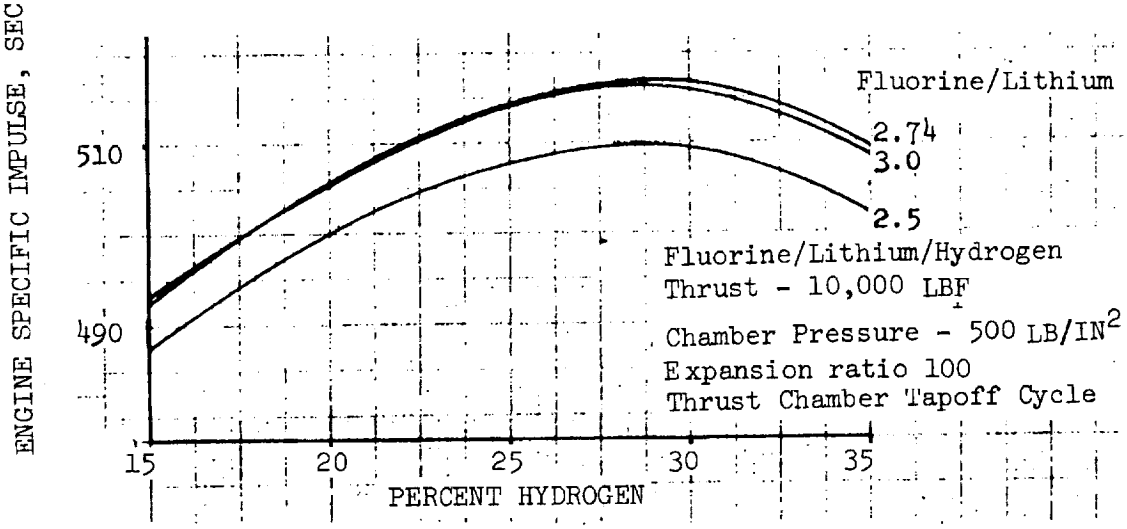

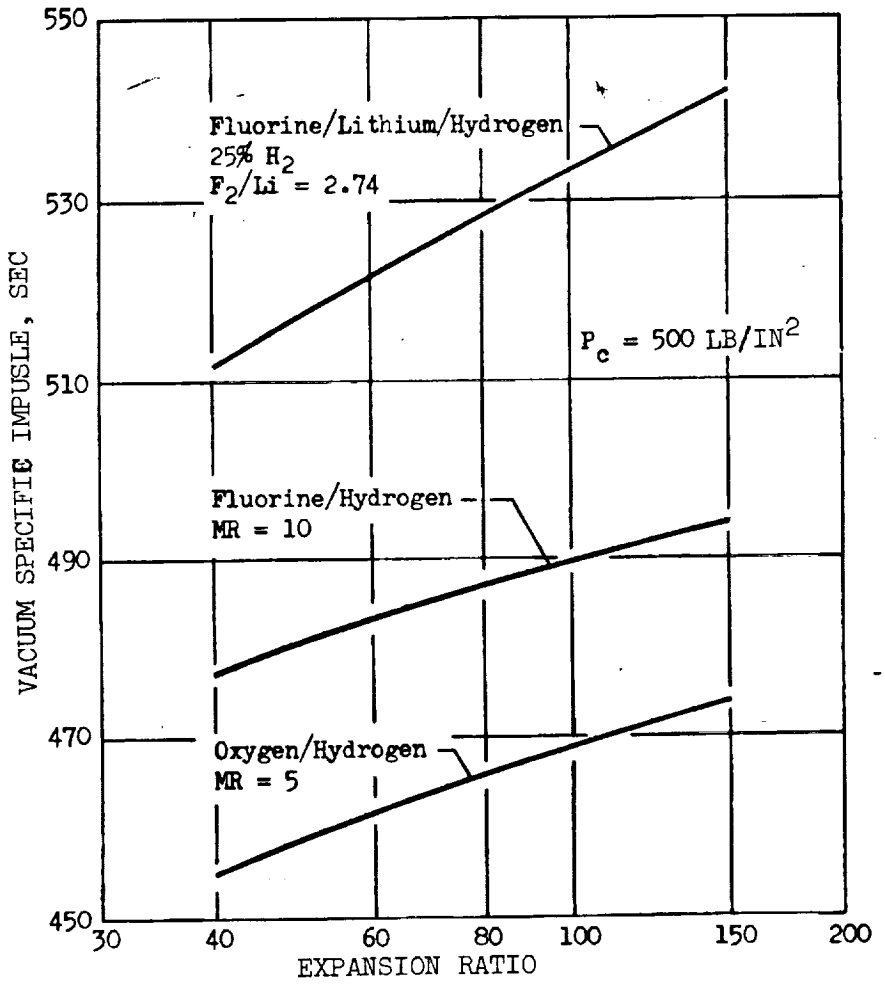

Fig. 81 Theoretical Shifting Equilibrium Performance for Current and Advanced Propellants

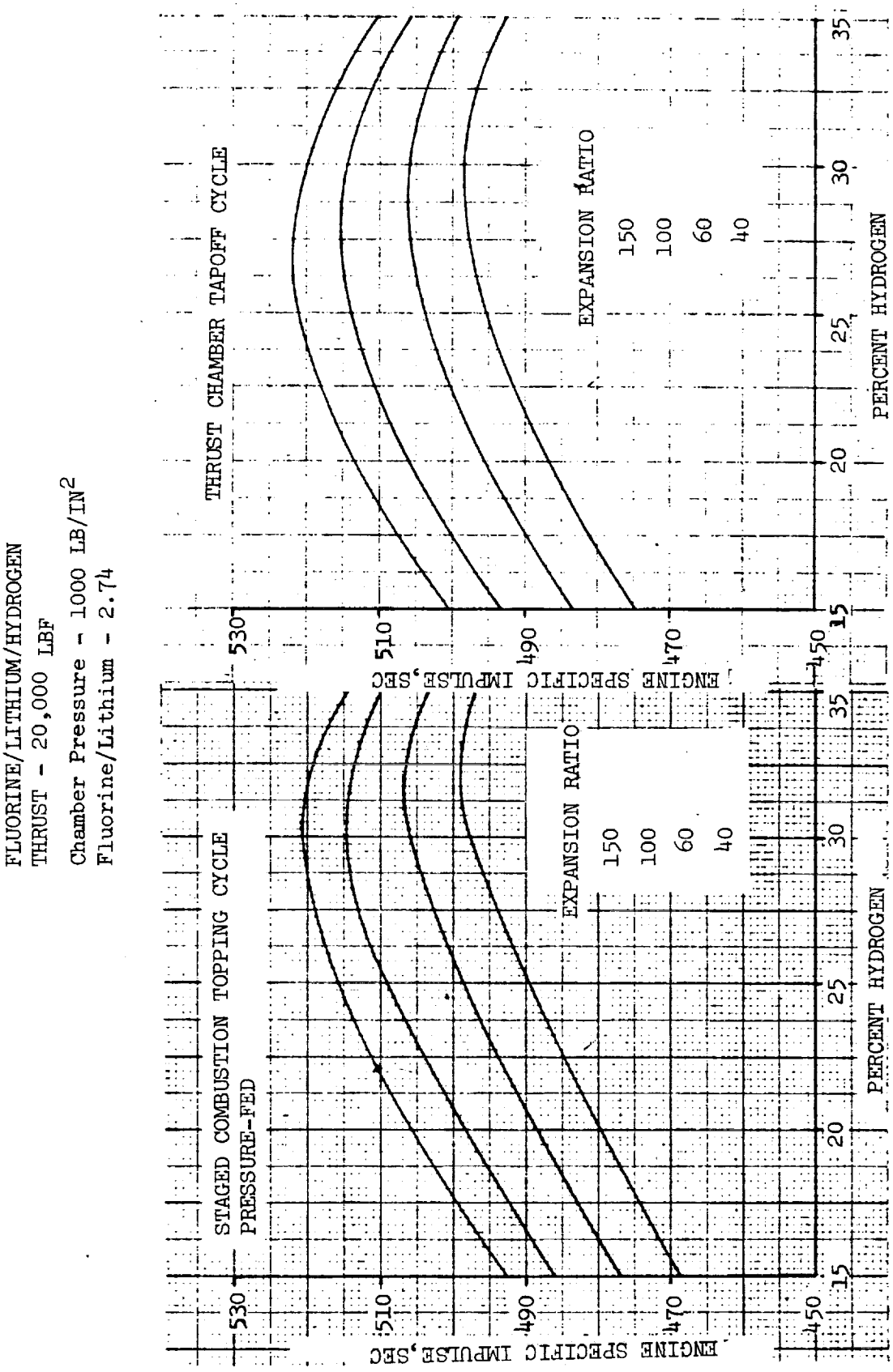

Figure 82 Specific Impulse (Fluorine/Lithium/Hydrogen)

There are several effects contributing to the satisfaction of the damping ratio requirements. These are:

1. Wall viscous damping (without baffles)
2. Ring baffles
3. Generalized mass factors
4. Vortex shedding (for small amplitude where the ratio of baffle double amplitude/baffle width is less than one)

The mathematical determination of the damping ratio fraction contributed by each of the above as a function of the various parameters is given by Cole in Reference 39.

The weight of the ring slosh baffle may be defined as:

$$W_{SB} = SN\rho$$

where

W_{SB} = Total Weight of slosh baffles kg (lb)

S = Baffle surface area m^2 (ft^2)

N = Number of baffles required

ρ = Unit surface weight of baffle kg/m^2 (lb/ft^2)

The value of baffle surface area is expressed as

$$S = \pi \left[r^2 - (r - w)^2 \right]$$

and

$$N = \frac{h}{s}$$

where

r = Tank radius m (ft)

W = Baffle width m (ft)

h = Fluid height = $W_p / (\rho_p \pi r^2)$

s = Baffle spacing m (ft)

Also the value of ρ varies with the tank radius as

$$\rho = \frac{r}{5} \rho_o$$

$\rho_o \triangleq 1$ lb/ft^2 for a 5-foot tank radius

Thus, the ring baffle weight may be expressed as

$$W_{SB} = \frac{\pi r h [r^2 - (r - w)^2] \rho_o}{5 s} \qquad (90)$$

Figure 83 is a plot of slosh baffle spacing versus damping ratio (ζ) for a baffle width/radius ratio w/r = 0.1 and slosh amplitude at wall/radius ratio (η/r) = 0.10. This plot was developed from data given in Reference 40 and has been approximated by

$$s = r \left(\frac{0.01726}{\zeta} \right)^{1.0493} \qquad (91)$$

Substituting Equation 91 and the w/r = 0.1 into Equation 90 results in the ring slosh baffle weight equation of:

$$W_{SB} = 0.00153 \left(\frac{hr^2}{\frac{0.01726}{\zeta}} \right)^{1.0493} \quad ; \quad \text{kg}$$

$$W_{SB} = 0.119 \left(\frac{hr^2}{\frac{0.01726}{\zeta}} \right)^{1.0493} \quad ; \quad \text{lb} \qquad (92)$$

but

$$hr^2 = W_P / (\rho_p \pi)$$

ρ_p = propellant density kg/m^3 (lb/ft^3)

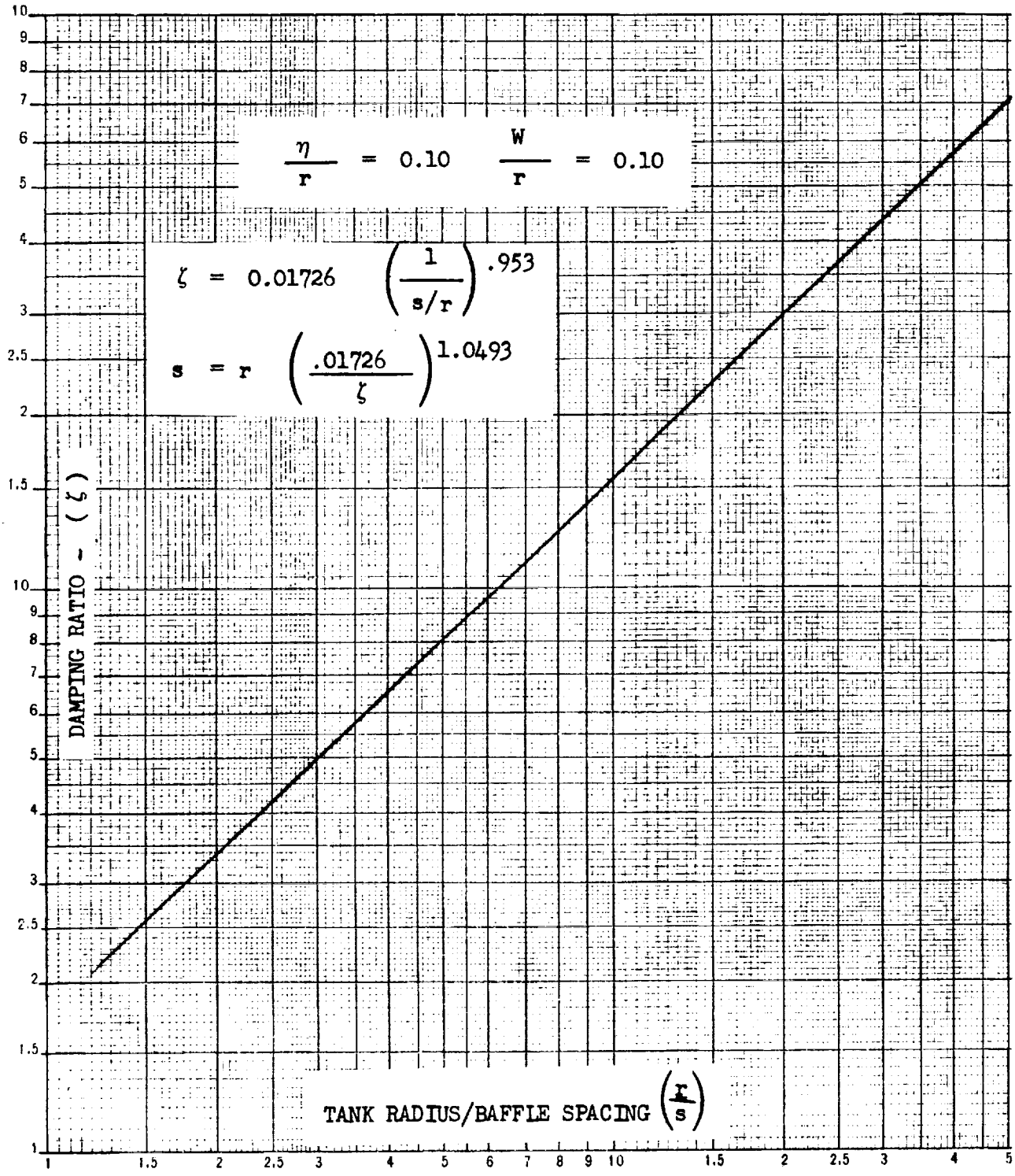

Figure 83 Slosh Baffle Spacing

Figure 84 shows the ring slosh baffle weight for various values of damping ratio (ζ) where w/r = 0.1 and η/r = 0.1. The effect of η/r on ζ is to the 0.35 power and is thus assumed not critical to the weight estimate. Baffle widths with different values of w/r have second order effects on the weight estimate, since as the baffle width is increased, the required spacing increases also for a fixed damping ratio. Althouth the total baffle area increases somewhat with lower values of w/r the unit weight per square area of the baffle is lower, thus compensating for the higher area in the final weight. The weight Equation 92 and Figure 84 can be used for weight estimation of ring type slosh baffles for any practical values of η/r and w/r.

6.1.2.2 Engine Base Heat Protection

The propulsion system base heat protection provides protection to the structure from heat emanating from the rocket engines. There are numerous parameters and conditions affecting the weight of the base heat protection. The following are considered the most influential and are used in the weight estimation.

1. Altitude - space (vacuum) versus atmosphere (earth)
2. Thrust level
3. Radiation from products of combustion
4. Thrust/weight ratio of propulsion stage
5. Length/diameter ratio of propulsion stage (L/D)

The basepoint weight data (Figure 85) were from the following systems:

SYSTEM	ENVIRONMENT	RELATIVE COMBUSTION PRODUCED RADIATION	THRUST kgf(lbf)	WEIGHT kg (lb)
Saturn S-II	Space	Low	454000 (1000000)	285.8 (630)
Saturn S-IVB	Space	Low	104000 (230000)	90.7 (200)
Apollo SM	Space	High	9100 (20000)	36.3 (80)

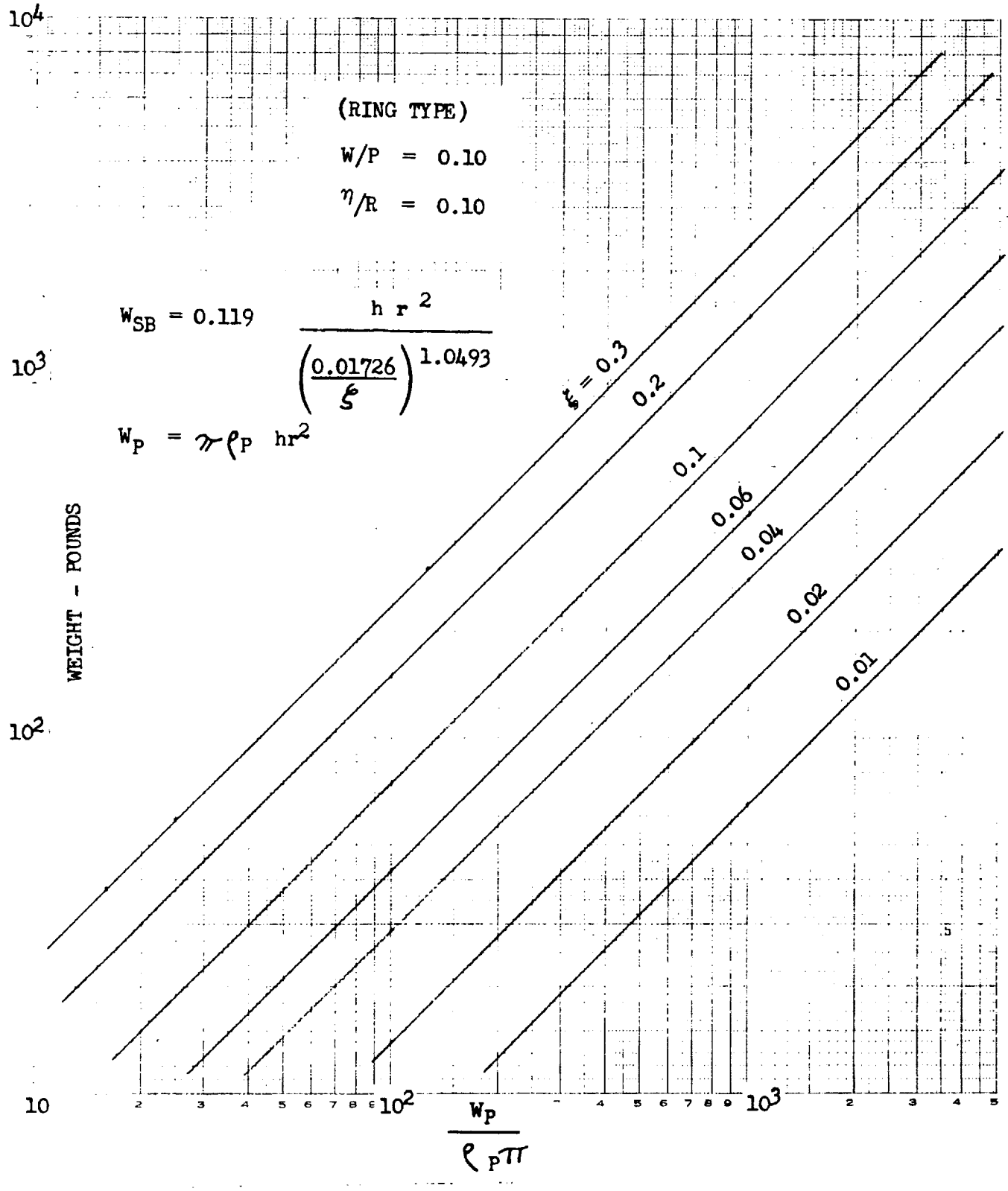

Figure 84 Slosh Baffle Weight

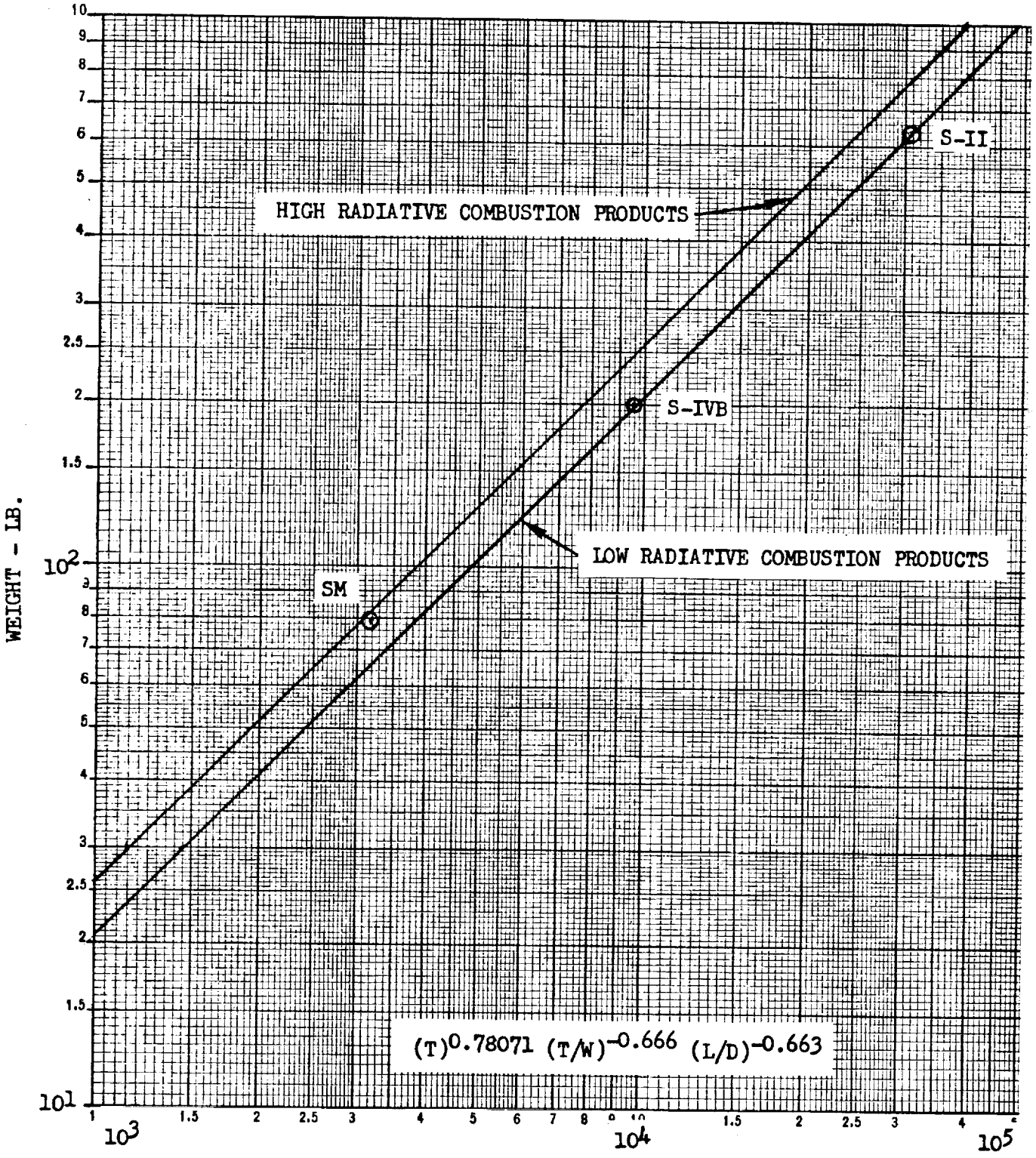

Figure 85 Propulsion System Base Heat Protection Weight

The scaling laws must consider the effects of thrust to weight, since space modules will have a thrust-to-weight ratio much lower than Earth launch systems. Decreasing the thrust-to-weight results in a larger base area for a given thrust- and stage- fineness ratio (L/D), thus the thrust-to-weight correction factor is $(T/W)^{-0.666}$. A variation of the fineness ratio, L/D, with fixed propellant weight also affects the base area to be protected and the weight correction factor is $(L/D)^{-0.663}$.

The form of the scaling law should be

$$W = K F_t \left(\frac{T}{W}\right)^{-0.666} \left(\frac{L}{D}\right)^{-0.663}$$

Correlating this law with basepoint weight data, it was found that appropriate sealing equations are:

for low radiative combustion products

$$W = 0.0172(T/W)^{-0.667} (L/D)^{-0.663} F^{0.7807} \text{ ; kg}$$
$$W = 0.0205 \; T/W^{-0.666} \; (L/D)^{-0.663} \; F^{0.7807} \text{ ; lb.}$$

for high radiative combustion products

$$W = 0.0233 (T/W)^{-0.668} (L/D)^{-0.663} F^{0.7807} \text{ ;kg} \qquad (93)$$
$$W = 0.0277 (T/W)^{-0.666} \; (L/D)^{-0.663} \; F^{0.7807} \text{ ;lb}$$

As a guide, the propellant combinations are listed below with respect to their product of combustion radiation.

Low Radiation	High Radiation
LF_2/LH_2	OF_2/B_2H_6
LO_2/LH_2	OF_2/CH_4
LF_2/Li $\%H_2$	$FLOX/CH_4$
	N_2O_4/MMH

6.1.2.3 Propulsion Feed Systems

The weights of the oxidizer and fuel feed systems were derived from system data of the SA-516 Saturn launch vehicle and other flight hardware. The systems include all the propulsion system elements necessary for a complete stage including: (1) feed lines, joints, valves and insulation; (2) fill, drain & vent provisions; (3) propellant level and mensuration systems. The parameters used in the equations include the number of lines (N_E), the thrust level and specific impulse (F_E and Isp) and the propellant density (ρ_{ox}, oxidizer, ρ_f, fuel) for the line routing. The scaling equations have been supplied separately for the oxidizer and fuel feed systems for two engine thrust ranges; small to medium thrust 2270 - 90720 kgf (5000-200,000 lbf) and thrust levels greater than 90,720 kgf (200,000 lbf).

Oxidizer System

$$W_{oxid\,sys} = 600 + 1.10\, N_E \left(\frac{F}{Isp\,\rho_{ox}}\right)^{\frac{1}{2}} \left(\frac{W_{ox}}{1000}\right)^{0.73} \quad ;\text{lb} \quad 200{,}000 \text{ lbf} \leq F$$

$$= 80 + 5.30\, N_E \left(\frac{F}{Isp\,\rho_{ox}}\right)^{\frac{1}{2}} \left(\frac{W_{ox}}{1000}\right)^{0.73} \quad ;\text{lb} \quad 5000 \text{ lbf} \leq F < 200{,}000 \text{ lbf}$$

Fuel System

(94)

$$W_{fuel\ sys} = 880 + 1.75\, N_E \left(\frac{F}{I_{sp}\,\rho_f}\right)^{\frac{1}{2}} \left(\frac{W_f}{1000}\right)^{0.68} \quad ;\text{lb} \quad 200{,}000 \leq F$$

$$= 18 + 16.70\, N_E \left(\frac{F}{Isp\,\rho_f}\right)^{\frac{1}{2}} \left(\frac{W_f}{1000}\right)^{0.68} \quad ;\text{lb} \quad 5000 < F < 200{,}000$$

The equivalent scaling laws using the metric units are quoted later in Section 7.2.

6.1.2.4 Pressurization Systems

Propellants are delivered to the engine thrust chamber by either an engine-mounted pump or tank-head pressure. In either mode, it is necessary to pressurize the propellant tankage. The pump fed system tankage must be pressurized to meet the net-positive-suction head (NPSH) requirement of the engine whereas the entire propellant delivery energy is provided by the tankage pressure in a pressure-fed system. Both techniques are classified as pressurization systems, but differ markedly in size, weight, design criteria, and performance. Pressure-fed systems are usually employed on smaller spacecraft - the Apollo service module is the largest pressure-fed system to be flown. A precise crossover between pump- and pressure-fed systems cannot be identified - the Agena and Centaur are examples of pump-fed systems with smaller propellant capacity than the Apollo. Pump-fed systems are universally employed in such large stages as S-IC, S-II, S-IVB and the liquid propellant ICBM systems. The subsequent material will discuss the pressurization systems associated with both pump-and pressure-fed systems.

The controlling factor in defining the size and weight of the pressurization system is the mass of pressurant required for complete pressurization and expulsion of the propellants. The propellant flow rate to the thrust chamber(s) dictates the size (and weight) of such components as lines, valves, regulators, orifices, etc.

Major weight items in a pressurization section include the pressurant components, pressure storage bottles and auxiliary tankage or increased propellant tank volume to accommodate pressurant. The pressurization system weight-scaling relationships are assigned to the propellant module weight for purposes of stage synthesis.

The operation of the pressurizations system may be conveniently divided divided into two categories: restart pressurization, and steady state pressurization (i.e., during engine firing). For small capacity propellant tanks, helium stored under high pressure (Figure 86) is most commonly used for restart and can also be used for steady tank pressurization requirements. In the case of larger propellant tanks, helium heat exchangers (Figure 87) are generally used to increase the temperature of the pressurant gases to minimize the pressurant storage requirements. The heat exchanger derives heat energy by use of a burner unit which uses either the stage propellants or separately stored propellants. During engine operation, engine-oriented heat exchangers can be used as an energy source for increasing pressurant temperatures, or an independent heat exchanger can continue to be used throughout the engine operation. Systems of these types are generally used for pressure-fed propulsion systems. Helium is most commonly used as the pressurant because of its low molecular weight and high heat capacity. Nitrogen gas is also commonly used as a pressurant gas, but its high molecular weight results in larger pressurant-gas weight penalties compared with helium. For cryogenic propellants, nitrogen is unsatisfactory because of the relatively high boiling temperature.

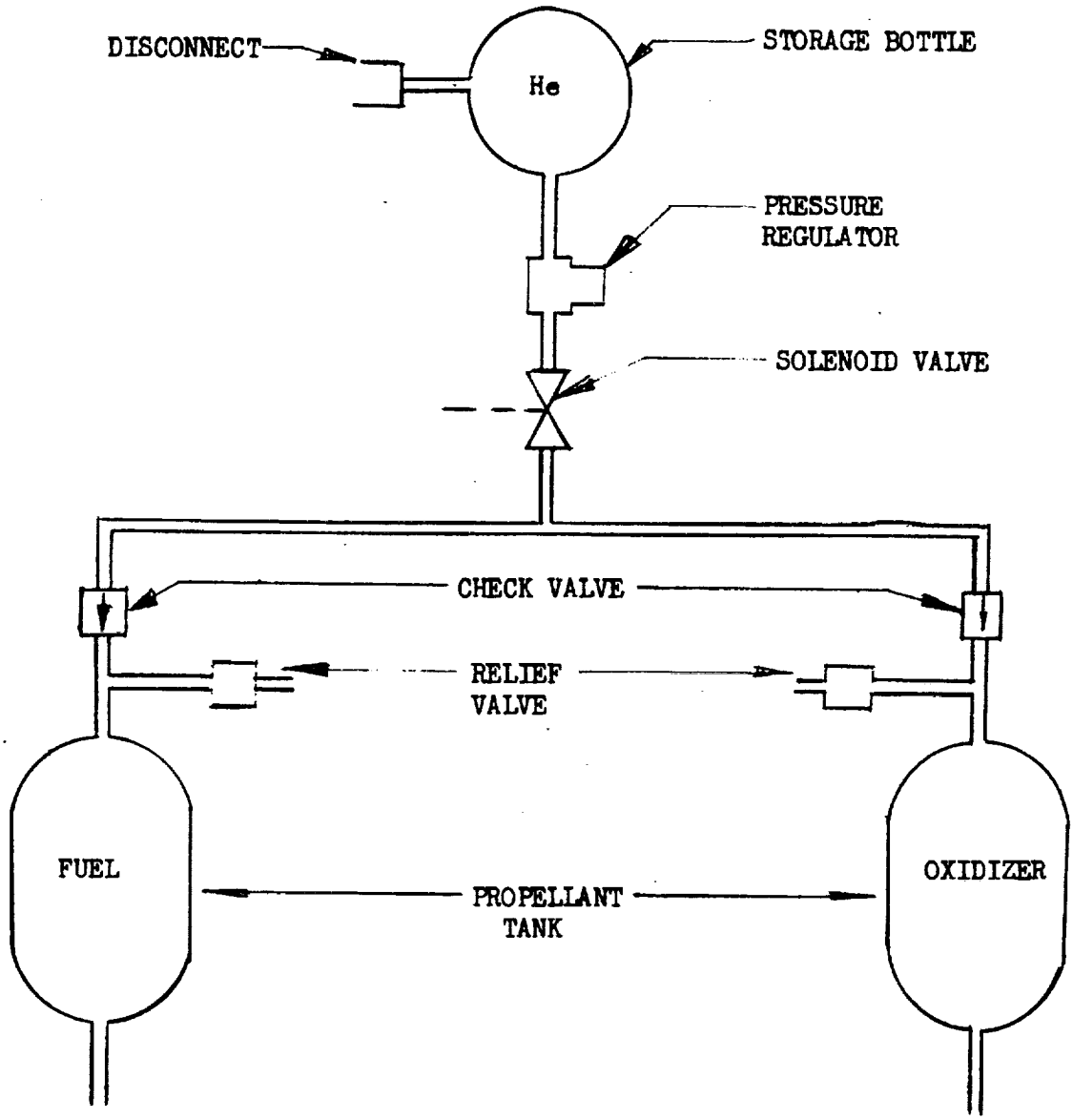

Figure 86. High-Pressure Stored Helium

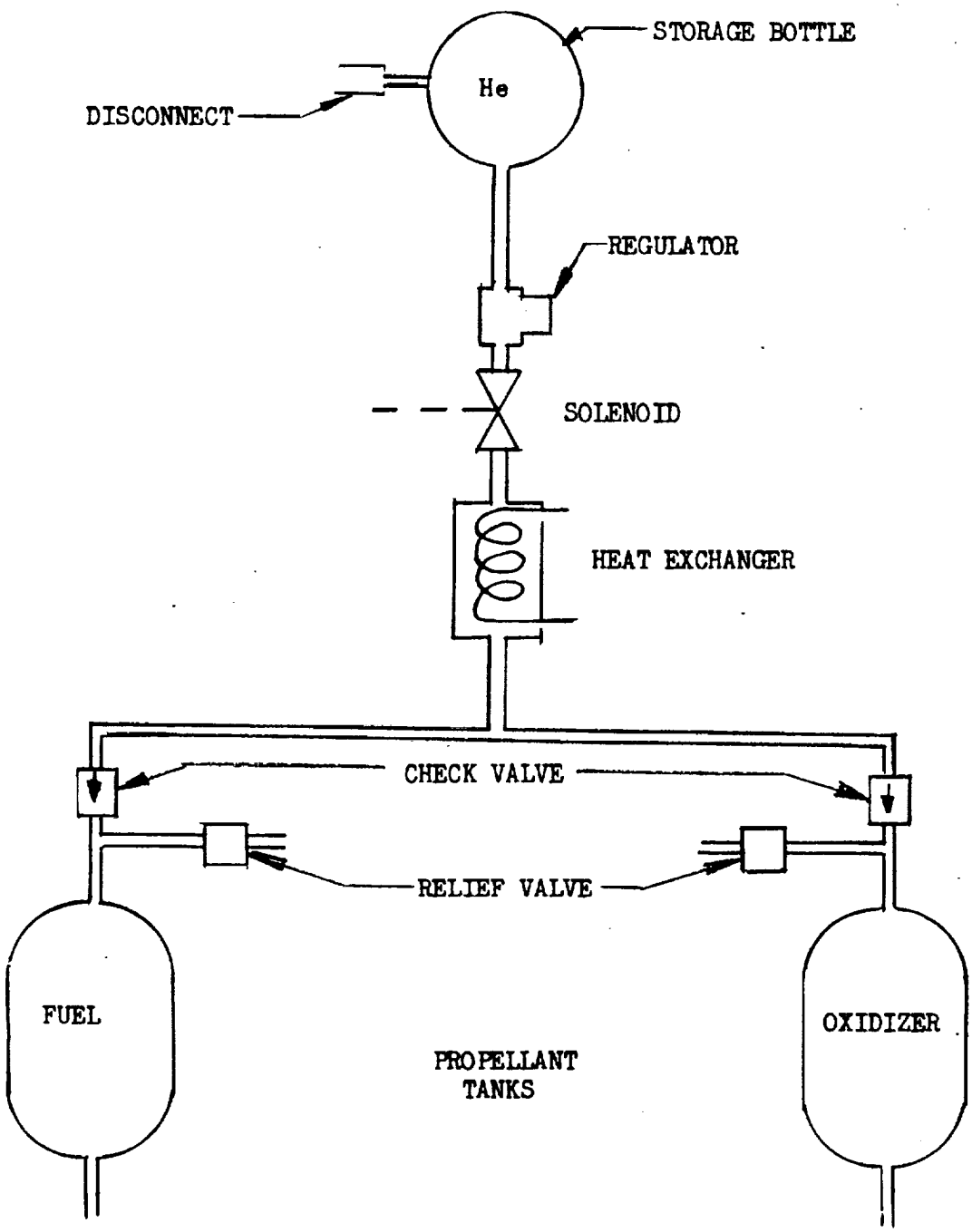

Figure 87 High-Pressure Heated Helium

In the case of large volume earth-storable pressure-fed (or pump-fed) propulsion systems, an attractive restart and steady state pressurization scheme uses a gas-generator pressurization system, Figure 88. The system consists of an independently-stored propellant supply system (fuel and oxidizer) which feeds two gas generators, one of which operates fuel rich (O/F ratio ∿0.5) to provide fuel rich gases for the fuel tank and the other oxidizer rich to provide oxidizer-rich (O/F ∿20) gases for the oxidizer tank pressurization. An advantage of the gas generator system is that pressurizing gases can be stored initially as a liquid, minimizing the weight associated with the storage bottles. Gas temperature of the gas-generator system can be controlled either by adjusting the mixture ratio or by using a heat exchanger to lower the temperature of the gases before they enter the propellant tank ullage. The effective molecular weights of these gases range from 12 to 15 lb/lb-mole and 28 to 33 lb/lb-mole for oxidizer rich and fuel rich gases, respectively. Although gas-generator pressurization systems are feasible for space-storable and cryogenic propulsion systems, the high temperature of the gas generator would result in propellant heating which is undesirable from a propulsion system standpoint.

Pump-fed propulsion systems provide two convenient sources of heat energy that can be used to vaporize liquid propellant for pressurizing the propellant tanks. One source is engine heat. Most pump-fed engines rely on regeneratively cooled thrust chambers assemblies, or at least a portion of the thrust chamber assembly uses regenerated cooling techniques (i.e., even when other cooling techniques are used, such as transpiration cooling, some part of the engine uses regenerative cooling techniques. Propellant pressurization gases, Figure 89, are tapped off the regenerative-cooling system just prior to entering the engine injector. In almost all cases the gas is above the critical temperature at this point. Fuels are usually used for regenerative cooling, since the oxidizer is much more sensitive to system contamination, particularly at the high operating temperatures and pressures associated with pump-fed engine operation.

The other source of heat energy on pump-fed propulsion systems is the exhaust from the gas generator turbine, preburner, chamber-tapoff or gases exhaust products. A heat exchanger is located in the turbine exhaust lines and is used for vaporizing and heating liquid propellant for tank pressurization. The S-II is an example of a vaporization pressurization system. Gaseous hydrogen is bled off from the engine regenerative-cooling system for hydrogen tank pressurization and liquid oxygen is bled off from high pressure discharge side of the pump, and passed through a heat exchanger where it is vaporized for oxygen tank pressurization.

The pressurization-system concepts applicable to the various propellant combinations are shown in Table 29. High-pressure stored helium is generally used for pressure-fed propulsion systems with small- to medium-volume propellant tanks. For larger propellant tanks and/or requirement for a number of engine restarts, minimum pressurant requirements can be achieved by increasing the propellant-tank gas inlet temperature by means of a heat exchanger. Propellant tank pressurization for large-volume earth-storable propellant tanks may also be achieved by employing a gas-generator pressurizing system.

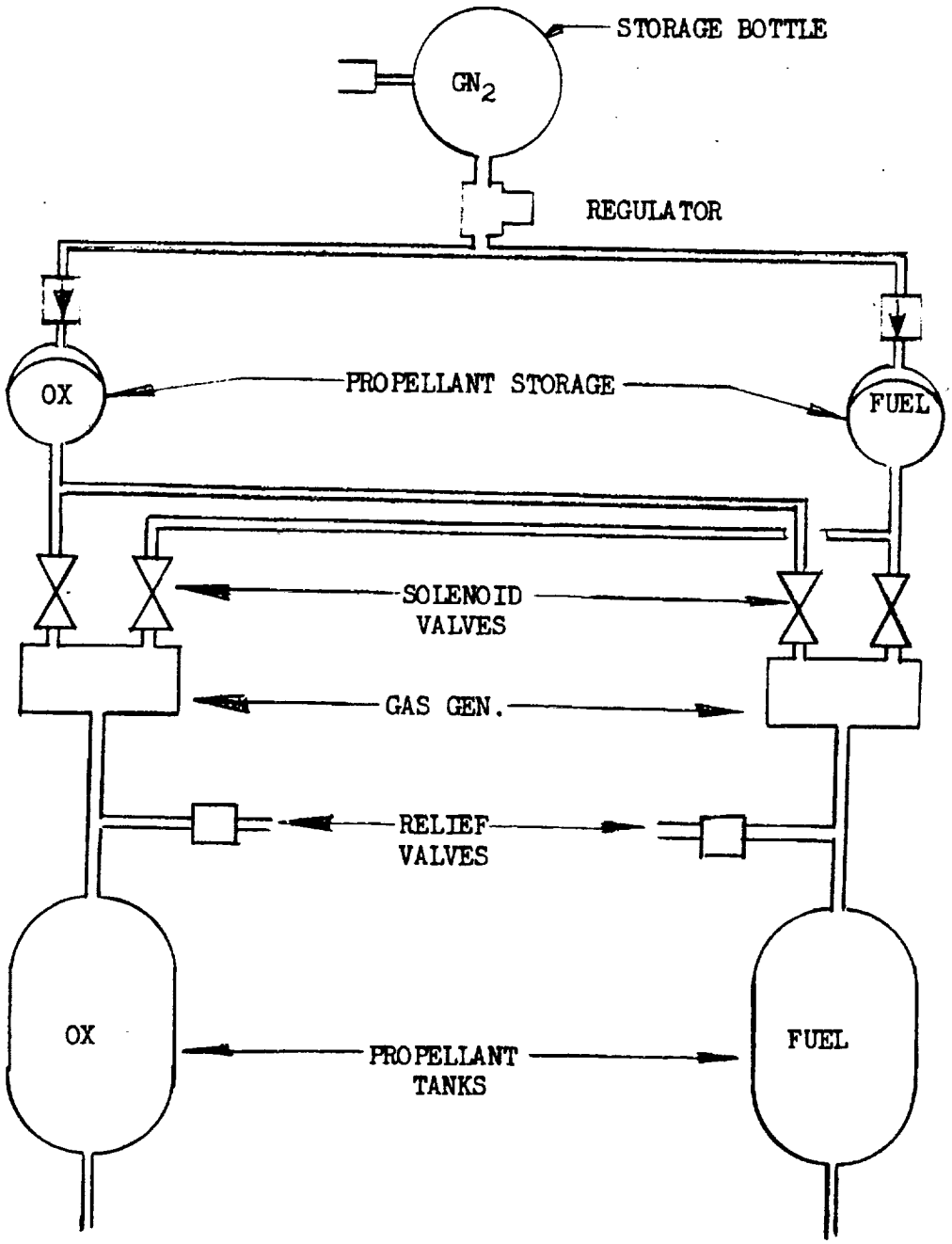

Figure 88 Gas Generator System

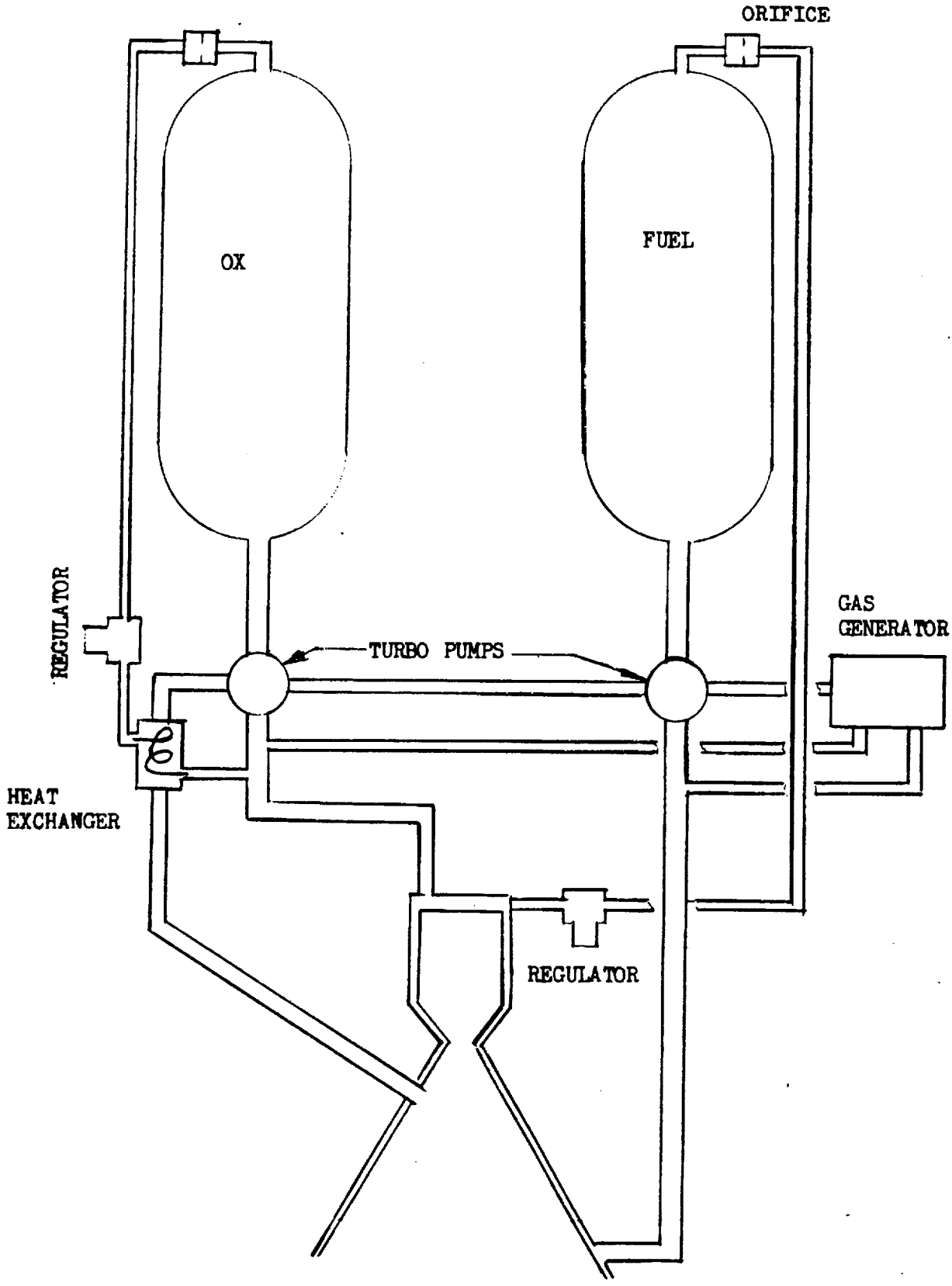

Figure 89 Vaporization Pressurization System

Table 29. Restart and Steady State Pressurization Systems

System Concept	Propellant Combinations													
	NTO/MMH		FLOX/CH_4		OF_2/CH_4		OF_2/B_2H_6		LOX/LH_2		LF_2/LH_2		$LF_2/Li/LH_2$	
	Pump Fed	Pressure Fed	Pump Fed	Pressure Fed	Pump Fed	Pressure Fed	Pump Fed	Pressure Fed	Pump Fed	Pressure Fed	Pump Fed	Pressure Fed	Pump Fed	Pressure Fed
High pressure stored Helium/GN_2		RS	RS	RS	RS	RS		RS	RS	RS	RS	RS	RS	RS
High pressure stored helium with heat exchanger		RS	RS	RS	RS	RS		RS	RS	RS	RS	RS	RS	RS
2 gas generators, one fuel rich and one oxidizer rich, with separate propellant supply		RS												
Supercritically stored propellants with heat exchanger			RS	RS	RS	RS			RS	RS	RS	RS		
Evaporative system using engine bleed and/or heat exchanger			S		S				S		S		S	

R = Restart
S = Steady state.

Pressurization system parameters are listed in Table 30 for the various propellant combinations. The data show representative high-pressure storage temperatures, approximate ullage-gas temperatures(for computing pressurant weight), and molecular weight of the pressurizing gases.

The amount of pressurant required for propellant-tank pressurization can be calculated using appropriate thermodynamic and heat transfer relationship. However, the precise calculations are complicated by the transient temperature-time relationship for the pressurizing gas, storage system, and propellant tank. The most complex step in estimating the amount of pressurant required for tank pressurization is that of calculating the gas temperature in the tank ullage. The mass of pressurant is computed using the gas law based on the known tank volume and ullage pressure. Estimate of pressurant requirements for scaling purposes can be made from an assumed ullage gas temperature based on past experience.

For purpose of pressurant-weight estimates the following simplified equations are recommended for restart and steady-state system pressurization.

Restart

Weight of ambient stored pressurant, W_{sc_i}

$$W_{sc_i} = \frac{(P_u - P_{vap})\, V_u}{R'T_{sc_i}} \cdot \frac{M\, K'}{\left[1 - \frac{P_{sc_f}\, Z_{sc_i}}{P_{sc_i}\, Z_{sc_f}}\right]}$$

where

W = pressurant weight kg (lb)

P = pressure, kg/cm^2 (lb/in^2)

V = volume, cm^3 (in^3)

M = pressurant gas molecular weight kg/kg (lb/lb)

K' = effective rate of specific heat

R' = modified gas constant

T = temperature degrees K (degrees R)

Z = compressibility factor

Table 30. Pressurization System Parameters

Propellant Combination	Restart				Steady State			
	Gas	Molecular Weight lb/lb-mole	Stored Temperature (deg R)	Average Ullage* Temperature (deg R) Heated	Gas	Molecular Weight lb/lb-mole	Storage Temperature (deg R)	Average Ullage* Temperature (deg R) Heated
NTO / MMH	He	4	530	530	He	4	530	520
NTO / MMH	Gas Generator	14/33	liq.	~600	Gas Generator	14/33	liq	~600
FLOX / CH_4	He	4	155	327/350	FLOX / CH_4	33/16	liq	385/400
OF_2 / CH_4	He	4	201	360/350	He / CH_4	4/16	200/liq.	410/400
OF_2 / B_2H_6	He	4	154	365/412	He	4	154	410/440
LO_2 / LH_2	He	4	37	331/263	O_2 / H_2	32/2	liq	385/280
LF_2 / LH_2	He	4	37	326/263	F_2 / H_2	38/2	liq	385/280
LF_2 / Li / LH_2	TBD	TBD	TBD	TBD				

*Average ullage temperature based on pressurant collapse factor of ~1.5 steady state 2. restart assumes heated restart and steady presurrant (~500 degrees R)

subscripts

u = ullage

vap = vapor

sc = storage container gas

f = final

i = initial

The above equation ignores heat and mass transfer between the pressurant, propellant, and the tank walls. An effective ratio of specific heats (K) of the pressurizing gas is used which corresponds to experimental data. The "K" is lower than theoretical, as the gases (cooled from adiabatic expansion) absorb heat from the propellants when the gas storage container is located in the propellant tanks.

Heated stored pressurant

$$W_{s_i} = \frac{(P_u - P_{vap})\ VM}{R'\ T_u \left[1 - \frac{P_{s_f}\ T_{s_i}\ Z_{s_i}}{P_{s_i}\ T_{s_f}\ Z_{s_f}}\right]}$$

The steady-state tank pressurization requirements are treated in a similar fashion as the restart requirements.

Ambient stored pressurant

$$W_{sc_i} = \frac{P_t\ V_t\ M\ K'}{R'\ T_{sc_i}\left[1 - \frac{P_{s_f}\ Z_{s_i}}{P_{s_i}\ Z_{s_f}}\right]}$$

where subscript

t = propellant tank

Heated Stored Gas

$$W_{sc_i} = \frac{P_u V_u M_u}{R' T_u \left[1 - \frac{P_{sc_f} T_{sc_i} Z_{sc_i}}{P_{sc_i} T_{sc_f} Z_{sc_f}} \right]}$$

Vaporization System

$$W_g = W_{g_o} + W_{g_f}$$

$$= f_o \frac{P_{u_o} V_{u_o} M_o}{R' T_{u_o}} + f_f \frac{P_{u_f} V_{u_f} M_{u_f}}{R' T_{u_f}}$$

where

f = factor which accounts for a collapse in the pressurant gas temperature after entering the tank

Subscripts

o = oxidizer

f = fuel

Initital estimates of the ullage pressurant gas requirements can be made by use of the equations and by selecting appropriate gas temperatures. Pressure requirements in the gas-weight equations are basically a function of the type of propulsion system employed (pressure- or pump-fed). For pressure-fed systems the ullage pressure may be estimated as

$$P_u = 1.5\, P_c + \Delta P_{line}$$

where

P_c = chamber pressure, kg/cm^2 (lb/in^2)

ΔP_{line} = line loss, kg/cm^2 (lb/in^2)

The interface pressure is assumed to be one and a half times the chamber pressure.

Ullage pressure requirements for pump-fed system can be expressed by the following equation:

$$P_u = P_{NPSH} + \Delta P_{line} + P_{vap}$$

where

NPSH = Net-positive-suction-head pressure requirements for the engine pump.

A large number of pressurization system schemes exist in present day designs and proposals for Space propulsion systems. In order to provide an adequate means of weight scaling for all designs, the pressurization system was divided into the following elements.

1. Pressurant Gas
2. Pressurant Storage Tank
3. Pressurant Transmission

   (Plumbing, valves, regulators, heaters, supports, etc.)

The equations for pressurant gas presented in the pressurization system discussion in this section were reduced to one equation of the following form for use in all pressurization designs.

$$W_f = (.1)\left(\frac{P_t\ V_t}{T_u}\right) M\ K' \quad (lb)$$

$$W_f = (126.5)\left(\frac{P_t\ V_t}{T_u}\right) M\ K' \quad (kg) \qquad (95)$$

where;

W_f = pressurant weight ~ kg (lb)

P_t = propellant tank pressure ~ kg/cm^2 (lb/in^2)

V_t = propellant tank volume ~ m^3 (ft^3)

T_u = ullage temperature ~ °K (°R)

M = molecular weight of pressurant gas

K' = pressurant gas collapse factor

The equation can be applied to either pump-fed or pressure-fed systems by varying the propellant tank pressure used. The ullage temperature for each propellant combination can be obtained from Table 30 of the pressurization system discussion. Helium has the smallest molecular weight of pressurant gases, 4.0, and provides the lightest pressurant gas weight. The pressurant gas collapse factor accounts for cooling of the pressurant gas contained in the propellant tank between multiple burns. A plot of helium pressurant weight versus propellant tank volume is presented in Figure 90 for a series of tank pressures. The pressurant weights are based upon a collapse factor of 1.17.

Both spherical and cylindrical tanks were considered for storage of the pressurant fluids. The following general assumptions have been made for the weight analysis.

(1) All pressurants stored as cryogenics will be submerged in cryogenic propellants, thus eliminating the weight penalty associated with dual wall insulated tanks.

(2) High pressure gas pressurants stored at 256°K (460°R)

(3) Cylindrical tanks will have hemi-spherical ends.

The weight equation of the pressurant tank may be expressed as

$$W_{tk} = N_o \rho_m \ (A_s t_s + A_c t_c) \qquad (96)$$

where:

W_{tk} = Tank weight - kg (lb)

N_o = Non-optimum factor

ρ_m = Tank wall material density - kg/cm^3 (lb/in^3)

A_s = Area of spherical portion of tank - cm^2 (in^2)

t_s = Thickness of spherical portion of tank - cm (in)

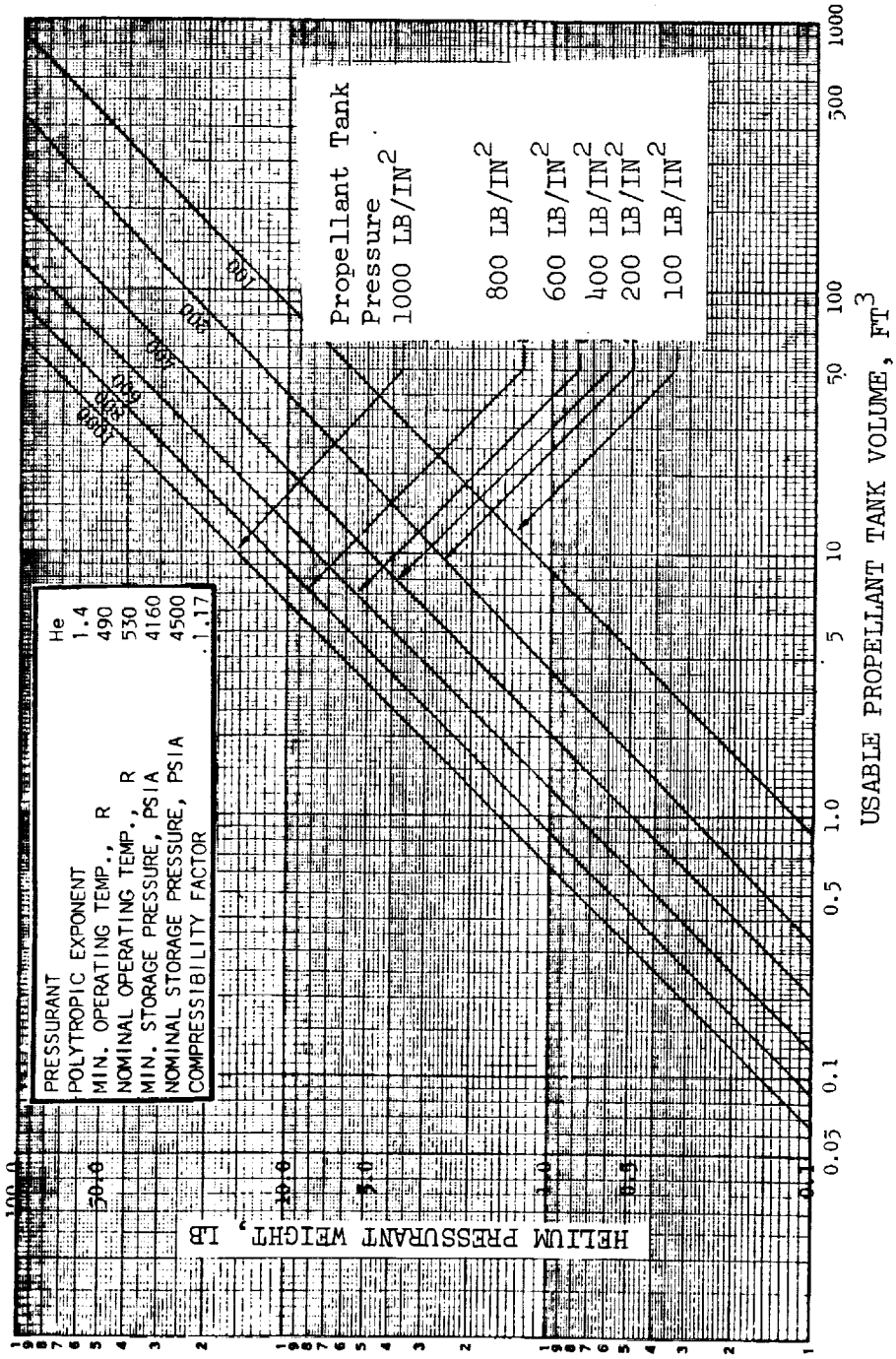

Figure 90. Helium Pressurant Weights

A_c = Area of cylindrical portion of tank - cm^2 (in^2)

t_c = Thickness of cylindrical portion of tank - cm (in)

The total required tank volumes for the pressurants may be expressed as follows:

For Liquids

$$V_T = W_f/\rho_f$$

For Gases

$$V_T = \frac{K_v W_f RT}{P} \qquad K_v = 100 \text{ (Metric); } 12 \text{ (English)}$$

where

V_T = Tank total volume - cm^3 (in^3)

W_f = Pressurant fluid weight - kg (lb)

ρ_f = Density of liquid pressurant - kg/cm^3 (lb/in^3)

R = Gas Constant - m-kg/°K/kg (ft-lb/°R/lb)

T = Temperature °K (°R)

P = Pressure - kg/cm^2 (lb/in^2)

The surface area for the pressurant tanks is given as

$$A = \pi \left(1+\frac{L}{d}\right)\left[\frac{W_f}{0.5236\ \rho_f\ (1+1.5L/d)}\right]^{2/3} \quad \text{- Liquid tanks}$$

$$= \left(1+\frac{L}{d}\right)\left[\frac{22.918\ W_f\ RT}{P(1+\ 1.5\ L/d)}\right]^{2/3} \quad \text{- Gas tanks}$$

where L/d is the finess ratio for the tank.

The tank wall thickness is proportional to the pressure and radius and inversely proportional to the material stress allowable. Using the material thickness and surface area relationships, the pressurant tank weight can be expressed as

$$W_{tank} = N_o \rho_m \left[\frac{1.5P\ \eta\ W_f\ (1+2\ L/d)}{\sigma\rho_f\ (1 + 1.5\ L/d)}\right] \quad \text{- liquids}$$

$$= N_o \rho_m \left[\frac{18\ \eta\ W_f R T\ (1+2\ L/d)}{\sigma\ (1+1.5\ L/d)}\right] \quad \text{- gas} \qquad (97)$$

where

η = safety factor

σ = material stress allowable kg/cm^2 (lb/in^2)

It should be noted that these weight equations apply to either spherical tanks or cylindrical tanks with spherical ends., i.e., the L/d term becomes zero for a spherical tank.

There are several factors that must be considered in the weight estimate of a pressure vessel which contribute to and increase the actual weight over the idealized weight. Some of these factors are:

(a) Stress at reinforced openings

(b) Plastic stress

(c) Fatigue

(d) Stress discontinuity at spherical/cylindrical juncture

Several actual pressure vessels were checked with the weight equations and were found to be quite consistent in the non-optimum factor (N_o). There was very close agreement amongst the gaseous spherical pressure vessels with only a slight variation of N_o. The non-optimum weight factor for gaseous spherical pressure vessels is presented in Figure 91 as a function of tank volume. There was greater dispersion of N_o for the spherical liquid tanks; however, the value of N_o for liquid spherical tanks in Table 31 should produce acceptable weights for the pressurant tanks. A plot of pressurant tank weight versus propellant tank volume is presented in Figure 92 for a helium pressurant gas system. The pressurant tank design parameters are shown on the figure.

The weight of plumbing, valves, regulators, heaters, and supports for a pressurization system is related directly to the pressurant or propellant flow rate. The following scaling relationships for pressurant transmission were obtained from Reference 39.

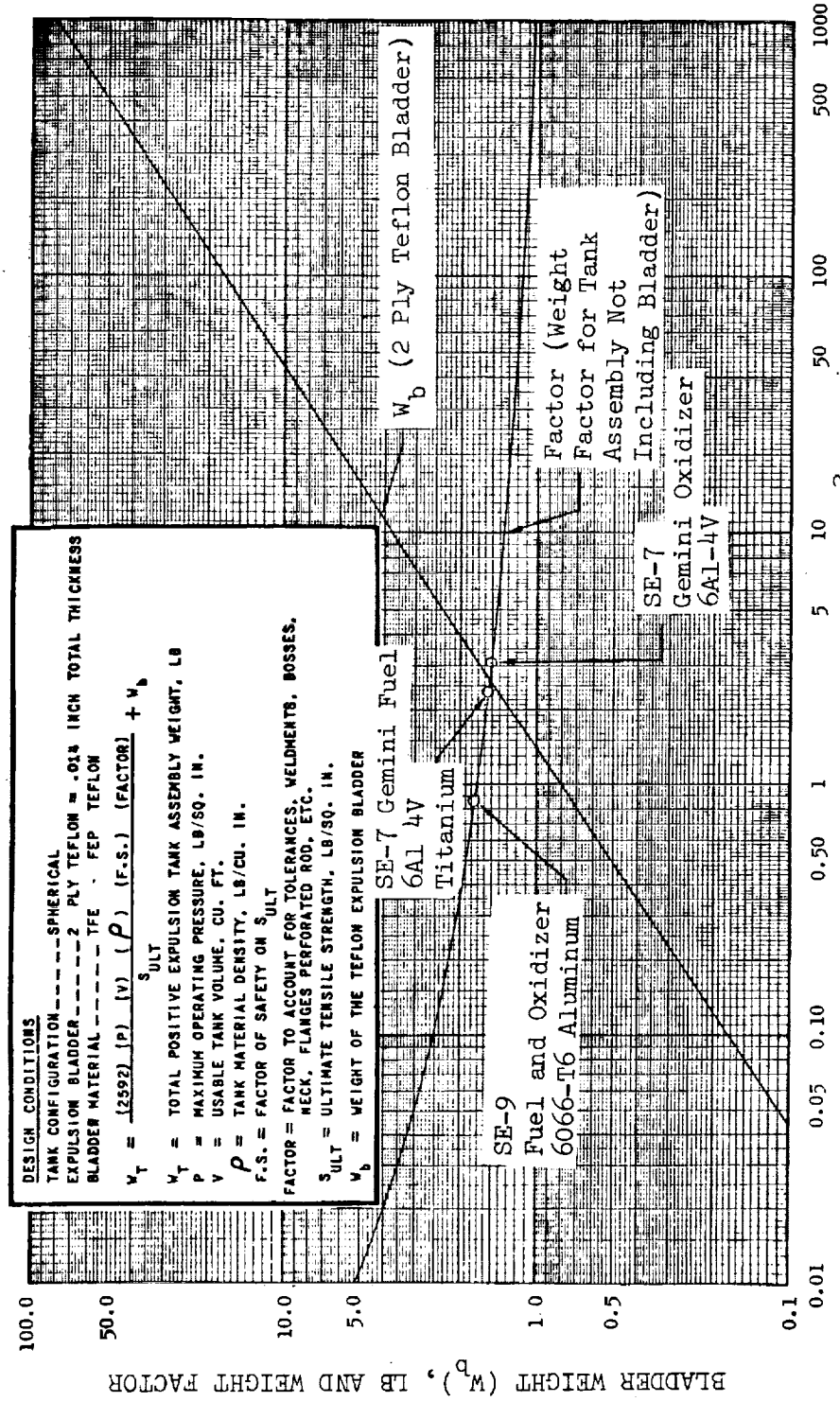

Figure 91 Weight Factor and Expulsion Bladder/Weight

Table 31. Pressurant Storage Parameters

	Cryogenic					Gas	
	H_2	O_2	N_2	He	CH_4	N_2	He
Gas Constant (R)	-	-	-	-	-	54.99	386
Storage Pressure (P)-psi	275	1000	690	46	940	3000	3000
Temperature - °R	59.8	278	227	9.4	343	460	460
Density - lb/in^3 (ρ_f)	.002557	.041186	.029085	.004514	.015318	-	-
Safety Factor (η) Proof	1.5	1.5	1.5	1.5	1.5	1.7	1.7
Safety Factor (η) Burst	2.0	2.0	2.0	2.0	2.0	2.3	2.3
Non-Optimum Factor (N_o) (Sphere)	1.32	1.32	1.32	1.32	1.32	1.41	1.41
Non-Optimum Factor (N_o) (Cylin)	1.4	1.4	1.4	1.4	1.4	1.5	1.5

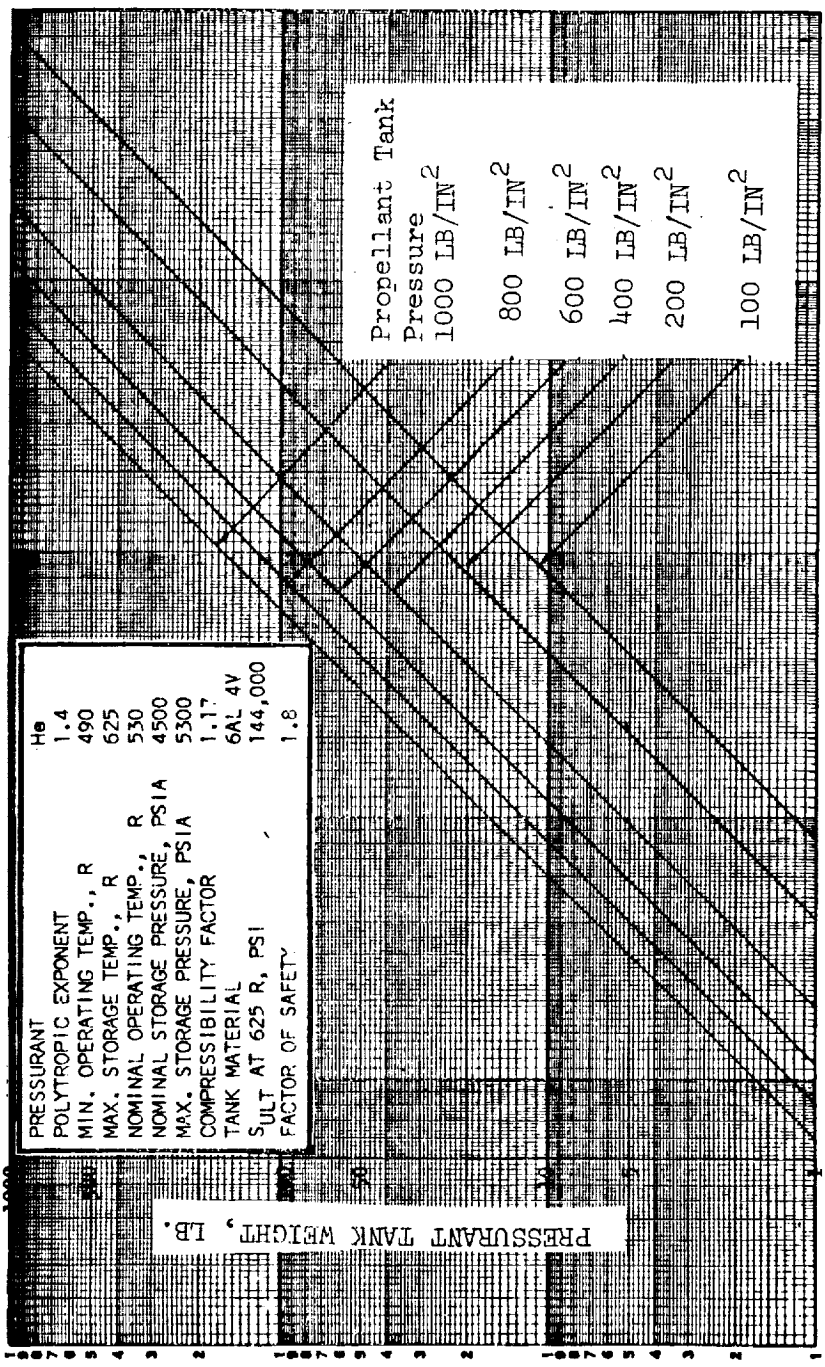

Figure 92 Pressurant Tank Weight

$$W_{pp} = 10.70 \quad EXP \left(\frac{1565\ \dot{W}}{\rho}\right)^{.125} \quad lb \text{ (Pump-fed System)}$$

$$W_{pp} = 4.85 \quad EXP \left(\frac{55200\ \dot{W}}{\rho}\right)^{.125} \quad kg$$

$$W_{pp} = 18.06 \quad EXP \left(\frac{1565\ \dot{W}}{\rho}\right)^{.125} \quad lb \text{ (Pressure-fed system)} \qquad (98)$$

$$W_{pp} = 8.18 \quad EXP \left(\frac{55200\ \dot{W}}{\rho}\right)^{.125} \quad kg$$

where;

W_{pp} = pressurant transmission weight ~ kg (lb)

$\dot{W}$ = propellant flow rate kg/sec (lb/sec)

ρ = propellant bulk density kg/m^3 (lb/ft^3)

The equation for pressure-fed systems accounts for hardware (heaters) necessary to increase the pressurant's temperature and pressure.

A typical example has been evaluated for a LOX/LH_2 pressurization system to demonstrate the procedure, weight data have been correlated with the S-II pressurization system. The design parameters for the stored gas system are

Propellants: LOX/LH_2

Pressurant: Helium stored at 3500 lb/in^2 and $400^{\circ}R$ (max) (Common storage for LOX and LH_2)

The pressurant weight is given by Equation 95 for a range of mixture ratios -

$$W_f = (7.2 \times 10^{-5})\ K'\ (P_t)\ W_P \qquad MR = 5$$

$$W_f = (6.4 \times 10^{-5})\ K'\ (P_t)\ W_P \qquad MR = 6$$

$$W_f = (5.82 \times 10^{-5})\ K'\ (P_t)\ W_P \qquad MR = 7$$

where W_P = Propellant weight ~ lb

MR = Propellant mixture ratio ($LOX:LH_2$)

For a single burn the pressurant collapse factor (K') equals 1.0. The pressurant weight is plotted versus propellant weight in Figure 93. The pressurant tank weight is based on a titanium spherical tank which has

N_o = 1.25 (Non-optimum weight factor)

and η = 2.0 (factor of safety)

By substituting these values into the pressurant tank weight-scaling Equation 97, the following relationship is arrived at

$$W_{tank} = 6.6\ W_f$$

Substituting for the pressurant weight gives;

$$W_{tank} = (47.52 \times 10^{-5})\ K'\ (P_t)\ W_P \qquad MR = 5$$

$$W_{tank} = (42.24 \times 10^{-5})\ K'\ (P_t)\ W_P \qquad MR = 6$$

$$W_{tank} = (38.412 \times 10^{-5})\ K'\ (P_t)\ W_P \qquad MR = 7$$

The pressurant tank weight is plotted versus propellant weight in Figure 94. Weight allowances for the plumbing are based on a propellant flow rate of 4.70 lb/sec, and the bulk density, ρ, for each specific mixture ratio is

ρ = 20.2 lb/ft^3 MR = 5

ρ = 22.4 lb/ft^3 MR = 6

ρ = 25.5 lb/ft^3 MR = 7

The resulting pressurization plumbing weights are shown in Table 32.

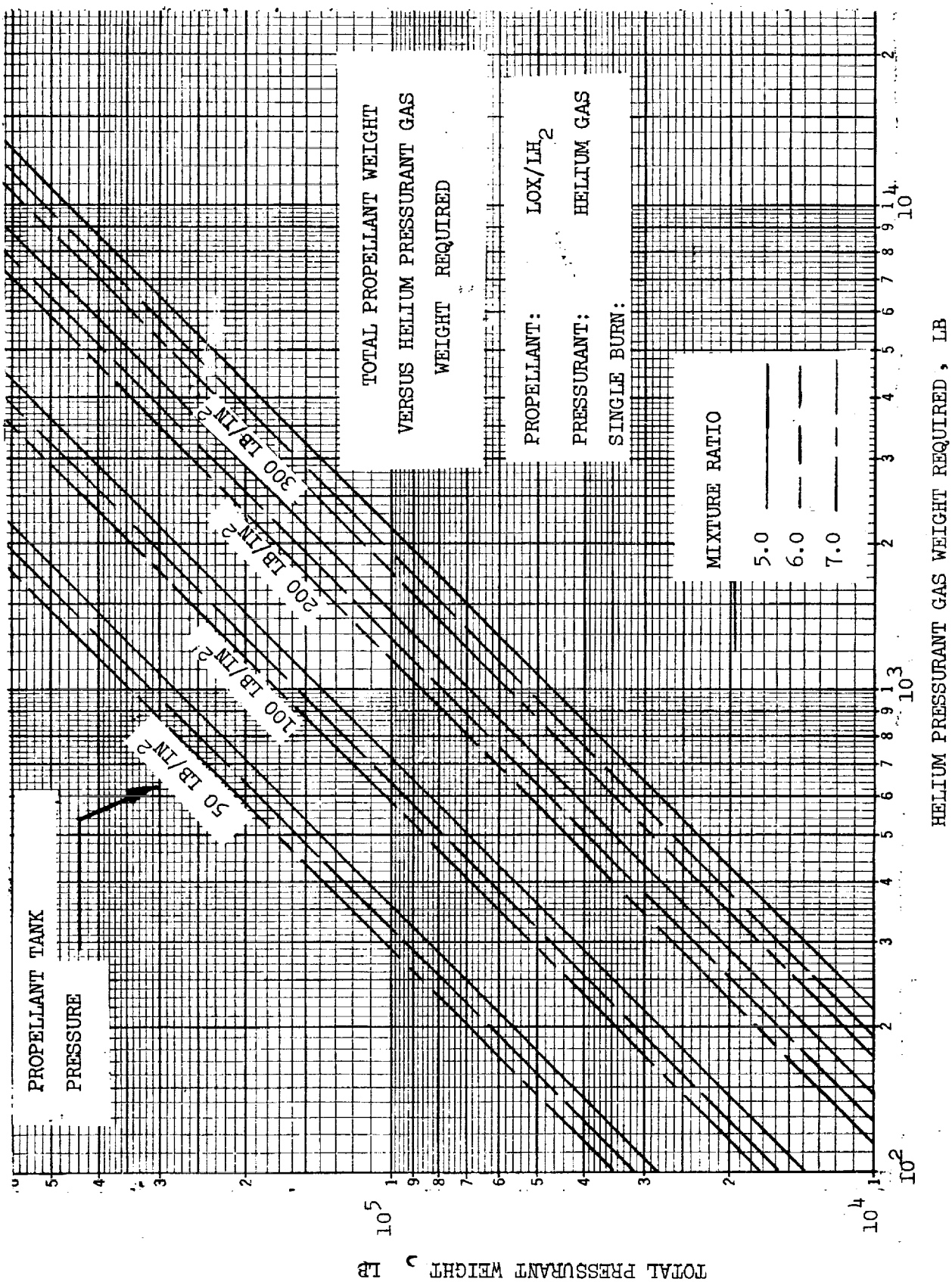

Figure 93 Helium Pressurant Gas Versus Propellant Weight

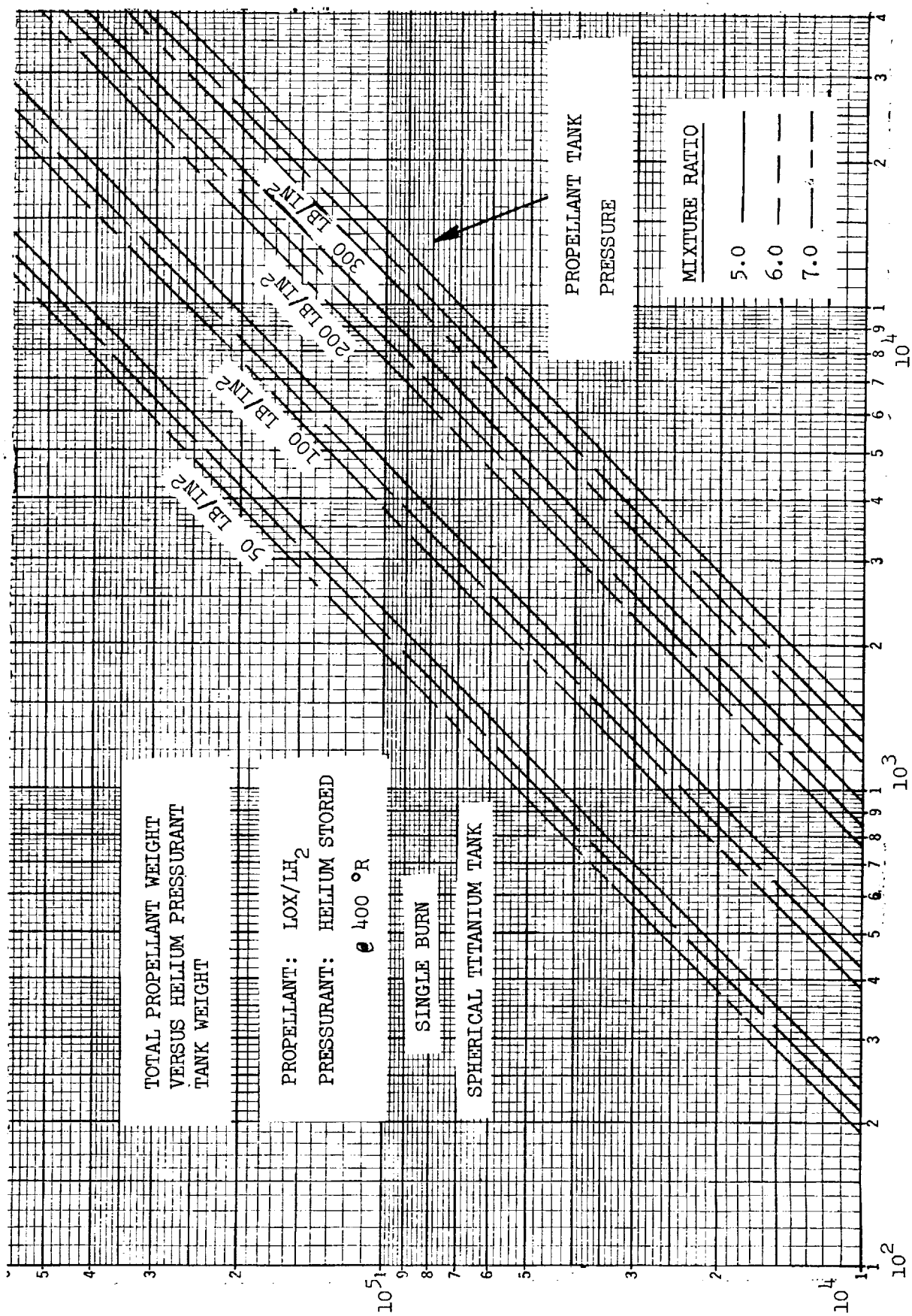

Figure 94 Pressurant Tank Weight Versus Propellant Weight

Table 32. Pressurization System Plumbing Weight

	PLUMBING WEIGHT (W_{Plumb}), LB		
	Mixture Ratio		
	5	6	7
Stored Gas System	439	417	396
Stored Gas System with Heater	741	705	669

The total weight of the stored gas pressurization system used as an example is given by

$$W_{press} = W_f + W_{tank} + W_{plumb}$$

$$W_{press} = (5.47 \times 10^{-4})\, K' \, (P_t)\, W_P + W_{plumb} \quad (MR=5)$$

$$W_{press} = (4.87 \times 10^{-4})\, K' \, (P_t)\, W_P + W_{plumb} \quad (MR=6)$$

$$W_{press} = (4.43 \times 10^{-4})\, K' \, (P_t)\, W_P + W_{plumb} \quad (MR=7)$$

A second example is for a gas generator system using the LOX/LH_2 propellants with a mixture ratio of 5.0 to pressurize the tanks. The pressurant gases in this example are GOX and GH_2 obtained at the main engine during propellant burn. The system requires no gas pressurant tanks but must include plumbing weight allowances for transfering the GOX and GH_2 to the LOX and LH_2 tanks, respectively.

Pressurization system weights for the S-II stage of the Saturn V were computed from the pressurization scaling relationship and compared to actual stage weights in Table 33.

Table 33 S-II Pressurization System Weight Comparison

	S-II PRESSURIZATION SYSTEM WEIGHTS (LBS)	
	SCALED	ACTUAL
GOX	5700	5600
GH_2	1600	1775
Plumbing	1000	1032
TOTAL	8300	8407

6.1.2.5 Thrust Structure Weight (W_{TS})

The thrust structure weight, W_{TS}, includes the thrust cone if there is a separate structure, the engine mounts and thrust posts, the end rings and cross beams. Thrust cones have varied types of construction and different cone angles and are usually based on stiffness criteria rather than direct loading in the structure. A universal scaling law has been used to express all types of thrust structure,

$$W_{TS} = 3.6 \times 10^{-3} \; F \; (N_E)^{0.3} \quad ; \; \text{kg (lb)}$$

F = stage total thrust ; kgf (lbf)

N_E = number of engines

6.2 SUBSYSTEM WEIGHT SCALING

Several of the smaller subsystems cannot be rigorously modeled to define their respective weights. These subsystems have their specifications dictated by specific mission requirements which could be quantitative. Weight scaling laws for these subsystems are related to historical data from definable hardware and are assumed to be applicable to future proposed space propulsion modules. Weights from these subsystems for the larger space propulsion stages result in only a few percent of the vehicle's inert mass.

6.2.1 Intelligence Module

Weight scaling relationships for a space vehicle's intelligence module (IM) were derived by separating the IM weight into hardware and support structure. The IM was assumed to be composed of IM hardware mounted inside a support ring, the same diameter as the space vehicle stage. The IM hardware includes the following items:

1. Guidance and Navigation
2. Control electronics
3. Communication equipment
4. Electrical power sources
5. Instrumentation
6. Environmental Control

IM hardware weight is plotted versus gross stage weight in Figure 95 using weight data obtained from Apollo, Saturn, Titan, and the present NR Space Tug project. The following scaling relationships were then derived for IM hardware.

Autonamous IM Hardware

Multiple purpose and completely independent of ground based control.

$$W_{IM_H} = 544 + 0.0075\ W_G \ ; \text{kg} \qquad (99)$$

$$W_{IM_H} = 1200 + 0.0075\ W_G \ ; \text{lb}$$

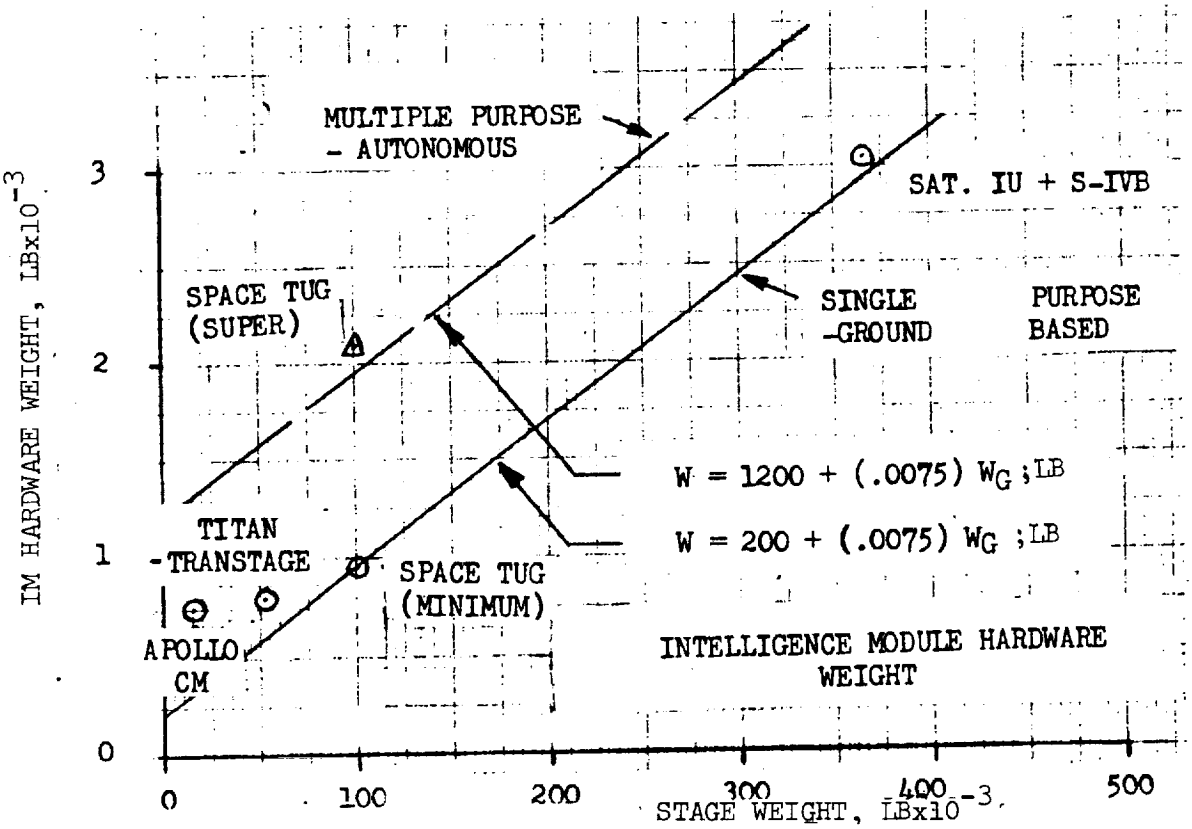

Figure 95. IM Hardware Weight

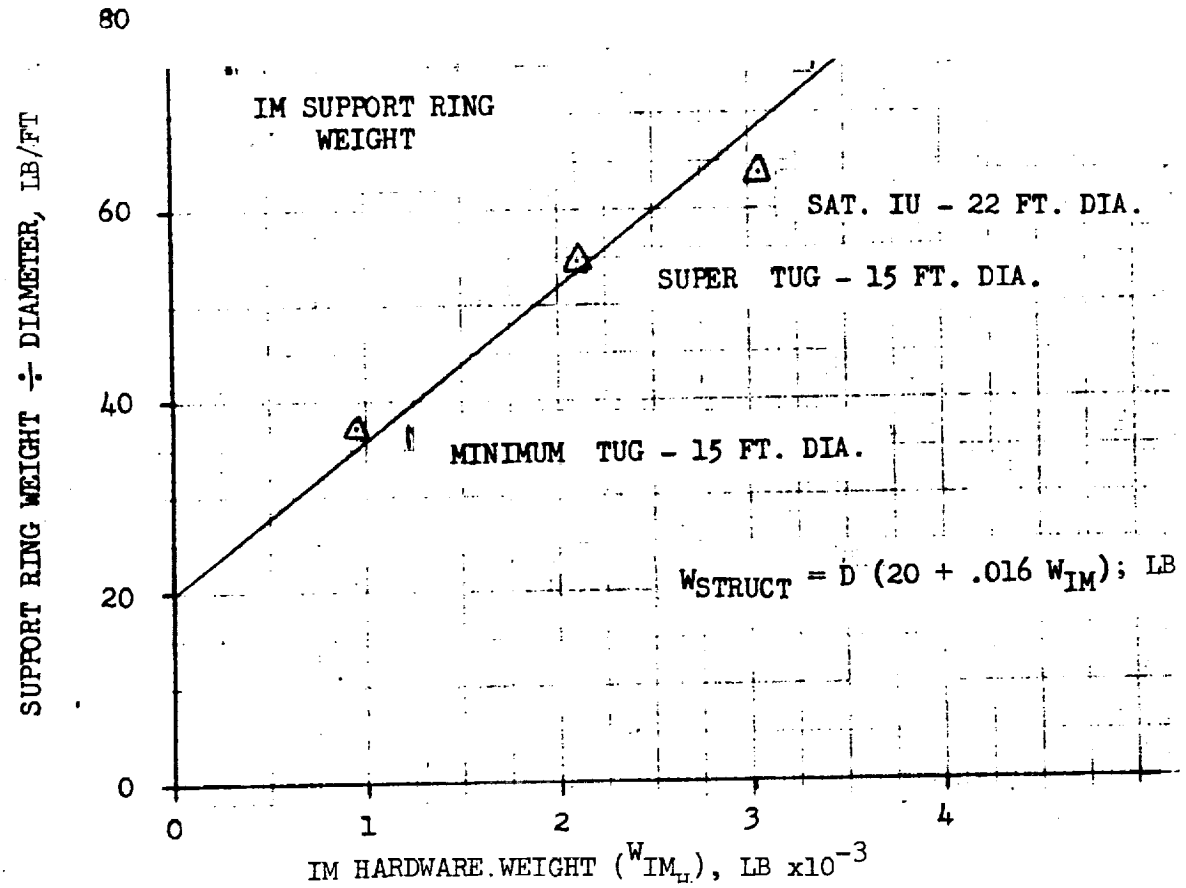

Figure 96. IM Support Ring Weight

Ground-Based-IM Hardware

Single purpose dependent upon ground-based control.

$$W_{IM_H} = 91 + 0.0075\ W_G \quad ; \text{ kg}$$

$$W_{IM_H} = 200 + 0.0075\ W_G \quad ; \text{ lb} \qquad (100)$$

W_G = Stage Weight, kg (lb)

The IM support weight was assumed to be related to the ring diameter and the weight of the IM hardware supported in the ring. The ratio of diameter-to-weight of the ring is plotted versus IM hardware weight in Figure 96. Data from the Saturn Instrument Unit (IU) and NR Space Tug IM are shown for comparison. A scaling relationship for the IM support ring weight is

$$W_{IM_{Ring}} = D\ (29.8 + 0.052\ W_{IM_H}) \quad ; \text{ kg}$$

$$W_{IM_{RING}} = D\ (20 + .016\ W_{IM_H}) \quad ; \text{ lb} \qquad (101)$$

where; D = support ring diameter, m(ft)

W_{IM_H} = IM hardware weight, kg (lb)

The scaling relationships derived for the IM hardware and support ring weights represent a preliminary method of obtaining these weights. A detailed analysis of the entire space mission would be required if better definition of the IM weight was desired.

6.2.2 Attitude Control System

The attitude control system (ACS) for space vehicles is composed of two main groups of hardware, the propulsion group and the computational group. The weight of the computational group has been included in the IM hardware weight under controls. For weight scaling purposes the ACS propulsion group was broken into propellants and hardware. The ACS hardware was assumed to include reaction control jets, plumbing, and propellant tanks. Figure 97 shows the ACS hardware weight versus gross stage weight This figure was prepared from Apollo, Titan, Saturn S-IVB, and NR Space Tug data. A scaling relationship for the ACS hardware can be represented as:

$$W_{ACS_H} = 150 + (0.002)\ W_G \quad ; \text{ lb} \qquad (102)$$

$$= 68 + (0.002)\ W_G \quad ; \text{ kg}$$

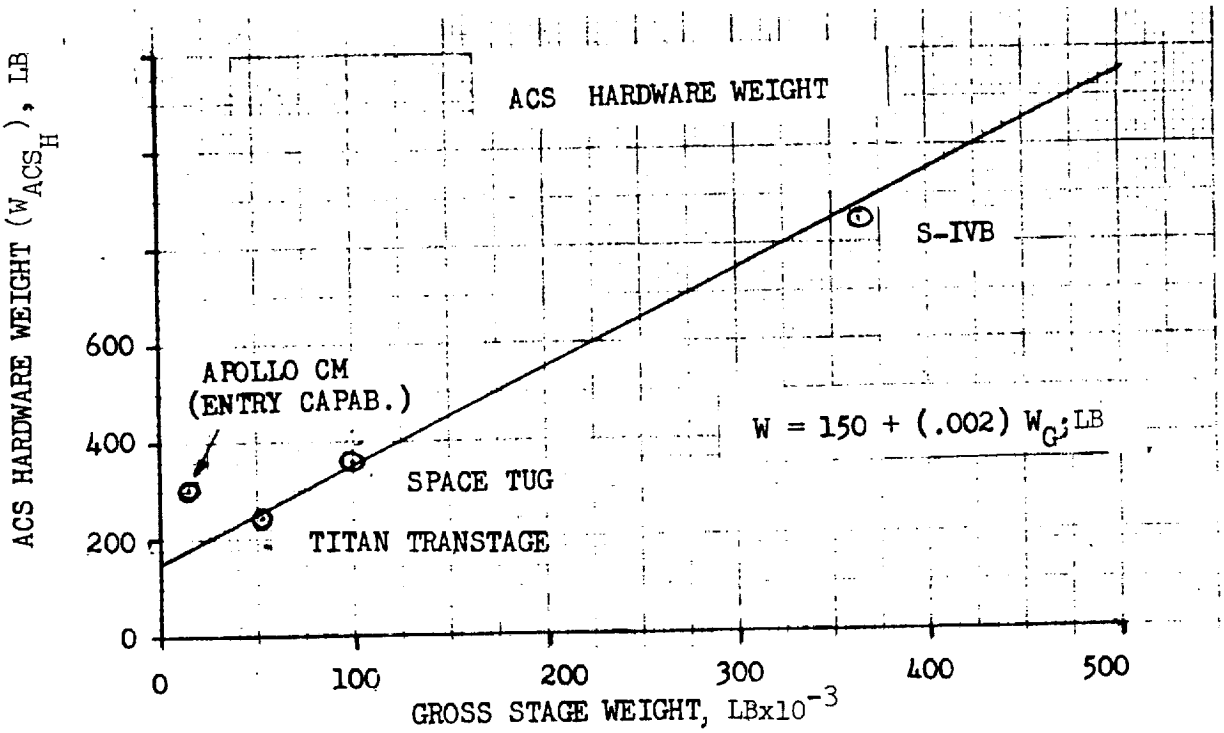

Figure 97 ACS Hardware Weight

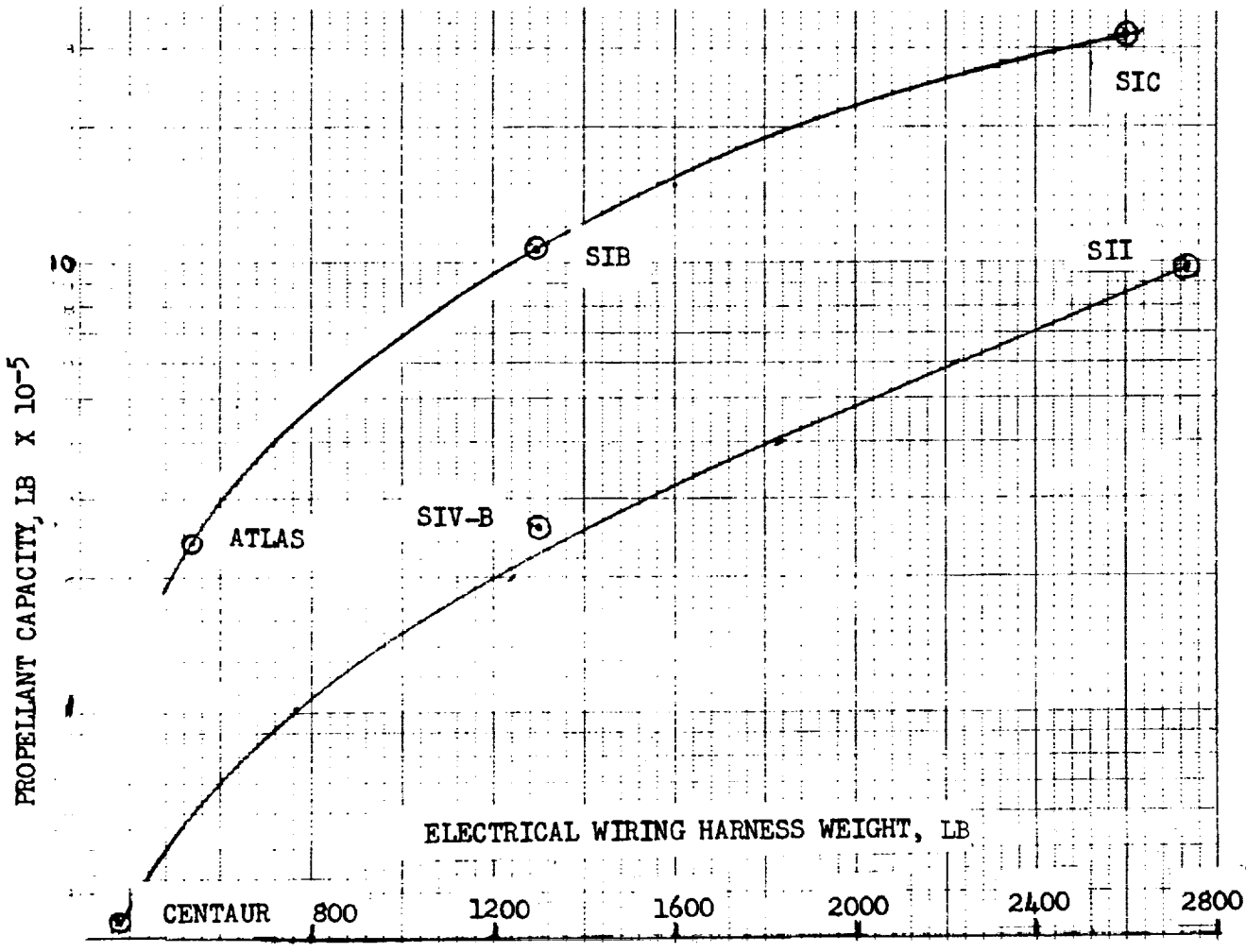

Figure 98. Electrical Wiring Harness Weight

The amount of ACS propellant required for a particular mission is dependent upon the type and accuracy of attitude control desired, the mission duration, ACS maneuver requirements, and the amount of contingency propellant required for losses and uncertainties. The ACS is made up of a system of jets which control the vehicles attitude about the pitch, yaw, and roll axes. The attitude accuracy of the system is defined by the dead band width of control about each axis. Fine control may be defined as $\pm$ 0.5 degrees and coarse control as $\pm$ 5 degrees from the desired attitude reference. The fine control requires jet pulses more often and consequently more propellant. The amount of ACS propellant required for a particular mission can be computed from the following relationship.

$$W_{ACS} = K \sum_{i=1}^{n} \left(\frac{P_i}{I_{SP}} \right)$$

where;

W_{ACS} = total ACS propellant

K = contingency factor for losses and uncertainties (1.25)

P_i = total impulse required for i^{th} mission leg

I_{SP} = specific impulse of ACS propellant

n = total number of mission legs

The amount of ΔV required for short duration maneuvers such as docking or small mid-course corrections must be defined. The required translational impulse can then be computed from the following expression.

$$P_{Ti} = \left(\frac{W_i}{g} \right) \left(\Delta V_i \right)$$

where;

P_{T_i} = translational impulse for leg

W_i = Vehicle weight at start of mission leg i

ΔV_i = total velocity change;

The total impulse for attitude hold or rate stabilized modes is a direct function of the control accuracies required for the mission. The ACS will be in primarily a limit cycle mode due to the extremely small disturbance torques acting on the vehicle. The total impulse for limit cycle operation is a direct function of the ACS dead-band width and minimum impulse of the ACS jets.

$$P_{R_i} = \frac{(57.3)(900)(24)(t_i)(I_{min})^2}{\phi_{DB}} \left(\frac{2}{(I/L)_{P_i}} + \frac{1}{(I/L)_{R_i}} \right)$$

where;

P_{R_i} = impulse required for rotational control of mission leg i (lb-seconds)

t_i = duration of mission leg i; (days)

I_{min} = minimum impulse of ACS jet (lb-sec)

ϕ_{DB} = dead-band width of ACS; (degrees)

$(I/L)_{P_i}$ = ratio of inertia over control lever arm in pitch or yaw plane for mission leg i; (slug-ft)

$(I/L)_{R_i}$ = ratio of inertia over control lever arm in roll plane for mission leg i (slug-ft)

The inertia ratios are as follows:

$$(I/L)_{P_i} = \frac{W_i}{6\ g\ L_v} (3/4\ D^2 + L_v^2)$$

$$(I/L)_{R_i} = \frac{W_i\ D}{4\ g}$$

where;

W_i = vehicle at start of mission leg (lb)

L_v = vehicle length (ft)

D = vehicle diameter (ft)

The total propellant required is the sum of the translational and rotational requirements. If the dead band width for fine and coarse attitude control

is assumed to be 0.5 and 5.0 degrees respectively, the ACS propellant is approximated by

$$W_{ACS} = 0.037\left[\frac{\Delta V}{I_{SP}} + 1.5 \times 10^{-4} t_{coarse} + 7.5 \times 10^{-2} t_{fine}\right] W_0 \quad ;lb \qquad (103)$$

where

t_{coarse} = transplanetary mission duration in days if vehicle pointing accuracy is to be obtained for propellant shielding.

t_{fine} = mission time (days) during which fine control and docking procedures are required.

6.2.3 Electrical Wiring Harness

The weight requirements for the electrical wiring for the vehicle models are influenced by the overall dimensions of the individual stage. Weight data were obtained for LOX/RP vehicles, and for Centaur, S-IVB and S-II and are shown on Figure 98. It was found the weight scaling could be expressed in terms of the stage propellant capacity

$$\begin{aligned} W_{ELEC} &= 300 + 9.7 \times 10^{-4} W_P - 7 \times 10^{-11} W_P^2 \quad ; \text{LOX/RP (lb)} \\ &= 300 + 4.78 \times 10^{-3} W_P - 2.36 \times 10^{-9} W_P^2 \quad ; \text{LOX/LH}_2 \text{ (lb)} \\ &= 136 + 9.7 \times 10^{-4} W_P - 15.5 \times 10^{-11} W_P^2 \quad ; \text{LOX/RP (kg)} \\ &= 136 + 4.78 \times 10^{-3} W_P - 5.2 \times 10^{-9} W_P^2 \quad ; \text{LOX/LH}_2 \text{(kg)} \end{aligned} \qquad (104)$$

These two different sets of scaling coefficients are the result of the different bulk densities for the LOX/RP and LOX/LH_2 stages. The equation for LOX/RP can be used for the denser fuel combinations (above 30 lb/ft^2) and the other equation for LOX/LH_2 employed for the lower bulk densities.

6.2.4 Parallel Attachment

Propellant modules or stages can be attached in parallel to other modules. The weight of the attachment mechanism and local strengthening of the stage depends upon the module diameter and the loads transmitted from one module to the center core module. Loads in the attachment structure have to be transformed from a concentrated load into the module structural shell. The weight increment to each module for the parallel staging is

Center Core Module

$$W_{T_{ATTACH}} = K_2 K_1 F^* D SF \quad ; \quad \text{kg (lb)}$$

Each Outer Module

$$W_{T_{ATTACH}} = 1.25 K_2 F^* D SF$$

where K_1 = No. of outer modules attached to center core module

$K_2 = 6.25 \times 10^{-7}$ (metric); 1.59×10^{-6} (English)

$F^* = \text{Maximum} \left\{ W_{O_{Module}} \left(T/W_o\right)_{Max}, F_{Module} \right\}$

D = Diameter of module; cm (in)

SF = Safety factor

7.0 SUMMARY OF IMPROVED SCALING LAWS

Space propulsion systems have been categorized into four independent modules for the weight-scaling laws. These modules will completely describe the vehicle stage and provide the stage weight and size description. Each of the major modules is composed of several primary subelements as shown in Table 34.

Table 34. Weight Modules for Scaling Laws

Engine Module	Propellant Module	Environmental Protection	Other Subsystems
Thrust Chamber Assembly	Tank Wall	Cryogen Insulation	Guidance
Thrust Vector Controls	Bulkheads	Insulation Attachment	Navigation
Skirt Enclosing Engines	Forward Skirt	Meteoroid Bumpers	Attitude Control
Thrust-Structure	Intertank	Secondary Structure	Docking
	Aft Skirt		Electrical
	Pressurization		Instrumentation
	Propellant Feed		Parallel Attmt. Structure

Each of these four modules is influenced by the type of space mission, its profile and duration, and individual design concepts/systems envisaged for the space vehicle. The engine module weight/size is determined by the type and number of engines. The inert weight of the propellant module is based on the propellant weight and volume, tankage arrangement, loading environment, and material/design selected. The stage mission exposure time history will define the thermal and meteoroid flux environment. This environment, the stage's surface area and type of propellant are used to determine the weights associated with the environmental protection systems. Other subsystems for the stage will be dictated by the type of mission, manned or unmanned, etc. These subsystem laws are based on historical data rather than explicit analysis of each subsystem's functional requirement which perhaps would not be completely defined during the conceptual studies.

7.1 ENGINE MODULE

The improved scaling laws for the engine module have been developed for the following system elements.

1. Thrust Chamber Assembly
   (a) Pressure and pump-fed
   (b) Cryogens, space- and earth-storable propellant
   (c) Fixed and stowed nozzles
   (d) Base heat protection
2. Thrust vector controls
3. Structure
   (a) Thrust structure
   (b) Skirt enclosing engine system

Thrust Chamber Assembly Weight (W_{ENG})

The scaling laws for the TCA, W_{ENG}, have been provided for the different classes of engine systems for a series of thrust ranges. Engine weights provided from these laws are considered to include:

1. Thrust attachment points
2. Turbo-pumps
3. Preburner assembly (where applicable)
4. Combustion Chamber assembly
5. Expansion of nozzle and translating mechanism (where applicable)
6. Controls, shut-off valves
7. Engine plumbing

Weight-scaling laws are provided in metric units, Table 35 and English units, Table 36. Since scaling laws are empirical in nature, the scaling equations are not dimensionally consistent, therefore, the conversion factors from metric to english units are not a single factor for all equations. In fact, each individual equation has to have its own conversion factor.

Engine dimensional data, length and overall diameter have been provided in Table 37. This information is required for determination of the length and hence weight of the stages' aft skirt which surrounds the engine(s). The Base Heat Protection (W_{BH_P}) is related to the combustion radiation of the propellants and the thrust level of the engine.

$$W_{BH_P} = K_1 \, (T/W)^{-0.666} \, (L/D)^{-0.663} \, F^{0.7807} \quad ; \quad \text{kg (lb)}$$

T/W = stage thrust to weight ratio

L/D = stage fineness ratio (length to diameter)

Table 35. Engine Weight Scaling Law (Metric Units)

$$W_{ENG} = K_1 F^{K_2} P_c^{K_3} \epsilon^{K_4} t_b^{K_5} + K_6 F^{K_7} P_c^{K_8} \epsilon + K_9 \epsilon + K_{10} \quad \text{(kg)}$$

Propellant Combination	K_1	K_2	K_3	K_4	K_5	K_6	K_7	K_8	K_9	K_{10}	Thrust Range Kgf	Remarks
Pressure Fed												
LO_2/LH_2	0.0336	0.853	-0.757	0.24	0.297	NA	NA	NA	NA	NA	450-13600	Ablative Fixed Nozzle
N_2O_4/MMH	0.218	0.538	-0.703	0.206	0.297						450-13600	Ablative/Radiation Fixed Nozzle
N_2O_4/UDMH	0.037	0.853	-0.757	0.24	0.297						450-13600	Ablative Stowed Nozzle
	0.24	0.538	-0.703	0.206	0.297						450-13600	Ablative/Radiation Stowed Nozzle
LF_2/LH_2	0.0403	0.853	-0.757	0.24	0.297	NA	NA	NA	NA	NA	450-13600	Ablative Fixed Nozzle
OF_2/CH_4	0.262	0.538	-0.703	0.206	0.297						450-13600	Ablative/Radiation Fixed Nozzle
OF_2/B_2H_6	0.0444	0.853	-0.757	0.24	0.297						450-13600	Ablative Stowed Nozzle
FLOX/CH_4	0.288	0.538	-0.703	0.206	0.297						450-13600	Ablative/Radiation Stowed Nozzle
Tripropellant	0.00161	1.22	-0.70	0.5	NA	NA	NA	NA	NA	9.07	450-13600	
Pump Fed												
LO_2/LH_2	$1.758X10^{-6}$	1.0	-1.0	2.0	NA	0.0183	1.0	0.0	NA	2.268	450-3630	Fixed Nozzle
LF_2/LH_2	$1.758X10^{-6}$	1.0	-1.0	2.0		0.0105	1.0	0.0		36.3	3630-13600	Fixed Nozzle
	$1.758X10^{-6}$	1.0	-1.0	2.0		0.00966	1.0	0.0		49.9	13600-113400	Fixed Nozzle
	0.00106	1.0	-1.0	1.0		0.0189	1.0	0.0		2.268	450-13600	Stowed Nozzle
	0.00106	1.0	-1.0	1.0		0.00966	1.0	0.0		49.9	13600-113400	Stowed Nozzle
	$2X10^{-9}$	1.5	-1.0	1.0		$1.065X10^{-6}$	1.0	1.0	2.5	454	90000-340000	High Pressure
OF_2/CH_4	0.3257	0.814	-0.43	0.05	NA	NA	NA	NA	NA	NA	450-22700	Fixed Nozzle
FLOX/CH_4	0.112	0.9269	-0.467	0.094							22700-113400	Fixed Nozzle
	0.3908	0.814	-0.43	0.05							450-22700	Stowed Nozzle
	0.117	0.9269	-0.467	0.094							22700-113400	Stowed Nozzle
Tripropellant	$6.4X10^{-3}$	1.1	0.0	0.0	NA	$1.4X10^{-5}$	1.1	0.0	NA	11.4		Fixed Nozzle

NA = Not Applicable

Table 36. Engine Weight Scaling Laws (English Units)

$$W_{ENG} = K_1 F^{K_2} P_c^{K_3} \epsilon^{K_4} t_b^{K_5} + K_6 F^{K_7} P_c^{K_8} \epsilon + K_9 \epsilon + K_{10} \text{ (lb)}$$

Propellant Combination	K_1	K_2	K_3	K_4	K_5	K_6	K_7	K_8	K_9	K_{10}	Thrust Range lbf	Remarks
Pressure Fed												
LO_2/LH_2	0.282	0.853	-0.757	0.24	0.297	NA	NA	NA	NA	NA	1000-30000	Ablative Fixed Nozzle
N_2O_4/MMH	2.03	0.538	-0.703	0.206	0.297						1000-30000	Ablative/Radiation Fixed Nozzle
$N_2O_4/UDMH$	0.31	0.853	-0.757	0.24	0.297						1000-30000	Ablative Stowed Nozzle
	2.23	0.538	-0.703	0.206	0.297						1000-30000	Ablative/Radiation Stowed Nozzle
LF_2/LH_2	0.338	0.853	-0.757	0.24	0.297	NA	NA	NA	NA	NA	1000-30000	Ablative Fixed Nozzle
OF_2/CH_4	2.44	0.538	-0.703	0.206	0.297						1000-30000	Ablative/Radiation Fixed Nozzle
OF_2/B_2H_6	0.372	0.853	-0.757	0.24	0.297						1000-30000	Ablative Stowed Nozzle
$FLOX/CH_4$	2.68	0.538	-0.703	0.206	0.297						1000-30000	Ablative/Radiation Stowed Nozzle
Tripropellant	0.008672	1.22	-0.70	0.5	NA	NA	NA	NA	NA	20	1000-30000	
Pump Fed												
LO_2/LH_2	$2.5X10^{-5}$	1.0	-1.0	2.0	NA	0.0183	1.0	0.0	NA	5.0	1000-8000	Fixed Nozzle
LF_2/LH_2	$2.5X10^{-5}$	1.0	-1.0	2.0		0.0105	1.0	0.0		80.0	8000-30000	Fixed Nozzle
	$2.5X10^{-5}$	1.0	-1.0	2.0		0.00966	1.0	0.0		110.0	30000-250000	Fixed Nozzle
	0.015	1.0	-1.0	1.0	0.0	0.0189	1.0	0.0		5	1000-30000	Stowed Nozzle
	0.015	1.0	-1.0	1.0	NA	0.00966	1.0	0.0		110.0	30000-250000	Stowed Nozzle
	$2X10^{-8}$	1.5	-1.0	1.0		$1.02X10^{-5}$	1.0	1.0	2.5	1000.0	200000-750000	High Pressure
OF_2/CH_4	1.1819	0.814	-0.43	0.05	NA	NA	NA	NA	NA	NA	1000-50000	Fixed Nozzle
$FLOX/CH_4$	0.41054	0.9269	-0.467	0.094							50000-250000	Fixed Nozzle
	1.30	0.814	-0.43	0.05							1000-50000	Stowed Nozzle
	0.43	0.9269	-0.467	0.094							50000-250000	Stowed Nozzle
Tripropellant	$5.94X10^{-3}$	1.1	0.0	0.0	NA	$1.4X10^{-5}$	1.1	0.0	NA	25.0		Fixed Nozzle

NA= Not Applicable

TABLE 37 Engine Dimensional Data

PROPELLANT COMBINATION	NOZZLE TYPE	K_1	K_2	K_3	K_4	K_5	THRUST RANGE
CRYOGENIC -, SPACE-AND EARTH - STORABLE PROPELLANTS	FIXED	102	1.05	0.5	1.0	0.815	>4540 kgf
	FIXED	40	1.05	0.5	1.0	0.815	>10000 lbf
	FIXED	12.7	1.45	0.5	1.0	0.815	<4540 kgf
	FIXED	5	1.45	0.5	1.0	0.815	<10000 lbf
	STOWED	102	0.53	0.5	1.0	0.815	>4540 kgf
	STOWED	40	0.53	0.5	1.0	0.815	>10000 lbf
	STOWED	12.7	0.73	0.5	1.0	0.815	<4540 kgf
	STOWED	5	0.73	0.5	1.0	0.815	<10000 lbf
TRIPROPELLANT	FIXED	0	2.31	0.4	0.0	0.815	-

LENGTH

$$L_{ENG} = K_1 + K_2 \left(\frac{F}{P_c}\right)^{1/2} \left(\epsilon^{K_3} - K_4\right) \quad ; \quad \text{cm (in)}$$

DIAMETER

$$D_{ENG} = K_5 \left(\frac{F}{P_c}\right)^{1/2} \quad ; \quad \text{cm (in)}$$

NOTE: VALUES IN PARENTHESIS ARE FOR ENGLISH UNITS

Table 38. Coefficients K_1 For Base Heat Protection Weight

COMBUSTION RADIATION LEVEL	Propellant	Metric K_1	English K_1
Low	LF_2/LH_2, LO_2/LH_2 $LF_2/LI/LH_2$	0.0172	0.0205
High	OF_2/B_2H_6, OF_2/CH_4 $FLOX/CH_4N_2O_4/MMH$	0.0233	0.0277

Thrust Vector Control (W_{TVC})

The thrust vector control system ($Weight_{TVC}$) is directly related to the engine thrust level which it is required to deflect

$$W_{TVC} = K_1 + K_2 F \quad ; \text{ kg (lb)}$$

Table 39 Thrust Vector Control Weight Coefficients

Thrust	K_1	K_2
$F < 13600$ kgf	0	0.002209
$F > 13600$ kgf	22.7	0.000542
$F < 30000$ lbf	0	0.002209
$F > 30000$ lbf	50	0.000542

Thrust Structure Weight (W_{TS})

The thrust structure weight W_{TS}, includes the thrust cone if there is a separate structure, the engine mounts and thrust posts, the end rings and cross beams. Thrust cones have varied types of construction and different cone angles and are usually based on stiffness criteria rather than direct loading in the structure. A universal scaling law has been used to express all types of thrust structure,

$$W_{TS} = 3.6 \times 10^{-3} \; F \; (N_E)^{0.3} \quad ; \text{ kg (lb)}$$

F = stage total thrust ; kgf (lb)

N_E = number of engines

Interstage Shell Weight (W_{INST})

The outer shell structure weight encasing the engine(s) is included in the engine module weight. The surface area of the shell is determined from the engine length (Table 37) and the stage diameter (D). Unit structural weight (W_{SHELL}) can be obtained from the structural synthesis equations of section 7.2

$$W_{INST} = \pi \, L_{ENG} D \; W_{SHELL}$$

7.2 PROPELLANT MODULE

The propellant module consists of the structural elements for the propellant containers, and the support structure between tanks and stages. Weight-scaling relationships are quoted for the various types of materials and construction for different environments, pressure and/or compressive stresses, and the component geometry. Weight data were statistically reduced from the design synthesis data for a large spectrum of design points.

The pressurized components are the tank wall and tank bulkheads. Surface area for these components are obtained from equations defining the tankage models and the volume required to contain the propellant. The six different tank arrangements are:

Tank Shape

1) 2 tandem tanks, identical radii and separate bulkhead

2) 2 tandem tanks, identical radii and common bulkhead

3) Single forward tank and 3 internally suspended aft tanks

4) Single forward tank and 4 internally suspended aft tanks

5) 2 spherical tanks with separate bulkheads

6) Single cylindrical forward tank and aft toroidal tank

Propellant Module Surface Areas

The stage geometry can be specified either by its diameter or the module fineness ratio (length to diameter). If the fineness ratio (L/D) and volume of oxidizer and fuel are given, the diameter is obtained from

$$D = \left\{ \frac{K_1 V_1 + K_2 V_2}{\pi \left[(K_3 (L/D) - K_4 (b/a) \right]} \right\}^{1/3}$$

where b/a = the bulkhead aspect ratio,

V_1 = forward tank volume; $W_{P_1} / \rho_1 (1+UF)$

V_2 = aft tank volume; $W_{P_2} / \rho_2 (1+UF)$

W_{P_1}, W_{P_2} = total weight of either the oxidizer or fuel including the boil-off weights

UF = the ullage factor

Table 40 Propellant Module Diameter Coefficients

Tank Shape	K_1	K_2	K_3	K_4
1	1.0	1.0	0.25	0.167
2	1.0	1.0	0.25	0.0835
3	1.0	1.78	0.25	0.1195
4	1.0	2.0	0.25	0.113
5 fwd	1.0	0.0	0.0	-0.167
5 aft	0.0	1.0	0.0	-0.167
6	1.0	0.0	0.0	-0.167

The tank module surface areas vary for the different tank arrangements and are evaluated from the following equations

Forward tank bulkheads

$$A_{Bulk\ 1} = KK_1 D_1^2$$

Aft tank bulkheads

$$A_{Bulk\ 2} = KK_2 D_2^2$$

Forward tank wall

$$A_{cy_1} = K_3 D \left(K_4 \frac{V_1}{D_1^2} - K_5 D_1 \frac{b}{a} \right)$$

Aft tank wall

$$A_{cy_2} = K_6 D \left(K_7 \frac{V_2}{D_2^2} - K_8 D_2 \frac{b}{a} \right)$$

Forward Skirt

$$A_{FWD} = K_9 D_1^2 \frac{b}{a}$$

Aft Skirt

$$A_{AFT} = K_{10} D_2^2 \frac{b}{a}$$

Intertank shell

$$A_{INT} = K_{11}\left(A_{FWD} + A_{AFT} \right) + K_{12} A_{cy_2}$$

where $K = 2.0\pi \left[1 + \frac{(b/a)^2}{2E} \ln \left(\frac{1+E}{1-E} \right) \right]$

$$E = \left[1 - (b/a)^2 \right]^{0.5}$$

Table 41 Propellant Module Surface Area Coefficients

Tank Shape / K_I	1	2	3	4	5	6
K_1	0.25	0.25	0.25	0.25	0.25	0.25
K_2	0.25	0.25	0.047	0.0313	0.25	(2)
K_3	3.142	3.142	3.142	3.142	0.0	3.142
K_4	1.275	1.275	1.275	1.275	0.0	1.275
K_5	0.667	0.0	0.667	0.667	0.0	0.667
K_6	3.142	3.142	1.365	1.11	0.0	0.0
K_7	1.275	1.275	2.27	2.55	0.0	0.0
K_8	0.667	0.667	0.289	0.237	0.0	0.0
K_9	1.571	1.571	1.571	1.571	1.571	1.571
K_{10}	1.571	1.571	0.68	0.555	1.571	(3)
K_{11}	1.0	0.0	1.0	1.0	(1)	1.0
K_{12}	0.0	0.0	2.32	2.83	0.0	0.0

(1) $$A_{INT} = \pi\left(\frac{D_1+D_2}{4}\right)\left(\frac{b}{a}\right)^2\left[(D_1+D_2)^2 + (D_2-D_1)^2\right]^{0.5}$$

(2) $$A_{Bulk\ 2} = 4\,\pi^2\,R.(RR)$$

(3) $$A_{AFT} = \pi\,D\,R$$

R and RR are the minor and major radii of the toroid.

Structural Shell Weights

The design loading intensity, N_x, has to be developed for all the structural components of each model and depends upon the design conditions which are:

1) Earth launch fully loaded as payload of expendable vehicle system
2) Earth launch fully loaded as payload in earth orbital shuttle cargo bay
3) Space launched

The unit structural weights are scaled by

Tank Wall Unit Weight

$$W_{Tank} = K_1 PR\sigma^{-1} + K_2 N_x^{K_3} R^{K_4} P^{K_5} \left(\frac{E}{10^6}\right)^{K_6}$$

Values for K_1 - K_6 are given in Table 4 metric and Table 5 English units.

Tank Bulkhead Weight

$$W_{Bulk} = K_1 \rho \left(\frac{b}{a}\right)^{K_2} R^3 P \sigma^{-1} \quad ; 0.707 \leq \frac{b}{a} \leq 1.0$$

$$= K_1 \rho \left(\frac{b}{a}\right)^{K_2} R^3 \left(K_3 - \frac{b}{a}\right)^{K_4} P^{\left(K_5 + \frac{b}{a}\right)^{K_6}} E^{K_7}$$

$$; 0.5 \leq \frac{b}{a} \leq .707$$

Values for K_1 - K_7 for bulkhead weight are shown in Table 9 (metric) and Table 10 (English units).

Unpressurized Shell Unit Weight

$$W_{Shell} = K_1 N_x^{K_2} \sigma^{K_3} (R+K_4)^{K_5} E^{K_6}$$

Values for K_1 - K_6 for different material and construction are supplied in Tables 2 and 3.

Where

P = tank maximum pressure times ultimate safety factor kg/cm^2 (lb/in^2)

N_x = ultimate load intensity accounting for pressure relief kg/cm (lb/in)

σ = $MIN \left(\frac{F_{ty}}{FS_y}, \frac{F_{tu}}{FS_u}\right)$

F_t = material stress kg/in^2 (lb/in^2)

FS = factor of safety

y yield, u ultimate

E = Young's Modulus depending on material temperature kg/cm^2 (lb/in^2)

The actual component weight, W_{COMP}, is the components surface area, A, the unit weight, W, and the non-optimum weight factors F_{NOM} and F_{NOC}.

$$W_{COMP_i} = W_i A_i F_{NOM_i} F_{NOC_i}$$

where F_{NOM} is the non-optimum weight factor depending upon the type of construction and material, and F_{NOC} varies with the structural component.

Table 42. Material Non-optimum Weight Factor F_{NOM}

Material \ Construction	Monocoque	Skin Stringer	Waffle	Sandwich
Aluminum	1.04	1.05	1.05	1.07
Titanium	1.05	1.06	1.06	1.08
Berylium	1.05	1.06	1.06	1.08
Composites	1.06	1.07	1.07	1.09

Table 43 Component Non-optimum Weight Factor F_{NOC}

Forward Skirt	1.02
Forward Bulkhead	1.02
Aft Bulkhead	1.05
Tank Wall	1.03
Intertank	1.03
Aft Skirt	1.03
Interstage	1.06

Propellant Baffles

The propellant baffles, W_{SB}, and secondary structure for the propellant module can be expressed as

$$W_{SB} = K_1 \left(\frac{W_{P_O}}{\rho_O R_O} + \frac{W_{P_f}}{\rho_F R_f} \right) \quad ; \text{ kg (lb)}$$

K_1 = 0.92 metric; 0.19 English

ρ = propellant density kg/in^3 (lb/ft^3)

W_P = propellant weight kg (lb)

R = tank radius m (ft)

subscripts O, oxidizer ; f, fuel

Bulkhead to Tank Wall Attachment (W_{INTER})

Additional weight, W_{INTER}, is considered for the attachment of the bulkheads, tank walls and the outer unpressurized shell

$$W_{INTER} = K_1 \; F^{1.083} \; P^{0.5} \quad ; \text{ kg (lb)}$$

$$K_1 = 1.94 \times 10^{-4} \text{ (metric)} \quad ; \quad 4.9 \times 10^{-5} \text{ (English)}$$

Propellant Feed System (W_{PF})

The weights for the propellant feed systems, W_{PF}, are itemized for the oxidizer and fuel systems.

$$W_{PF_i} = K_1 + K_2 \, N_E \left(\frac{F}{I_{sp} \; \rho_i}\right)^{1/2} \left(\frac{W_i}{1000}\right)^{K_3} \quad ; \text{ kg (lb)}$$

F = engine thrust level kg (lb)

I_{sp} = specific impulse

W_i, ρ_i = weight, kg (lb) and density, kg/cm^3 (lb/in^3), of propellant i = 1 oxidizer; i = 2 fuel

Table 44 Propellant Feed System Weight Coefficients

System	Thrust lbf (kgf)	Metric			English		
		K_1	K_2	K_3	K_1	K_2	K_3
Oxidizer	> 200,000 (90700)	272	0.22	0.73	600	1.10	0.73
	< 200,000 (90700)	36.3	1.06	0.73	80	5.30	0.73
Fuel	> 200,000 (90700)	399	0.35	0.68	880	1.75	0.68
	< 200,000 (90700)	8.2	3.34	0.68	18	16.7	0.68

Pressurization System

The pressurization system consists of the pressurant gas, its container (if any), and the pressurant transmission.

Pressurant Weight (W_f)

$$W_f = K_1 \frac{P_t V_t}{T_u} MK^1 \quad ; \text{ kg (lb)}$$

K_1 = 126.5 (metric); 0.1 (English)

K^1 = collapse factor {1.0 single burn; 1.2 multiple burn}

P_t = propellant tank pressure, kg/cm^2 (lb/in^2)

T_u = ullage temperature ^oK (^oR), Table 45

V_t = main propellant tank volume m^3 (ft^3)

M = molecular weight of pressurant gas

Pressurant Tank Weight (W_{PT})

If the pressurant used for pressurization is propellant from the main tank which has been cycled through a heat exchanger, then there will be no tank required to contain the pressurant. Otherwise, separate pressurant tanks must be supplied and their weight scaling relationships are

Table 45. Pressurant Design Physical Parameters

		Liquid Storage					Gas	
		H_2	O_2	N_2	He	CH_4	N_2	He
Gas Constant (R)		-	-	-	-	-	54.99	386
Storage Pressure (P)-psi		275	1000	690	46	940	3000	3000
Temperature - °R		59.8	278	227	9.4	343	460	460
Density - $Lb/In^3(\rho f)$		.002557	.041186	.029085	.004514	.015318	-	-
Safety Factor (η) Proof		1.5	1.5	1.5	1.5	1.5	1.7	1.7
Safety Factor (η) Burst		2.0	2.0	2.0	2.0	2.0	2.3	2.3
Non-Optimum Factor (N_o) (Sphere)		1.32	1.32	1.32	1.32	1.32	1.41	1.41
Non-Optimum Factor (N_o) (Cylin)		1.4	1.4	1.4	1.4	1.4	1.5	1.5
Molecular Weight Lb/lb Mole		2.0	32.0	-	4.0	16.0	-	4.0
Propellant		LH_2	LO_2	LF_2/FLOX	OF_2	CH_4	B_2H_6	Earth Storable
Average Ullage Temperature	°K	145	185	185	200	195	230	320
	°R	260	330	330	360	350	410	580

$$W_{PT} = N_o \rho_m \left[\frac{1.5 P \eta W_f \ (1 + 2L/D)}{\rho_f \sigma (1 + 1.5\ L/D)} \right] \quad \text{- liquids storage}$$

$$= N_o \rho_m \left[\frac{18 \eta W_f \ RT_f \ (1 + 2\ L/D)}{\sigma (1 + 1.5\ L/D)} \right] \quad \text{- gas storage}$$

where

P = tank pressure kg/cm^2 (lb/in^2)

η = safety factor

σ = material stress allowable kg/cm^2 (lb/in^2)

R = gas constant m - $kg/^oK/kg$ ($ft\text{-}lb/^oR/lb$)

ρ_f = density of liquid pressurant kg/cm^3 (lb/in^3)

T_f = temperature of pressurant ^oK (^oR)

Pressurant Transmission Weights (W_{PP})

The plumbing valves, heaters, regulators, etc., which constitute the pressurant transmission can be scaled from

$$W_{PP} = K_1 \exp \left(\frac{K_2 \dot{\omega}}{\rho} \right)^{0.125} \quad ; \text{ kg (lb)}$$

where W_{PP} = pressurant transmission weight

$\dot{\omega} \approx T/I_{sp}$ - propellant flow rate kg /sec (lb/sec)

ρ = propellant bulk density kg/m^3 (lb/ft^3)

Table 46 Pressurant Transmission Weight Coefficients

System	Metric		English	
	K_1	K_2	K_1	K_2
Pump-fed	4.85	55200	10.70	1565
Pressure-fed	8.18	55200	18.06	1565

7.3 ENVIRONMENT PROTECTION

7.3.1 Meteoroid Protection

Both the meteoroid and thermal environments vary throughout the mission profile and their fluxes are integrated during each mission segment.

The meteoroid flux distribution is represented by

$$\text{Log}_{10} F = K_1 + K_2 \ \text{Log}_{10} m + f(R) + \text{Log}_{10} \bar{V} \qquad \text{Table 47}$$

and the relative velocity between the meteoroid particle and the spacecraft is

$$\bar{V} = R^{-0.5} \ u_1 \left(\mu_2 - u_3 \ \sigma \cos\gamma + \sigma^2 \right)^{0.5} \qquad \text{m/sec}$$

where F = flux of particles of mass $\geq m$, m^{-2} sec^{-1}

m = meteoroid mass grams

$f(R)$ = solar system distribution for particles: asteroidal, (Figure 99); cometary, $- 1.5 \log_{10} R$; stream, not applicable.

R = distance from sun (Au)

σ = ratio of vehicle speed to circular speed

γ = angle between vehicle velocity vector and circular velocity vector.

Modification factors are applied to the undisturbed flux to account for gravitational and shielding effects of planets.

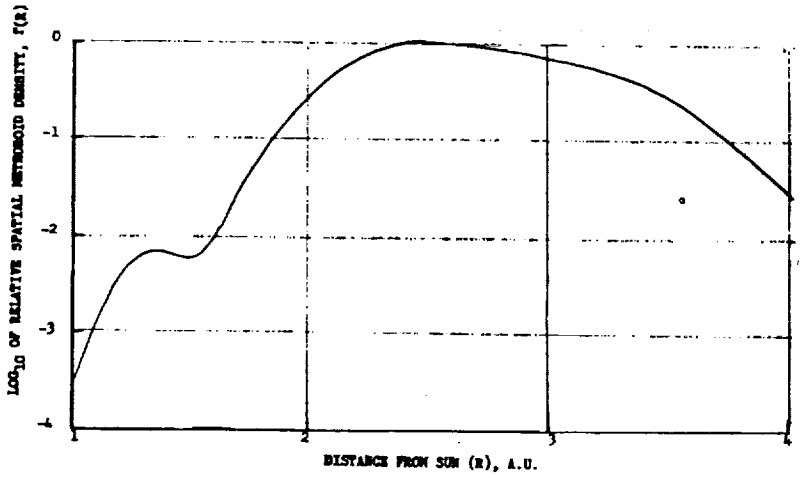

Figure 99. Radial Distribution of Asteroidal Meteoroid

Table 47. Meteoroid Environment Density and Velocity Coefficients

Environment (1)	Mass Range Grams	K_1	K_2	Density Gram/cm^2
Cometary	$10^{-6} \leq m \leq 10^{2}$	-18.776	-1.213	0.5
Asteroidal	$10^{-9} \leq m \leq 10^{2}$	-16.392	-0.84	3.5
Stream	$10^{-6} \leq m \leq 10^{2}$	-11.475	-1.213	0.5

R	U_1	U_2	U_3	Meteoroids
1.7 AU	30.05×10^3	1.2292	2.1334	Asteroidal
2.5 AU	29.84×10^3	1.0391	1.9887	Asteroidal
4.0 AU	29.93×10^3	0.9593	1.9230	Asteroidal
	31.29×10^3	1.30	1.9235	Cometary
	20.0×10^3	- 0 -	- 0 -	Stream

Gravitation $$G = 1 + 0.76 \left(\frac{R\, V_P^2\, r_P}{V_e^2\, r} \right)$$

Shielding $$\eta = \frac{1}{2} + \frac{1}{2} \left(1 - \frac{r_P^2}{r^2} \right)^{0.5}$$

where r = spacecraft's distance from the planet's center

V_e = Escape velocity from the surface of Earth

r_P = planet's radius (km)

R = planet's average radius from the sun (AU)

V_P = Escape velocity from the surface of the planet

Table 48 . Escape Velocities from the Surface of the Planets

Planet	Average Distance from Sun (AU)	V_P (m/sec)	r_P Planet Radius (km)
Mercury	0.39	4.3×10^3	2330
Venus	0.72	10.4×10^3	6700
Earth	1.00	11.2×10^3	6375
Mars	1.52	5.1×10^3	3415
Jupiter	5.20	61.0×10^3	71335
Saturn	9.54	36.7×10^3	60950
Uranus	19.19	22.4×10^3	23525
Neptune	30.07	25.6×10^3	24900

Penetration Probability Assignment

Optimum assignment of probabilities is based on the weight requirements for asteroidal and cometory protection being identical. The solution of the following equation determines the apportionment of the probability of no penetration, P_o; between the asteroidal flux (P_{oa}) and the cometary (P_{oc}).

$$K_a^* \left(1 - P_{oa}\right)^{1/K_{2a}} = K_C^* \left(1 - P_{oc}\right)^{1/K_{2c}}$$

$$K_i^* = \frac{\rho_i^{0.4735} \, \bar{V}_i^{2.486}}{\left(A \sum_{j=1}^{J} FLUX_{ij}\right)^{1/K_{2i}}}$$

$$FLUX_{ij} = \int_0^{T_j} \dot{G}\eta \; 10^{K_{1i}} \; 10^{f(R)_i} \; \bar{V}_i \; dt$$

Stage overall probability

$$P_o' = P_{oa} \, P_{oc}$$

where i = a asteroidal ; c cometary

j = mission leg

The probability assignment can also be specified and the individual weight requirements for both the asteroidal and cometary flux have to be determined individually, and the maximum weight selected. The particle diameter d_P is given by

$$d_{P_i} = \left\{ \frac{6}{\pi \rho_i} \left[\frac{1 - P_{o_i}}{A \sum_{j=1}^{J} FLUX_{ij}} \right]^{1/K_{2i}} \right\}^{1/3}$$

and the average particle velocity is

$$V_i = \frac{\sum_{j=1}^{J} FLUX_{ij} \; V_i}{\sum_{j=1}^{J} FLUX_{ij}}$$

The shielding weight depends on the particle diameter, density and velocity, and the type of shielding concept (single sheet, or multiple bumper). Shielding weight is given as the weight of the rear sheet W_{m2} and weight of the outer bumper, W_B.

$$W_{m2} = K_1 \; d_P^{\alpha} \; V_P^{\beta}$$

$$W_B = \text{Maximum} \left[K_2 d_p \; , K_3 + \left(\frac{K_4 - d}{K_5} \right) \left(\frac{V_p - K_6}{V_p} \right) \right]$$

Values for K_1 through K_6, α and β are supplied for the single sheet (Table 49), single bumper (Table 50) and dual bumper (Table 51).

Table 49. Scaling Coefficients - Single Sheet

α	β	K_1	Material	Meteoroid
1.0535	0.667	0.713	Aluminum	Asteroidal
1.0535	0.667	0.825	Titanium	Asteroidal
1.0535	0.667	0.259	Aluminum	Cometary
1.0535	0.667	0.300	Titanium	Cometary

Table 50. Scaling Coefficients for Single Bumper

METEOROID	MATERIAL	VELOCITY m/sec	K_1	K_2	K_3	α	β
Cometary	Aluminum	V > 8000	0.0412	1.77	1.71	1.12	0.667
Cometary	Aluminum	V ≤ 8000	2225	1.77	1.71	1.12	-0.546
Cometary	Titanium	V > 8000	0.0332	3.18	2.77	1.11	0.667
Cometary	Titanium	V ≤ 8000	4360	3.18	2.77	1.11	-0.645
Cometary	Gloss Epoxy	V > 8000	0.0467	2.28	1.27	1.09	0.667
Cometary	Gloss Epoxy	V ≤ 8000	1092	2.28	1.27	1.09	-0.453
Asteroidal	Aluminum	V > 8000	0.105	5.5	1.71	1.11	0.667
Asteroidal	Aluminum	V ≤ 8000	8960	5.5	1.71	1.11	-0.6
Asteroidal	Titanium	V > 8000	0.0866	7.7	2.77	1.12	0.667
Asteroidal	Titanium	V ≤ 8000	7270	7.7	2.77	1.12	-0.595
Asteroidal	Gloss Epoxy	V > 8000	0.139	8.01	1.27	1.09	0.667
Asteroidal	Gloss Epoxy	V ≤ 8000	4205	8.01	1.27	1.09	-0.485

Table 51. Scaling Coefficients for Dual Bumper

METEOROID	MATERIAL	VELOCITY m/sec	K_1	K_2	K_3	K_4	K_5	K_6	α	β
Cometary	Aluminum	V > 8000	0.0073	3.01	2.71	0.9	0.52	15000	1.15	.667
Cometary	Aluminum	V ≤ 8000	7.445×10^9	3.01	2.71	0.9	0.346	3550	1.15	-2.45
Cometary	Titanium	V > 8000	0.0062	2.32	2.32	1.0	.286	7350	1.09	.667
Cometary	Titanium	V ≤ 8000	1.42×10^{10}	2.32	2.32	1.0	1.8	4000	1.09	-2.5
Asteroidal	Aluminum	V > 8000	0.0165	6.87	2.71	0.3	2.0	0	1.04	.667
Asteroidal	Aluminum	V ≤ 8000	3.77×10^{10}	6.87	2.71	9.3	2.01	16000	1.04	-2.5
Asteroidal	Titanium	V > 8000	0.0098	9.9	4.95	0.5	2.0	0	1.12	.667
Asteroidal	Titanium	V ≤ 8000	5.59×10^{10}	9.9	4.95	0.5	4.0	0	1.12	-2.6

The weight (W_{m2}) is based upon a 25% penetration and can be modified for the unpressurized shell where complete penetration is allowed.

$$W_{m2\ \text{unpressurized}} \approx 0.445\ W_{m2\ \text{tank}}$$

If the shell or tank consists of material other than aluminum

$$W_{m2} = K_1\ W_{m2\ al} \qquad K_1 = 1.15\ \text{, titanium} \quad = 0.83\ \text{, glass epoxy}$$

For shielding with insulation between the bumper and rear sheet, the rear sheet weight requirements are reduced further by

$$W_{m2\ \text{insulated}} = \frac{W_{m2}}{\text{EXP}\ (14.9\ \rho_{ins}\ \ \tau_{ins}/d)}$$

ρ_{ins} = insulation density gm/cm^3

τ_{ins} = insulation thickness (cm)

Existing tank or unpressurized shell thickness for structural integrity, W_S, is subtracted from the rear sheet thickness requirements to determine the additional weight accredited to the meteoroid shielding weight

$$W_{mp} = W_{m2} + W_B - W_S$$

The meteoroid shielding unit weight is to be applied to all of the exposed outer structure; the tank bulkheads are assumed to be shielded by adjacent surrounding structure.

7.3.2 Thermal Protection

The thermal conductivity, k, of the multi-layer high performance insulation is dependent upon the type of insulation, number of layers/inch and the temperature differential across the insulation.

$$k = A^*T + BT^3 \qquad \frac{\text{Btu FT}}{\text{HR FT}^2\ {}^{o}R}$$

where $A^* = K_c\ 1.168 \times 10^{-13}\ N^{2.725}$

$B = K_r\ (8.68 \times 10^{-12})\ N^{-1}$

T = the average temperature of any insulation layer

N = the insulation layers per inch

Table 52 gives the conductivity properties of the individual layers for the different insulations. For typical HPI, with the layer densities shown in Table 52, the resulting coefficient A* and B for the conductivity equation are quoted in Table 52.

Table 52. High Performance Insulation Thermal Conductivity Factors

HPI	K_c	K_r	Layer/ Inch	A * $\frac{\text{Watt-cm}}{\text{cm}^2\ {}^\circ\text{K}^2}\left(\frac{\text{Btu Ft}}{\text{HR FT}^2\ {}^\circ\text{R}^2}\right)$	B $\frac{\text{Watt-cm}}{\text{cm}^2\ {}^\circ\text{K}^4}\left(\frac{\text{Btu Ft}}{\text{HR FT}^2\ {}^\circ\text{R}^4}\right)$
DAM/NM	1.0	4.7	50	1.71×10^{-12} (5.49×10^{-9})	8.24×10^{-14} (8.16×10^{-13})
Superfloc	35.4	1.922	30	1.48×10^{-11} (4.77×10^{-8})	5.61×10^{-14} (5.56×10^{-13})
GAC-9	65.0	1.118	38	5.22×10^{-9} (1.6779×10^{-7})	2.58×10^{-14} (2.554×10^{-13})
NRC-2	2.96	5.12	80	1.835×10^{-11} (5.919×10^{-8})	5.61×10^{-14} (5.56×10^{-13})
NARSAM	1.885	2.3	93	1.785×10^{-11} (5.703×10^{-8})	2.17×10^{-14} (2.147×10^{-13})

Solar Flux Integration

Integration of the solar heat flux throughout the mission leg will provide the total heat input Q_{IN}

$$Q_{IN} = \frac{8766\ A}{\pi\ d}\left[\frac{C_1\ a\sqrt{1-e^2}\ (\Delta E) + C_2\ (\Delta\nu)}{\sqrt{a\ (1 - e^2)}} - C_3\ (\Delta t)\right] +$$

$$\left[\frac{S\ \theta\ (1 + B_{eff})}{\sigma\ R_P{}^2} + E_{ff}\right]\ t_{stay}\left(\frac{\alpha_s\ A_A}{\varepsilon\ A_E}\right)$$

$$C_1 = \frac{A^*}{2}\left[\left(\frac{\alpha_s}{\epsilon}\right)\left(\frac{A_A}{A_E}\right)\left(\frac{S_\oplus}{\sigma}\right)\right]^{0.5}$$

$$C_2 = \frac{B}{4}\left[\left(\frac{\alpha_s}{\epsilon}\right)\left(\frac{A_A}{A_E}\right)\left(\frac{S_\oplus}{\sigma}\right)\right]$$

$$C_3 = \frac{A^*}{2} T_c^{\,2} + \frac{B}{4} T_c^{\,4}$$

The changes in anomalies are evaluated from the departure (R_0) and arrival points (R_f) of the mission leg.

$$E = \cos^{-1}\ (1/e - R/ea)$$

$$\nu = \cos^{-1}\left(\frac{\cos E - e}{1 - e\cos E}\right)$$

$$\Delta t = \frac{8766\ a^{3/2}}{2\pi}\left[E_f - E_0 - e\ (\sin E_f - \sin E_0)\right] \text{ hours}$$

where

a = semimajor axis of the heliocentric conic , AU

e = eccentricity

ΔE = change in eccentric anomaly

$\Delta\nu$ = change in true anomaly

Δt = exposure time, hours

A = the total surface area, cm^2 (ft^2)

d = the insulation thickness, cm (ft)

t_{stay} = stop-over time at planet, hours

α_s = the surface coating absorptivity

ϵ = the surface coating emissivity

A_A = the effective absorbing area (m^2)

A_E = the effective emitting area (m^2)

$S_\oplus$ = the solar constant

σ = the Stefan-Boltzmann constant

The planet's albedo contribution B_{eff} is a function of the planet's radius r_p and the spacecraft orbital attitude h and can be approximated for a sphere by

$$B_{eff} = B\left(1 - \frac{\sqrt{h\,(2\,r_p + h)}}{(r_p + h)}\right)$$

The planet's emitted radiation contribution is expressed as

$$E_{ff} = \frac{6.325 \times 10^{10}}{R_p^{\,2}}\left(1 - \frac{\sqrt{h\left(2\,r_p + h\right)}}{\left(r_p + h\right)}\right)(1-B)$$

R_p = planet's solar distance (AU)

Table 53. Near Planet Albedo (B) and Surface Temperature

Planet	Mercury	Venus	Earth	Mars	Jupiter	Saturn	Uranus	Neptune	Pluto
Albedo	0.058	0.76	0.39	0.15	0.51	0.50	0.66	0.62	0.16
Maximum Surface Temp °F	750	210	140	90	-200	-240	-270	-330	-370

Insulation Thickness and Propellant Boil-off

The insulation thickness and propellant boil-off are optimized in terms of the stages overall mission performance. The optimization of the oxidizer and fuel containers are treated separately. For a single stage with a single burn we have for the oxidizer tanks and fuel tanks respectively,

Optimum Insulation

$$d_{l_o} = \frac{f_{l_o} K_{l_o}}{L_o} + \frac{1}{L_o}\sqrt{\frac{K_{l_o}}{\mu_l \rho_{ins_o}}\left(L_o \mu_l G_{l_o} + L_o + \mu_l K_{l_o} f_{l_o}^2 \rho_{ins_o}\right)}$$

$$d_{l_f} = \frac{f_{l_f} K_{l_f}}{L_f} + \frac{1}{L_f}\sqrt{\frac{K_{l_f}}{\mu_l \rho_{ins_f}}\left(L_f \mu_l G_{l_f} + L_f + \mu_l K_{l_f} f_{l_f}^2 \rho_{ins_f}\right)}$$

Propellant boil-off

$$W_{B_{l_o}} = A_{l_o}\sqrt{\frac{\mu_l \rho_{ins_o} K_{l_o}}{\left(L_o \mu_l G_{l_o} + L_o + K_{l_o} f_{l_o}^2 \mu_l \rho_{ins_o}\right)}}$$

$$W_{B_{I_F}} = A_{l_f}\sqrt{\frac{\mu_l \rho_{ins_f} K_{l_f}}{\left(L_f \mu_l G_{l_f} + L_f + K_{l_f} f_l \mu_l \rho_{ins_f}\right)^2}}$$

A two-stage vehicle will have different insulation thicknesses for each propellant container, depending upon the relative mission performance requirements and coast duration for each stage. The two-stage vehicle optimization requirements for insulation thicknesses for single burn per stage are, for either oxidizer or fuel

$$d_{l_{opt}} = \frac{f_1 K_1}{L_1} + \frac{1}{L_1}\sqrt{\frac{L_1 K_1}{\rho_{ins}}\left(G_1 + \frac{1}{\mu}\right) + f_1^2 K_1^2}$$

$$d_{2_{opt}} = \frac{f_2 K_2}{L_2} + \frac{1}{L_2}\sqrt{\frac{L_2 K_2}{\rho_{ins}}\left[G_2 + \frac{1}{\mu_1 \mu_2}\left(1 + \frac{K_{21}(\mu_1 - 1)}{K_2}\right)\right] + f_2^2 K_2^2}$$

The optimum boil-off propellant requirements for the two stages are

$$W_{B_1}{}_{opt} = A_1 \sqrt{\frac{K_1 \rho_{ins} \mu_1}{L_1(G_1 \mu_1 + 1) + f_1^2 K_1 \mu_1 \rho_{ins}}}$$

$$W_{B_2}{}_{opt} = A_2 \sqrt{\frac{K_2 \rho_{ins} \mu_1 \mu_2}{\left\{L_2\left(G_2 \mu_1 \mu_2 + 1 + \frac{K_{21}}{K_2}(\mu_1 - 1)\right) + \right. \\ \left. f_2^2 K_2 \mu_1 \mu_2 \rho_{ins}\right\}}}$$

where $G = W_{stBo}/W_B$

additional structure weight required to contain the boil-off propellant divided by the boil-off propellant

f = additional surface area divided by the boil-off propellant

μ_{ij} = the performance mass ratio for the j^{th} burn of the i^{th} stage

L = the latent heat of vaporization

K_i = the total normalized heat absorbed by the i^{th} stage

K_{ij} = normalized heat absorbed by the i^{th} stage between the j^{th} and $j+1^{th}$ burn of the entire stage

$K = \frac{Q_{in}\, d}{A}$

No Propellant Boil-off with Increased Tank Pressure

For the case of allowing the tank pressure to increase and have no propellant boil-off, the heat input per volume of propellant Q/V_L is expressed empirically from the data shown in Figures 56 and 57.

$$Q/V_L = K_1 \; EXP \left\{\frac{K_2}{K_3 - P}\right\} \; UF^{1.25} \; ; \; \frac{\text{Watt-hr}}{m^3} \left(\frac{BTU}{ft^3}\right)$$

where UF = tank ullage factor

P = tank maximum pressure

V_L = volume of liquid

Table 54. Coefficients for Insulation with No Propellant Boil-off

Propellant	K_1				K_2	K_3
	LH_2	LO_2	LF_2	B_2H_6		
Metric	0.315×10^5	2.93×10^5	3.7×10^5	3.15×10^5	0.045	1.05
English	0.305×10^4	2.84×10^4	3.6×10^4	3.06×10^4	13.5	15.0

The insulation thickness (d) required is

$$d = \frac{K \quad A}{(Q/V_L)\ V_L}$$

Insulation is applied to the walls and bulkheads of the tanks which contain propellant requiring thermal protection. The unpressurized shells adjacent to the tank will result in heat leaks into the tank.

The heat input rate is

$$\dot{Q}_2 = \frac{Q_{IN}\ FACT}{t}$$

where t is the exposure time (hours).

The same insulation thickness, d, is used for the unpressurized shells as for the tank and the optimum length L_2 of insulation covering the outer surface is

$$L_2 = \frac{1.61\ K_2\ \bar{t}_2\ \omega_2\ \Delta T}{\dot{Q}_2}$$

where

K_2 = thermal conductivity of support structure

$\bar{t}_2$ = thickness of support structure

ω_2 = perimeter of propellant tank πD

ΔT = temperature difference between hot and cold temperature of support structure

The additional weight of insulation W_{ins_S} for each tank support is then

$$W_{ins_S} = 2\rho_{ins}\ d_{ins}\ \omega_2\ L_2$$

7.4 OTHER SUBSYSTEMS

Generally other subsystem weights are included in the stage's inert mass estimation. Most of these subsystem weights cannot be rigorously evaluated until their particular operational mode and functional requirements are specified. Empirical weight estimates are based on existing hardware designs and proposed studies of discrete bases point concepts.

Intelligence Module Weight (W_{IM})

The vehicle's intelligence module will include weight allowances for

1. Guidance and navigation
2. Control electronics
3. Communication equipment
4. Electrical and thermal power
5. Miscellaneous electronic equipment

The weight-scaling laws are

$$W_{IM} = K_1 + K_2 W_G + D (K_3 + K_4 W_G); \text{ kg} \quad (\text{lb})$$

W_G = stage weight, kg (lb)

D = stage diameter, m (ft)

Table 55. Intelligence Module Weight Coefficients

Intelligence Module	K_1	K_2	K_3	K_4	
Multi-purpose	544	.0075	58.3	3.94×10^{-4}	Metric
Independent of Ground Control	1200	.0075	39.2	1.2×10^{-4}	English
Single Purpose	90.5	.0075	34.5	3.94×10^{-4}	Metric
Ground base control	200	.0075	23.2	1.2×10^{-4}	English

Attitude Control System Weights (W_{ACS})

Attitude control systems weights are provided for the hardware and the amount of expellant required during the mission.

$$W_{ACS} = K_1 + 0.002\, W_G$$

where $$K_1 = \left[K_2 \frac{\Delta V}{I_{SP}} + 1.5 \times 10^{-4}\, t_{coarse} + 7.5 \times 10^{-2}\, t_{fine} \right] W_O + K_3$$

K_2 = 0.0113 (metric); 0.037 (English)

K_3 = 68 (metric); 150 (English)

ΔV = total translational velocity changes to be supplied by the ACS m/sec (ft/sec)

t_{coarse} = transplanetary mission duration (days) when vehicle requires pointing accuracy

t_{fine} = time (days) for fine control, docking, etc.

I_{sp} = specific impulse of ACS propellant

Docking Mechanism Weight (W_{DOCK})

Docking mechanisms will be applied only to the upper stage where there is attachment and reattachment of the vehicle to the payload. Two basic designs are being employed, the Apollo drogue and probe and the NASA Neuter concept used for heavier vehicle. It will be assumed that the female (heavier) portion of the mechanism is attached to the stage.

$$W_{DOCK} = K_1 \quad ; \quad \text{kg (lb)}$$

Table 56. Docking Mechanism Weight Coefficients

Docking Type	BASIC		PRESSURIZED	
	METRIC	ENGLISH	METRIC	ENGLISH
Drogue & Probe	79	175	90	200
Neuter	218	480	236	520

Electrical System Weight (W_{elec})

Electrical wiring, junction bases, switches, sensors, etc., are a function of the stage length, type and number of measurements and electrical functions required. The scaling laws are identified for stages whose propellant bulk density is low (propellant combinations containing hydrogen) and for high bulk densities (space- and earth- storable propellants).

$$W_{elec} = K_1 + K_2 W_p - K_3 W_p^2 \quad ; \quad \text{kg (lb)}$$

Table 57. Electrical System Weight Coefficients

Bulk Density	Thrust Level	K_1	K_2	K_3	
LOW	< 13600 kgf	0	0.0147	0	Metric
	< 30,000 lbf	0	0.0147	0	English
	> 13600 kgf	136	478×10^{-3}	5.2×10^{-9}	Metric
	> 30000 lbf	300	478×10^{-3}	2.36×10^{-9}	English
HIGH	< 13600 kgf	0	0.011	0	Metric
	< 30000 lbf	0	0.011	0	English
	> 13600 kgf	136	9.7×10^{-4}	15.5×10^{-11}	Metric
	> 30000 lbf	300	9.7×10^{-4}	7×10^{-11}	English

Parallel Attachment Weight

Propellant modules or stages can be attached in parallel to other modules. The weight of the attachment mechanism and local strengthening of the stage depends upon the module diameter and the loads transmitted from one module to the center core module. Loads in the attachment structure have to be transformed from a concentrated load into the module structural shell. The weight increment to each module for the parallel staging is

Center Core Module

$$W_{T_{ATTACH}} = K_2 K_1 F^* D SF \quad ; \quad \text{kg (lb)}$$

Each Outer Module

$$W_{T_{ATTACH}} = 1.25 K_2 F^* D SF$$

where K_1 = No. of outer modules attached to center core module

K_2 = 6.25×10^{-7} (metric); 1.59×10^{-6} (English)

F^* = Maximum $\left\{ W_{O_{Module}} \left(T/W_o \right)_{Max} , F_{Module} \right\}$

D = Diameter of module; cm (in)

SF = Safety factor

8.0 PROPULSION STAGE SYNTHESIS

The improved scaling laws for the stage inert mass are to be used to synthesize propulsion stage(s) to meet specific mission requirements. The mission spectrum should encompass the planetary system and be capable of differentiating between the mission profiles and environments, and their relative effect on the propulsion stages with respect to stage weight and performance. Scaling laws developed during this study are in sufficient detail that stage weight changes can be identified for the different missions, subsystem selection, design concept and materials.

A synthesis procedure has been identified that allows the improved scaling laws to be used in sizing total vehicle systems which will meet the mission requirements. The propulsion system may be a multi-stage vehicle with multiple restarts per stage and contain cryogenic propellants which suffer boil-off during the coast phases of the mission. Basic synthesis performance equations developed in this section will estimate the total vehicle weights for designs fulfilling these complex missions. A Space Propulsion Automated Synthesis Modeling (SPASM) program has been developed which is capable of synthesizing these multi-stage vehicles for the spectrum of space missions, using various design concepts and materials.

There are two separate performance criteria used in vehicle synthesis. One requires minimization of initial mass in earth orbit for a specified payload and mission profile. The other involves maximizing the payload for a fixed GLOW. In the latter case the method is straight forward for vehicle systems that have up to four stages and as many as five burns per stage but do not have any propellant boil-off. The maximization of the vehicle payload requires starting with the lower stage and progressively working up towards the payload. The payload for any stage (mission payload plus upper stages) can be evaluated for a fixed but unknown stage payload. However, if propellant boil-off occurs, the change in weight during the mission coast periods causes a problem. Although the boil-off percentages could be assumed, there is no method of determining the actual propellant weights of the upper stages until these upper stages are synthesized. An iteration scheme is used to resolve the difficulty.

No such difficulty is encountered when the mission payload is given and the initial mass in earth orbit is to be found. The procedures consider the uppermost stage first and proceeds down the stack.

In both methods described above, the approaches used in the computer program are much the same. Figure 100 shows an outline of the procedure.

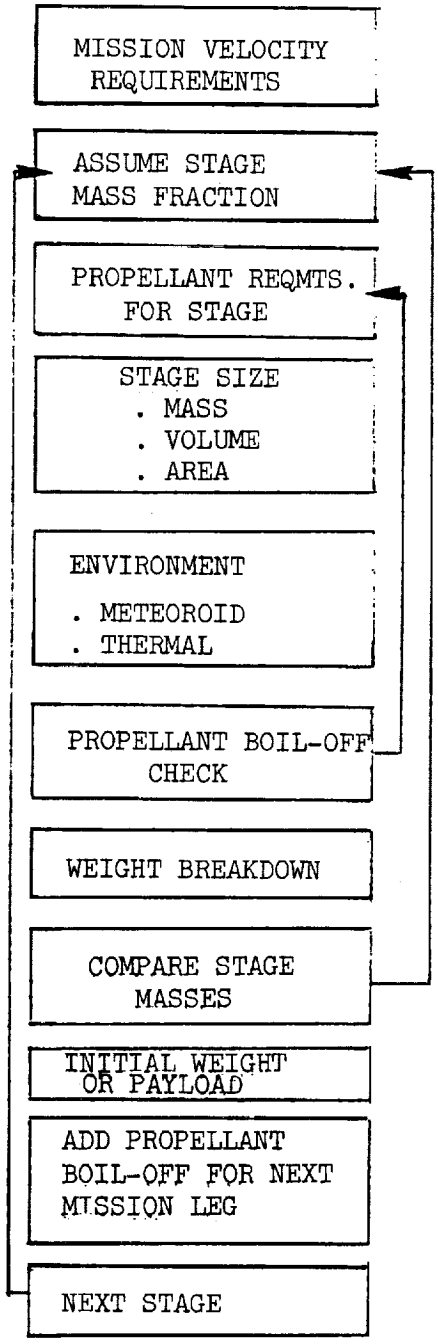

Figure 100. Stage Synthesis Procedure

Preliminary sizing is based on an initial estimate for the stage mass fraction ν_B which is used with input data to obtain a starting value for stage initial mass. The stage mass fraction is then varied until the mass of usable propellants calculated from this stage initial mass agrees with that obtained by using the scaling laws to calculate stage inerts and boil-off, or until the variation of ν_B decreases to less than 1×10^{-6}. An updated value of the stage mass is obtained as the sum of the stage inert masses and of the total mass of usable, boil-off and reserve propellants. The procedure is then repeated with the updated value replacing the starting value of the stage initial mass until the difference between the new updated value and the previous value is no greater than 0.01% of the latter, or until the allowable sum of iterations is exceeded.

$$\nu_B = \frac{W_P^*}{W_P^* + W_{ST}} \tag{105}$$

where W_P^* = the total usable propellant W_P and boil-off weight contained in the stage

W_{ST} = the stage burn-out weight including the inert stage weight plus any trapped or residual weights

From Equation 105. the burn-out weight of the stage is expressed as a function of the stage propellant capacity

$$W_{ST} = \left(\frac{1}{\nu_B} - 1\right) W_P^* \tag{106}$$

The final burn-out weight W_{BO} of the vehicle is the stage weight plus the payload weight (W_{PAY})

$$W_{BO} = W_{PAY} + W_{ST} \tag{107}$$

The payload weight for the top stage is the mission payload, while payload for any other stages will include the weights of stages to be used subsequently and the mission payload.

Each of the vehicle stages can have several engine firings to attain a selection of velocity requirements. The general performance equation is given as

$$W_0 = W_{BO}\, e^{V/I_g} \qquad V = \sum_{b=1}^{B} V_b \tag{108}$$

B = number of burns per stage

where W_0 = the initial weight of vehicle at engine ignition

V_i = the total velocity increment required from each engine firing including any gravity losses

I = the specific impulse performance from the engine system

Minimum Initial Weight with Fixed Payload

The following equations and procedures are used to find the initial mass in Earth orbit.

If no boil-off occurs, $W_P^* = W_P$; by combining Equations 106, 107 and 108, the initial weight can be expressed as follows:

$$W_O = \left[W_{PAY} + \left(\frac{1}{\nu_B} - 1\right) W_P\right] e^{V/Ig} \tag{109}$$

For a single burn condition for a stage, it is relatively straight forward to determine the propellant weight since

$$W_P = W_O - W_{BO} \tag{110}$$

Therefore the stage will require the following propellant weight

$$W_P = \frac{W_{PAY}\left(e^{V/Ig} - 1\right)}{1 - \left(\frac{1}{\nu_B} - 1\right)\left(e^{V/Ig} - 1\right)} \tag{111}$$

Substituting Equation 111 for the propellant weight into Equation 109 will provide the initial vehicle weight. The stage weight, W_G, can be obtained from

$$W_G = \frac{W_P}{\nu_B}$$

and the stage inert structure weight is given by Equation 106.

For stage designs that contain cryogenic propellants and suffer propellant boil-off losses during the mission, the sizing and performance equations are modified as shown below.

The allowance for propellant boil-off prior to ignition is added to Equation 111 as follows.

$$W_P^* = \left[\left(\frac{MR}{MR+1}\right)\left(1+\Delta BO_{Ox}\right)+\left(\frac{1}{MR+1}\right)\left(1+\Delta BO_f\right)\right] W_P \qquad (112)$$

where MR = the mixture ratio of propellants used for the engine performance

ΔBO_f = the fraction of fuel boil-off to usable fuel

ΔBO_{O_X} = the fraction of oxidizer boil-off to usable oxidizer

W_P = the total usable propellant weights used by the engine system

Using Equations 109, 110 and 112, the total propellant requirements can be found.

$$W_P^* = \frac{W_{PAY}\left(e^{V/Ig}-1\right)\left(1+\Delta BO\right)}{\left[1-\left(\frac{1}{\nu_B}-1\right)\left(1+\Delta BO\right)\left(e^{V/Ig}-1\right)\right]} \qquad (113)$$

where

$$\Delta BO = \left(\frac{MR}{MR+1}\right)\Delta BO_{ox}+\left(\frac{1}{MR+1}\right)\Delta BO_f$$

For the case of multiple stages and multiple burns, the propellant boil-off further complicates the stage sizing. The performance equation uses the stage inert weights of the upper stages which are of an unknown propellant capacity, only to be defined several steps later. Also, for vehicle payload weights which include upper stages, the upper stage weights will change with mission time due to their propellants boiling off. Equation 109 can be modified for the multi-stage vehicle as follows.

$$W_{o_i} = \left[W_{PAY}+\sum_{k=i+1}^{N} W_{G_k}+W_{ST}\right]E^B+\sum_{b=1}^{B-1}\sum_{k=i}^{N}\left(\Delta BO_k\right)_{b+1}X$$

$$W_{P_k}E^b+\sum_{b=1}^{B-1} W_{JET_{i,b}}E^b \qquad (114)$$

where

N = total number of stages

B = total number of burns per stage

W_{G_k} = the k^{th} stage weight at final burn of the i^{th} stage

$(\Delta BO_k)_{b+1}$ = the fraction of propellant boiled off from the k^{th} stage during the time between the b^{th} burn and the $b+1^{th}$ burn of the i^{th} stage

$$E^b = \prod_{m=1}^{b} e^{V_m/Ig}$$

$W_{JET_{i,b}}$ = the weight jettisoned between the b^{th} and the $b+1^{th}$ burn of the i^{th} stage

Substituting Equation 114 into Equation 113 and rearranging, the propellant used by the engines of the i^{th} stage can be expressed as

$$W_{P_i} = \frac{\left(W_{PAY} + \sum_{k=i+1}^{N} W_{G_k}\right)\left(E^B-1\right) + \sum_{b=1}^{B-1}\left(E^b-1\right)\left(W_{JET_{i,b}} + \sum_{k=i+1}^{N}\left(\Delta BO_k\right)_{b+1} W_{P_k}\right)}{\left[1-\left(\frac{1}{\nu_B}-1\right)\left(1+\Delta BO\right)\left(E^B-1\right) - \sum_{b=1}^{B-1}\left(\Delta BO_i\right)_{b+i} E^b\right]} \qquad (115)$$

where

ΔBO_i is the fraction which includes all the propellant boil-off from the i^{th} stage

$$\Delta BO_i = \left(\frac{MR_i}{MR_i+1}\right)\sum_{b=1}^{B}\left(\Delta BO_{ox_i}\right)_b + \left(\frac{1}{MR_i+1}\right)\sum_{b=1}^{B}\left(\Delta BO_{f_i}\right)_b$$

The total amount of propellant including boil-off propellant for the i^{th} stage is given by

$$W_{P_i}^{*} = W_{P_i} (1+\Delta BO_i)$$

and the stage initial weight is

$$W_{G_i} = W_{ST_i} + W_{P_i}$$

and the total vehicle initial weight prior to any boil-off can be obtained from

$$W_{Oi}^{*} = W_{PAY} + \sum_{k=i}^{N} \left(W_{G_k} + W_{JET_k} + W_{P_k}^{*} \right)$$

Maximum Payload with Fixed Initial Weight

If no propellant boil-off occurs, the stage mass sizing for the maximum payload performance for a specified initial launch weight is given by

$$W_P = W_O \left(1-e^{-V/Ig}\right) \tag{116}$$

and the stage payload mass is given by

$$W_{PAY} = W_O \; e^{-V/Ig} - \left(\frac{1}{\nu_B} - 1\right) W_\Gamma \tag{117}$$

If there is propellant boil-off from the vehicle stages and the weight prior to ignition and after boil-off, W_0, can be estimated, then Equations 116 and 117 can be modified to account for the propellant losses

$$W_P^* = W_0 \left(1-e^{-V/Ig}\right)\left(1+\Delta BO\right) \qquad (118)$$

and the stage payload mass is given by

$$W_{PAY} = W_o\, e^{-V/Ig} - \left(\frac{1}{\nu_B} - 1\right) W_P^* \qquad (119)$$

A difficulty arises in estimating the initial launch weight and an iteration is required to determine the boil-off from as yet an undefined propellant volume.

9.0 SIMPLIFIED SCALING LAWS

The improved scaling laws developed during this study were intended to be used by the SPASM synthesis program. A subset of these laws in a greatly simplified form are provided in this section. The simplified scaling laws are amenable to manual manipulation for the synthesis of individual vehicle stages while still considering the major design and mission parameters. A single stage synthesis example is included to demonstrate the systematic approach and use of the simplified data and scaling laws.

The procedure described below is recommended to obtain the performance of a single stage or of a multi-stage system. One stage at a time is considered in systems having more than one stage. If the mission payload is known, synthesis starts with the last stage to be used. If the initial gross mass is known, the first stage to be ignited is synthesized first to obtain the initial mass of the next stage and so on until the payload of the last stage is determined. The synthesis procedure involves iteration through the following five steps:

1. Calculation of total propellant weight.
2. Propellant module inert weight evaluation, W_{PM}
3. Engine module weight estimation, W_{EM}
4. Environmental module weight calculation, W_{EMP}
5. Other system module weight estimation, W_{SYS}.

An initial estimate is made for the mass fraction, $\nu_B = W_P^* / (W_P^* + W_{ST})$, where W_P^* is the sum of the weights of usable and boil-off propellants.

The weights of the four modules calculated later in steps 2 through 5, and the residual propellant weight, W_{PR}, are used to obtain the stage inert mass, W_{ST},

where

$$W_{ST} = W_{PM} + W_{EM} + W_{EMP} + W_{SYS} + W_{PR}$$

The stage mass fraction is computed next and compared with the initial estimate of the stage mass fraction. If the estimated and calculated values of the mass fraction are not within a specified tolerance (0.001), then steps 1 through 5 are repeated with an updated estimate of the mass fraction until convergence is obtained. When one stage has been successfully evaluated the complete process is repeated for subsequent stages.

During the iteration loop for convergence of the stage mass fractions, module weights are expressed in terms of the propellant loading of the stage. This procedure greatly reduces the amount of calculation and table look-up required during the iteration loop. A final check of the module scaling

law can be conducted during the stage iteration if the mass fraction greatly departs from the initial mass fraction estimate. An example of expressing the module weights as functions of the propellant loading is demonstrated in Section 9.6.

9.1 TOTAL PROPELLANT WEIGHT

The propellant weight requirement (W_P^*) is obtained from specifying the fraction of usable fuel that will boil off, ΔBO_f, and the fraction of usable oxidizer that will boil off, ΔBO_{ox}, and using the following equations.

$$\Delta BO = \left(\frac{MR}{MR+1}\right) \Delta BO_{cx} + \left(\frac{1}{MR+1}\right) \Delta BO_f$$

Where ΔBO is the ratio of the total weight of boil-off to the weight of usable propellants. The term MR is the mixture ratio by weight, oxidizer/fuel. The initial weight of propellants W_P^*, including that which will boil-off, is given by

$$W_P^* = W_P \ (1 + \ \Delta BO)$$

Where W_P, the usable propellant, is calculated from one or the other of the two following equations, depending upon whether the mission payload W_{PAY}, or the initial gross mass W_0 (including payload and any other upper stages) is given.

For given payload

$$W_P = \frac{W_{PAY} \left(e^{V/Ig} - 1 \right)}{1 - \left(\frac{1}{v_B} - 1\right) (1 + \Delta BO) \left(e^{V/Ig} - 1\right)}$$

For given initial gross mass

$$W_P = W_0 \left(1 - e^{-V/Ig}\right)$$

Where I is the specific impulse of the stage, I_g is the jet velocity c of the rocket-engine exhaust, and V is the total velocity increment to be supplied by the stage.

Residual and reserve propellants are considered as part of the inert total weight W_{ST}, since they receive the same velocity increment as the tank and other structures generally thought of as inert weight. For obtaining the weight of the propellant module, expressed as a function of its total propellant capacity, these propellants as well as an ullage volume should be taken into account as shown in the next step.

9.2 PROPELLANT MODULE INERT WEIGHT

The inert weight of the propellant module W_{PM} consists of the weights of propellant tanks, W_{PT}, of the pressurization systems, W_{PRESS}, and of the propellant feed systems, W_{PF}, all for both oxidizer and fuel where applicable.

$$W_{PM} = W_{PT} + W_{PRESS} + W_{PF}$$

Propellant Module Structural Weight (W_{PT})

There are many different design concepts, materials and construction, loading conditions and pressure ranges which can influence the structural weight estimate for the propellant module. For the simplified laws a conventional basepoint design has been considered.

Figure 101 provides the weight estimated for the propellant module structure W_{PT}, for either LO_2/LH_2 or LF_2/LH_2 propellant and indicates the weight variations with mixture ratio for both the separate and common bulkhead design tank arrangements. The effects of changing to the denser fuel combinations are shown in Figure 102 which has weight data for stages using space-and earth-storable propellant combinations. The latter propellants are assumed for a pressure-fed engine system which have tank pressures ranging from 7.03 kg/cm^2 (100 lb/in^2) to 21.09 kg/cm^2 (300 lb/in^2). These high pressures would produce prohibitively heavy designs for the larger stage diameters; therefore the pressure-fed engine systems should be limited to stages with initial gross weight less than 45,000 kg (100,000 lb).

To obtain W_{PT} from Figure 101, the total propellant capacity of both tanks $W_{P_{tot}}$ should be used. This capacity is computed from the following equations

$$W_{P_{tot}} = W_{P_{tot,ox}} + W_{P_{tot,f}}$$

For oxidizer tank:

$$W_{P_{tot,ox}} = W_P \left(\frac{MR}{MR+1} \right) \left[1 + \Delta BO_{ox} + W_{PR_{ox}} + W_{PRV_{ox}} \right] x \left[1 + UF_{ox} \right]$$

For fuel tank:

$$W_{P_{tot,f}} = W_P \left(\frac{1}{MR+1} \right) \left[1 + \Delta BO_f + W_{PR_f} + W_{PRV_f} \right] \left[1 + UF_f \right]$$

Where, in addition to the terms already defined in Section 9.1,

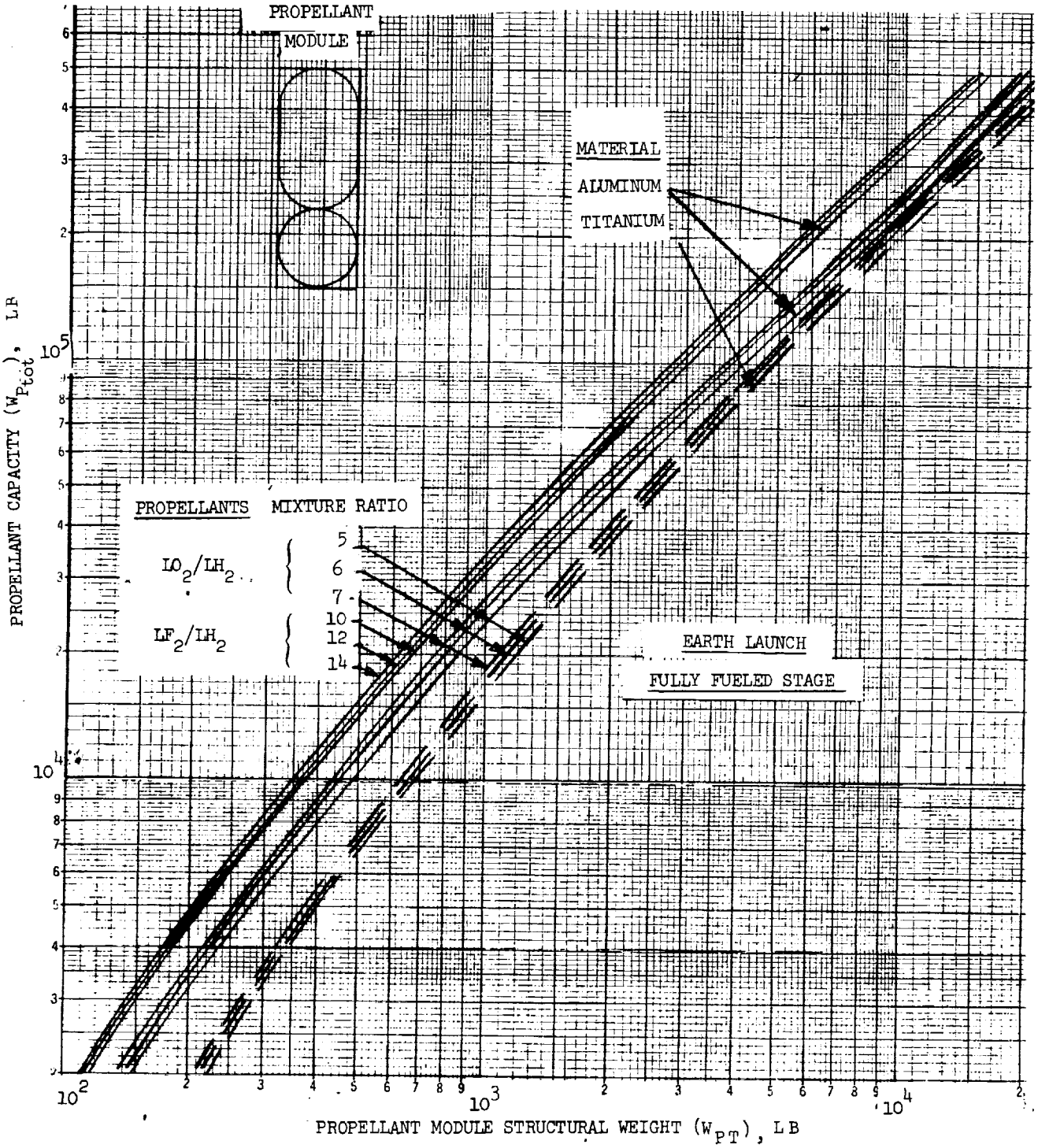

Figure 101. Propellant Module Structural Weight - Cryogen Fuels

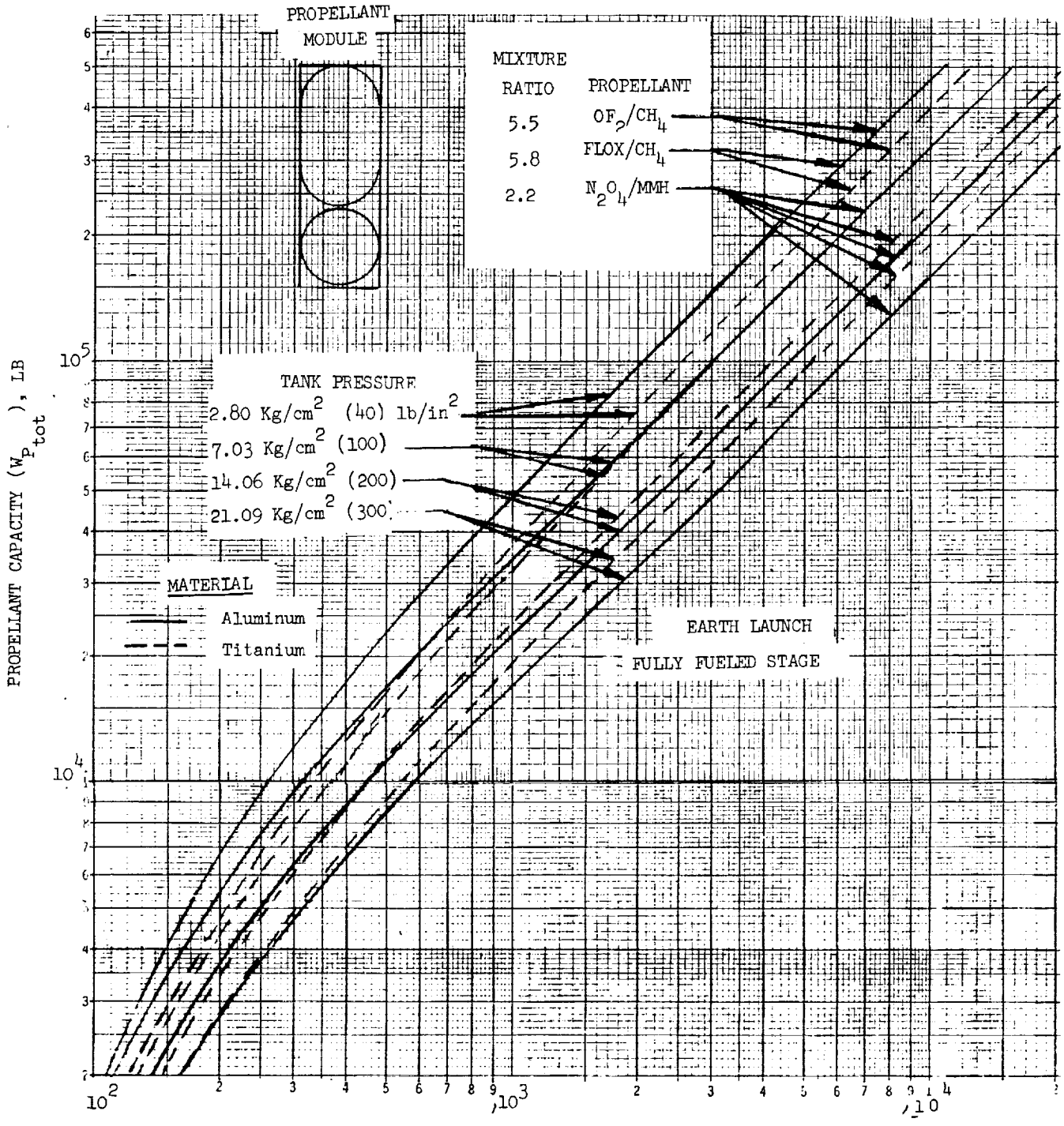

Figure 102. Propellant Module Structural Weight - Storable Fuels

$W_{PR_{ox}}$, W_{PR_f} = fraction of usable (oxygen, fuel) trapped in plumbing, sumps

$W_{PRV_{ox}}$, W_{PRV_f} = fraction of usable (oxygen, fuel) provided for contingencies

UF_{ox}, UF_f = tank ullage factor, or fraction of tank volume (based on propellant requirements) added to provide for gaseous oxidizer or fuel

ρ_{ox}, ρ_f = density of (oxidizer, fuel) at estimated tank pressure and propellant boiling-point temperature just prior to ignition.

W_{PR} may be taken equal to 0.5% for small tanks (diameter less than ten feet) or 0.25% for larger tanks.

W_{PRV} will vary between 1% and 5% depending on mission planner's assessment of accuracy of velocity requirements for mission. One method often used is to provide an increase of 0.75% in the velocity increment V and thus set W_{PRV} to zero.

UF_{ox}, UF_f are generally taken as 3% to 5%

The propellant tankage weights were obtained from the SPASM synthesis program. The weight, W_{PT}, include weights for the tank bulkheads and walls, baffles, tank/shell intersection, forward and aft skirts and intertank structure.

Pressurization System Weight (W_{PRESS})

The pressurization system weights are for the pressurant gases, pressurant tankage if any, and the pressurant transmission (plumbing, valves, etc.). One scaling law is used to represent the combination of both pressurization systems for the bi-propellant stages.

Weight for the pressurization systems is

$$W_{PRESS} = K_1 K_2 \frac{W_P}{\rho^*}$$

ρ^* = the propellant combinations bulk density

$$= \frac{(MR+1)\,\rho_{ox}\,\rho_f}{\rho_{ox} + MR\,\rho_f} \quad ; \ kg/m^3 \ (lb/ft^3)$$

where

$K_2 = 1.0$ for steady state continuous pressurization

$$K_2 = \left(\frac{MR}{MR+1}\right)\left(\Delta BO_{ox} + UF_{ox}\right) + \left(\frac{1}{MR+1}\right)\left(\Delta BO_f + UF_f\right)$$

for engine start pressurization only

Table 58. Pressurization System Weight Coefficients

Propellant	Pressurant	Pressure kg/cm^2	Pressure (lb/in^2)	K_1 English	K_1 Metric
Cryogen	Helium	1.76	(25)	0.400	6.40
	Nitrogen	1.76	(25)	0.625	10.00
Space Storable	Helium	2.81	(25)	0.335	5.35
	Nitrogen	2.81	(25)	0.525	8.40
Earth Storable	Helium	7.03	(100)	0.775	12.40
Storable	Helium	14.06	(200)	1.525	24.4
Storable	Helium	21.09	(300)	2.275	36.4
Storable	Nitrogen	7.03	(100)	1.225	19.1
Storable	Nitrogen	14.06	(200)	2.425	38.8
Storable	Nitrogen	21.09	(300)	3.625	58.0

Propellant Feed System Weight (W_{PF})

The propellant feed systems for both the oxidizer and fuel tanks are combined into one simplified scaling law, which is given by

$$W_{PF} = 100 + 2.5 \times 10^{-3} W_P$$

9.3 ENGINE MODULE WEIGHT

The engine module weight W_{EM} is the sum of the weights of the engine, W_{ENG}, the thrust structure, W_{TS}, and of the shell enclosing the engine, W_t.

$$W_{EM} = W_{ENG} + W_{TS} + W_t$$

Engine Weight (W_{ENG})

Thrust/weight ratios for the different engine types shown in Figure 103 include the thrust chamber assembly and the thrust vector control

$$W_{ENG} = \frac{F\, K_p\, K_\varepsilon}{(T/W)_{ENG}}$$

K_p and K_ε are modification factors to account for changes in the chamber pressure and expansion ratio, Figure 103. K_p for pump fed engine systems can be assumed to be equal to 1.0 for the normal range of operating pressure. The weights for high pressure shuttle type engines are quoted as a separate curve in Figure 103. The stage thrust level required can be estimated from the given initial gross weight W_0, or from a first estimate for W_0 when the payload is given. In the latter case, for an initial guess on ν_B,

$$W_0 = W_{PAY} + W_P \left(\frac{1+\Delta BO}{\nu_B} - \Delta BO \right); \text{ (Payload given)}$$

For departure from an Earth parking orbit, a value of 0.4 to 0.6 for the ratio of engine thrust/gross weight is generally close to that required for maximum performance. For capture at or escape from target planets, the optimum value of F/W_0 varies with the mass of the planet and with the radius and eccentricity of the capture or departure orbit. For orbits no smaller than 2 planet radii, the ratio of F/W_0 (in Earth g's) that provides essentially maximum performance at target planets lies between about 0.2 and 0.4.

The engine thrust level, F, required can be obtained from

$$F = \left(\frac{F}{W_0}\right) \frac{W_0}{N_E}$$

where N_E = the number of engines per stage

Pressure-fed engine weights quoted are for an ablative/radiation-cooled nozzle. Engines with an all ablative nozzle would increase the engine weight by 25%. Propellants of the halogen-family used in the pressure-fed engine system require an additional 20% weight for the change of nozzle material.

Thrust Structure Weight (W_{TS})

Weight of the thrust structure W_{TS} is a function of the total thrust level and the number of engines.

$$W_{TS} = 3.6 \times 10^{-3}\, F\, (N_E)^{0.3}$$

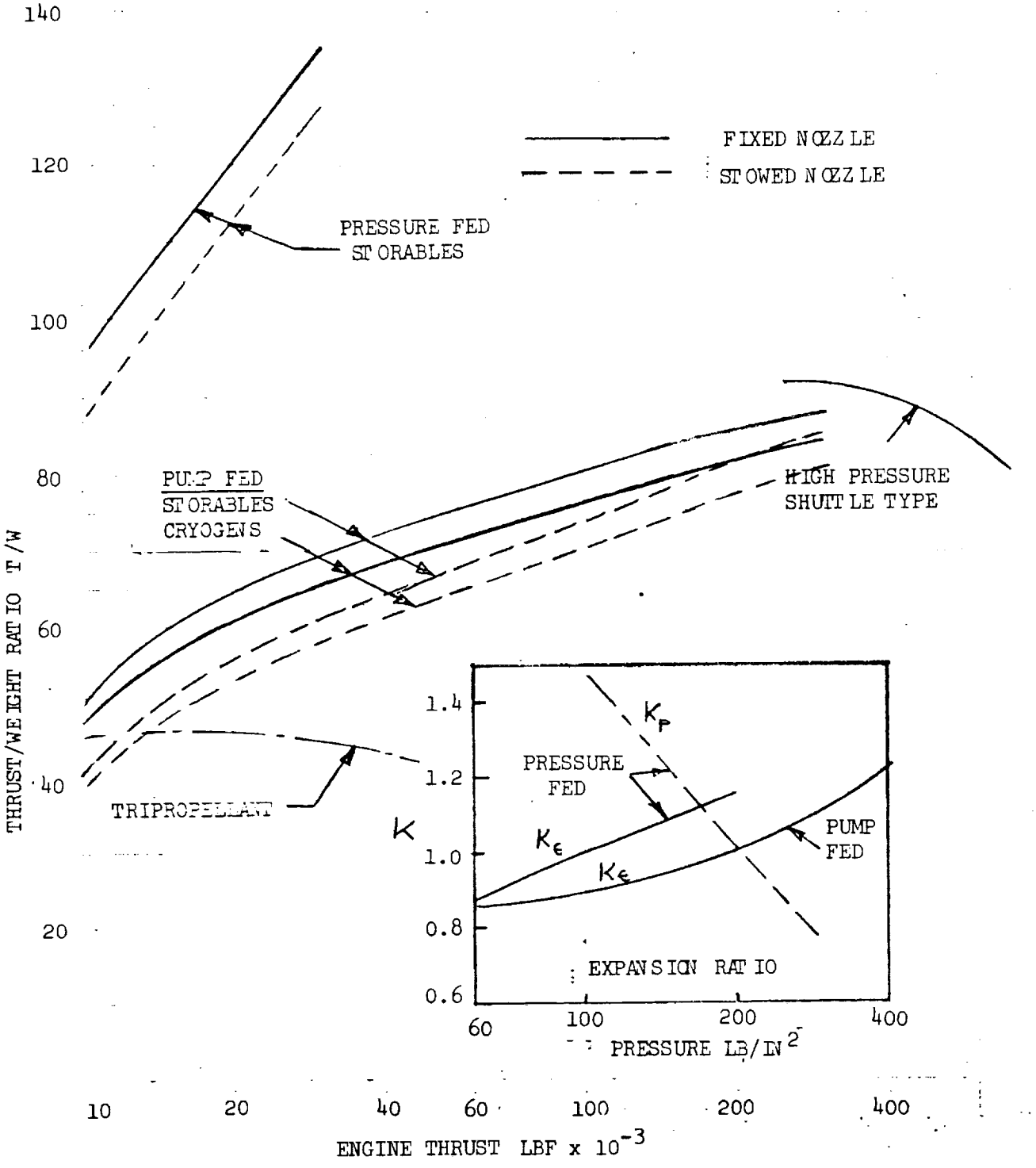

Figure 103. Engine Thrust/Weight for Different Engine Classes

Outer-Shell Weight (W_t)

The weight of the outer shell W_t of the engine module is a function of the stage diameter and engine length:

$$W_t = K_1 W_p^{*} \left(\frac{D}{2}\right)^{K_2} L_{ENG}^{K_3} \quad (kg, lb)$$

where

K_1, K_2, K_3 are given in Table 59

D and L_{ENG} are in inches

and the stage diameter D is the larger of the values obtained from Figure 104 with a selected L/D and volumes obtained from one or another of

$$V_{OX} = \frac{W_{P_{tot,ox}}}{\rho_{ox}}$$

$$V_F = \frac{W_{P_{tot,ox}}}{\rho_{ox}}$$

} Separate tanks for oxidizer, fuel

or from

$$V = \frac{W_{P_{tot}}}{\rho^{*}}$$, Single tank with common bulkhead

Table 59. Outer Shell Weight Coefficients

Material	K_1	K_2	K_3	
Aluminum	1.76×10^{-4}	0.47	0.85	Metric
	5.92×10^{-4}	0.47	0.85	English
Titanium	6.7×10^{-5}	0.36	0.85	Metric
	2.45×10^{-4}	0.36	0.85	English

The length of the engine module is obtained from Figure 105 by selecting the thrust level, chamber pressure and expansion ratio for the engine.

9.4 ENVIRONMENTAL MODULE WEIGHT

The inert weight of the environmental shielding module, W_{EMP}, consists of the total weight penalty for the meteoroid shielding, $W_{MP_{tot}}$, and the stage insulation weight, $W_{INS_{tot}}$.

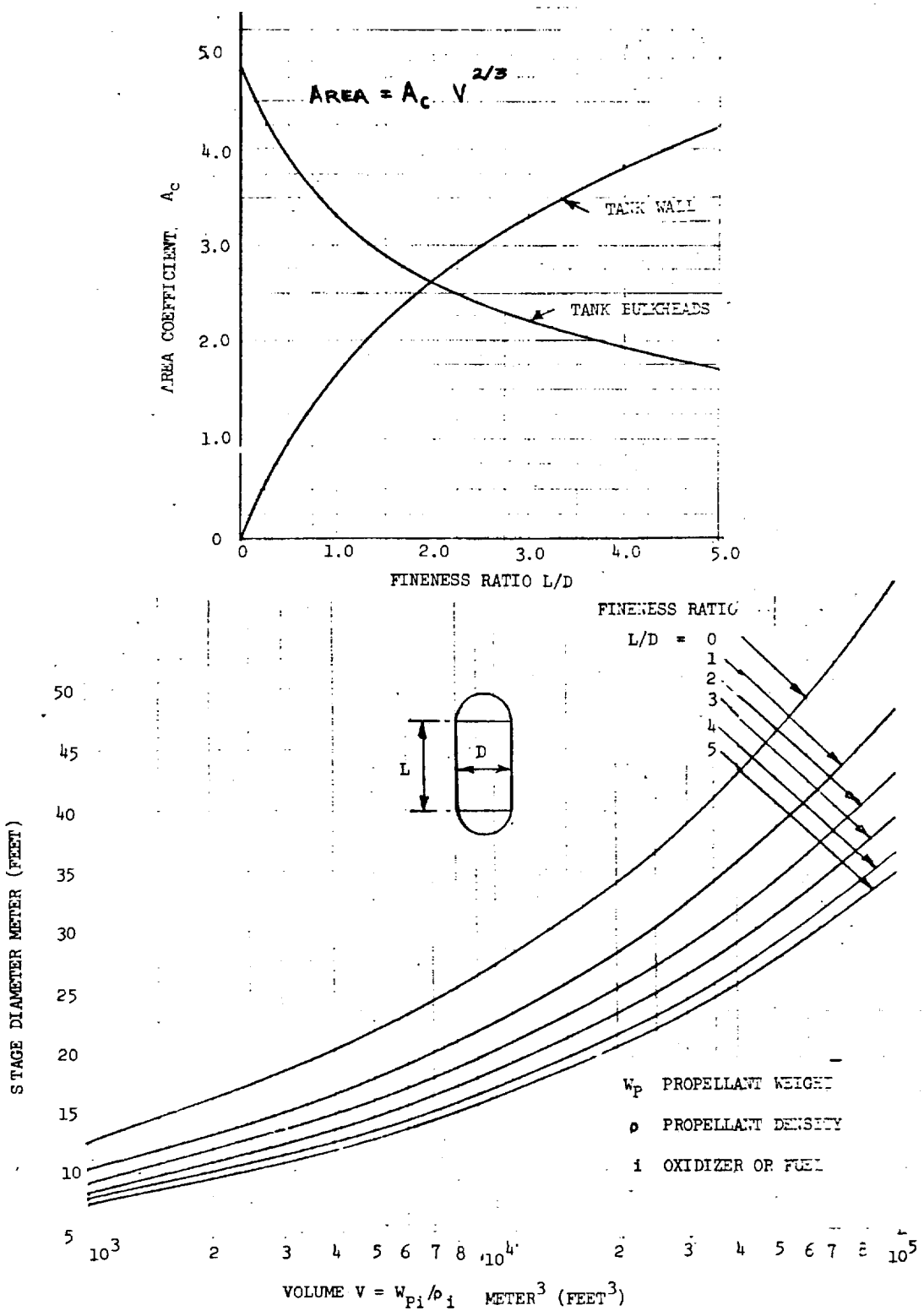

Figure 104. Tank Diameter Versus Volume and Fineness Ratio

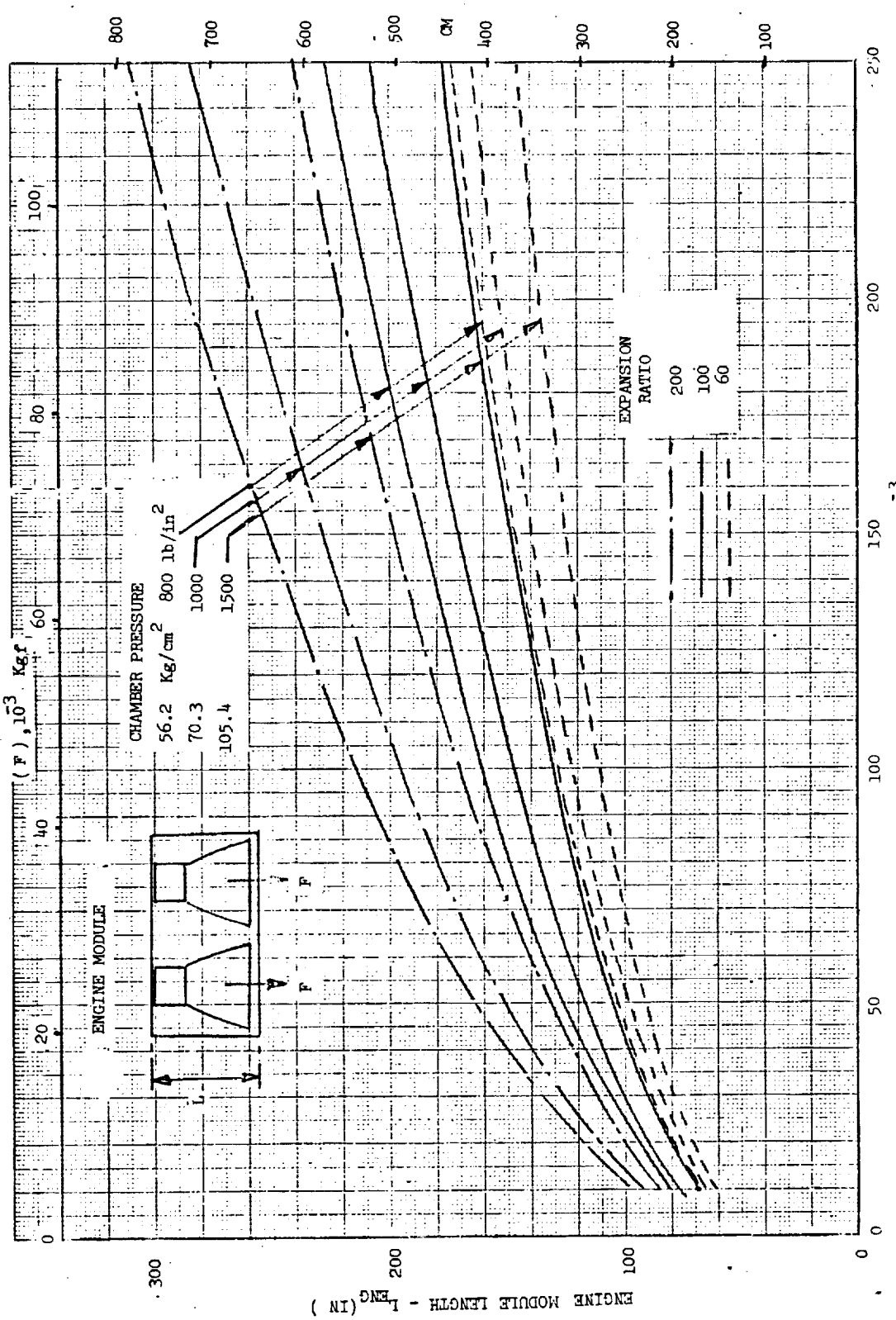

Figure 105. Engine Module Length

$$W_{EMP} = W_{MP_{tot}} + W_{INS_{tot}}$$

Meteoroid Shielding Weight ($W_{MP_{tot}}$)

It is necessary to use a series of figures and charts to evaluate the meteoroid environment, particle diameter and finally the shielding weight requirements. The accuracy of estimation will depend upon graphical interpolation and should be within one or two percent error for the unit shielding weight estimation.

The results obtained from the synthesis program SPASM for the meteoroid flux integration have clearly indicated that there is a strong dependency upon the mission duration and the mission profile. Figures 41 through 44 show that the flux integrals and flux-velocity integrals are non-linear with mission duration and trajectory semi-major axis. It should be noted that these figures are limited to interplanetary trajectories with central angles no larger than 180 degrees.

A simplified worksheet, Table 60, is provided and the look-up procedure is capable of handling multi-mission legs with varying flux density, asteroidal and cometary particles, single sheet, single and dual bumper design concepts, and different materials, and of optimizing the overall penetration requirements.

The procedure is identified for the weight estimation together with the data source.

The mission leg parameters are identified as the solar distance of the arrival planet, planet stop-over time, periapse, r_1, and apoapse, r_2, around the planet. The average modification factor is

$$G\eta_{AV} = 8.3 \frac{G\eta_2\left(\frac{r_2}{r_p}\right) - G\eta_1\left(\frac{r_1}{r_p}\right)}{\left(\frac{r_2}{r_p} - \frac{r_1}{r_p}\right)}$$

where r_p = the planet radius

$G\eta_1$, $G\eta_2$ are given in Figure 106

The undisturbed flux at planet distances, Table 61, is corrected by the flux modification factor $G\eta_{AV}$ to obtain FLX_A and FLX_C.

The velocity integral is evaluated by

$$VxFLX_A = \overline{V} \times FLX_A$$

Table 60 Meteoroid Shielding Requirements

MISSION FLUX INTEGRATION

	MISSION LEG STAGE IS EXPOSED				
	1	2	3	4	Total
Departure Planet Arrival Planet Solar Distance AU Planet Orbit Radii Stop-Over Time (hrs) Modification Factor G_η					
Sporadic V_X FLX_A Asteroidal FLX_A					
Sporadic V_X FLX_C Cometary FLX_C					

SHIELDING WEIGHT

	SPORADIC ASTEROIDAL	SPORADIC COMETARY
Average Velocity, m/sec Stage Surface Area, m^2 Po of No Penetration Particle Diameter , cm Diameter Factor α Bumper Wt , W_B; kg/cm^2 Rear Sheet Factor W_m/d^α Rear Sheet Wt , W_m; kg/cm^2		

$$P_o = P_{o_a} \times P_{o_c} =$$

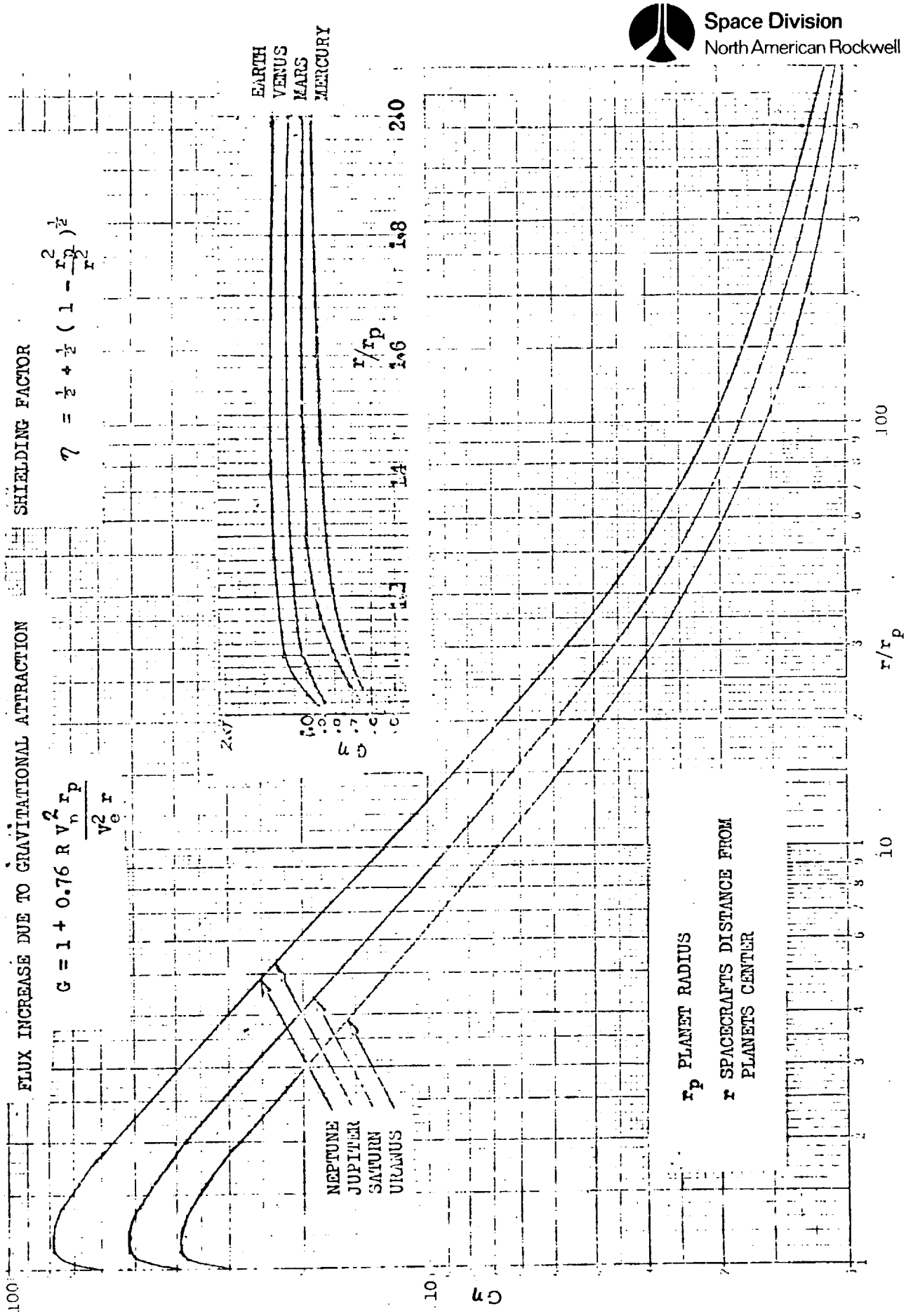

Figure 106. Meteroid Modification Factor Due to Planets

where $\bar{V}$ is given in Table 61.

Table 61. Meteoroid Fluxes at Planet Distances

PLANET	COMETARY FLUX		ASTEROIDAL FLUX	
	F_{pC}* $\frac{\text{Particles}}{m^2 \text{ Year}}$	$\bar{V}$ m/sec	F_{pA}* $\frac{\text{Particles}}{m^2 \text{ Year}}$	$\bar{V}$ m/sec
Mercury	6.822×10^{-7}	31000		24900
Venus	1.955×10^{-7}	22700	1.399×10^{-10}	10900
Earth	1.021×10^{-7}	19300	3.761×10^{-9}	9300
Mars	4.399×10^{-8}	15600	6.365×10^{-8}	7500
Jupiter	3.774×10^{-9}	8450	1.0105×10^{-10}	2580
Saturn	1.123×10^{-9}	6240	-	1850
Uranus	2.777×10^{-10}	4400	-	1300
Neptune	1.131×10^{-10}	3500	-	1040
Pluto	6.569×10^{-11}	3070	-	910

The transplanetary mission segment flux and flux-velocity integrals for a particular planet pair are obtained from Figures 41 through 44.

The procedure is repeated for each mission leg and the total mission flux is the sum of all the flux integrals and the weighted particle velocity V_P is

$$V_{Pa,c} = \frac{\Sigma \text{ Vx FLX}_{a,c}}{\Sigma \text{ FLX}_{a,c}}$$

A representative exposed surface area for each stage is considered based on the initial estimate of the propellant volume.

$$A = \left(A_{cox_{BULK}} + A_{cox_{WALL}}\right) V_{ox}^{2/3} + \left(A_{cf_{BULK}} + A_{cf_{WALL}}\right) V_f^{2/3} + \pi D L_{ENG} \quad ; \ M^2$$

Area coefficients for both tanks are obtained from the engine module section using Figure 104.

A probability of no penetration for the cometary flux (P_{oc}) is selected where $P_o < P_{oc} < 1$ and the meteoroid particle for design purposes is obtained from

$$d_{Pa,c} = \left[\frac{6}{\pi \rho_{a,c}} \left(\frac{1-P_{oa,c}}{A \sum \int F^*_{a,c} \, dt} \right)^{1/K_{2a,c}} \right]^{1/3}$$

where K_2 = -0.84 (asteroidal); -1.213 (cometary)

ρ = 3.5 (asteroidal); 0.5 (cometary)

For the single and dual bumper design concepts, the unit weight of the outer bumper, W_B, is given in Figure 107 and depends on the particle diameter and the bumper material.

The rear sheet weight requirements can be determined with the aid of Figure 108 and the meteoroid impact velocity V_P. An exponent α associated with the particle diameter is given in Table 62 as a function of the material and the shielding concept. The unit weight for the rear sheet is

$$W_{M_2} = \left(\frac{W_{M_2}}{d^{\alpha}} \right) d^{\alpha}$$

Table 62. Meteoroid Particle Diameter Exponent

Meteoroid	Material	Single Sheet	Single Bumper	Dual Bumper
Cometary	Aluminum	1.0535	1.12	1.15
	Titanium	1.0535	1.11	1.09
	Glass Epoxy	-	1.09	-
Asteroidal	Aluminum	1.0535	1.11	1.04
	Titanium	1.0535	1.12	1.12
	Glass Epoxy	-	1.09	-

Actual meteoroid shielding unit weight penalty (W_{mp}) considers the shell material, unpressurized/pressurized and insulation shielding allowances

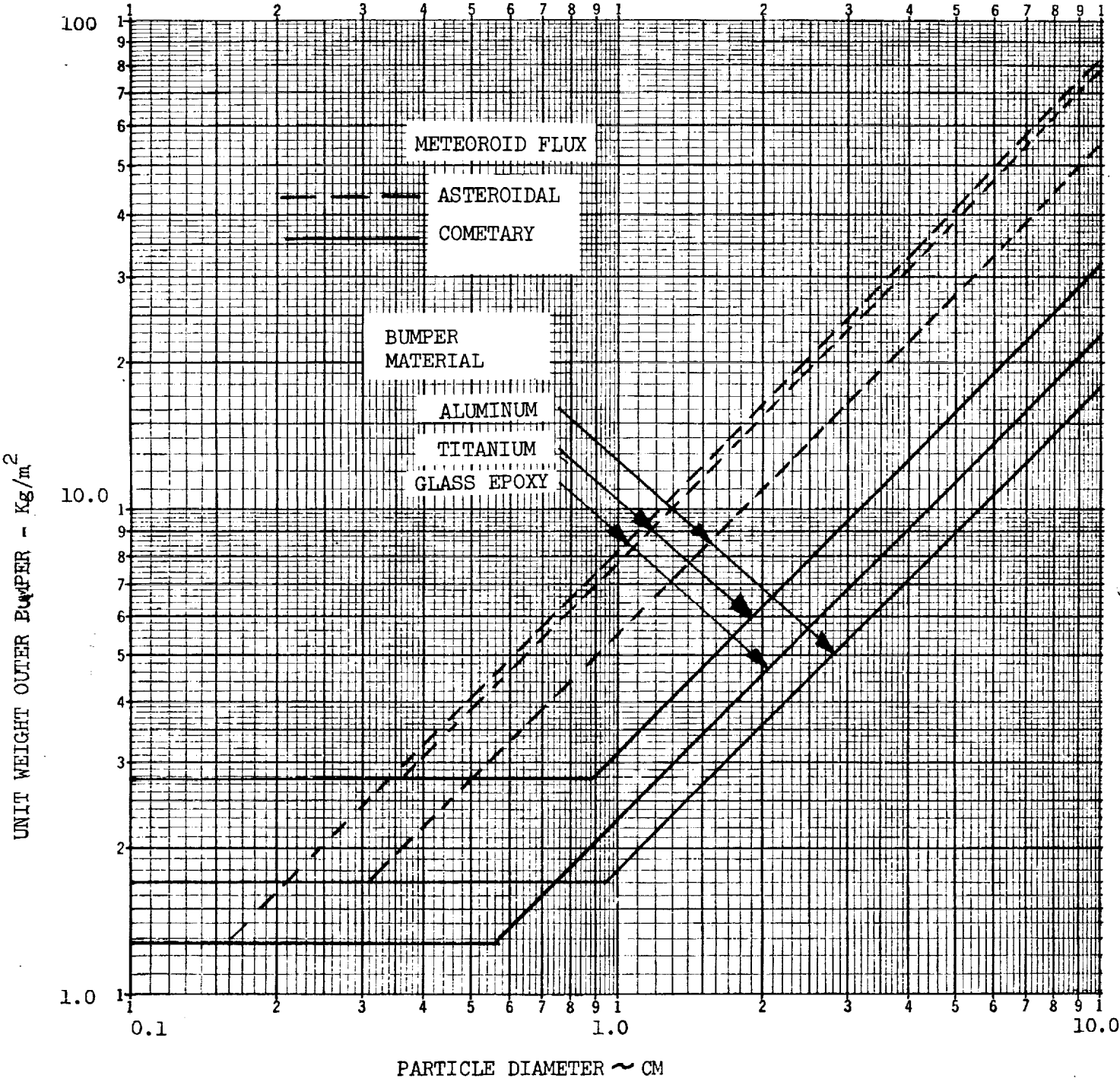

Figure 107. Meteoroid Bumper Unit Weight

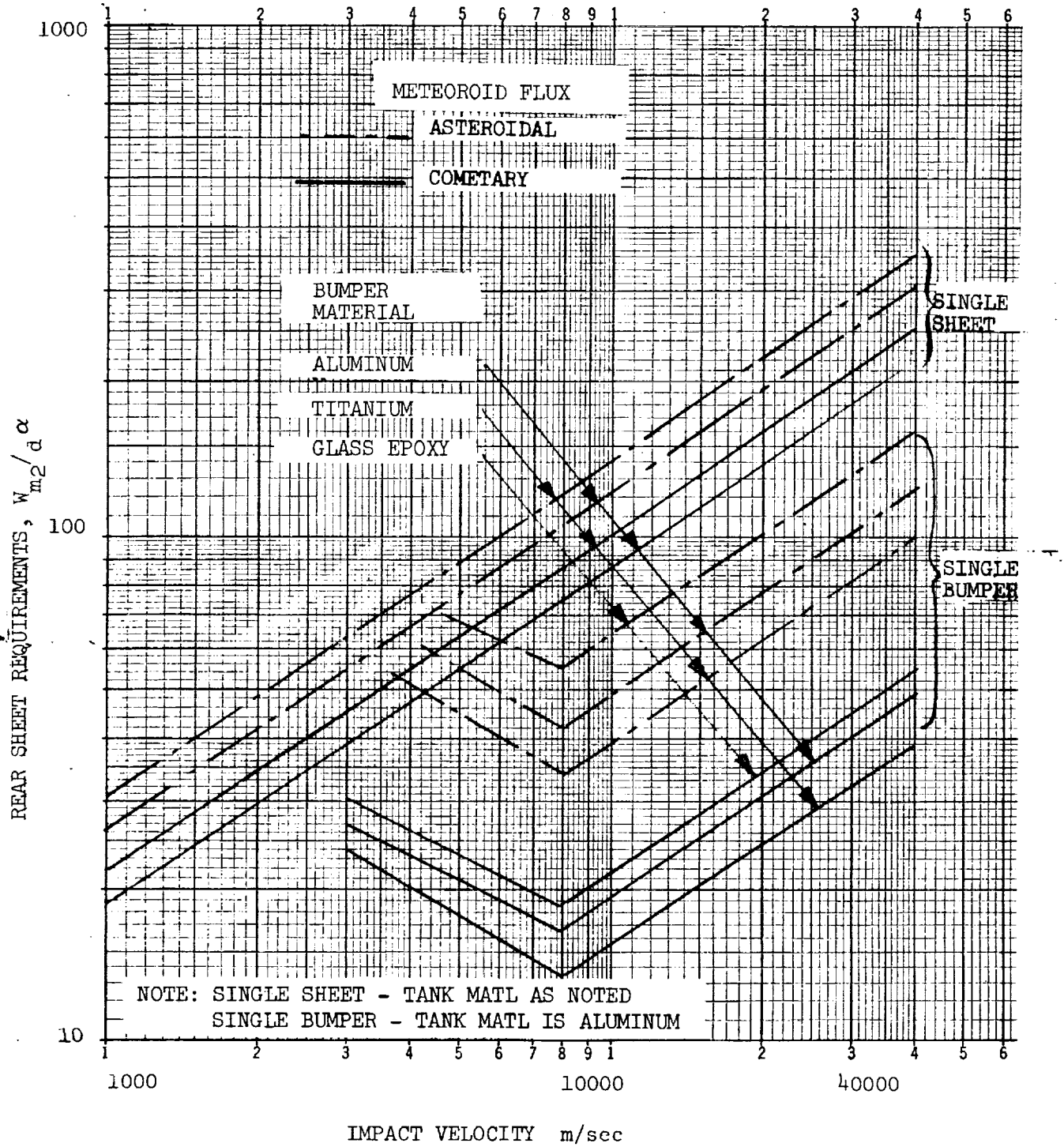

Figure 108. Meteoroid Shielding Rear Sheet Requirements

$$W_{mp} = W_B + \frac{K_1 K_2 W_m}{EXP\ (14.9\ \rho_{ins}\ \tau_{ins}/d^*)} - W_S$$

where K_1 = 1.0 for pressure tanks
= 0.445 for unpressurized shells

K_2 = 1.0 aluminum
= 1.15 titanium
= 0.83 Glass Epoxy

ρ_{ins} = insulation density (gm/cm^3)

τ_{ins} = insulation thickness (cm)

d^* = max (d_p, 1.0) (cm)

W_S = existing unit weight for structural integrity

The procedure is repeated for the asteroidal flux and the shielding penalty is taken as the maximum W_{mp} due to the cometary or asteroid fluxes. The stage overall mission penetration probability P_o is

$$P_o = P_{oa} \times P_{oc}$$

The total meteoroid shielding weight penalty, $W_{MP_{tot}}$ is given by

$$W_{MP_{tot}} = A_{unp}\ W_{mp_{unp}} + A_p\ W_{mp_p}$$

where subscript unp is for the unpressurized structural elements (skirts, intertank, interstage) and the subscript p refers to the pressurized structural elements (tank walls).

Stage Insulation Weight ($W_{INS_{tot}}$)

A simplified approach for predicting thermal requirements will use simple models and several charts depicting the integrated thermal properties of various insulation/propellant combinations. The following procedure will provide the insulation weight estimates.

Planet stop-over mission legs subject the stage to planet albedo and emitted radiation, B_f,

$$B_f = \left(1 - \frac{\sqrt{h(r_p+h)}}{(r_p + h)}\right)\left(B + 0.25\ (1-B)\right)$$

where R_p = planet's solar distance AU
B = planet's albedo
r_p = planet's radius
h = average radius of spacecraft orbit

The equilibrium temperature T_H of the outer surface during planet stop-over is

$$T_H = K_1 \left[\left(\frac{\alpha_s}{\varepsilon} \right) \left(\frac{1+B_f}{R_P^2} \right) \right]^{1/4}$$

where K_1 = 281 (metric); 505 (English)
α_s/ε = absorptivity/emissivity ratio (0.20)

For the transplanetary mission segments the equilibrium temperature is

$$T_H = K_1 \left[\left(\frac{\alpha_s}{\varepsilon} \right) \left(\frac{1}{R^2} \right) \right]^{1/4}$$

where R = solar distance of the spacecraft, AU

The normalized unit flux, H_n, is obtained for each mission leg from Figure 109 for the specific propellant and the type of thermal insulation used for the tank protection. The total flux integral K is

$$K = \sum H_n \times \text{Time} \times (1+C)$$

where C = correction factor to account for heat leaks through support structure 0.5 (aluminum); 0.4 (titanium); 0.25 (structure with heat blocks)

A thickness-heating parameter (d/k) is evaluated from the thermal insulation sizing nomograph Figure 110 for a fixed percent propellant boil-off. The required insulation thickness is obtained from

$$d_{INS} = (d/k)\, K$$

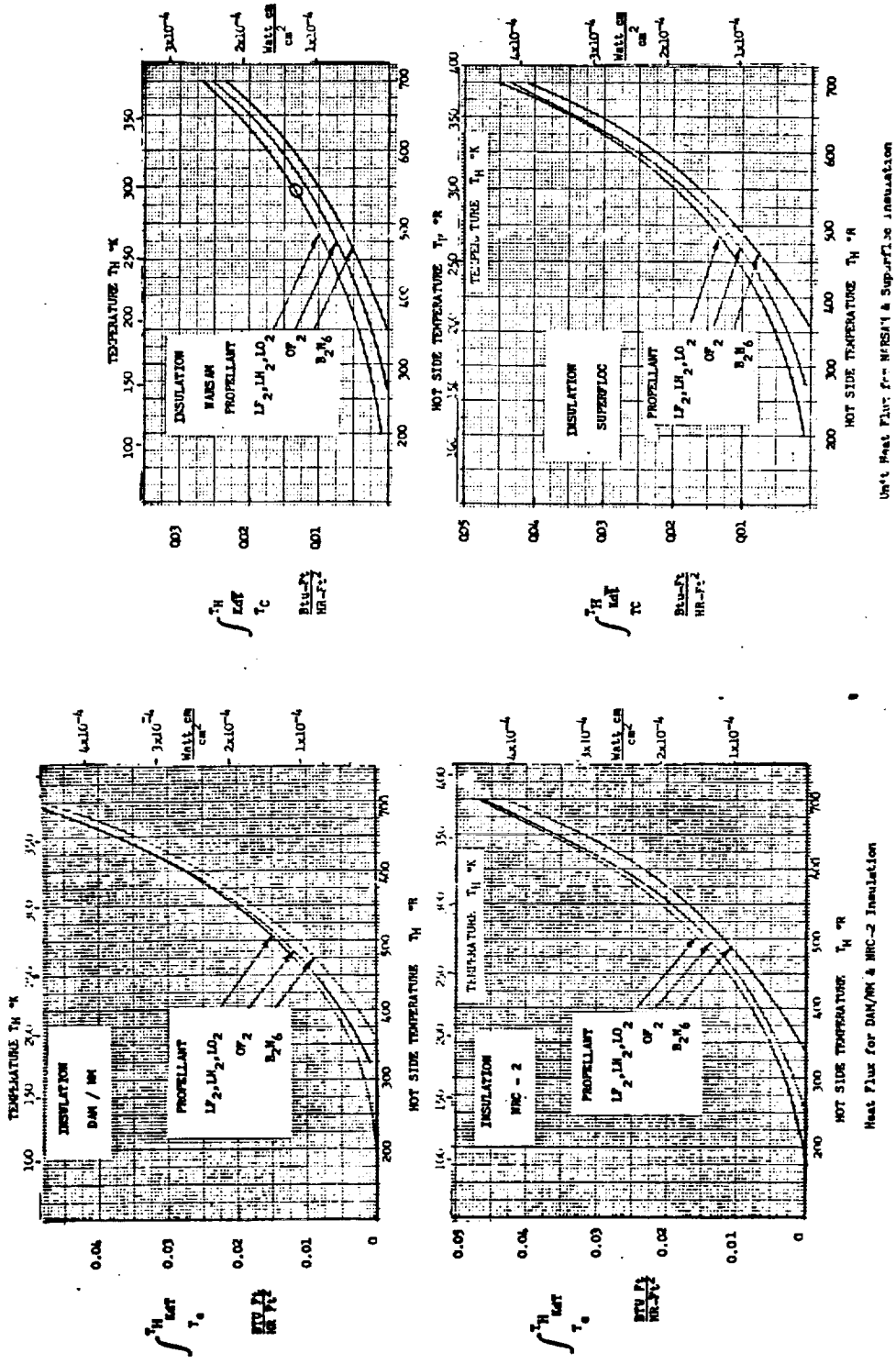

Figure 109. Unit Heat Flux With High Performance Insulation

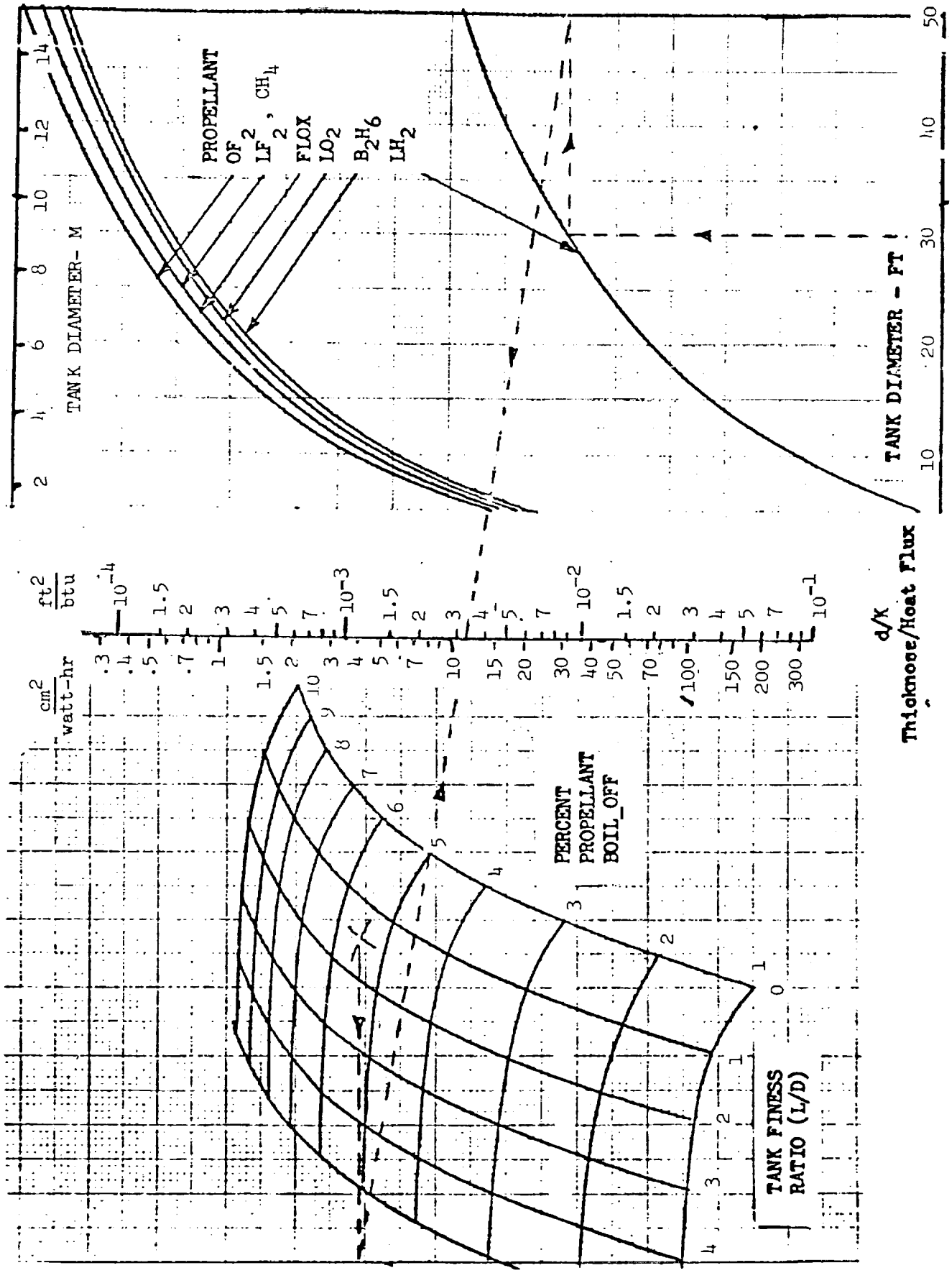

Figure 110. Thermal Insulation Sizing Nomograph

The stage insulation weight is given as

$$W_{INS_{tot}} = \left(\rho_{INS} \, d_{INS} + W_{INS} \right) A_T$$

where

A_T = thermal protected area including tank walls and bulkheads (if exposed) and unpressurized shells

W_{INS} = 6×10^{-5} kg/cm^2; 0.12 lb/ft^2 for ground hold

= 2×10^{-4} kg/cm^2; 0.40 lb/ft^2 if insulation is exposed to aerodynamic pressure forces during the Earth boost

= 0.0 for space exposure with an outer meteoroid bumper

No Propellant Boil-off - Increased Pressure

The allowable heat input per unit volume of propellant Q/V_L, is evaluated for a particular propellant tank pressure, P, and a specified ullage percent (UF).

$$Q/V_L = K_1 \; EXP \left(\frac{K_2}{K_3 - P} \right) UF^{1.25}$$

Table 63. Heat Input Coefficients

	K_1				K_2	K_3
Propellant	LH_2	LO_2	LF_2	B_2H_6		
Metric	0.315×10^5	2.93×10^5	3.7×10^5	3.15×10^5	0.945	1.05
English	0.306×10^4	2.84×10^4	3.6×10^4	3.06×10^4	13.5	15.0

The required insulation thickness is given by

$$d_{INS} = \frac{K}{(Q/V)} \quad \frac{A}{V}$$

where A = surface area of tank

K = total heat flux integral

Insulation Optimization

There are several ways to optimize the insulation requirements; each method based on different performance criteria. The usual method is to minimize the weight of the propellant boiled-off, insulation and additional tank structure and neglect the effect on the stage performance. A second approach is to minimize the vehicles initial weight for a specified mission performance requirement for the vehicle. The optimized insulation thicknesses for a two stage vehicle using the second method are

$$d_{1_{INS}} = \frac{f_1 K_1}{L_1} + \frac{1}{L_1}\sqrt{\frac{L_1 K_1}{\rho ins_1}\left(G_1 + \frac{1}{\mu_1}\right) + f_1^2 K_1^2}$$

$$d_{2_{INS}} = \frac{f_2 K_2}{L_2} + \frac{1}{L_2}\sqrt{\frac{L_2 K_2}{\rho ins_2}\left[G_2 + \frac{1}{\mu_1 \mu_2}\left(1 + \frac{K_{21}}{K_2}(\mu_1 - 1)\right)\right] + f_2^2 K_2^2}$$

The weight of propellant boil-off for each of the two stages with the optimum insulation thickness is

$$W_{B_i}{}_{opt} = \frac{A_i K_i}{d_{i_{INS}} L_i - f_i K_i} \qquad i = 1 \text{ or } 2$$

9.5 OTHER SYSTEMS MODULE WEIGHT

The weight estimation for the other systems module, W_{SYS}, can be obtained from the equations and empirical coefficients detailed in Section 7.4.

9.6 STAGE SYNTHESIS EXAMPLE

An example of synthesizing the upper stage of a two-stage Jupiter Orbiter mission will indicate the use of the simplified scaling laws. The mission/design data requirements for the upper stage of a two-stage Jupiter Orbiter having a 22000 lb payload requirement are shown in Table 67.

The sizing procedure is to estimate initially the stage mass fraction, obtain the gross size of the stage for its volume and surface areas. The weights of each module are developed as a function of the usable propellant weight, the scaling coefficients are obtained from the appropriate figures relating to the particular system and design. The performance, mass fraction and inert weight equations are iterated to obtain convergence on a vehicle stage which is constant with the mission requirements. The propellant used by the main engines is obtained from

$$W_P = \frac{W_{PAY}\,(e^{V/Ig} - 1)}{1 - (\frac{1}{\nu_\beta} - 1)\,(1 + \Delta Bo)\,(e^{V/Ig} - 1)}$$

$$= \frac{120700}{1 - (\frac{1}{\nu_\beta} - 1)\,5.759}$$

Let the initial mass fraction estimate be 0.9 and the stage and vehicle weight data are

W_P = 335200 lb

W_P^* = 352000 lb

W_O^* = 413100 lb

W_O = 396300 lb

W_G^* = 391100 lb

W_G = 374300 lb

ΔBO_{ox} = 0.05
ΔBO_f = 0.05
ΔBO = 0.05
} Boil-off

$W_{PR_{ox}}$ = 0.0025
W_{PR_f} = 0.0025
} Residual

UF_{ox} = 0.03
UF_f = 0.03
} Ullage

ρ_{ox} = 91.06 lb/ft^3

ρ_f = 23.24 lb/ft^3

Table 64. Mission/Design Data for Jupiter Orbiter

2 MISSION LEGS

a/ Earth Orbit Assembly
b/ Transplanetary Trajectory
e = 0.774; a = 4.346 AU; Duration = 600 days

VELOCITY REQUIREMENTS

Earth Escape - 23,100 ft/sec
Jupiter Capture - 24,380 ft/sec

PROPELLANT CHARACTERISTICS

Oxidizer - Flox -85%/O_2		Fuel - Methane	
Boiloff	5%	Boiloff	5%
Ullage	3%	Ullage	3%
Residual	0.25%	Residual	0.25%

ENGINE CHARACTERISTICS

Single pump-fed engine with fixed nozzle
Thrust to initial weight = 0.5
Chamber pressure = 1000 lb/in^2
Expansion ratio = 200
Mixture ratio = 5.75
Specific impulse = 405 sec

DESIGN CONCEPT

Two cylindrical tandem tanks with spherical bulkheads
Ring-stiffened aluminum construction
Tank pressure = 40 lb/in^2
Safety factor = 1.4
Meteoroid single bumper with Po_c = 0.995
Thermal insulation with NRC-2 α_s/ϵ = 0.2

Earth launch boost of 5 g longitudinal

Engine Module

The volume and surface areas are as follows

$$V_{ox} = \left(\frac{MR}{MR + 1}\right) \frac{W_P^*}{\rho_{ox}} \left(1 + \Delta BO_{ox} + W_{PR_{ox}}\right)$$

$$= 3399 \text{ ft}^3$$

and similarly

$$V_f = 2316 \text{ ft}^3$$

Selecting the smaller volume for a spherical tank, L/D = 0, Figure 104 shows the stage diameter is 17 feet. In the same figure, using V_{OX} and D, obtain L/D = 0.5 for the oxygen tank and the area coefficients A_C.

	L/D	$A_{c\ BULK}$	$A_{c\ WALL}$
Fuel	0	4.85	0
Oxidizer	0.5	3.925	1.0

$A_{BULK} = A_{c\ BULK} (V)^{2/3}$; 863.3 ft^2 - fuel and 894.9 ft^2 - oxidizer

$A_{WALL} = A_{c\ WALL} (V)^{2/3}$; 0.0$\text{ft}^2$ - fuel and 228.0 ft^2 - oxidizer

Engine Thrust Level

$$F = 0.5\ W_0$$

$$= 198200 \text{ lbf}$$

Using Figures 105 and 103, the engine module length is 256 in, the engine thrust/weight is 86 and the modification factors are $K_\varepsilon = K_P = 1.0$. Thus the engine weight is

$$W_{ENG} = \frac{F\ K_P\ K_\varepsilon}{(T/W)_{ENG}}$$

$$= \frac{(198200)(1.0)(1.0)}{86} = 2305 \text{ lb}$$

$$= 0.01527\ W_P^*$$

The thrust structure weight is

$$W_{TS} = 3.6\text{x}10^{-3} F\ (N_E)^{0.3} = 3.6\text{x}10^{-3}\ (198200)\ (1)^{0.3}$$

$$= 713.5 \text{ lb} = 0.00493\ W_P^*$$

Interstage stage shell weight and its protection shields are jettisoned prior to the second stage ignition. Therefore, the interstage weight is included in the performance equation of the first stage but not included in the weight statement for the orbiter stage.

$$W_t = K_1\ W_P^{*\,K_2} \left(\frac{D}{2}\right)^{K_3} L_{ENG}$$

$$= 5.92\text{x}10^{-4}\ W_P^{*\,0.47} \left(\frac{204}{2}\right)^{0.85} (256)$$

$$= 7.68\ W_P^{*\,0.47}$$

The total weight of the engine module is

$$\boxed{W_{EM} = 0.0202\ W_P^*}$$

Propellant Module

The weight of the propellant module from Figure 102 is 7700 lb. Since the weight curve can be linearized about the basepoint propellant capacity of 362700 lb, it will allow the propellant module to be expressed as a function of the propellant requirements

$$W_{PT} = 0.0154\ W_P^{*\,1.03}$$

The pressurization requirements are determined from the engine start-up conditions with an evaporative system using fluids from the main tanks (included in the residual propellants).

$$W_{PRESS} = 0.0$$

The propulsion feed system for both the oxidizer and fuel tanks is

$$W_{PF} = 100 + 0.0025\ W_P^*$$

Total weight for the propellant module is

$$\boxed{W_{PM} = 100 + 0.0025\ W_P^* + 0.0154\ W_P^{*\,1.03}}$$

Environmental Module

The surface areas which are exposed to the meteoroid flux are based on the area coefficients from Figure 104. The pressurized area is for the oxidizer tank wall.

$$A_{PRESS} = 1.0 \left(\frac{W_P^*\ 1.03}{91.06}\right)^{2/3} = 0.05\ W_P^{*\,2/3}\ \text{ft}^2$$

The fuel tank has no tank wall. The unpressurized areas include the forward and aft skirt, intertank and interstage structure.

$$A_{UNPRESS} = (4.85 + 3.925)\left(\frac{W_P^* \, 1.03}{91.06}\right)^{2/3} + \pi(17)\left(\frac{256}{12}\right)$$

$$= 0.438 \; W_P{}^{*2/3} + 1140 \; ft^2$$

$$AMET = 0.488 \; W_P{}^{*2/3} + 1140 \; ft^2$$

The interstage shell is included in estimating the meteoroid shielding requirements although the stage is jettisoned prior to stage two ignition. The surface areas requiring thermal insulation are all the outer shell (excluding the interstage) plus the four bulkhead surfaces, therefore

$$A_{THERM} = \left[2(0.438) + 0.05\right] W_P{}^{*2/3} \; ft^2$$

The flux and flux velocity integrals for the transplanetary mission and the meteoroid requirement are evaluated in Table 68. Assuming an average unit skin weight of 1.36 lb/ft^2 based on the propellant module weight and surface area, the rear sheet requirements for the meteoroid shielding are

$$W_{M \; TANK} = 1.87 - 1.36$$
$$= 0.51 \; lb/ft^2$$

$$W_{M \; UNPRESS} = 1.87 (0.445) - 1.36$$
$$= 0.0 \; lb/ft^2$$

The bumper weight $W_B = 0.362 \; lb/ft^2$ has to be added as a weight penalty. The thermal flux changes between Earth orbit and arrival at Jupiter. Temperatures at the departure and arrival points are specified as follows:

$$T_{H_{EARTH}} = 505 \; (.2)^{1/4} = 340°R$$

$$T_{H_{JUPITER}} = 505 \left(\frac{.2}{5.2^2}\right)^{1/4} = 150°R$$

The normalized flux from Figure 109 using NRC2 insulation is

PROPELLANT	TEMP FLUID	$\int K \, dT_{EARTH}$	$\int K \, dT_{JUPITER}$
Oxidizer	155°R	0.005	0.0
Fuel	200°R	0.004	0.0

The total averaged heat input throughout the mission

$$K_{ox} = 24\left(\frac{0.005 + 0.0}{2}\right)(600)\,(24)$$
$$= 36 \; \frac{btu/ft}{ft^2}$$

$$K_f = \frac{(0.004 + 0.0)}{2} (600) (24)$$

$$= 28.8 \frac{\text{btu/ft}}{\text{ft}^2}$$

Table 65. Meteoroid Shielding Requirements - Jupiter Orbiter

MISSION FLUX INTEGRATION

	MISSION LEG STAGE IS EXPOSED				
	1	2	3	4	Total
Departure Planet	Earth				
Arrival Planet	Jupiter				
Solar Distance AU	-				
Planet Orbit Ratio	-				
Stop-Over Time (Years)	-				
Modification Factor Gη	-				
Sporadic VX FLX_A					
Asteroidal FLX_A					
Sporadic VX FLX_C	9.5×10^{-4}				
Cometary FLX_C	4.40×10^{-8}				

SHIELDING WEIGHT

	SPORADIC ASTEROIDAL	SPORADIC COMETARY
Average Velocity m/sec		21600 m/sec
Stage Surface Area M^2	333 m^2	
Po of No Penetration	0.995	0.995
Particle Diameter d (cm)	Negligible	0.31 cm
Diameter Factor α		1.12
Bumper Wt W_B Kg/cm^2		1.77 kg/m^2
Rear Sheet Factor W_m/d^α		34.0
Rear Sheet Wt W_m		9.16 kg/m^2

$$P_o = P_{o_a} \times P_{o_c} = 0.995 \times 0.995 = 0.99$$

Using the nomograph, Figure 110, for a 17 ft diameter tank with 5 percent boil-off, the insulation thickness is

$$d_{ox} = 0.9 \times 10^{-3} \ (36) = 0.0324 \text{ ft}$$

$$d_f = 1.0 \times 10^{-3} \ (28.8) = 0.0288 \text{ ft}$$

The average insulation weight is

$$W_{INS} = d \times \rho_{INSTALL} \times (1 + \text{Leak Factor}) + \Delta W_{INS}$$

$$= \left(\frac{0.0324 + 0.0288}{2} \right) (2.17) \ (1.0 + 0.5) + 0.12$$

$$W_{INS} = 0.22 \text{ lb/ft}^2$$

Total weight for the environmental module is

$$W_{EMP} = A_{MET} \times W_M + A_{THERM} \times W_{INS}$$

$$= 0.203 \ W_P{}^{*2/3} + 413 + 0.204 \ W_P{}^{*2/3}$$

$$\boxed{W_{EMP} = 0.407 \ W_P{}^{*2/3} + 413}$$

Other System Elements

Single purpose ground base

$$W_{IM} = 586 + 0.01155 \ W_P{}^*$$

Attitude control

$$W_{ACS} = 150 + 0.005 \ W_P{}^*$$

Electrical system

$$W_{ELEC} = 300 + 4.78 \times 10^{-3} \ W_P{}^* - 2.36 \times 10^{-9} \ W_P{}^{*2}$$

Total module weight reduces to

$$\boxed{W_{SYS} = 1036 + 0.02133 \ W_P{}^* - 2.39 \times 10^{-9} \ W_P{}^{*2}}$$

The stage inert weight is the total of the various module weights plus the residual propellant weight of 0.0025 W_P*.

$$W_{ST} = 1549 + 0.04653\ W_P^* + 0.1407\ W_P^{*2/3} - 2.39 \times 10^{-9}\ W_P^{*2} + 0.0154\ W_P^{*1.03}$$

The stage mass fraction is

$$\nu_B = \frac{W_P^*}{W_P^* + W_{ST}}$$

and the performance equation

$$W_p^* = \frac{120700\ (1 + .05)}{1 - \left(\frac{1}{\nu_B} - 1\right)\ 5.759}$$

These three equations are used for the iteration process to converge on a constant stage design as summarized in Table 66.

Table 66. Mass Fraction Iteration

MASS FRACTION $\nu_{B\ EST}$	PROPELLANT W_p^*	INERT WEIGHT W_{ST}	MASS FRACTION $\nu_{B\ CALC}$
0.9	351933	27607	.9273
0.9273	231059	18859	.9245
0.9245	239147	19448	.9248
0.9248	238354	19390	.9248

A two-stage Jupiter Orbiter vehicle synthesized by the SPASM program had an upper stage weight of 252515 lb while the stage evaluated manually (Table 66) has a stage weight of 257743 lb. The earth departure stage is evaluated in an identical fashion using the mission payload weight and stage two weight as the payload weight W_{PAY}.

10.0 REFERENCES

1. Space Storable Propellant Rocket Engine Parametric Data Florida Research and Development Center, Pratt & Whitney Aircraft, PDS-2686 (19 Jan. 1968)

2. Rocket Engine Design Criteria as a Basis for Propellant Selection for Spacecraft Propulsion Systems Sacramento Plant, Aerojet-General Corporation, (Aug. 1967)

3. Influence of Structure and Material Research on Advanced Launch Systems Weight, Performance, and Cost Phase III Final Report, Volume II Users Manual for Vehicle and Structural Design Syntheses Program. Space Division, North American Rockwell Corporation, SD67-1204-2 (Jan. 1968)

4. Dow, N. F., and Rosen, B. W. Structural Effiency of Orthothropic Cylindrical Shells Subjected to Axial Compression AIAA Journal, Volume 4, No. 3, (March 1966), pp. 481-485

5. Nominal Natural Environment for Application to Advanced Manned Planetary Mission Program Studies, ASTD, Space Environment, NASA-MSC, 1 July 1964

6. Weidner, Don, et al., Space Environment Criteria Guidelines for Use in Space Vehicle Development (1969 Revision), George C. Marshall Space Flight Center Report N70-22208, 17 October 1969

7. Study of Unmanned Systems to Evaluate the Martian Environment, Final Report, NAA/S&ID, SID65-1172, September 1965

8. Meteoroid Environment Model - 1970 (Interplanetary & Planetary), NASA Space Vehicle Design Criteria, (Environment), NASA SPS038, 6-70

9. Smith, R. E. and Weidner, D. K., Space Environment Criteria Guidelines for Use in Space Vehicle Development (1968) Revision George C. Marshall Space Flight Center, NASA TMS-53798, 1968

10. Dycus, R. D., and Richardson, A. J., A Meteoroid Stream Model for Evaluation of the Stream Hazard to Interplanetary Flight, Journal of Spacecraft and Rockets, Vol. 6, No. 9, September 1969, pp 1070-1072

11. Summers, J. L., and A. C. Charters, High Speed Impact of Metal Projectiles in Targets of Various Materials. Third Hypervelocity Symposium, Vol. 1 (October 1958)

REFERENCES (CONT.)

12. Charters, A. C., and J. L. Summers. Some Comments on the Phenomena of High-Speed Impact. Paper presented at Decennial Symposium at U. S. Naval Ordnance Laboratory, White Oak, Silver Springs, Md. (May 26, 1959)

13. Hermann, W., and A. H. Jones. Survey of Hypervelocity Impact Information. A.S.R.L. Report No. 99-1, MIT (September 1961)

14. Bohn, J. L., and O. P. Fuchs. High Velocity Impact Studies Directed Towards the Determination of the Spatial Density. Mass and Velocity of Micrometeroids at High Altitudes. Scientific Report No. 1 ASTIA AD 243 106.

15. Hypervelocity Impact Penetration Equation for Metal by Multiple Regression Analysis. NR/SD STR 153 (March 1966)

16. Meteoroid Damage Assessment, NASA SP-8042, May 1970

17. Kinard, W. H., C. H. Lambert, D. R. Schryer, and F. W. Casey, Jr. Effect of Target Thickness on Cratering and Penetration of Projectiles Impacting at Velocities to 13,000 fps. NASA memo 10-18-58L (December 1958).

18. Richardson, A. J., Theoretical Penetration Mechanics of Multisheet Structures Based on Discrete Particle Modeling, AIAA Paper No. 69-371, Proc. AIAA Hypervelocity Impact Conference (April 1969)

19. Handbook of Thermal Design Data for Multi-layer Insulation Systems - Volume VI - Design of High Performance Insulation Systems, Lockheed Missiles and Space Co. Report No. LMSC-A742593-VI, August 1965

20. Thermal Protection Systems for Cryogenic Propellants on Interplanetary Spacecraft - Volume III - Analytical Methods. General Dynamics Fort Worth Division Report No. FZA-416-111, September 1966.

21. Development of Materials and Materials Application Concepts for Joint Use as Cryogenic Insulation and Micro-Meteoroid Bumpers, NASA Contract No. NAS8-11747, Goodyear Aerospace Corporation Report No. GER 11676 8/36, June 1967

22. Tri-propellant Engine System Study-Final Report: Contract NASw-1838 NR Rocketdyne R-7877 (June 1969)

23. J-25 Interface Criteria. Contract NAS8-19. NR Rocketdyne R-7211. (16 October 1967)

REFERENCES (CONT.)

24. Reusable Spacecraft Engines. Aerojet-General Corp. (20 March 1969)

25. Parametric Data for Liquid Bipropellant Engine Designs at Thrust Levels of 100-7000 lbs. Aerojet-General Corp. (2 June 1969)

26. Space Shuttle Main Propulsion Engine Interface Data. Aerojet-General Corp. (1 July 1970)

27. Technical Data for Fluorine Hydrogen Rocket Engines for Small Upper Stage Applications. Bell Aerospace Co. D 8500-953019 (May 1964)

28. Parametric Data for Space Shuttle Main Engine 400K. Aerojet Liquid Rocket (26 May 1970)

29. Parametric Data for Space Shuttle Main Engine 1,000K. Aerojet Liquid Rocket (20 July 1970)

30. Parametric Data for TRW Space Engines. TRW System Group

31. Space Engine Design Handbook. NR Rocketdyne R-8000P-1 (1 Jan. 1969)

32. Design Criteria for Spacecraft Propulsion Systems. Final Report Vol. III-A and III-B, Detailed Propulsion Scaling and Design Data. Contract NAS7-519. Aerojet General Space Division SGC 1069 FR-1 (October 1967)

33. Evaluation of Advanced Propulsion Systems for Upper-Stage Applications. McDonnell Douglas Astronautics Co. NASA-CR 105935 (July 1969)

34. Masters, A. I. et al Flox/Methane Pump Fed. Engine Systems. AIAA 5th Propulsion Joint Specialist Conference, Colorado AIAA Paper No. 69-510 (June 1969)

35. Propellant Selection for Spacecraft Propulsion Systems. Final Report Vol. II Missions & Vehicles. Contract NASw-1644. Lockheed Missiles & Space Co. K-19-68-6 Vol. II (August 1968)

36. Propellant Selection for Spacecraft Propulsion Systems. Final Report Vol. III. Thermodynamic and Propulsion Contract NASw 1644 Lockheed Missile & Space Co. 1C-19-68 Vol. 111 (August 1968)

37. Space Shuttle Engine Stowed Length Study for Space Division & General Dynamics/Convair. NR rocketdyne SSE 552-158 (29 June 1970)

REFERENCES (CONT.)

38. Oxygen/Hydrogen and Fluorine (Hydrogen Rocket Engine Parametric Data Pratt and Whitney Aircraft PDS-2687 (19 Jan. 1968)

39. Cole, Henry A. Jr., Effects of Vortex Shedding on Fuel Slosh Damping Predictions, NASA TN F-5705 (March 1970)

40. Slosh Suppression, NASA SP-8031 (May 1969)

APPENDIX A

A-1 Becker, H., Handbook of Structural Stability, Part II, Buckling of Composite Elements, NACA TN 3782, (July 1957)

A-2 Structures Manual, NR, Space Division

A-3 Shanley, F. R., Weight-Strength Analysis of Aircraft Structures, Dover, N. Y. (1960)

A-4 Jones, T. B., The Derivation of Statements of Weight, Enclosed Volume, and Geometry of Monocoque and Stiffened Cylindrical Tank Component", NR SD Internal Letter

A-5 Seide, P., The Effectiveness of Integral Waffle-Like Stiffening for Long, Thin Circular Cylinders Under Axial Compression, Part 1 - Chemically Milled Sheet, Ramo-Wooldridge GM TR-15 (April 1965)

A-6 Schmit, L. A. and T. P. Kicher, Structural Synthesis of Symmetrical Waffle Plate, NASA Technical Note D-1691, (December 1962)

A-7 Thielemon, W., New Developments for the Nonlinear Buckling Theory of Thin Cylindrical Shells. Proceeding of the Durona Conference, Stanford, California (August 1959)

A-8 Baker, E. H., Design Procedure for Integrally Stiffened Waffle Cylinders under Axial Compression, NR/Space Division, STR 71 (May 1961)

APPENDIX A (CONT.)

A-9 Baker, E. H., General Instability of Waffle Cylinders Subjected to Combined Loads, NR/Space Division STR 96 (September 1963)

A-10 Dow, N. F., C. Libove and R. E. Hubka, Formulas for the Elastic Constants of Plates with Integral Waffle-Like Stiffening, NACA RM-L63 E 13a (August 1953)

A-11 Influence of Structure and Material Research on Advanced Launch Systems Weight, Performance and Cost Phase III Final Report, Volume II Users Manual for Vehicle and Structural Design Syntheses Program. Space Division, North American Rockwell Corporation, SD67-1204-2 (Jan. 1968)

APPENDIX B

B-1 Summers, J. L., and A. C. Charters. High Speed Impact of Metal Projectiles in Targets of Various Materials. Third Hypervelocity Symposium, Vol. 1 (October 1958)

B-2 Charters, A. C., and J. L. Summers. Some Comments on the Phenomena of High-Speed Impact. Paper presented at Decennial Symposium at U. S. Naval Ordnance Laboratory, White Oak, Silver Springs, Md. (May 26, 1959

B-3 Hermann, W., and A. H. Jones, Survey of Hypervelocity Impact Information. A.S.R.L. Report No. 99-1, MIT (September 1961)

B-4 Bohn, J. L., and O. P. Fuchs. High Velocity Impact Studies Directed towards the Determination of the Spatial Density, Mass and Velocity of Micrometeoroids at High Altitudes. Scientific Report No. 1 ASTIA AD 243 106.

B-5 Kinard, W. H., C. H. Lambert, D. R. Schryer, and F. W. Casey, Jr. Effect of Target Thickness on Cratering and Penetration of Projectiles Impacting at Velocities to 13,000 fps. NASA Memo 10-18-58L (December 1958)

B-6 Meteoroid Damage Assessment NASA SP-8042 (May, 1970)

B-7 Richardson, A. J., Theoretical Penetration Mechanics of Multisheet Structures Based on Discrete Particle Modeling, AIAA Paper No. 69-371, Proc. AIAA Hypervelocity Impact Conference (April 1969)

APPENDIX B (CONT.)

B-8 Richardson, A. J., and J. P. Sanders, Penetration Damage to Multisheet Structures Based on Debris Particles of Two Materials, North American Rockwell Report SD-70-463, to be issued.

APPENDIX A. STRUCTURAL SHELL ANALYSIS

A.1 Cylindrical Shells

The primary failure modes considered in the stress analysis of the cylindrical shell are material failure, general instability, and local instability.

The classes of loads used for design are defined as:

1. AL - limit compressive axial load
2. BM - absolute value of the limit bending moment
3. P - propellant tank pressures.

The safety factors are:

1. FS_Y - yield factor of safety
2. FS_U - ultimate factor of safety.

The following strength criteria were used to analyze the shell structures for material failure. A tensile stress resulting from ultimate (yield) pressure loads and/or inertia loads will not exceed the tensile ultimate (yield) strength F_{tu} (F_{ty}) of the material. If the inertial loads are additive to the tensile stresses, ultimate (yield) inertia loads are used. Limit inertia loads are used if the inertia loads are subtractive from the tensile stresses.

$$F_{t_i} \geq \frac{1}{\bar{t}} \left[\frac{BM}{\pi R^2} + \frac{PR}{2} - \frac{AL}{2\pi R} \right] FS_i \qquad \text{if } AL < 0$$

$$F_{t_i} \geq \frac{1}{\bar{t}} \left\{ \left[\frac{BM}{\pi R^2} + \frac{PR}{2} \right] FS_i - \frac{AL}{2\pi R} \right\} \qquad \text{if } AL \geq 0$$

where $\bar{t}$ = the equivalent shell longitudinal extensional thickness

subscript i = u for ultimate condition

= y for yield condition

A compressive stress resulting from ultimate (yield) inertia loads and stresses due to pressure will not exceed the allowable (yield) compressive strength, F_{cu} (F_{cy}), of the material. If the pressure is additive to the compressive stresses, ultimate (yield) pressure is used. Minimum pressure is used when the stresses due to pressure are subtractive from the compressive stresses.

$$F_{c_i} \geq \frac{1}{t} \left\{ \left[\frac{BM}{\pi R^2} + \frac{AL}{2\pi R} \right] FS_i - \frac{P_{MIN} R}{2} \right\} \qquad \text{if } AL \geq 0$$

$$F_{c_i} \geq \frac{1}{t} \left\{ \frac{BM}{\pi R^2} FS_i + \frac{AL}{2\pi R} - \frac{P_{MIN} R}{2} \right\} \qquad \text{if } AL < 0$$

A primary mode of structural failure is the general instability of the shell. The general instability considered orthotropic and isotropic shells for column buckling and used small-deflection theory with the theoretical results modified with appropriate "knock-down" correction factors. These correction factors are based on experimental data. All the shell structures were designed not to buckle at ultimate design conditions (no post-buckle analysis required). The small-deflection theory coupled with the correction factors will produce realistic weight estimates for the structural shells. For the design of structural shells for general instability, it is usual to rely on design curves based on statistical reduction of test data. When data are insufficient to obtain the statistical design allowable buckling load, the design recommendations have been made by comparing similar designs of equivalent constructions (i.e., equating honeycomb structural shell stiffness parameters to an equivalent monocoque parameters). In general, this technique involves using recommended correction factors to reduce the theoretical buckling loads. Because of the lack of data on some types of shells and loading, as well as the question of applicable ranges, the recommendations may be too conservative for some cases. Although the design buckling load could be based on applying a correction factor to the theoretical large deflection buckling load, the results will be identical to those obtained by applying a somewhat larger correction factor to the small deflection theory buckling load.

Another mode of structural failure is the local instability of the skin panel and the stiffener elements buckling as plates with simply supported edges or one edge simply supported and the other edge free.

The skin-stringer cylinder, Figure A1 , is a built-up structure consisting of a thin face sheet stiffened by longitudinal stringers and transverse ring frames. The stringer configurations analyzed are integral, "z," "I," and hat section. The primary failure modes considered are material failure and instability of the composite structure.

The method utilized in this optimization procedure is based on the premise that for minimum weight, all elements of a structure fail simultaneously in all instability modes. For the skin-stringer constructions, the instability modes are as follows:

1. Local instability of the element: skin panels, stringer webs and lips.

2. General instability of the structures: flexural and torsional.

The following assumptions were made:

1. The skin and stringer sections behave as panels simply supported at the ends by the frames.

2. Thin plate buckling theory is applicable.

3. "Strip theory" as described for general instability of wide panels is sufficiently accurate for application to orthotropic cylinders for the long radii considered.

4. The nonbuckled designs assume that the Euler instability or the Johnson parabola approximation and the initial buckling occur simultaneously.

5. Frames are included for the buckling modes for general instability but do not restrain local buckling.

6. The effect of transverse loads produced by internal pressure are neglected when considering buckling failure.

The material failure criteria are used to determine the minimum equivalent thickness required. The general form of the equations is

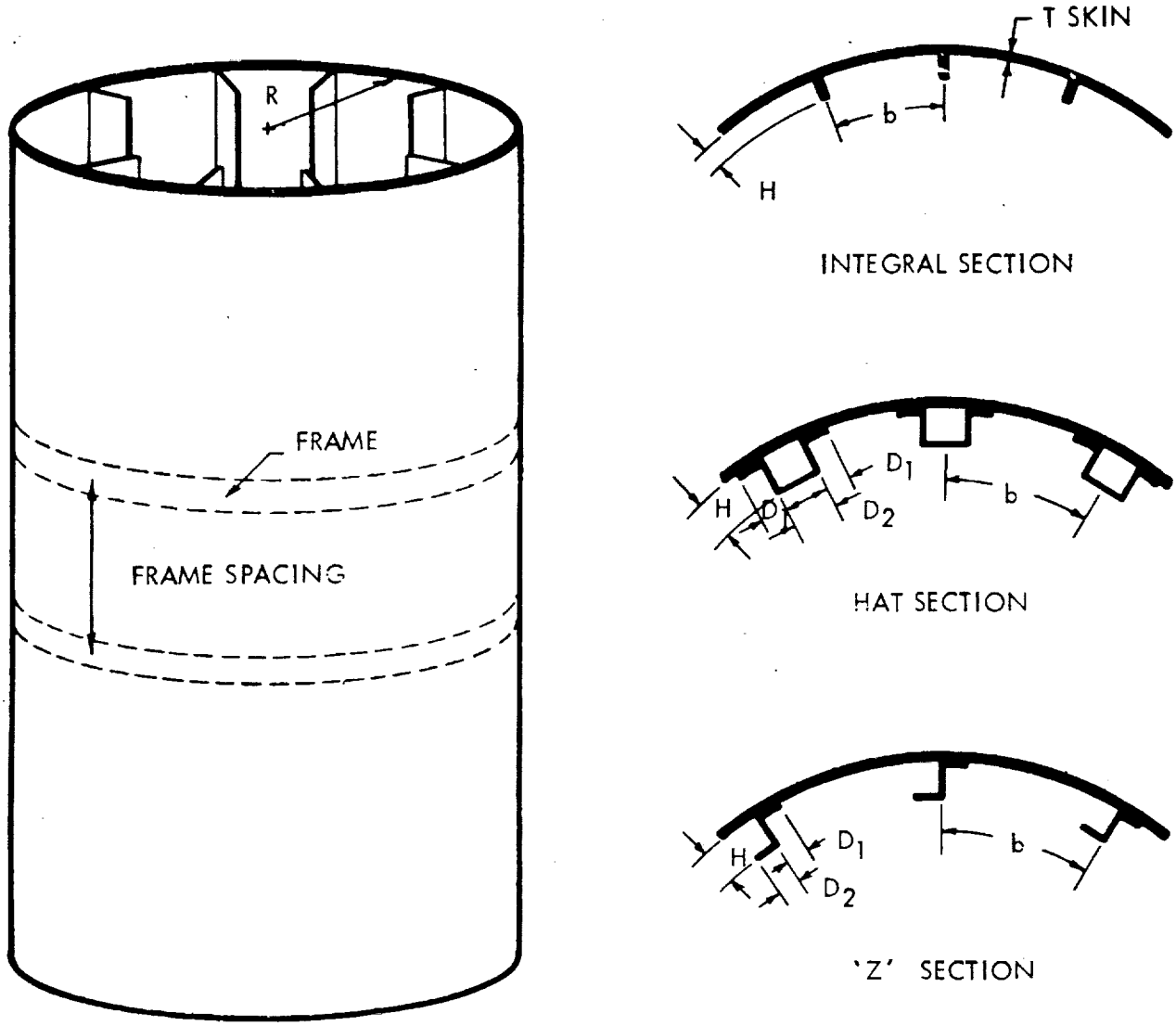

Figure A-1. Skin-Stringer Cylindrical Shell

$$\bar{t} = t_{skin} + \frac{Astr}{b} = \max\left\{\frac{f\,(loads)}{f_1(matl\ allowables)},\ min\ gauges\right\}$$

$$t_{skin} = \max\left\{\frac{f\,(pressure)}{f_1\,(matl\ allowables)},\ min\ gauges\right\}$$

The procedure to achieve the optimum combination of skin and stringer sizes is systematic in nature. It requires a knowledge of the unit loading intensity N_X at the section under consideration and the material properties.

The local instability modes considered are panel instability of the face sheets and crippling of the stringer.

If the stiffened-skin structure has sufficiently stiff ring frames, the first failure mode generally encountered is panel instability. In this failure mode, the ring frames and stringers effectively divide the shell into small panels, whose principal dimensions are the spacings of the ring frames and stringers.

In general, the structure does not fail because of panel instability. Instead, the load is redistributed, and the composite structure is able to carry additional loads before failure. However, if the design criteria specify that the skin panels shall not buckle, panel instability is a primary failure mode.

The critical buckling stress for the plate element (Reference A1) is

$$\frac{\sigma_{CR}}{\eta} = KE\left(\frac{t}{b}\right)^2$$

The crippling stress for the stringer is determined by

$$\sigma_{cc} = \sum_{i=1}^{N} \frac{Ai\ Cei\ \sqrt{\sigma_{cyi}\ Ei}\left(\frac{t}{b}\right)_i^{3/4}}{\Sigma Ai}$$ Reference A2

The critical flexural buckling stress for stringer column instability is given by the Euler equation

$$\sigma_{CR_E} = \frac{\pi^2 E}{\left(\frac{L'}{\rho}\right)^2}$$

where L' is the effective length of the stringer and ρ is the radius of gyration of the section.

For the low L'/ρ ratios, the column does not fail in the classical Euler manner through elastic bending but in a combination of failure modes, each contributing to a reduced general instability. The elements of column section may experience initial buckling, but the column can continue to carry load until ultimate failure occurs. This ultimate failure is predicted by a modified Johnson parabola, which is influenced by both the ultimate crippling strength of the section elements and also by the general instability of the section. The Euler and tangent modulus equation is given by

$$\sigma_{CR_E} = \frac{\pi^2 Et}{\left(\frac{L'}{\rho}\right)^2}$$

The modified Johnson parabola can be expressed

$$\sigma_{CR} = \sigma_{cc} - \frac{\sigma_{cc}^2}{4\sigma_{CR_E}}$$

where σ_c is the crippling stress of the sectional elements.

General instability occurs when the ring frames are not stiff enough to force buckling modes to occur at the ring frame. Therefore, the

deflected shape for this failure mode extends over several panels and ring frames. The general procedure for preventing this failure mode is by designing ring frames of sufficient stiffness. Shanley, Reference A3 determines the required ring frame stiffness as

$$(EI)_f = \frac{BMD^2}{16000L}$$

The cross-sectional area of the frame can be written as

$$I_f = A_f^2 K_4$$

where K4 is a form factor approximately 5.2. If the frames are not stiff enough, they will allow the cylinder to buckle across the ring plane. Therefore, an empirical analysis was used to check this failure mode that takes into account the ring and stringer inertias, Reference A1

The critical general instability stress for the stiffened cylinder is given by

$$\sigma_{CR} = \frac{KE}{R} \left(\frac{\rho_s^3 \rho_f^3}{bL} \right)^{1/4}$$

This equation is modified in Reference A4 to include the effects of internal pressure. The resulting equation is

$$\sigma_{CR} = \left[C_c + C_p\right] \left[\frac{t}{b} \frac{t}{L} \frac{t}{R}\right]^{1/4} \left[\frac{\rho_f}{R} \frac{\rho_s}{t}\right]^{3/4}$$

The cylinder buckling coefficient due to internal pressure can be approximated by

$$C_p = \gamma \left[\frac{P}{E} \left(\frac{R}{t}\right)^2\right]^{\alpha}$$

The variation of C_c and C_p with the cylinders design parameters is taken from Reference A2

The waffle cylinder, Figure A2, is a composite structure consisting of a face sheet stiffened by internal ribs. The ribs are oriented at angles of $\pm\theta$ degrees with respect to the axis of the cylinder.

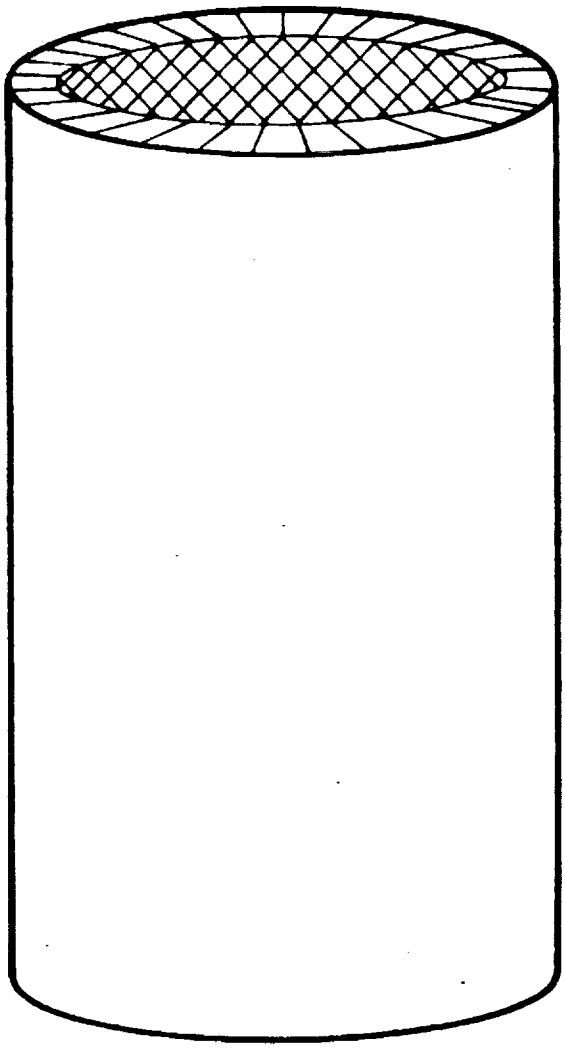

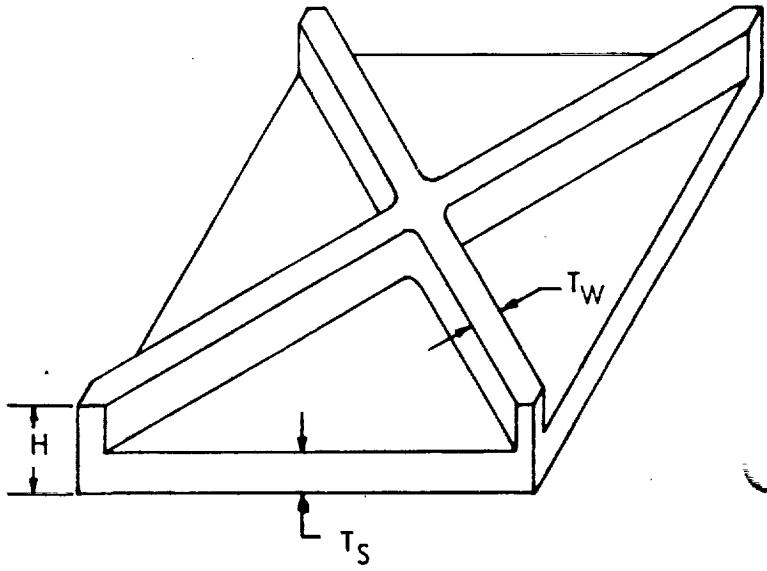

WAFFLE SECTION

A-2. Waffle Grid Cylindrical Shell

In Reference A5 , the influence of rib orientation on the strength of unpressurized, axially compressed cylinders is evaluated. For this loading condition, the optimum rib orientation is approximately ±15 degrees. However, the weight penalty associated with a ±45-degree orientation is small for the range of parameters considered. In this study, the influence or rib orientation on the weight of cylindrical shell subjected to combined loading conditions is assumed to be negligible. The 45-degree orientation is selected for all computations. Synthesis of symmetrical section waffle concepts is illustrated in Reference A6.

The primary failure modes considered for the waffle cylinder are material failure, local instability of the face sheet and ribs, and general instability of the composite structure.

Material Failure

The failure criteria presented in this section is used to prevent material failure. The effective skin thickness is determined by equations of the general form.

$$t = \max \left\{ \frac{f\ (\text{applied loads})}{f_1\ (\text{matl allowables})},\ \text{minimum gauge} \right\}$$

$$t_{skin} = \max \left\{ \frac{f\ (\text{pressure})}{f_1\ (\text{matl allowables})},\ \text{minimum gauge} \right\}$$

Local Instability

When the ribs are sufficiently stiff to force buckling nodes to occur at the ribs, the critical buckling stress for the plate element is given by

$$\sigma_{CR} = KE \left(\frac{t}{b}\right)^2$$

where

K = a plate shape factor, and

b = the rib spacing.

For the ribs oriented at ±45 degrees, the plate element is subjected to uniform compression and shear stress equal to one-half the applied stress on the composite structure. For this loading condition and plate shape, the value of K is 3.87, Reference A2.

The crippling stress for the rib is given by

$$\sigma_{CRIP} = Kr\ E \left(\frac{t_r}{L_r}\right)^2$$

where

K_r = a shape factor

E = the modulus of elasticity

t_r = the rib thickness

L_r = the rib width.

The numerical value of the coefficient K_r is a function of the rotational constraint provided by the face sheets. For plates with one edge fixed, the approximate value of K_r is 0.43.

The waffle cylinder, with sufficiently small rib spacing will respond similarly to an orthotropic shell. However, a generally accepted procedure does not exist for determining the design buckling load for orthotropic shells. The theoretical buckling load predicted by classical small deflection theory is unconservative and the minimum postbuckling load predicted on large deflection theory is usually very conservative. Consequently, neither of the loads is generally acceptable for design analysis. The situation is further complicated by the absence of sufficient test data for waffle constructions.

For this study, the critical buckling load for the waffle cylinder is determined by a joint consideration of large and small deflection theory for an orthotropic shell.

The buckling load of an axially compressed orthotropic shell can be characterized by three primary parameters, Reference A7. These parameters are:

1. H, the extensional stiffness parameter of the orthotropic shell

$$H = \frac{H_{12} + \frac{1}{2} H_{33}}{\sqrt{H_{11} H_{22}}}$$

2. D, the bending stiffness parameter

$$D = \frac{D_{12} + 2D_{33}}{\sqrt{D_{11} D_{22}}}$$

3. γ, the principal stiffness parameter

$$\gamma = \frac{D_{11} H_{11}}{D_{22} H_{22}}$$

where

11 = longitudinal direction

22 = circumferential direction

33 = in plane through material thickness

12 = shear stiffness perpendicular to plane 1 in the direction of plane 2.

These three parameters provide an efficient method for evaluating the buckling and postbuckling behavior of orthotropic shells. The most important parameter for studying the buckling behavior is γ. For small γ (γ less than 1) the cylinder is assumed to be circumferentially stiffened. For γ greater than unity, the cylinder is longitudinally stiffened. The ratio of the minimum post buckling load to the classical buckling load is inversely proportional to γ. When γ is very small ($\gamma \ll 1$) the minimum theoretical postbuckling load is approximately equal to the classical buckling load. When γ is large ($\gamma \geq 1$), the post-buckling load is approximately ten percent of the classical buckling load.

For waffle cylinders with ribs oriented at ± 45 degrees, the value of γ is unity. γ is also equal to 1 for monocoque shells; therefore, it appears that a reasonable estimate, for the correction factor to be used with the classical buckling load, can be obtained by using test data for isotropic monocoque shells, Reference A5.

When extrapolating the test data for isotropic cylinders to 45-degree waffle cylinders, it is necessary to remember that all of the orthotropic shell parameters are equal to unity for the isotropic shell, while two may not be equal to unity for the waffle. This is significant because the classical buckling loads are identical for axisymmetric and asymmetric buckling of isotropic shells, but may be different for orthotropic shells.

The unpressurized isotropic cylindrical shells generally buckle asymmetrically. Since the theoretical axisymmetric and asymmetric buckling loads for isotropic shells are identical, it is not important which theoretical buckling load is corrected to obtain a design load. However for orthotropic shells, the correction factor should not be identical for both buckling modes. The observed postbuckling deformation patterns for longitudinal stiffened shells is generally asymmetric, and the corresponding buckling load is a small percentage of the theoretical load. The postbuckling deformation pattern changes as the cylinder is stiffened circumferentially and the ratio of the postbuckling load to the classical load increases. With sufficient circumferential stiffening, and/or with sufficient internal pressure, the axisymmetric buckling pattern is observed, and the classical buckling load obtained.

For these reasons, the isotropic correction factor is only applied to the asymmetric buckling load. No correction factor is used for axisymmetric buckling. The design buckling load is based on the minimum buckling load obtained by this procedure. For most cases, the design load for the 45-degree waffle cylinder will be based on asymmetric buckling.

The critical buckling stress for asymmetric buckling of a 45-degree waffle cylinder is given by References A5, A8 and A9.

$$\frac{N_c R}{EH^2} = 2\gamma \sqrt{\bar{D}_2 \bar{E}_1 \frac{1 + \mu_x + \frac{2\bar{D}_K}{\bar{D}_2}}{1 - \mu_1 + \frac{\bar{E}_1}{2\bar{G}_K}}}$$

where the elastic constants, Reference A10, are defined in the following nomenclature list. For symmetric buckling, the critical buckling load is Reference A9.

$$\frac{N_c R}{EH^2} = 2\sqrt{\bar{D}_2 \bar{E}_1}$$

Definition of waffle elastic constants

A_{W_S} Twice the cross-sectional area of the ribs

b_s Spacing or ribs

$\bar{D}_k$ Twisting stiffness

$\overline{D}_2$	Bending stiffness
$\overline{E}_1$	Extensional stiffness
$\overline{G}_k$	Shear stiffness
H	Total height of waffle
Iw_s	Twice the moment of inertia of the ribs
Kw_s	Dimensionless distance from middle surface of sheet to centroid of ribs
N_c	Critical axial stress per unit width
t_s	Skin thickness
μ_1	Poisson's ratio associated with stretching
μ_x	Poisson's ratio associated with bending

$$\overline{D}_2 = Iy - \frac{As^2\, Ay}{\overline{As}^2}\,(\overline{Ky} - \overline{Ks})^2$$

$$\overline{E}_1 = \frac{\overline{As}^2}{Ay}$$

$$\overline{D}_k = \frac{Ixy}{4}$$

$$\overline{G}_k = Axy$$

$$\mu_x = \frac{\overline{Is}^2}{\overline{As}^2 \overline{D}_2}$$

$$\mu_1 = \frac{As}{Ay}$$

$$Ay = \frac{1}{1-\mu^2}\frac{t_s}{H} + \frac{A_{W_s}}{b_s H}\cos^4\theta$$

$$As = \frac{\mu}{1-\mu^2}\frac{t_s}{H} + \frac{A_{W_s}}{b_s H}\sin^2\theta\cos^2\theta$$

$$Axy = \frac{1}{2(1+\mu)}\frac{t_s}{H} + \frac{A_{W_s}}{b_s H}\sin^2\theta\cos^2\theta$$

$$\overline{As}^2 = Ay^2 - As^2$$

$$\overline{Ky} = \frac{A_{W_s}}{b_s H}\frac{Kw_s}{Ay}\cos^4\theta$$

$$\overline{Ks} = \frac{A_{W_s}}{b_s H}\frac{Kw_s}{As}\cos^2\theta\sin^2\theta$$

$$\overline{Kxy} = \frac{A_{W_s}}{b_s H}\frac{Kw_s}{Axy}\sin^2\theta\cos^2\theta$$

A.2 Ellipsoidal Bulkheads

The principal failure modes used to estimate the "theoretical" membrane weight of monocoque ellipsoidal bulkheads are material failure due to pressure stresses that exceed the material allowables and buckling due to internal or external pressure.

Material failure: The Von Mises criteria are used to determine the minimum skin thickness required to prevent material failure. This minimum skin thickness is given by

$$t_i = \frac{\sqrt{N_{\theta_i}^2 - N_{\theta_i} N_{\phi_i} + N_{\phi_i}^2}}{\sigma}$$

where

N_{θ_i} = circumferential stress resultant at the ith station

N_{ϕ_i} = meridional stress resultant at the ith station

t_i = the membrane thickness at selected points of the bulkhead

t_{min} = minimum membrane thickness based on constraints imposed by available material gauges, fabrication considerations, etc.

σ = allowable material stress, including safety factors

The circumferential and meridional stress resultants are given by

$$N_{\theta_i} = Pr_2 \left(1 - \frac{r_2}{2r_1}\right)$$

$$N_{\phi_i} = \frac{Pr_2}{2}$$

where

a = major semi-axis of bulkhead

b = minor semi-axis of bulkhead

P = the bulkhead pressure

$$r_1 = a^2 b^2 / (a^2 \text{ SIN}^2 \phi + b^2 \text{ COS}^2 \phi)^{3/2}$$

$$r_2 = a^2 / (a^2 \text{ SIN}^2 \phi + b^2 \text{ COS}^2 \phi)^{1/2}$$

Stability analysis: An elliptical isotropic monocoque bulkhead subjected to external pressure is evaluated for the critical buckling stress by converting the elliptical bulkhead into an equivalent hemispherical dome and using the classic Von Karmen-Tsien formula to predict buckling of the monocoque spherical shells. This buckling equation is given by

$$\frac{\sigma_{cr}}{\eta} = \frac{0.606 \text{ CE t}}{R (\text{SIN } \beta)^{1/3}}$$

where

C = 0.25, the buckling correction factor required to correlate theoretical with experimented results.

η = plaslicity correction factor

R = radius of the equivalent spherical shell

In order to convert the ellipsoidal bulkhead to the equivalent spherical bulkhead, the following equations are used, Figure A3.

$$\beta = \pi - 2 \text{ ARCTAN } \left(\frac{a}{b}\right)$$

$$R = a/\text{SIN } \beta$$

For equivalent stresses at the apex of the elliptical and spherical bulkhead, the pressure on the spherical bulkhead is given by

$$P_{eq} = \frac{Pa \text{ SIN} \beta}{b}$$

Hence, the buckling equation may be rewritten

$$\frac{\sigma_{cr}}{\eta} = 0.15 \text{ E } \left(\frac{t}{a}\right) \text{ SIN}^{2/3} \beta$$

Therefore, the minimum skin thickness required to prevent buckling due to external pressure is given by

$$t = \left[\frac{P \; a^3}{0.30 \; Eb \; SIN^{2/3} \; \beta \quad \eta} \right]^{1/2}$$

To determine the membrane unit weight of any ellipsoidal shell of monocoque construction, the following is used.

$$\omega = \left(\frac{\rho \; t}{12} \right) F_b$$

where F_b is a fabrication factor which accounts for non-calculated items. The fabrication factor is used to assess the weights due to weld lands, close-outs, additional thicknesses at the junction of bulkhead and tank walls and any secondary structure. These factors will provide correlation between the theoretical membrane weights and actual detail design study or hardware weights. The total weight is calculated as ω times the surface area, where the surface area, A_s, is given by

$$A_s = \frac{\pi \; a}{144 \; b^2} \left\{ Y \sqrt{(a^2 - b^2) \; Y^2 - b^4} + \frac{b^4}{\sqrt{a^2 - b^2}} \; \ln \left[Y \sqrt{a^2 - b^2} + \sqrt{(a^2 - b^2) \; Y^2 + b^4} \right] \right\}_{Y_o}^{Y_{max}}$$

Ellipsoidal domes with an aspect ratio greater than $\sqrt{2}$ are subject to buckling stresses near the lower edges of the bulkhead when there is an internal pressure. The actual stress resultant can be obtained from the previous equations, and the shell stability is checked as an equivalent cylindrical shell. The buckling stress is approximated by

$$\sigma_{cr} = \frac{CEt}{a}$$

The buckling coefficient factor, C, is given by

$$C = C_c + \Delta C_P$$

where

C_c = the stability coefficient for cylindrical shell with equivalent radius-to-thickness ratio

ΔC_p = the increase in the cylindrical shell stability coefficient due to internal pressure

The stability coefficients C_c and ΔC_p are derived from reference A-2 and are shown in figures A4 and A5.

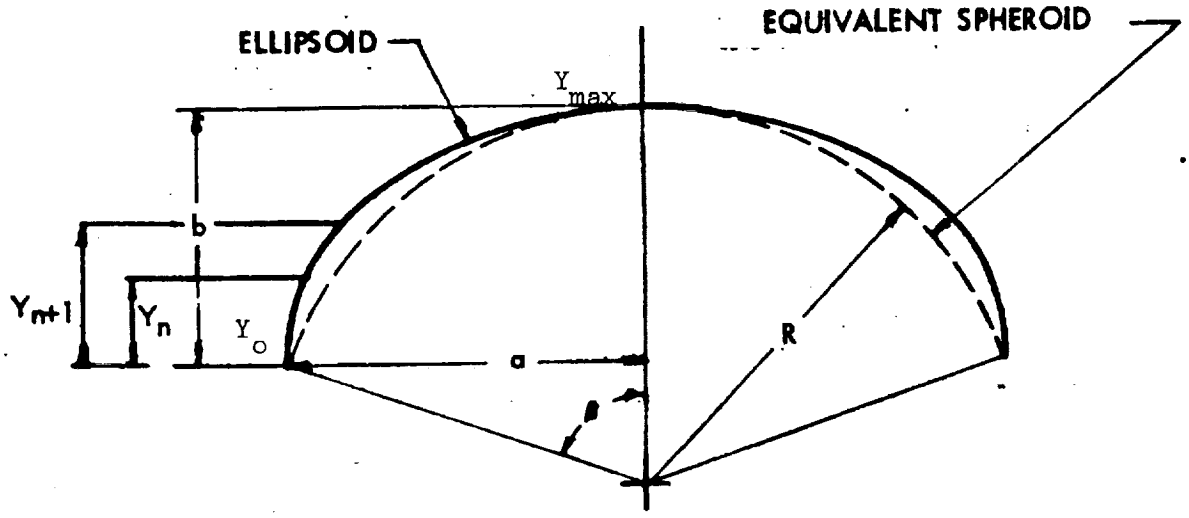

Figure A-3. Ellipsoid-to-Spheroid Conversion for Bulkheads

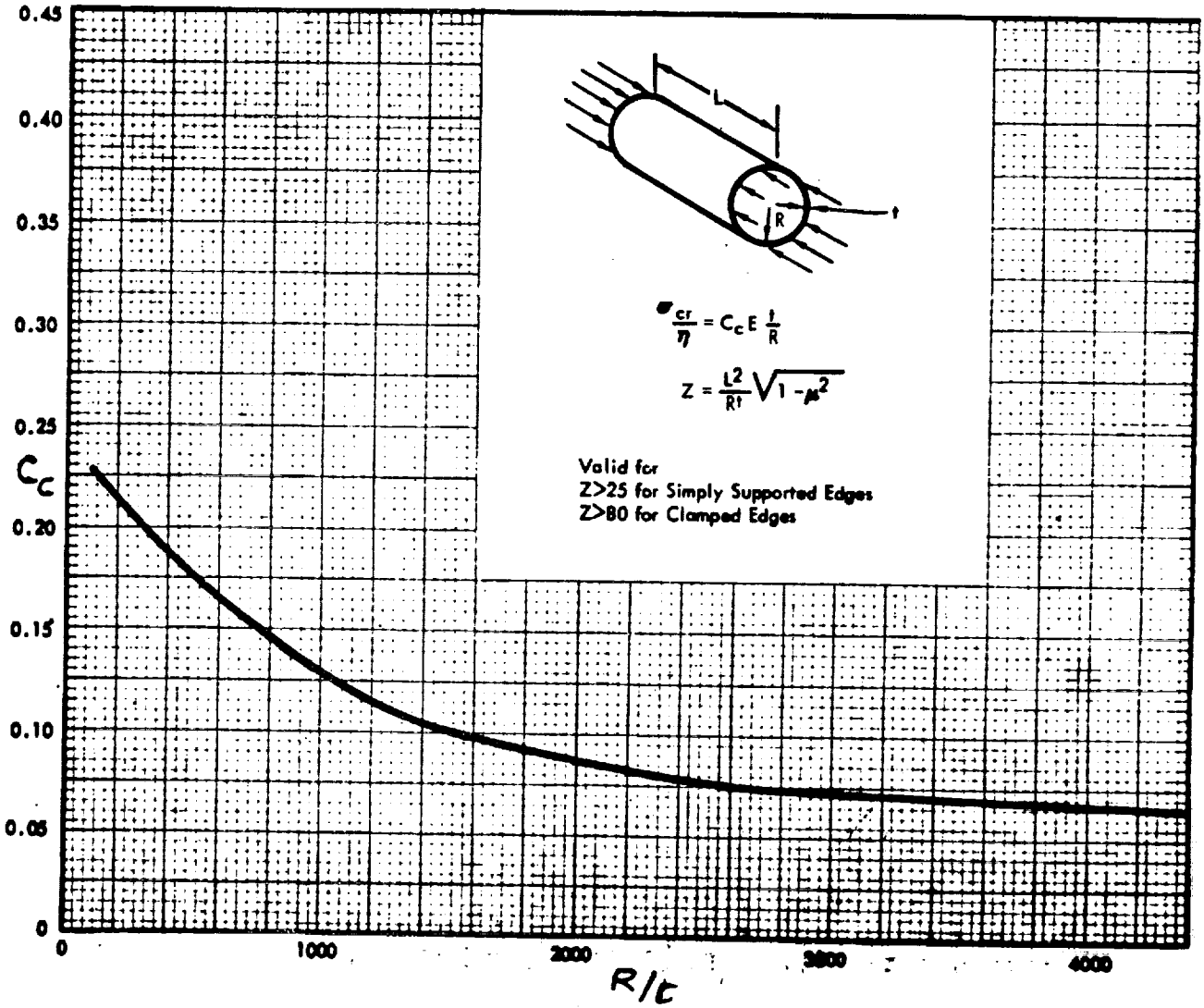

Figure A-4. Buckling Stress Coefficient, C_c, for Unstiffened, Unpressurized Circular Cylinders in Axial Compression

Hence, the minimum skin thickness required to prevent buckling due to internal pressure is given by

$$t_{stab} = \left[\frac{N\theta_c \, a}{C\,E}\right]^{1/2}$$

where $N\theta_c$ = circumferential stress resultant at the equator of the elliptical bulkhead.

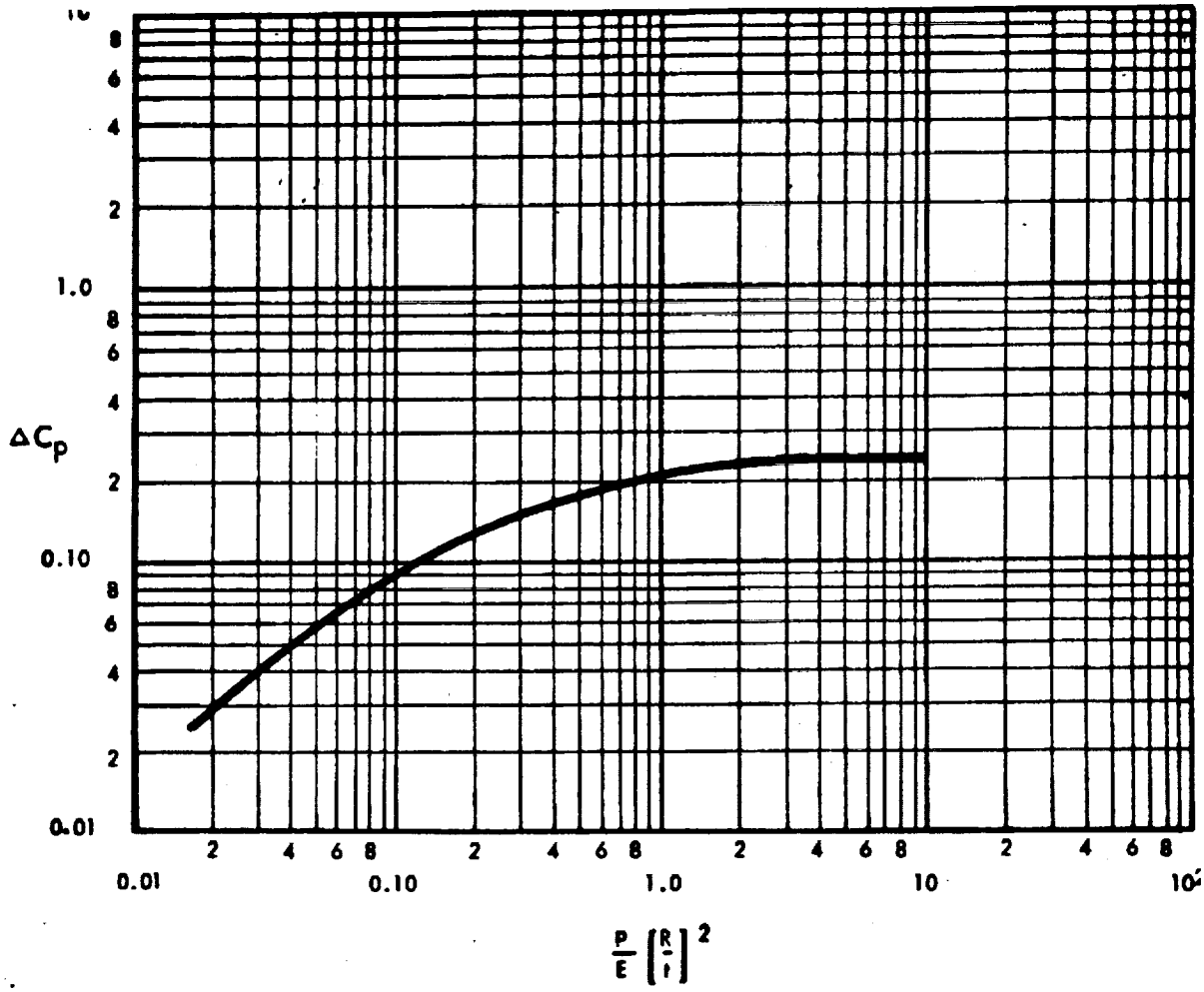

Figure A-5. Increase in Axial-Compressive Buckling-Stress Coefficient of Cylinders Due to Internal Pressure

A.3 Composite Structures

The burst pressure for a metal lined composite pressure vessel is given by

$$P_b = (P_o - 41.5\ t_l)\ 2.5$$

where

t_L = thickness of the metal liner

P_o = operating pressure

P_b = burst pressure (Figure A6)

If a rubber liner is used, the burst pressure is given by

$$P_b = 1.25\ P_o$$

The volume contained in the pressure vessel's bulkhead is a function of the chamber diameter, the boss diameter, and the percent of the meridian load carried by the liner. The resulting equation is

$$V_H = K_V D_C^3$$

where

V_H = head volume

D_C = chamber diameter

and K_V is given by Figure A7.

The percentage load carried by the liner at the equator of the head is used in Figure A7 to position the volumes for one boss diameter on a single curve. This percentage is calculated by the following equation:

$$k = \frac{4\,\sigma_L\,t_L}{P_b D_c} \times 100$$

where

k = percent of load carried by the liner

σ_L = stress in liner at composite failure level for titanium

= 0 for rubber liner

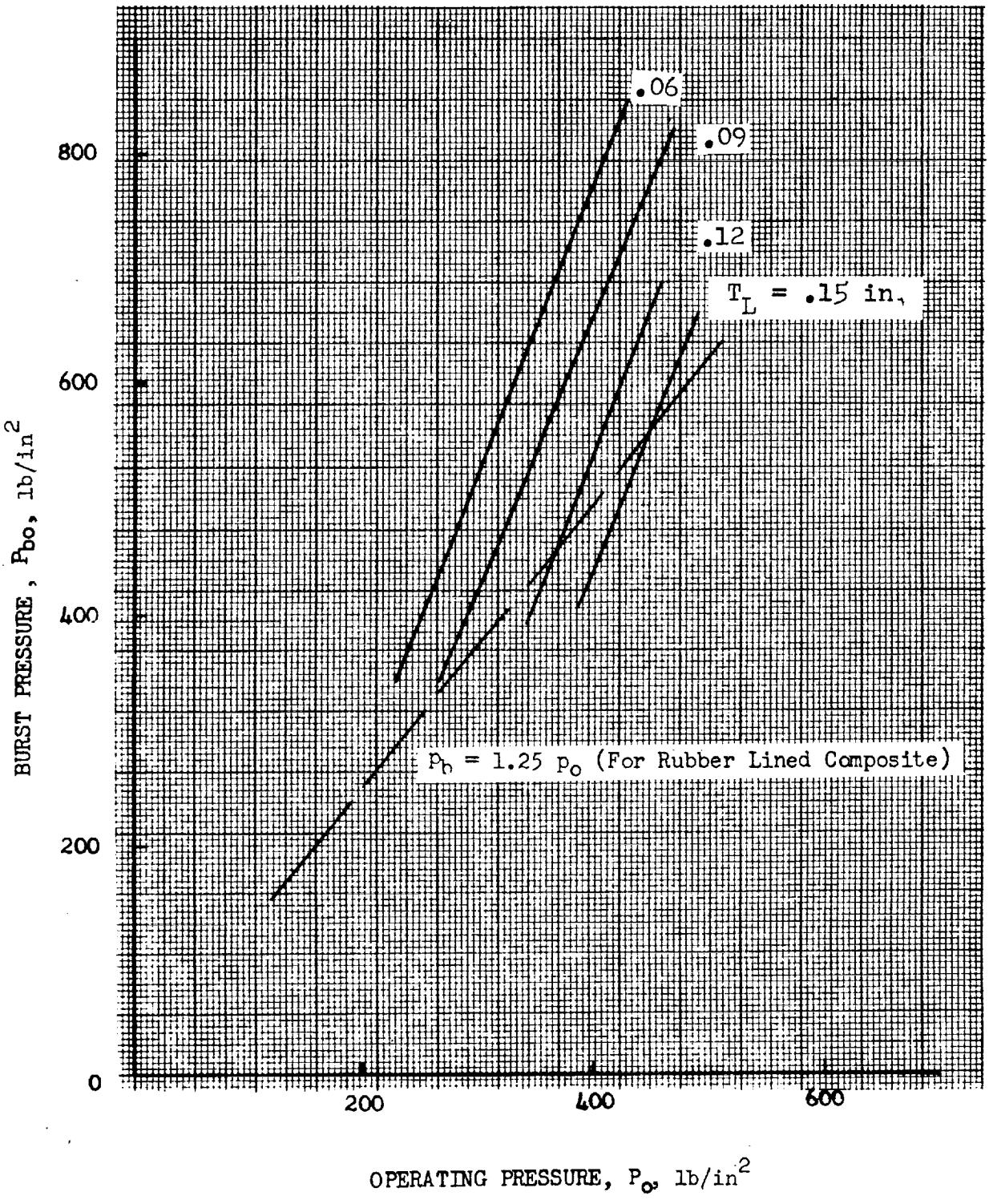

Figure A-6. Burst Pressure vs. Operating Pressure Titanium Lined Composite Tanks

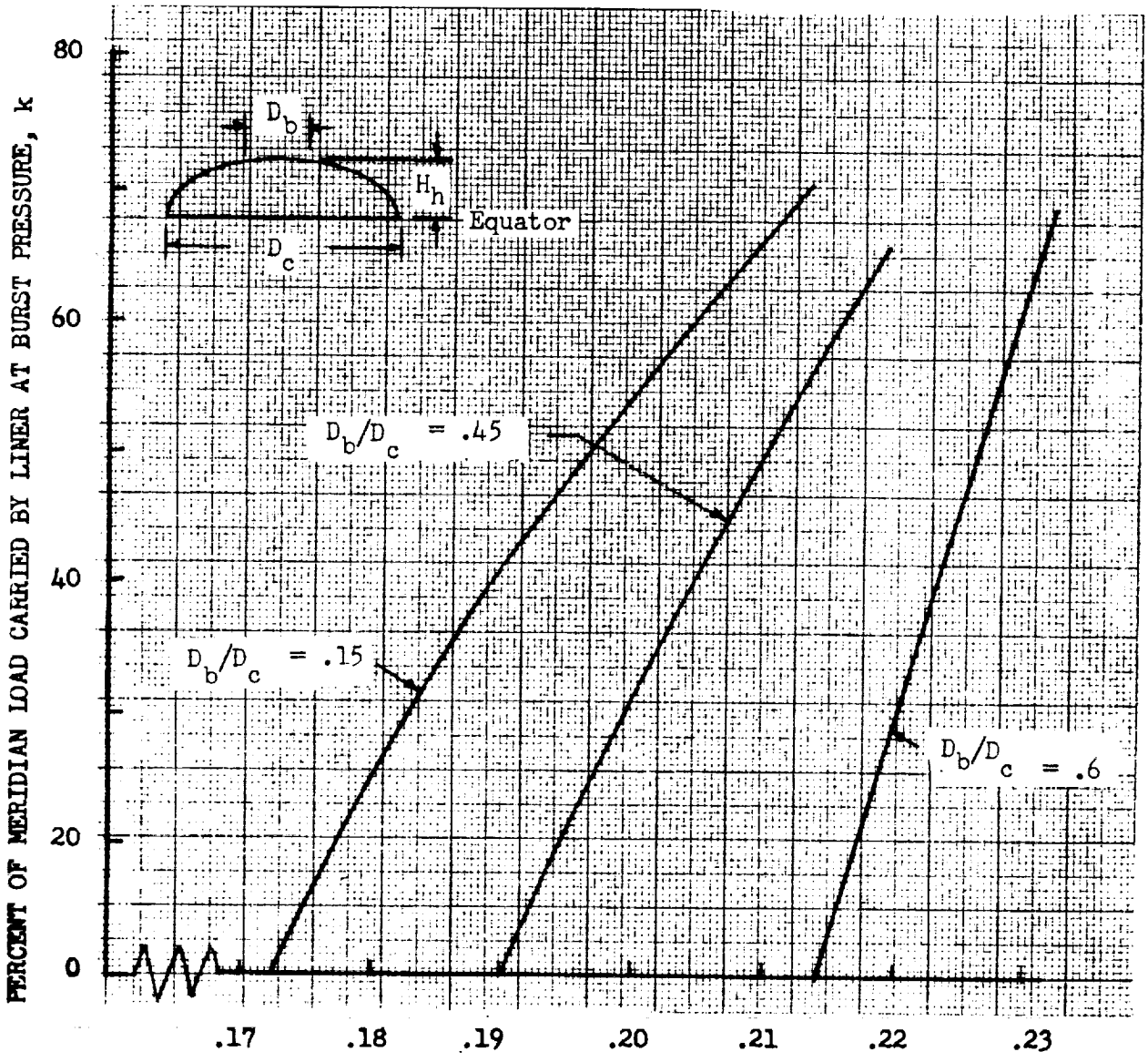

Figure A-7. Head Volume, Titanium Lined Tanks

The height of the pressure vessel's bulkhead is also a function of the boss diameter, the chamber diameter, and the percentage of the meridian load carried by the liner. This height H_H is given by

$$H_H = \frac{1}{2} K_H D_c$$

K_H is obtained from Figure A8. The weight of the bulkhead is given by

$$WT_H = K_1 \rho_c D_c^2 t_L$$

where

WT_H = bulkhead weight

ρ_c = composite density

and K_1 is given by Figure A9 or by the following formula:

$$K_1 = A \frac{\rho_L}{\rho_c} + \left(\frac{P_b D_c}{4 t_L} - \sigma_L \right) \frac{B}{\sigma_c \left[1 - \left(\frac{D_b}{D_c} \right)^2 \right]^{1/2}}$$

where

ρ_L = liner density kg/cm^3
(0.0044 kg/cm^3 for titanium; 0.00125 kg/cm^3 for rubber)

D_b = boss diameter, cm

σ_c = composite unidirectional ultimate strength 15500 kg/cm^2 for S-glass/epoxy

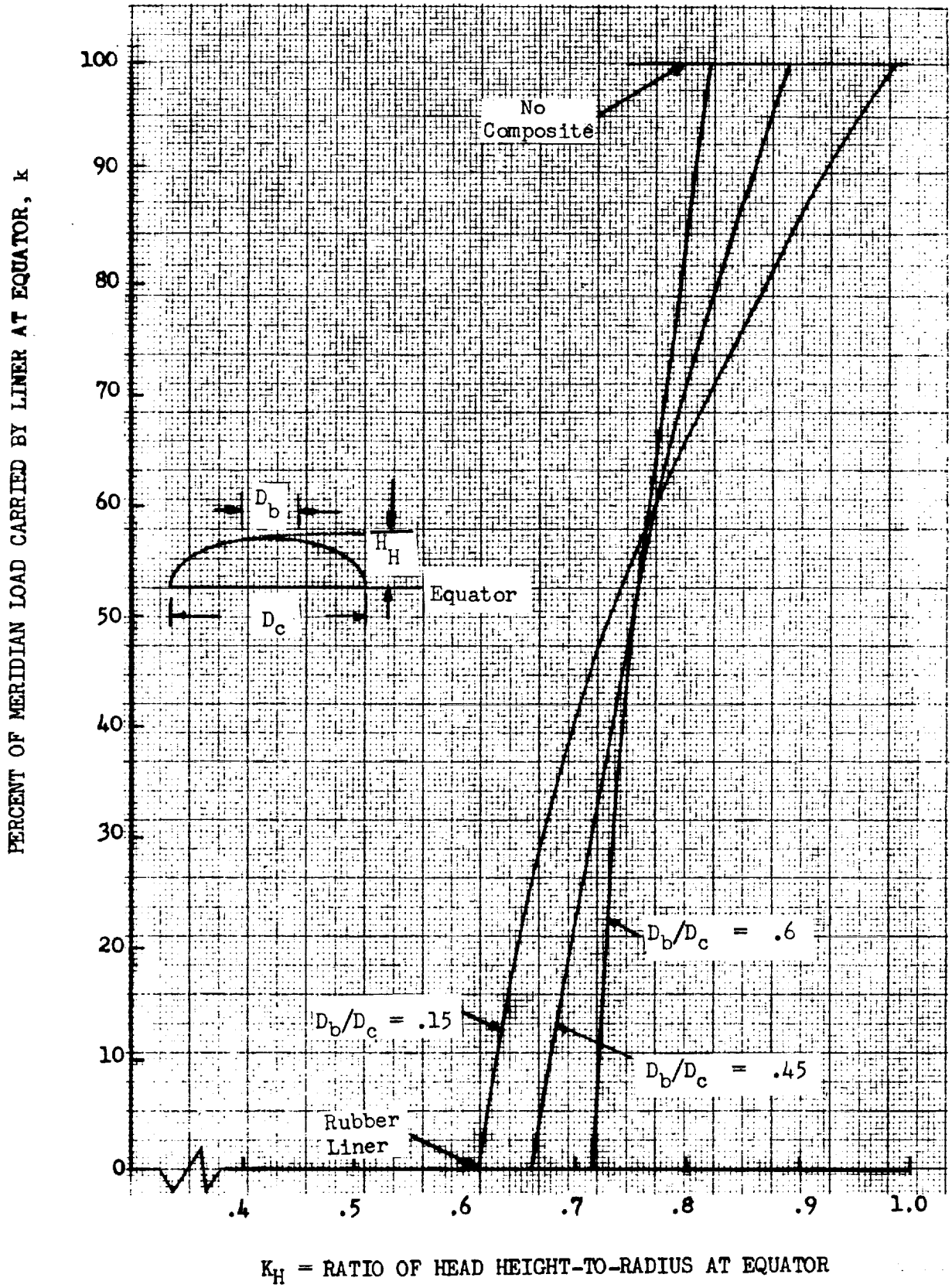

Figure A-8. Head Heights, Titanium Lined Composite Tankage

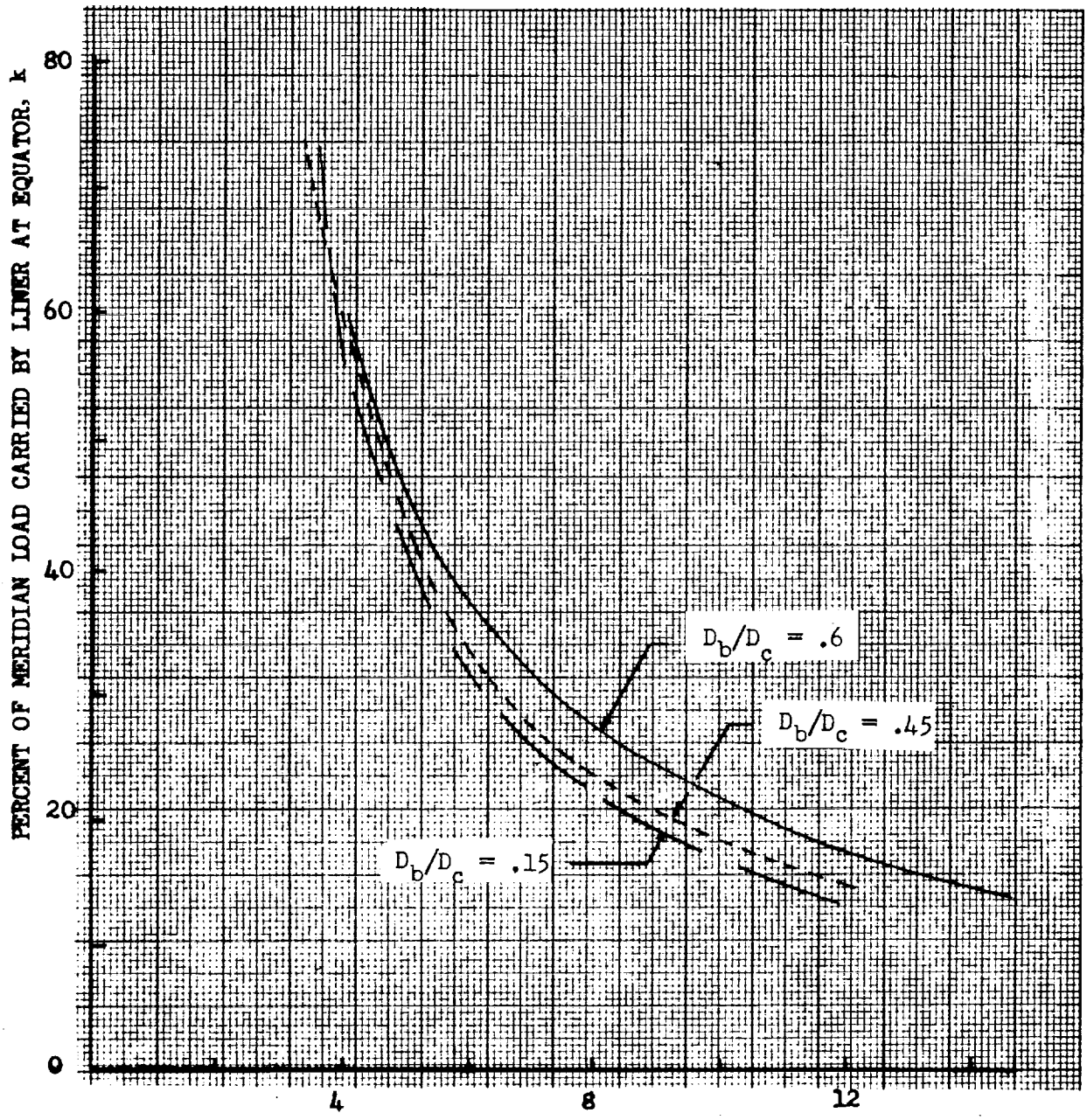

Figure A-9. Head Weights, Titanium Lined Composite Tanks

$$A = A_1 + A_2\ t_L$$

$$B = B_1 + B_2\ t_L$$

The A's and B's are described in Table A1.

The weight of the boss in the bulkhead is calculated by the following equation:

$$WT_b = K_2\ \rho_b\ D^3$$

where

WT_b = Boss weight kg

ρ_b = Density of the boss

For metal-lined tanks, the boss should be made of the same material as the liner.

Therefore,

$$\rho_b = \rho_L$$

For rubber-lined tanks either steel or titanium bosses should be used.

The factor K_2 is shown as a function of the ratio of boss diameter-to-chamber diameter and chamber burst pressure in Figure A10. The data in this figure pertain only to bosses with an ultimate tensile strength of 10540 kg m^2. K_2 may also be calculated by the following equation:

$$K_2 = \left[55.5\ P_b^{\,2} + \left(8.3 + 5.08\ \frac{D_c}{D_b}\right) \times \left(59.5 + 942.P_b\ \frac{D_c}{D_b}\right)^{1/2} P_b^{3/2} \right] \times 10^{-8}$$

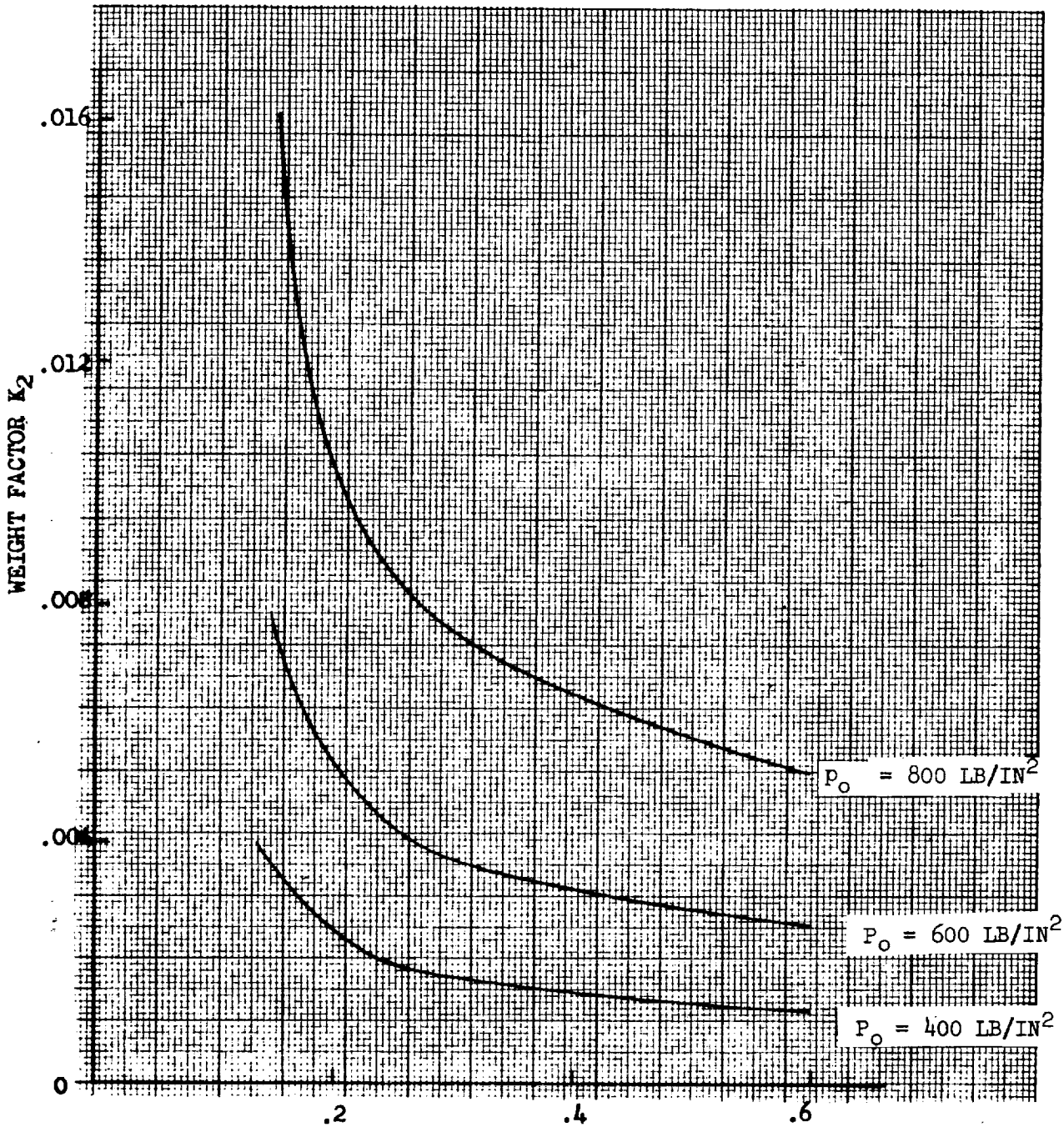

Figure A-10. Boss Weight Factor, Composite Tanks

Table A1. Weight Coefficients for Liner Material

Liner Material	Liner Weight Coefficients				
	D_b/D_c	A_1	A_2	B_1	B_2
Titanium	0.15	1.178	0.394	2.0	0.656
Titanium	0.45	1.121	0.263	2.07	0.524
Titanium	0.60	1.137	0.0180	2.31	0.263
Rubber*	0.15	1.22	0	0.515	0
Rubber*	0.45	1.141	0	0.527	0
Rubber	0.60	1.130	0	0.575	0
*Rubber liner at constant thickness t_L = .304 cm					

The weight of the cylindrical portion of the pressure vessel is given by the expression:

$$WT_c = 0.703\ K_3\ L\ D_c$$

where

WT_c = cylinder weight, kg

L = cylinder length, cm

D_c = chamber diameter, cm

and K_3 is obtained from Figure A11 or from the following equation:

$$K_3 = 14.3\ \pi\ \rho_c \left[t_L \frac{\rho_L}{\rho_c} + \frac{(0.75\ P_b D_c - 1.5\ \sigma_L\ t_L)}{\sigma_c} \right]$$

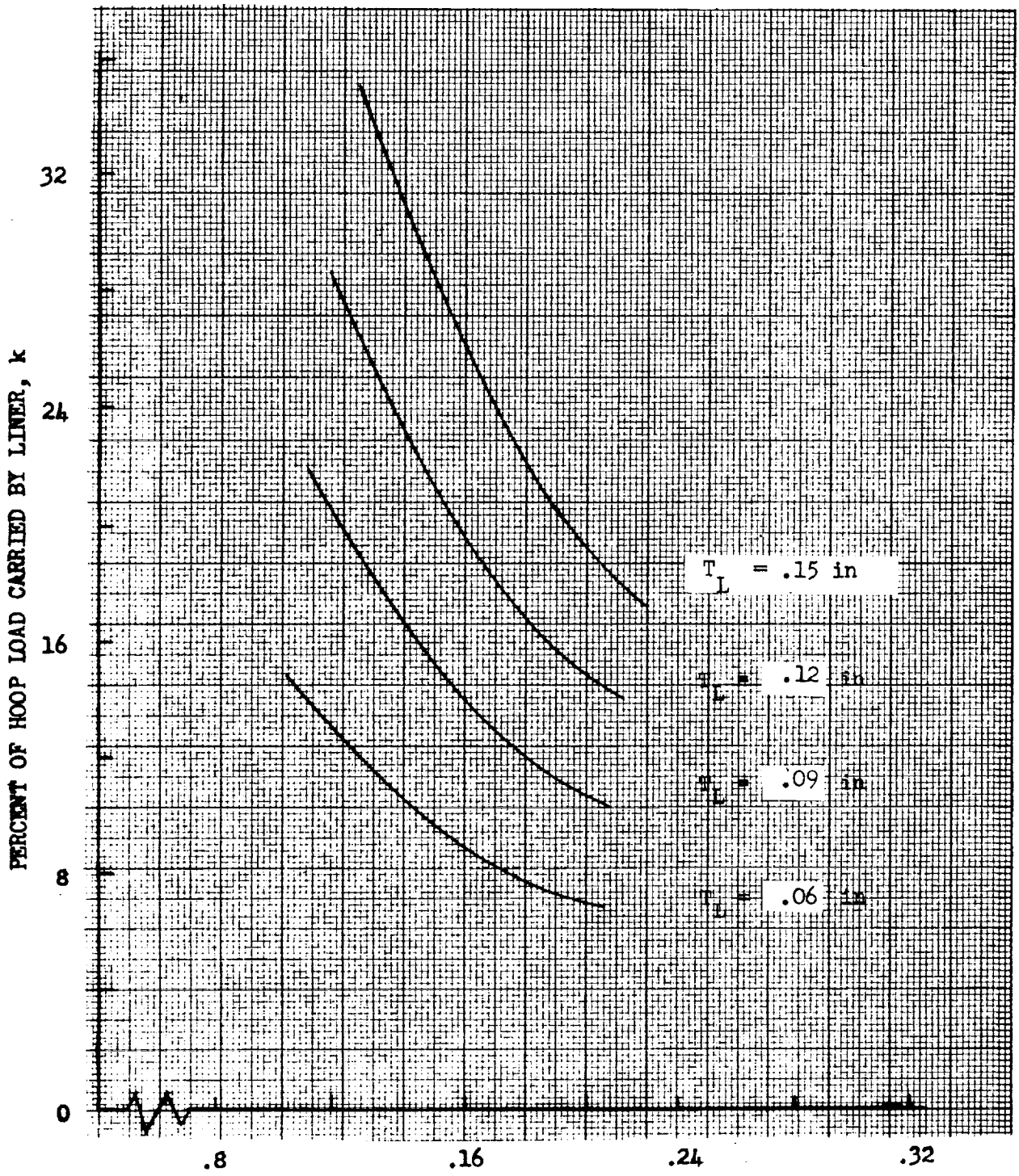

Figure A-11. Cylindrical Weight, Titanium Lined Composite Tanks

The length of the cylindrical portion of the pressure vessel is calculated from the volume requirements of the chamber, the chamber diameter, and the volumes of the bulkheads.

A composite stub skirt is required to provide the transition from the composite chamber to other structural shells such as the interstage and the intertank structures. The length of this skirt is given by

$$L_s = 0.1\ D_c$$

The weight of the skirt is

$$WT_s = 6.33 \times 10^{-7}\ D_c^{\,2}\ P^{\frac{1}{2}}$$

where

WT_s = skirt weight

P = maximum axial load on the unpressurized structure in kg (ultimate load)

The effect of material changes on the dimensions and weights of composite reinforced tankage can be effectively handled by use of the parameter k, which is defined as the percent of load carried by the liner. For the heads,

$$k_H = \left[\frac{F_{Tu'}\ L\ t_L}{\frac{P_b D_c}{4}}\right] \times 100$$

This parameter is used with Figures A7 and A8 to calculate head heights and head weights. For the cylinder

$$k_{cyL} = \left[\frac{F_{Tu'}\ L\ t_L}{\frac{P_b D_c}{2}}\right] \times 100$$

This equation is used to calculate the weight per unit length of cylinder.

A.4 Cylindrical Shell Weight Scaling Relationships

A discussion of the methods employed in developing weight scaling relationships for structural cylindrical shells is presented in this section. Weight scaling laws were developed for the materials and types of construction tabulated below.

Materials

Aluminum
Titanium
Beryllium

Shell Construction

Integral Skin Stringer
Hat section skin stringer
Waffle

Unit shell weights for the nine combinations of material and construction type were computed with the aid of a structural shell analysis program, Reference A11. The structural shell analysis program was developed in accordance with the previously described shell analysis. Unit shell weights were computed for the following shell design parameters.

1. Radius

   50, 100, 150, 200, 250, 300 inches

2. Pressure

   0, 15, 30, 45, 100, 200, 300 lb/in^2

3. Temperature

   Ambient, 70-100°F
   Cryogenic, -300 (Titanium)
   -423 (Aluminum)

4. Load Intensity

   500 to 10000 lb/in

A sampling of the computed shell weights have been plotted versus load intensity and are presented herein for descriptive purposes Figures A12 through A33. The shell weight data were computed in English units but scaling laws have been developed for both English and metric units.

By examining the shell weight figures, it can be seen that the pressurized and unpressurized shell weights have separate distinctively shaped curves. Therefore, the approach taken in deriving scaling laws was to find curve fits for the unpressurized and pressurized data separately. A multi-regression analysis was performed on the computed shell weight data to determine if curve fits of the following form were feasible.

Unpressurized:

$$W = K_1 N_x^{K2} \sigma^{k3} (R + K_4)^{K5} E^{K6}$$

Pressurized:

$$W = K_1 PR\sigma^{-1} + K_2 N_x^{K3} R^{K4} P^{K5} E^{K6}$$

where;

K_i = weight scaling coefficient and exponents

N_x = load intensity

σ = ultimate stress

R = cylinder radius

E = modulus of elasticity

P = pressure

A sample of the regression analysis performed for unpressurized titanium integral skin stringer shell weights is shown in Table A2. In this case, nine types of curve fits were examined. Different curve fits were accomplished by constraining or eliminating one or more of the weight scaling coefficients. The multi-regression program used for this analysis computed a curve fit correlation coefficient which is a measure of curve fit accuracy. A perfect curve fit would have a correlation coefficient of 1 . In all cases the curve fits chosen were decided upon by examining the correlation coefficient as well as maintaining consistency between materials and types of construction. The particular case chosen in the example had a correlation coefficient of 0.9965. The maximum error at any data point was not greater than 5 percent for this case.

Table A2. Curve Fitting of Titanium Shell Weight Data

Titanium Unpressurized Shell Weights
(English Units)

Example of Scaling Law Development from a Multi-Regression Analysis of Titanium Shell Weight Data

$$W = K_1 N_x^{K_2} R^{K_3} \sigma^{K_4} (R+50)^{K_5} (R+100)^{K_6} E^{K_7}$$ (Equation used for multi-regression analysis)

Case	Computed Coefficients							Curve Fit Correlation Coefficient
	K_1	K_2	K_3	K_4	K_5	K_6	K_7	
1	2.16×10^{-13}	.4031	.210	-1.45	0	0	2.59	.9955
2	4.69×10^{-10}	.4031	0	-1.09	.3026	0	1.85	.9965
3	2.88×10^{-8}	.4031	0	-.894	0	.387	1.424	.9967
4	113.1	.4031	.210	0	0	0	-.465	.9955
*5	64.46	.4031	0	0	.3026	0	-.465	.9965
6	37.54	.4031	0	0	0	.387	-.465	.9968
7	169.05	.425	.210	0	0	0	-.500	.9500
8	96.3	.425	0	0	.3026	0	-.500	.9590
9	56.10	.425	0	0	0	.387	-.500	.9618

* Case used for scaling law

The scaling laws for unpressurized shell weights are tabulated in Tables 3 and 2 for English and metric units respectively. The scaling laws for pressurized shell weights are given in Tables 5 and 4 for English and metric units respectively. All of the scaling laws were developed in the same manner as the example case. The metric unit scaling laws were determined from the English unit scaling laws with the use of conversion factors. The computed weight of unpressurized shells must be checked against a minimum weight determined by the material, minimum skin gages, and type of construction.

$$\begin{matrix}\text{Unpressurized} \\ \text{Shell Weight}\end{matrix} = \text{Maximum} \left[\left(\begin{matrix}\text{Scaling Law} \\ \text{Weight-Unpress}\end{matrix} \right) , \left(\begin{matrix}\text{Minimum} \\ \text{Gage Weight}\end{matrix} \right) \right]$$

The computed weight of pressurized shells must be checked against the unpressurized weight as well as the minimum gage weight.

$$\begin{matrix}\text{Pressurized} \\ \text{Shell Weight}\end{matrix} = \text{Maximum} \left[\begin{matrix} \left(\begin{matrix}\text{Scaling Law} \\ \text{Weight-Press.}\end{matrix} \right) , \left(\begin{matrix}\text{Scaling Law} \\ \text{Weight-Unpress.}\end{matrix} \right) \\ , \left(\begin{matrix}\text{Minimum} \\ \text{Gage Weight}\end{matrix} \right) \end{matrix} \right]$$

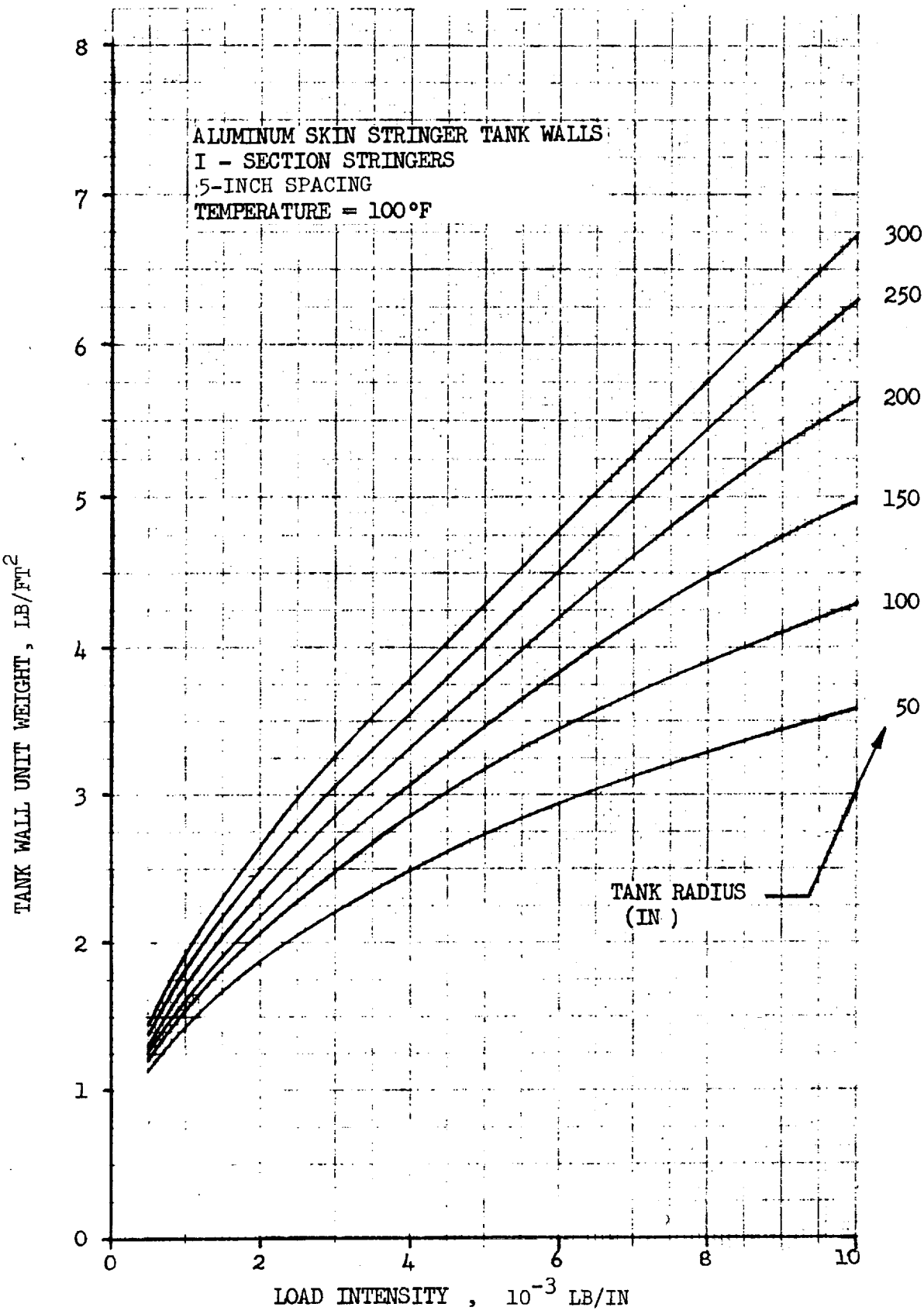

Figure A12. Tank Wall Unit Weight for Unpressurized Tanks of Aluminum Skin-I Stringer Construction (T = 100°F)

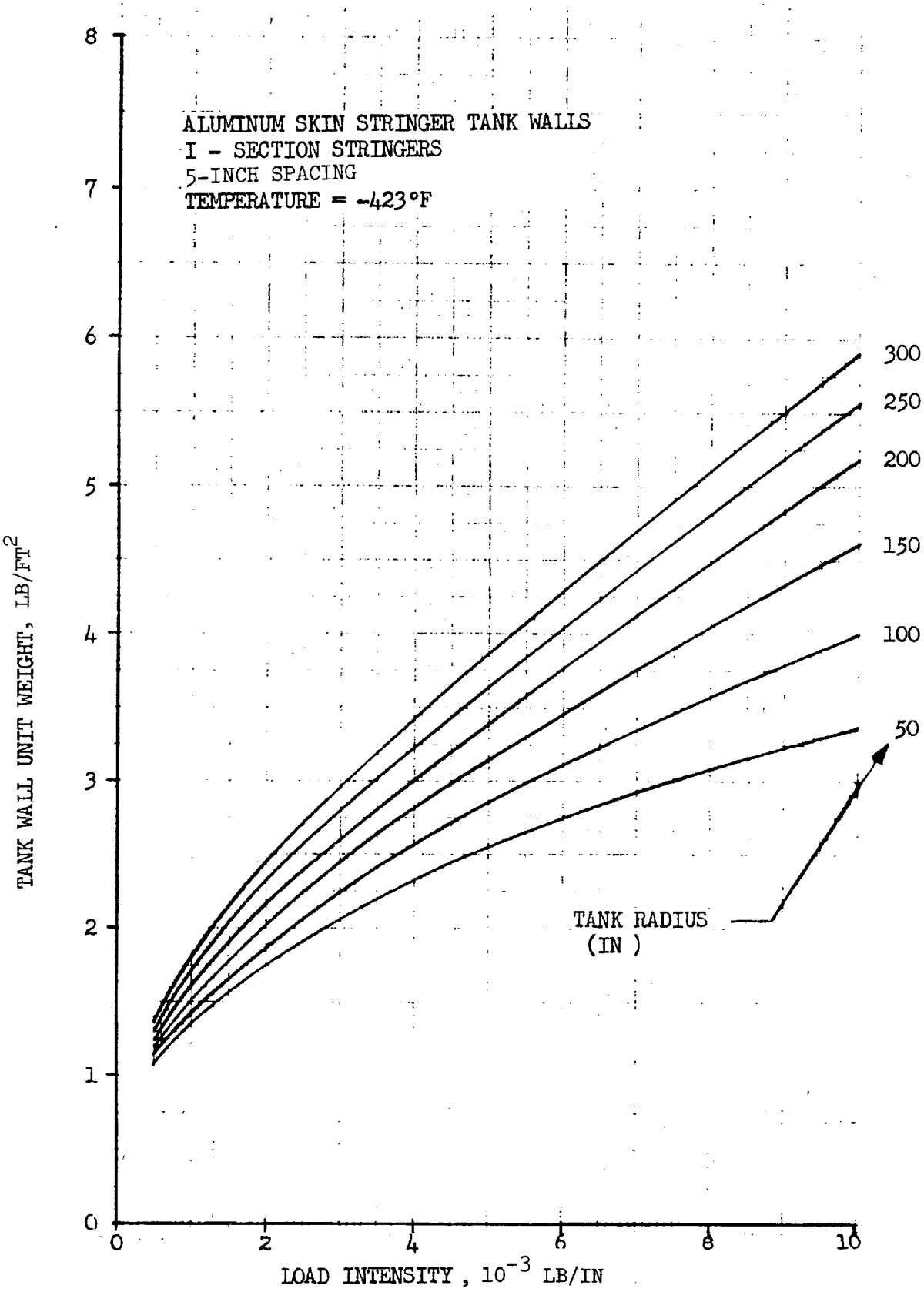

Figure A13. Tank Wall Unit Weight for Unpressurized Tanks of Aluminum Skin-I Stringer Construction (T = -423°F)

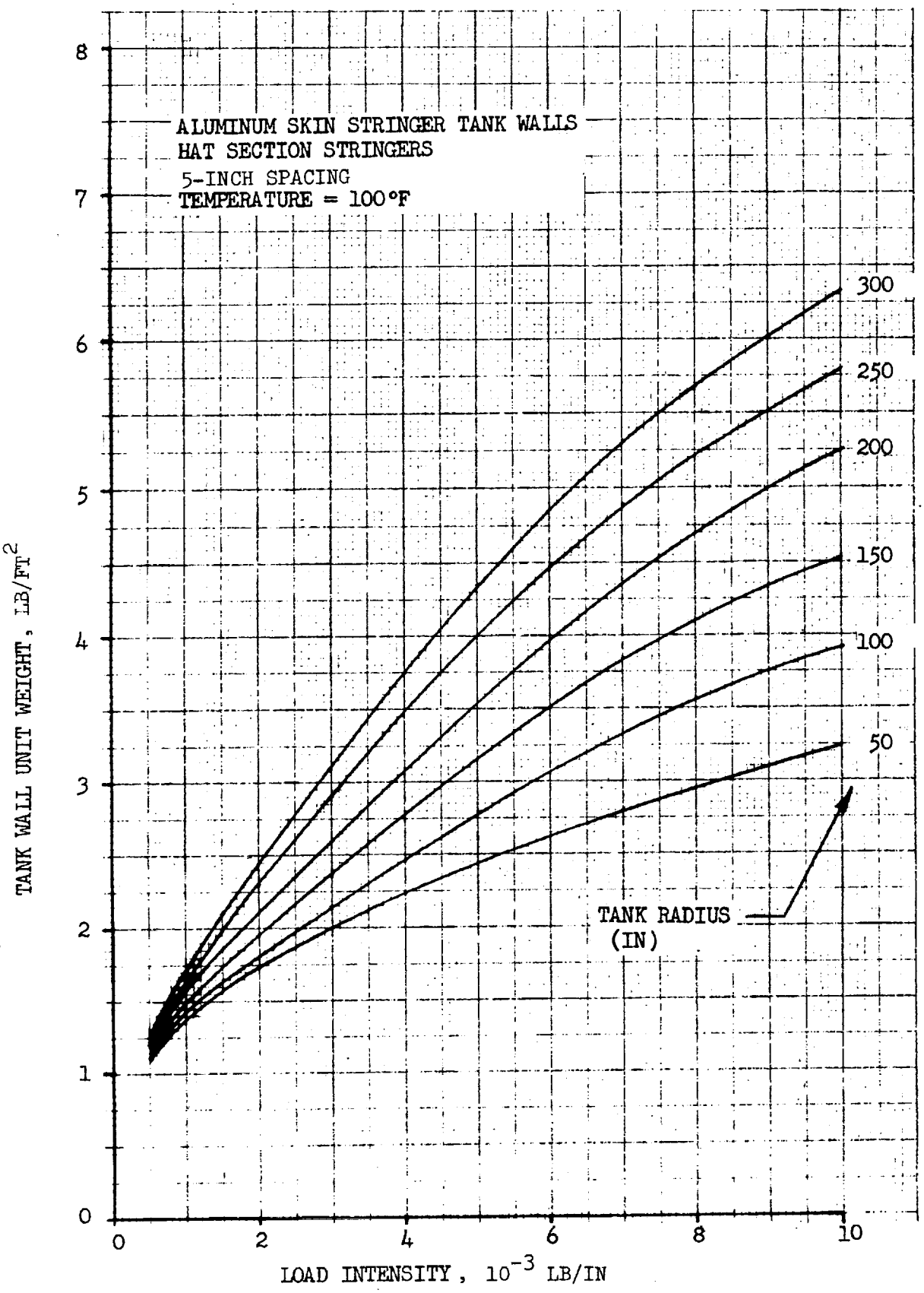

Figure A14. Tank Wall Unit Weight for Unpressurized Tanks of Aluminum Skin-Hat Stringer Construction (T = 100°F)

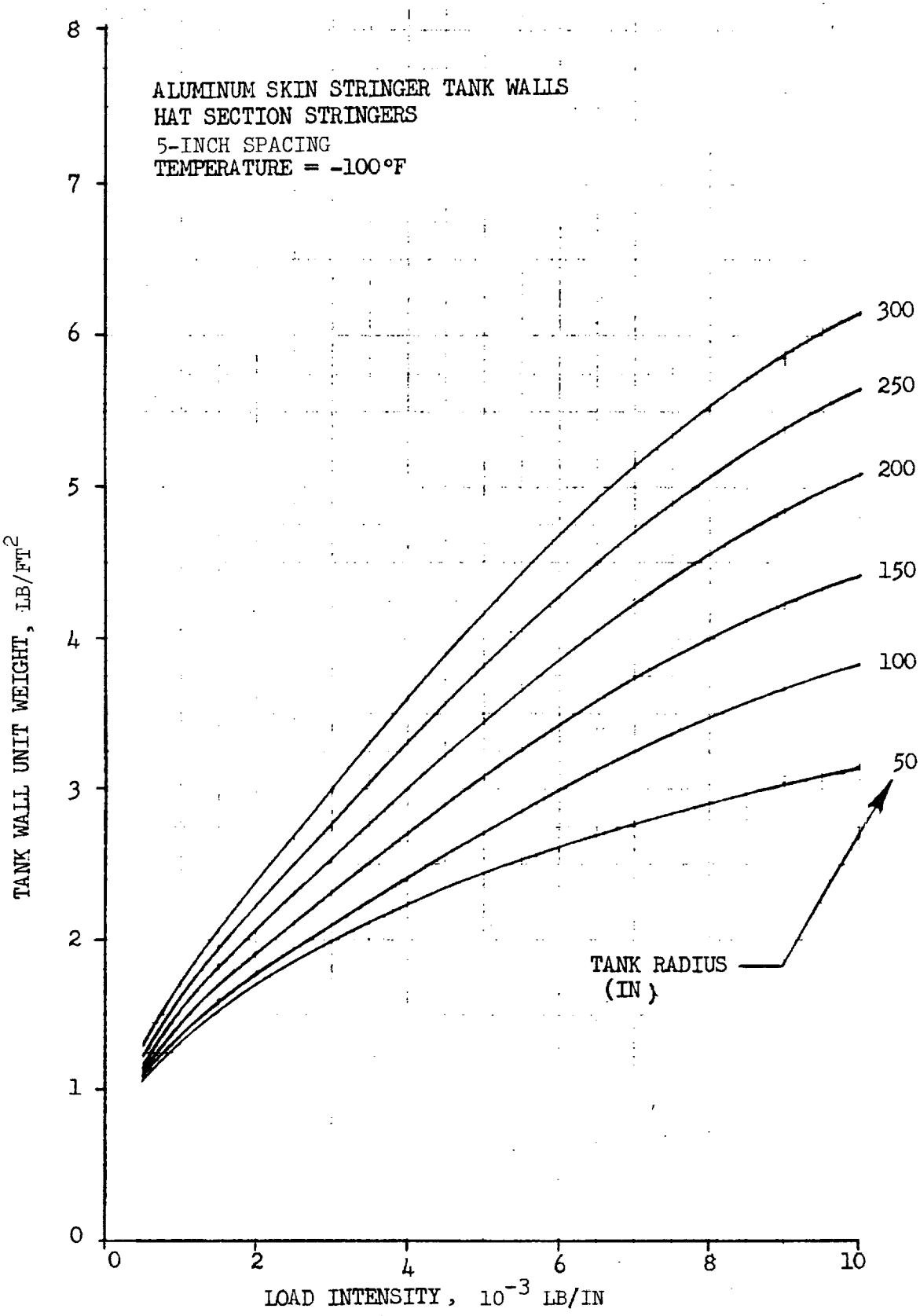

Figure A15. Tank Wall Unit Weight for Unpressurized Tanks of Aluminum Skin-Hat Stringer Construction (T = -100°F)

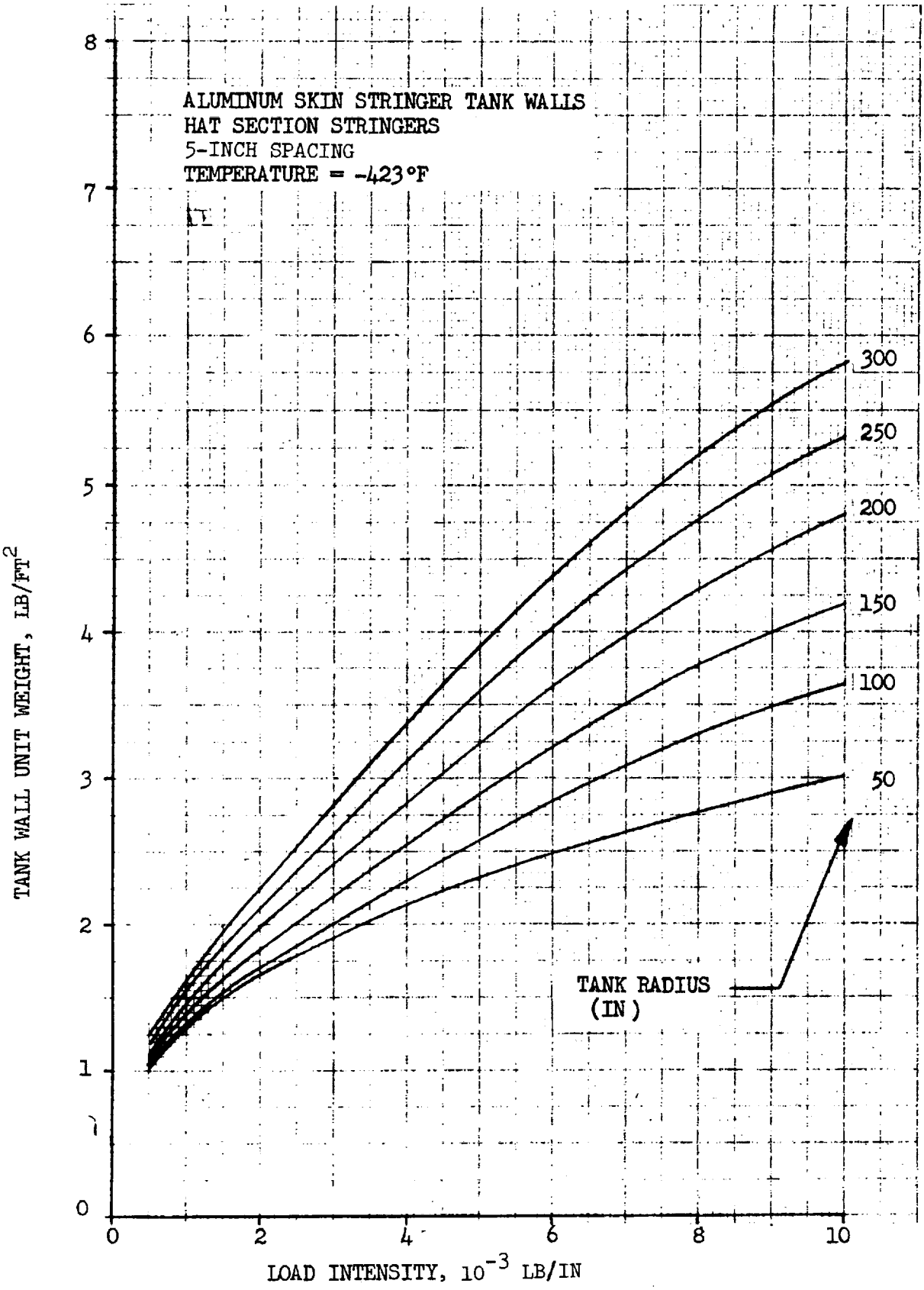

Figure A16. Tank Wall Unit Weight for Unpressurized Tanks of Aluminum Skin-Hat Stringer Construction (T = -423°F)

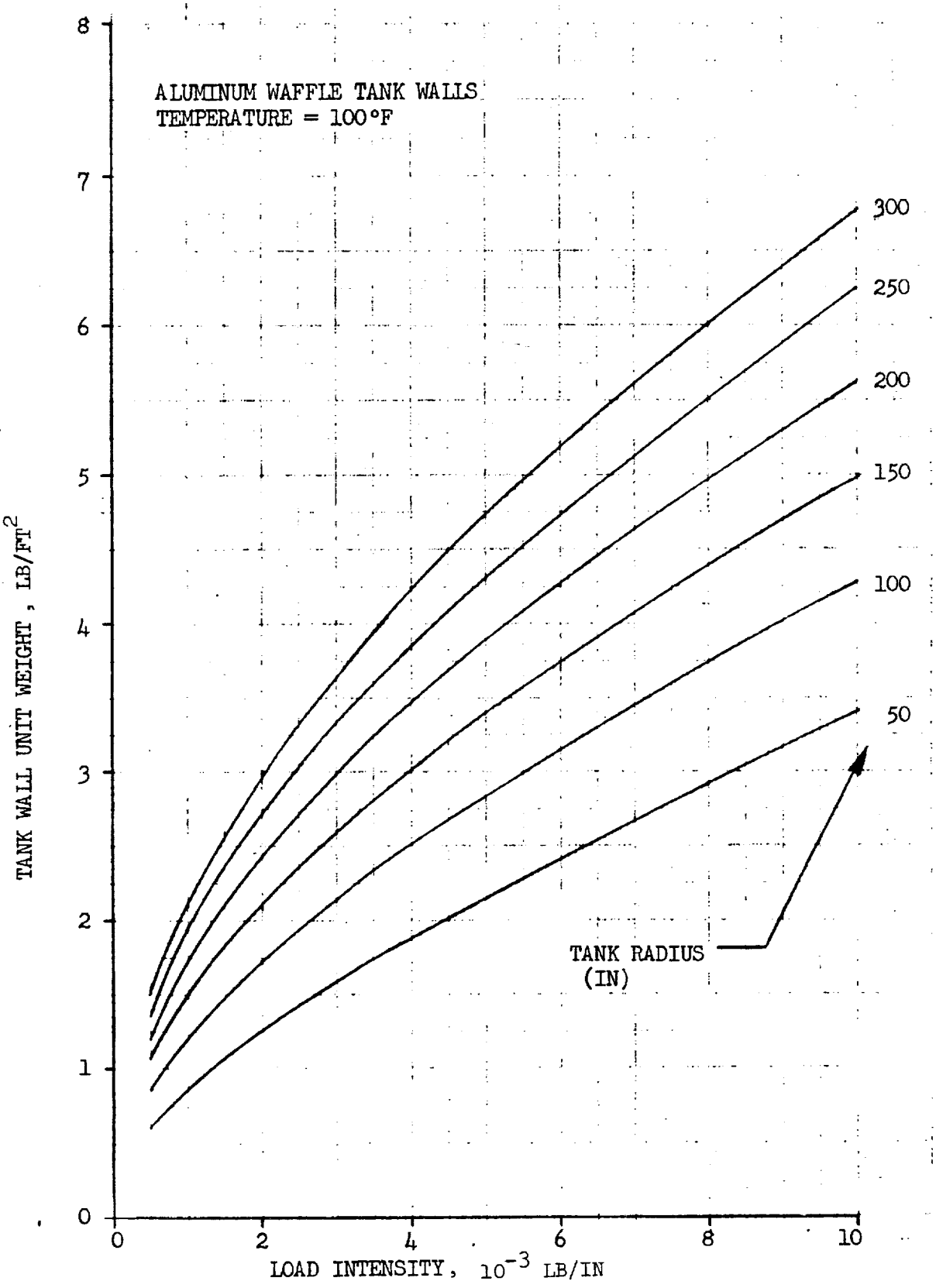

Figure A17. Tank Wall Unit Weight for Unpressurized Tanks of Aluminum Waffle Construction (T = 100°F)

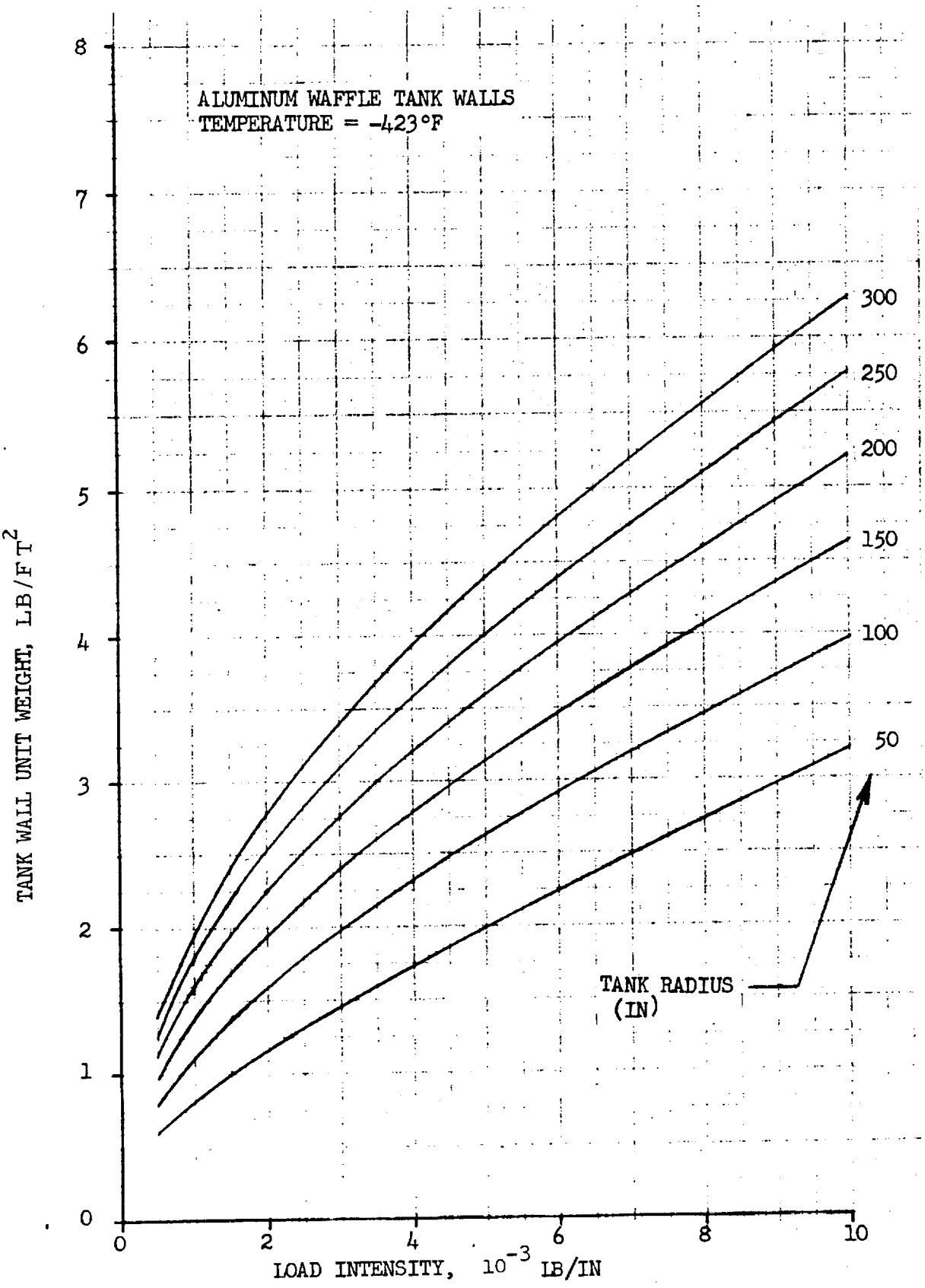

Figure A18. Tank Wall Unit Weight for Unpressurized Tanks of Aluminum Waffle Construction (T = -423°F)

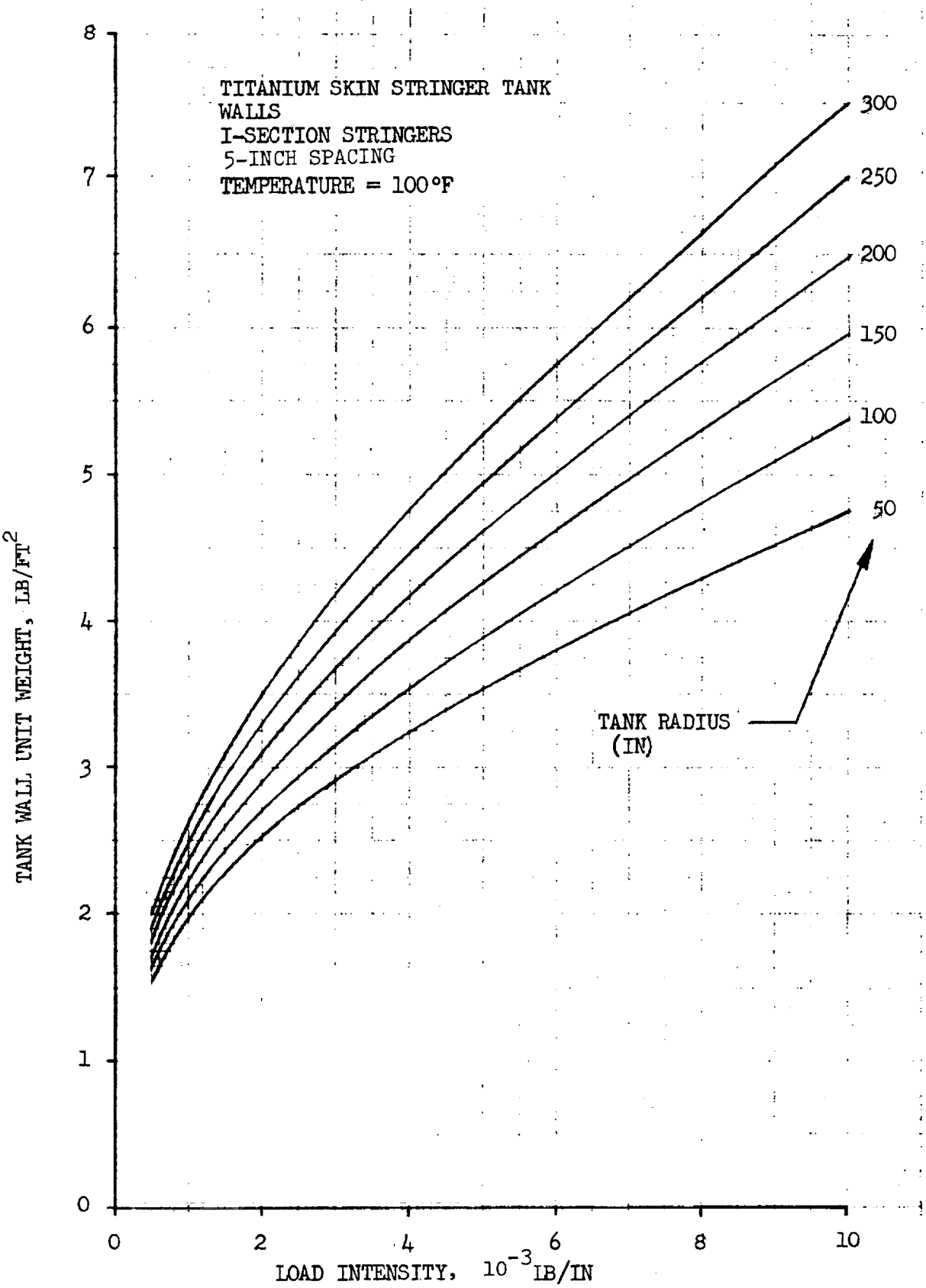

Figure A19. Tank Wall Unit Weight for Unpressurized Tanks of Titanium Skin-I Stringer Construction (T = 100°F)

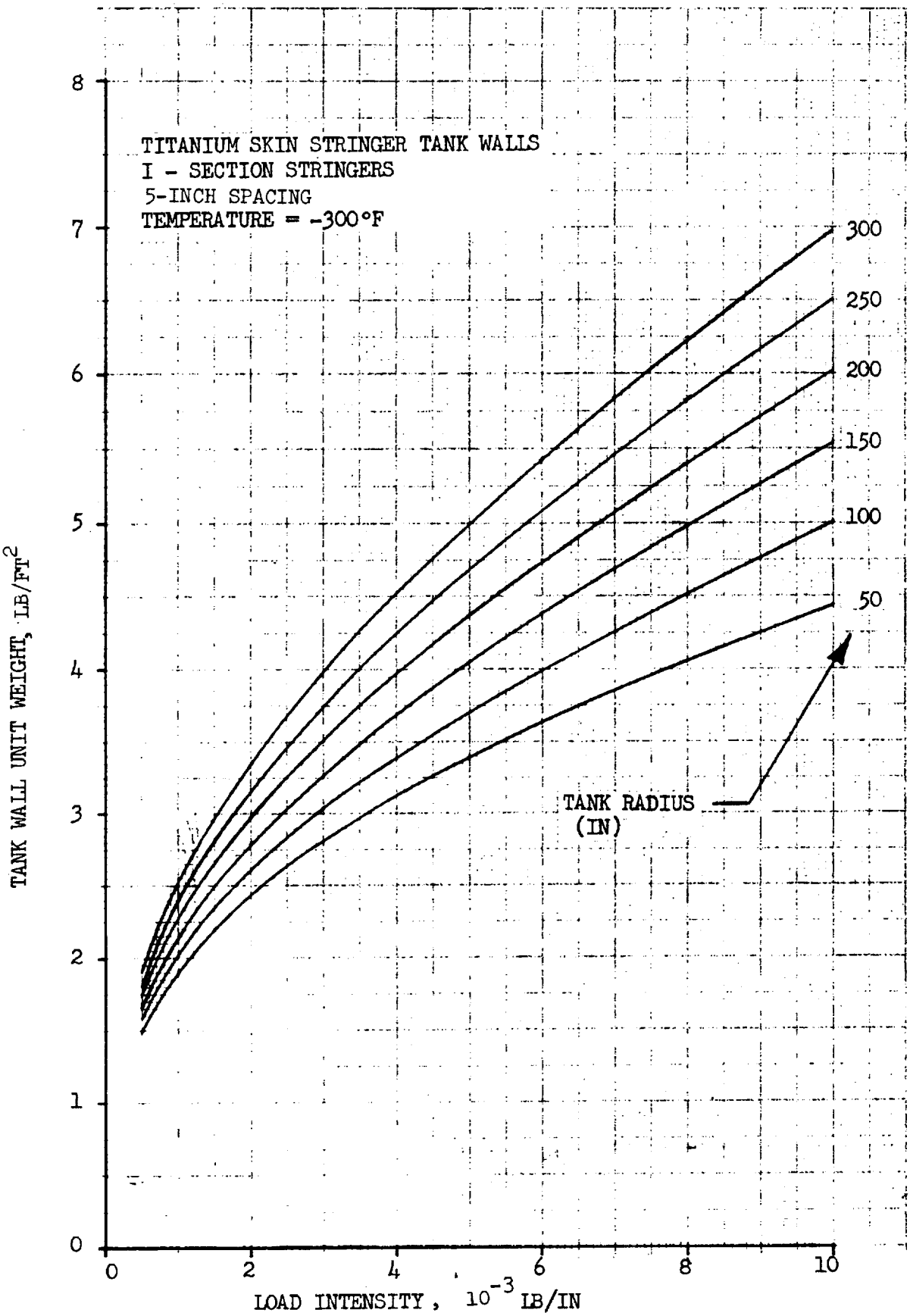

Figure A20. Tank Wall Unit Weight for Unpressurized Tanks of Titanium Skin-I Stringer Construction (T = -300°F)

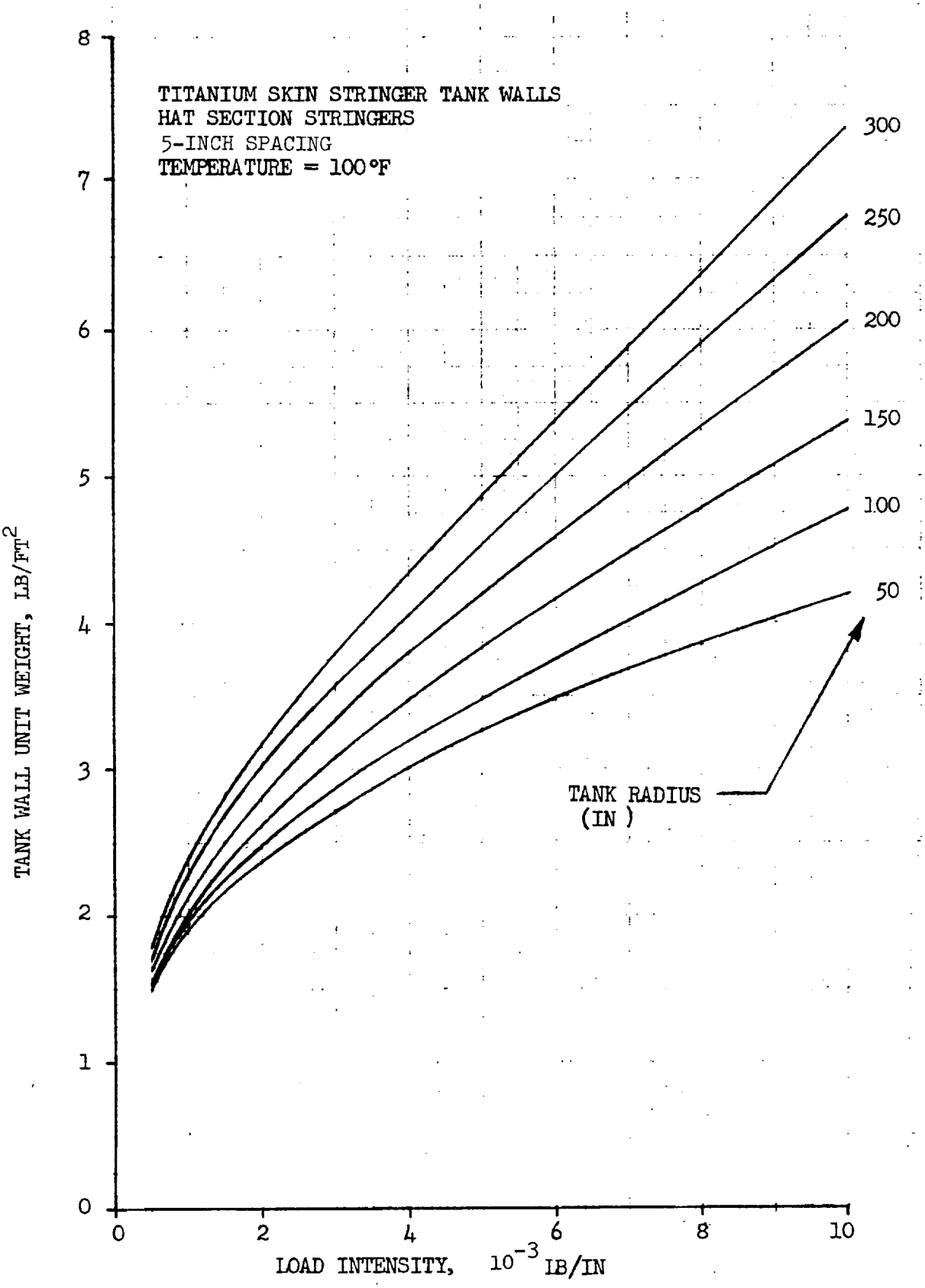

Figure A21 Tank Wall Unit Weight for Unpressurized Tanks of Titanium Skin-Hat Stringer Construction (T = 100°F)

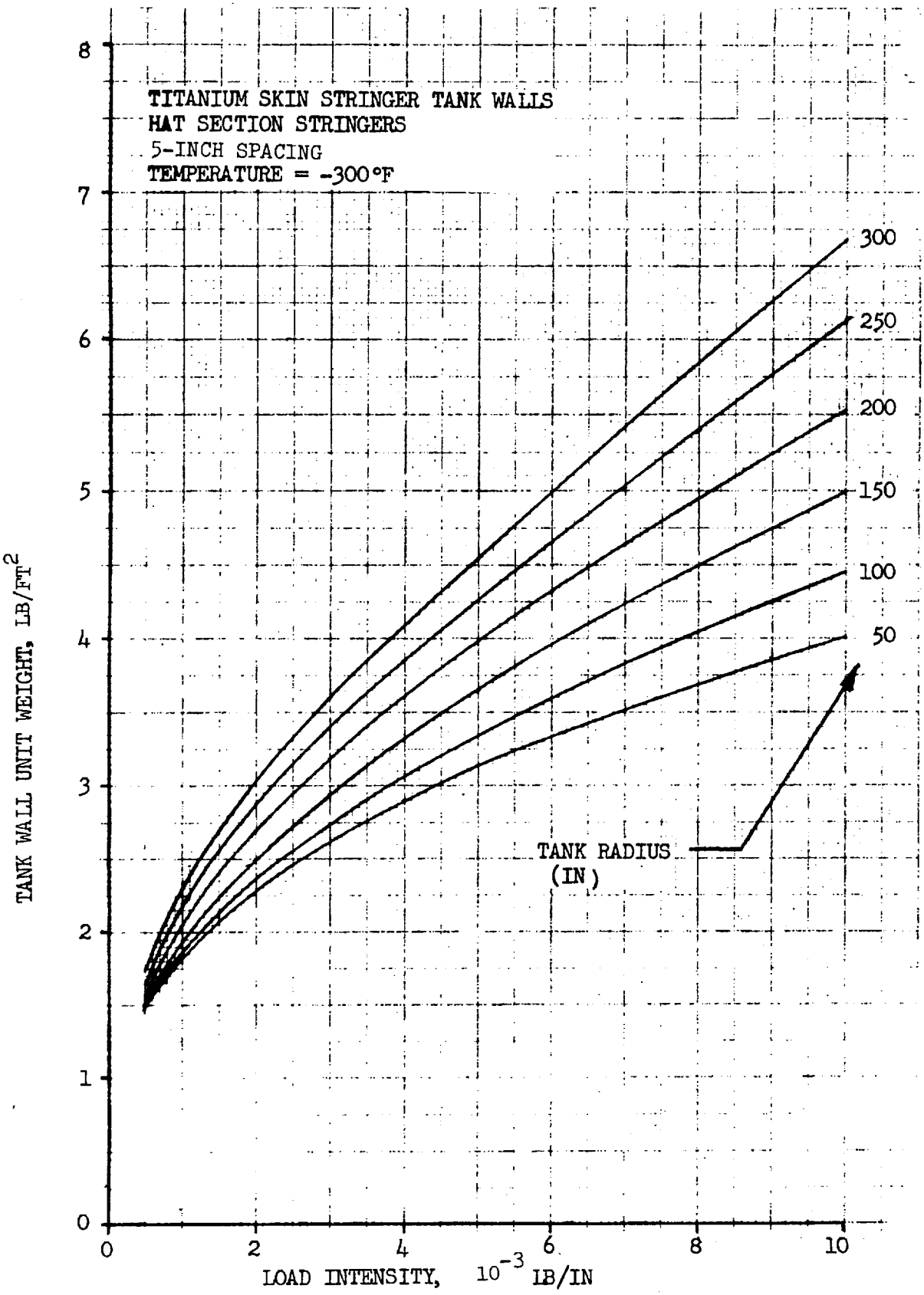

Figure A22. Tank Wall Unit Weight for Unpressurized Tanks of Titanium Skin-Hat Stringer Construction (T = -300°F)

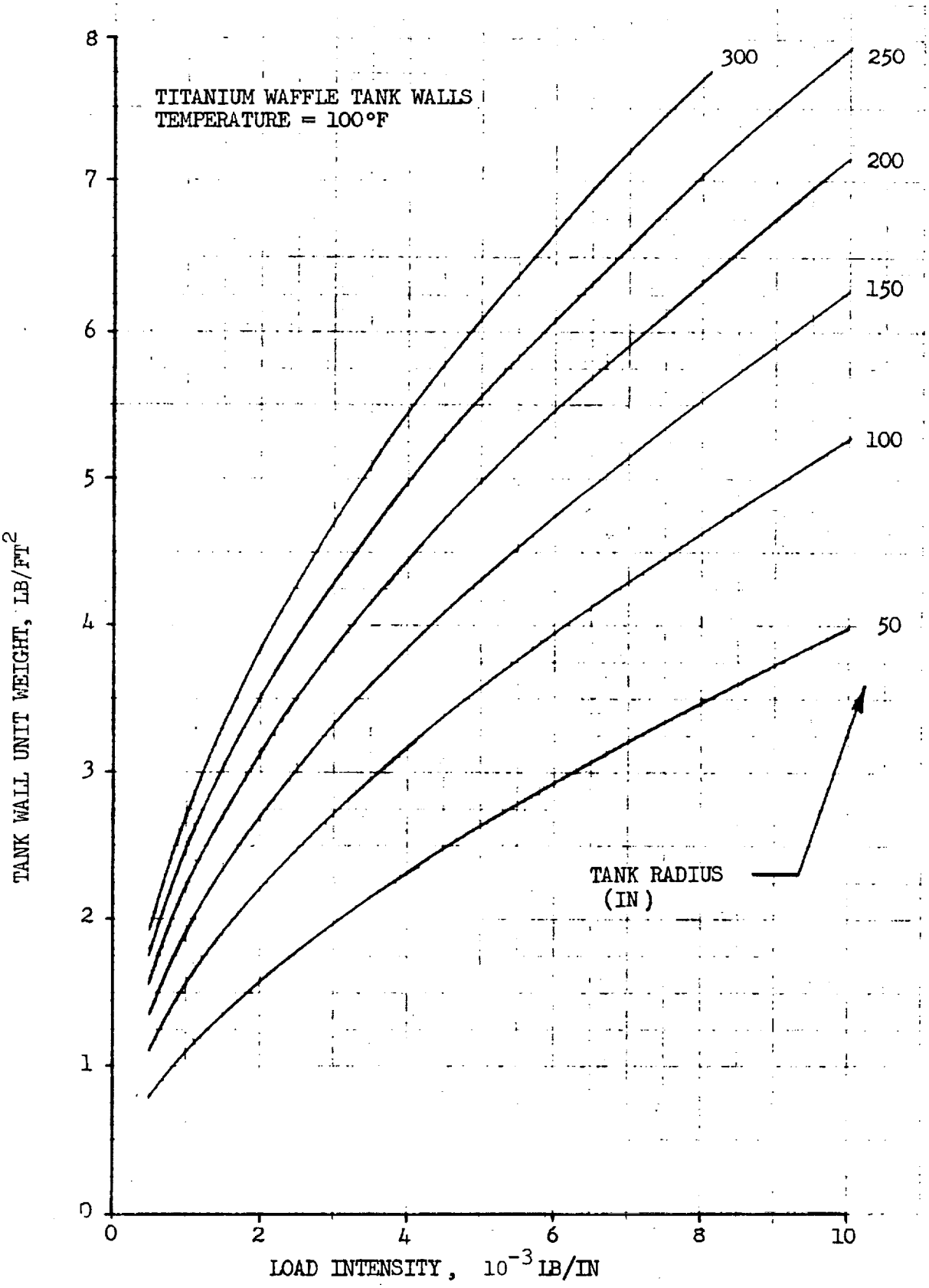

Figure A23. Tank Wall Unit Weight for Unpressurized Tanks of Titanium Waffle Construction (T = 100°F)

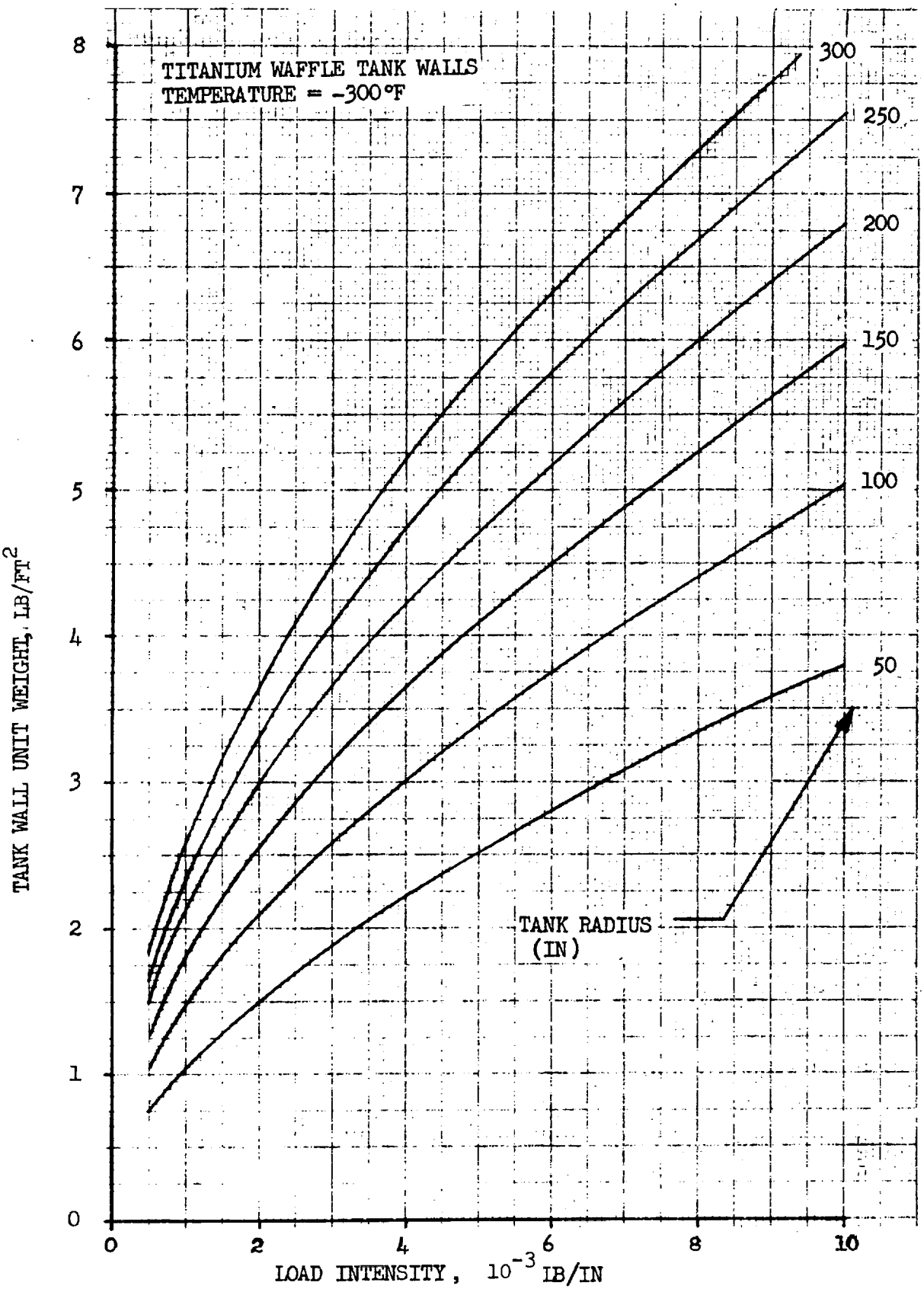

Figure A24. Tank Wall Unit Weight for Unpressurized Tanks of Titanium Waffle Construction (T = -300°F)

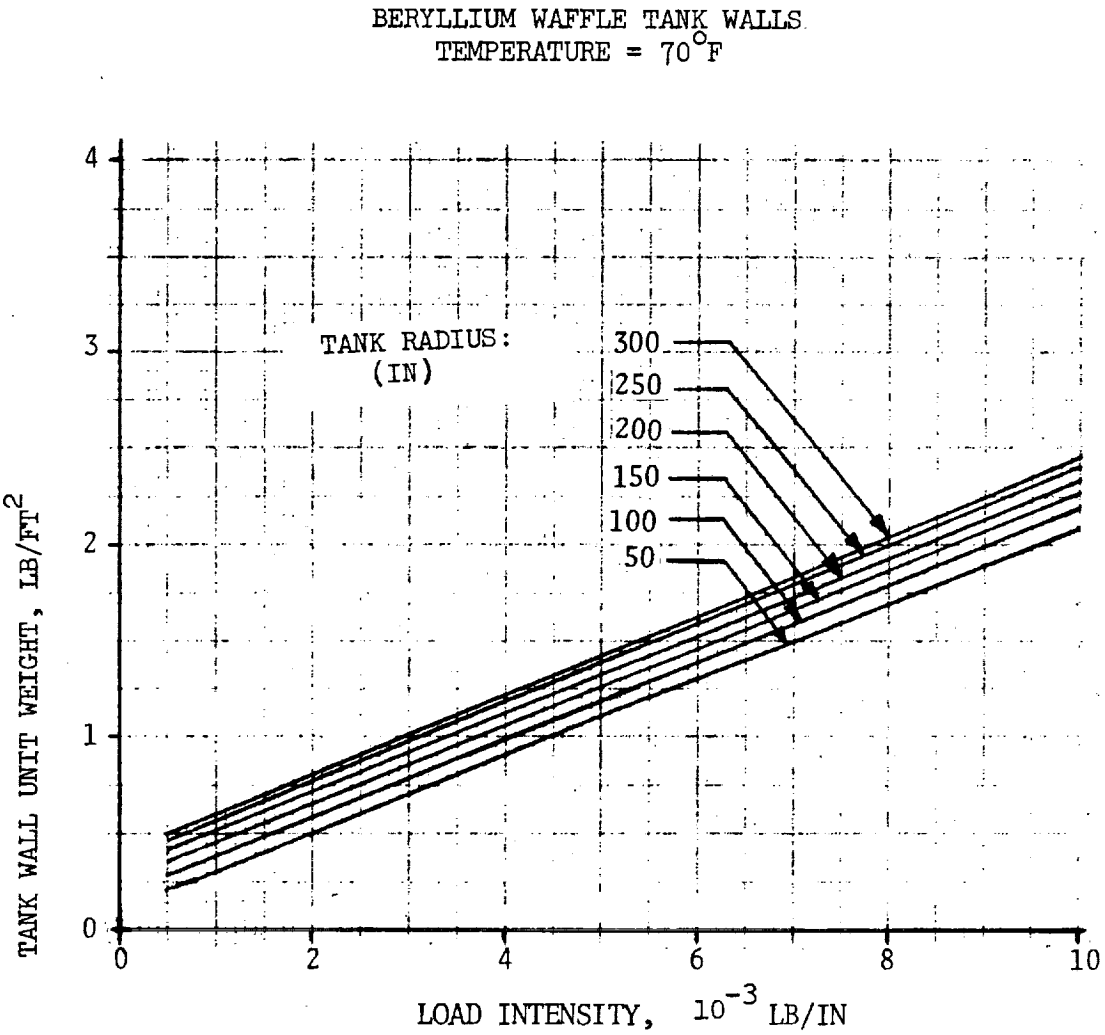

Figure A25 . Tank Wall Unit Weight for Unpressurized Tanks of Beryllium Waffle Construction (T=70°F)

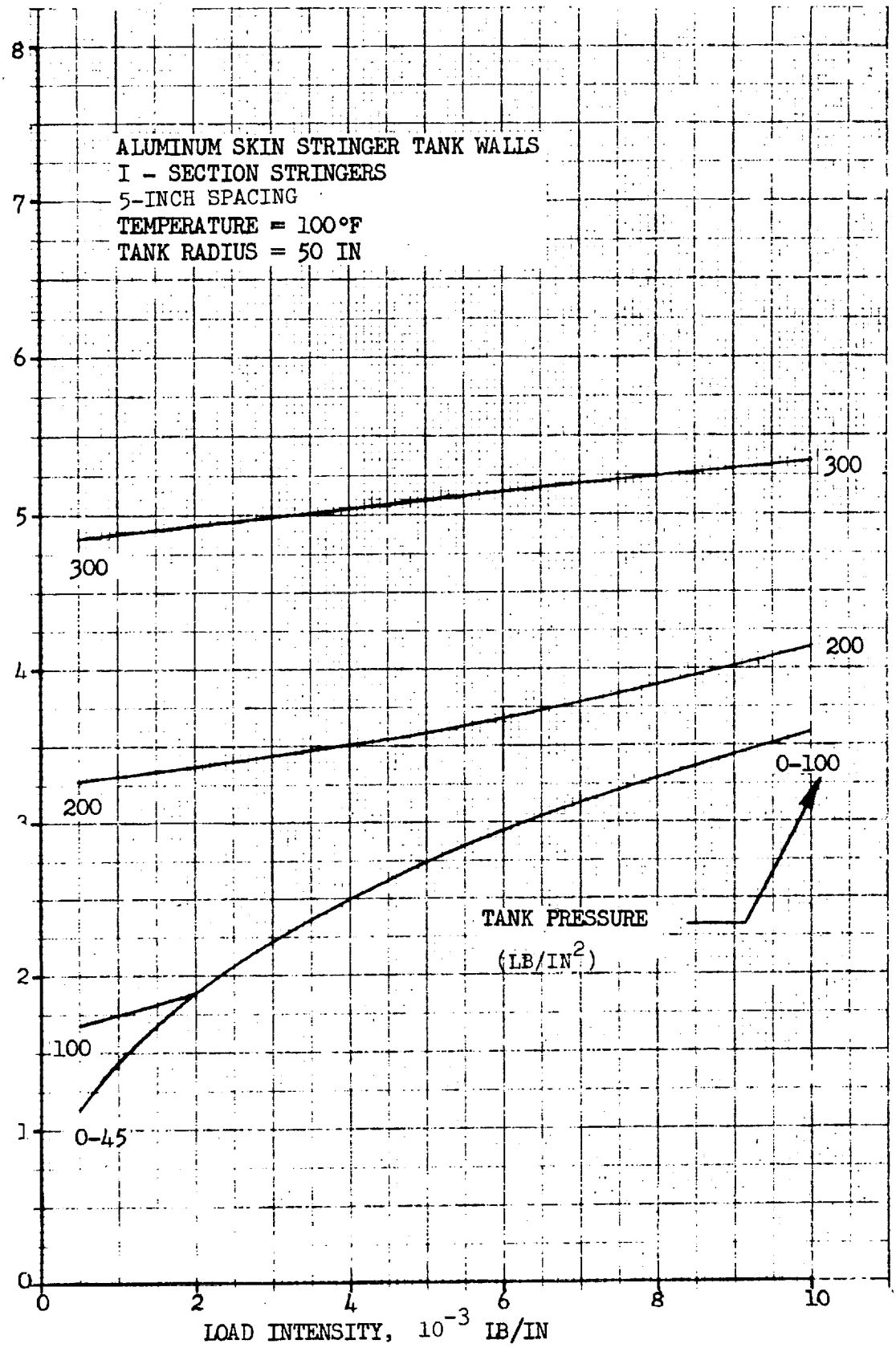

Figure A26. Tank Wall Unit Weight for Pressurized Tanks of Aluminum Skin I-Stringer Construction (R = 50 In., T = 100°F)

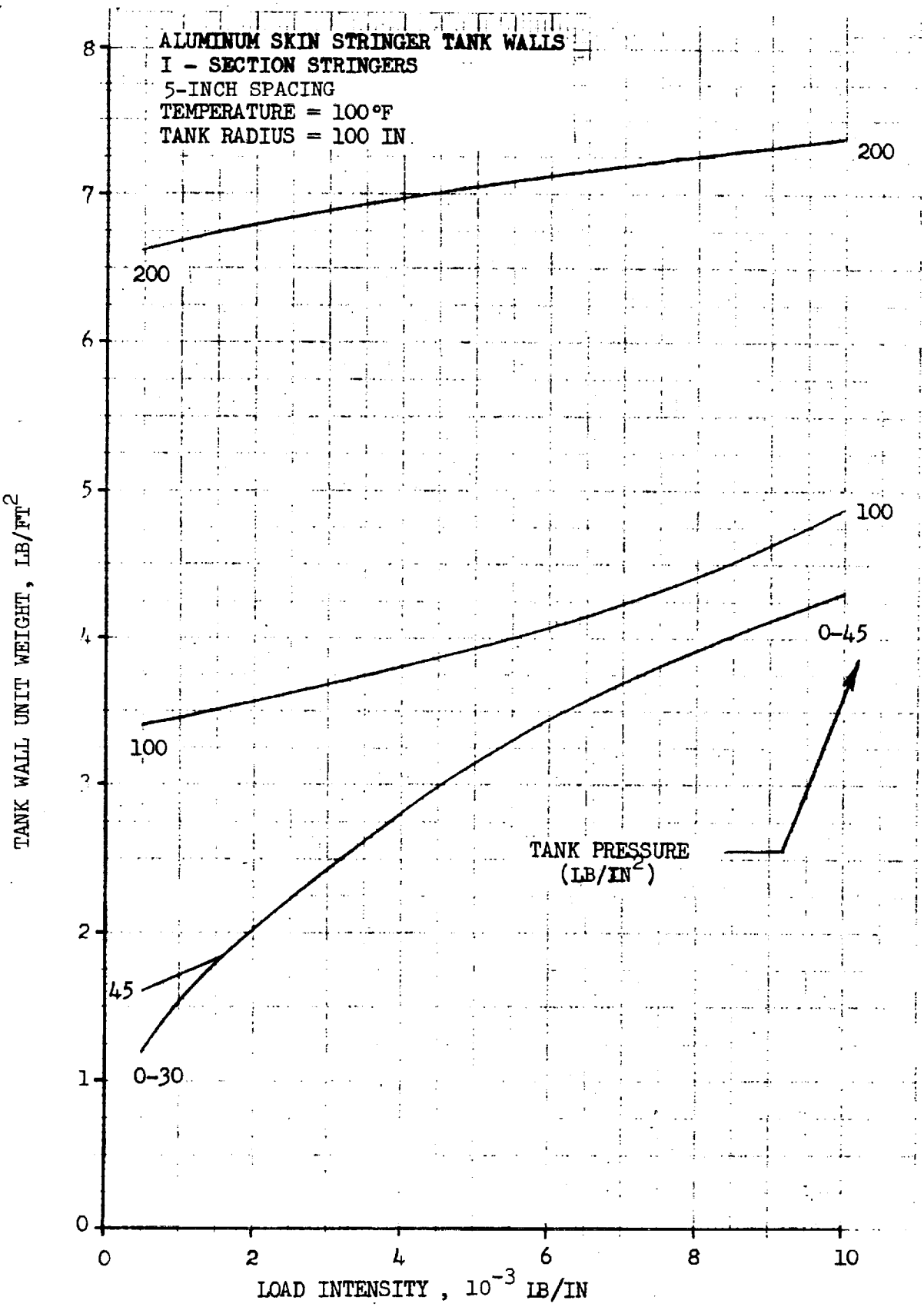

Figure A27. Tank Wall Unit Weight for Pressurized Tanks of Aluminum Skin I - Stringer Construction (R = 100 In., T = 100°F)

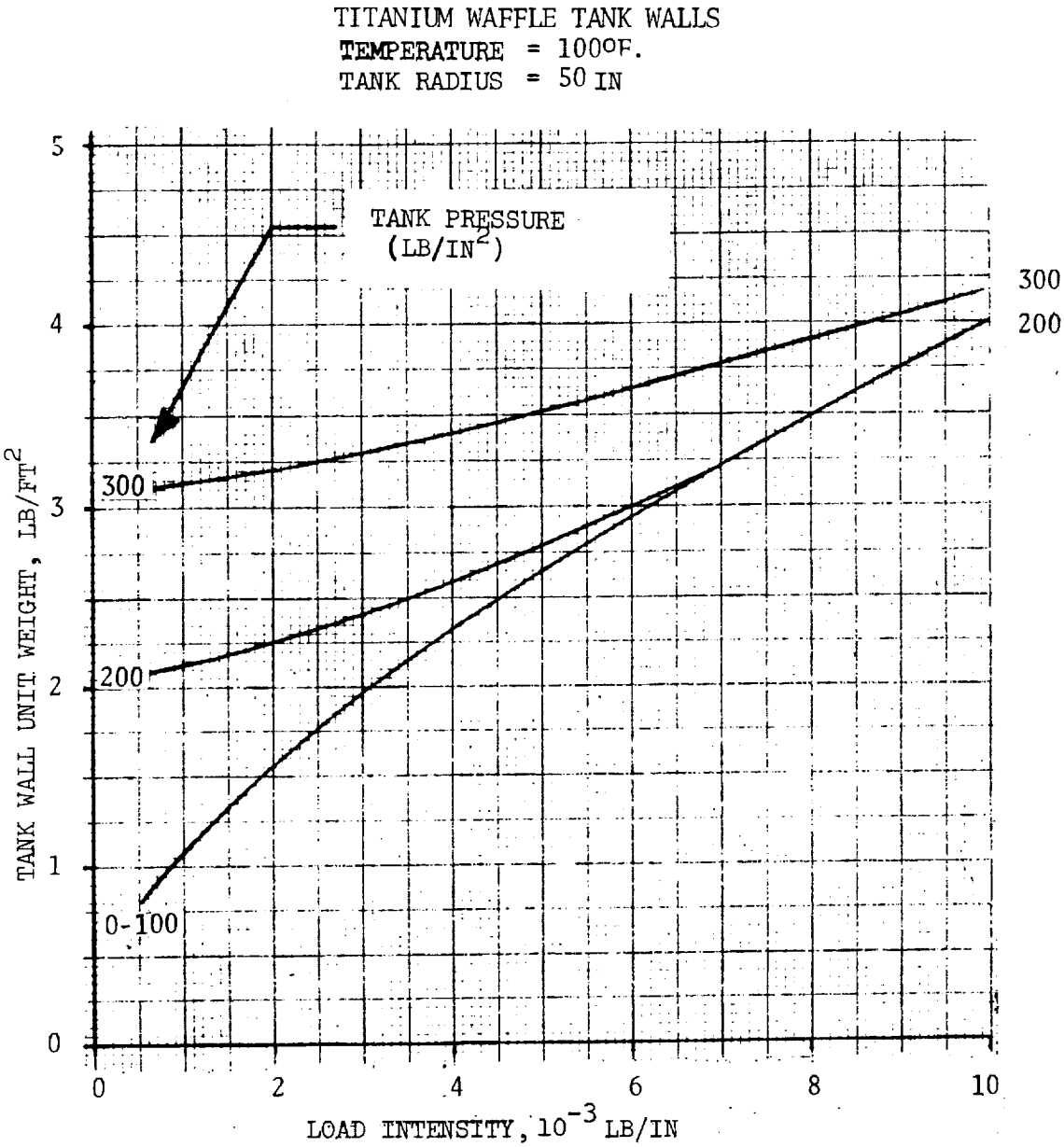

Figure A28. Tank Wall Unit Weight for Pressurized Tanks of Titanium Waffle Construction (R=50 inches, T=100°F)

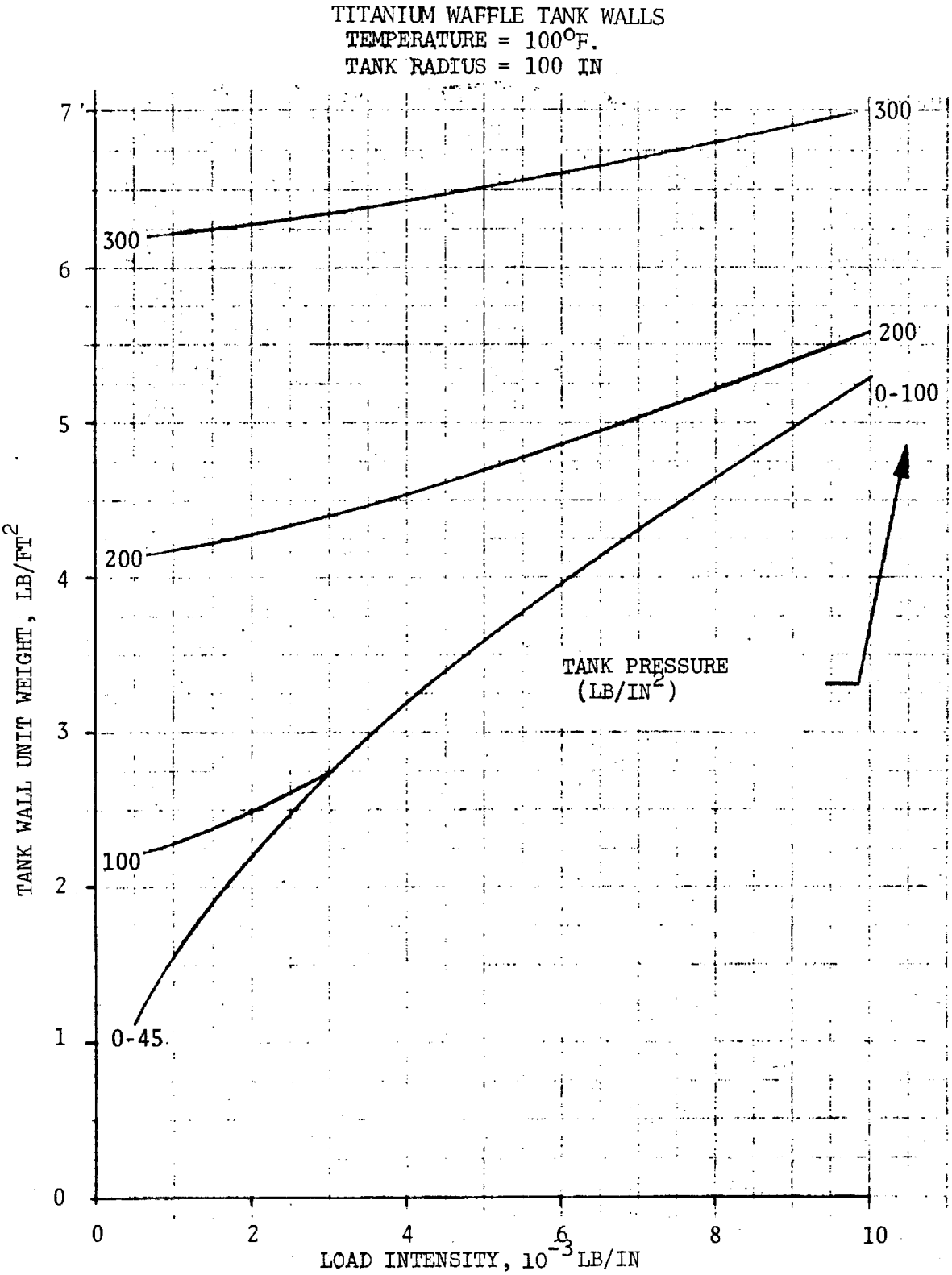

Figure A29 . Tank Wall Unit Weight for Pressurized Tanks of Titanium Waffle Construction (R=100 inches, T=100°F)

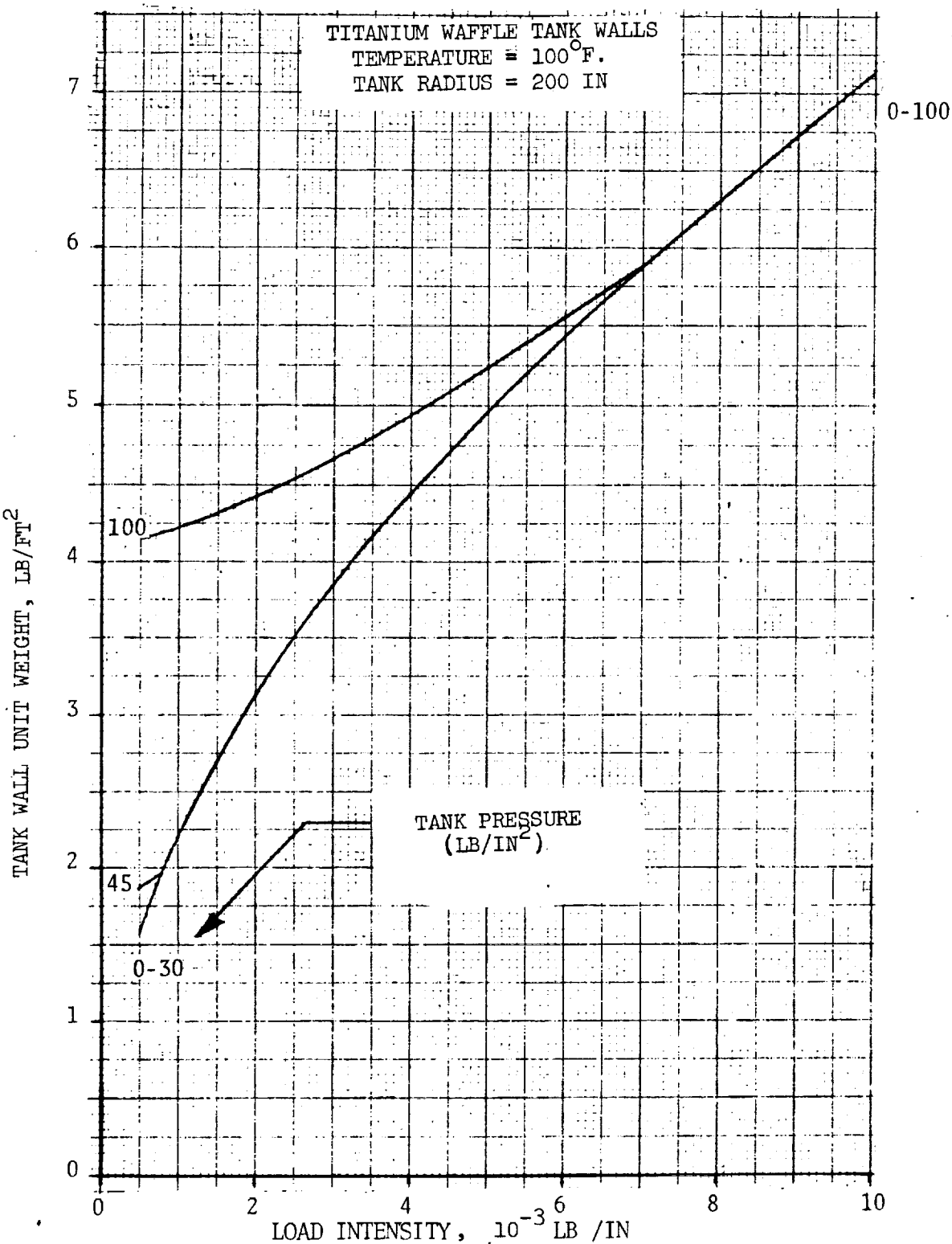

Figure A30: Tank Wall Unit Weight for Pressurized Tanks of Titanium Waffle Construction (R=200 in., T=100°F)

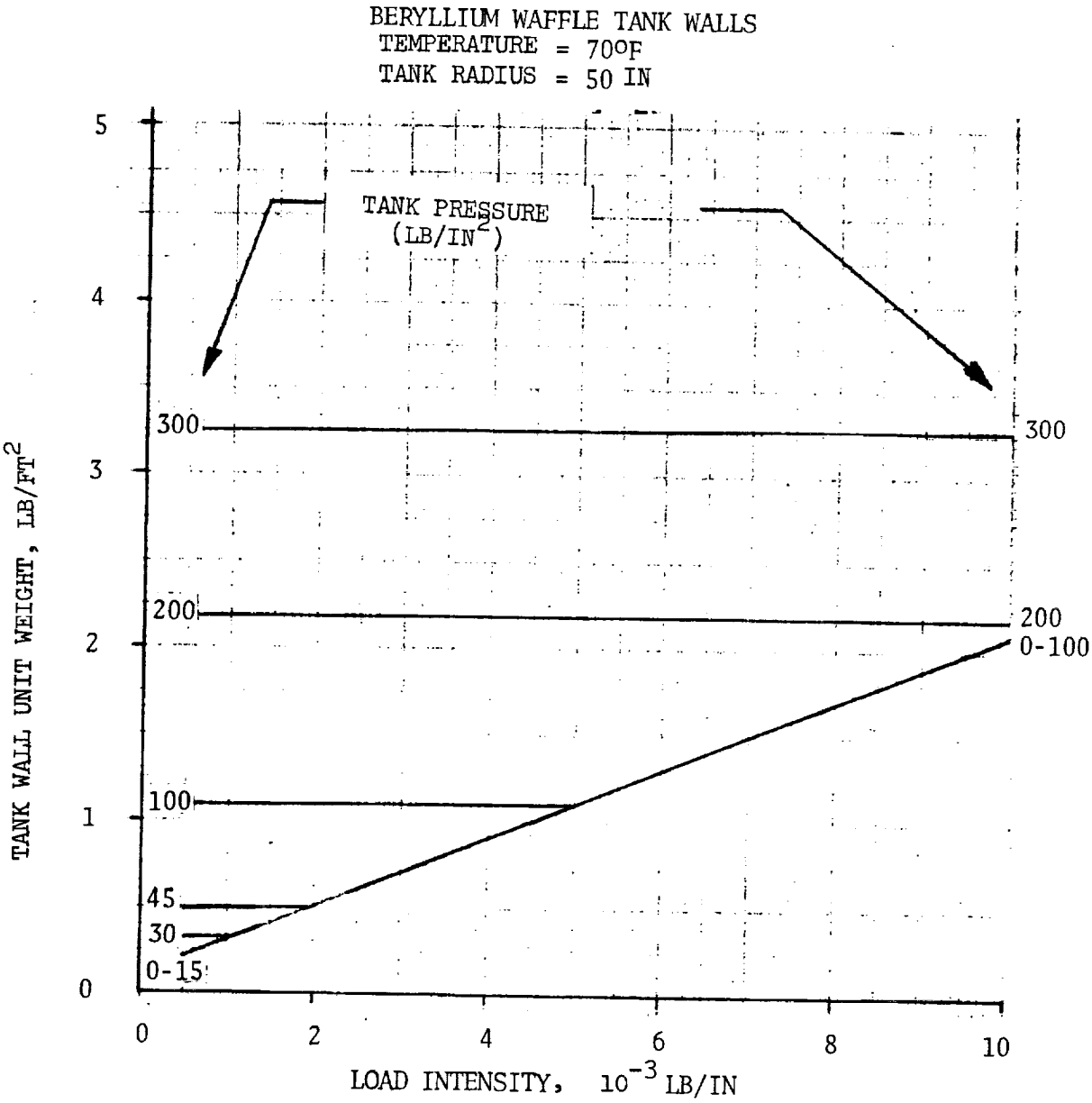

Figure A31 . Tank Wall Unit Weight for Pressurized Tanks of Beryllium Waffle Construction (R=50 in., T=70°F)

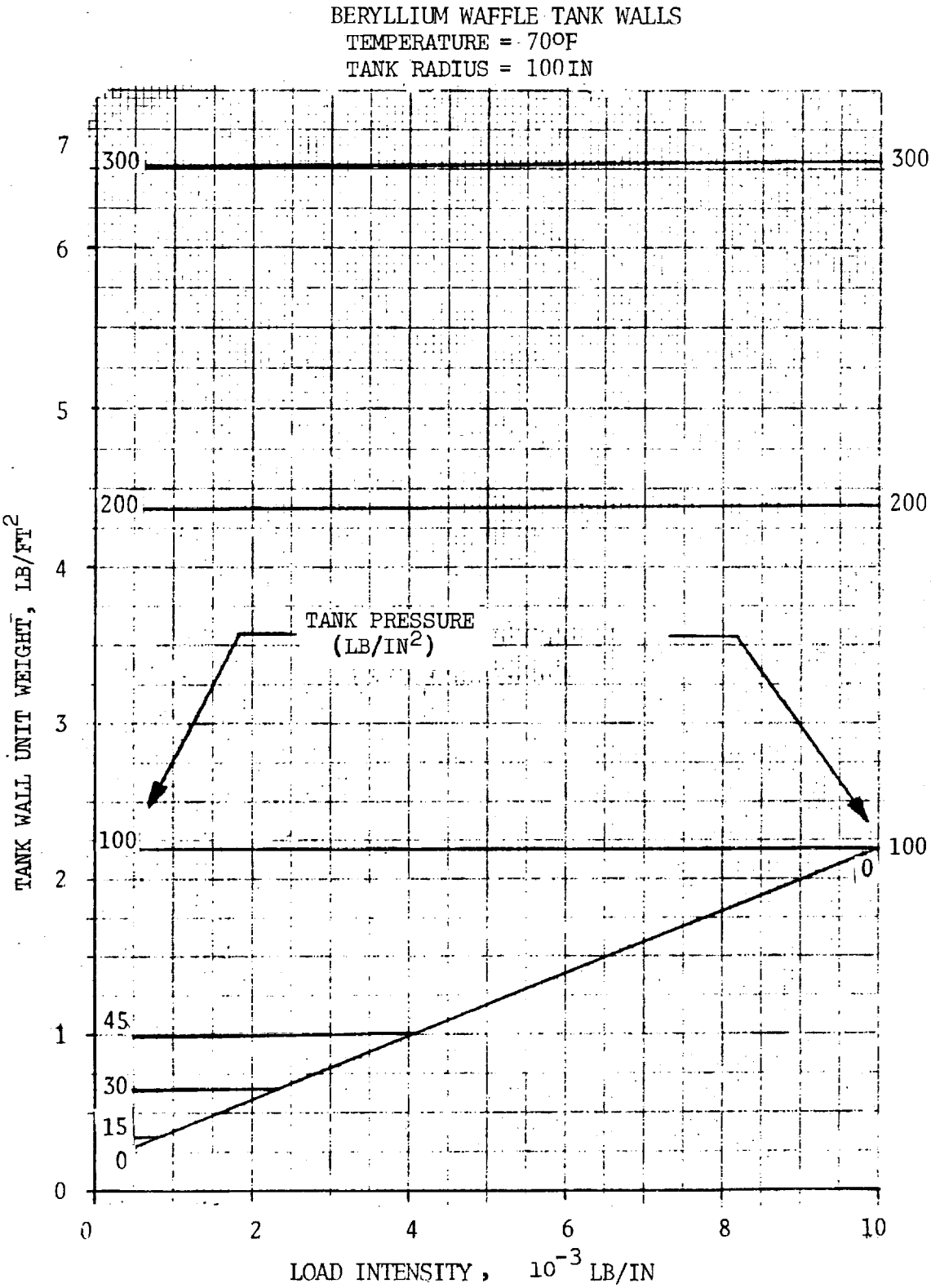

Figure A32 . Tank Wall Unit Weight for Pressurized Tanks of Beryllium Waffle Construction (R=100in., T=70°F)

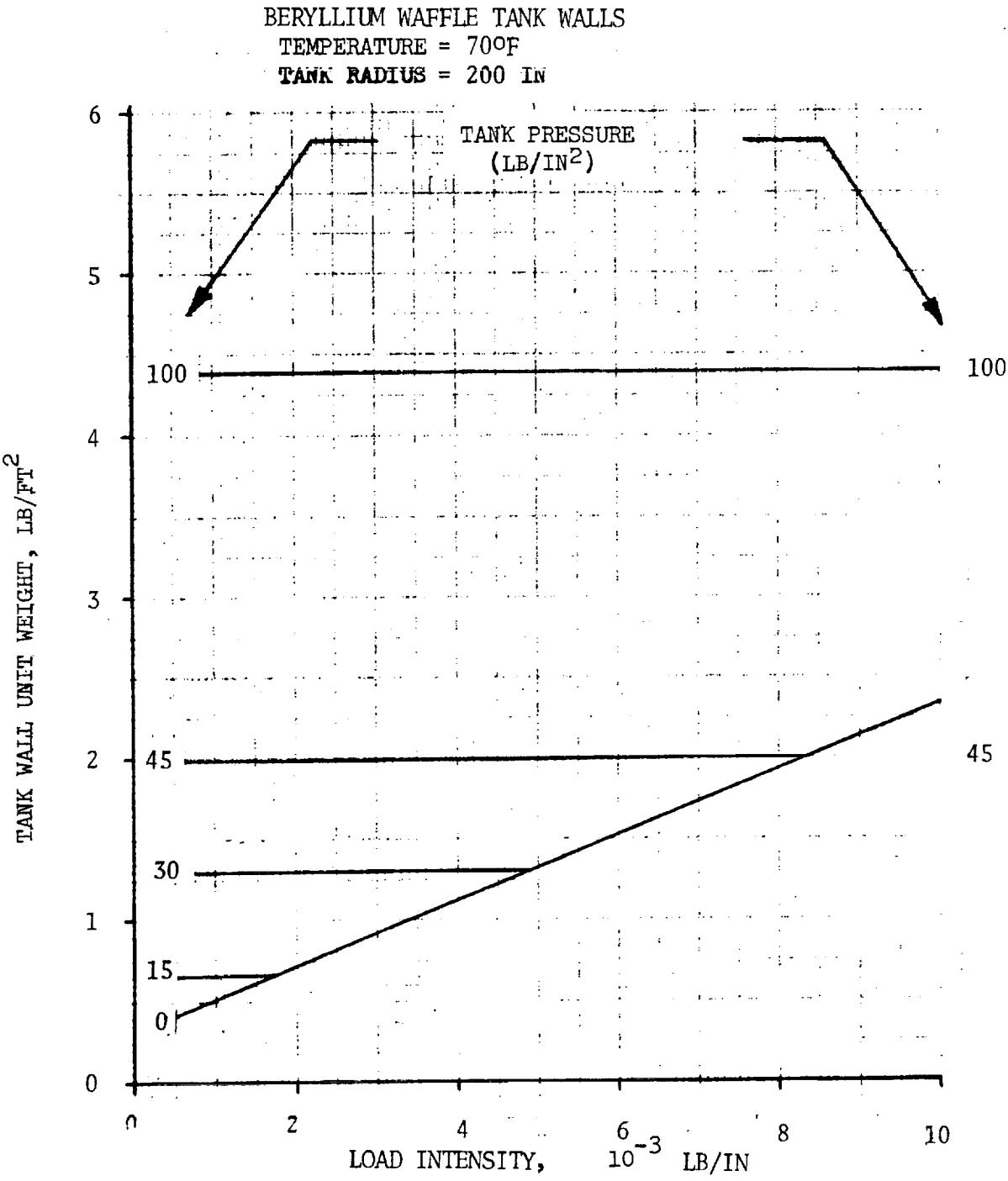

Figure A33 : Tank Wall Unit Weight for Pressurized Tanks of Beryllium Waffle Construction (R=200 in., T= 70°F)

APPENDIX B

METEOROID SHIELDING

Numerous methods have been used to describe the penetration mechanics of the meteoroid particles impacting upon quasiinfinite and finite metal targets. In the past, most investigators have chosen to relate penetration depth to the various projectile and target parameters by power expressions. (References B1 and B2). Others (References B3 and B4) have chosen to use a combination of power and logarithmic expressions.

A NASA monograph entitled "Meteoroid Damage Assessment" has a simplified expression for the penetration with an empirical coefficient K, which is determined experimentally for the particular target material.

The penetration depth for a quasiinfinite sheet is

$$P_{\infty} = K m_p^{0.352} \rho_p^{1/6} V_p^{2/3}$$

Typical values for K are 0.42 for several different aluminum alloys (Reference B6).

In the meteoroid protection analysis for a spacecraft, it is necessary to be able to compute the minimum thickness of material able to resist perforation by a given hypervelocity particle. Sufficient test data are available for this target to provide a gross understanding of the perforation process. As target thickness is reduced toward the minimum thickness that will just resist perforation (limit thickness), the projectile impact causes penetration and removal of material from the target rear surface. The amount of material removed can be substantial, the thickness in some cases being as much as 80 percent of the depth of penetration.

Early tests by Kinard (Reference B5) on aluminum targets indicated single finite sheet requirements to resist penetration were 1.5 times that of a quasiinfinite target. The NASA monograph, Reference B6 , has been used for this study to determine the single sheet requirements, and the empirical equation is

$$t_{ss} = K_1 m_p^{0.352} \rho_p^{1/6} V_p^{0.875}$$

where the coefficient K_1 is based on test results for various materials as shown in Table B1

Table B1. Single Sheet Penetration Coefficient K_1

Material	K_1	
	Visual	Pressure
2024 T3, T4 7075 T6 6061 T6	0.54	0.57
304 316	----	0.32
17-4 PH (annealed)	----	0.38
Magnesium Lithium 141-A	----	0.80
Columbium alloy CB-IZR	----	0.34

The penetration mechanics for multi-sheet concepts have not been identified in Reference B6 and it is proposed to use the discrete particle analysis of NR to define the weight estimates of advanced design concepts.

The penetration and bulge damage to the tank-shield by the impacting meteoroid debris can be predicted by the NR penetration mechanics of References B7 and B8 . In these methods the debris cloud resulting from the meteoroid and first sheet impact is modeled by an expanding sphere of bumper and projectile debris particles. The projectile debris particle mass m_{pl} is given by

$$m_{pl} = \frac{m_p}{n_p} ; \quad n_p \geq 1$$

where m_p = mass of impacting projectile (gm)

n_p = number of debris particles originating from impacting projectile

The ratio of the mass of shield material removed to the mass of the original particle (β) is

$$\beta = \frac{m_s}{m_p}$$

where m_s = mass of shield material removed as a result of shield perforation

The projectile fragmentation is given by

$$n_p = C_p \left[\rho_p \beta V_p^2 / 2(1 + \rho_p \beta / \rho_1)(1 + \beta)\right]^{\eta_p}$$

where η_p = projectile fragmentation factor based on test results

ρ_p = density of impacting particle (gm/cm^3)
ρ_1 = density of first sheet material (gm/cm^3)
V_p = velocity of impacting projectile (cm/sec)

After fragmentation, the velocity of the leading particle in the debris cloud, V_{1x} is represented by

$$V_{1x} = V_p(1 + \beta^{1/2})/(1 + \beta)$$

The discrete particles from the original projectile and bumper shield material comprise the debris cloud and their maximum penetration into the second shielding sheet, P_2, is

$$P_2 = m_p^{\gamma} R_p \left[V_p^{2/3}(1 + \cos S) - V_{1x}^{2/3}(\cos S)/n_p^{\gamma}\right]$$

$$- t_1 C_1 (1 + \cos S), \quad (h \leq \bar{h})$$

where

$$S = \pi(h + \bar{h})/2\bar{h}$$

$$R_p = 8.15 \times 10^{-4} \rho_p^{(1/2-\gamma)} / H_2^{1/4} \rho_2^{1/6}$$

$$C_1 = (H_1/H_2)^{1/4} (\rho_1/\rho_2)^{1/6}$$

where H_1 H_2 = Brinell hardness of first and second sheets.
t_1 t_2 = Thickness of first and second sheets (cm).
ρ_1 ρ_2 = Density of first and second sheets (gm/cm^3).
h = Actual spacing between the bumper and rear sheet.
$\bar{h}$ = Maximum spacing, h, where any additional spacing does not contribute to the efficiency of the shielding.
γ = Penetration empirical exponent based on available test data.

Treatment of penetration by first sheet debris is also incorporated in the method.

The second sheet or tank wall can also fail by bulge and tear. In testing and in theory, this is found to become the dominant mode of failure when n_p is greater than 600 for the single bumper case. The above methods have been extended to treat this form of damage as well, by consideration of the energy imparted to the rear sheet in the form of kinetic energy, and its dissipation in metal deformation. The diameter of the bulge D_b formed is:

$$D_b = h\,\beta^{1/2}\,C_{bd}$$

where C_{bd} = the bulge diameter coefficient

The bulge depth h_b is

$$h_b = \frac{C_{dis} D_b}{2}\left\{\left[1/(1 - 10.18\,E_{bc}/\eta t_2\,F_{ty} D_b^2)\right]^2 - 1\right\}^{1/2}$$

C_{dis} = bulge depth coefficient

F_{ty} = second sheet tensile yield stress (lb/in^2)

where the energy imparted to the bulge material by the debris cloud, E_{bc} (ergs) is based on the mass of the bulge material, m_b and is given by

$$E_{bc} = 2m_b\left[V_p/(1 + \beta_{c2})\right]^2\left[\left(1 + \frac{1}{2}\beta^{1/2}\right)/(1 + \beta)\right]^2$$

β_{c2} = Ratio of the maximum of the bulge material to the mass of the debris particles in the front half of the debris cloud

The strain in the bulge material is

$$\epsilon = \left(1 + 4\,(h_b/D_b)^2\right)^{1/2} - 1,\ \text{in./in.}$$

Failure strain, ϵ_f, in the bulge mode occurs when $\epsilon = \epsilon_f$

The coefficients C_{dis}, C_{bd}, C_p, n_p, and γ are empirical constants. Values have been obtained for each by correlation with tests performed by NR and others. Details are presented in References B7 and B8

The performance of the single bumper can be improved by considering the effective stopping power of the thermal insulation which can significantly reduce the velocity of the smaller particles before they impact the propellant tank. Figures B16 through B18 include cometary meteoroids and aluminum shielding having an insulation of 2 lb/ft^3 and show the effects of varying the insulation thickness from 1 inch to 4 inches. The relative efficiencies of insulation density are presented in Figures B19 and B20, various materials are shown in Figure B21, and asteroidal particles illustrated in Figures B22 and B23.

Insulation acts as a drag barrier which slows down the impacting particle and results in a shallower penetration in the rear sheet. Since the front bumper is a thin sheet which disintegrates the particle, the velocity of the cloud can be considered to be approximately the original particle velocity. Reference B8 and tests at NR/SD have verified the proposed approach for estimating the efficiency of the insulation shielding concept. Reference B8 states that the final velocity, V_f, of the particle hitting the rear sheet is

$$V_f = \left\{ \left(V_P^2 + \frac{2\beta}{C_D \rho_{ins}} \right) \mathrm{EXP} \left[(X_o+\tau)^2 \left(\frac{1-C_F}{2h} \right) + C_F \tau - X_o^2 \left(\frac{1-C_F}{2h} \right) \right] \left[\frac{C_D A_P \rho_{ins}}{M_P} \right] - \frac{2\beta}{C_D \rho_{ins}} \right\}^{\frac{1}{2}} \quad \text{(B-1)}$$

where C_D = the effective drag coefficient of the insulation

τ = insulation thickness (cm)

X_o = shield spacing between bumper and insulation (cm)

h = overall spacing of shield (cm)

β = mass ratio of particles

C_F = test correlation coefficients

Since weight-scaling laws are desired, the expression for final velocity can be drastically simplified by considering the relative magnitude of the individual terms.

In Equation (B-1) the second term $\frac{2\beta}{C_D \rho_{ins}}$ can be neglected when compared to the first term and also $V_P^2 \gg 2\beta \; C_D \rho_{ins}$

Therefore,

$$\frac{V_f}{V_P} \approx \mathrm{EXP} \left[\frac{(2X_o\tau + \tau^2)}{2h} (1-C_F) + C_F \tau \right] \frac{1}{2} \left[\frac{C_D \; A_p \; ins}{M_P} \right]$$

For the design arrangements considered, the front spacing (X_o) is approximately equal to the overall dimension (h). Treating the particle as a sphere, the velocity ratio is further reduced to

$$\frac{V_f}{V_p} = EXP\left[\frac{3C_D \tau \rho ins}{4\, d_p}\right]$$

The allowable penetration depth of the rear sheet without insulation is 25 percent for pressurized tank walls.

$$P_\infty = \left(\frac{W_M - W_B}{4\rho}\right)$$

The penetration depth (P_∞) for a single sheet is a function of the impacting velocity

$$P_\infty = f\ (V^{2/3})$$

Shielding designs containing insulation help reduce the particles impacting velocity and hence the penetration depth; therefore, the ratio of rear sheet requirements is as follows.

$$\frac{W_{2_{ins}}}{W_2} = EXP\left(\frac{1}{\left[\frac{A\tau\ \rho ins}{d_p}\right]}\right)$$

Where A is an adjustment coefficient derived from the unit weight data requirements for meteoroid shielding. Equation B-2 shows that the important term is the density thickness product (i.e., a design with 5 cm of 16 kg/m^2 insulation will be similar to 2.5 cm of 32 kg/m^3 insulation).

From the data of Figures B16 through B23 the insulation effects can be accounted for by the following scaling equation

$$W_M = \frac{K_1 d_p^{\alpha} V_p^{\beta}}{EXP(14.9\rho\tau/d_p)} + W_B \quad ; \text{Kg/m}^2$$

where W_B = Maximum $(K_2 d, K_3)$

ρ = insulation thickness (cm)

τ = insulation density (gm/cm)

The empirical coefficient K_1, K_2 and K_3 are obtained from the shielding unit weight data. Shielding weight data have been provided for a spectrum of design conditions and concepts. The weight data are shown for a range of particle diameters and velocity for both pressurized tankage and unpressurized shells for the following concepts and materials.

Concepts
- (a) Single sheet
- (b) Single bumper
- (c) Dual bumper

Material
- (a) Aluminum
- (b) Titanium
- (c) Glass epoxy
- (d) High performance insulation

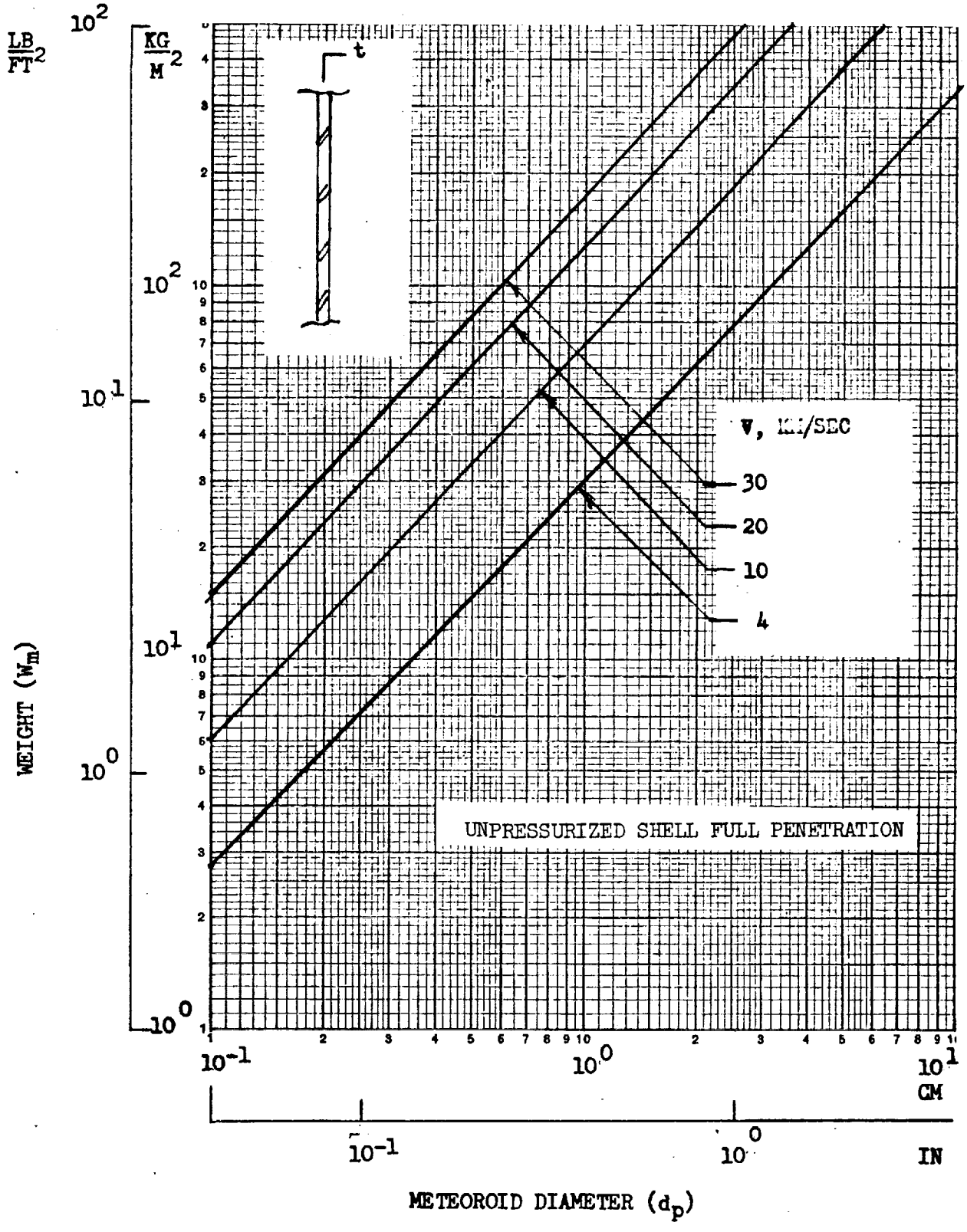

Figure B-1. Single Sheet Protection Weight — Cometary Meteoroids — Aluminum Material

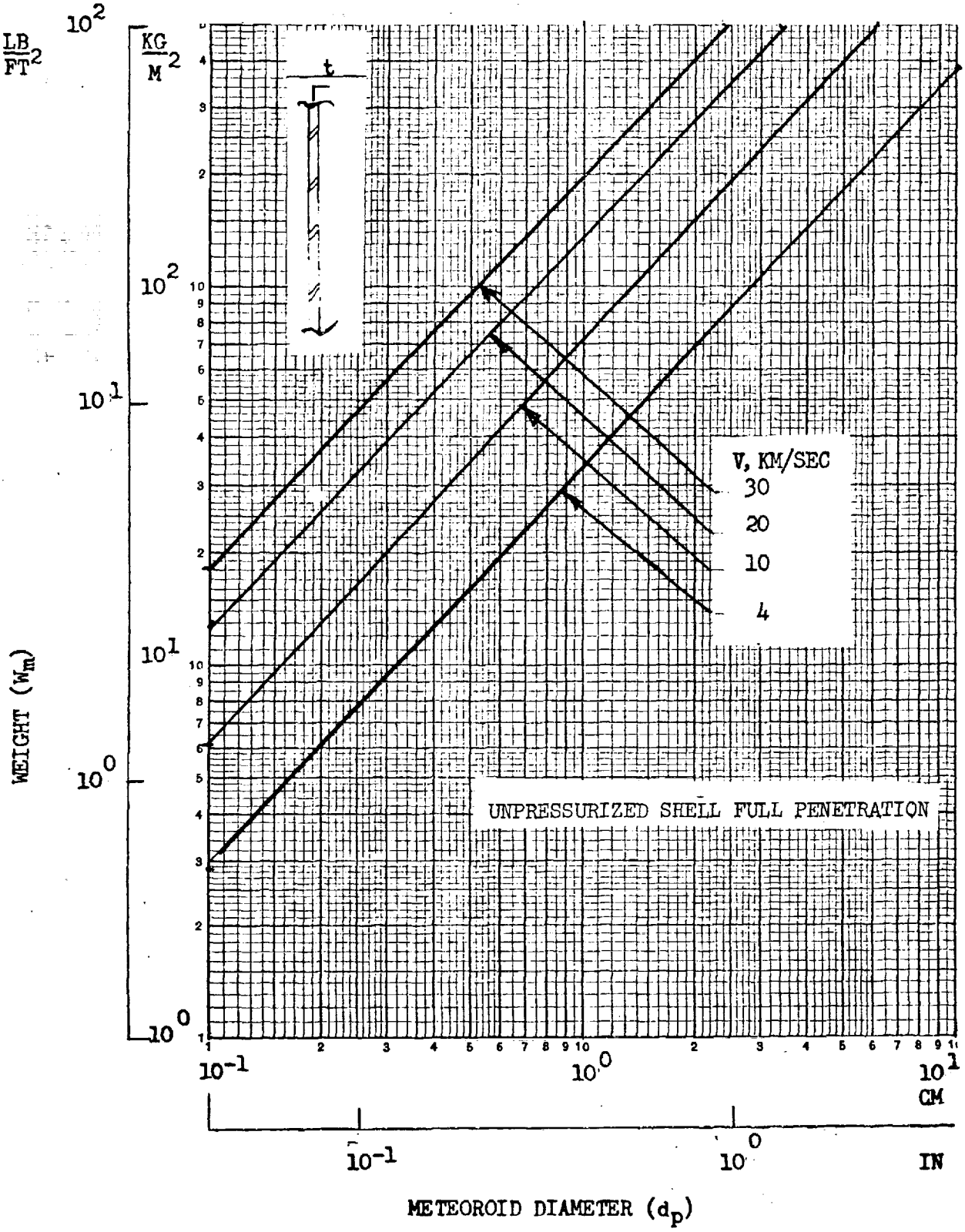

Figure B-2. Single Sheet Protection Weight — Cometary Meteoroids — Titanium

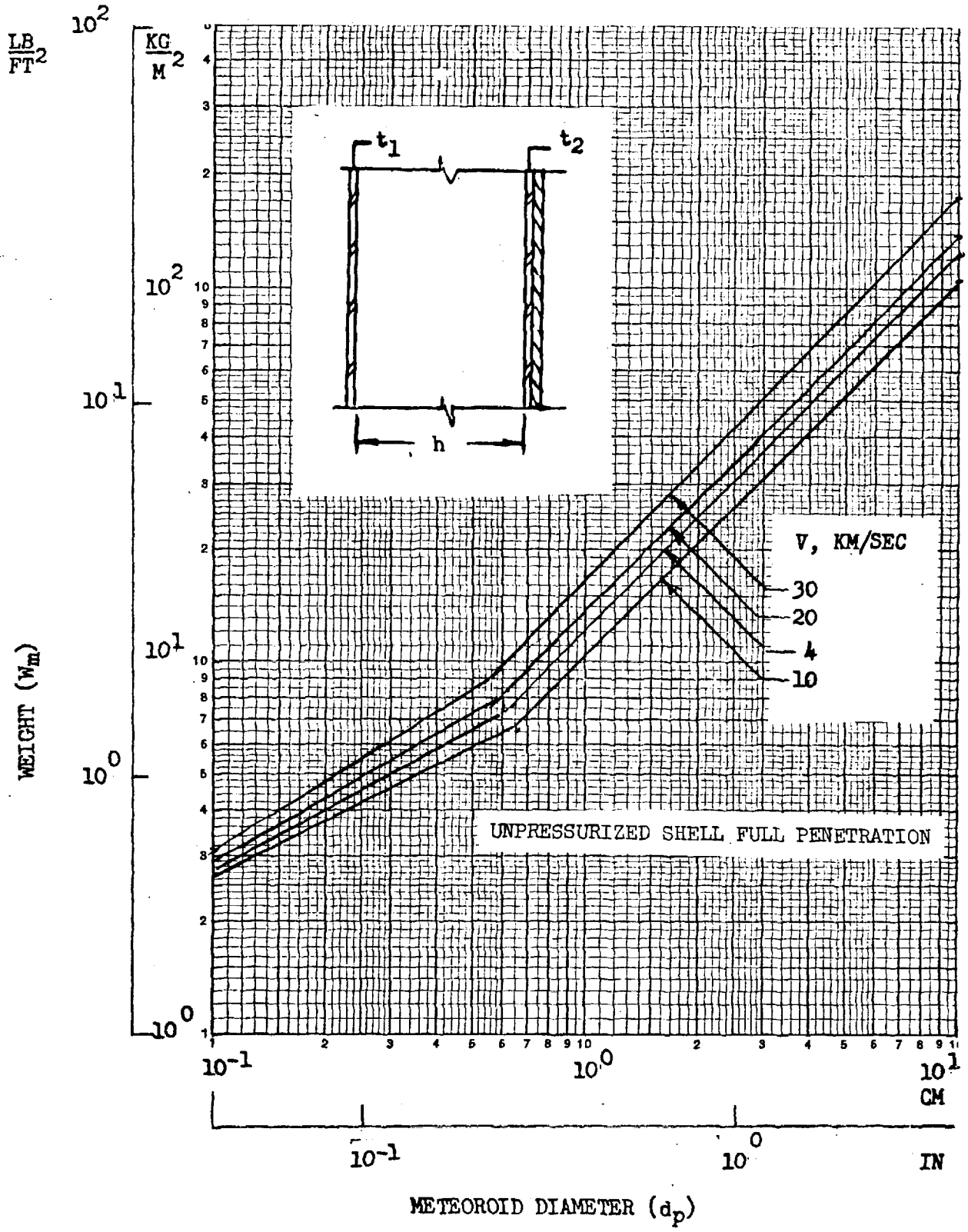

Figure B-3. Single Bumper Protection Weight – Cometary Meteoroids – Aluminum Material

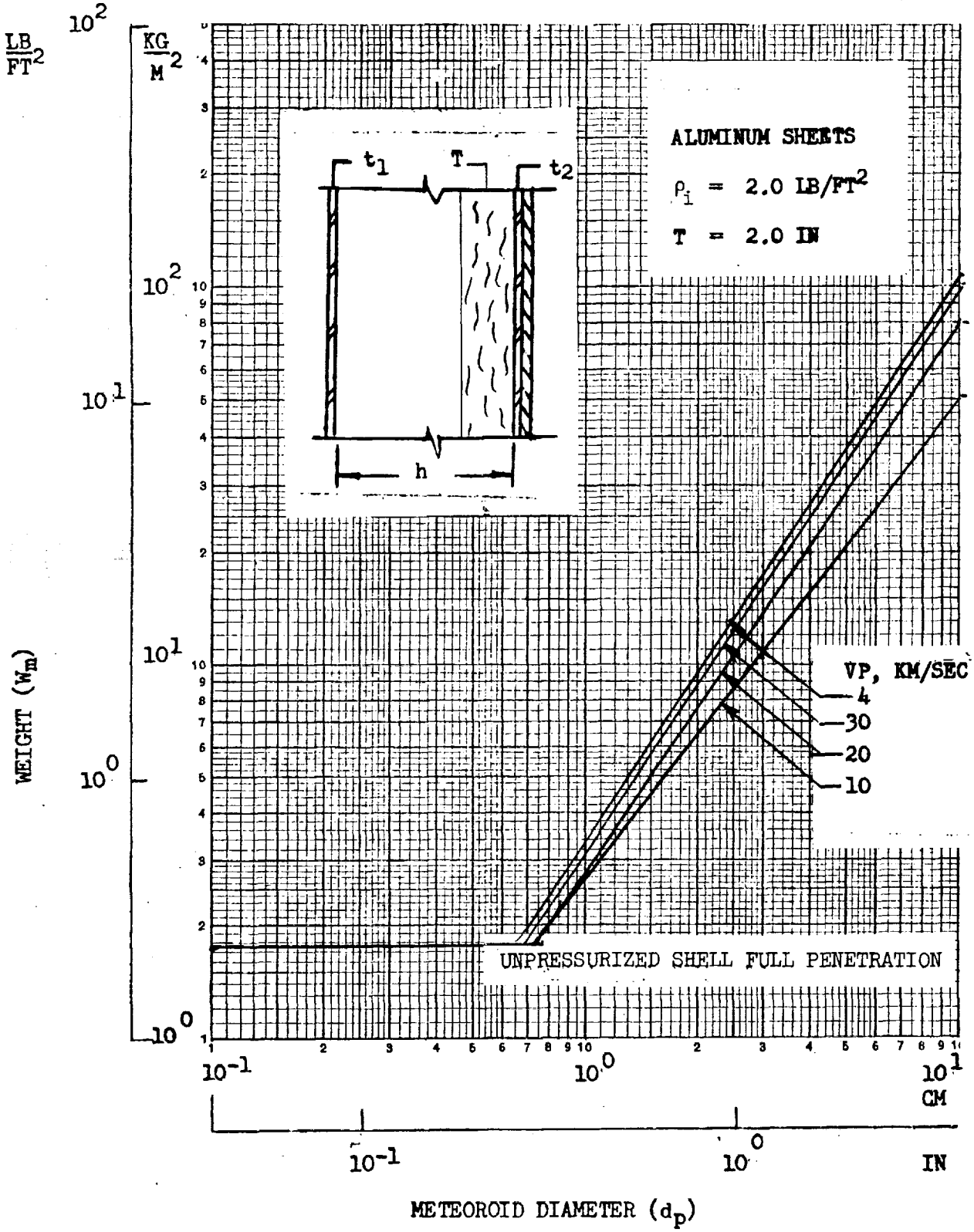

Figure B-4. Single Bumper Protection Weight — Asteroidal Meteoroids — Aluminum Sheets with Insulation

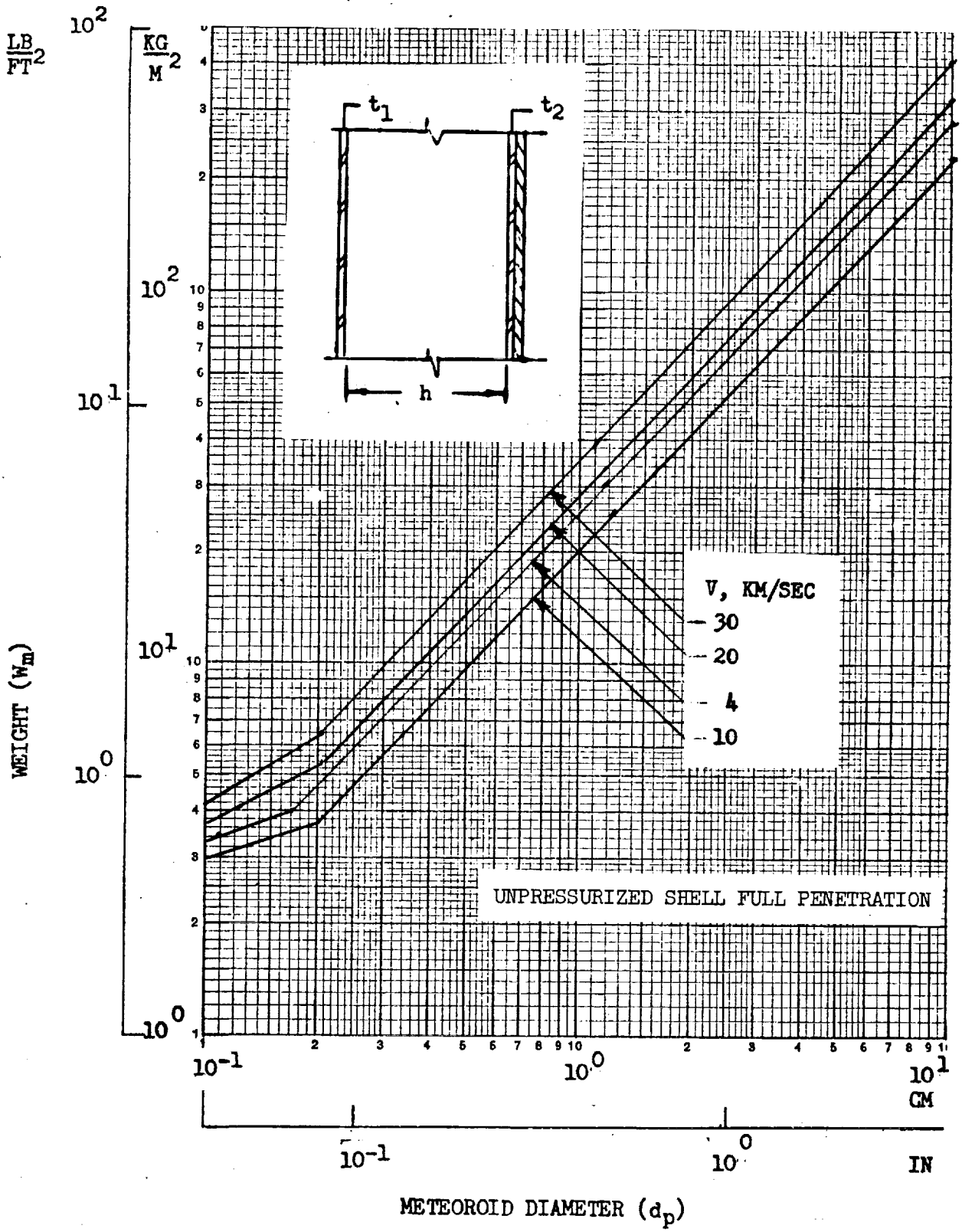

Figure B-5. Single Bumper Protection Weight — Asteroidal Meteoroids — Aluminum Material

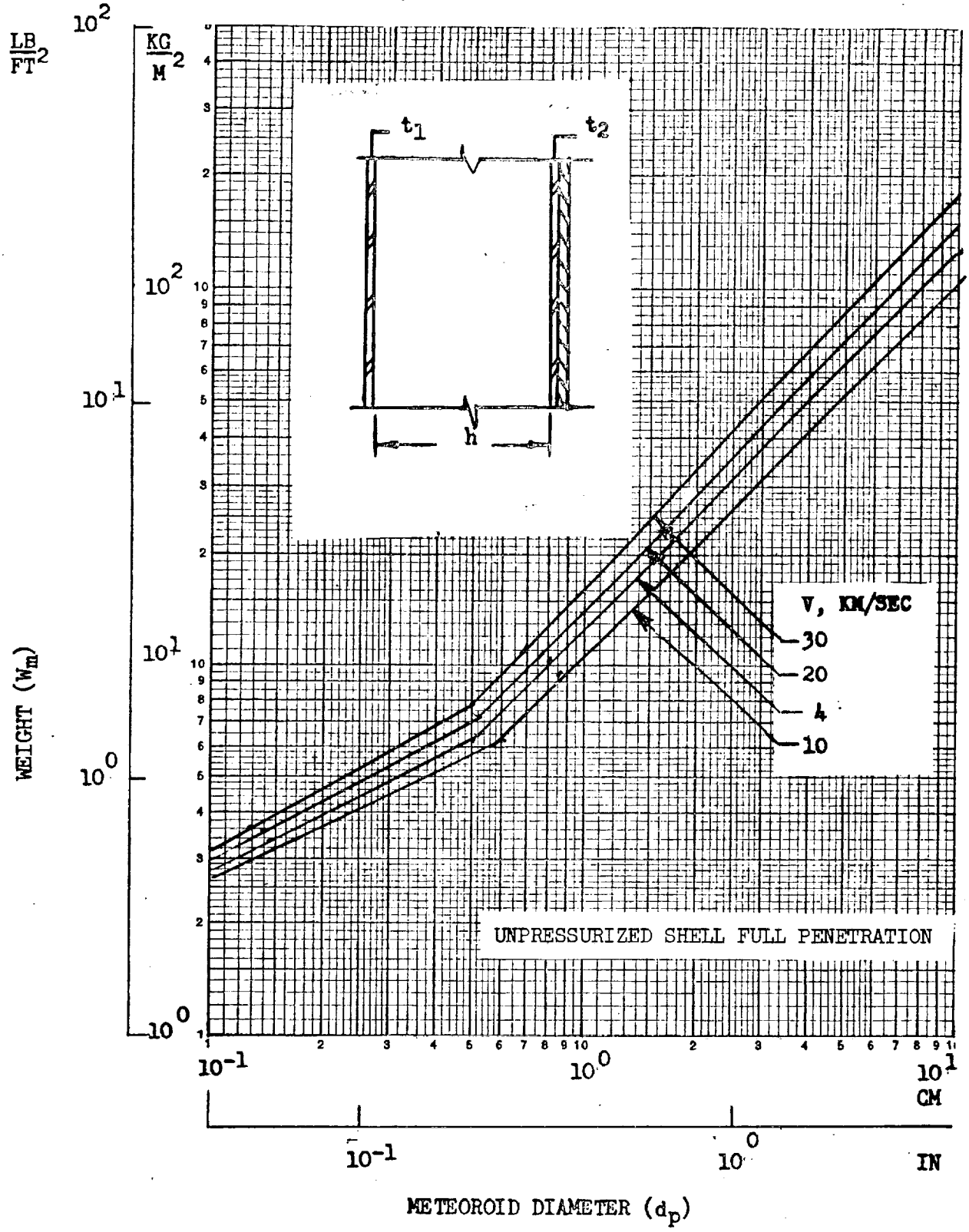

Figure B-6. Single Bumper Protection Weight — Cometary Meteoroids — Titanium Material

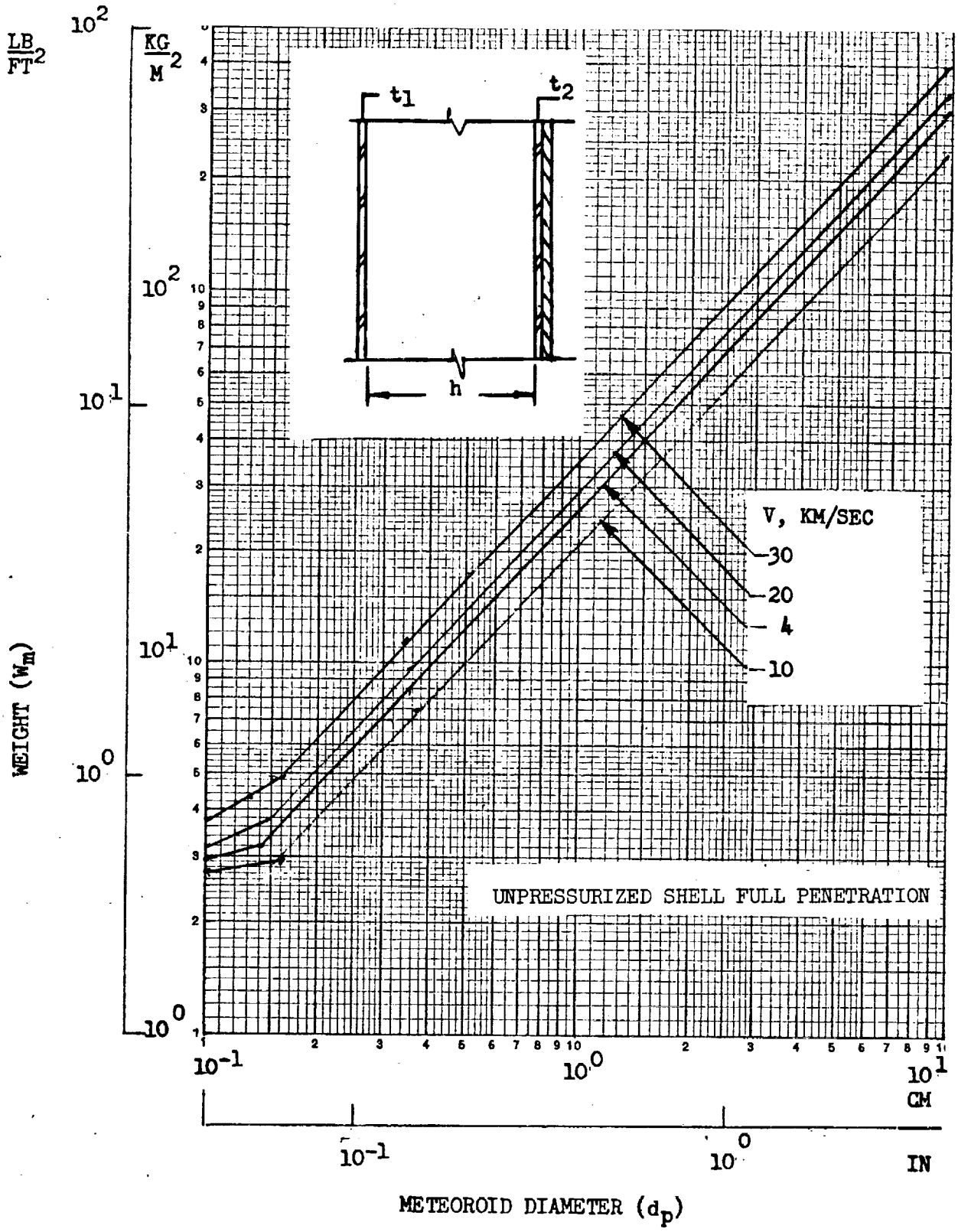

Figure B-7. Single Bumper Protection Weight — Asteroidal Meteoroids — Titanium Material

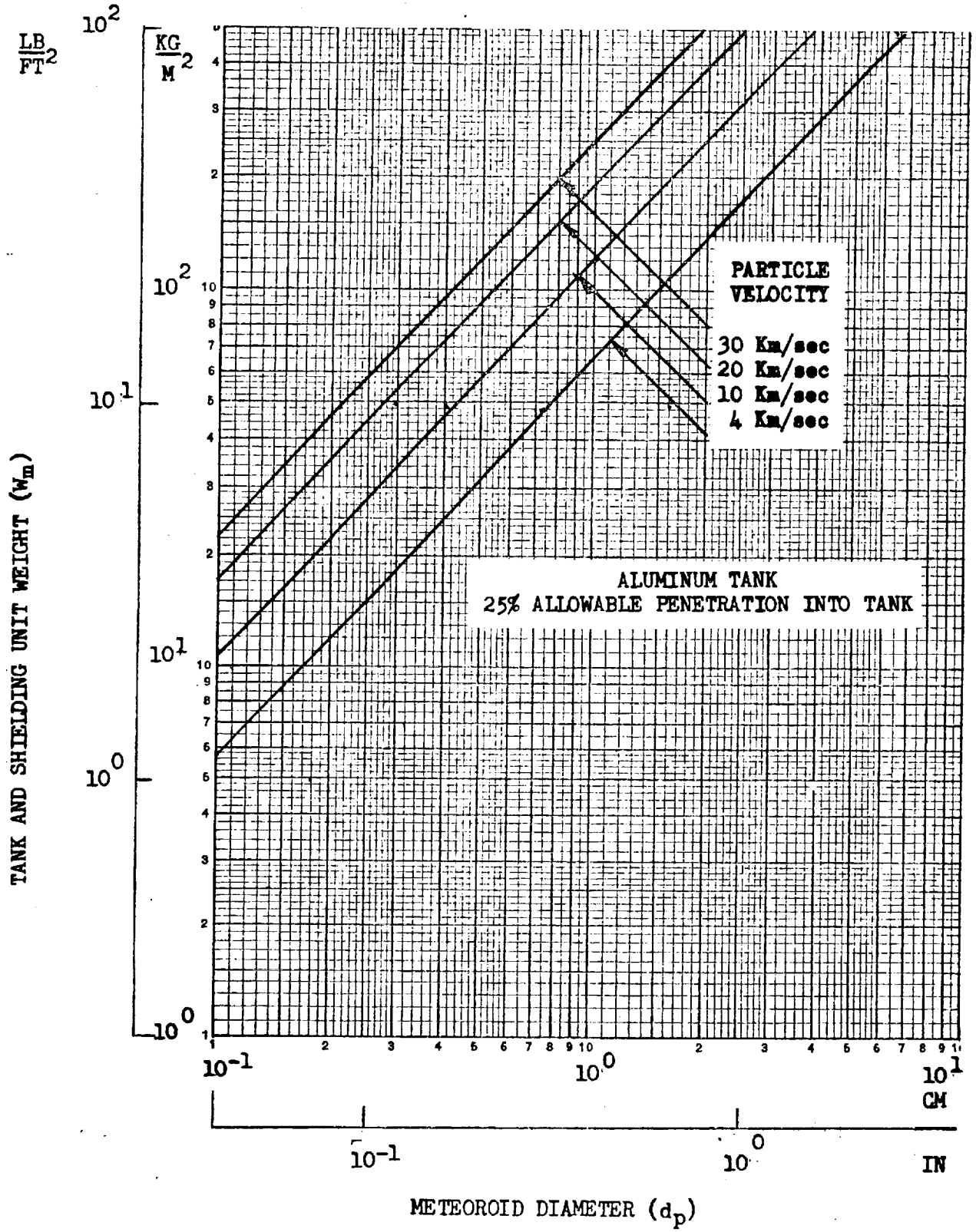

Figure B-8. Single Sheet Protection Weight - Cometary Meteoroids - Aluminum Material

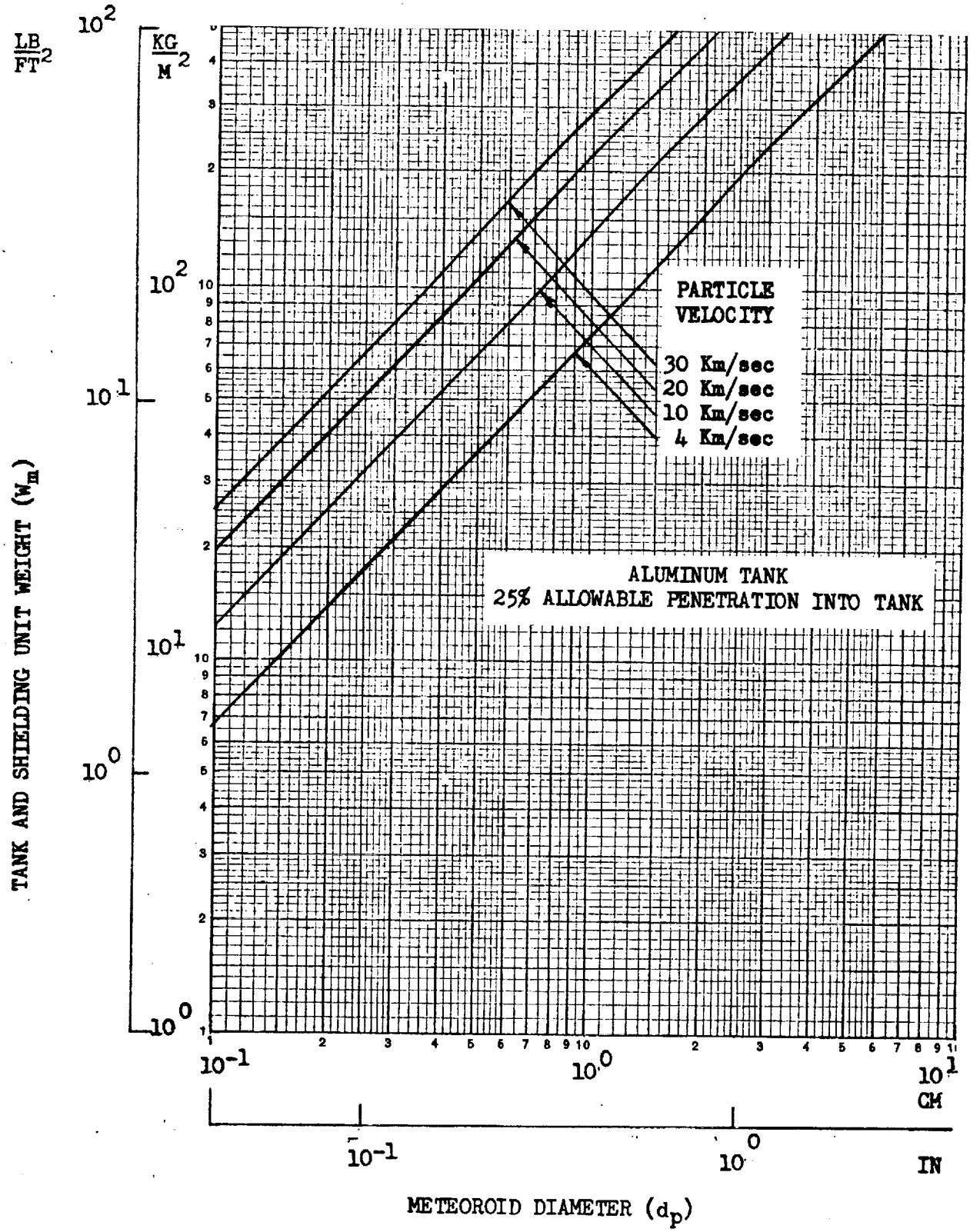

Figure B-9. **Single Sheet Protection Weight - Cometary Meteoroids - Titanium Material**

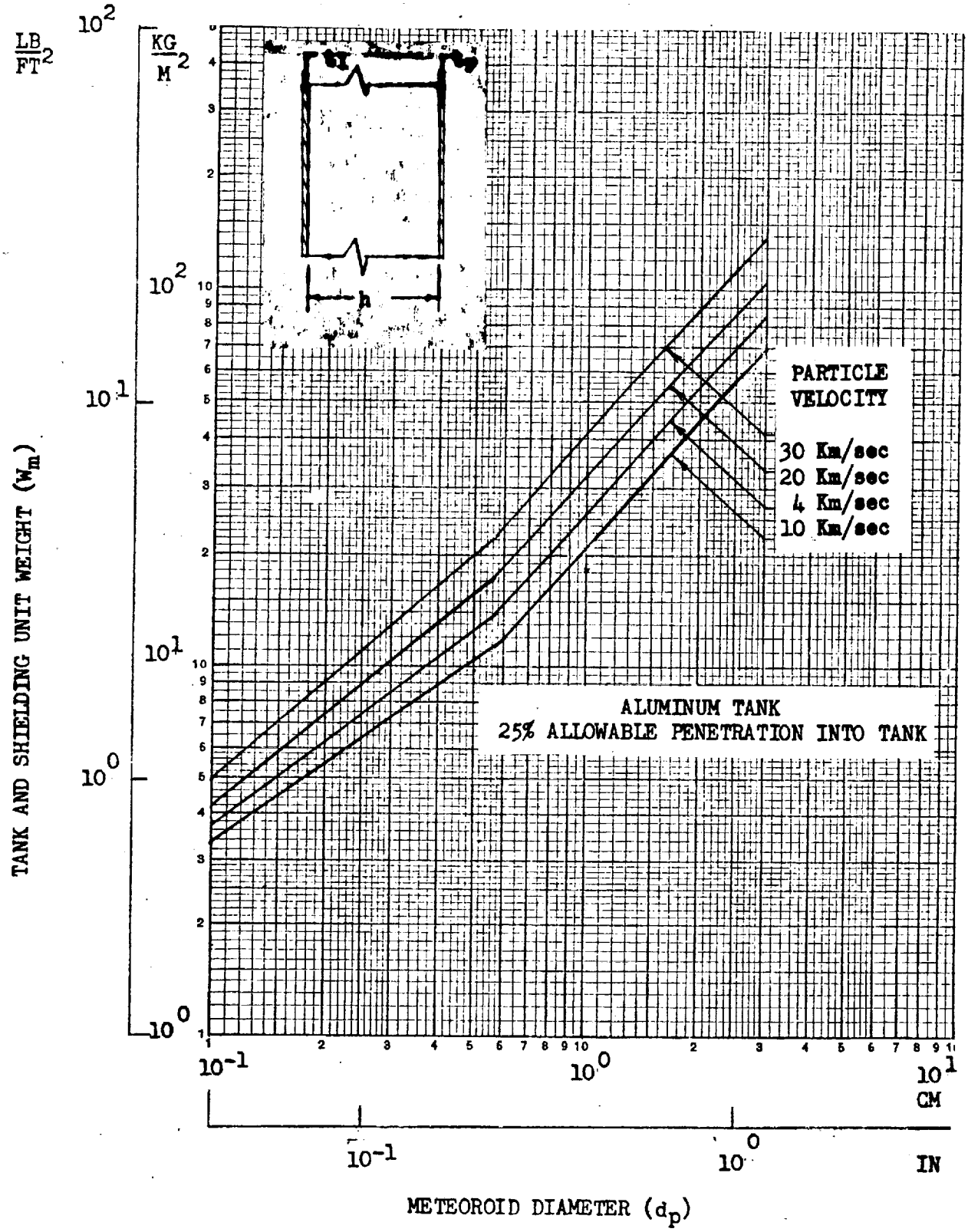

Figure B-10. **Single Bumper Protection Weight - Cometary Meteoroids - Aluminum Material - Zero Insulation**

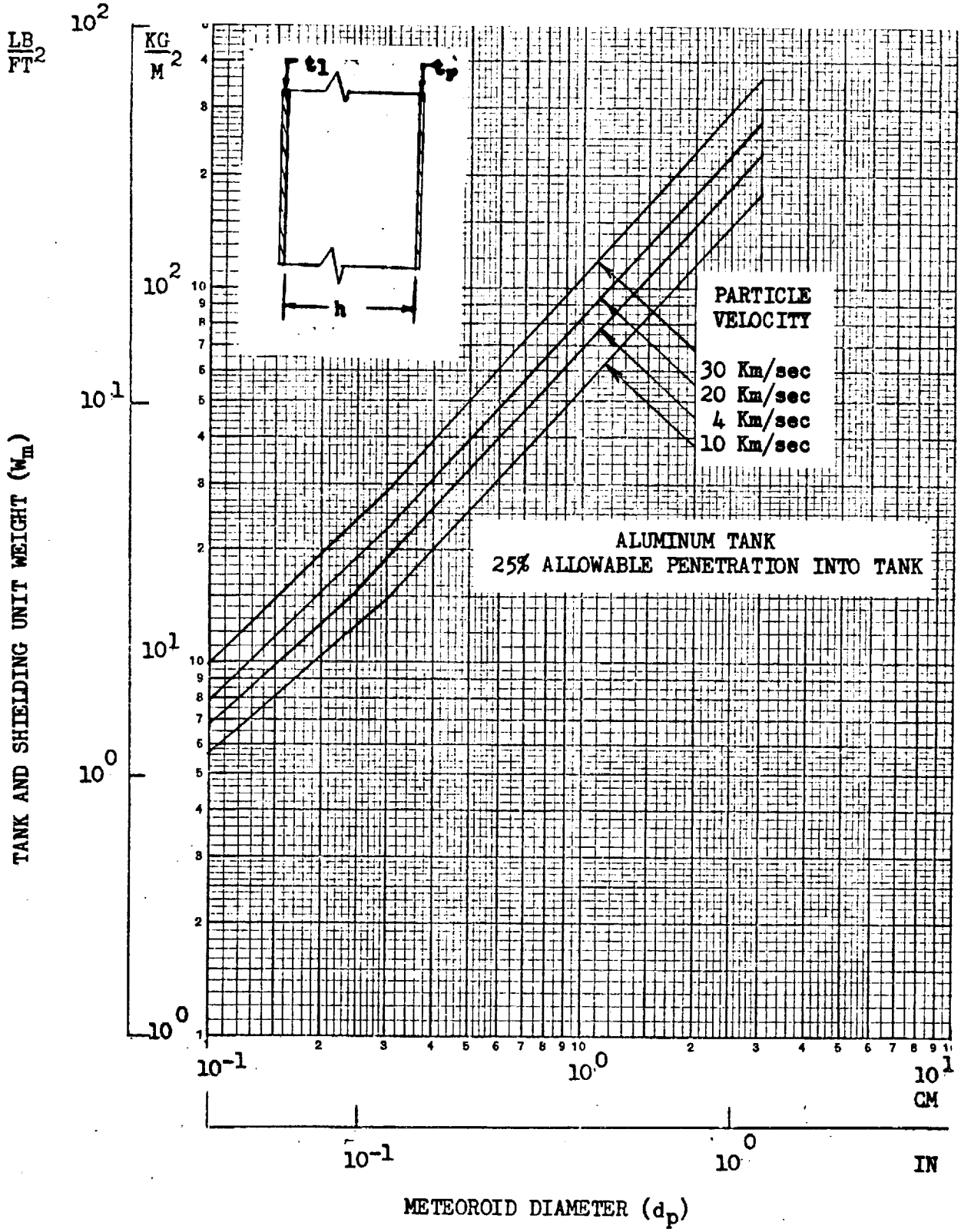

Figure B-11. Single Bumper Protection Weight - Asteroidal Meteoroids - Aluminum Material - Zero Insulation

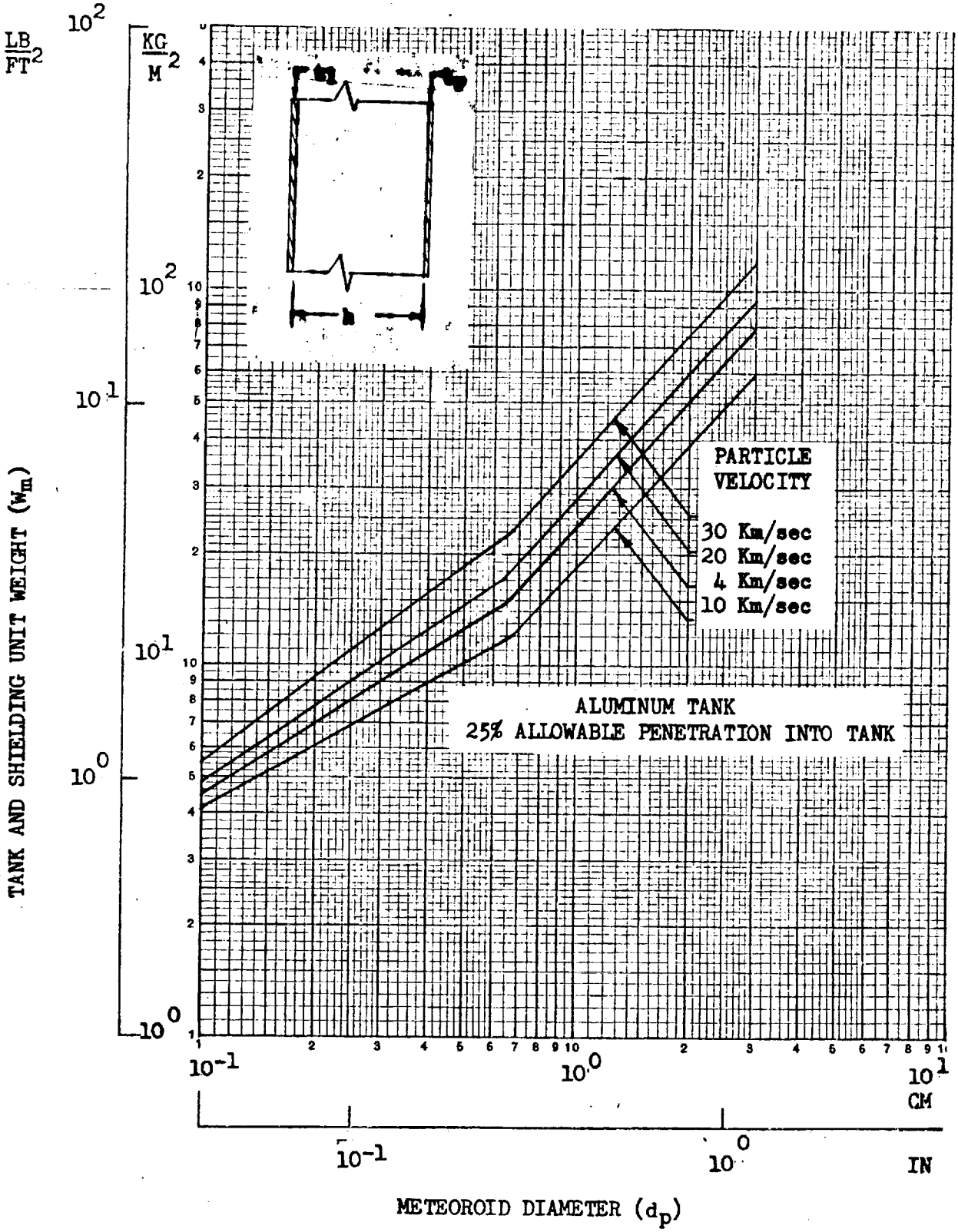

Figure B-12. **Single Bumper Protection Weight - Cometary Meteoroids - Titanium Material - Zero Insulation**

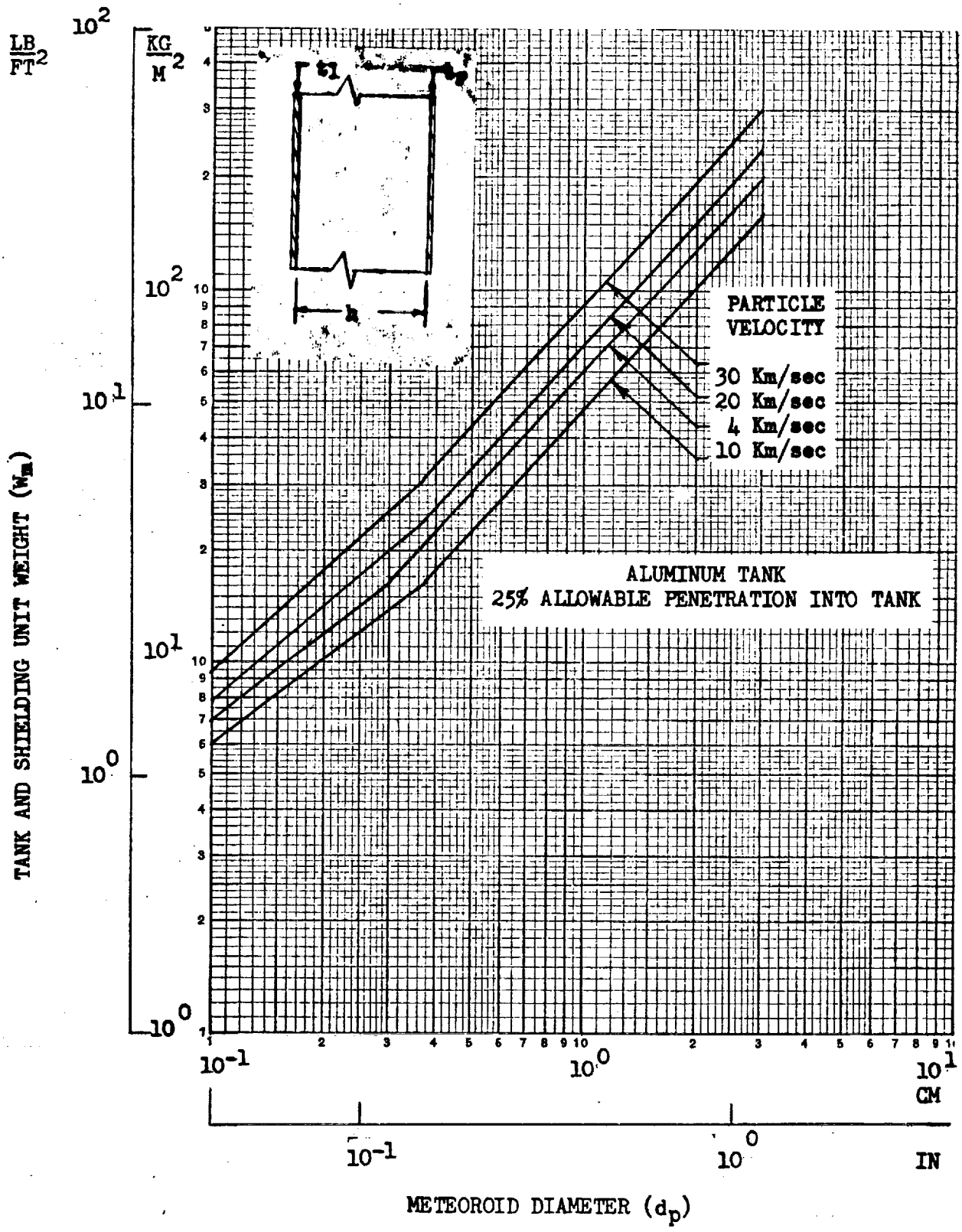

Figure B-13. **Single Bumper Protection Weight - Asteroidal Meteoroids - Titanium Material Zero Insulation**

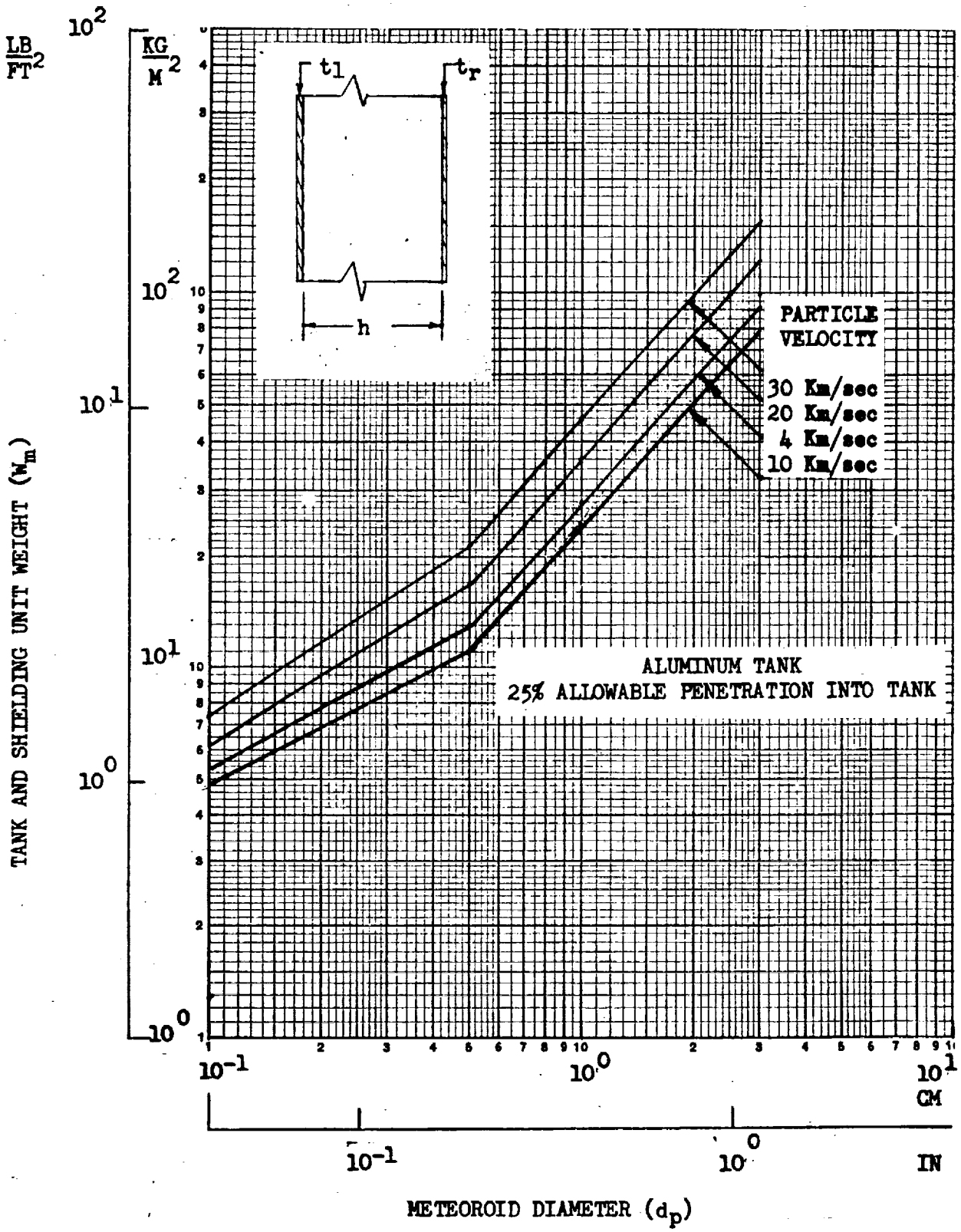

Figure B-14. Single Bumper Meteoroid Protection - Cometary Meteoroids - Glass Epoxy Material - Zero Insulation

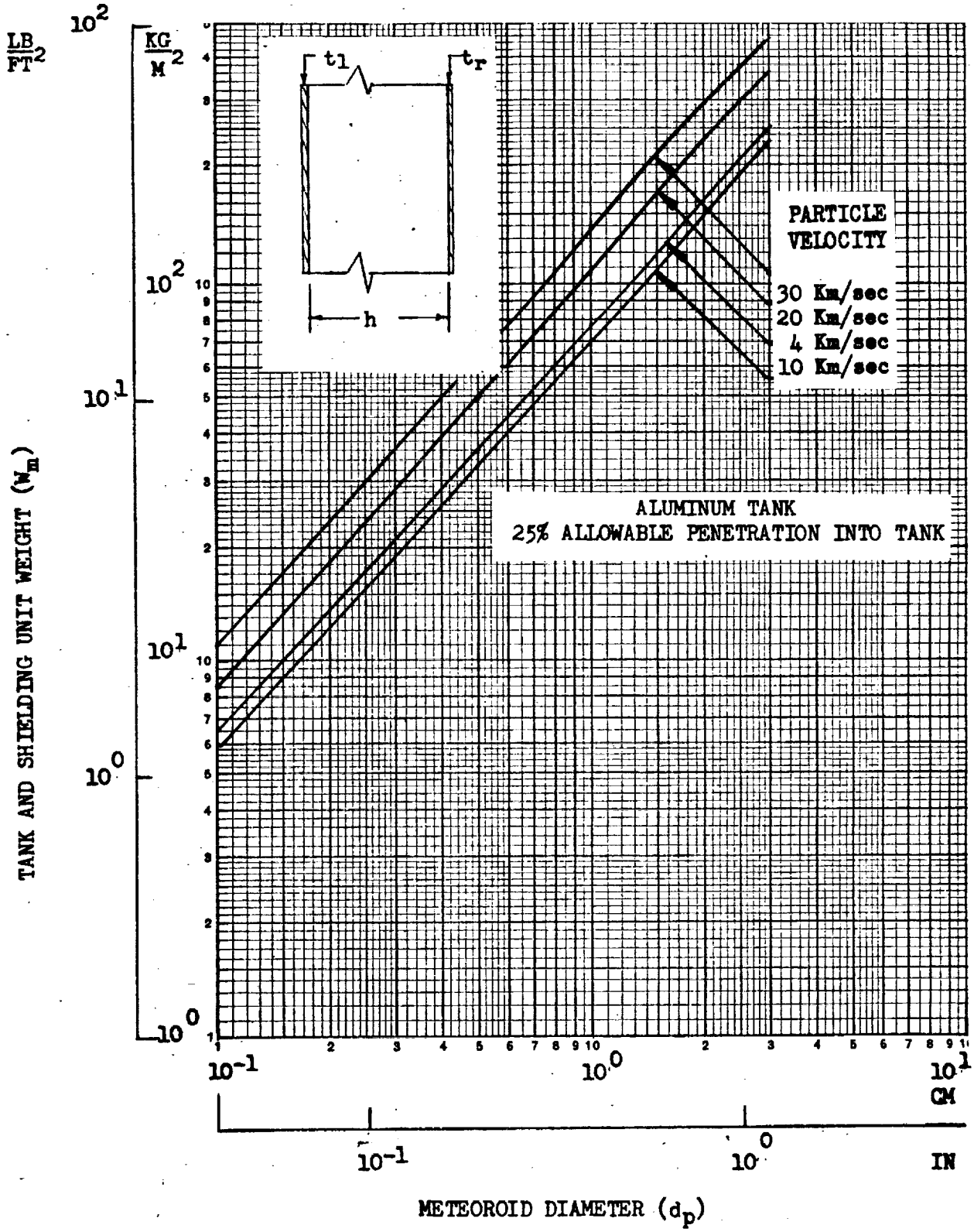

Figure B-15. Single Bumper Meteoroid Protection - Asteroidal Meteoroids - Glass Epoxy Material - Zero Insulation

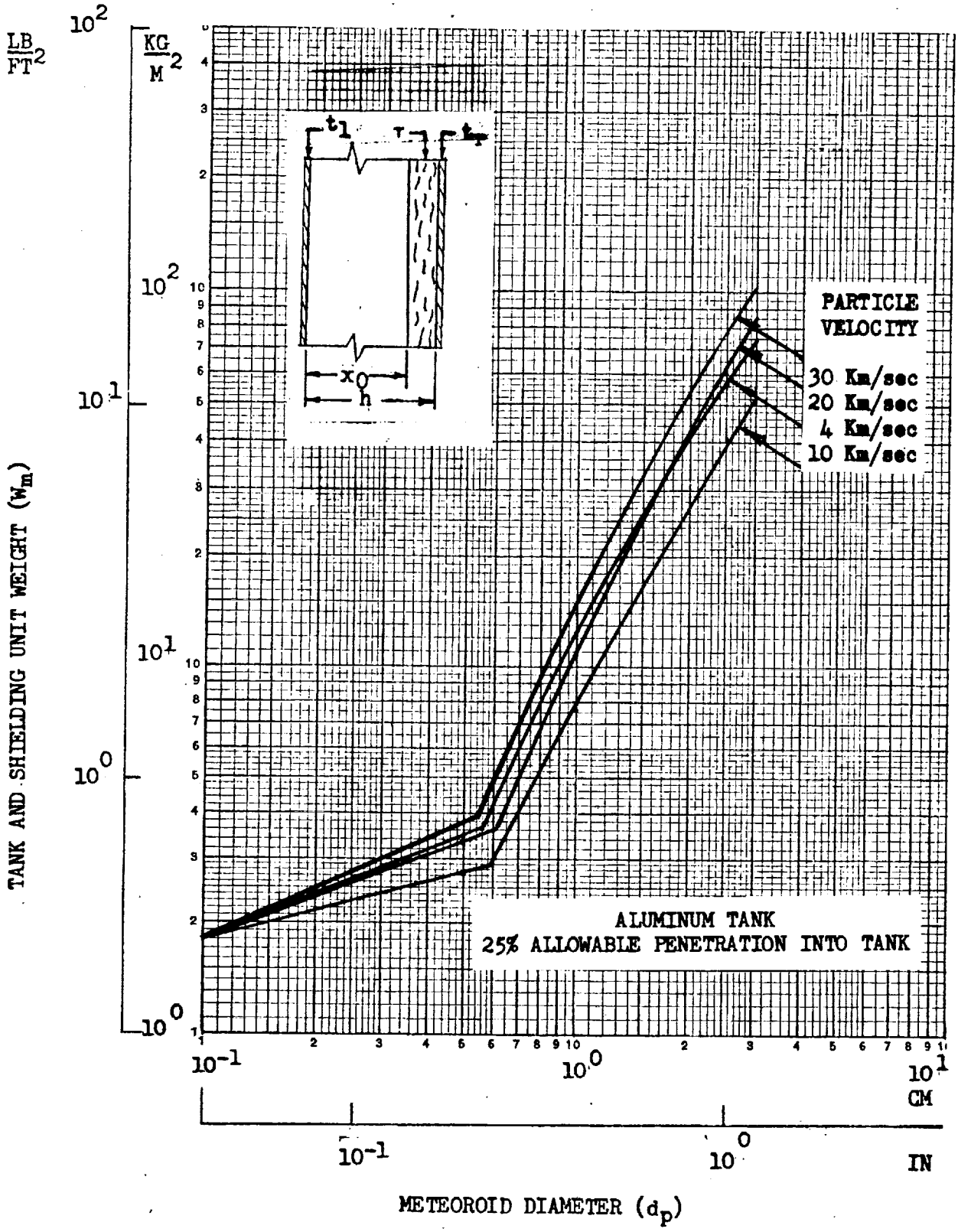

Figure B-16. Single Bumper Protection Weight - Cometary Meteoroids - Aluminum Material - 1 Inch/2lb/ft^3 Insulation

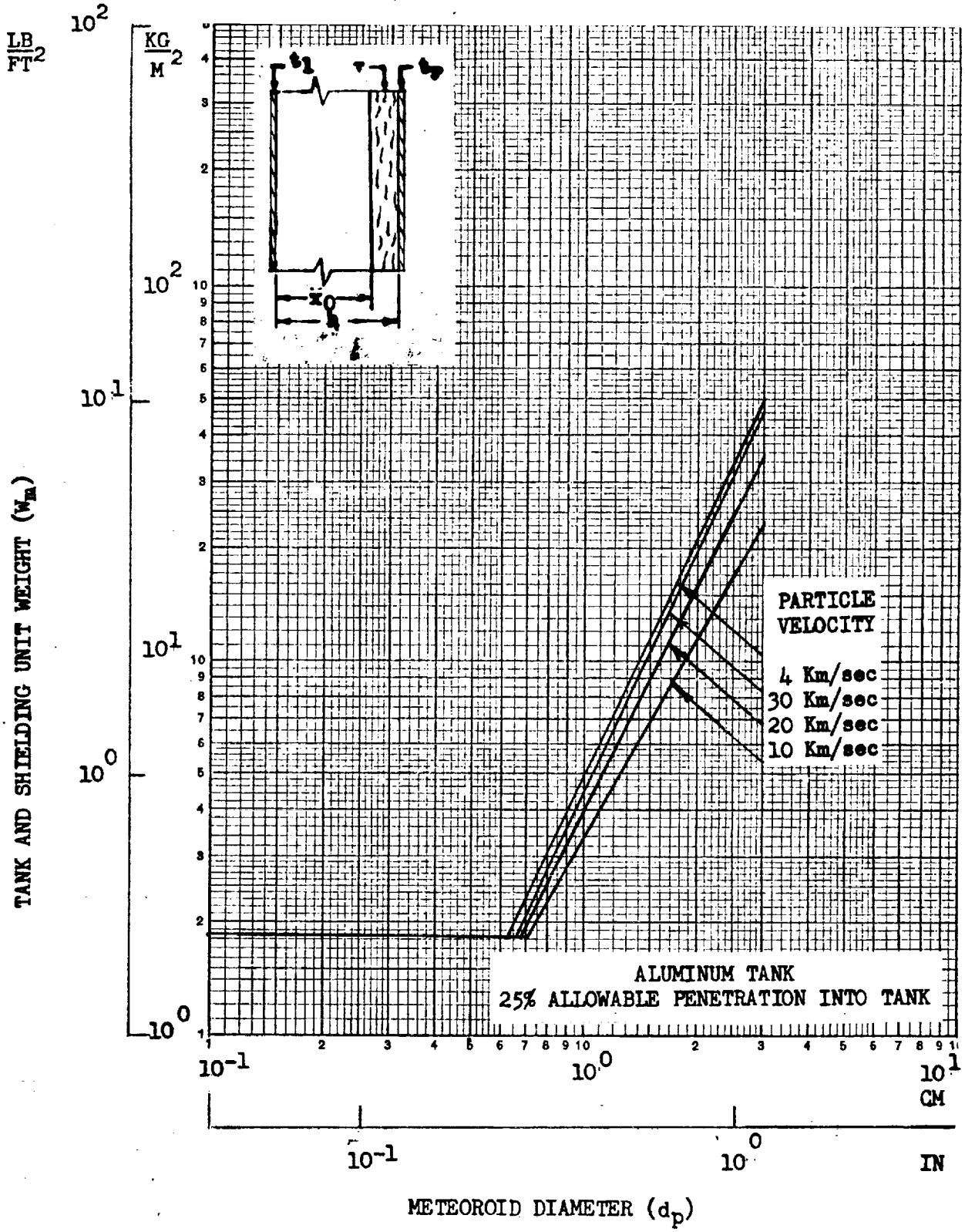

Figure B-17. Single Bumper Protection Weight - Cometary Meteoroids - Aluminum Material - 2 Inch/2lb/ft^3 Insulation

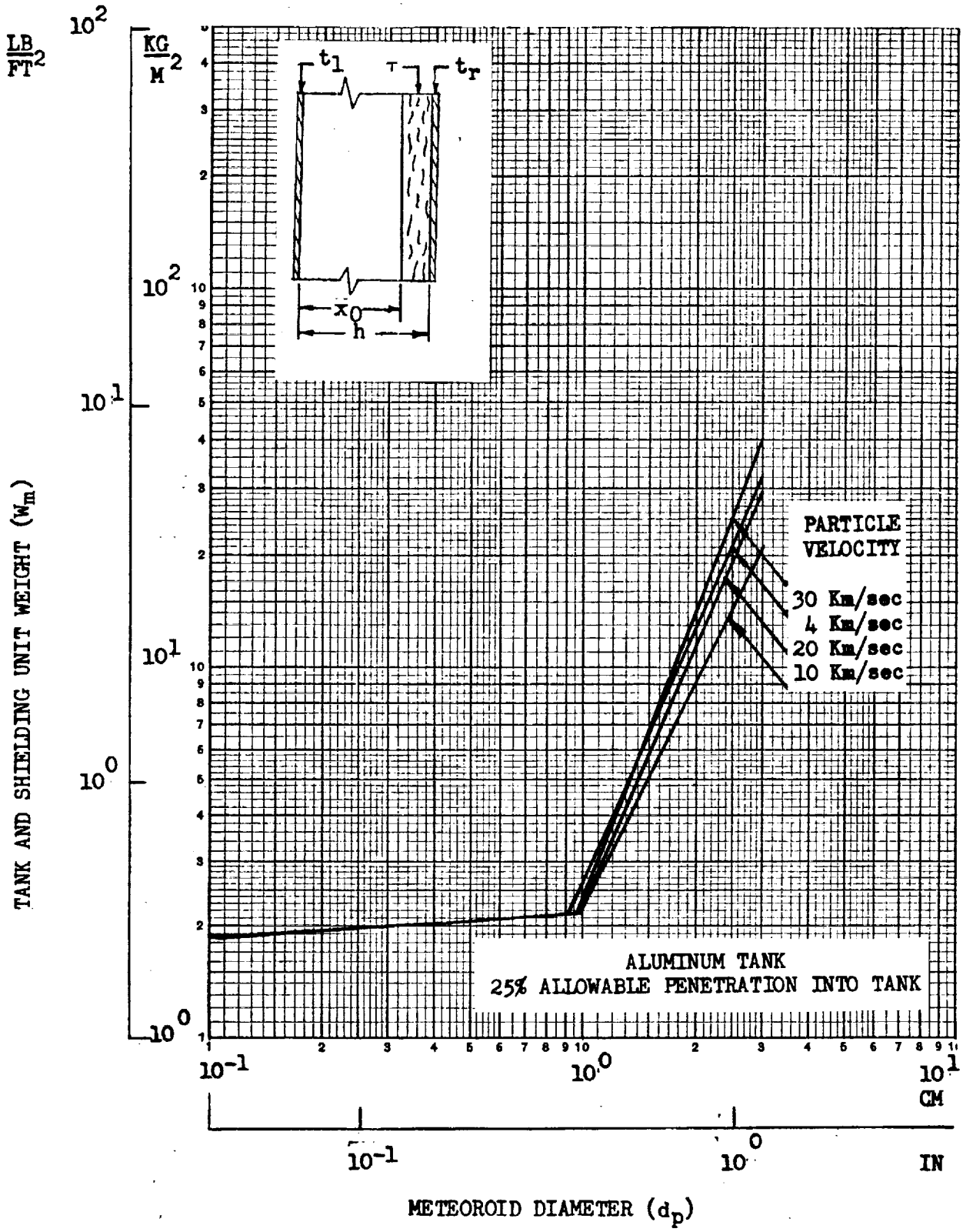

Figure B-18. Single Bumper Protection Weight - Cometary Meteoroids - Aluminum Material - 4 Inch/2lb/ft^3 Insulation

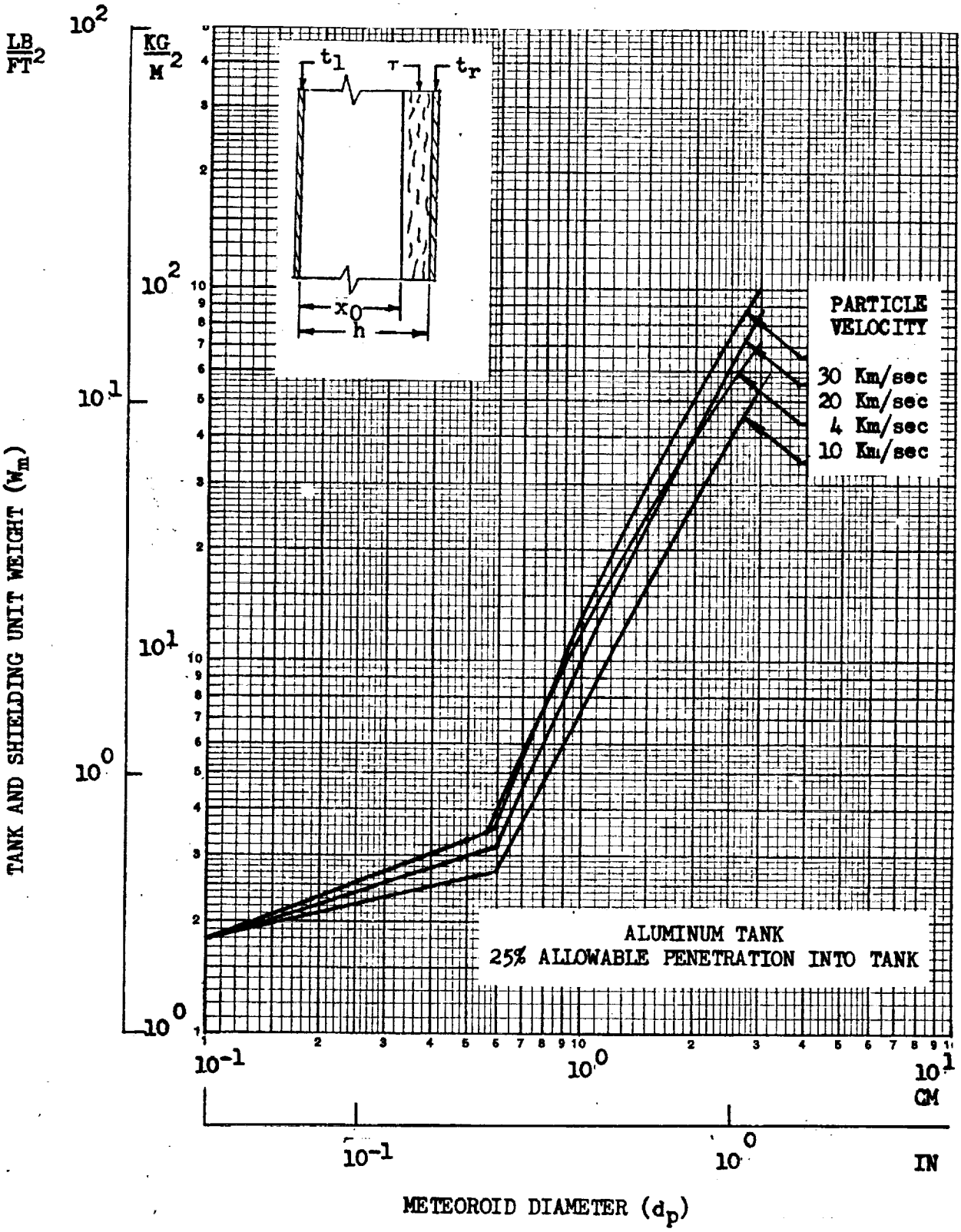

Figure B-19. Single Bumper Protection Weight - Cometary Meteoroids - Aluminum Material - 2 Inch/11b/ft^3 Insulation

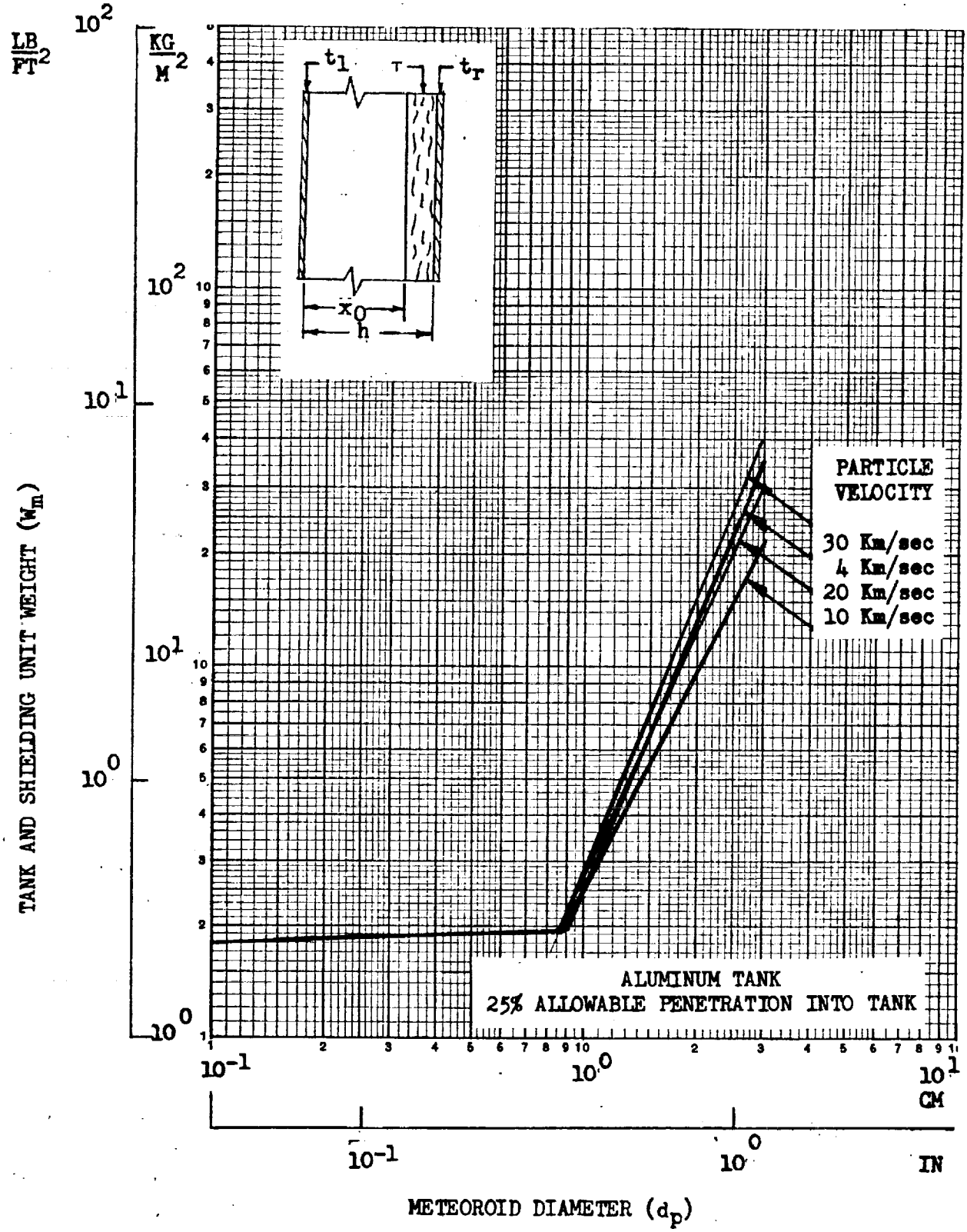

Figure B-20. Single Bumper Protection Weight - Cometary Meteoroids - Aluminum Material - 2 Inch/4lb/ft^3 Insulation

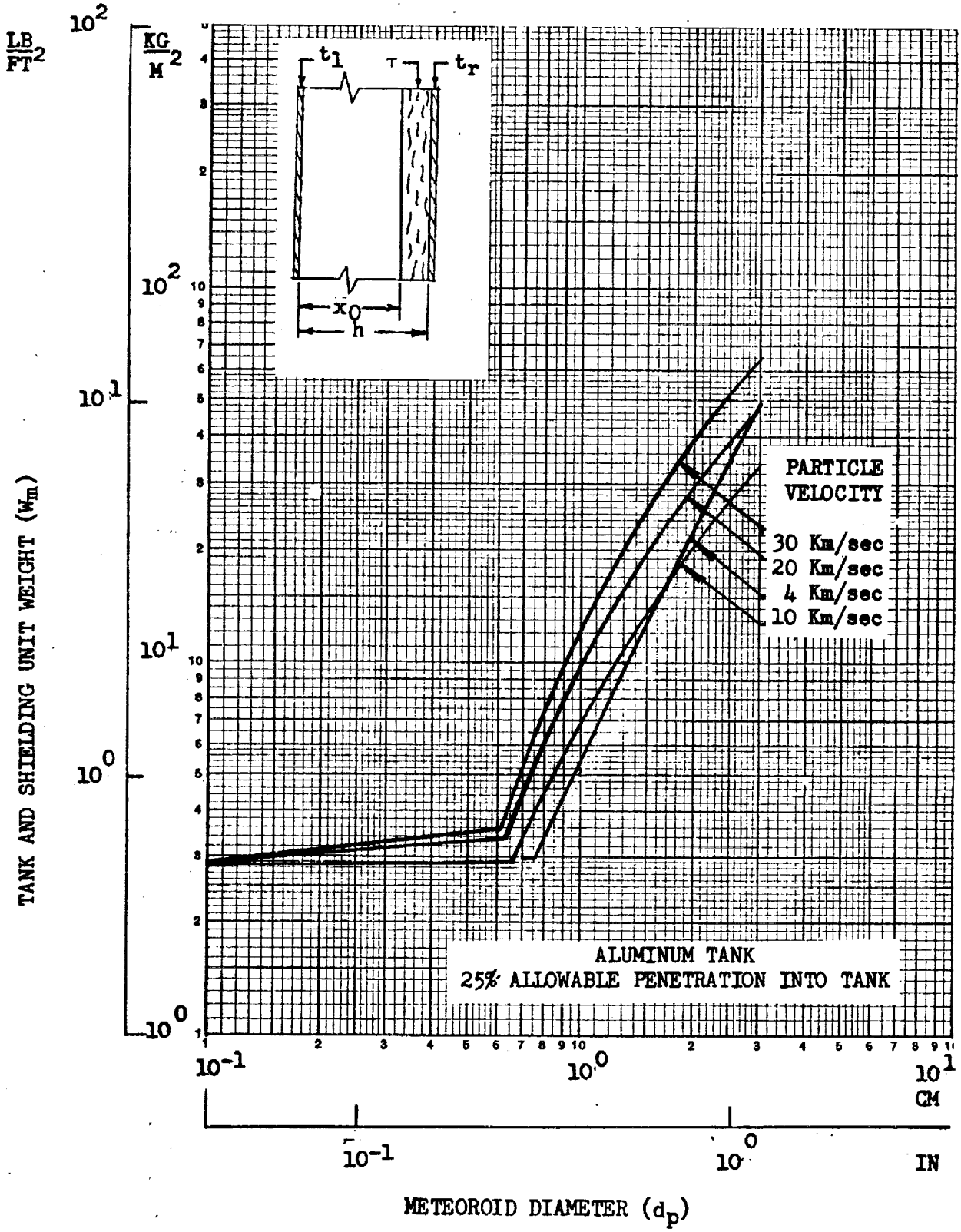

Figure B-21. Single Bumper Protection Weight - Cometary Meteoroids - Titanium Material - 2 Inch/2lb/ft^3 Insulation

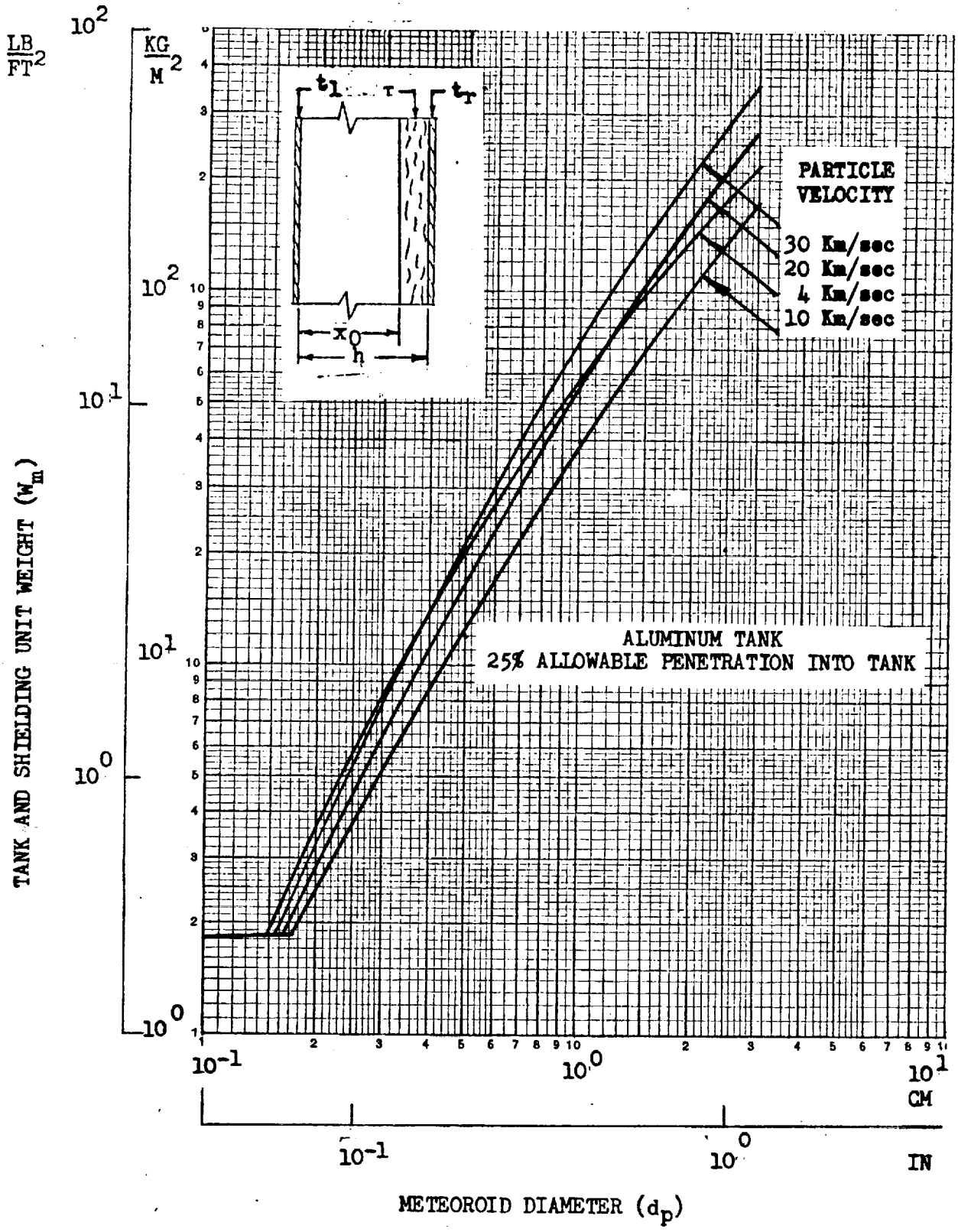

re B-22. **Single Bumper Protection Weight - Asteroidal Meteoroids - Aluminum Material - 2 Inch/2lb/ft^3 Insulation**

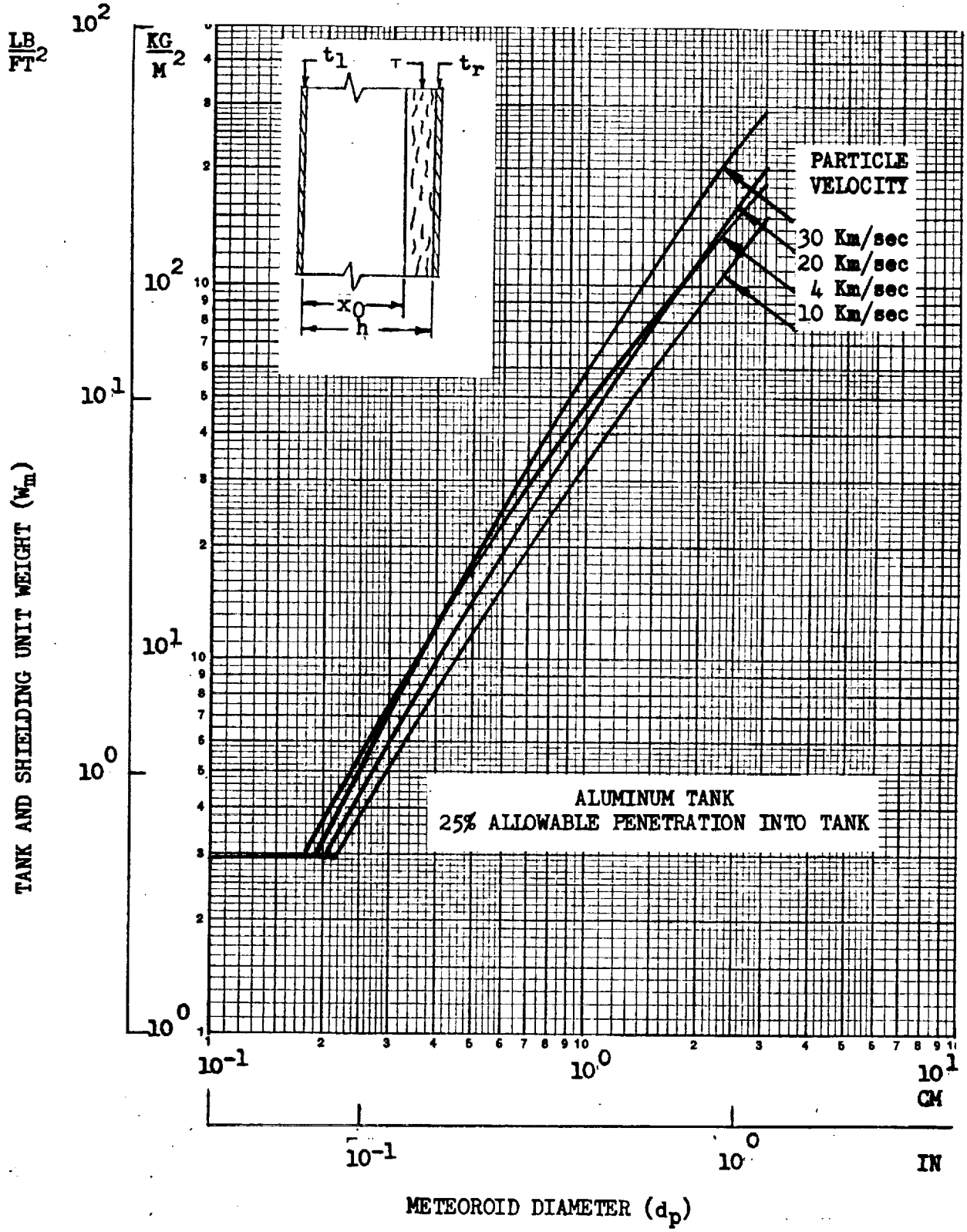

Figure B-23. Single Bumper Protection Weight - Asteroidal Meteoroids - Titanium Material - 2 Inch/2lb/ft^3 Insulation

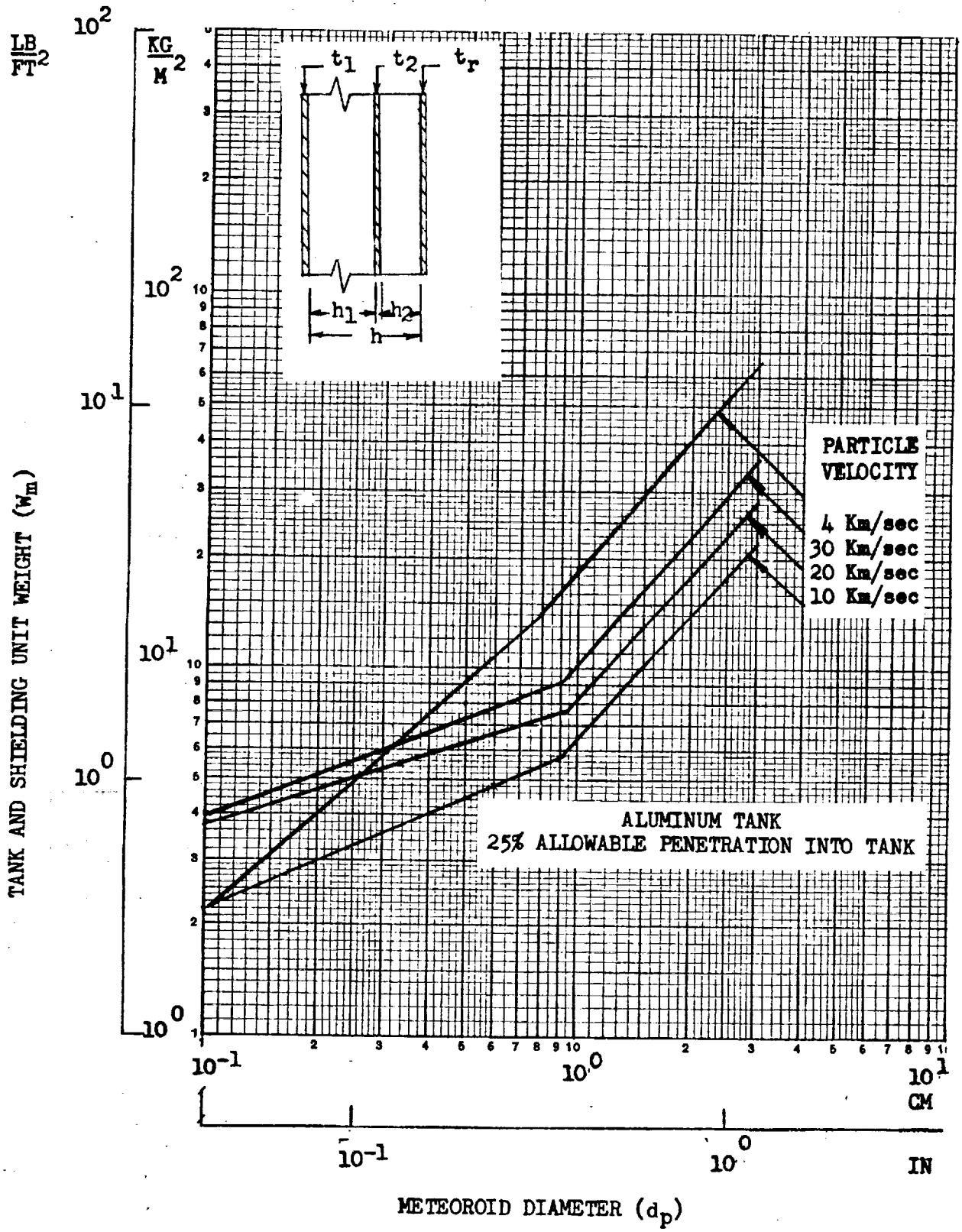

gure B-24. Dual Bumper Meteoroid Protection - Cometary Meteoroids - Aluminum Material - Zero Insulation

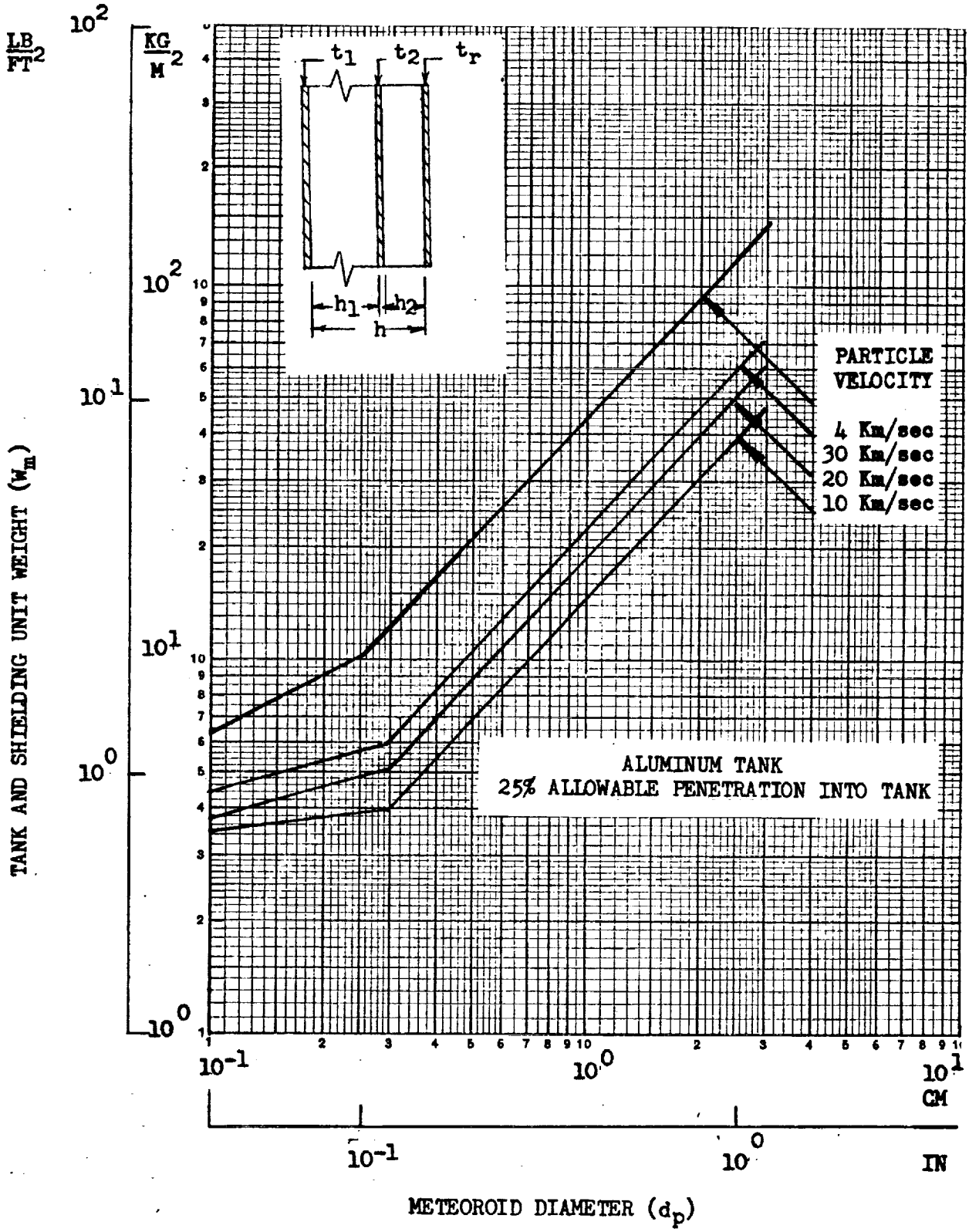

igure B-25. Dual Bumper Meteoroid Protection - Asteroidal Meteoroids - Aluminum Material - Zero Insulation

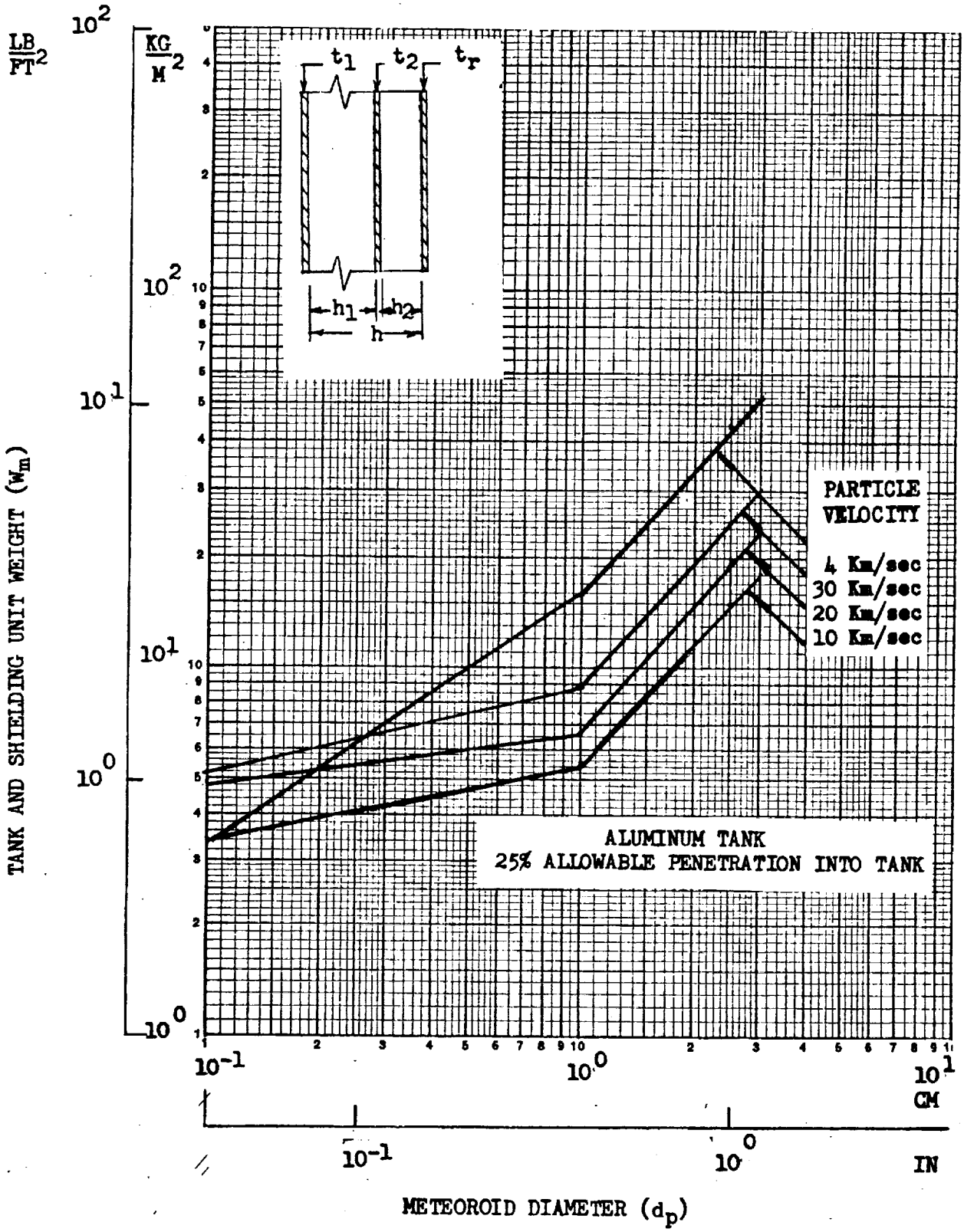

Figure B-26. Dual Bumper Meteoroid Protection - Cometary Meteoroids - Titanium Material - Zero Insulation

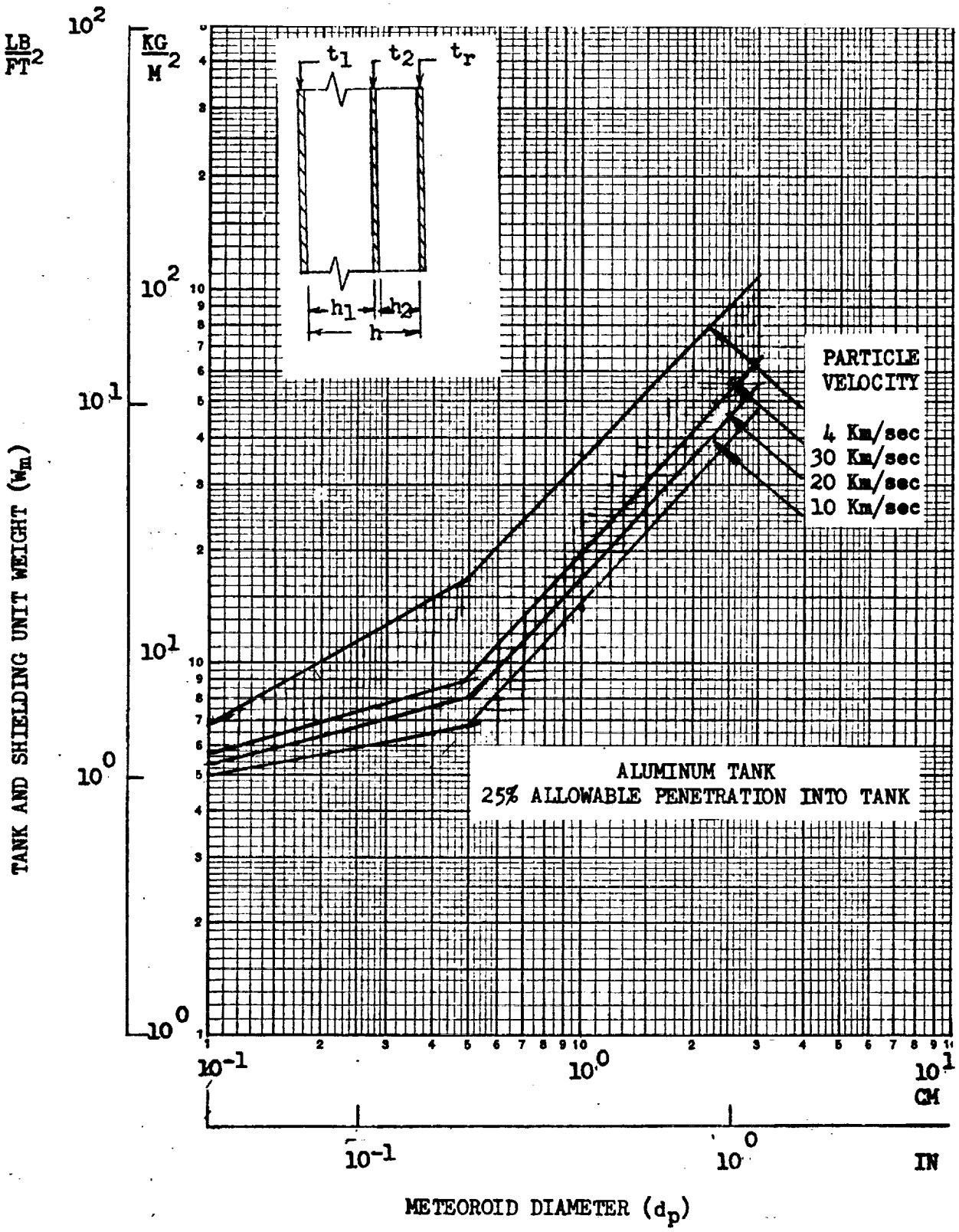

Figure B-27. Dual Bumper Meteoroid Protection - Asteroidal Meteoroids - Titanium Material - Zero Insulation

APPENDIX C

THERMAL INSULATION OPTIMIZATION FOR PROPELLANT TANK

A one dimensional thermal model will provide a representative assessment of the insulation requirements and the heat input into the propellant tanks. The optimum relationship between the boil-off propellant and the insulation thickness is obtained by minimizing the total vehicle mass. The following expression for the propellant boil-off mass (W_B) is the total heat input divided by the heat of vaporization of the propellant.

$$W_B = \frac{Q_{in}}{L} \qquad \text{(C1)}$$

where L = the heat of vaporization

An analytical approach to the insulation optimization was suggested in Reference C1 which provides an explicit approach rather than the usual iterative techniques. Reference C1 considered the insulation optimization only for a fixed stage size. This study is concerned with the sizing and weight estimation for propulsion stages and therefore the model used in Reference C1 has been expanded to include the additional tank volume required to contain the propellant prior to boil-off. Figure C1 is a schematic representating the tankage optimization modeling. For the actual vehicle systems, optimization is considered for a two-stage vehicle, with up to two burns per stage and each stage having bipropellant tankage. The performance mass ratios (μ) for a two stage vehicle are given by the following:

Stage one performance mass ratios -

$$\mu_{11} = \frac{W_{PL}+W_{S1}+W_{S2}+W_{INS1}+W_{INS2}+W_{P11}+W_{P12}+W_{P21}+W_{P22}+W_{B11}+W_{B21}+W_{B22}+W_{B23}}{W_{PL}+W_{S1}+W_{S2}+W_{INS1}+W_{INS2}+W_{P12}+W_{P21}+W_{P22}+W_{B11}+W_{B21}+W_{B22}+W_{B23}}$$

$$\mu_{12} = \frac{W_{PL}+W_{S1}+W_{S2}+W_{INS1}+W_{INS2}+W_{P12}+W_{P21}+W_{P22}+W_{B22}+W_{B23}}{W_{PL}+W_{S1}+W_{S2}+W_{INS1}+W_{INS2}+W_{P21}+W_{P22}+W_{B22}+W_{B23}} \qquad \text{(C2)}$$

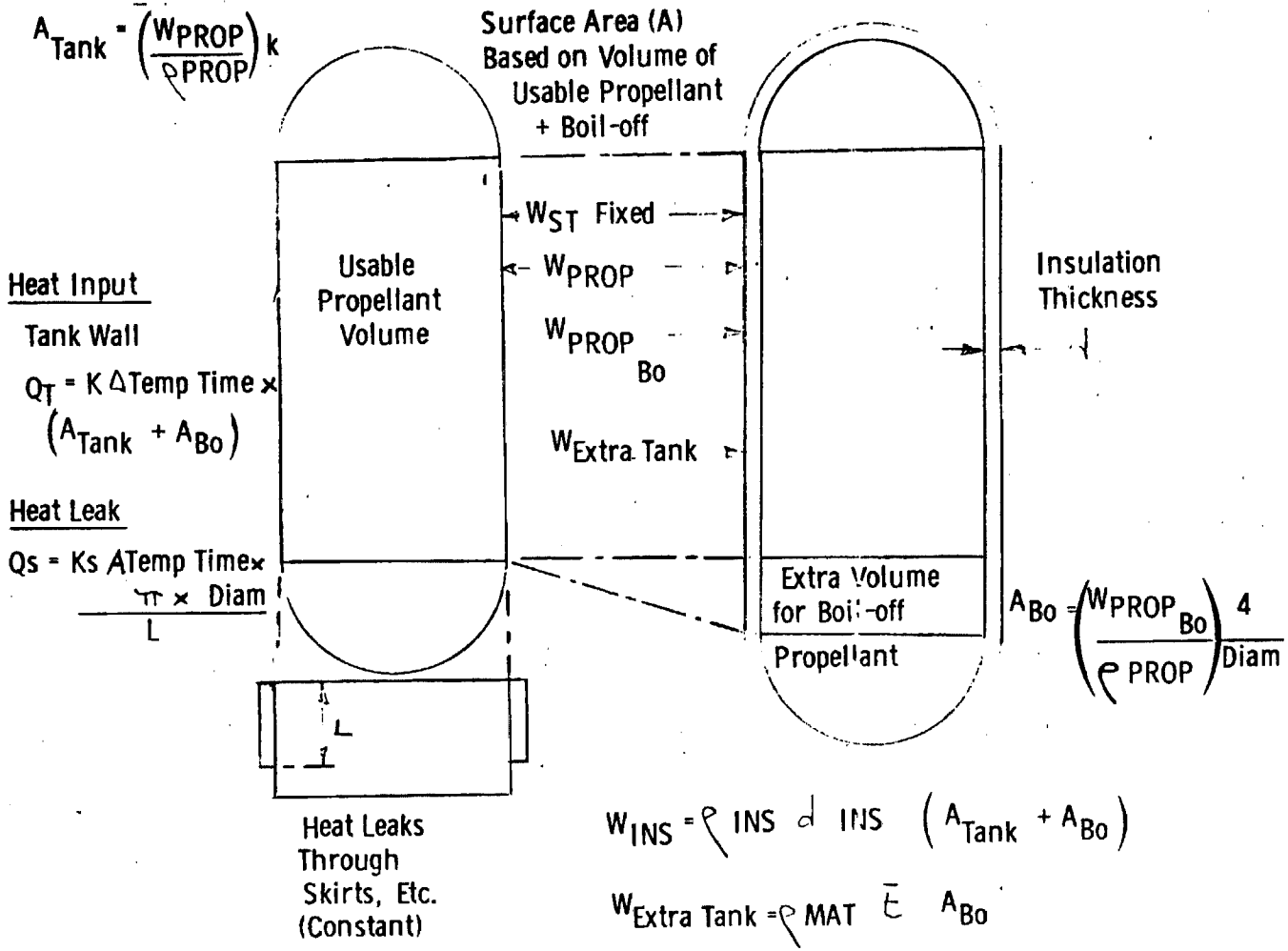

Figure C-1. Thermal Insulation Optimization Model

Stage two performance mass ratios

$$\mu_{21} = \frac{W_{PL}+W_{S2}+W_{INS2}+W_{P21}+W_{P22}+W_{B23}}{W_{PL}+W_{S2}+W_{INS2}+W_{P22}+W_{B23}} \qquad (C3)$$

$$\mu_{22} = \frac{W_{PL}+W_{S2}+W_{INS2}+W_{P22}}{W_{PL}+W_{S2}+W_{INS2}}$$

where W_{PL} = payload mass

W_S = inert weight of stage with no insulation

W_{INS} = weight of stage insulation

W_P = weight of useful propellant per stage

W_{Bij} = weight of boil-off propellant from the ith stage between the jth and the j+1th velocity increment of the total vehicle

μ_{ij} = the performance mass ratio for the jth burn of the ith stage.

The initial vehicle mass is given by

$$W_o = W_{PL}+W_{S1}+W_{S2}+W_{INS1}+W_{INS2}+W_{P11}+W_{P12}+W_{P21}+W_{P22}+W_{B1}+W_{B2} \qquad (C4)$$

Where in addition to the previously defined variables

W_{Bi} = total boil-off propellant weight for the i^{th} stage

Combining Equations C2, C3 and C4.

$$W_o=\mu_{11}(W_{B11}+W_{B21}+\mu_{12}(W_{S1}+W_{INS1}+W_{B22}+\mu_{21}(W_{B23}+\mu_{22}(W_{PL}+W_{S2}+W_{INS2}))))$$
$$-W_{B11}-W_{B21}W_{B22}-W_{B23}+W_{B1}+W_{B2} \qquad (C5)$$

C.1 MONOPROPELLANT STAGE

A monopropellant stage will be considered initially and afterwards expanded to the bipropellant combinations. The inert stage weight (W_S) is composed of a fixed inert weight ($W_S{}^1$) for a stage with no propellant boil-off and the additional tank weight ($W_{ST_{BO}}$), required to contain the boil-off propellant.

$$W_S = W_S{}^1 + W_{ST_{BO}}$$

If the stage diameter remains fixed and the tank length increases to contain the additional propellant, the tank weight increase will be linear with the weight of propellant boil-off.

$$W_S = W_S{}^1 + G_1 W_B \qquad (C6)$$

The amount of propellant boil-off due to solar heating of the tanks with no other heat leaks

$$W_B = \frac{A^1 K}{dL} \qquad (C7)$$

where $K = Q_{IN} \frac{d}{A}$

Unfortunately the surface area of the tank (A^1) is not a fixed value but is dependent on the amount of boil-off. Therefore, Equation C7 is modified to

$$W_B = \frac{(A + f W_B) K}{dL} \qquad (C8)$$

L = Propellant heat of vaporization

where (A) is the fixed area based upon the useful propellant and ($f W_B$) is the additional surface area incurred by propellant boil-off. Equation C8 can be rearranged to give

$$W_B = \frac{AK}{dL - f\ K} \qquad (c9)$$

The insulation weight (W_{INS}) is given by

$$W_{INS} = (A + f\ W_B)\ d\ \rho_{INS} \qquad (C10)$$

where ρ_{ins} is the insulation density.

C.1.1 Two-Stage Vehicle-Single Burn

Considering a two-stage vehicle with a single burn during each stage, and substituting Equations C6, C8 and C10 into Equation C5, the following results:

$$\mu_1 = \mu_{11} \quad \text{for a single burn}$$

$$W_o = \mu_1 \left[W_{S1}{}^1 + \mu_{21}(W_{PL} + W_{S2}{}^1) \right]$$

$$+ \frac{A_1}{d_1 L_1 - f_1 K_1} \left[K_1 \mu_1\ G_1 + f_1\ d_1\ \rho_{ins}\ \mu_1\ K_1 + K_1 \right]$$

$$+ \mu_1\ A_1\ d_1\ \rho_{ins} + \mu_1\ \mu_{21}\ A_2\ d_2\ \rho_{ins} \qquad (C11)$$

$$+ \frac{A_2\ K_2}{d_2 L_2 - f_2\ K_2} \left[\mu_1\ \mu_{21}\ G_2 + \mu_1\ \mu_{21}\ f_2\ d_2\ \rho_{ins} + 1 + K_{21}(\mu_1 - 1)/K_2 \right]$$

where

K_i = total normalized heat absorbed by the i^{th} stage

K_{ij} = normalized heat absorbed by the i^{th} stage between the j^{th} and $j+1^{th}$ burn of the entire vehicle

Differentiating Equation C11 with respect to the insulation thickness, the optimum thicknesses are found to be

$$d_{1_{opt}} = \frac{f_1 K_1}{L_1} + \frac{1}{L_1}\sqrt{\frac{L_1 K_1}{\rho_{ins}}\left(G_1 + \frac{1}{\mu_1}\right) + f_1^2 K_1^2}$$

$$d_{2_{opt}} = \frac{f_2 K_2}{L_2} + \frac{1}{L_2}\sqrt{\frac{L_2 K_2}{\rho_{ins}}\left[G_2 + \frac{1}{\mu_1 \mu_{21}}\left(1 + \frac{K_{21}(\mu_{11}-1)}{K_2}\right)\right] + f_2^2 K_2^2} \qquad \text{(C12)}$$

If the additional tank volume is neglected (i.e., a fixed tank volume), then Equation C2 reduces to the following results as identified in Reference C1.

$$d_1 = \sqrt{\frac{K_1}{\mu_1 \rho_{ins} L}}$$

$$d_2 = \sqrt{\frac{K_2 + K_{21}(\mu_1 - 1)}{\mu_1 \mu_2 \rho_{ins} L}}$$

The optimum boil-off propellant requirement for the two stages are obtained from Equations C12 and C9.

$$W_{B_{1_{opt}}} = A_1\sqrt{\frac{K_1 \rho_{ins} \mu_1}{L_1(G_1 \mu_1 + 1) + f_1^2 K_1 \mu_1 \rho_{ins}}}$$

$$W_{B_{2_{opt}}} = A_2\sqrt{\frac{K_2 \rho_{ins} \mu_1 \mu_2}{\left\{L_2\left(G_2 \mu_1 \mu_2 + 1 + \frac{K_{21}}{K_2}(\mu_1 - 1)\right) + f_2^2 K_2 \mu_1 \mu_2 \rho_{ins}\right\}}} \qquad \text{(C13)}$$

C.1.2 Two Stages - Two Burns Per Stage

The next step considers two burns per stage and shows how the optimum equations for the two stage vehicle are modified for the additional burns. The mass ratios for two burns for a single stage are:

$$\mu_{11} = \frac{W_{PL}+W_{S1}+W_{INS_1} + W_{P11} + W_{P12} + W_{B_1}}{W_{PL} + W_{S1} + W_{INS1} + W_{P12} + W_{B1}} \qquad \text{(C14)}$$

$$\mu_{12} = \frac{W_{PL} + W_{S1} + W_{INS1} + W_{P12}}{W_{PL} + W_{S1} + W_{INS1}}$$

The initial vehicle weight can be expressed as:

$$W_o = \mu_{11}\mu_{12}\left(W_{PL} + W_{S1}{}^{1} + A_1 d_1 \rho_{ins}\right) + \frac{A_1 K_1}{d_1 L_1 - f_1 K_1}\left[\mu_{11}\mu_{12} G_1 + f_1 \; d_1 \rho_{ins} \mu_{11}\mu_{12} + 1 + \frac{K_{21}}{K_1}(\mu_{11}-1)\right] \qquad \text{(C15)}$$

The optimum results obtained from Equation C15 are:

Insulation Thickness

$$d_{1_{opt}} = \frac{f_1 K_1}{L_1} + \frac{1}{L_1}\sqrt{\frac{L_1 K_1}{\mu_{11}\mu_{12}\rho_{ins}}\left[1+\frac{K_{11}}{K_1}\right] + \frac{L_1 K_1 G_1}{\rho_{ins}} + K_1{}^2 f_1{}^2} \qquad \text{(C16)}$$

Boil-Off Propellant

$$W_{B_1\,opt} = A_1\sqrt{\frac{K_1 \rho_{ins}\mu_{11}\mu_{12}}{L_1\left[1+\frac{K_{11}}{K_1}(\mu_{11}-1)\right] + L_1 G_1 \mu_{11}\mu_{12} + K_1{}^2 f_1{}^2 \mu_{11}\mu_{12}\rho_{ins}}} \qquad \text{(C17)}$$

Equation C17 for the two-burn condition is similar to Equation C13 for the single burn, with an additional term to accounts for the boil-off between the two burns of the first stage, namely

$$\frac{K_{11} \quad (\mu_{11}-1)}{K_1 \ \mu_{11}\mu_{12}}$$

Similarly, considering the double burn for the second stage, the following is obtained:

$$d_{2_{opt}} = \frac{f_2 K_2}{L_2} + \frac{1}{L_2}\sqrt{\frac{L_2K_2}{\mu_{11}\mu_{12}\mu_{21}\mu_{22}\rho_{ins}} \times\left[1+\frac{K_{21}}{K_2}(\mu_{11}-1)+\frac{K_{22}}{K_2}(\mu_{11}\mu_{12}-1)+\frac{K_{23}}{K_2}(\mu_{11}\mu_{12}\mu_{21}-1)\right] + \frac{L_2K_2G_2}{\rho_{ins}} + K_2{}^2 f_2{}^2} \quad \text{(C18)}$$

$$W_{B_{o_2}}{}_{opt} = A_2\sqrt{\frac{K_2 \rho_{ins}\mu_{11}\mu_{12}\mu_{21}\mu_{22}}{\left\{L_2\left[1+\frac{K_{21}}{K_2}(\mu_{11}-1)+\frac{K_{22}}{K_2}(\mu_{11}\mu_{12}-1)+\frac{K_{23}}{K_2}(\mu_{11}\mu_{12}\mu_{21}-1)\right]\right\}} + L_2 G_2 \mu_{11}\mu_{12}\mu_{21}\mu_{22} + K_2 f_2{}^2 \mu_{11}\mu_{12}\mu_{21}\mu_{22}\rho_{ins}} \quad \text{(C19)}$$

C.2. Bipropellant Stages

For the bipropellant stage, the stage inert for a single stage and single burn is given by:

$$W_{S1}{}^1 = W_{S1} + G_{1_0} W_{B1_0} + G_{1_f} W_{B1_f} \quad \text{(C20)}$$

Surface area change with boil-off is as follows:

$$A_{l_O} = A_{l_{O_{fixed}}} + f_{l_O} (W_{B_{l_O}})$$

$$A_{l_f} = A_{l_{f_{fixed}}} + f_{l_f} (W_{B_{l_f}}) \qquad \text{(C21)}$$

$$\text{Area} = A_{l_O} + A_{l_f} + f_{l_O} (W_{B_{l_O}}) + f_{l_f} (W_{B_{l_f}})$$

where subscript "O" and "f" refer to the oxidizer and fuel respectively

The initial vehicle weight is given by the following:

$$W_o = \mu_1 \left[W_{Sl} + A_{l_O} d_{l_O} \rho_{ins_O} + A_{l_f} d_{l_f} \rho_{ins_f} + W_{PL} \right]$$
$$+ \frac{A_{l_O} K_{l_O}}{d_{l_O} L_O - f_{l_O} K_{l_O}} \left[\mu_1 G_{l_O} + f_{l_O} \mu_1 d_{l_O} \rho_{ins_O} + 1 \right] \qquad \text{(C22)}$$
$$+ \frac{A_{l_f} K_{l_f}}{d_{l_f} L_f - f_{l_f} K_{l_f}} \left[\mu_1 G_{l_f} + f_{l_f} \mu_1 d_{l_f} \rho_{ins_f} + 1 \right]$$

The terms for oxidizer and fuel are completely independent in Equation C22. Therefore, the optimization can be performed independently for the oxidizer and fuel.

Optimum Insulation

$$d_{l_O} = \frac{f_{l_O} K_{l_O}}{L_O} + \frac{1}{L_O} \sqrt{\frac{K_{l_O}}{\mu_1 \rho_{ins_O}} (L_O \mu_1 G_{l_O} + L_O + \mu_1 K_{l_O} f_{l_O}^2 \rho_{ins_O})}$$

$$d_{l_f} = \frac{f_{l_f} K_{l_f}}{L_f} + \frac{1}{L_f} \sqrt{\frac{K_{l_f}}{\mu_1 \rho_{ins_f}} (L_f \mu_1 G_{l_f} + L_f + \mu_1 K_{l_f} f_{l_f}^2 \rho_{ins_f})}$$

Propellant boil-off

$$W_{B_{l_o}} = A_{l_o} \sqrt{\frac{\mu_l \rho_{ins_o} K_{l_o}}{(L_o \mu_l G_{l_o} + L_o + K_{l_o} f_{l_o}^2 \mu_l \rho_{ins_o})}}$$

$$W_{B_{I_F}} = A_{l_f} \sqrt{\frac{\mu_l \rho_{ins_f} K_{l_f}}{(L_f \mu_l G_{l_f} + L_f + K_{l_f} f_l^2 \mu_l \rho_{ins_f})}}$$

This independency of fuel and oxidizer insulation optimization can be applied to the two-stage process, Equation C13 and the multi-burn case, Equations C16, C17, C18 and C19.

APPENDIX D

OPTIMUM THERMAL SHIELDING FOR TANK SUPPORTS

A typical tank/skirt insulation model is shown in Figure D1 where insulation not only encases the tank but additional insulation is required along the skirt length. This insulation length along the skirt is defined in an optimum fashion to effectively minimize the heat input down the skirt and into the tank. A simplified thermal model for this support structure is shown in Figure D1 where the tank is considered as the cold surface. The uninsulated support structure away from the tank is the hot surface exposed either to the solar heat flux or another heat source such as an engine system or tank with propellant at a higher temperature.

The total heat leak per unit time into the tank of Figure D1 is given by

$$\dot{Q}_T = \dot{Q}_1 + \sum_{i=2}^{n} \dot{Q}_i , \qquad (D1)$$

where:

Q_1 = heat leak per unit time through wall surfaces

Q_i = heat leak per unit time through support i

n = number of heat leak paths

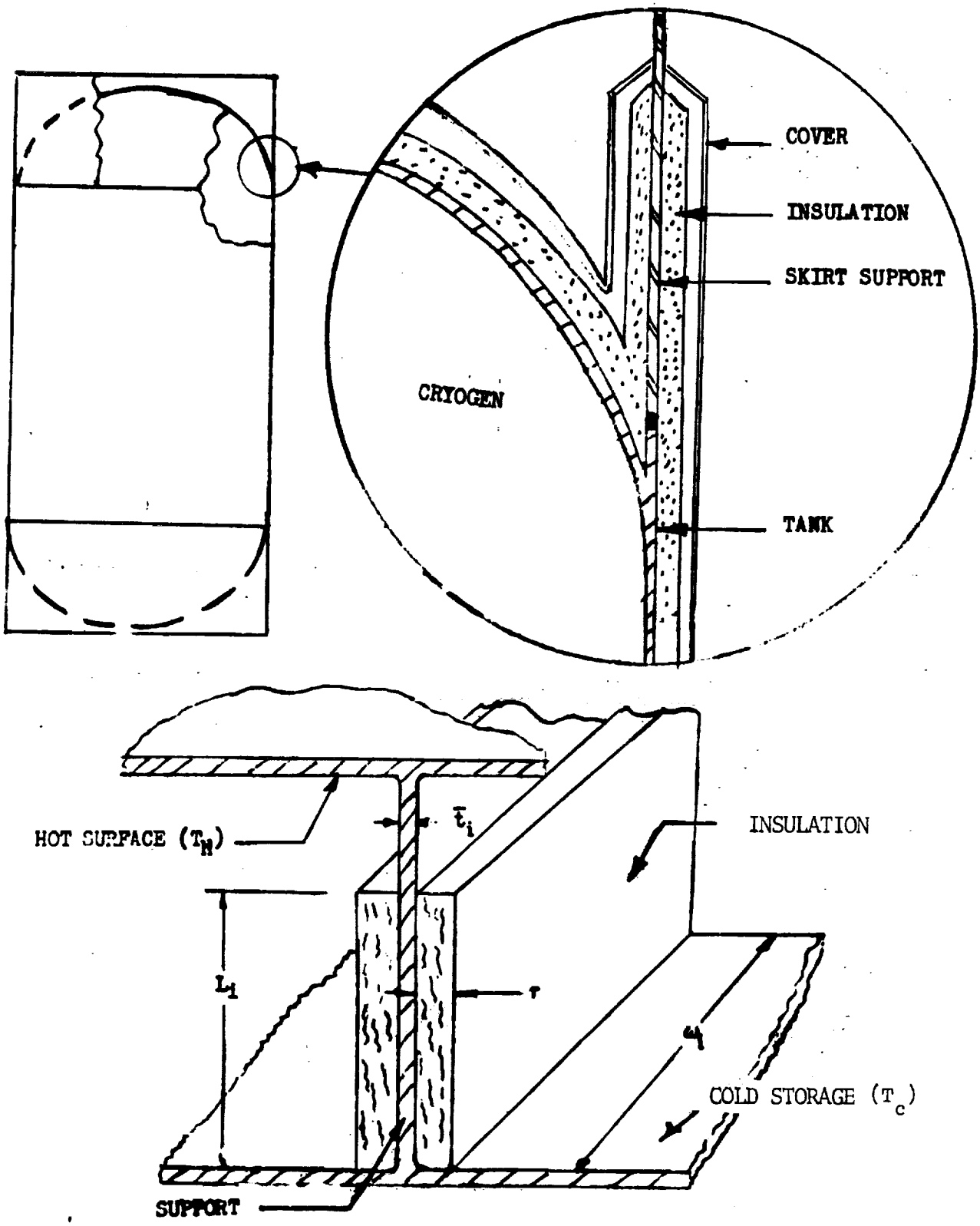

FIGURE D1. TANK SUPPORT INSULATION MODEL

The heat leak rate through wall surfaces is given by

$$\dot{Q}_l = \frac{kA_l \Delta T}{\tau_l} \qquad (D2)$$

where

k = mean value of the thermal conductivity for the insulation

$$k \approx \frac{1}{T_H - T_C} \int_{T_C}^{T_H} k_{ins} \, dT$$

where k_{ins} = thermal conductivity of a layer of insulation at temperature T

Average surface temperatures, T_H, throughout the mission are used. These temperatures are obtained from a heat balance which neglects the heat transmitted through the insulation. This amount of heat is small compared to the heat absorbed and reflected by efficient insulation systems. Surface temperatures for the interplanetary phase of the missions are a function of the tank orientation relative to the sun and of the optical surface properties such as solar absorptivity of surface coatings, and surface emissivity . For cryogenic propellants where low temperatures are required, the surface should be coated with an optical solar reflector ($\alpha_s/\epsilon = 0.06$) or with a white paint that has undergone ultraviolet degradation ($\alpha_s/\epsilon = 0.4$), (Reference D1).

The heat transfer through any support shown in Figure D1 can be approximated by neglecting the edge effects as follows.

$$\dot{Q}_i = \Delta T \omega_i \sqrt{\frac{2\bar{t} K_i k}{\tau_i}} \, \mathrm{COTH} \left(\sqrt{\frac{2k}{K_i \bar{t}_i \tau_i}} \right) \qquad (D3)$$

where

K_i = thermal conductivity of support.

The effective design time (θ_ϵ) for the thermal analysis can be represented by the mission phase duration (θ), plus an additional time to account for the boost ascent to earth orbit. During the ascent and initial earth orbits, thermal conductivity has been degraded due to insulation out-gassing.

From previous studies it was found that an additional 1200 hours would account for this initial boost phase. The allowable total rate of heat input for a specified fractional propellant boil-off, β , is given by

$$\dot{Q}_T = \frac{\beta L W_P}{(\theta + 1200)}$$

where

L = propellant heat of vaporization of

W_p = weight of propellant

The minimum heat rate input of a propellant module $\dot{Q}_T$ is obtained when for a fixed Q_1 the support structure is insulated to the length LO_i.

$$\dot{Q}_T = \sum_{i=2}^{n} \frac{\Delta T \omega_i K_i \bar{t}_i}{L_{oi}} + \dot{Q}_1$$

The insulation length (L_i) of Figure D1 can be adjusted to any value desired. There are numerous combinations of τ_i and L_i which can result in specified heat rate input through the supports ($\dot{Q}_i$). The combination which yields minimum insulation weight addition to the support is desired.

Insulation weight is given by

$$m_i = 2\rho_i \tau_i \omega_i L_i$$

Rearranging Equation D3, the insulation length L_i is

$$L_i = \coth^{-1}\left(\frac{\dot{Q}_i}{\Delta T \omega_i}\sqrt{\frac{\tau_i}{2\bar{t}_i K_i k}}\right)\left(\sqrt{\frac{K_i \bar{t}_i \tau_i}{2k}}\right) \qquad (D4)$$

and the insulation weight will become

$$m_i = 2\rho_i \tau^{3/2} \omega_i \sqrt{\frac{K_i \bar{t}_i}{2k}} \quad \mathrm{COTH}^{-1}\left(\frac{\dot{Q}_i}{\Delta T \omega_i}\sqrt{\frac{\tau_i}{2\bar{t}_i K_i k}}\right)$$

To obtain the minimum insulation weight for a specified heat input, the weight is differentiated with respect to the insulation thickness. Therefore for a minimum weight

$$3\,\mathrm{COTH}^{-1}\left(\frac{\dot{Q}_i}{\Delta T_{\omega_i}}\sqrt{\frac{\tau_i}{2\bar{t}_i K_i k}}\right) + \frac{\left(\frac{\dot{Q}_i}{\Delta T_{\omega_i}}\sqrt{\frac{\tau_i}{2\bar{t}_i K_i k}}\right)}{1-\left(\frac{\dot{Q}_i}{\Delta T_{\omega_i}}\right)^2\frac{\tau_i}{2\bar{t}_i K_i k}} = 0 \qquad \text{(D5)}$$

A solution of Equation D5 is

$$\frac{\dot{Q}_i}{\Delta T_{\omega_i}}\sqrt{\frac{\tau_i}{2\bar{t}_i K_i k}} = 1.125 \qquad \text{(D6)}$$

with the optimum insulation thickness for support " i " is given by

$$\tau_i = \frac{2.53\Delta T^2 \omega_i^2 \bar{t}_i K_i k}{\dot{Q}_i^2} \qquad \text{(D7)}$$

Substituting the optimum thickness in Equation D4 and using Equation D6 give the optimum value for insulation length as

$$L_i = 1.61\,\frac{K_i \bar{t}_i \Delta T_{\omega_i}}{\dot{Q}_i} \qquad \text{(D8)}$$

Equations D7 and D8 define the insulation thickness and length of insulation for the support components, provided the allowable heat leak for the support is given. A method is derived which allocates the insulation to the various heat leak paths, supports and wall surfaces, of the tank.

By rearranging Equation D7, the heat rate leak for the i^{th} support is

$$\dot{Q}_i = C_{1i}\sqrt{\frac{\bar{t}_i}{\tau_i}} \qquad \text{(D9)}$$

where

$$C_{1i} = 1.585\Delta T\omega_i\sqrt{K_i k} \tag{D10}$$

For simplicity, the insulation thickness of the overall components was set equal. Previous analysis showed that the optimum allocation of insulation required nearly uniform insulation thickness, provided material for all heat blocks was the same. Using Equation D9, the following can then be written:

$$\left.\begin{aligned} \dot{Q}_3 &= \sqrt{\frac{\bar{t}_3}{\bar{t}_2}\frac{C_{13}}{C_{12}}}\,\dot{Q}_2 \\ \dot{Q}_4 &= \sqrt{\frac{\bar{t}_4}{\bar{t}_2}\frac{C_{14}}{C_{12}}}\,\dot{Q}_2 \end{aligned}\right\}$$

Using Equations D2 and D9 the heat rate input $\dot{Q}_1$ through the tank wall can be expressed as a relationship of the support heat rate input $\dot{Q}_2$ for a given support.

$$\dot{Q}_1 = \dot{Q}_2^2\frac{kA_1\Delta T}{\bar{t}_2 C_{12}^2} \tag{D11}$$

Substituting the expression derived above for $\dot{Q}_3$, $\dot{Q}_4$ and $\dot{Q}_1$ in terms of $\dot{Q}_2$ and Equation D11 in Equation D1 and rearranging gives the heat rate input from the second support ($\dot{Q}_2$) as a function of the insulation properties, support thickness and the total heat rate input $\dot{Q}_T$.

$$\dot{Q}_2 = \frac{1}{2}\left\{ -\frac{1+\sqrt{\frac{\bar{t}_3}{\bar{t}_2}\frac{C_{13}}{C_{12}}}+\sqrt{\frac{\bar{t}_4}{\bar{t}_2}\frac{C}{C_{12}}}}{\frac{kA_1\Delta T}{\bar{t}_2 C_{12}^2}} + \sqrt{\left(\frac{1+\sqrt{\frac{\bar{t}_3}{\bar{t}_2}\frac{C_{13}}{C_{12}}}+\sqrt{\frac{\bar{t}_4}{\bar{t}_2}\frac{C_{14}}{C_{12}}}}{\frac{kA_1\Delta T}{\bar{t}_2 C_{12}^2}}\right)^2 + \frac{4\dot{Q}_T\bar{t}_2 C_{12}^2}{kA_1\Delta T}}\right\}$$

The other heat leak allocations can be determined from Equation D10 and the relationships developed previously for $\dot{Q}_1$, $\dot{Q}_3$ and $\dot{Q}_4$ with $\dot{Q}_2$. Once $\dot{Q}_2$ is determined, insulation thickness can be obtained from the Equation D9.

$$\tau = \frac{\bar{t}_2 C_{12}^2}{\dot{Q}_2^2}$$

and the mass of insulation for the tank supports can be obtained from

$$m = \frac{\rho \bar{t}_2 C_{12}^2 A_1}{\dot{Q}_2^2} + \sum_{i=2}^{n} \frac{2\rho \omega_i L_i \bar{t}_2 C_{12}^2}{\dot{Q}_2^2}$$